Synthesis, Characterization and Applications of Aqua-Stable Metal-Organic Frameworks and their Composites for the Environmental Remediation and Bio-Molecule Sensing

A Dissertation Submitted to the

Indian Institute of Technology Guwahati

as Partial Fulfilment for the Degree of

DOCTOR of PHILOSOPHY

in

CHEMISTRY

by

Subhrajyoti Ghosh

Roll No. 196122037

DEPARTMENT OF CHEMISTRY

INDIAN INSTITUTE OF TECHNOLOGY GUWAHATI

GUWAHATI-781039

INDIA

March 2024

DECLARATION:

I hereby affirm that the thesis titled as " **Synthesis, Characterization and Applications of Aqua-Stable Metal-Organic Frameworks and their Composites for the Environmental Remediation and Bio-Molecule Sensing**" is the culmination of my research conducted at the Department of Chemistry, Indian Institute of Technology Guwahati. I conducted this research under the guidance of Dr. Shyam P. Biswas. I confirm that this work has not been previously submitted to any other institution or university. I have duly acknowledged collaborative efforts in obtaining results and have appropriately credited materials sourced from other references in the thesis.

Adhering to scientific traditions, I assert that all information presented in this thesis is accurate to the best of my knowledge.

IIT Guwahati

March 2024

Subhrajyoti Ghosh

Candidate

Dr. Shyam P. Biswas
Associate Professor
Department of Chemistry
Indian Institute of Technology Guwahati
Guwahati – 781039, India
Tel: +91-361-258 3309
Email: sbiswas@iitg.ac.in

CERTIFICATE

This is to certify that the work presented in the thesis entitled "**Synthesis, Characterization and Applications of Aqua-Stable Metal-Organic Frameworks and their Composites for the Environmental Remediation and Bio-Molecule Sensing**" by Mr. Subhrajyoti Ghosh, was carried out by the candidate at the Department of Chemistry, Indian Institute of Technology Guwahati, under my supervision and has not been submitted elsewhere for a degree.

IIT Guwahati
March 2024

Shyam Biswas

Thesis supervisor
Department of Chemistry
Indian Institute of Technology Guwahati
Guwahati – 781039, Assam, India

ACKNOWLEDGEMENT

My heartfelt gratitude to all those who played a pivotal role in enabling the successful completion of this dissertation. Foremost, I express my sincere thanks to my supervisor, Dr. Shyam P. Biswas, who introduced me to the fascinating realm of Metal-Organic Frameworks (MOFs). His unwavering motivation, inspiration, encouragement, and consistent guidance were instrumental in navigating the scientific journey documented in this thesis.

In addition to my supervisor, I seize this opportunity to convey my deep appreciation and indebtedness to the members of my doctoral committee, namely Prof. Chandan Mukherjee, Prof. A. S. Achalkumar, and Dr. Kalyan Raidongia for their insightful suggestions and invaluable guidance throughout the research journey.

I express my profound thanks to our collaborators, namely Dr. Amarajothi Dhakshinamoorthy, Dr. Matthias Vandichel, Dr. Felix Steinke, Dr. Uttam Manna, and Prof. Debasis Manna, whose contributions significantly enriched my research work.

The Department of Chemistry and the Central Instrument Facility (CIF) of IIT Guwahati deserve my gratitude for providing access to sophisticated instruments crucial for the characterization of my targeted compounds. My Special thanks go to the faculty and staff members of the Department of Chemistry. I am grateful to the technical officers and operators in the Chemistry Department and CIF for their assistance in data collection.

Heartfelt appreciation is extended to my lab seniors, Dr. Rana Dalapati, Dr. Mostakim SK, Dr. Aniruddha Das, Dr. Soutick Nandi, Dr. Chiranjib Gogoi, and Mr. Masud Alam for their skillful and invaluable support during this undertaking. My list of acknowledgments never becomes complete without saying a special thanks to my lab colleagues, Paltan da, Abhijeet, Srijan, Sakir, Nazir, Arindam, Sandip, Priti and Jyotismita. They are more than my brothers and sisters. Along with their timely help, and support, the joyful atmosphere they maintained in the laboratory made me more enthusiastic to work hard in a friendly environment. I express my thanks to Ravindra Meena, Dinesh Kumar, Pratip Bhattacharyya, and Debjit Mal for their contributions during their project work.

A heartfelt thanks to my friends, Pranam, Rakesh da, Siddhartha, Rupkumar, Subhankar, Hirendra, Abhay, Jagajiban, Sukesh, Santanu, Swarup, Souman, Amit, Bikram and Avishek for their unasked assistance during my research. I am indebted to the teachers and professors from my school, college, and university whose guidance provided direction and insightful information for advancing in this field. A special thanks to my first chemistry teacher Mr. Milan Chandra Low for making me admirable in this colourful world.

I am highly appreciative of the Ministry of Human Resource Development (MHRD), Government of India, and Prime Minister Research Fellowship (PMRF) for providing me with financial and research grand support.

I owe a debt of gratitude to my family my grandparents, Sukumar Ghosh and Malati Ghosh and my parents Subhas Chandra Ghosh and Parbati Ghosh, for their unconditional love and sacrifices throughout my career as a student.

I would like to express my deep love and gratitude to my dear sister Sudipa and Babli and my elder brothers Subir, Suken, and Subhandu daa for their invaluable support. I am also thankful to my sister-in-law Laboni Das for her immense care and support. I extend my

heartfelt thanks to my uncle Arijit Ghosh and my aunt Joly Ghosh for their unwavering support. I express my love to my cousin Soumay. I am sincerely grateful to my two pici Suchitra Ghosh and Uttra Das for their kindness and encouragement.

My deepest regards to the Almighty for granting me the courage to navigate life's complexities and successfully complete this dissertation. Many individuals have contributed, and while their names may not be explicitly mentioned, their efforts and assistance are duly acknowledged.

Subhrajyoti Ghosh

Dedicated to My Loving Family

TABLE OF CONTENTS

Ph.D. Synopsis Report

Thesis Title: Synthesis, Characterization and Applications of Aqua-Stable Metal-Organic Frameworks and their Composites for the Environmental Remediation and Bio-Molecule Sensing

Name of the Candidate: Subhrajyoti Ghosh

Roll No.: 196122037

Thesis Supervisor: Dr. Shyam P. Biswas

Department: Chemistry

Institute: Indian Institute of Technology Guwahati, Assam, India

Thesis Overview:

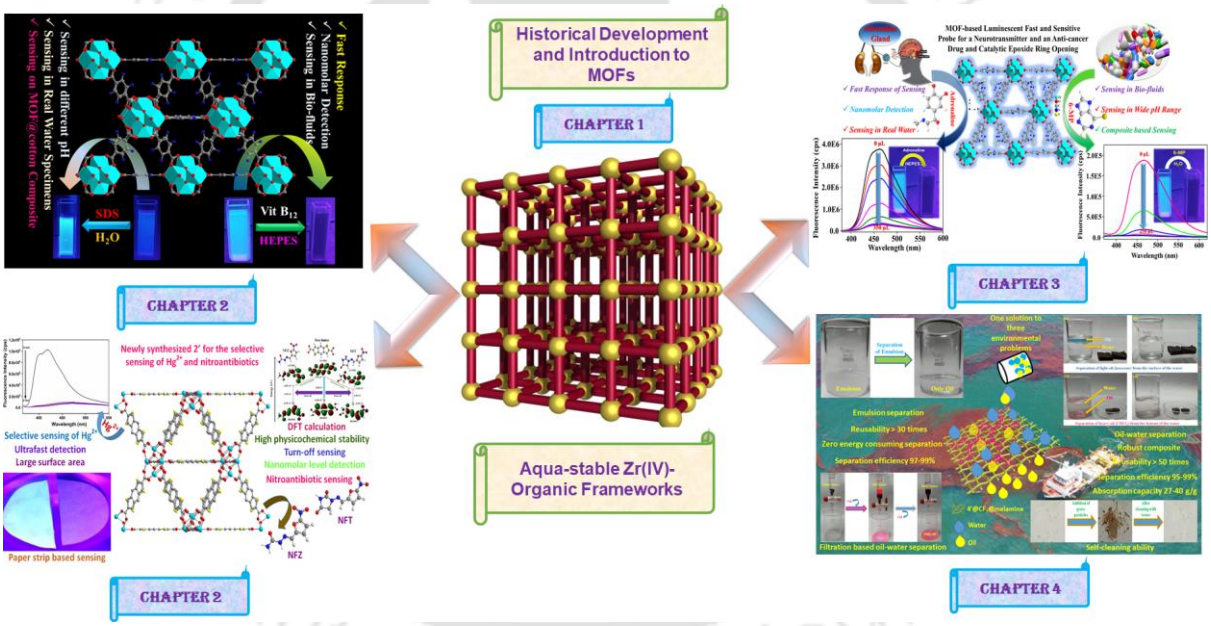

Chapter 1: Historical Evolution of Metal-Organic Frameworks (MOFs) and their Prospective Applications in Targeted Sensing and Adsorption

This chapter provides an overview of the historical development of coordination compounds and the discovery of metal-organic frameworks (MOFs). It explores the synthetic revolution in creating aqua-stable robust MOFs, driven by the imperative to address modern environmental pollution resulting from industrialization, urbanization, population-driven socioeconomic development, modern agricultural practices, and the excessive use and arbitrary disposal of pharmaceutical wastes. Within this thesis, my focus lies on utilizing MOFs as potential fluorescent sensors for various toxic cations, anions, and organic molecules, as well as adsorbents for oil spills. Aqua-stable MOFs are exceptionally versatile materials capable of exhibiting fluorescence properties through the electrical communication between metal ions and conjugated polytopic organic linkers. Furthermore, they can adsorb toxic pollutants using their porous structures. Thus, the introduction comprehensively outlines the synthesis methods for aqua-stable MOFs, elucidates the origins of their fluorescence properties, and delves into the mechanistic aspects of diverse sensing processes. The central theme of this thesis revolves around the creation and applications of various aqua-stable MOFs based on Zr(IV) ions. Detailed discussions are provided on the structures of different Zr(IV)-based MOFs. The introduction also summarizes the pivotal role of aqua-stable MOFs in combating water pollution stemming from drugs, antibiotics, herbicides, pesticides, toxic heavy metal ions, volatile organic compounds, oil spills, and other emerging pollutants over the past few decades. This thesis primarily employs two approaches to monitor water pollution and mitigate environmental risks using MOFs: measuring pollutant concentrations and removing toxic substrates from water. I strategically employed fluorescence sensing for the rapid and accurate measurement of the concentration of foreign substrates in water. The thesis introduces functionalized, target-specific, fluorescent MOFs designed for the selective sensing of organo-toxins and bio-molecules. Additionally, a porous hydrophobic MOF is presented for the efficient and selective removal of oil spills from water, offering substantial reusability.

Chapter 2: A Functionalized MOF for Selective Fluorometric Detection of Sodium Dodecyl Sulphate and Vitamin B_{12} using MOF@Cotton Composite

This chapter provides detailed insights into the synthesis and analytical characterization of a di -NH_2 functionalized aqua-stable metal-organic framework (MOF) (**1**) and the application of its activated forms (**1′**) for the sensing SDS surfactant and vitamin B_{12}. Notably, this MOF represents the pioneering instance of a MOF-based sensor for SDS and vitamin B_{12}, boasting remarkable features such as the lowest reported limits of detection (LOD) values of 108 and 45.3 nM for SDS and vitamin B_{12}, respectively. The sensor exhibits a swift response time, exceptional selectivity, and noteworthy reusability.

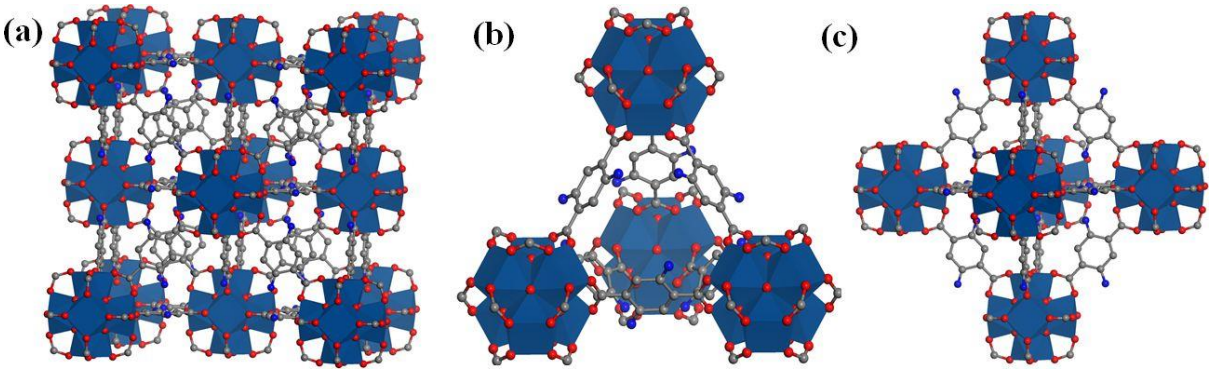

Figure 1 Cubic structure of **1** (a), and its tetrahedral (b) and octahedral (c) cages.

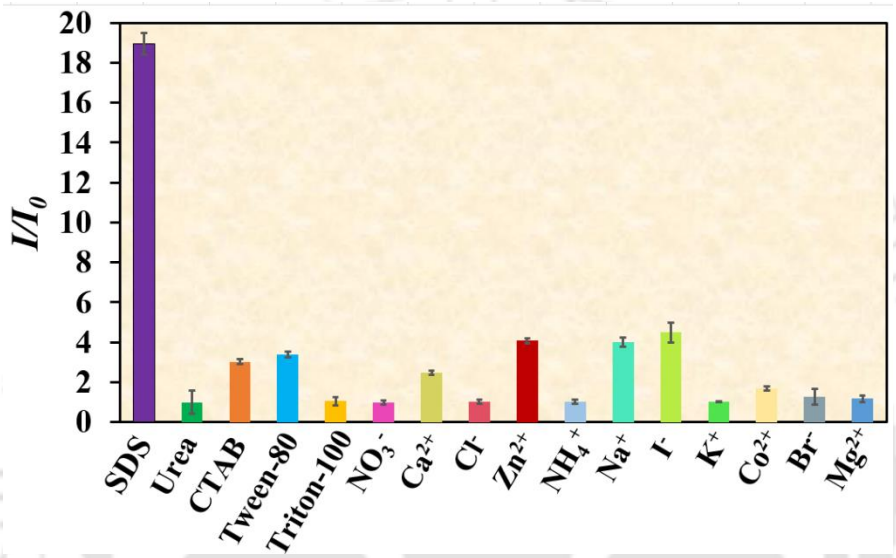

Figure 2 Selectivity test of **1′** for the sensing of SDS (error bars represent the standard deviations of three individual measurements).

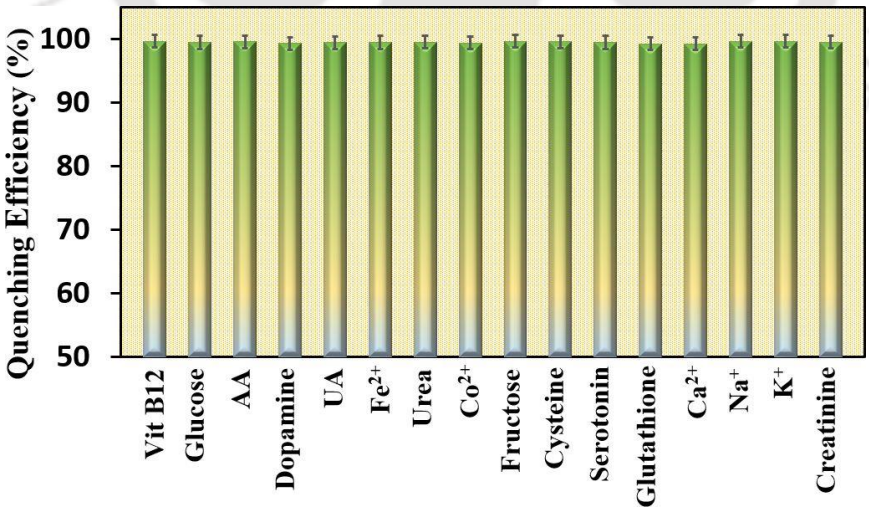

Figure 3 Selectivity test for the sensing of vitamin B_{12} in the presence of other competitors (error bars represent the standard deviations of three individual measurements).

To assess the practical utility of the sensor, its sensing capability was evaluated across various real-water specimens and biofluids. MOF@cotton composites were ingeniously crafted for on-

field detection of both targeted analytes. Even upon treatment with nanomolar concentrations of analyte solutions, observable alterations in the color of the composites were evident. The sensor's selective turn-on sensing of SDS is attributed to electrostatic interactions between the $–NH_2$ groups in the linker and the $–SO_3^-$ group of SDS. In the case of vitamin B_{12}, fluorescence resonance energy transfer (FRET) from the probe to vitamin B_{12} leads to the quenching of the MOF's fluorescence.

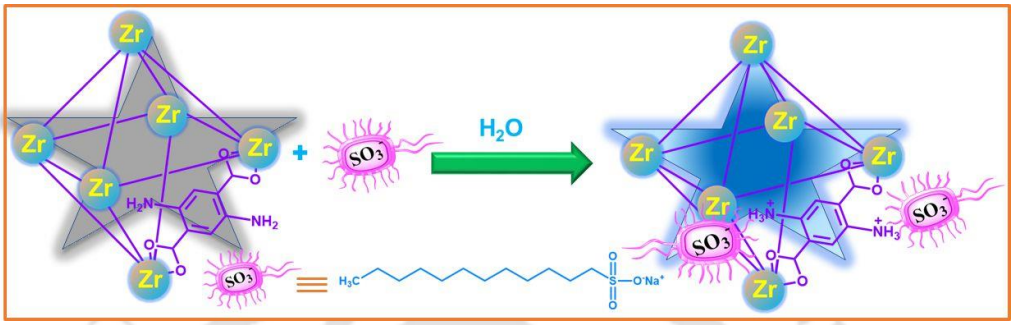

Scheme 1 Schematic representation of SDS sensing by **1′**.

In summary, this research not only introduces a novel aqua-stable MOF but also showcases its exceptional sensing capabilities for SDS and vitamin B_{12}, demonstrating promising potential for practical applications, particularly in the realm of real-world water specimens and biofluids. The fabrication of MOF@cotton composites further extends the sensor's utility, enabling visible color changes in response to low concentrations of the target analytes.

Chapter 3: A Fluorescent Zirconium Organic Framework Displaying Rapid and Nanomolar Level Detection of Hg(II) and Nitroantibiotics

In this chapter, a zirconium (Zr) metal-organic framework (MOF) bearing the rigid benzo[1,2-b:4,5-b']dithiophene-2,6-dicarboxylic acid linker was prepared and its solid structures were characterized with the help of X-ray powder diffraction (XRPD) and Rietveld refinement techniques. Other characterization methods like thermogravimetric analysis, FE-SEM, EDX, Fourier transform infrared spectroscopy, and elemental analysis were applied to verify the phase purity of the compound. Both as-synthesized (**2**) and activated (**2′**) compounds are thermally stable up to 415 °C in N_2 environment. The BET surface area of **2′** was found to be 1228 $m^2 g^{-1}$.

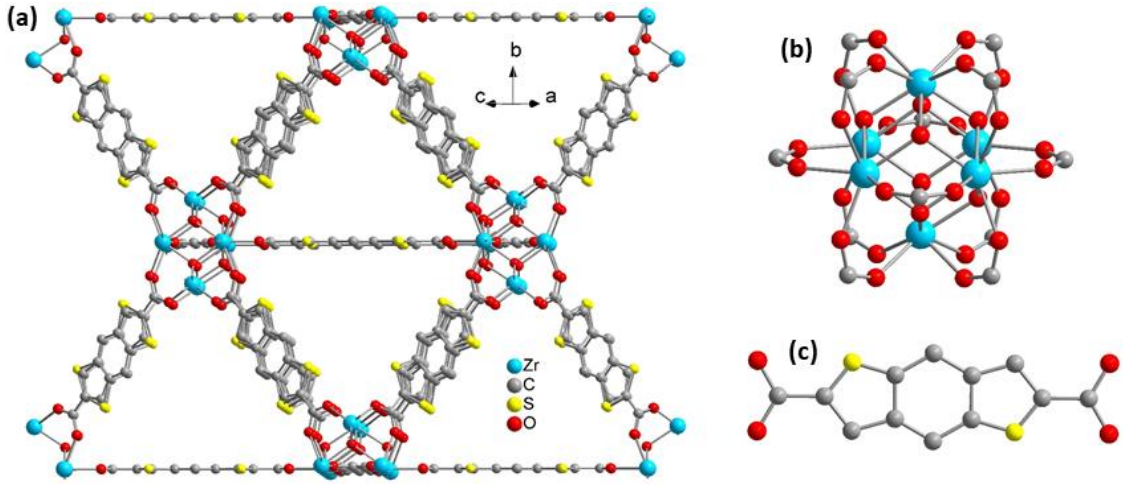

Figure 4 Structure of compound **2** (a), its SBU (b), and corresponding linker (c).

Fluorescence titration experiments showed that **2′** exhibits highly selective and sensitive fluorescence turn-off behavior towards mercury (Hg^{2+}) and nitroantibiotics (nitrofurazone and nitrofurantoin). The interference experiments suggested that other cations and antibiotics did not interfere in the detection of Hg^{2+} and nitroantibiotics. Moreover, rapid response times (1 min) were shown by the probe **2′** for both the sensing experiments. Together with rapid response, very low limit of detections (LODs) were observed for the sensing of all the targeted analytes (LOD of Hg^{2+}, nitrofurazone (NFZ) and nitrofurantoin (NFT) were 5, 156.7, and 96.3 nM, respectively). The LOD values are lower than the value regulated by WHO and lower than most of the reported chemodetectors of Hg^{2+} and nitroantibiotics (nitrofurazone and nitrofurantoin). Activated MOF (**2′**) can also be effective for the on-site detection of the targeted analytes by using portable paper strips.

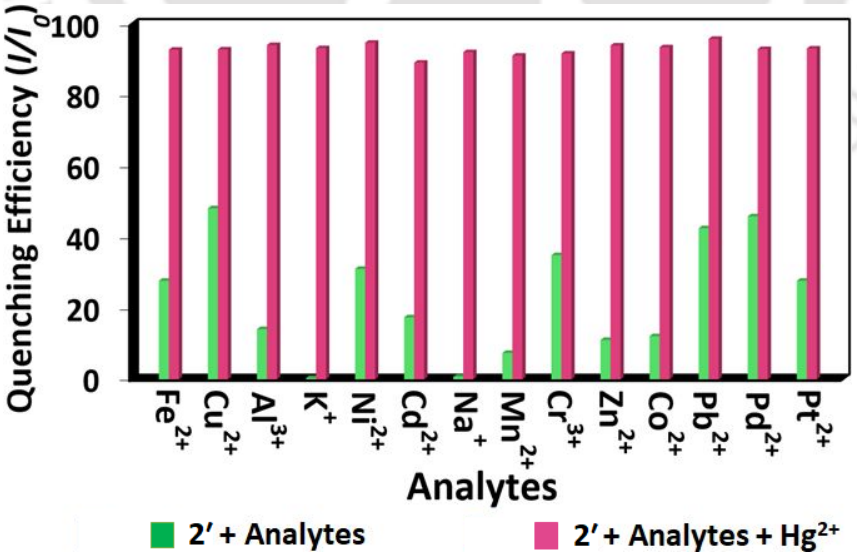

Figure 5 Change in emission response of **2′** after the inclusion of 75 µL of 10 mM Hg^{2+} in the co-existence of 75 µL of 10 mM solutions (in H_2O) of various competitor metal ions (λ_{ex} = 320 nm, λ_{em} = 420 nm).

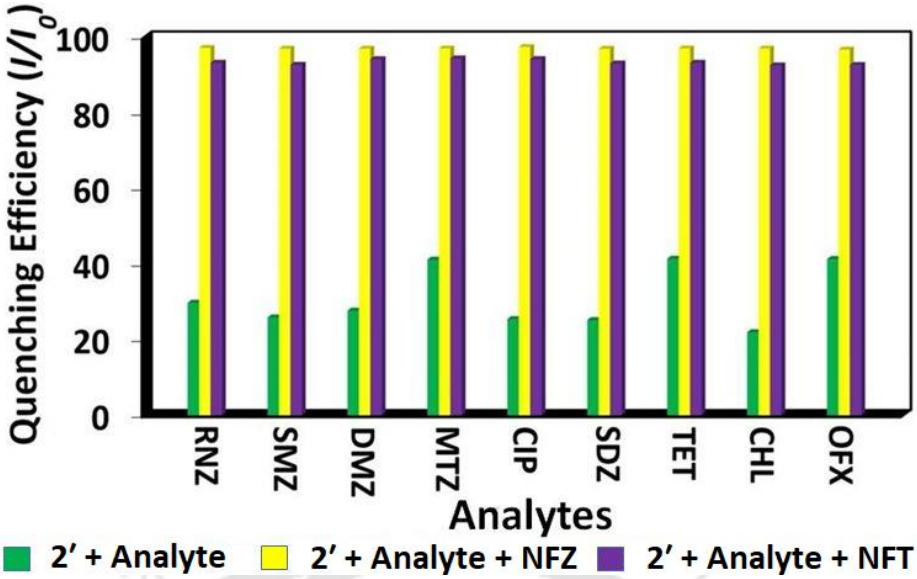

Figure 6 Switch-off in fluorescence emission intensity of **2′** after addition (100 µL) of 10 mM of NFZ and NFT solutions in the presence of 100 µL of 10 mM solutions (in MeOH) of other competitor antibiotics (λ_{ex} = 370 nm, λ_{em} = 442 nm).

The experimental studies about the possible turn-off sensing mechanism of Hg^{2+} revealed the energy transfer through the coordination of Hg^{2+} with the sulfur atoms of the linker was the reason behind the switch-off fluorescence response. The above-discussed reaction mechanism was proved by the PXRD, XPS, TRPL, EDX, and UV-Vis analysis. Furthermore, the resonance energy transfers from **2′** to the nitro-antibiotics were the possible reason behind the quenching in fluorescence intensity which was supported by the decrease in fluorescence lifetime value and maximum overlap between the absorption spectra of nitro-antibiotics and the emission spectra of **2′**. A theoretical HOMO-LUMO energy calculation was also performed using Gaussian 09 software. The theoretical results displayed good agreement with the experimental results. The sensor showed reusability up to five times with no appreciable change in its selectivity and sensitivity. Also, the structural integrity and morphology after five-times reused solids remained similar to the fresh solid which was confirmed by the PXRD analysis.

Chapter 4: MOF-Fabric Composites Based on a Multi-Functional MOF as Luminescent Sensor for a Neurotransmitter and an Anti-Cancer Drug

This chapter contains the construction of a highly physicochemically stable, porous, thiourea-functionalized zirconium metal-organic framework which was applied as a potential probe for the selective ‘turn-on’ fluorometric detection of adrenaline in HEPES buffer (pH = 7.4) medium and 6-mercaptopurine (6-MP) in aqueous medium. The probe displayed fast response times of 5 s for both the targeted analytes with the lowest ever reported detection limit of 1.9 nM and 0.028 nM for the sensing of adrenaline and 6-MP, respectively. Furthermore, the probe was employed for the detection of adrenaline in different bio-fluids (human urine and blood serum) and 6-MP in real samples (environmental water specimens). Impressive performances

were observed during all the detection experiments. Rigorous statistical analyses were performed to determine the reproducibility, originality, and precision of the measurements.

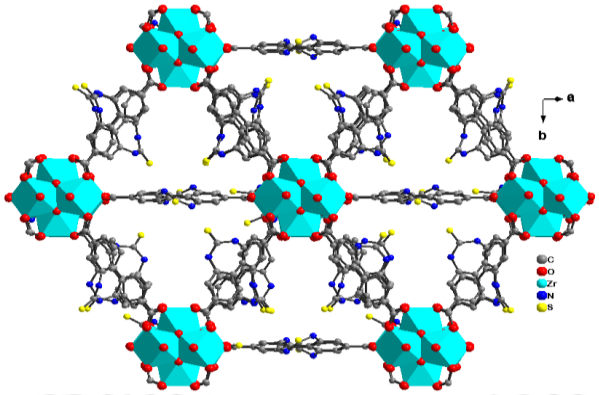

Figure 7 Structure of **3**.

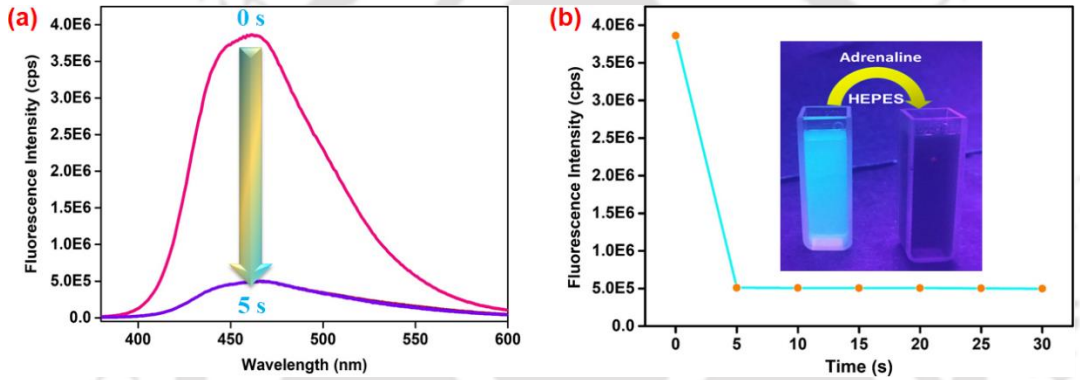

Figure 8 (a) Change in luminescence intensity of **3′** with respect to time. (b) Time-dependent saturation plot of fluorescence intensity of **3′** (change in fluorescence under UV-light is shown in the inset of Figure 8b).

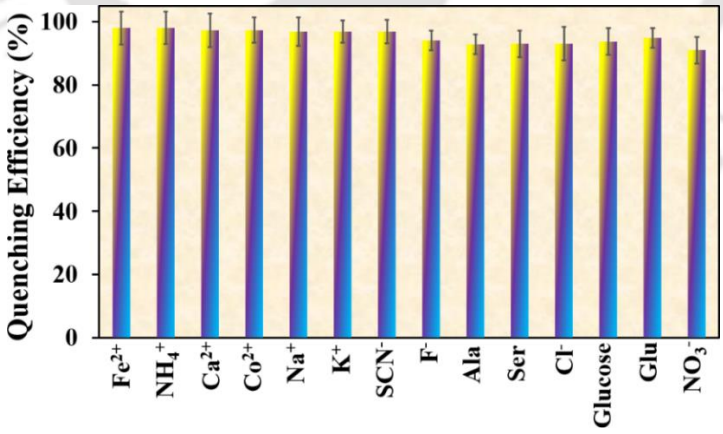

Figure 9 Selectivity of **3′** towards the sensing of 6-MP in the existence of other competitors (error bars signify the standard deviations of three individual measurements).

MOF-coated cotton composite was fabricated for the rapid and on-site detection of both the targeted analytes. The inexpensive, reusable cotton composite displayed nanomolar level sensing ability towards both the analytes. Systematic investigations were executed in search of plausible reasons for 'turn-off' behaviour of the probe in the presence of quenchers. Various

instrumental outcomes indicated that FRET in the presence of adrenaline and IFE in the presence of 6-MP are the most possible reasons behind the quenching of fluorescence intensities of the MOF. All the experimental results indicate that the newly developed sensor will help us for rapid monitoring of the concentrations of adrenaline in human bio-fluids and 6-MP in real water.

Chapter 5: A Self-Cleaning Hydrophobic MOF-Based Composite for Highly Efficient and Recyclable Separation of Oil from Water and Emulsion

This chapter outlines an environmentally friendly, rapid, efficient, and cost-effective strategy for separating diverse oils from water and water-in-oil emulsions under varying challenging conditions. The approach demonstrates remarkable efficiency and high recyclability, offering a sustainable solution for oil separation. In this chapter, a Zr-UiO-66-OH metal-organic framework was post-synthetically modified with 2,2,2-trifluoroacetyl (-$COCF_3$) group. Using the modified MOF (**4′@CF_3**) hydrophobic **4′@CF_3@melamine** composite was prepared using a commercially available melamine sponge. Initially, the melamine sponge was coated with PDA followed by dipping into a mixture of **4′@CF_3** and PDMS-co-PMHS polymer suspension. After the addition of **4′@CF_3** the WCA of the **4′@CF_3@melamine** composite was increased from 106 ± 1° to 145 ± 1°.

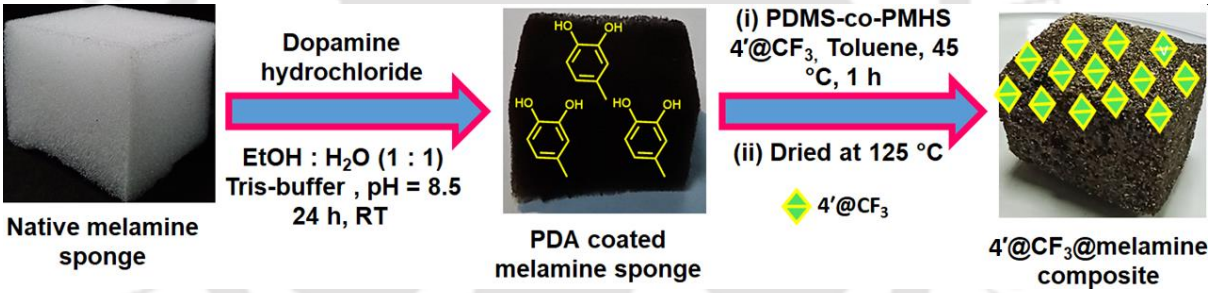

Scheme 2 Schematic representation for the preparation of **4′@CF_3@melamine** composite.

The hydrophobic **4′@CF_3@melamine** composite possesses remarkable efficiency towards both heavy and light oil separation from the oil-water mixture (95-99%) with 50 times reusability. The observed absorption capacity for different oils was found to be 27-40 g/g. The efficiency of oil-water separation has remained unaltered even in harsh conditions like in different environmental water samples and pH solutions.

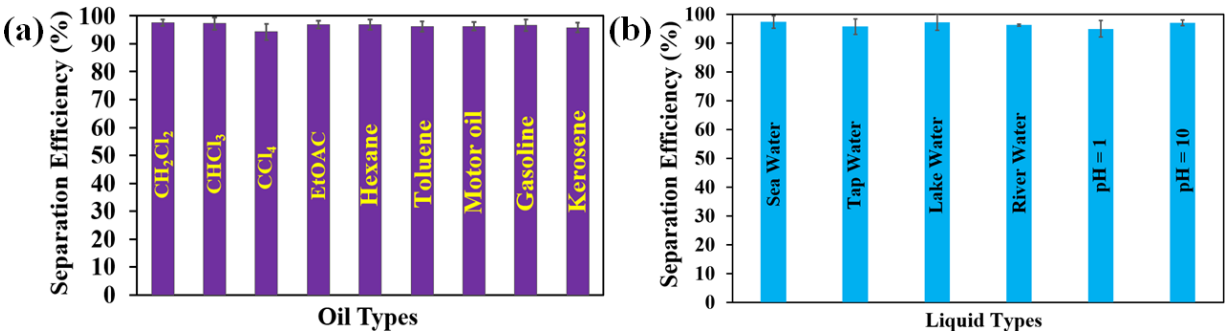

Figure 10 Bar plot of separation efficiency (%) of **4′@CF$_3$@melamine** composite towards separation of (a) various oils from oil-water mixtures, and (b) EtOAc from different types of aqueous media. Each measurement was repeated six times.

The emulsion separation efficiency of the **4′@CF$_3$@melamine** composite was between 97-99% for various water-in-oil emulsions with the flux range of 1461-2288 L/m^{2}h. The emulsion separation efficiency of the composite remained almost the same up to 30 consecutive cycles of separation. Moreover, the hydrophobic surface of the **4′@CF$_3$** MOF was also applied for the self-cleaning purpose.

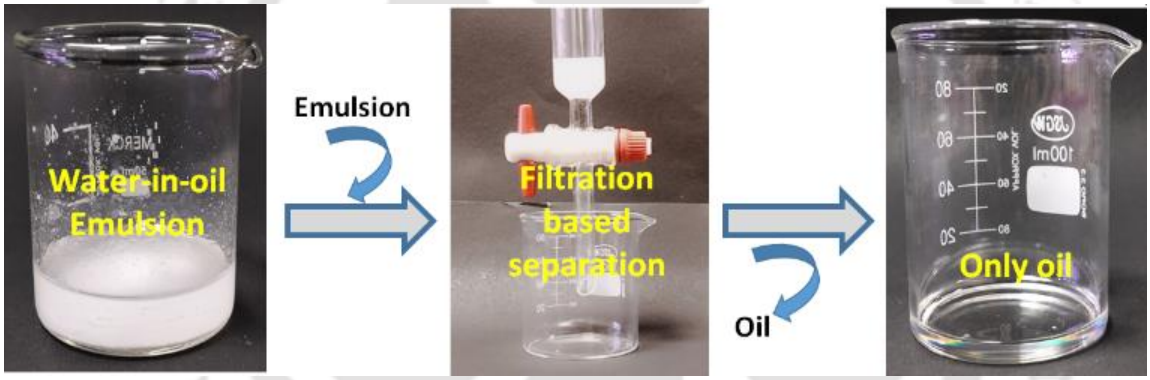

Figure 11 Digital photographs of selective separation of oil by gravity-driven method from water-in-oil emulsion.

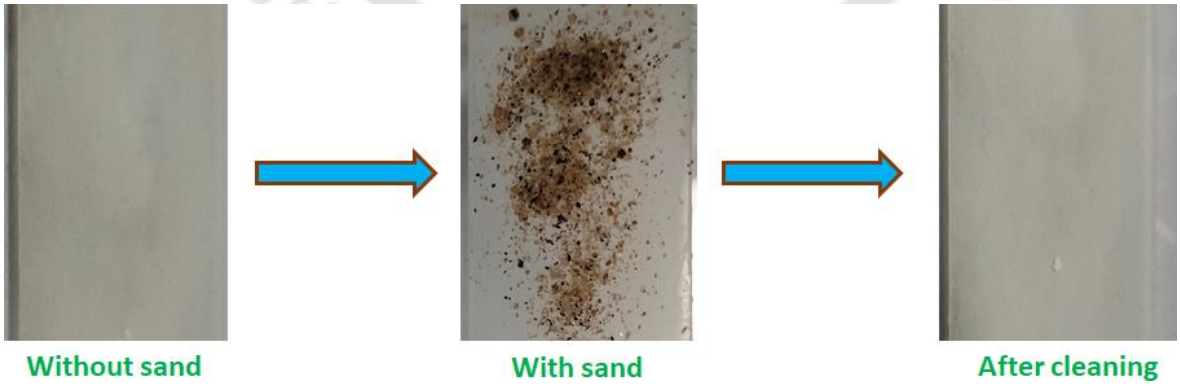

Figure 12 Digital image of **polymer@4′@CF$_3$** glass slide displaying self-cleaning nature.

Conclusion

The main theme of this thesis is centered on the development of various aqua-stable MOFs and their utilization for environmental remediation and bio-molecules detection. It embraces comprehensive discussions on the intricate structures of diverse functionalized Zr(IV) metal ion-containing MOFs. Here, the functionality of a MOF was deliberately integrated into the MOF linker, enabling its practical application in the fluorescence-based detection and quantification of bioactive compounds and organo-toxins. Additionally, the thesis investigates the synthetic methodology of a hydrophobic MOF designed for the selective and efficient adsorption of oil spills. We assert that the findings presented in this thesis hold significant importance for promoting the sustainable development of a clean environment and contribute to the accurate diagnosis of certain diseases associated with the uncontrolled release of specific bio-molecules.

Chapter 1

Historical Evolution of Metal-Organic Frameworks (MOFs) and their Prospective Applications in Targeted Sensing and Adsorption

The discovery of a novel class of highly crystalline porous materials in the late 90's garnered significant attention, owing to their potential applications in gas storage and separation, as a heterogeneous catalysis, for drug delivery, as a luminescent sensor of bio-active and toxic chemicals, for carbon capture, and more. These materials were originated by the combination of metal clusters and organic linkers known as metal-organic frameworks (MOFs). Unlike other porous materials such as zeolites, activated carbons, and silica MOFs offer a distinct advantage as they can be purposefully designed by selectively choosing the metal ion and organic linker and their structural modification is possible even after its synthesis. This chapter provides a comprehensive overview of the brief history of MOFs, encompassing different synthesis procedures and highlighting diverse applications. This chapter also elucidates how the precise tuning of MOFs is achieved by including specific functionalities in the linker moiety which enhances their efficacy in detecting targeted applications. The discussion emphasizes the significance of fine-tuning MOFs for tailored applications in chemical sensing and toxic pollutant (oil) adsorption showcasing their potential capability in addressing specific analytical challenges and environmental sustainability.

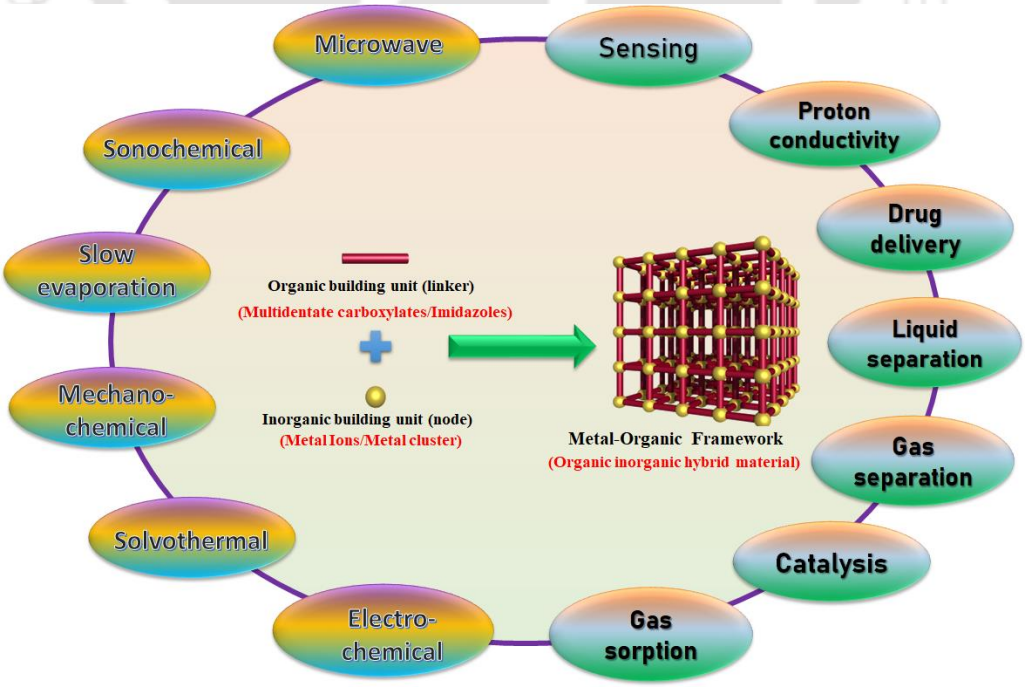

1.1 Introduction

Coordination compounds are the ions, or molecules that embrace one or more metal centers bonded to linkers through coordination bonds.[1] The history of coordination chemistry started with the synthesis of blue-colored Cu(II) and ammonia complex (i.e., $[Cu(NH_3)_4]^{2+}$) by German chemist Prof. Andreas Libavius in the year 1597.[2] Thereafter, slow but continuous development of various colorful coordination compounds continued in the different parts of the world. Synthesis of Prussian blue complex ($KFe[Fe(CN)_6]$), yellow-colored K_2PtCl_6 and orange-colored $CoCl_3 \cdot 6NH_3$ by various rewound chemists in 18th century are a few examples of such coordination complexes.[3-5] Famous German chemist Prof. Karl W. Hofmann first synthesized a coordination complex (properly known as Hofmann clathrate complex) with extended 2D network in 1897.[6] Meanwhile, two important theories of coordination chemistry, i.e. chain theory (1869) by Swedish chemist Prof. C. W. Blomstrand and coordination theory (1893) by Prof. Alfred Werner were developed.[7, 8] It is assumed that Prof. Alfred Werner's theory of coordination compounds is the first foundation of the coordination chemistry whatever we practice in modern day.[9] This theory not only taught us to assign the oxidation state and coordination number of a complex but also inspired us to develop complexes with higher dimensions (2D and 1D) from the 0D molecular regime.[6] Prof. Pedersen and his co-workers (in 1960) first showed that complementary small molecules might display intermolecular recognition via noncovalent interactions which led to the development of supramolecular polygons and polyhedra based on metal-linker coordination.[10] Up to that point, all the synthesized compounds are purely inorganic and non-porous in nature.

In the year 1756, Swedish chemist Prof. Axel Frederik Cronstedt first discovered the porous, natural zeolites.[11] But modification of pore radius and flexibility of incorporation of required functional groups are not possible for the zeolites. Thus, the application of such materials became limited. For a long time, chemists have been trying to rectify such issues. The wait came to an end when Prof. Robson and Prof. Hoskins synthesized the first functionalized microporous coordination polymer between the tetrahedral Cu(I) metal nodes and TCTPM (4,4′,4″,4‴-tetracyanotetraphenylmethane).[12] This cage was porous in nature (pore volume = 700 Å^3) and BF_4^- ions of the complex could be exchanged with PF_6^-.[6] They also showed that synthesis of similar coordination polymers with different porosity can be possible by using different sized linkers.[12, 13] Two similar coordination networks with Cu(II) and bipyridine linker were published in 1995. The discovery of these complexes was very much essential for the synthesis of metal-organic frameworks (MOFs) by Prof. O. M. Yaghi. In the year of 1999, Yaghi and co-workers first discovered a solvothermal synthesis pathway for the synthesis of a porous, crystalline organic-inorganic combined framework, named as MOF-5 which had porosity comparable to the activated carbon and zeolite.[6] The measured Langmuir surface area of MOF-5 was 3800 m^2/g.[6] It was a Zn-organic framework with pcu-topology, which was synthesized by heating a mixture of $Zn(CH_3COO)_2$ and benzene-1,4-dicarboxylic acid in DMF medium (Figure 1.1). Thus, the journey of beautiful reticular chemistry was inaugurated.[6, 14]

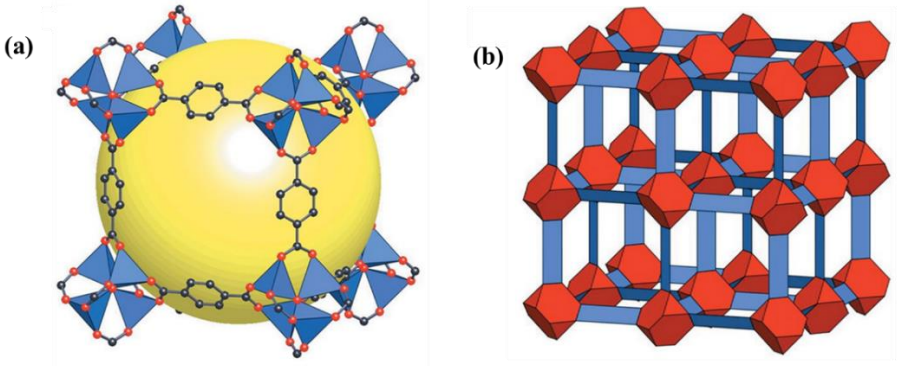

Figure 1.1 (a) The structure of MOF-5 is shown as ZnO_4 tetrahedra (blue polyhedra) joined by benzene-1,4-dicarboxylate linkers (O, red and C, black) to give an extended 3D cubic framework with interconnected pores of 8 Å aperture width and 12 Å pore (yellow sphere) diameter (yellow sphere represents the pore). (b) The structure is shown as the envelopes of $(Zn_4O)O_{12}$ clusters (red truncated tetrahedron) and benzene-1,4-dicarboxylate (BDC) ion (blue slat). These images are collected with permission from ref. no. 14. Copyright 2003, Nature.

Now days, MOFs are defined as a class of organic-inorganic hybrid giant coordination polymers where organic linkers are surrounded by the positively charged metal ions in one, two, or three-dimensional manners.[15, 16] After the synthesis of the first MOF (MOF-5) in the late 1990s by Prof. Omar Yaghi, over 90,000 different MOF structures have been reported to date.[17] MOFs have attracted the attention of inorganic and materials science researchers because of their tuneable surface area, porosity, and functional group.[18] Extremely high physicochemical stability, outstanding catalytic activity, and selective and fast detection of analytes have made them more interesting in the last few decades.[19, 20] Together with these applications, MOFs can also be used for chemical separation, gas storage, drug delivery, etc.[21-24] Now-a-days, MOF materials are used for the separation of miscible and immiscible solids and liquids from water and a particular gas from a gas mixture.[25-27] Among various applications, luminescence sensing based on luminescent MOFs has attracted immense attention due to their high selectivity, quick response, operability, and reversibility.[28-31] Various cations, anions, bio-active molecules, reactive oxygen species, reactive nitrogen species, and volatile organic compounds, etc. have been successfully and selectively detected by various functionalized MOF materials in the past few years.[32-35]

MOFs are a special type of porous materials.[36] The surface area values of MOF materials are typically within the range of 1000 to 10,000 m^2/g.[37] Their porosity can be tuned with the variation of organic linker size and the functional groups attached to the linker molecules.[38] Unlike other traditional porous materials (zeolites, mesoporous silica, carbon nanotubes, and activated carbons), MOF materials can be functionalized even after the synthesis of the materials.[39] Such an easy scope to modify the linker molecules (as required) makes these porous materials different from other adsorbent porous materials.

Outstanding physicochemical stability is another fascinating feature of a MOF material.[40] Depending upon the different kinds of metal ions and organic linker's combination, a large assortment of MOFs bear different types of porosity and physicochemical stability.[41] From the

development of physicochemically stable MOFs in the past two decades, it can be concluded that the stability of the framework depends upon the oxidation state of the metal ions and the lability of metal-linker bonds. Highly robust MOF materials were synthesized by the use of metal ions with high oxidation states such as Cr(III), Fe(III), Ti(IV), Al(III), Zr(IV), and Hf(IV).[42-46] Although different types of MOFs are still growing with date but their stability in various drastic conditions (in highly acidic and basic conditions, at high temperatures and sometimes in moisture) limits their applications at the industrial level. It is a challenge to synthesize ultra-robust physiochemically stable MOF materials which can survive in drastic industrial conditions. In recent times, the synthesis of superhydrophobic MOFs and their applications for oil-water separation, self-cleaning, dye-separation, anti-icing, and corrosion resistance have grasped a lot of attention from many famous material science research groups.[47-52] Although over 90,000 different MOF structures have been reported to date, out of them, only around 100 are hydrophobic, few of them (~30) are superhydrophobic, and very few of them have been used for oil/water separation.[53-55] Therefore, it is another new and interesting area of research. In this thesis, I focused on the synthesis, characterization, and application of Zr(IV)-based UiO (UiO = University of Oslo) series MOFs (UiO-66 and 67). These types of MOFs are always preferable for various application purposes due to the higher oxidation state of zirconium (for highly physicochemically stable MOF synthesis), and its non-toxic and eco-friendly nature. Because of that, during the last decade, a significant number of research publications have been reported on 'UiO' series of MOF materials (Figure 1.2). Hence, I have focused on the synthesis, characterization and application of different 'UiO' type of MOF materials for the sensing of various analytes and oil/water separation.

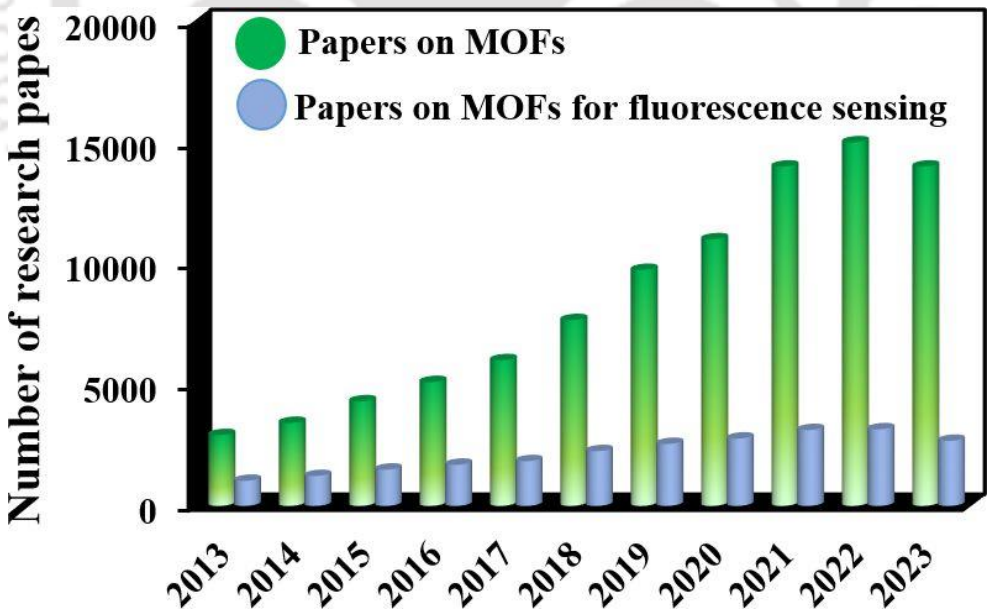

Figure 1.2 Number of research papers per year from 2013-2023 on the topics of "metal-organic framework" and "metal-organic framework for fluorescence sensing". The figure was drawn according to the database of Scifinder. Search was conducted in November 2023. The search employed keywords such as "metal-organic framework" and "water-stable metal-organic framework" specifically focusing on applications in fluorescence sensing.

1.2 Modern-Day Water Pollution and Necessity of MOFs

Environmental problems associated with industrialization, population-driven socioeconomic development, urbanization, intensified modern agricultural practices, and an increase in bacterial and viral diseases result in water quality being compromised by the pollution from drugs, antibiotics, herbicides, pesticides, toxic heavy metal ions, volatile organic compounds, oil spills, and other emerging pollutants.[56, 57] The effect of such water pollution not only ends with a short-term notice of killing the fish and other aquatic animals, but it also can carry forward to higher class animals via the food chain which ultimately affects the biodiversity, atmosphere and economy.[58, 59] Therefore, minimizing environmental pollution and assuring the comfort of the modern day is one of the great challenges of environmental science researchers in the 21st century. Thus, appropriate and regular monitoring of domestic and urban water pollution is highly necessary.

There are two best possible ways to monitor water pollution and nullify the environmental risks, i.e., by measuring the concentration of such pollutants and by removing such toxic substrates from water.[60-63] One of the finest, fastest, and well-established ways to measure the concentration of such foreign substrates in water is fluorescence sensing.[62, 64] Among the other possible sensing techniques, fluorescence-based sensing is one of the easiest, fastest, most economical, and most reliable ways to find out whether such contaminants are present in environmental water bodies.[65] These good qualities have elevated the fluorescence-based way of sensing over the other conventional approaches. e.g., LC-MS, electrochemical detection, capillary electrophoresis, different types of chromatography, atomic emission, and absorption spectroscopy, HPLC, etc.[29, 66, 67] For that fluorescence sensing in aqueous medium, we need a water-stable fluorescent probe which can selectively change its fluorescence emission signal in presence of targeted foreign species up to the safety level of living organisms.

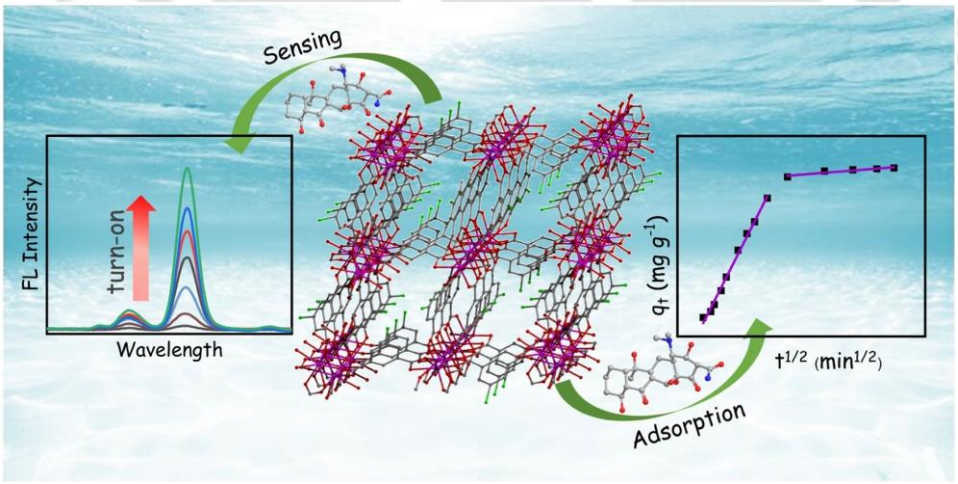

Figure 1.3 Graphical representation of MOF as a sensor and as an adsorbent. This image is collected with permission from ref. no. 63. Copyright 2021, Elsevier.

Aqua-stable MOFs are such a diverse materials that can display their fluorescence property through the electrical communication between the metal ions and the conjugated polytopic organic linkers and also can adsorb toxic pollutants using their pores.[68-70] Therefore, an aqua

stable, porous and luminescent MOF has the potential capability to monitor or remove the pollutants from environmental water bodies. Because of significant porosity, physicochemical stability, diverse functionality and reusability, thousands of Zr(IV) MOFs have been employed for aqueous phase fluorescence detection and adsorption of various pollutants during the past twenty years.[65, 70-72]

Along with the pollution due to various micropollutants, the pollution of water due to oil spills has become a great threat to the environment which is continuously increasing with the upgradation of modern civilization.[73, 74] Oil spill contamination does not just harm the water, it also has an impact on the neighboring land ecology, air humidity and the emission of greenhouse gases as a result of the burning of the oil.[75] Every time there is an oil leak, the oil settles into a thin layer over the water, blocking the sunlight. The aquatic food chain producers are immediately interrupted by the decreased sunshine, which has an impact on the entire food chain.[76] Due to the pollution caused by the oil spills, the seaside animals, fish nurseries, and birds are most dangerously affected.[77] The consumption of seafood exposes individuals to the harmful and persistent component of oil that is introduced into an organism.[78] It is also a huge loss from an economical point of view, since after mixing the oils with water, we can't selectively separate the oils from water.[79] It is one of the major reasons of hike in oil price in the world market.[79]

Therefore, it is urgently needed to develop a simple oil spill clean-up method to get rid of the aforementioned environmental and economic disturbances. The conventional techniques for cleaning up oil spills, such as in situ burning, bioremediation, dispersants, physical labour, etc., are insufficient,[80] as harmful gases are released during in situ burning. Therefore, this process is not ecologically beneficial.[80] A strategic design of porous hydrophobic MOFs can be effective for the selective removal of oil spills from water with huge efficiency and reusability. Lots of articles have been recently published where researchers have used hydrophobic polymers, MOFs, and other hydrophobic surfaces to resolve these environmental pollutions (Table 1.5).

1.3 Fundamental Construction Strategies of MOFs

As previously mentioned, MOFs consist of two components, i.e., inorganic metal ions/clusters and organic linkers. During the construction of a targeted MOF, the choice of a particular metal ion and linker is very crucial. Strong bonding between metal ions and organic SBUs (SBU = secondary building units) generates the final three-dimensional structures of MOFs.[81] The organic linker and metal ions used for the construction of MOFs are defined as 'primary building units'.[81] During the formation of a MOF, the metal ion acts as a junction point and the organic linkers interconnect these metal nodes.[81, 82] Therefore, the coordination number and oxidation state of the metal ion regulate the geometry of the constructed MOF.[83] The selection of alkali metal ions, transition-metal ions, alkaline-earth metal ions, or rare-earth metal ions for a particular linker may construct MOFs with different porosity and geometry.[81, 84] Since there are many vertices with distinct topologies and numerous possible ways to connect those vertices, there are an unlimited number of conceivable net topologies. Because of versatile coordination numbers and geometries, including octahedral, tetrahedral, trigonal-bipyramidal,

square planar, square-pyramidal, and linear coordination geometry of the transition metal ions, they are often utilized for the synthesis of a stable MOF. Figure 1.4 is an example, of how the geometry, porosity, and metal-linker linkage can be varied according to the availability of coordination sites of the metal clusters.

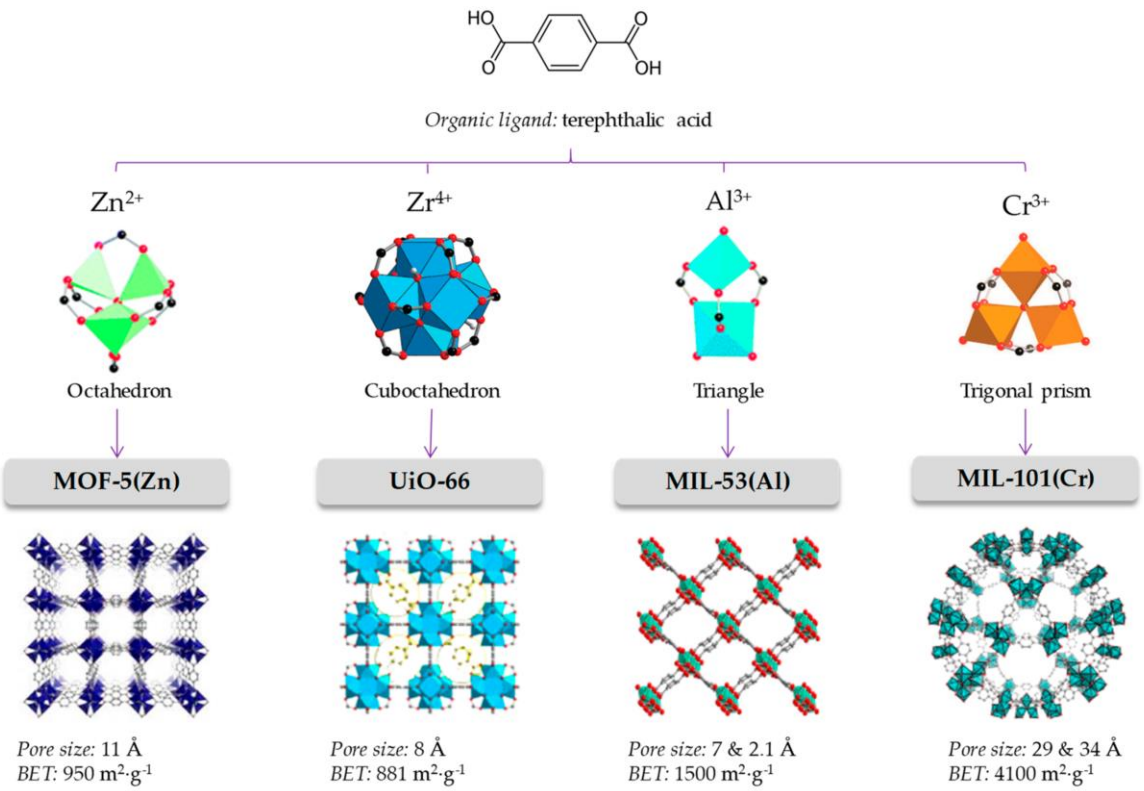

Figure 1.4 The node and connector approach to prepare MOFs. The adequate selection of the organic linker (linear in the case of terephthalic acid) and connection geometry of the metal cluster lead to the desired topology. Each framework topology has its characteristic pore size and available surface. This image is collected with permission from ref. no. 84. Copyright 2019, MDPI.

The choice of the linker with definite coordination sites is also another important factor that controls the pore size, rigidity, stability and geometry of a MOF. The linker commonly used for the construction of a MOF can be categorized in two basic things i.e., according to its ionic nature (neutral, cationic, and anionic) and according to its accessible coordination sites (ditopic, tritopic, tetratopic, hexa, and octatopic) (Figure 1.5). Generally, a hard-soft acid-base theory is followed for the choice of a linker. Soft metal ions form a stable framework with the linker having soft binding sites (N-donor) and metal ions with high positive charge prefer the hard coordination centers (O-donor) (Figure 1.5).[85] But there are some common fetches of a linker, such as rigidity, which will allow them to maintain the open pore structure even after the guest molecules have been evacuated from the pores of the MOF.[86] Because of this, hard organic linkers with phenyl rings are frequently chosen for the construction of MOF instead of flexible long-chain compounds like alkanes. The linkers with multiple binding sites are always preferable for the synthesis of MOFs as they can link up with different metal centres to create

extensive networks.[86] The longer oxygen (benzene-1,4-dicarboxylic acid) or nitrogen (4,4′-bipyridine) donating organic linkers are generally utilized in the MOF synthesis process as longer linker facilities with more vacant space for adsorption in the synthesized MOF. Since the cationic linkers have poor affinity for positively charged metal ions, they are rarely used in the construction of MOFs.[87]

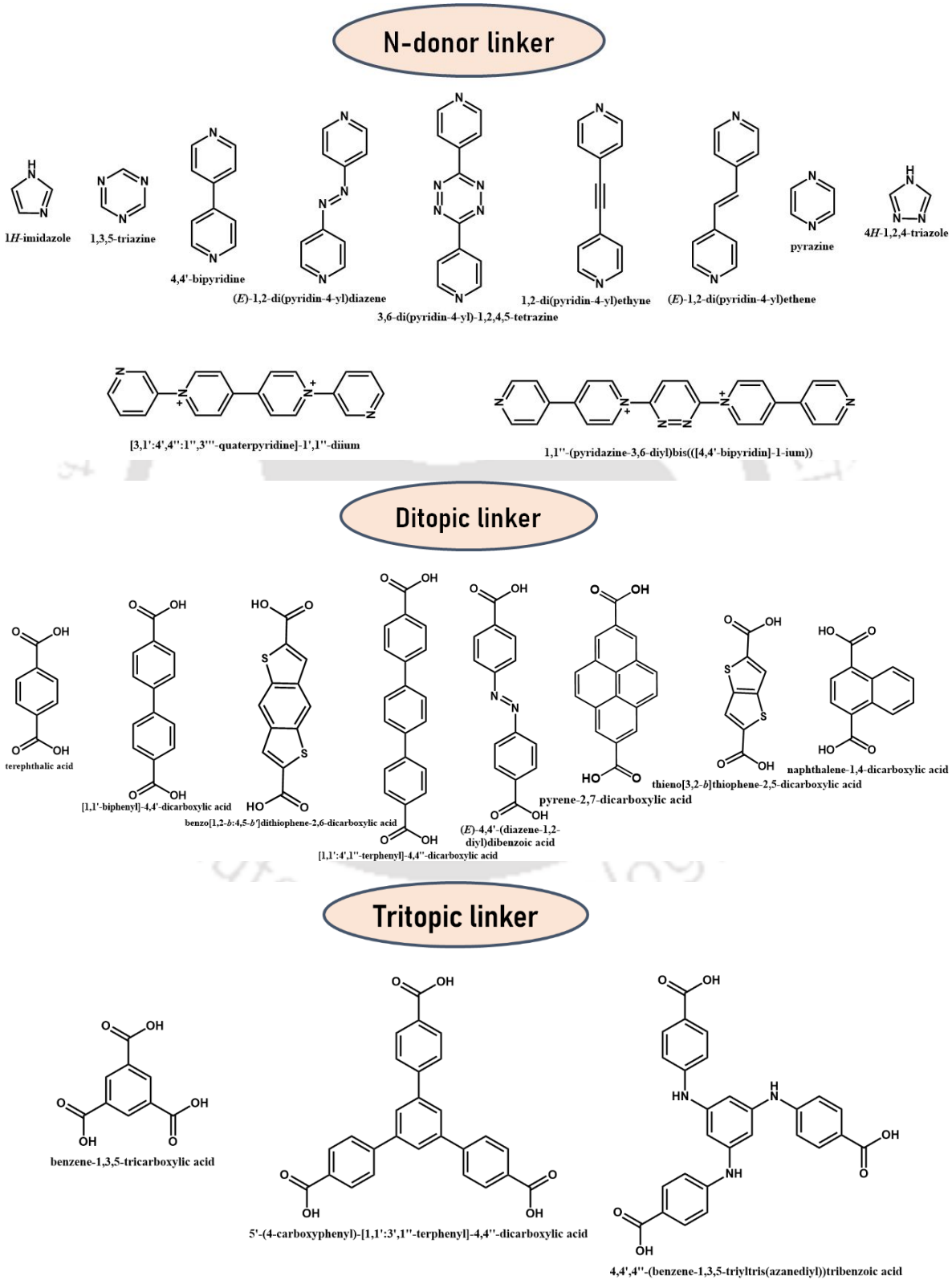

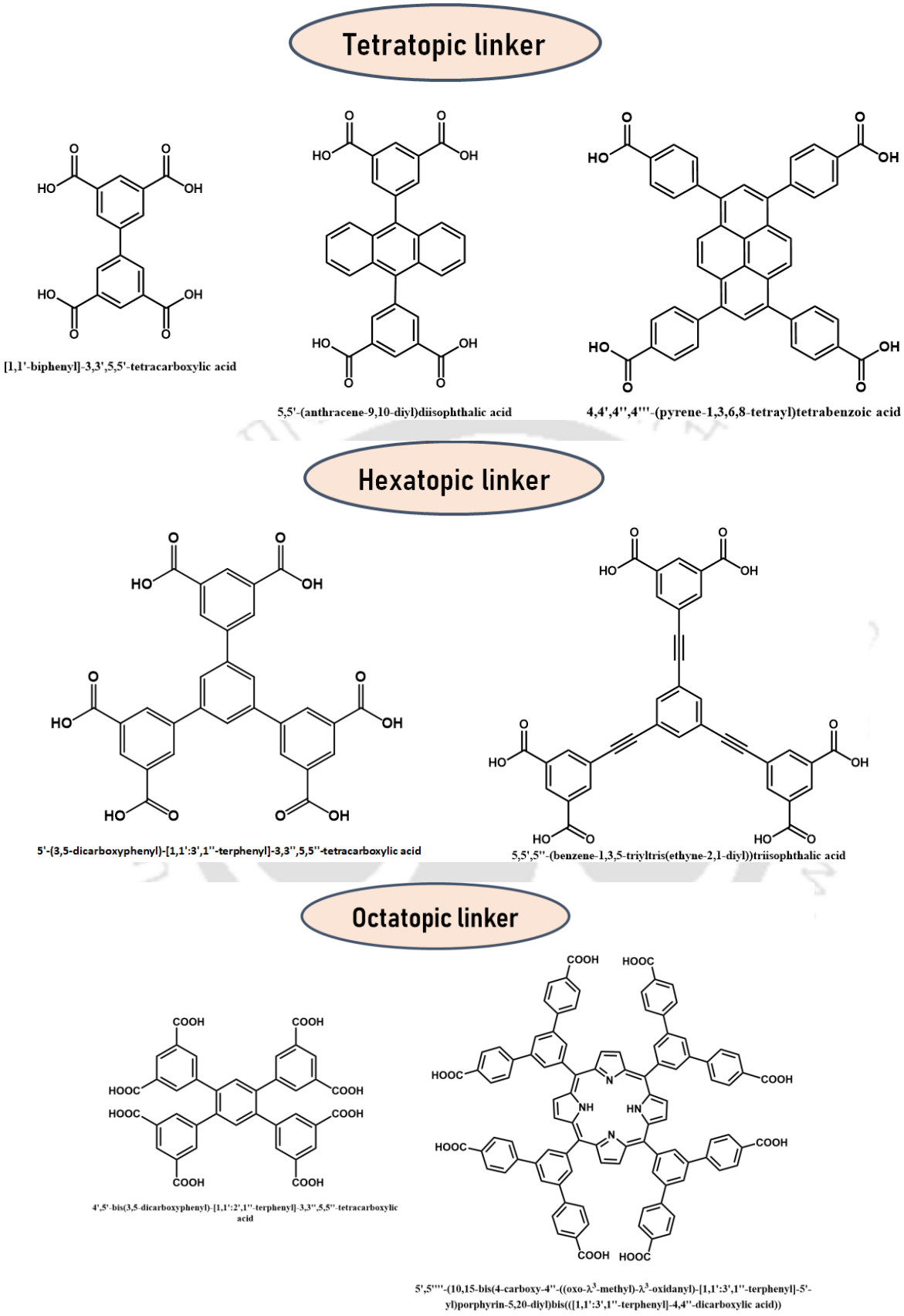

Figure 1.5 Different types of rigid organic linkers that have been used for the synthesis of MOFs.

Recognizing the concept of SBUs is very crucial when looking at the structures of MOFs, as it determines the ultimate topology of a framework. SBUs are mostly made of metal-containing clusters, which are produced when metal ions and multi-donating linkers combine to create a definite coordination geometry.[88] Basically, SBUs are molecular complexes and cluster entities by the interconnection of which (by the polytopic organic linkers) the metal fragments convert into extended periodic porous networks.[88] Prof. Yaghi and his co-workers first introduced the SBU strategy for the synthesis of MOFs.[89] They also displayed that after the judicious construction of a particular SBU, it can be utilized for the construction of periodic ordered frameworks and the chemistry of the synthesized network can be easily predicted.[89] The shape of a SBU depends on different factors i.e., coordination geometry of metal and linker, the used solvents and the used metal to linker ratio.[90] Overall, the final topology of the constructed MOF is determined by the combination of both SBUs and organic linkers.[90] This kind of MOF synthesis strategy is popularly known as "reticular synthesis" which is applied for the successful construction of many MOFs.[14, 91, 92] Some of SBUs of different MOFs are summarized in Figure 1.6.

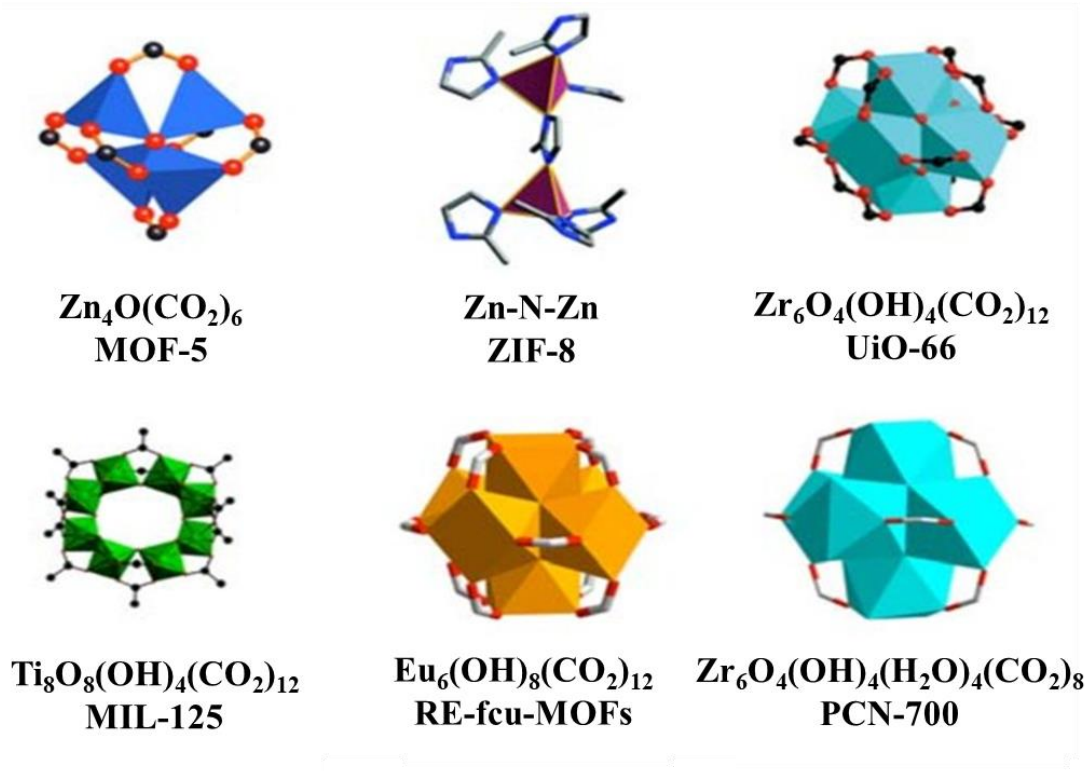

Figure 1.6 Graphic illustration of common SBUs within MOFs. This image is collected with permission from ref. no. 92. Copyright 2018, Bentham Science.

1.4 Different Synthesis Methods of MOFs

With the continuous development of different types of MOFs with different crystal structures, porosity and functional groups, different types of MOF synthesis procedures were developed.[93] In most of the developed methods, synthesis of MOF was performed in liquid phase.[93] Despite the challenges of the formation of single crystals, solid-state synthetic techniques have

occasionally been employed for the synthesis of MOFs.[93] MOF crystals have frequently been grown via slow evaporation of the reaction solution.[94] The traditional diffusion method produces single crystals of MOFs. However, this is a very slow process and often it takes a few weeks to a month for the synthesis of MOF with a very low yield. The majority of the time, MOFs are synthesized via solvo(hydro)thermal processes at high pressures and temperatures.[93] The solvothermal method is the "classic" way to prepare MOFs with high yield and crystallinity.[93] In recent years, new synthetic techniques such as slow evaporation, electrochemical, mechanochemical, microwave, sonochemical and post-synthetic modification techniques have been developed (Figure 1.7).

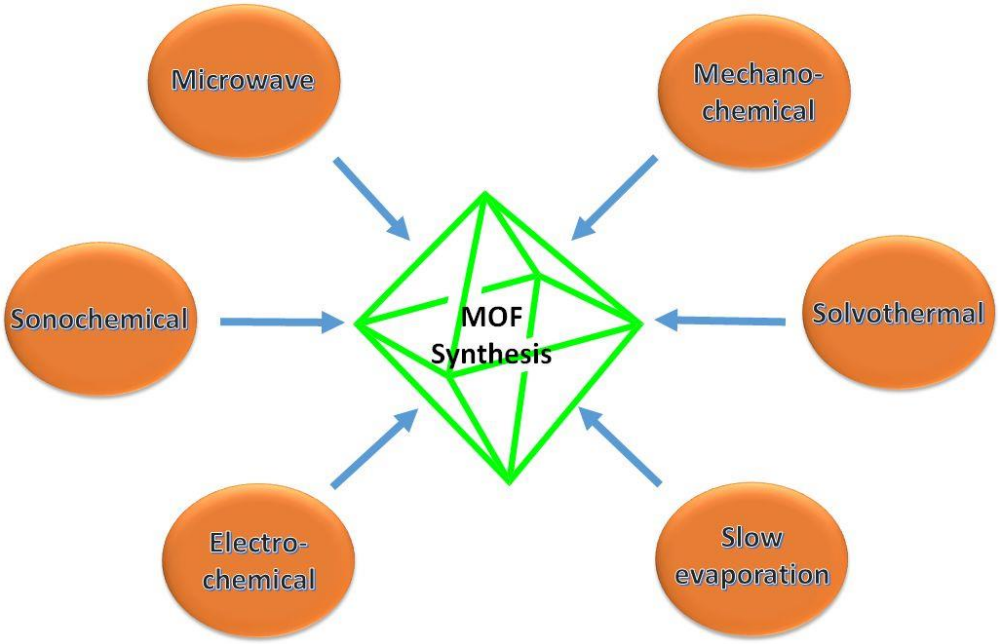

Figure 1.7 Different processes for the synthesis of MOFs.

1.4.1 Slow Evaporation or Diffusion Method

The slow evaporation technique is a traditional, zero energy consuming, room temperature synthesis procedure of a single crystal.[93] In this process, a homogeneous solution of participating reagents is kept at room temperature for the evaporation of solvents, and single crystals are formed as the starting materials reach their critical concentration.[93] Generally, low boiling solvents are preferred for this process to accelerate the crystal growing process. The homogeneous solutions of reagents are layered on top of one another, separated by a solvent layer, or progressively dispersed by descending physical barriers during the diffusion process. Gels are occasionally utilized as diffusers in the crystallization media. After the slow diffusion of the precipitating solvent into the separated layers, crystals are formed at the contact between the layers.[95] Single crystals of MOF-5 were synthesized using this method. In that case, a small amount of Et_3N was placed in between the solution of $Zn(NO_3)_2$ and H_2BDC in DMF and chlorobenzene and a small amount of hydrogen peroxide was added to assist the formation O^{2-} bound SBU.[96]

1.4.2 Solvothermal Method

It is the most widely used MOF synthesis procedure.[97, 98] This method was first developed for the synthesis of zeolites.[99] Nowadays, it has become one of the most popular MOF synthesis methods. Solvothermal reactions are carried out in closed containers (sealed Pyrex tube or stainless-steel autoclaves) which can survive at autogenous pressures produced by solvent's evaporation. Polar, high boiling solvents are usually used for this method in between 50 and 220 °C for several hours or even days. For reactions at very high temperatures greater than 150 °C, Teflon-lined autoclaves are utilized. The shape of the crystals is also influenced by temperature and longer reaction durations might result in the decomposition of final product.[100] Solvents with high boiling points are most often employed. Dimethyl formamide (DMF), H_2O, diethyl formamide (DEF), dimethylacetamide (DMA), MeOH, MeCN, EtOH, and methoxyformamide (Me_2CO) or their combinations are the most often used. When such reactions are executed in water, they are often called hydrothermal reactions. If the ionic liquid is used as a solvent, it is known as an ionothermal method.[101] At high temperature, the dielectric constant of the solvent increases which favours the solvation of the reacting components and the diffusion of the chemicals increases as the viscosity of the superheated solvent decreases.[102] Crystal growth by this process is also impacted by the cooling rate, which should be extremely slow. In solvothermal process, after the synthesis of MOF, the encapsulated solvent molecules need to be removed by stirring it with low boiling solvent. Further, the low boiling solvent needs to be removed by heating the MOF at a high temperature (Figure 1.8).[103] This synthesis method has been widely explored in the recent past for the synthesis of UiO-66, BUT-30 and DUT-52 MOFs.[104-106]

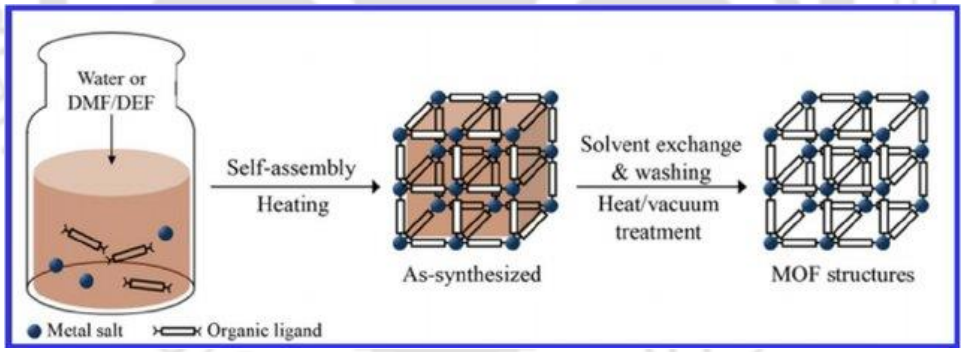

Figure 1.8 Conventional solvothermal synthesis of MOFs. This image is collected with permission from ref. no. 104. Copyright 2015, Elsevier.

1.4.3 Microwave-Assisted Method

This technique is frequently used to create organic and inorganic nanoporous materials.[107] Metal clusters and MOFs have been recently synthesised using this technique.[108] In this type of synthesis, the reactants' dipoles line up with the electromagnetic radiation.[109] As a result, the heat is produced by the collision of precursor molecules. The method's benefits include the quick reaction time, high yield and low cost. In comparison to its traditional hydrothermal synthesis, the microwave-assisted synthesis of MOFs enhances yield and crystallinity within a shorter reaction time. Even if the specific method cannot produce crystals, microwaves aid in

the mobility of the molecules, causing nucleation and the production of crystals with a regulated shape and size by correctly controlling the reaction's concentration and temperature.[109]

1.4.4 Electrochemical Method

The most common technique used to produce MOF powders on an industrial basis is electrochemical method.[110] The method's advantages over solvothermal synthesis include low reaction temperature and rapid reaction times. An ion source and two conducting electrodes are necessary for this method. For the production of MOF materials, an electrolyte, an organic linker, and a protic solvent are required (Figure 1.9).[111] Use of protic solvents prevents metal deposition from the cathode. The in-situ generation of metal ions close to the support surface reduces the unfavorable growth of crystals during membrane formation and causes a constraint in crystallization on a bulk scale.[110] The electrochemical synthesis approach also has more parameters for fine-tuning than solvothermal procedures since it just requires a simple voltage change or the imposition of specific signals.[110] After the first synthesis of MOFs in large scale by Mueller et al. using the electrochemical method, several MOFs (Al-MIL-53, ZIF-8 and MIL-100 (Fe)) were synthesized using this approach.[112, 113]

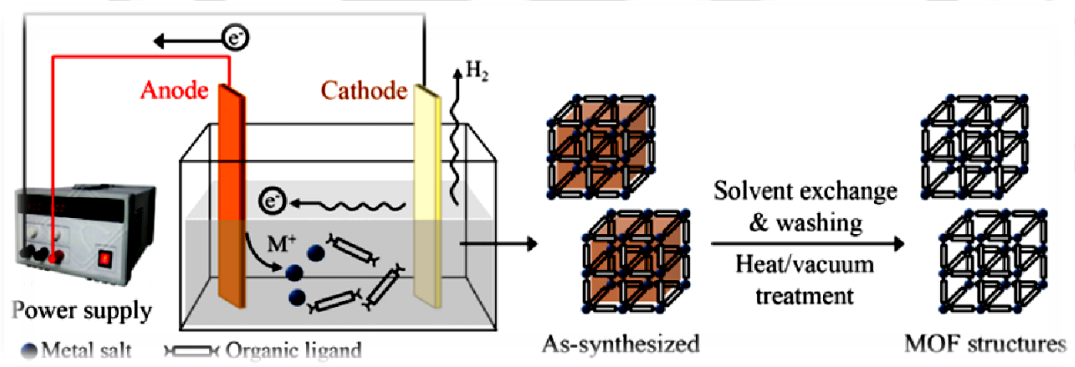

Figure 1.9 Microwave-assisted synthesis of MOFs. This image is collected with permission from ref. no. 111. Copyright 2013, Springer.

1.4.5 Mechanochemical Method

It is a solid-state synthesis pathway for MOFs. In this procedure, chemicals are required to grind manually or more frequently in ball mills to create coordination bonds at room temperature without the use of any solvent.[114] 1D, 2D, and sometimes 3D coordination polymers can be synthesized by adding a small quantity of solvent to the solid reaction mixture.[114] The mechanochemical approach speeds up the reaction time by facilitating mass transfer, reducing particle size, heating, and locally melting the chemicals. It is a process of green chemistry that is safe for the environment and generates materials with high efficiency and purity in a short amount of time.[115] These facilities appealing the use of mechanical chemistry in the production of MOFs over the high-temperature and pressure solvothermal synthesis. The formation of unwanted products (in the solvothermal process) can be avoided by using this approach. This method is also suitable for the synthesis of thermal and solvent labile functional groups containing MOFs. James et al. first reported a Cu(II) MOF using this

method. Thereafter, this approach was adapted for the synthesis of HKUST-1, MOF-74 and ZIF-8, etc. MOFs.[116, 117] Sometimes, the synthesis of MOFs with a different topology is possible by using this method. For example, the solvothermal reaction between $Ni(OAc)_2 \cdot 4H_2O$ with 2-methyl imidazole in the presence of ZnO produced BIT-12 MOF but BIT-11 was produced by using the mechanochemical method (Figure 1.10).[118]

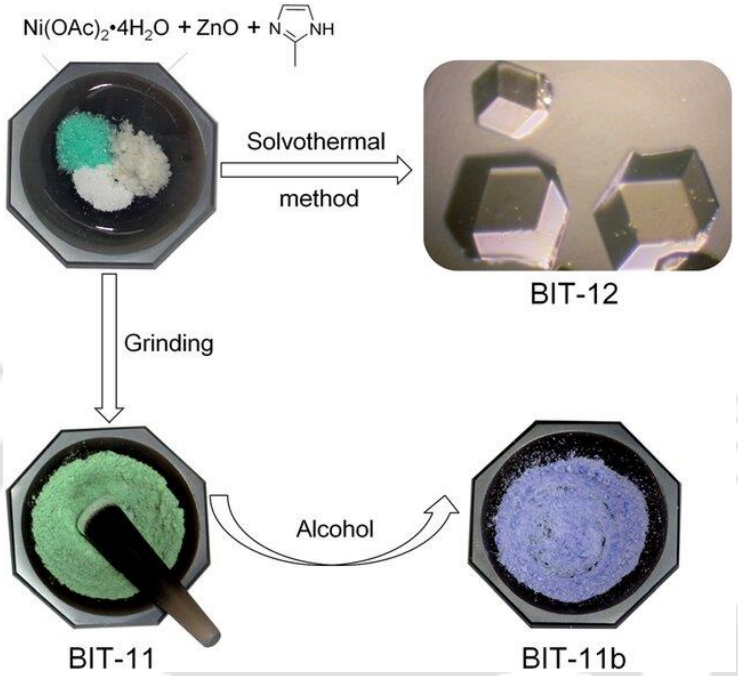

Figure 1.10 Schematic representation of the mechanochemical synthesis of BIT-11 and-11b, as well as the microscopic photo of BIT-12 single crystals synthesized solvothermally. This image is collected with permission from ref. no. 118. Copyright 2014, Royal Society of Chemistry.

1.4.6 Sonochemical Method

Intense ultrasonic radiation between 10 and 20 MHz is utilized in sonochemical synthesis of nanostructures. The major goal of this synthesis strategy is to develop an energy-effective, ambient-temperature, and ecologically responsible process for MOF synthesis.[119, 120] In comparison to the traditional hydrothermal process, this technique can produce uniform nucleation centres, take less time to crystallize and provide a larger yield of MOFs. The first sonochemically fabricated MOF was described by Qiu et al. It is reported that altering the reaction temperature and time in sonochemical synthesis, morphologies and particle size of MOFs can be varied. Many more MOFs, including MOF-177, MOF-556, HKUST-1, have been produced recently utilizing sonochemical synthesis technique.[121]

1.4.7 Microemulsion Method

The technique has recently been employed to synthesize MOFs and is often used in the fabrication of nanoparticles. During this process, tiny nanometer-sized water droplets are immobilized on the organic phase of water microemulsions by a surfactant. The microemulsions' micelles serve as nanoreactors and regulate the kinetics of crystal

formation.[122, 123] By adjusting the water-to-surfactant ratio and the kind of surfactant, the size and quantity of micelles in the microemulsion may be changed. The process has the benefit that it can regulate the dimensions of nanoscale materials, but it also has significant drawbacks due to its high cost and the fact that the majority of the surfactants it uses are harmful to the environment.[93]

1.4.8 Post-Synthetic Modification

The scope of post-synthetic modification (PSM) even after the synthesis of the framework has made the MOF materials more application-friendly than the other porous materials (zeolite, silica, and activated carbon). PSM strategy was first introduced by Hoskins and Robson in the early 90's but the detailed implication of such an idea in IRMOF-3 was executed by Wang and Cohen in 2007.[124] They modified the free amine groups of the MOF by acetic anhydride and corresponding acetamide derivative was synthesized.[124] Afterwards, along with MOF synthesis with pre-synthesized linkers, PSM became a widely acceptable, interesting, and useful synthesis strategy. Sometimes the functional groups aren't able to tolerate the typical solvothermal synthesis conditions of the MOF. In that case, PSM is the only way to introduce the required functional group for the application purpose.

PSM strategy increases the functional group scope of MOFs. PSM can take many different forms, but there are primarily two approaches: (i) covalent PSM and (ii) coordinative PSM.[125] In covalent PSM, the organic linkers of the MOF are modified with a reagent to produce new functional groups.[126] Generally, the $–NH_2$ or –OH functionalized MOFs are modified using this approach after reacting with some electrophilic centres (aldehydes, isocyanates, anhydrides, acyl chlorides, and alkyl bromides).[126, 127] Sometimes, more complicated reactions like the modification of azide group by click reaction is also reported.[128] PSM strategy is also crucial in the synthesis of MOF-polymer matrix.[129]

In the case of coordinative PSM, organic molecules containing metal ligating groups are incorporated into the secondary building units (SBUs) of the MOF. Moreover, hierarchal MOFs, porous liquids based on MOFs, as well as other unique MOF materials have been developed via covalent and coordinative PSM. MOF containing open N-donor sites (2,2′-bipyridine (bpy)) may be post-synthetically modified by a soft metal ion i.e., Cu^{2+} and Pd^{2+}.[130] Sometimes, to enhance CO_2 absorption, the empty coordination sites in certain Cr and Cu-based MOFs are altered with alkane amines. Through straightforward acid/base interactions, the coordinatively unsaturated Zr_6-clusters can also bond to carboxylates.[130] For instance, the coordinatively unsaturated Zr-cluster of NU-1000 was altered to improve CO_2 adsorption using the solvent-assisted linker incorporation (SALI) approach.[131] Coordinative PSM was also employed by Mirkin and colleagues to adhere phosphate-modified nucleic acids to MOF surfaces (Figure 1.11). It has been demonstrated that the SBU of nine distinct MOFs with a range of metals (Zr^{4+}, Cr^{3+}, Fe^{3+} and Al^{3+}) can coordinate with oligonucleotides with terminal phosphate linkers.[132] All MOFs were examined both before and after PSM and revealed a thick DNA surface coating.[132] Importantly, following coordinated PSM, the particles' porosity and crystallinity were preserved. Along with these two types PSMs, various other approaches e.g., metal exchange, metal incorporation, linker exchange, linker installation, guest incorporation

inside the pores of the MOF and linker removal have been reported.[133] With the use of PSM, MOFs may be functionalized with substances that change the properties of the finished MOFs, such as hydrophobicity, hydrophilicity, porosity, luminescence property, catalytic activity and other properties.[125]

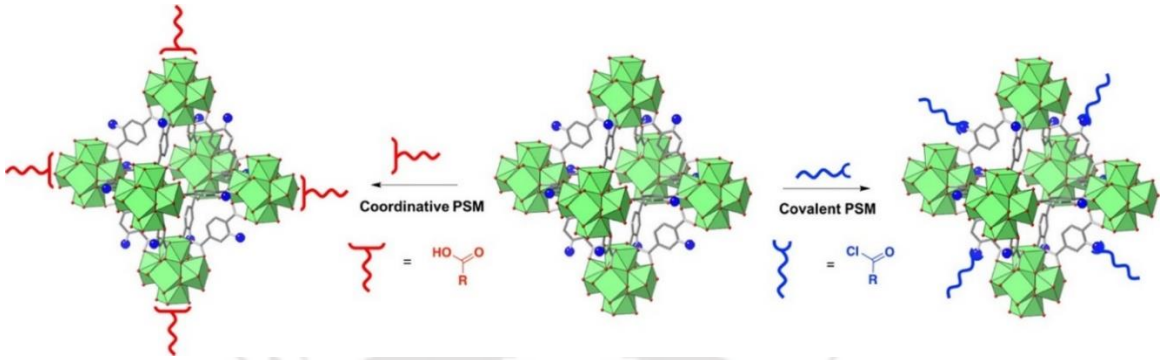

Figure 1.11 Illustrative schematic of MOFs and PSM. Depiction of covalent PSM using reactive groups on the MOF linker (blue spheres representing amine groups) for modification by an organic reagent (blue lines: acid chloride reagent). Depiction of coordinative PSM using a coordinating organic molecule (red lines: acid reagent) to bind to the MOF SBU. This image is collected with permission from ref. no. 125. Copyright 2020, American Chemical Society.

1.5 Parameters Controlling Synthesis of MOFs

Acquiring the proper synthesis conditions is one of the primary goals during the synthesis of a predictable crystalline structure. MOFs are a type of crystalline compounds. Thus, the synthesis of MOFs is also influenced by plenty of factors, including reaction time and temperature, molar ratio of metal and linker, solvent type, pressure, pH of the reaction medium and the kinetics of crystallization, which should result in nucleation and crystal growth with definite shape and size. Therefore, mixing of metal ion and linker with proper stoichiometric ratio, choice of appropriate solvent and setting of exact temperature are highly necessary for the synthesis of the desired MOF structure. The aforementioned parameters can be categorized into parts. The solvent, molar ratio of starting materials, pH and concentration of counter ions are within the compositional parameters, and time of reaction, pressure and temperature are considered as process parameters.[134]

1.5.1 Effect of Solvent

The choice of proper solvent for the MOF synthesis is very crucial. Generally, solvents are chosen according to their reactivity, basicity, solubility of the reacting components and redox behaviour. The reaction's thermodynamics and activation energy are significantly influenced by the solvent. For the synthesis of MOF materials, high boiling amide solvents (DMF, DEF or DMA) are mainly used. The use of amide solvents has mainly two advantages, (i) their boiling point is very high which is required for a solvothermal reaction and (ii) amide solvents are converted to their corresponding amines which are basic in nature. They favour the deprotonation of acidic hydrogen atoms which enhances the coordination process.[135]

In 2012, Luo's group found three different MOF structures after reacting $Cd(NO_3)_2 \cdot 4H_2O$ with biphenyl tricarboxylic acid (H_3BPT) in three different solvents like DMF, DEF and DMA.[136] The chemical composition and coordination networks of these compounds are completely different. In DMF, a 3D framework with vast Cd-O-Cd chains was observed where DMF made a bridge with neighbouring Cd_1 and Cd_2 centers. In the case of DMA, 3D compound with many metal-carboxylate chains was found. Here, the DMA molecule coordinated with one of the Cd(II) centres. In the presence of DEF, a 2D honeycomb-type net is formed by the mononuclear metal ion with the BPT linker, which is then layered to create a 3D supramolecular architecture.[136] There are many other reports where solvent molecules take a vital role in the formation of framework structure.[137-139]

1.5.2 Effect of Molar Ratio of Reacting Components

Since the topological structure of MOFs depends on the stoichiometry of the reactants, the molar ratio of the reactants is another crucial component in the synthesis of MOFs. Luan et al. were able to synthesize three different Cu-based coordination polymers with interlaced triple-stranded molecular braid topologies by regulating linker-to-metal molar ratios. The chemical composition, geometry, properties and ratio of metal ions and linkers in the synthesized compound are completely different.[140]

Carlucci et al. discovered two different Mn(II) complexes by the reaction of flexible linker 1,4-bis(imidazol-1-ylmethyl)benzene (bix) and $Mn(NO_3)_2$. Complex with molecular formula $[Mn_2(1,4\text{-bix})_3(NO_3)_4]_n 2n \cdot CHCl_3$ was formed after the reaction of metal ion and linker with 1:3 ratio but the complex with molecular formula $[Mn(1,4\text{-bix})_{1.5}(NO_3)_2]_n$ was produced after varying the ratio to 1:1.5.[141]

1.5.3 Effect of Reaction Temperature

Since most of the MOFs are synthesized under solvothermal conditions, reaction temperature has some crucial roles in the successful formation of a desired MOF. The temperature range of 80-200 °C is generally used for the synthesis of MOFs. At high temperatures, the dielectric constant of the solvent increases and viscosity decrease which favours the solvation of the interacting components and increases the collision between the metal ions and linkers.[102]

The complex formed between Ho(III) ion and succinic acid under solvothermal conditions and room temperature is a classic example of the effect of temperature in MOF synthesis. Narda and his co-workers were able to prepare two Ho(III) complexes i.e., $[Ho_2(C_4H_4O_4)_3(H_2O)_2] \cdot H_2O$ and $[Ho_2(C_4H_4O_4)_3(H_2O)_4] \cdot 6H_2O$ under solvothermal and ambient conditions, respectively. These two complexes are not only different in their chemical compositions, but their magnetic property and thermal stability are also completely different.[142]

Similarly, the synthesis of Zn(II) MOF with 5-iodoisophthalic acid was possible both in hydrothermal and room-temperature synthetic conditions. It was observed that under the solvothermal conditions, the more thermodynamically stable conformer formation occurs at high temperatures, and kinetics at low temperatures would result in distinct kinetically stable conformer.[143] The research showed that hydrothermal conditions are more suited for producing

denser, less-hydrated, higher-dimensional solids with expanded M-O-M networks and superior thermal stability.

1.5.4 Effect of pH of Reaction Medium

A proper understanding of the acidity or basicity of a coordinating linker is very important for the synthesis of the required MOF. The acidity or basicity of the reaction medium has a significant impact on the crystallization and development of inorganic-organic hybrid materials. A polycarboxylate linker will be more likely to be connected to a metal ion based on the acid-base principle depending on the degree of deprotonation of an organic linker. Numerous research teams have reported different works addressing the impact of pH on the synthesis of MOFs.[144, 145] For example, Hu et. al. reported two different Cd(II)-coordinating frameworks at two different pH media (5.5 and 7.5) by using 4-carboxy-4,2′,6′,4″-terpyridine (CTPy) and oxalic acid as binding linkers. It was observed that the MOF obtained at pH = 7.5 coordinated with the oxalate group but no such coordination was observed for the MOF synthesized at pH = 5.5. It was evident that at a highly basic pH (7.5), the carboxylic acid groups of oxalic acid were completely deprotonated and it participated in the coordination bond formation.[146]

By adjusting the pH level, three distinct Co-BTC-L (L = 3,3′,5,5′-tetra(1H-imidazole-1-yl)-1,1′-biphenyl) MOFs were reported by Luo et al. Pink coloured crystals with the molecular formula $[Co(L)(HBTC)_2(\mu_2\text{-}H_2O)(H_2O)_2]\cdot 3H_2O$ was obtained at pH = 5. The colour of the crystal converted to purple at pH = 7 and the corresponding molecular formula became $[Co_3(L)_2(BTC)_2]\cdot 4H_2O$. Upon further increasing the pH to 9, the molecular formula became $[Co_2(L)(BTC)(\mu_2\text{-}OH)(H_2O)_2]\cdot 2H_2O$ and the colour turned brown.[144] According to the above discussions, it can be concluded that MOF synthesis with different coordination environments, topology, and physicochemical behavior is possible just by adjusting the pH of the synthesis medium.

1.5.5 Effect of Modulator

From the very basic theory of crystallography, we know that crystal formation is a slow process. Without making the process slow, the synthesis of ordered crystalline compounds is not possible. Here the modulator chemistry is generally applied for the synthesis of MOFs containing metal ions with highly positive oxidation states (Zr(IV), Al(III) or Hf(IV)), as there is a possibility of rapid reaction between the highly positive charged hard metal ion and the hard carboxylate groups (generally used for the synthesis of these MOFs) of the linker. Rapid nucleation often produces amorphous products. Before the development of modulators, these types of MOFs were often obtained in gel form. Therefore, a modulator not only controls the kinetics of MOF formation process, but also has a vital role in the formation of the final texture of the product, its porosity, yield, crystallinity, and coordination geometry.

In general, modulators frequently consist of a single carboxylic acid coupled to a carbon chain with the formula R-COOH, where R is any one of the following: -Ph, $-CH_3$, -H, or $-CF_3$ (acetic acid, benzoic acid, trifluoroacetic acid, and formic acid). The binding affinity of these monocarboxylic acids with the metal ion is faster than the dicarboxylate group containing

organic linkers but this type of binding is reversible in nature. Although these lone carboxylate groups rapidly interact with the metal nodes, the crystal structure cannot develop since there isn't another carboxylate group. As a result, a balance is preserved during coordination with the linker molecules and the crystal formation process becomes sluggish, which is necessary for proper crystal formation.[147] But, the use of excess modulators can entirely stop the crystallization process.[147] Moreover, modulators facilitate the crystal formation process for the formation of M(IV) based MOFs through the formation of $M_6O_4(OH)_4$ SBUs.[148]

The critical role of modulators in the synthesis of various MOFs was judiciously investigated by many famous research groups all over the world. The term "coordination modulation" was first introduced by the Kitagawa group in 2009 to describe the employment of modulators to regulate the size and grow crystals of HKUST-1 and $[Cu_2(NDC)_2(dabco)]_n$.[149, 150]

Recently, De Vos and his co-workers synthesized the terephthalic acid containing Zr(IV) based UiO-66 MOF by using different amounts of TFA modulator (0-20 equivalent concerning the linker). Although the crystallinity and particle size of the synthesized MOFs did not widely vary after using the different modular concentrations, their reactivity as a catalyst towards "ene"-type cyclization dramatically increased with the gradual increase in the concentration of TFA.[151]

A thorough investigation of the modulator effect on the synthesis of Zr(IV)/Hf(IV) MOFs with fumarate linker was executed by Zhao et al.[148] They used acetic acid, trifluoroacetic acid and formic acid with different concentrations for the synthesis of these MOFs. The effect of the modulator on the resulting MOFs' crystallinity, morphology, yield, pore size, CO_2 separation ability, defects and stability were examined in detail in this study. They discovered that the underlying parameters dictated by the acidity rather than the kind of modulators have a remarkable influence on the crystallinity and yield of MOFs. According to this study, both increasing and reducing modular acidity had the same impact on the crystallinity of synthesized MOF.[148]

1.5.6 Template Strategies

Novel MOFs, which are challenging to produce using conventional synthetic techniques, can be produced by using template molecules in the reaction mixture.[152] Small organic molecules, such as organic solvents, carboxylic acids, organic amines, *N*-heterocyclic aromatic compounds, surfactants, ionic solutions, and other organic molecules have been often utilized as templates. Different organic molecules in this class have different effects on the production and crystallization of the MOF.[93] For instance, organic amines regulate reaction solution pH and make it easier for organic linkers to deprotonate. Aromatic heterocyclic compounds act as counter ions when they are protonated as weak organic bases. Carboxylate compounds bind to metal centers and can fill MOF pores and sometimes bind with metal ion and slow down the crystallization process. Ionic liquids function as solvents as well as counter ions and surfactants form micelles in solvent and can capture a specific ion. With mesoporous and microporous channels for hosting big molecules like proteins and enzymes, the template synthesis approach is employed to create hierarchical porous materials. However, the most popular method for

making hierarchical MOFs is reticular chemistry, which involves employing linkers of varying lengths to create MOFs with the same topology but different pore sizes.[93]

1.6 Synthesis of Aqua-Stable MOFs via Linker Design

The development stages of MOFs over the past three decades can be categorised into three important parts.[153] The early research on MOF stability was primarily concerned with its mechanical and thermal stability. The second stage of MOF development began with a thorough knowledge of the framework collapse of MOFs in the air. To overcome such issues, several air and water-stable MOFs have been developed. In the third stage, several highly physicochemical stable MOFs were synthesized using various crystal growth and crystal structure determination techniques, greatly expanding their potential applications and assisting in their commercialization.[153]

Under typical circumstances, the stability of a MOF depends on mainly thermodynamic and kinetic factors.[154] The thermodynamic factor mainly depends on the strength of the coordination bonds between the metal ion and the coordinating linker.[155] The hard soft acid-base (HSAB) theory of Pearson may be able to forecast the coordination bond strength.[155] However, the stability of a framework can be widely varied, even if, the thermodynamic factors are the same. The chemical stability of 'UiO' and SUMOF-7 series MOFs gradually declines with the lengthening of the linker and the widening of pore size.[156, 157] This is mostly caused by kinetic considerations, which are primarily connected to the linker's stiffness, surface hydrophobicity, coordination number and framework interpenetration. Various innovative approaches have been adopted by many researches over the last 20 years for the synthesis of aqua-stable MOFs.[153] Some of them are enlisted below.

1.6.1 Synthesis of MOF with High Connectivity

In the early stage of MOF synthesis, soft divalent metal ions were generally considered for the synthesis of MOFs with hard carboxylate groups. As a result, the basic principle of HSAB theory was violated which ultimately generated MOFs with low chemical stability. The stability of the MOFs completely has become reverse after using high-valent hard metals (Zr^{4+}, Al^{3+}, Cr^{3+} and Fe^{3+}) with hard O-donor linkers. The large number of metal cluster connections and the reduction of several structural defects may take the major responsibility for improving the stability of the resulting MOFs.[158] From the kinetic perspective, the gradual replacement of coordinating moieties by small nucleophiles (water) is the primary cause of the disintegration of MOFs in solutions. For a defective structure, the formation of aqua-complex with the metal ion is much more favourable which eventually results in the breakdown of the whole structure.[158] On the other hand, a framework with more connectivity (for the metal ions with a high coordination number) slows the linker dissociation process which increases the stability of the framework. Using this principle, Férey and his co-workers synthesized Cr(III)-based MIL-101(Cr) MOF which has a large BET surface area (~4000 m^2/g) and pore sizes (2.9 and 3.4 nm) with high chemical stability. It is capable to resist the attack of alkali and acid. Moreover, it retains its crystalline nature in wide ranges of pH (0-12) for 2 months. [159]

Fabrication of a stable framework with low valent metal ions is also possible by using soft (N-donor) coordinating linkers. For example, the zeolitic imidazolate framework (ZIF-8), formed by the coordination of imidazole with tetra-coordinated Zn^{2+} ion, displays its structural integrity even in 8 M aqueous NaOH for a day at 100 °C.[160]

1.6.2 Synthesis of Mixed-Metallic MOF

The stability of a MOF can also improve by using mixture of metal ions, instead of using a single metal ion. This strategy is mainly applied to bivalent metal ions. For example, the stability of MOF-5 in an aqueous medium can be increased by doping Ni^{2+} in the pristine MOF.[161] Appling similar strategy, synthesis of hydrolytically stable STU-1 MOF was possible by doping of various metal (Cd^{2+}, Fe^{2+} and Cu^{2+}). All metal-doped STU-1 MOFs were observed to maintain their crystallinity and morphology even after soaking in boiling water for seven days.[162] There might be several reasons responsible behind these observations: formation of stronger coordination bonds in the MOFs than pristine MOF, improvement of inertness in the metal cluster, or increase of surface hydrophobicity of the metal-doped MOF.[153]

1.6.3 Use of Rigid Linker for Synthesis of MOF

The stiffness of the coordinating linker plays a vital role in the formation of a stable framework. The stability of the framework is inversely proportional to the flexibility of the linker.[163] This is one of the main reasons for using aromatic conjugated linkers for the preparation of MOFs instead of flexible aliphatic linkers. As the flexibility of the linker increases, the number of degrees of freedom increases and its bending ability increases which reduces the stability of MOFs. For examples, 'UiO' and SUMOF-7 series of MOFs have the same coordination geometry and coordinating ions are also same. But, with increasing the coordinating linker size, the stability of the MOFs gradually decreases.[156] According to the literature reports, the MOF with a longer linker has lower activation energy of solvation. Therefore, shorter and more rigid linkers are always preferable for the construction of aqua-stable frameworks.[164]

1.6.4 Use of Hydrophobic Linkers

Most of the metal ions form stable hydroxides with water. Therefore, it is very difficult to prepare an aqua-stable MOF. One of the most popular ways to keep the framework free from nucleophilic attack by water is to use hydrophobic linkers for the synthesis of MOFs. The weak coordination bonds between the metal ion and the linker can be protected by the introduction of water-repellent functional groups through linker modification around the metal cluster. Such hydrophobicity in a MOF can also be incorporated by the PSM technique. Long-chain alkyl, long-chain fluorine-containing groups, $-CF_3$, -F, $-CH_3$, $-C_2H_5$ or –Ph groups are very effective in introducing hydrophobicity in a MOF.[165] Sometimes, the use of a pyrene linker also makes a MOF hydrophobic.[166] The introduction of hydrophobicity in a MOF not only enhanced the stability of a MOF in an aqueous medium but also increased its stability in highly acidic and basic pH media for a long time.[166]

A copper-based MOF, USTC-6, containing 4,4′-(perfuoropropane-2,2-diyl)diphthalic acid linker was reported by Jiang's group.[167] Due to the hydrophobicity of the corrugated $-CF_3$

surface, USTC-6 demonstrates extraordinary endurance to water and in the pH range of 2 to 10, even though the majority of Cu-O coordination bonds in MOFs are susceptible to hydrolysis. The position of the hydrophobicity-introducing functional group also takes a vital role in making a MOF aqua stable. For example, Li and his co-workers reported bipyridine containing MOF-508 and its two analogous MOFs i.e., SCUTC-18 and SCUTC-19 where -CH_3 groups are in ortho and meta position to the coordinating N atoms, respectively. After 30 days of exposure to humidity, it was observed that only in the case SCUTC-18, the porosity was preserved due to the presence of methyl substituents closer to the metal clusters.[165]

Many other chemists reported various methods e.g., insertion of stabilizing pillars and generation of interpenetrated frameworks for the synthesis of aqua-stable MOFs.[153]

1.7 Zr(IV)-Carboxylate Frameworks

One of the frequently available transition metal atoms on earth is zirconium, which is mostly produced from the mineral zircon.[168] Zr(IV) is a hard metal ion and it has a very strong affinity towards the hard oxygen atoms of carboxylate groups. Sometimes, it has been found that the carbon-carbon bonds in the organic compounds break down before the Zr-O coordination bonds.[169] This extraordinary stability of Zr-O coordination bonds helped Lillerud et al. for the first synthesis of ultra-stable UiO-66 MOF material in the year 2008 (UiO = University of Oslo).[156] $Zr_6(\mu_3\text{-}O)_4(\mu_3\text{-}OH)_4(CO_2)_{12}$ is present as an inorganic building unit in the UiO-66 MOF structure.[169] It contains an inner $Zr_6O_4(OH)_4$ core in which the triangular faces of Zr_6 octahedron are alternatively coordinated with μ_3-O and μ_3-OH groups. Carboxylate groups of the linker molecules interconnect all the polyhedral edges and form a cluster. In that cluster, each Zr-atom resides in a square anti-prismatic coordination environment with a coordination number of 12. The framework structure has larger-sized octahedral and smaller-sized tetrahedral cages. In the cluster, one square face is formed by the two carboxylate groups of the linker molecules and another square face is formed by the μ_3-O and μ_3-OH groups.[156] In the first synthesized Zr-MOF, the synthesis was carried out without using any modular. This type of synthesis condition often results in an amorphous material than crystalline product. Thereafter, the research started in order to convert the amorphous material to a crystalline material.[147]

In the year of 2011, Schaate et al. first reported a highly crystalline, powdered Zr-UiO-66 MOF material.[169] They achieved the result after using a modulator during the synthesis of MOF. In that work, they studied the effects of a modulator (benzoic acid, acidic acid and H_2O) during the synthesis of Zr-UiO-66 MOF. It was observed that, with the increase of concentration of modulators, the synthesis of the MOF materials can be controlled. The larger size crystals were obtained after using more concentration of modulators. It is now understood that modulators may be used to competitively and reversibly bind to the metal node, slowing the crystallization process and allowing for crystal nucleation and controlled growth.[147] These modulators are often a single carboxylic acid connected to a carbon chain with the formula R-COOH (where R = -Ph, -CH_3, -H and -CF_3). These single carboxylate groups bind with the metal nodes but due lack of another carboxylate group, the crystal structure can't propagate.[147] Thus, a balance during coordination with the linker molecules was maintained and the

formation of the crystal process became slow which is required for a good crystal formation. However, the use of more amount of modulators can completely inhibit the crystal formation process.[169] Using a similar modular strategy in the same year, Schaate et al. reported the first single crystal of -NH_2 functionalized UiO-66 MOF.[147] The first synthesized UiO-66 MOF had a BET surface area of 1187 m^2/g.[147] Just after the discovery of UiO-66 MOF, two other isoreticular MOFs e.g., Zr-UiO-67 (using H_2BPDC linker) and Zr-UiO-68 (using H_2TPDC linker) were developed (Figure 1.12).[154] The UiO-67 and UiO-68 MOFs were obtained by extending two to three benzene rings with the increased surface area of 2400 and 3000 m^2/g, respectively.[170, 171] Thereafter, during a short period, several Zr(IV) and Hf(IV) based 'UiO' series of MOFs were synthesized by various prominent research groups of reticular chemistry and their versatile applications were investigated.[172-174]

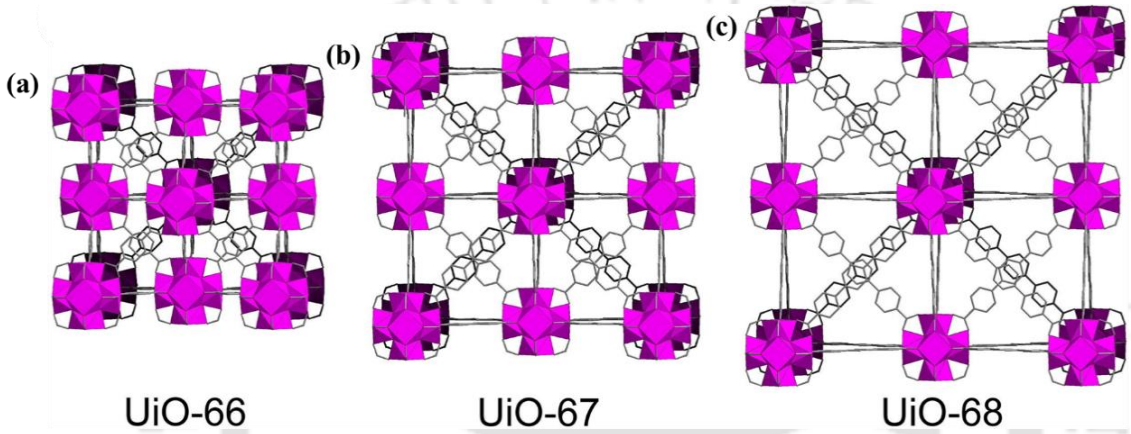

Figure 1.12 (a) Structures of (a) UiO-66, (b) UiO-67 and UiO-68 based on the connection of $[Zr_6O_4(OH)_4]^{12+}$ clusters via BDC^{2-}, $BPDC^{2-}$ and $TPDC^{2-}$, respectively. Color code: ZrO_8 polyhedra: pink; O: red; C: grey and H atoms are omitted. This image is collected with permission from ref. no. 171. Copyright 2017, Elsevier.

Kaskel *et al.* in 2013 reported another single crystal of 12-connected Zr(IV) MOF by using 2,6-naphthalene dicarboxylic acid linker (named as DUT-52) (DUT = Dresden University of Technology).[105] Structure of DUT-52 is closely similar to the 'UiO' series MOFs. Similar to the UiO MOFs, in DUT-52, hexanuclear $[Zr_6O_4(OH)_4]^{12+}$ are present as secondary building units (SBUs).[105] These SBUs are interconnected by 12 dicarboxylate linker molecules.[105] Thereafter, the use of different types of carboxylic acid linkers generated Zr-MOFs with different topologies and network connectivities (Table 1.1). Ten-coordinated Zr-MOF was obtained (MOF-802) after using *1H*-pyrazole-3,5-dicarboxylate linker.[171] Similarly, the coordination number became six in MOF-808 when 1,3,5-benzenetricarboxylate was used as a linker.[171, 173] The 1,3,6,8-tetrakis(*p*-benzoate)pyrene based NU-1000 MOF has eight linked clusters (Figure 1.13).[171, 173]

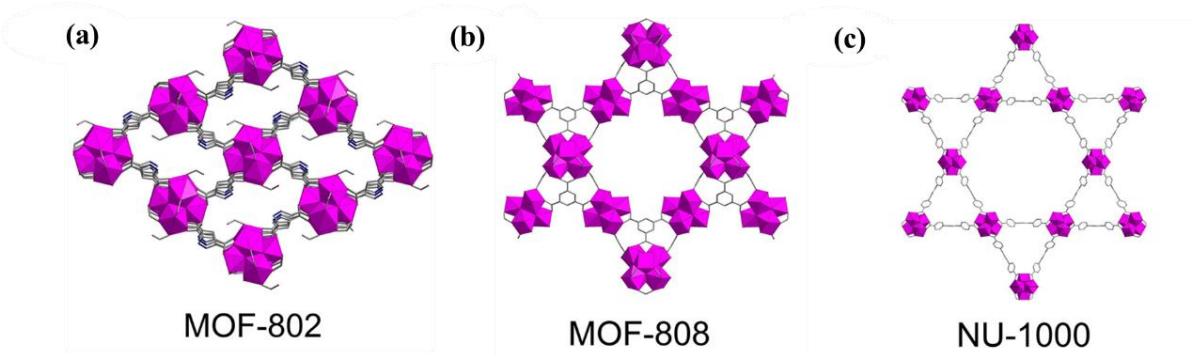

Figure 1.13 Crystal structures of (a) MOF-802, (b) MOF-808 and (c) NU-1000 (c) Colour code: ZrO_8 polyhedra: pink; O: red; C: grey; N: blue. H atoms are omitted. This image is collected with permission from ref. no. 171. Copyright 2017, Elsevier.

There are some Zr-based MOFs where the framework connectivity of is 3 or 4 (DUT-84, PCN-94, Zr-AP-2 etc.).[173] Recently, Biswas *et al.* reported one 10-connected benzo[1,2-*b*:4,5-*b'*]dithiophene-2,6-dicarboxylate containing Zr-MOF with cubic space group.[175] In most of the reported Zr(IV)-based MOFs, $[Zr_6O_4(OH)_4]^{12+}$ is present as a SBU.[173] There are some Zr-MOFs which has some other SBU units. For instance, the Zr-MOFs of MIL-140 series are made up of polymeric double chains of ZrO_7 polyhedra with shared edges that are joined by linear linkers.[176] Devic et al. reported MIL-153 and -154 MOF where Zr(IV) is present as ZrO_8 coordination geometry with network connectivity of 8.[177] A few of Zr-MOFs (e.g. Zr-TPDC) with $[Zr_{12}(\mu_3\text{-}O)_8(\mu_3\text{-}OH)_8(\mu_2\text{-}OH)_6(COO)_{18}]$ clusters have been reported in recent past.[178] In these MOFs, six μ_2-OH groups interconnect two Zr_6 clusters that are face-to-face in these frameworks. The cooperation of different linkers with different shapes and coordination numbers of metal ions regulates the crystal structure and porosity of various Zr-MOFs.[178] In Table 1.1, a summary of clusters, topology and network connectivity of some popular, physicochemically stable, and porous Zr-MOFs are presented.

Table 1.1 Summary of clusters/cores, linker used, coordination number and topology and surface area of some previously reported Zr(IV)-MOFs.

MOFs	Clusters	Linker Used	Topology and Connectivity	BET Surface Area (m^2/g)	Ref.
UiO-66	$Zr_6(\mu_3\text{-}O)_4(\mu_3\text{-}OH)_4$	BDC	**fcu**, 12-connected	1187	156
UiO-67	$Zr_6(\mu_3\text{-}O)_4(\mu_3\text{-}OH)_4$	BPDC	**fcu**, 12-connected	3000	156
UiO-68	$Zr_6(\mu_3\text{-}O)_4(\mu_3\text{-}OH)_4$	TPDC	**fcu**, 12-connected	4170	156
NU-1000	$Zr_6(\mu_3\text{-}OH)_8$	TBAPy	**csq**, (4,8)-connected	2320	179
NU-1100	$Zr_6(\mu_3\text{-}O)_4(\mu_3\text{-}OH)_4$	PTBA	**ftw**, (4,12)-connected	4020	180
MOF-801	$Zr_6(\mu_3\text{-}O)_4(\mu_3\text{-}OH)_4$	FUM	**fcu**, 12-connected	990	181
MOF-802	$Zr_6(\mu_3\text{-}O)_4(\mu_3\text{-}OH)_4$	PZDC	**bct**, 10-connected	<20	181
MOF-808	$Zr_6(\mu_3\text{-}O)_4(\mu_3\text{-}OH)_4$	BTC	**spn**, (3,6)-connected	2060	181
MOF-812	$Zr_6(\mu_3\text{-}O)_4(\mu_3\text{-}OH)_4$	MTB	**ith**, (4,12)-connected	2335	181
MOF-841	$Zr_6(\mu_3\text{-}O)_4(\mu_3\text{-}OH)_4$	MTB	**flu**, (4,8)-connected	1390	181
MOF-525	$Zr_6(\mu_3\text{-}O)_4(\mu_3\text{-}OH)_4$	TCPP	**ftw**, (4,12)-connected	2620	182
MOF-545	$Zr_6(\mu_3\text{-}O)_8$	TCPP	**csq**, (4,8)-connected	2260	182
DUT-51	$Zr_6(\mu_3\text{-}O)_6(\mu_3\text{-}OH)_2$	DTTDC	**reo**, 8-connected	2335	183
DUT-52	$Zr_6(\mu_3\text{-}O)_4(\mu_3\text{-}OH)_4$	2,6-NDC	**fcu**, 12-connected	1399	105
DUT-84	$Zr_6(\mu_3\text{-}O)_8$	2,6-NDC	**(4,4)IIb**, 6-connected	637	105
DUT-67	$Zr_6(\mu_3\text{-}O)_6(\mu_3\text{-}OH)_2$	TDC	**reo**, 8-connected	1064	184
DUT-68	$Zr_6(\mu3\text{-}O)_6(\mu_3\text{-}OH)_2$	TDC	8-connected	891	184

PCN-221	$Zr_8(\mu_4\text{-}O)_6$	TCPP	**ftw**, (4,12)-connected	1936	185
PCN-222	$Zr_6(\mu_3\text{-}OH)_8$	TCPP	**csq**, (4,8)-connected	2223	186
PCN-223	$Zr_6(\mu_3\text{-}O)_4(\mu_3\text{-}OH)_4$	TCPP	**shp**, (4,12)-connected	1600	187
PCN-224	$Zr_6(\mu_3\text{-}O)_4(\mu_3\text{-}OH)_4$	TCPP	**she**, (4,6)-connected	2600	188
Zr-TPDC	$Zr_{12}(\mu_3\text{-}O)_8(\mu_3OH)_8(\mu_2\text{-}OH)_6(COO)_{18}$	TPDC	-	1967	178
IITG-5	$Zr_6(\mu_3\text{-}O)_4(\mu_3\text{-}OH)_4$	$C_{12}O_4H_4S_2$	10-connected	1228	175
MIL-140A	$Zr(\mu_3\text{-}O)_3O_4$	BDC	-	415	189
MIL-140B	$Zr(\mu_3\text{-}O)_3O_4$	2,6-NDC	-	460	189
Zr-BTBA	$Zr_6(\mu_3\text{-}O)_4(\mu_3\text{-}OH)_4$	BTBA	**ftw**, (4,12)-connected	4342	190
MIL-153	ZrO_8	pgal	-	-	177
MIL-154	ZrO_8	Hgal, Hsal	-	-	177

BDC = terephthalate; BPDC = biphenyl-4,40-dicarboxylate; TPDC = [1,1′:4′,1″-terphenyl]-4,4″-dicarboxylate; TBAPy = 1,3,6,8-tetrakis(p-benzoate)pyrene; PTBA = 4-[2-[3,6,8-tris[2-(4-carboxylatephenyl)-ethynyl]-pyren-1-yl]ethynyl]-benzoate; FUM = fumarate; PZDC = 1H-pyrazole-3,5-dicarboxylate; BTC = benzene-1,3,5-tricarboxylate; MTB = 4,4′,4″,4‴-methanetetrayltetrabenzoate; TCPP = meso-tetrakis(4-carboxylate-phenyl)porphyrin; DTTDC = dithieno[3,2-b;20,30-d]-thiophene-2,6-dicarboxylate; 2,6-NDC = naphthalene-2,6-dicarboxylate; TDC = 2,5-thiophenedicarboxylate; TCPP = meso-tetrakis(4-carboxylate-phenyl)porphyrin; BTBA = 4,4′,4″,4‴-(biphenyl-3,30,5,50-tetrayltetrakis(ethyne-2,1-diyl))tetrabenzoate; $C_{12}O_4H_4S_2$ = benzo[1,2-*b*:4,5-*b*′]dithiophene-2,6-dicarboxylic acid; H_3Pgal = pyrogallol; gal = gallate; sal = salicylate.

1.8 Origin of Luminescence in MOFs

The photophysical process by which the electrons of a material absorb photons, leap to a higher energy state, subsequently re-radiate the photons and then return to the lower energy state is known as luminescence. It is a conversion process of absorbed energy in the form of light. Concerning the required time of the process and energy states involved in this conversion process, it can be categorized into two parts: fluorescence and phosphorescence. In the case of fluorescence, the electronic transition occurs between two electronic states of the same spin multiplicity value but in the case of phosphorescence, such transition happens with the electronic states having different spin multiplicity values. The average time required for fluorescence (~10 ns) is much less as compared to phosphorescence (microseconds to seconds) (Figure 1.14a).[191] There are a few MOFs reported in the literature that display phosphorescence whereas thousands of fluorescent MOFs are explored. In MOFs fluorescence properties can arise due to the presence of highly π-conjugated fluorescent organic linkers, the antenna effect of lanthanide metal ions, the electronic communication between the metal ions and π-conjugated polytopic organic linkers (LMCT and MLCT), aggregation-induced emission and diffusion of guest molecules in the framework (Figure 1.14b).

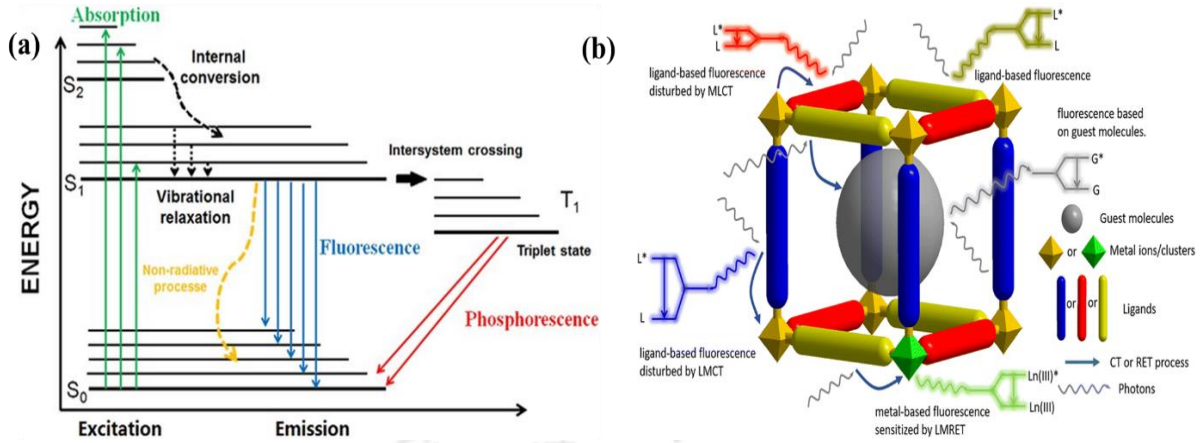

Figure 1.14 (a) Jablonski diagram of fluorescence and phosphorescence. This image is collected with permission from ref. no. 191. Copyright 2021, Springer. (b) Schematic diagram showing the different sources of fluorescence signals in MOF-based fluorescence sensors. CT: charge transfer, RET: charge transfer, MLCT: metal-to-linker charge transfer, LMCT: metal-to-linker charge transfer, LMRET: linker-to-metal resonance energy transfer. This image is collected with permission from ref. no. 29. Copyright 2014, Royal Society of Chemistry.

1.8.1 Linker-Based Fluorescence

Except for the f-block metal ion-containing MOFs, in most of the fluorescent MOFs the origin of fluorescence is due to the presence of highly π-conjugated fluorescent organic linkers. In the free linker, the electronic circulation through π-bonds makes them fluorescent and after the formation of coordination complexes with the metal ion, its fluorescence property is further enhanced due to the reduction of unwanted relaxation of the linker in the excitation state. The formation of strong coordination bonds also makes a change in the quantum efficiency and fluorescence lifetime of the linker. For example, Li and his co-workers synthesized a Cd-based *N*-2-aryl-triazole (NAT) linker containing MOF. They displayed that the MOF's fluorescence intensity (Φ = 26%) was much higher than the corresponding linker (Φ = 6.7%).[192] Zhou and his team synthesized Zr-based PCN-94 using H_4ETTC (H_4ETTC = 4′,4‴,4⁗,4⁗′-(ethene-1,1,2,2-tetrayl)tetrakis(([1,1′-biphenyl]-3-carboxylic acid)) linker and displayed that after rigidifying the fluorescent linker by the formation of MOF, the fluorescence intensity and quantum yield of the linker can be improved.[68] Twisted linker conformation, framework stiffness and intramolecular hindrance are thought to be the causes of these peculiar photoluminescence characteristics.[68] The observed spectral property, color of the linker and MOF are also completely different from each other. The solid-state photoluminescence spectrum of H_4ETTC linker has a broad absorption profile with two distinct peaks, whereas PCN-94 displays a significantly sharper absorption profile. H_4ETTC linker shows a brilliant yellow color after absorbing blue light, but PCN-94 displays a white color with a minor decolouration since it only absorbs UV radiation but reflects all visible light.[68]

1.8.2 Metal-Based Fluorescence

Lanthanide-based MOFs frequently exhibit metal-based fluorescence because of the f-f transition. Such transition of 4f orbital electors is responsible for the origin of various colours of lanthanide ions. Because of the f-f transition, Eu^{3+}, Sm^{3+}, Tb^{3+} and Tm^{3+} ions emit red, orange, green and blue color lights, respectively. But these f-f transitions are spectroscopically forbidden. As a result, lanthanide ions exhibit low luminescence efficiency. In MOF, through the "antenna effect," organic linkers can make lanthanide ions more fluorescence active. During this process, the organic linkers first absorb the energy from the light and transfer the energy via its triplet state to the closely lying energy state of the lanthanide ion through an intersystem crossing mechanism. Moreover, to maximize the energy transfer process, the triplet state of lanthanide should stay in such a position that it can reduce the back-transfer process. Therefore, the location of energy states of the metal ions and the organic linkers are very crucial for the production of particular fluorescence color emissive MOF. Although many of the fluorescent f-block metal-containing MOFs are reported, Eu(III) and Tb(III)-based MOFs are frequently used for sensing applications. Distinctive fluorescent color at different excitation wavelengths is the main reason behind such selection (Figure 1.15).[193-195]

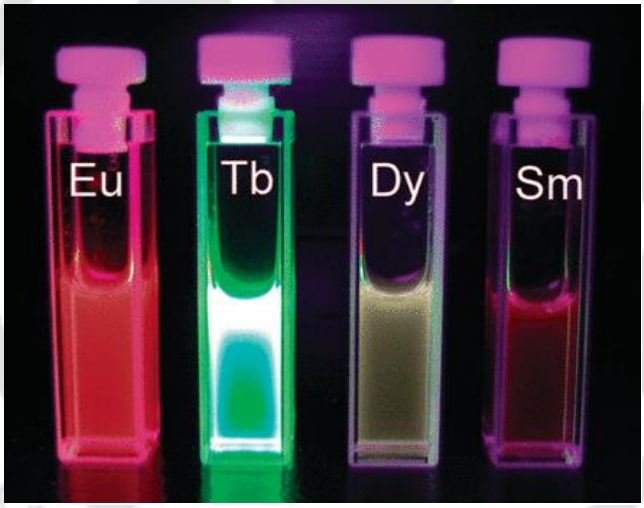

Figure 1.15 Digital image of the fluorescence emission of aqueous solutions (0.01 M Tris buffer (10^{-4} M), pH = 8.5) of the various lanthanide organic complexes illuminated by a standard laboratory UV lamp (λ_{ex} = 354 nm). This image is collected with permission from ref. no. 195. Copyright 2003, American Chemical Society.

1.8.3 Charge Transfer Fluorescence

In MOFs, two different kinds of charge transfers are generally observed: metal-to-linker charge transfer (MLCT) and linker-to-metal charge transfer (LMCT).[196, 197] For MLCT, transfer of electron occurs from an excited state of a metal ion to the ground state of an organic linker. In the case of LMCT, the exact opposite scenario is observed.[196, 198]

The fluorescence emission maxima and nature of the spectrum of a MOF closely resemble that of the original linker when there isn't any charge transfer or resonance energy transfer between the metal ion and the linker. The emission maxima of the linker can be shifted to a

higher wavelength if there is any MLCT and for LMCT, that is shifted to the lower wavelength.[29] Sometimes, linker-to-linker charge transfer (LLCT) is also observed within different linkers or the different parts of the same linker. Similar to the MLCT and LMCT, a change in emission intensity and wavelength of the MOF was observed in LLCT.[29]

1.8.4 Guest-Induced Fluorescence

The porosity of MOF allows the loading of certain fluorescent compounds inside its cavity. The most often utilized guest fluorescent molecules include precious metal complexes,[199] organic and inorganic dyes[200] and lanthanide ions.[29] A MOF can enhance the stability of guests and avoid their agglomeration with various interactions. Sometimes, the fluorescence of MOF is found to be increased through charge transfer or resonance energy transfer between MOF and the guests. By combining numerous fluorescent sources into one MOF, many MOF-based fluorescent sensors have been developed for multiple fluorescent signals. Two distinct fluorescence signals based on two separate fluorescent linkers can also be observed in the fluorescence spectrum of a MOF. It is an interesting and useful technique to create a multi-responsive fluorescent MOF-based sensor by loading a guest fluorescent molecule without hampering the linker and metal-based fluorescent signals. Additionally, partial sensitization can be used to create multiple fluorescence signals. For instance, an imperfect "antenna effect" causes the sensors to exhibit both linker-based and metal-based fluorescence signals when the energies of the linkers and the lanthanide ions are not well matched.[29, 201]

1.8.5 Aggregation-Induced Fluorescence

Due to the unique emission feature of aggregation-induced emission (AIE), AIE-based luminescent MOFs have become attractive candidates for various sensing applications. In reality, the introduction of AIEgens in MOFs is very difficult. It was observed that the AIEgen sites become rigid after the formation of a coordination bond with the metal ions.[202] However, the significant tuning of electronic transitions was observed in some of the reported AIE (tetraphenylethene)-based MOFs. Rapid rotation of phenyl rings and twist vibrations of ethylenic C–C bond in tetraphenyl ethane-based MOFs should cause the fluorescence quenching, but the reduction of such rotation and twist in the aggregated state results in fluorescence turn-on. Utilizing this concept, Omary et al. prepared a Zr-based MOF using tetrakis(4-carboxyphenyl)ethylene as a binding linker. The synthesized MOF was highly fluorescent and displayed a high quantum yield due to the AIE of the binding linker.[68] Likewise, Yang et al. were able to fabricate Hf-based 2D layer based on AIE effect of the H_4ETTC (4',4",4'",4""-(ethene-1,1,2,2-tetrayl)tetrabiphenyl-4-carboxylic acid) linker. Because of the AIE effect, a 27.6% increase in electrochemiluminescence (ECL) efficiency of the layer was observed which is due to the inhibition of the intramolecular motions of the linker, shortened diffusion distances of metal ions and electron density of the linker.[203]

1.9 Mode of Fluorescence Response and its Reasons

The fluorescence signal of a fluorophore can be changed due to a change in the pathway of electronic transition of the fluorophore or by the change in the excited state energy of the fluorophore.[29] Four types of fluorescence responses are reported in the literature: (i) increase in emission signal (turn-on), (ii) decrease in emission signal (turn-off), (iii) shift of emission signal and (iv) combination of third one with any of the first two.[29] Among the aforementioned responses, the quenching (turn-off) of fluorescence in the presence of an external analyte is very common. However, due to poor recyclability, loss of signal and vulnerability issues, turn-off response is not user-friendly. On the other hand, the turn-on response is more responsive and instinctive than the turn-off type. Because the of short range of change in emission signals, poor linearity and low sensitivity the wavelength-shift type responses are not much investigated. However, the combination type has shown enough potential and significant interest in the scientific community since both wavelength and emission intensity are changed at the same time. Several reasons are reported in the literature which can be responsible for these observations. Some of them are summarized below:

1.9.1 Structural Change of the Fluorophore

In the presence of external molecules, some organic or inorganic reactions can take place between the fluorophore and the foreign substrate which can make a change in the signal output of the fluorophore. These types of reactions can occur in the ground state (ground state complexation) and can also occur in the excited state of the molecule (exciplex).[175, 204, 205] Such reaction-based changes in fluorescence can be irreversible and can also be reversible. In reversible cases, the fluorophore (MOF) recovers its fluorescence after removing the external analyte which is not possible for reversible case.

1.9.2 Resonance Energy Transfer

Resonance energy transfer (RET) is a pathway of a non-reaction-based energy transfer process by which excess energy is transferred from an excited molecule to an energy-deficient molecule. Proper distance and orientation are mandatory for this type of energy transfer. Fluorescence resonance energy transfer (FRET) is one of the widely acceptable energy transfer mechanisms of MOF-based sensing. FRET is a dipole-dependent, long-range, intermolecular energy transfer process.[206] The efficiency of FRET is inversely proportional to the sixth power of intermolecular distance. The typical FRET distance is 10–100 Å.[206] This type of energy transfer can directly occur from MOF to analytes and vice-versa. For this process, a significant overlap between the emission spectrum of the MOF and the absorption spectrum of the analyte is required.[206] The resulting emission response is turned off when the energy transfer takes place from the MOFs to the analytes and it will be turned on when the reverse occurs.[206]

1.9.3 Photo-induced Electron Transfer (PET)

It is an excited state redox process.[207] During this process electron transfer occurs from an excited state molecular orbital of a molecule to a low-lying vacant orbital of another molecule. Moreover, PET can also occur in between two parts of the same molecule. Through this

process, both an increase and decrease in fluorescence emission intensity of the fluorophore can occur.[207] When the excited state orbital energies of the sensor (LUMO) lie above the lowest unoccupied orbital (LUMO) of the analyte, then electrons in the excited state can be shifted from the LUMO of the sensor (MOF) to the LUMO of the analyte. In this typical case, a turn-off in the fluorescence response of the MOF can be noticed. Similarly, the transfer of electrons from the LUMO of the external analyte to the LUMO of MOF results turn-on in fluorescence.[208, 209]

1.9.4 Internal Filter Effect (IFE)

IFE can be responsible for quenching of fluorescence intensity of a fluorophore if the excitation wavelength of the MOF is nearly close to the absorption maxima of the analyte.[210] In this scenario, there is a possibility of absorption of a part of the excitation beam of light by the external analyte. This phenomenon can interrupt the complete excitation of the probe, which eventually results in less emission signal output of the probe.[211] IFE can also occurred if the part of emitted light of a probe is absorbed by the external analyte. Based on these phenomena, IFE can be categorized into two parts: competitive absorption and resonance energy transfer (RET). RET arises when the analyte's UV-Vis absorption overlaps with the sensor's emission, whereas competitive absorption occurs when the analyte's UV-Vis absorption overlaps with the sensor's excitation.[29] The fluorescence of the sensor is turned off by both RET and competitive absorption. Although the IFE was once believed to be a fault in fluorescence measurement, it has now been revealed to be a non-irradiative energy transformation model in the spectroscopic approach and has been used in the development of several photoluminescent-based detection systems.[212, 213]

1.10 Applications of MOFs

Like the other commercially available porous materials the applicability of MOFs did not end with gas adsorption and separation. Structural diversity and tenability, physicochemical stability and scope of introducing required functional groups have made MOF materials applicable in miscellaneous fields. Because of the huge internal surface areas, high degree of crystallinity and vast porosity, MOFs are frequently compared to zeolites. But, modern-day research displays that MOFs are capable of fulfilling more requirements of upgrading civilization. Now-a-days, MOFs are used for different industrial, technological, environmental and biological applications including gas storage and separation, separation of miscible and immiscible liquids and solids from water, proton-conductivity, ion exchange, drug delivery, heterogeneous catalysis of various organic reactions, sensing of toxic or biological important molecules, etc. (Figure 1.16).

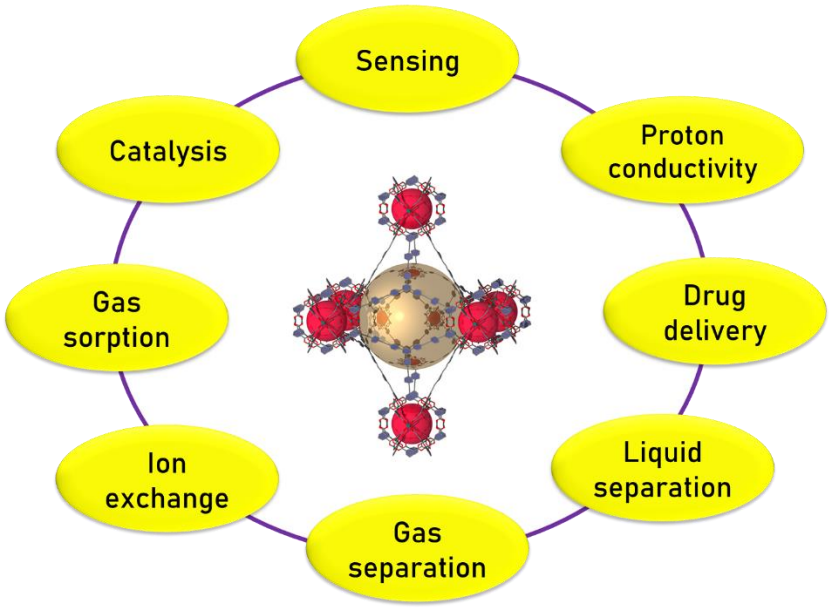

Figure 1.16 Different applications of MOFs.

The spontaneous development of modern civilization, socioeconomic growth, industrialization, urbanization and intensification in the use of modern agricultural practices and uncontrollable increase in bacterial and viral diseases have drastically increased the water and environmental pollution caused by toxic heavy metal ions, drugs, herbicides, antibiotics, pesticides, toxic anions, volatile organic compounds, oil spills, and other emerging pollutants. Detection and quantification of such pollutants in an aqueous body is one of the finest, easiest and popular ways to remote such pollution. The critical diagnosis of various human diseases, pharmacokinetics study of various drugs and forensic science require the determination of the exact concentration of various biomolecules in body fluids is very crucial. For the remediation of the aforementioned environmental pollution and measurement of the concentrations of biomolecules, various quantification techniques have been developed by the scientific community. Among them, fluorescence-based sensing is one of the most accessible, cost-effective, swiftly responsive and consistent methods for the determination of various pollutants present in environmental water bodies and biomolecules in living organisms. These qualities have made the fluorescence-based method a better and more promising sensing technique than most of the other traditional techniques e.g., HPLC, LC-MS, capillary electrophoresis, atomic emission and absorption spectroscopy etc. The detection of the targeted analytes can be enabled by the selective selection of suitable fluorophore molecules. A fluorescent MOF can act as a fluorophore and nullify the above-mentioned issues. In this thesis, I have mainly focused on developing some functionalized MOFs to control water pollution and biological diseases by sensing and adsorption of environmentally toxic and biologically important molecules.

1.10.1 Toxic Heavy Metal Sensing

Water pollution due to toxic, non-decomposable, soft and heavy metals is one of the premium concerns in 21st century. The world already has faced many disasters due to the harmful effects of lead, arsenic, cadmium and mercury. Japan's Minamata disease in 1956 is only one example

of such a disaster that occurred due to toxic effects of mercury.[175, 214] Now-a-days, the presence of excess amounts of arsenic in drinking water is one of the major reasons behind the crisis of drinking water in South Asia (India and Bangladesh).[214] Cardiovascular disease, incidence of hypertension, increased blood pressure and decreased function of kidneys can occur due to the abnormal presence of lead in drinking water.[214] Symptoms of Itai-Itai disease can be observed by cadmium contamination in water. Realizing such urgency, several MOF-based fluorescence sensors have been developed for the detection and quantification of heavy metal ions during the last 10 years.

As mercury is the softest heavy metal and in the biological environment, inorganic Hg^{2+} readily converts to more soft and lipophilic methyl mercury, pollution due to soft mercury is one of the major concerns among the pollution caused by various metals.[175] When a trace quantity of mercury interacts with soft, sulfur-containing amino acid molecules the immunological and central neurological systems are quickly damaged. Higher mercury concentrations can induce a variety of health problems such as nephrotic syndrome, respiratory problems, cancer, motion disorders, renal failure and transient blindness.[175]

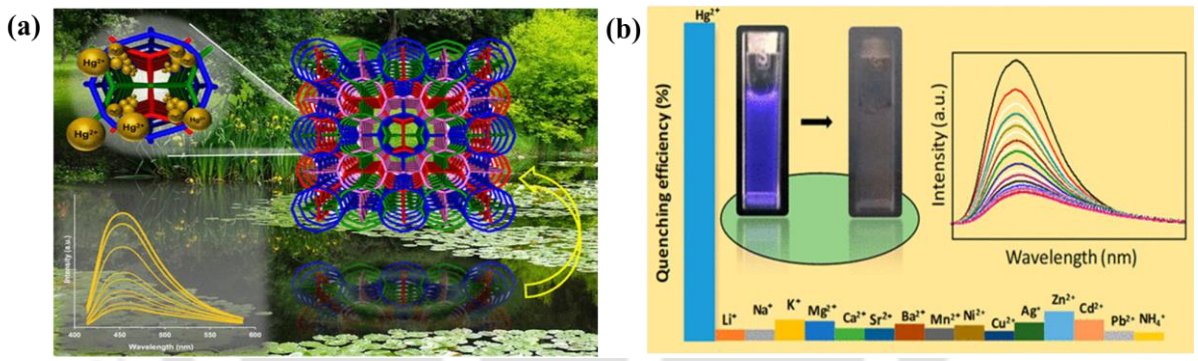

Figure 1.17 (a) Sensing and adsorption of toxic heavy metal ions by MOF and (b) sensing of Hg^{2+} by a fluorescent Zn-MOF. This image is collected with permission from ref. no. 215 and 31. Copyright 2016 and 2019, American Chemical Society.

Several research groups in the world have developed MOF-based fluorescent sensors of Hg^{2+}. For instance, Li and his co-workers developed a series of sulfone-functionalized, water-stable, fluorescent Zn-MOFs for the detection of Hg^{2+} up to ppb level.[215] Another Zn(II)-MOF was developed by Mandal et al. for the selective sensing of the same metal ion (Figure 1.17).[31] A Ni(II) containing MOF with the molecular formula $[Ni(3\text{-bpd})_2(NCS)_2]_n$ was developed by Roy et al. for the detection of Hg^{2+}. A porphyrinic zirconium framework with an exposed pyrrole Lewis basic site was prepared by Safarifard and his co-workers for the fluorescence sensing of Hg^{2+}. A butyne-functionalized UiO-66 MOF was synthesized by Ghosh et al. for the nanomolar detection of Hg^{2+} in water. They showed that the interaction between the triple bond and Hg^{2+} was the reason behind the selective sensing of Hg^{2+} by the MOF. G. Qian and his co-workers developed a Tb(III) MOF for the fast and selective sensing of mercury. The reported response time of the probe was only 3 s and LOD was 47.8 nM. Recently, Biswas et al. developed two sulfur-containing MOFs named IITG-5 and Hf-UiO-66-$NHCSNHCH_3$ for the ultrafast and nanomolar level detection of Hg^{2+} in various environmental waters.[216] Many other reports are

available in the literature for the specific fluorometric sensing of Hg^{2+} by utilizing MOFs. Some of them are summarized in Table 1.2.

Table 1.2 Examples of some literature reported fluorescent MOFs and their response time, detection limit and sensing media used for the sensing of Hg^{2+}.

Sl. No.	Sensor Material	Sensing Medium	Detection Limit (nM)	Response Time (min)	Ref.
1	$[Ni(3\text{-}bpd)_2(NCS)_2]_n$	water	-	120	217
2	[PCN-221]	water	10	1	218
3	[Cu(Dcbb)(Bpe)]·Cl	HEPES buffer	3.2 and 3.3	30	219
4	UiO-66@ Butyne	water	10.9	3	220
5	$Ln(TATAB)\cdot(DMF)_4(H_2O)(MeOH)_{0.5}$	water	4.4	-	221
6	Eu^{3+}/CDs@MOF-253	water	47.88	3	222
7	$[Cu(Cdcbp)(H_2O)2\cdot 2H_2O]_n$	water	(2.3 ± 0.8)	2	223
8	Al-MOF (TAM)	water	2.94	0.5	224
9	$[Cu(Cbdcp)(Dps)(H_2O)_3]\cdot 6H_2O_n$	HEPES buffer	2.6	10	225
10	Cd−EDDA	water	2	0.25	226

1.10.2 Toxic Anion Sensing

The contamination of water by toxic anions, such as CN^-, PO_4^{3-}, AsO_4^{3-}, CrO_4^{2-}, SO_3^- and MnO_4^- etc. from various industrial, environmental and human activities create several problems that harm both the environment and human health.[227] The Development of highly effective and widely applicable methods for detecting toxic anions is urgently needed since it is very necessary to monitor the concentration of toxic anions in various environmental water bodies and wastewater to prevent their penetration into the human body. Numerous MOF-based sensors for the detection of harmful anions have been developed during the last few decades.[227]

Along with these purely inorganic anions, excessive use of some lipophilic groups containing anions (e.g. surfactants) becomes a great treat for aquatic animals and indirectly for human beings. Recent reports evidenced that around 15 million tons of surfactants are synthesized worldwide every year to use as an emulsifier, cleaning agent and in the cosmetic industry. Most of the used surfactants are anionic surfactants (e.g., sodium dodecyl sulfate: SDS). Overusing these surfactants causes their discharge into the environment, which negatively impacts both human health and the health of aquatic species. Because surfactants may permeate the lipid barrier of the skin and other cells, prolonged contact with them can irritate and damage the skin.[228] When the concentration of surfactants in the water is very high, they can enter the gills, pancreas, kidneys, gallbladder, blood, and liver, which can impair the activities of these organs.[229] To monitor such pollution several polymers, organic molecules, carbon nanotubes and polymeric membranes have been developed for the colorimetric, potentiometric and electrochemical sensing of SDS. However, no fluorescent MOF-based sensors are reported.

For the first time Biswas et al. developed a diamine functionalized UiO-66 MOF for the fluorescent-based, nanomolar level detection of SDS.[230] The electrostatic interaction between the $–NH_3^+$ (produced after proton abstraction from water) of the MOF and $-SO_3^-$ of SDS is the reason behind this selective and reusable sensing.

1.10.3 Pharmaceutical Waste Sensing

The development of synthetic pharmaceuticals marks a significant turning point in the healthcare industry, altering the general public's overall health, aging and lifestyle.[231] These medications have become increasingly prevalent as possible environmental contaminants in water and soil samples due to the growth in their manufacturing and usage. These antibiotics have detrimental impacts on both human health and the ecology because of their high toxicity and poor biodegradability.[231] These medicinal substances are poisonous to microbes and aquatic animals and their presence in the aquatic environment also increases the growth of green algae. In addition to the environmental risks, the introduction of pharmaceutical residues into our ecosystem can promote the development of bacteria that are resistant to antibiotics.[231] This will decrease the effectiveness of present antibiotics by making common bacteria less susceptible to them.

Recent reports suggested that the use of various pharmaceutical drugs and antibiotics has increased by 10-15 times after the COVID-19 pandemic, directly enhancing the concentration of pharmaceutical waste in environmental water bodies.[232] The concentrations of these pharmaceutical wastes and their metabolized side products in urban wastewater have risen by more than 70% due to their misuse and careless disposal in the past 2-3 years.[231] It has become a worrying worldwide issue since the concentrations of these medications and their metabolites are rising so rapidly. These reasons make it essential to develop selective and sensitive sensor systems that continuously check the concentration of synthetic drug residues in our surroundings.

Several recent studies were executed for the development of rapid, reliable and reusable MOF sensors to monitor the pollution caused by antibiotics and other pharmaceutical drugs. For example, Pan et al. developed HNU-52 MOF for the micromolar level detection of nitrofuran antibiotics in DMF medium.[67] For the sensing of the same antibiotics in DMAc medium a Zn(II) MOF was developed by Zhao and his co-workers and a Cd(II) based MOF was synthesized by Teng et al. (Figure 1.18a).[233, 234] A double-walled bimetallic MOF was synthesized by Du et al. for the selective sensing of metronidazole (MDZ) in DMF medium.[235] Another lanthanide MOF was developed by Li and his co-workers for the detection of MDZ.[236] A sensor of tetracycline antibiotics was developed by Tan and his co-workers, and a sensor for the same antibiotic was also developed by Zheng and his co-workers.[237, 238] Along with the antibiotics, many other sensors for the detection of various pharmaceutical drugs have been also developed. Among them, favipiravir sensing by Serre et al. (Figure 1.18b), penicillamine sensing by Yang et al., alendronate sensing by Xu et al. and carbamazepine sensing by Li and his co-workers are only a few examples.[239-242] Some of the other reports are summarized in Table 1.3.

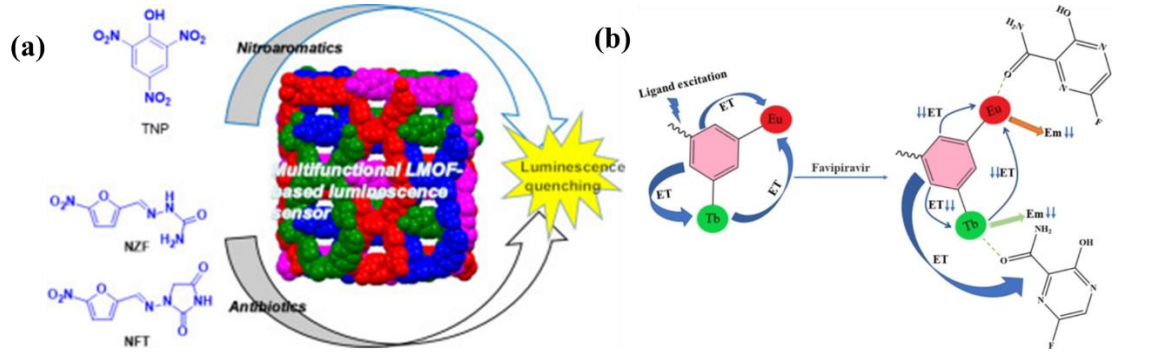

Figure 1.18 (a) Sensing of toxic antibiotics by MOF and (b) sensing of the drug (favipiravir) by a fluorescent Tb-MOF. This image is collected with permission from ref. no. 233 and 239. Copyright 2019, Elsevier and 2022, Wiley and Sons.

Table 1.3 Examples of some literature reported fluorescent MOFs and their response time, detection limit and sensing media used for the sensing of nitro antibiotics.

Sl. No	Sensor Material	Name of Antibiotic	Sensing Medium	Detection Limit (nM)	Response Time (min)	Ref.
1	CNDs	NFT	-	1400	-	243
2	$(Me_2NH_2)1.5[In1.5(FBDC)(BDC)]2.5DMF.CH_3CN$	NFT	water	1900	60	244
3	$[Cd_3(DBPT)_2(H_2O)_4]\cdot 5H_2O$	NFT	methanol	5000	-	245
4	Tb(IJTCPB)·DMF	NFZ NFT	water	55000 120000	120	246
5	$[Cd_3(TDCPB)\cdot 2DMAc]\cdot DMAc\cdot 4H_2O$	NFT NFZ	DMAc	60000	1.25	247
6	4⊃DEASM	NFZ	water	208	-	248

1.10.4 Biomolecules Sensing

First MOF based bio-sensor was developed by Asefa *et al.*in the year 2008.[249] After that, a huge number of MOFs were employed for the sensing of various macromolecules (protein/enzyme and nucleic acid) and small bioactive molecules (adrenaline, dopamine, amino acids and glucose).[249] Better biodegradability and compatibility, adaptable networks, scope of nanoscale design and topological diversity make MOFs a popular choice for sensing of biomolecules. According to toxicological research, some metals, such as Ca, Fe, Mn, Zn, Zr and Mg are considered to have extremely high fatal dosage limits of at least 1g/kg.[249] Therefore, MOFs with the aforementioned metal ions are generally preferred for biological application purpose. The science of biomolecule sensing has greatly benefited from the recent development of functional MOFs. Not only sensing and measuring the concentration of biomolecules in various bio-fluids, the in vitro study (inside the biological cell) of biomolecules is also possible using a fluorescent MOF.

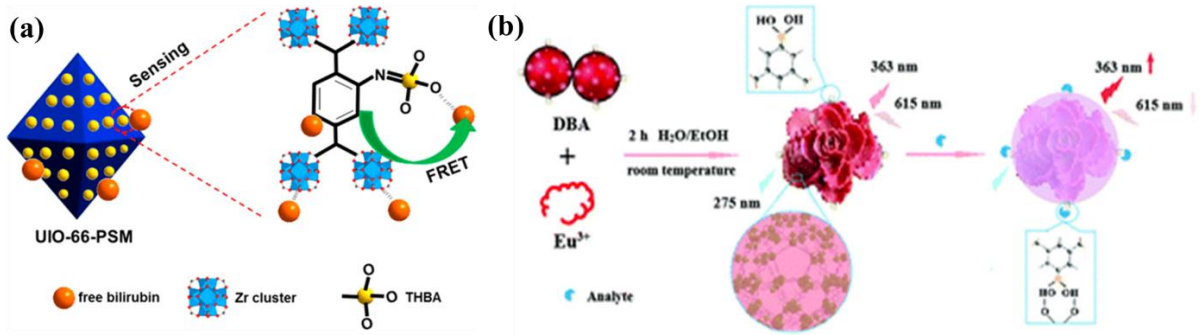

Figure 1.19 (a) Sensing of bilirubin by MOF and (b) sensing of dopamine by a fluorescent Cd-MOF. These images are collected with permission from ref. no. 250 and 251. Copyright 2017, American Chemical Society and 2018, Royal Society of Chemistry.

There are many fascinating MOF-based sensors for biomolecules reported in the literature. For example, Mirkin et al. first developed a nucleic acid-MOF hybrid by functionalizing UiO-66 MOF with oligonucleotides for the selective detection of DNA/RNA. Here, the DNA/RNA has been integrated on MOF surface.[252] In the year 2013, Chen et al. proposed a Cu(II) containing MOF which was able to detect HIV-1 DNA via quenching of fluorescence of the MOF.[253] A peptide nucleic acid modified 'MIL' MOF was synthesized by Mejia-Ariza et al. for the sensing of DNA.[254] Xie's group designed an aqua-stable Cu(II) MOF for the detection of Zika virus RNA.[255] Together with bio-macromolecule sensing, there are many reports of small biomolecule sensing. A ratiometric fluorescence boric-acid-functional Eu-MOF was developed by Yin et al. for the selective sensing of glucose and H_2O_2.[256] Turn-on in fluorescence was observed after the addition of the targeted analytes. LOD of the reported probe was at micromolar level for both the targeted analytes. A water-stable homochiral pyrene-tetraacetic acid containing Zn-MOF was synthesized by Moorthy et al. that demonstrated enantioselective distinction of histidine based on fluorescence quenching.[257] PSM strategy was adopted by Jia et al. and Biswas et al. for the selective sensing of bilirubin in various bio-fluids (Figure 1.19a).[250, 258] In both cases, quenching in fluorescence was observed after the addition of bilirubin in the MOF suspension. Ultra-fast response time and microlevel detection ability are the specialty of these probes. An Eu(III)-MOF of honeycomb topology was developed by Janczak and his co-workers for the nanomolar level detection of dopamine.[259] A Cd(II) containing MOF for dopamine sensing in various body fluids was developed by Y. Li and his co-workers (Figure 1.19b).[251] Another dopamine sensor was recently reported by Biswas et al. The sensor was capable of detecting dopamine in human serum and urine samples. Fast response and nanomolar level detection ability are the other specialties of this Al-based CAU-10 MOF.[260] A Tb(III)-metal ion containing MOF was recently reported by Yan and co-workers for the selective fluorometric detection of adrenaline. The reported sensor was able to detect adrenaline up to micromolar concentration level via turn-off pathway.[261] A ratiometric serotonin MOF sensor was reported by Liu et al. The sensor displayed good selectivity and rapid detection ability for the sensing of serotonin up to the micromolar level.[262] Many more MOF-based sensors for biomolecules are reported in the literature. A few of them are summarized in Table 1.4.

Table 1.4 Examples of some literature reported MOFs and their response time, detection limit and sensing media used for the sensing of different biomolecules.

Sl. No.	Sensor Material	Name of Biomolecule	Linear Range	Detection Limit	Ref.
1	PHIV/MIL-88B	DNA	0-5 nM	10 pM	263
2	Cu_3 (1,3,5-benzene tricarboxylicacid)$_2$ /GCE	dopamine	5.0×10^{-7} - 1.0×10^{-4} M	1.5×10^{-7} M	264
3	P-DNA@ZIF-8	HIV-1 ds-DNA	10 nM-100 nM	1.2 nM	265
4	NiCo-MOFNs array	glucose	1-8 mM	0.29 μM	266
5	AChE-ChO/Pt/MOF/Au	acetylcholine	0.01-500 μM	0.01-500 μM	267

1.10.5 Adsorption of Oil Spills from Water

Pollution of environmental water by oil spills is one of the primary levels of water pollution which continuously increasing day by day. Such pollution may occur due to the disposal of oily waste to the environmental water bodies from oil-based industries, from the waste of the kitchen, during the collection and transport of oils through water roots.[268] After mixing the oil spills with water, it develops a layer of oil above the water which frequently blocks the sunlight from coming inside the water. The aquatic food chain producers are immediately impacted by the decreased sunshine, which has an impact on the entire food chain. Due to the oil transported by the waves, seaside animals, fish nurseries and birds become most defenceless. The consumption of seafood exposes individuals to the harmful and persistent component of oil that is introduced into an organism. The mixing of crude oil spills with water can also enhance the oil price in the world market.[269]

Many industrial-level procedures, such as gravity separation, air flotation, centrifugation and coagulation have been developed for the separation of oil-water mixture. But, they are frequently ineffective, complex, time-consuming and expensive. Zeolites, linoleum, cotton and other porous adsorbents have also been used to separate oils from water. However, they often have low adsorption capacity, selectivity and limited reusability and can result in secondary contamination.[270] In recent times, material chemists have been looking to develop alternative materials that can resolve the pollution caused by oil spills.

Some of the recent reports suggested that a hydrophobic MOF can be a potential candidate to resolve the pollution caused by oil spills. The hydrophobic MOFs are appropriate for the selective separation of oil from oil/water mixture. Flexible absorbents made of MOFs can also be recycled. The recovery of absorbed oil by mechanical squeezing is also possible as the materials are stable enough to sustain the external pressure. Considering the aforementioned advantages, a huge number of hydrophobic MOFs have been developed for the selective separation of oil spills from oil/water mixture.

Since fluorides and alkyls have low surface free energies, therefore, long chain alkylated and highly fluorinated linkers are used for the building of hydrophobic MOFs. Due to the lack of free-standing ability of MOF powder, several hydrophobic MOF-based composites were

developed to make the separation process more user-friendly. For instance, a dialkoxyoctadecyl-oligo-(pphenylene ethynylene)dicarboxylate (OPE-C18) linker containing Zn(II)-MOF (NMOF-1) was developed by Roy and co-works in 2016.[271] This developed MOF was superhydrophobic in nature. The measured water contact angle (WCA) of the MOF was 162° and it was utilized for the self-cleaning and oil-water separation application. In the same year, a Cu(II) containing ultrahydrophobic MOF with WCA of 176° was developed by Ghosh et al. and they used that MOF for oil separation from oil-water and water-in-oil emulsion. By spraying a cross-linked mixture of polydimethylsiloxane and UHMOF-100 onto a polypropylene fabric a polypropylene-based membrane was fabricated. The membrane displayed an oil absorption capacity of 40-70 wt% with 10 times reusability (Figure 1.20).[272] Du and co-workers synthesized four highly stable hydrophobic Zr/Hf-UiO-66 MOFs by adding fluoroalkyl chains of various lengths (C6-C10) and using them for the same application.[273] Zhu et al. reported long-chain hydrocarbon containing Zr-UiO-67 MOF and applied the MOF for the separation of oil.[274] Another hydrocarbon chain containing Zr-UiO-66 MOF was synthesized by Rana et al. The developed MOF showed high absorption capacity towards various oils and the developed composite displays 70 times reusability. The observed separation efficiency for all the used oils was above 99%.[268] The one-pot synthesis of a ZIF-8 MOF with highly fluorinated graphene oxide (HFGO) was developed by Jayaramulu and his team which resulted in the formation of a hydrophobic ZIF-8@HFGO composite. The resultant superhydrophobic hybrid MOF with micro- and meso-porosity displayed a WCA of 162°. By utilizing the HFGO@ZIF-8 based sponge, a superb oil and polar/nonpolar organic solvent absorption capacity of 150-600 wt% was attained.[275] The same group reported a hydrophobic MIL-100(Al) MOF and prepared a composite with fluorinated graphene oxide which displayed oil absorption capacities of 200-500 wt%.[276] A superhydrophobic (WCA = 158°) ZIF-8@rGO@sponge composite was developed by Gu and his colleagues. The composite displayed an impressive oil absorption capacity of 1400-2900 wt% with excellent recyclability of 100 times.[277] Many other reports of superhydrophobic MOFs and their composites are available in the literature. Some of them are presented in Table 1.5. Increasing absorption capacity, reusability and improving composite stability was the main focus of the reported hydrophobic MOF composite based oil/water separators.

Table 1.5 Examples of some hydrophobic MOFs, functional groups responsible for hydrophobicity, their WCA, oil separation efficiency and flux of separation.

Sl. No.	MOF Used	Wettability Response Unit	WCA (°)	Separation Efficiency	Flux	Ref.
1	ODPA-ZIF-8(n)@ZIF-8/PDMS	octadecylphosphonic acid	163	separation factor = 17.4	0.64 kg m^{-2} h^{-1}	278
2	Ni_2(L-asp)$_2$ bipy@PDMS	polydimethylsiloxane	137.1	separation factor = 73.6	27.6 kg m^{-2} h^{-1}	279
3	ZIF-8/PAN	surface roughness	153	99.92%	2550 L kg m^{-2} h^{-1}	280
4	MXene@UIO-66-(COOH)$_2$	hierarchical roughness & hydrophilicity of composite	>150	>99%	713.3 L m^{-2} h^{-1} bar^{-1}	281

5	PAN@ZIF-8	surface roughness	155	>99.98%	>900 L m^{-2} h^{-1}	282
6	ZIF-90 membrane	Fluorinated alkyls and the ZIF-90 layer	170	99.98%	1260 L m^{-2} h^{-1}	283
7	ZIF-8-DMBIM	hydrophobic 5,6-dimethyl-benzimidazole linker	141.7	>99.9%	1411.8-1643.1 L m^{-2} h^{-1} bar^{-1}	284

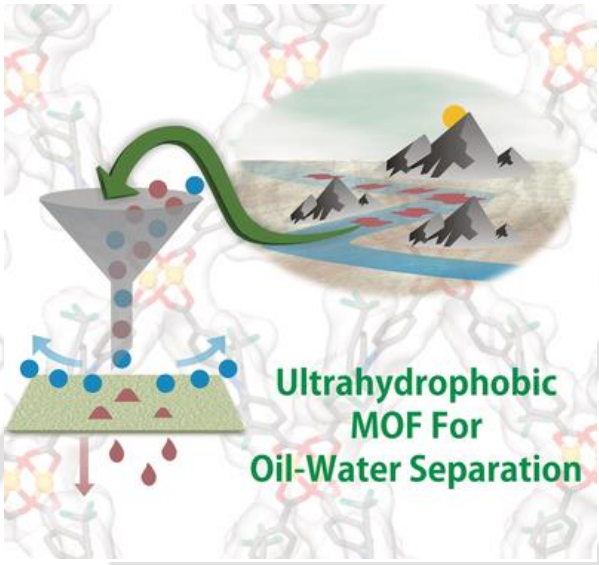

Figure 1.20 Selective separation of oil spills by superhydrophobic MOF. This image is collected with permission from ref. no. 272. Copyright 2016, John Wiley and Sons.

1.11 Conclusions and Outlook

This chapter provides an in-depth explanation of the historical development of highly physicochemically stable porous MOFs and their various implications. This introduction offers a comprehensive overview of the possible synthesis methods for MOFs, the underlying origins of their fluorescence properties and the mechanistic aspects underlying diverse sensing processes. The primary focus of this thesis revolves around the creation and applications of various MOFs based on Zr(IV) ion. Consequently, extensive discussions are presented on the detailed structures of different Zr(IV)-based MOFs. Moreover, the thesis delves into the applications of recently synthesized fluorescent MOFs, particularly in the context of fluorescence-based detection and quantification of bioactive compounds and organo-toxins. Additionally, it explores the synthetic approach for designing hydrophobic MOFs, tailored to selectively and efficiently adsorb oil spills. We firmly believe that the research encapsulated in this thesis is of utmost importance for fostering sustainable, environmentally friendly development and aiding in the precise diagnosis of certain diseases stemming from the uncontrolled secretion of specific neurotransmitters.

Fluorescent MOFs offer several advantages in the detection of drug molecules. But, they also come with certain challenges that need to be overcome for practical use. One primary drawback of MOFs is their stability in various environmental conditions, such as water, acidic, or alkaline mediums. Typically, MOFs based on metal-nitrogen coordination remain stable in alkaline pH

but tend to lose structural integrity in acidic environments, while MOFs based on metal-oxygen coordination are stable in acidic pH but less stable in alkaline pH. Achieving stability in both acidic and alkaline conditions can be addressed by utilizing hard Lewis acids (high-valent metal centers) with hard Lewis bases (polycarboxylates), or vice versa. Moreover, enhancing the hydrophobic properties of the linker can improve MOF stability in water. Robustly structured MOFs can be reused for sensing drug molecules over multiple cycles. Another challenge is the insolubility of MOFs in aqueous media, limiting their practicality for drug detection. This issue can be circumvented by designing MOF-based films or composites, making them suitable for real-world applications.

Furthermore, some fluorescent MOFs lack selectivity, limiting their usefulness for drug detection. To address this, researchers can synthesize pre-functionalized linkers or incorporate suitable functionalities into the MOF framework through post-synthetic modification or solvent-assisted linker installation. Additionally, introducing guest molecules into MOF pores can enhance selectivity for specific drug molecules. In cases of drug sensing, chirality is crucial, and the design of chiral luminescent MOFs becomes essential to detect the exact enantiomer of the clinically significant drug molecule. Numerous research groups, including our own, are actively developing functional luminescent MOFs to create selective, sensitive, reusable, and cost-effective MOF sensors that can address these challenges. Therefore, I believe that the idea developed in this thesis will be helpful to future researchers in the fields of materials science, pharmaceutical chemistry, environmental chemistry, metal-organic frameworks, fluorescence sensing, and related areas.

1.12 References

1. G. A. Lawrance, *John Wiley & Sons*, 2013.
2. E. C. Constable, *Chemistry*, 2019, **1**, 126-163.
3. R. E. Schöllhorn, J. Atwood, J. Davies and D. MacNicol, *Science*, 1984.
4. H. Buser, D. Schwarzenbach, W. Petter and A. Ludi, *Inorg. Chem.*, 1977, **16**, 2704-2710.
5. T. Iwamoto, T. Nakano, M. Morita, T. Miyoshi, T. Miyamoto and Y. Sasaki, *Inorg. Chim. Acta*, 1968, **2**, 313-316.
6. O. M. Yaghi, M. J. Kalmutzki and C. S. Diercks, *John Wiley & Sons*, 2019.
7. A. Werner, *Chemie Bd*, 1893, **21**, 201-229.
8. G. B. Kauffman, *ACS Publications*, 1994.
9. F. Basolo, R. C. Johnson and R. Carl, *Science*, 1986.
10. T. R. Cook, Y.-R. Zheng and P. J. Stang, *Chem. Rev.*, 2013, **113**, 734-777.
11. K. Margeta and A. Farkaš, *BoD-Books on Demand*, 2020, 1-10.
12. B. F. Hoskins and R. Robson, *J. Am. Chem. Soc.*, 1989, **111**, 5962-5964.
13. B. F. Hoskins and R. Robson, *J. Am. Chem. Soc.*, 1990, **112**, 1546-1554.
14. O. M. Yaghi, M. O'Keeffe, N. W. Ockwig, H. K. Chae, M. Eddaoudi and J. Kim, *Nature*, 2003, **423**, 705-714.
15. R. B. S, N. R. Champness, X.-M. Chen, J. G. -Martinez, S. Kitagawa, L. Öhrström, M. O'Keeffe, M. P. Suh and J. Reedijk, *Pure Appl. Chem.*, 2013, **85**, 1715–1724.
16. K. Biradha, A. Ramanan and J. J. Vittal, *Cryst. Growth Des.*, 2009, **9**, 2969-2970.

17. J. L. Rowsell and O. M. Yaghi, *Microporous Mesoporous Mater.*, 2004, **73**, 3-14.
18. P. G. -García, M. Müller and A. Corma, *Chem. Sci.*, 2014, **5**, 2979-3007.
19. A. Kirchon, L. Feng, H. F. Drake, E. A. Joseph and H.-C. Zhou, *Chem. Soc. Rev.*, 2018, **47**, 8611-8638.
20. V. Pascanu, G. G. Miera, A. K. Inge and B. M.-Matute, *J. Am. Chem. Soc.*, 2019, **141**, 7223–7234.
21. B. Li, H.-M. Wen, W. Zhou and B. Chen, *J. Phys. Chem. Lett.*, 2014, **5**, 3468–3479.
22. J. Cao, X. Li and H. Tian, *Curr. Med. Chem.*, 2020, **27**, 5949-5969.
23. J.-R. Li, J. Sculley and H.-C. Zhou, *Chem. Rev.*, 2012, **112**, 869-932.
24. P. Horcajada, C. Serre, M. Vallet-Regí, M. Sebban, F. Taulelle and G. Férey, *Angew. Chem.*, 2006, **118**, 6120-6124.
25. M.-L. Gao, S.-Y. Zhao, Z.-Y. Chen, L. Liu and Z.-B. Han, *Inorg. Chem.*, 2019, **58**, 2261–2264.
26. Q. Qian, P. A. Asinger, M. J. Lee, G. Han, K. Mizrahi Rodriguez, S. Lin, F. M. Benedetti, A. X. Wu, W. S. Chi and Z. P. Smith, *Chem. Rev.*, 2020, **120**, 8161-8266.
27. F. Ghanghermeh, F. Aghili and A. Rahimpour, *ACS Publications*, 2022, 245-282.
28. P. Kumar, A. Deep and K.-H. Kim, *Trends Anal. Chem.*, 2015, **73**, 39-53.
29. T. Wu, X.-j. Gao, F. Ge and H.-g. Zheng, *CrystEngComm*, 2022, **24**, 7881-7901.
30. X.-D. Zhu, K. Zhang, Y. Wang, W.-W. Long, R.-J. Sa, T.-F. Liu and J. Lü, *Inorg. Chem.*, 2018, **57**, 1060-1065.
31. A. Pankajakshan, D. Kuznetsov and S. Mandal, *Inorg. Chem.*, 2019, **58**, 1377-1381.
32. S. Nandi and S. Biswas, *Dalton Trans.*, 2020, **48**, 17612-17620.
33. A. Das, M. Alam, C. Gogoi, R. Dalapati and S. Biswas, *Dalton Trans.*, 2020, **49**, 16928-16934.
34. H.-Y. Li, S.-N. Zhao, S.-Q. Zang and J. Li, *Chem. Soc. Rev.*, 2020, **49**, 6364-6401.
35. S. Ghosh, A. Das and S. Biswas, *Microporous Mesoporous Mater.*, 2021, **323**, 111251.
36. B. M. Connolly, M. A. -Anglada, J. G. -Loe, N. A. Danaf, D. C. Lamb, J. P. Mehta, D. Vulpe, S. Wuttke, J. S. -Albero, P. Z. Moghadam, A. E. H. Wheatley and D. Fairen-Jimenez, *Nat. Commun.*, 2019, **2345-2355**.
37. O. K. Farha, I. Eryazici, N. C. Jeong, B. G. Hauser, C. E. Wilmer, A. A. Sarjeant, R. Q. Snurr, S. T. Nguyen, A. Ö. Yazaydın and J. T. Hupp, *J. Am. Chem. Soc.*, 2012, **134**, 15016–15021.
38. J. Lyu, X. Zhang, K.-I. Otake, X. Wang, P. Li, Z. Li, Z. Chen, Y. Zhang, M. C. Wasson, Y. Yang, P. Bai, X. Guo, T. Islamoglu and O. K. Farha, *Chem. Sci.*, 2019, **10**, 1186-1192.
39. R. Dalapati, S. Nandi and S. Biswas, *Dalton Trans.*, 2020, **49**, 8684-8692.
40. W. Fan, X. Wang, B. Xu, Y. Wang, D. Liu, M. Zhang, Y. Shang, F. Dai, L. Zhang and D. Sun, *J. Mater. Chem. A*, 2018, **6**, 24486-24495.
41. J. Krautwurst, D. Smets, R. Lamann and U. Ruschewitz, *Inorg. Chem.*, 2019, **58**, 8622–8632.
42. G. Férey, C. M. -Draznieks, C. Serre, F. Millange, J. Dutour, S. Surblé and I. Margiolaki, *Science*, 2005, **309**, 2040-2042.
43. H. Chevreau, T. Devic, F. Salles, G. Maurin, N. Stock and C. Serre, *Angew. Chem. Int. Ed.*, 2013, **52**, 5056 –5060.

44. K. Wu, X. Xu, F. Ma and C. Du, *ACS Omega*, 2022, **7**, 35970-35980.
45. B. Wang, Y. Ma, W. Xu and K. Tang, *Langmuir*, 2022, **38**, 8954-8963.
46. H. L. Nguyen, *New J. Chem.*, 2017, **41**, 14030-14043.
47. R. A. -Baah and H. Liu, *Materials*, 2018, **11**, 2250-2271.
48. Y. Sun, Q. Sun, H. Huang, B. Aguila, Z. Niu, J. A. Perman and S. Ma, *J. Mater. Chem. A*, 2017, **5**, 18770-18776.
49. X. Chen, P. Qian, T. Zhang, Z. Xu, C. Fang, X. Xu, W. Chen, P. Wu, Y. Shen, S. Li, J. Wu, B. Zheng, W. Zhang and F. Huo, *Chem. Commun.*, 2018, **54**, 3936-3939.
50. W. Gong, M. Kazem-Rostami, F. A. Son, S. Su, K. M. Fahy, H. Xie, T. Islamoglu, Y. Liu, J. F. Stoddart and Y. Cui, *J. Am. Chem. Soc.*, 2022, **144**, 22574-22581.
51. S. Leubner, R. Siegel, J. Franke, M. T. Wharmby, C. Krebs, H. Reinsch, J. r. Senker and N. Stock, *Inorg. Chem.*, 2020, **59**, 15250-15261.
52. S. Mollick, S. Saurabh, Y. D. More, S. Fajal, M. M. Shirolkar, W. Mandal and S. K. Ghosh, *Energy Environ. Sci.*, 2022, **15**, 3462-3469.
53. M. Zhang, B. Guo, Y. Feng, C. Xie, X. Han, X. Kong, B. Xu and L. Zhang, *Inorg. Chem.*, 2019, **58**, 5384–5387.
54. J. Gu, H. Fan, L. U. Hannover, C. Li and J. Caro, *Angew. Chem. Int.*, 2019, **16**, 58.
55. D. M. DeChellis, C. M. Ngule and D. T. Genna, *J. Mater. Chem. A*, 2020, **8**, 5848-5852.
56. C. Kumunda, A. S. Adekunle, B. B. Mamba, N. W. Hlongwa and T. T. Nkambule, *Front. Mater.*, 2021, **7**, 616787.
57. X. Ma, Y. Chai, P. Li and B. Wang, *Acc. Chem. Res.*, 2019, **52**, 1461-1470.
58. L. Lin, H. Yang and X. Xu, *Front. Environ. Sci.*, 2022, 975.
59. J. N. Halder and M. N. Islam, *J. Hum. Environ. Stud.*, 2015, **2**, 36-46.
60. F. Zadehahmadi, N. T. Eden, H. Mahdavi, K. Konstas, J. I. Mardel, M. Shaibani, P. C. Banerjee and M. R. Hill, *Environ. Sci. Water Res.* , 2023, **9**, 1305-1330.
61. X. Liu, Y. Shan, S. Zhang, Q. Kong and H. Pang, *Green Energy Environ.*, 2022, **8**, 2468-0257.
62. E. Zhang, L. Wu, L. Jiang, K. Guo, Z. Su and P. Ju, *J. Mol. Struct.*, 2022, **1264**, 133314.
63. Y. Zhao, Q. Wang, H. Wang, H. Zhangsun, X. Sun, T. Bu, Y. Liu, W. Wang, Z. Xu and L. Wang, *Sens. Actuators B: Chem.*, 2021, **334**, 129610.
64. X.-J. Zhang, F.-Z. Su, D.-M. Chen, Y. Peng, W.-Y. Guo, C.-S. Liu and M. Du, *Dalton Trans.*, 2019, **48**, 1843-1849.
65. X. Fang, B. Zong and S. Mao, *Nano-Micro Lett.*, 2018, **10**, 1-19.
66. A. Das, S. Ghosh, L. Bourda, S. Mostakim, K. Banerjee, K. Van Hecke and S. Biswas, *CrystEngComm*, 2022, **24**, 4723-4730.
67. Y. Yang, G. Ren, W. Yang, X. Qin, D. Gu, Z. Liang, D.-Y. Guo and P. Qinhe, *Polyhedron*, 2021, **194**, 114923.
68. Z. Wei, Z.-Y. Gu, R. K. Arvapally, Y.-P. Chen, R. N. McDougald Jr, J. F. Ivy, A. A. Yakovenko, D. Feng, M. A. Omary and H.-C. Zhou, *J. Am. Chem. Soc.*, 2014, **136**, 8269-8276.
69. J.-X. Wang, J. Yin, O. Shekhah, O. M. Bakr, M. Eddaoudi and O. F. Mohammed, *ACS Appl. Mater. Interfaces*, 2022, **14**, 9970-9986.
70. H. Liu, T. Fu and Y. Mao, *ACS Omega*, 2022, **7**, 14430-14456.

71. W. Cheng, X. Tang, Y. Zhang, D. Wu and W. Yang, *Trends Food Sci. Technol.*, 2021, **112**, 268-282.
72. L. E. Kreno, K. Leong, O. K. Farha, M. Allendorf, R. P. Van Duyne and J. T. Hupp, *Chem. Rev.*, 2012, **112**, 1105-1125.
73. G. N. Delin, H. Essaid and I. Cozzarelli, Ground Water Contamination By Crude Oil, *Science*, 2012.
74. S. Ismail and A. Dadrasnia, *PLoS One*, 2015, **10**, e0120931.
75. S. E. Chang, J. Stone, K. Demes and M. Piscitelli, *Ecol. Soc.*, 2014, **19**.
76. N. Andrews, N. J. Bennett, P. Le Billon, S. J. Green, A. M. Cisneros-Montemayor, S. Amongin, N. J. Gray and U. R. Sumaila, *Energy Res. Soc. Sci.*, 2021, **75**, 102009.
77. P. N. Wassenaar and E. M. Verbruggen, *Chemosphere*, 2021, **276**, 130113.
78. T. K. Collier, B. F. Anulacion, M. R. Arkoosh, J. P. Dietrich, J. P. Incardona, L. L. Johnson, G. M. Ylitalo and M. S. Myers, *Elsevier*, 2013, 33,195-255.
79. R. M. Atlas and T. C. Hazen, *ACS Publications*, 2011.
80. S. A. Zengel, J. Michel and J. A. Dahlin, *Spill Sci. Technol. Bull.*, 2003, **8**, 373-377.
81. S. Kitagawa, R. Kitaura and S. i. Noro, *Angew. Chem. Int. Ed.*, 2004, **43**, 2334-2375.
82. B. J. Burnett, P. M. Barron and W. Choe, *CrystEngComm*, 2012, **14**, 3839-3846.
83. X. Li, J. Liu, K. Zhou, S. Ullah, H. Wang, J. Zou, T. Thonhauser and J. Li, *J. Am. Chem. Soc.*, 2022, **144**, 21702-21709.
84. P. Rocío-Bautista, I. Taima-Mancera, J. Pasán and V. Pino, *Separations*, 2019, **6**, 33.
85. D. Wang, Y. Zhang, J. Gao, G. Ge and C. Li, *Cryst. Growth Des.*, 2019, **19**, 4571-4578.
86. D. J. Collins and H.-C. Zhou, *J. Mater. Chem.*, 2007, **17**, 3154-3160.
87. B. Chen, C. Liang, J. Yang, D. S. Contreras, Y. L. Clancy, E. B. Lobkovsky, O. M. Yaghi and S. Dai, *Angew. Chem. Int. Ed.*, 2006, **45**, 1390-1393.
88. M. Eddaoudi, D. B. Moler, H. Li, B. Chen, T. M. Reineke, M. O'keeffe and O. M. Yaghi, *Acc. Chem. Res.*, 2001, **34**, 319-330.
89. G. Férey, *Chem. Soc. Rev.*, 2008, **37**, 191-214.
90. P. V. Dau, K. K. Tanabe and S. M. Cohen, *Chem. Commun.*, 2012, **48**, 9370-9372.
91. C. S. Collins, D. Sun, W. Liu, J.-L. Zuo and H.-C. Zhou, *J. Mol. Struct.*, 2008, **890**, 163-169.
92. J. Zhang, Y. Cui and G. Qian, *Curr. Org. Chem.*, 2018, **22**, 1792-1808.
93. C. P. Raptopoulou, *Materials*, 2021, **14**, 310.
94. S. R. Halper, L. Do, J. R. Stork and S. M. Cohen, *J. Am. Chem. Soc.*, 2006, **128**, 15255-15268.
95. K. N. Lazarou, V. Psycharis, A. Terzis and C. P. Raptopoulou, *Polyhedron*, 2011, **30**, 963-970.
96. H. Li, M. Eddaoudi, M. O'Keeffe and O. M. Yaghi, *Nature*, 1999, **402**, 276-279.
97. O. Yaghi and H. Li, *J. Am. Chem. Soc.*, 1995, **117**, 10401-10402.
98. N. Stock and S. Biswas, *Chem. Rev.*, 2012, **112**, 933-969.
99. R. M. Barrer, *J. Chem. Soc.*, 1948, 127-132.
100. E. Biemmi, S. Christian, N. Stock and T. Bein, *Microporous Mesoporous Mater.*, 2009, **117**, 111-117.
101. P. Li, F.-F. Cheng, W.-W. Xiong and Q. Zhang, *Inorg. Chem. Front.*, 2018, **5**, 2693-2708.

102. X.-X. Zhao, J.-P. Ma, Y.-B. Dong, R.-Q. Huang and T. Lai, *Cryst. Growth Des.*, 2007, **7**, 1058-1068.
103. Y. Zhao, Z. Song, X. Li, Q. Sun, N. Cheng, S. Lawes and X. Sun, *Energy Storage Mater.*, 2016, **2**, 35-62.
104. M. Lammert, M. T. Wharmby, S. Smolders, B. Bueken, A. Lieb, K. A. Lomachenko, D. De Vos and N. Stock, *Chem. Commun.*, 2015, **51**, 12578-12581.
105. V. Bon, I. Senkovska, M. S. Weiss and S. Kaskel, *CrystEngComm*, 2013, **15**, 9572-9577.
106. X.-L. Lv, M. Tong, H. Huang, B. Wang, L. Gan, Q. Yang, C. Zhong and J.-R. Li, *J. Solid State Chem.*, 2015, **223**, 104-108.
107. Y. Hu, C. Liu, Y. Zhang, N. Ren and Y. Tang, *Microporous Mesoporous Mater.*, 2009, **119**, 306-314.
108. J. Klinowski, F. A. A. Paz, P. Silva and J. Rocha, *Dalton Trans.*, 2011, **40**, 321-330.
109. Z. Ni and R. I. Masel, *J. Am. Chem. Soc.* , 2006, **128**, 12394-12395.
110. U. Mueller, M. Schubert, F. Teich, H. Puetter, K. Schierle-Arndt and J. Pastre, *J. Mater. Chem.*, 2006, **16**, 626-636.
111. Y.-R. Lee, J. Kim and W.-S. Ahn, *Korean J. Chem. Eng.*, 2013, **30**, 1667-1680.
112. A. Martinez Joaristi, J. Juan-Alcañiz, P. Serra-Crespo, F. Kapteijn and J. Gascon, *Cryst. Growth Des.*, 2012, **12**, 3489-3498.
113. W.-J. Li, J. Lü, S.-Y. Gao, Q.-H. Li and R. Cao, *J. Mater. Chem. A* 2014, **2**, 19473-19478.
114. T. Friščić, I. Halasz, P. J. Beldon, A. M. Belenguer, F. Adams, S. A. Kimber, V. Honkimäki and R. E. Dinnebier, *Nat. Chem.*, 2013, **5**, 66-73.
115. A. L. Garay, A. Pichon and S. L. James, *Chem. Soc. Rev.*, 2007, **36**, 846-855.
116. A. Pichon and S. L. James, *CrystEngComm*, 2008, **10**, 1839-1847.
117. P. A. Julien, K. Užarević, A. D. Katsenis, S. A. Kimber, T. Wang, O. K. Farha, Y. Zhang, J. Casaban, L. S. Germann and M. Etter, *J. Am. Chem. Soc.*, 2016, **138**, 2929-2932.
118. R. Li, X. Ren, H. Ma, X. Feng, Z. Lin, X. Li, C. Hu and B. Wang, *J. Mater. Chem. A*, 2014, **2**, 5724-5729.
119. A. Aslani and A. Morsali, *Inorg. Chim. Acta*, 2009, **362**, 5012-5016.
120. J. Kim, S.-T. Yang, S. B. Choi, J. Sim, J. Kim and W.-S. Ahn, *J. Mater. Chem.*, 2011, **21**, 3070-3076.
121. W.-J. Son, J. Kim, J. Kim and W.-S. Ahn, *Chem. Commun.*, 2008, 6336-6338.
122. R. Ye, M. Ni, Y. Xu, H. Chen and S. Li, *RSC Adv.*, 2018, **8**, 26237-26242.
123. W. Zheng, X. Hao, L. Zhao and W. Sun, *Int. Eng. Chem. Res.*, 2017, **56**, 5899-5905.
124. Z. Wang and S. M. Cohen, *J. Am. Chem. Soc.*, 2007, **129**, 12368-12369.
125. M. Kalaj and S. M. Cohen, *ACS Cent. Sci.*, 2020, **6**, 1046-1057.
126. S. M. Cohen, *Chem. Rev.*, 2012, **112**, 970-1000.
127. Z. Wang and S. M. Cohen, *Chem. Soc. Rev.*, 2009, **38**, 1315-1329.
128. G. Tuci, A. Rossin, X. Xu, M. Ranocchiari, J. A. van Bokhoven, L. Luconi, I. Manet, M. Melucci and G. Giambastiani, *Chem. Mater.*, 2013, **25**, 2297-2308.
129. M. Kalaj, K. C. Bentz, S. Ayala Jr, J. M. Palomba, K. S. Barcus, Y. Katayama and S. M. Cohen, *Chem. Rev.*, 2020, **120**, 8267-8302.

130. E. D. Bloch, D. Britt, C. Lee, C. J. Doonan, F. J. Uribe-Romo, H. Furukawa, J. R. Long and O. M. Yaghi, *J. Am. Chem. Soc.*, 2010, **132**, 14382-14384.
131. P. Deria, J. E. Mondloch, E. Tylianakis, P. Ghosh, W. Bury, R. Q. Snurr, J. T. Hupp and O. K. Farha, *J. Am. Chem. Soc.*, 2013, **135**, 16801-16804.
132. S. Wang, C. M. McGuirk, M. B. Ross, S. Wang, P. Chen, H. Xing, Y. Liu and C. A. Mirkin, *J. Am. Chem. Soc.*, 2017, **139**, 9827-9830.
133. S. Mandal, S. Natarajan, P. Mani and A. Pankajakshan, *Adv. Funct. Mater.*, 2021, **31**, 2006291.
134. R. Seetharaj, P. Vandana, P. Arya and S. Mathew, *Arab. J. Chem.*, 2019, **12**, 295-315.
135. N. Stock and S. Biswas, *Chem. Rev.*, 2012, **112**, 933–969.
136. L. Li, S. Wang, T. Chen, Z. Sun, J. Luo and M. Hong, *Cryst. Growth Des.*, 2012, **12**, 4109-4115.
137. P. Pachfule, R. Das, P. Poddar and R. Banerjee, *Cryst. Growth Des.*, 2011, **11**, 1215-1222.
138. D. Banerjee, J. Finkelstein, A. Smirnov, P. M. Forster, L. A. Borkowski, S. J. Teat and J. B. Parise, *Cryst. Growth Des.*, 2011, **11**, 2572-2579.
139. M.-L. Cheng, E. Zhu, Q. Liu, S.-C. Chen, Q. Chen and M.-Y. He, *Inorg. Chem. Commun.*, 2011, **14**, 300-303.
140. X. J. Luan, X. H. Cai, Y. Y. Wang, D. S. Li, C. J. Wang, P. Liu, H. M. Hu, Q. Z. Shi and S. M. Peng, *Chem. Eur. J.*, 2006, **12**, 6281-6289.
141. L. Carlucci, G. Ciani, S. Maggini and D. M. Proserpio, *Crystal Growth and Design*, 2008, **8**, 162-165.
142. C. Livage, C. Egger and G. Ferey, *Chem. Mater.*, 2001, **13**, 410-414.
143. K.-L. Zhang, C.-T. Hou, J.-J. Song, Y. Deng, L. Li, S. W. Ng and G.-W. Diao, *CrystEngComm*, 2012, **14**, 590-600.
144. L. Luo, G.-C. Lv, P. Wang, Q. Liu, K. Chen and W.-Y. Sun, *CrystEngComm*, 2013, **15**, 9537-9543.
145. J. Gu, Z. Gao and Y. Tang, *Cryst. Growth Des.*, 2012, **12**, 3312-3323.
146. F. Yuan, J. Xie, H.-M. Hu, C.-M. Yuan, B. Xu, M.-L. Yang, F.-X. Dong and G.-L. Xue, *CrystEngComm*, 2013, **15**, 1460-1467.
147. J. Winarta, B. Shan, S. M. Mcintyre, L. Ye, C. Wang, J. Liu and B. Mu, *Cryst. Growth Des.*, 2019, **20**, 1347-1362.
148. Z. Hu, I. Castano, S. Wang, Y. Wang, Y. Peng, Y. Qian, C. Chi, X. Wang and D. Zhao, *Cryst. Growth Des.*, 2016, **16**, 2295-2301.
149. T. Tsuruoka, S. Furukawa, Y. Takashima, K. Yoshida, S. Isoda and S. Kitagawa, *Angew. Chem. Int. Ed.*, 2009, **121**, 4833-4837.
150. S. Diring, S. Furukawa, Y. Takashima, T. Tsuruoka and S. Kitagawa, *Chem. Mater.*, 2010, **22**, 4531-4538.
151. F. Vermoortele, B. Bueken, G. Le Bars, B. Van de Voorde, M. Vandichel, K. Houthoofd, A. Vimont, M. Daturi, M. Waroquier and V. Van Speybroeck, *J. Am. Chem. Soc.*, 2013, **135**, 11465-11468.
152. N. Zhao, K. Cai and H. He, *Dalton Trans.*, 2020, **49**, 11467-11479.
153. M. Ding, X. Cai and H.-L. Jiang, *Chem. Sci.*, 2019, **10**, 10209-10230.

154. S. Yuan, L. Feng, K. Wang, J. Pang, M. Bosch, C. Lollar, Y. Sun, J. Qin, X. Yang and P. Zhang, *Adv. Mater.*, 2018, **30**, 1704303.
155. N. C. Burtch, H. Jasuja and K. S. Walton, *Chem. Rev.*, 2014, **114**, 10575-10612.
156. J. H. Cavka, S. Jakobsen, U. Olsbye, N. Guillou, C. Lamberti, S. Bordiga and K. P. Lillerud, *J. Am. Chem. Soc.*, 2008, **130**, 13850-13851.
157. Q. Yao, A. Bermejo Gómez, J. Su, V. Pascanu, Y. Yun, H. Zheng, H. Chen, L. Liu, H. N. Abdelhamid and B. n. Martín-Matute, *Chem. Mater.*, 2015, **27**, 5332-5339.
158. T.-F. Liu, D. Feng, Y.-P. Chen, L. Zou, M. Bosch, S. Yuan, Z. Wei, S. Fordham, K. Wang and H.-C. Zhou, *J. Am. Chem. Soc.*, 2015, **137**, 413-419.
159. G. Férey, C. Mellot-Draznieks, C. Serre, F. Millange, J. Dutour, S. Surblé and I. Margiolaki, *Science*, 2005, **309**, 2040-2042.
160. X. C. Huang, Y. Y. Lin, J. P. Zhang and X. M. Chen, *Angew. Chem. Int. Ed.*, 2006, **45**, 1557-1559.
161. H. Li, W. Shi, K. Zhao, H. Li, Y. Bing and P. Cheng, *Inorg. Chem.*, 2012, **51**, 9200-9207.
162. X.-W. Zhu, X.-P. Zhou and D. Li, *Chem. Commun.*, 2016, **52**, 6513-6516.
163. N. M. Padial, E. Quartapelle Procopio, C. Montoro, E. López, J. E. Oltra, V. Colombo, A. Maspero, N. Masciocchi, S. Galli and I. Senkovska, *Angew. Chem. Int. Ed.*, 2013, **125**, 8448-8452.
164. K. Wang, X.-L. Lv, D. Feng, J. Li, S. Chen, J. Sun, L. Song, Y. Xie, J.-R. Li and H.-C. Zhou, *J. Am. Chem. Soc.*, 2016, **138**, 914-919.
165. D. Ma, Y. Li and Z. Li, *Chem. Commun.*, 2011, **47**, 7377-7379.
166. K. Wang, H. Huang, X. Zhou, Q. Wang, G. Li, H. Shen, Y. She and C. Zhong, *Inorg. Chem.*, 2019, **58**, 5725-5732.
167. Z.-R. Jiang, J. Ge, Y.-X. Zhou, Z. U. Wang, D. Chen, S.-H. Yu and H.-L. Jiang, *NPG Asia Mater.*, 2016, **8**, e253-e253.
168. L. Xu, Y. Xiao, A. Van Sandwijk, Q. Xu and Y. Yang, *J. Nucl. Mater.*, 2015, **466**, 21-28.
169. J. Winarta, B. Shan, S. M. Mcintyre, L. Ye, C. Wang, J. Liu and B. Mu, *Cryst. Growth Des.*, 2020, **20**, 1347−1362.
170. X. -LiangL, M. Tong, H. Huang, B. Wang, L. Gan, Q. Yang, C. Zhong and J.-R. Li, *J. Solid State Chem*, 2015, **223**, 104-108.
171. M. Taddei, *Coord. Chem. Rev.*, 2017, **343**, 1-24.
172. X. Wang, K. Ma, T. Goh, M. R. Mian, H. Xie, H. Mao, J. Duan, K. O. Kirlikovali, A. E. Stone and D. Ray, *J. Am. Chem. Soc.*, 2022, **144**, 12192-12201.
173. Y. Bai, Y. Dou, L.-H. Xie, W. Rutledge, J.-R. Li and H.-C. Zhou, *Chem. Soc. Rev.*, 2016, **45**, 2327-2367.
174. F. Xiao, X. Hu, Y. Chen and Y. Zhang, *ACS Appl. Mater. Interfaces*, 2019, **11**, 47390-47403.
175. S. Ghosh, F. Steinke, A. Rana and S. Biswas, *Inorg. Chem. Front.*, 2022, **9**, 859-869.
176. V. Guillerm, F. Ragon, M. Dan-Hardi, T. Devic, M. Vishnuvarthan, B. Campo, A. Vimont, G. Clet, Q. Yang and G. Maurin, *Angew. Chem. Int. Ed.*, 2012, **51**, 9267-9271.
177. L. Cooper, N. Guillou, C. Martineau, E. Elkaim, F. Taulelle, C. Serre and T. Devic, *Eur. J. Inorg. Chem.*, 2014, **2014**, 6281-6289.

178. P. Ji, K. Manna, Z. Lin, X. Feng, A. Urban, Y. Song and W. Lin, *J. Am. Chem. Soc.*, 2017, **139**, 7004-7011.
179. J. E. Mondloch, W. Bury, D. Fairen-Jimenez, S. Kwon, E. J. DeMarco, M. H. Weston, A. A. Sarjeant, S. T. Nguyen, P. C. Stair and R. Q. Snurr, *J. Am. Chem. Soc.*, 2013, **135**, 10294-10297.
180. O. V. Gutov, W. Bury, D. A. Gomez-Gualdron, V. Krungleviciute, D. Fairen-Jimenez, J. E. Mondloch, A. A. Sarjeant, S. S. Al-Juaid, R. Q. Snurr and J. T. Hupp, *Chem. Eur. J.*, 2014, **20**, 12389-12393.
181. H. Furukawa, F. Gandara, Y.-B. Zhang, J. Jiang, W. L. Queen, M. R. Hudson and O. M. Yaghi, *J. Am. Chem. Soc.*, 2014, **136**, 4369-4381.
182. W. Morris, B. Volosskiy, S. Demir, F. Gándara, P. L. McGrier, H. Furukawa, D. Cascio, J. F. Stoddart and O. M. Yaghi, *Inorg. Chem.*, 2012, **51**, 6443-6445.
183. V. Bon, V. Senkovskyy, I. Senkovska and S. Kaskel, *Chem. Commun.*, 2012, **48**, 8407-8409.
184. V. Bon, *Cryst. Growth Des*, 2013, **13**, 1231-1237.
185. D. Feng, H.-L. Jiang, Y.-P. Chen, Z.-Y. Gu, Z. Wei and H.-C. Zhou, *Inorg. Chem.*, 2013, **52**, 12661-12667.
186. D. Feng, Z. Y. Gu, J. R. Li, H. L. Jiang, Z. Wei and H. C. Zhou, *Angew. Chem. Int. Ed*, 2012, **124**, 10453-10456.
187. D. Feng, Z.-Y. Gu, Y.-P. Chen, J. Park, Z. Wei, Y. Sun, M. Bosch, S. Yuan and H.-C. Zhou, *J. Am. Chem. Soc.*, 2014, **136**, 17714-17717.
188. H.-L. Jiang, D. Feng, K. Wang, Z.-Y. Gu, Z. Wei, Y.-P. Chen and H.-C. Zhou, *J. Am. Chem. Soc.*, 2013, **135**, 13934-13938.
189. V. Guillerm, F. Ragon, M. Dan-Hardi, T. Devic, M. Vishnuvarthan, B. Campo, A. Vimont, G. Clet, Q. Yang and G. Maurin, *Angew. Chem., Int. Ed.*, 2012, **51**, 9267-9271.
190. S. B. Kalidindi, S. Nayak, M. E. Briggs, S. Jansat, A. P. Katsoulidis, G. J. Miller, J. E. Warren, D. Antypov, F. Corà and B. Slater, *Angew. Chem. Int. Ed.*, 2015, **54**, 221-226.
191. T. Schweizer, H. Kubach and T. Koch, *Int. J. Automot. Technol.*, 2021, **6**, 275-287.
192. J. Li, Y. He, L. Wang, G. Li, Y. Zou, Y. Yan, D. Li, X. Shi, Z. Song and X. Shi, *RSC Adv.*, 2020, **10**, 41921-41925.
193. M. Wu, Y. Zhuang, J. Liu, W. Chen, X. Li and R.-J. Xie, *Opt. Mater.*, 2020, **106**, 110006.
194. T. Sun, Y. Gao, Y. Du, L. Zhou and X. Chen, *Front. Chem.*, 2021, **8**, 624592.
195. S. Petoud, S. M. Cohen, J.-C. G. Bünzli and K. N. Raymond, *J. Am. Chem. Soc.*, 2003, **125**, 13324-13325.
196. X. Li, J. Yu, D. J. Gosztola, H. C. Fry and P. Deria, *J. Am. Chem. Soc.*, 2019, **141**, 16849-16857.
197. M.-X. Li, H. Wang, S.-W. Liang, M. Shao, X. He, Z.-X. Wang and S.-R. Zhu, *Cryst. Growth Des.*, 2009, **9**, 4626-4633.
198. Y. Zhou, D. Zhang, W. Xing, J. Cuan, Y. Hu, Y. Cao and N. Gan, *Anal. Chem.*, 2019, **91**, 4845-4851.
199. H. Li, Y. Han, Z. Shao, N. Li, C. Huang and H. Hou, *Dalton Trans.*, 2017, **46**, 12201-12208.

200. Z. Zhang, Z. Wei, F. Meng, J. Su, D. Chen, Z. Guo and H. Xing, *Chem. Eur. J.*, 2020, **26**, 1661-1667.
201. M. Lei, F. Ge, S. Ren, X. Gao and H. Zheng, *Sep. Purif. Technol.*, 2022, **286**, 120433.
202. M. Asad, M. I. Anwar, A. Abbas, A. Younas, S. Hussain, R. Gao, L.-K. Li, M. Shahid and S. Khan, *Coord. Chem. Rev.*, 2022, **463**, 214539.
203. Y. Yang, G.-B. Hu, W.-B. Liang, L.-Y. Yao, W. Huang, Y.-J. Zhang, J.-L. Zhang, J.-M. Wang, R. Yuan and D.-R. Xiao, *Nanoscale*, 2020, **12**, 5932-5941.
204. S. K. Panda, S. Mishra and A. K. Singh, *Dalton Trans.*, 2021, **50**, 7139-7155.
205. S.-L. Yao, S.-J. Liu, X.-M. Tian, T.-F. Zheng, C. Cao, C.-Y. Niu, Y.-Q. Chen, J.-L. Chen, H. Huang and H.-R. Wen, *Inorg. Chem.*, 2019, **58**, 3578-3581.
206. R. B. Sekar and A. Periasamy, *J. Cell Biol.*, 2003, **160**, 629.
207. D. Escudero, *Acc. Chem. Res.*, 2016, **49**, 1816-1824.
208. V. Ramamurthy, CRC Press, 1998.
209. X. Zhang, Y. Wu, S. Ji, H. Guo, P. Song, K. Han, W. Wu, W. Wu, T. D. James and J. Zhao, *J. Org. Chem.*, 2010, **75**, 2578-2588.
210. S. C. Chen, C. Y. Lin, T. L. Cheng and W. L. Tseng, *Adv. Funct. Mater.*, 2017, **27**, 1702452.
211. S. Ghosh, J. Krishnan, S. S. Hossain, A. Dhakshinamoorthy and S. Biswas, *ACS Appl. Mater. Interfaces*, 2023.
212. N. Nandi, K. Choudhury, P. Sarkar, N. Barnwal and K. Sahu, *ACS Appl. Nano Mater.*, 2022, **5**, 17315-17324.
213. L. Han, S. G. Liu, J. Y. Liang, Y. J. Ju, N. B. Li and H. Q. Luo, *J. Hazard. Mater.*, 2019, **362**, 45-52.
214. Y. Peng, H. Huang, Y. Zhang, C. Kang, S. Chen, L. Song, D. Liu and C. Zhong, *Nat. Commun*, 2018, **9**, 187.
215. N. D. Rudd, H. Wang, E. M. Fuentes-Fernandez, S. J. Teat, F. Chen, G. Hall, Y. J. Chabal and J. Li, *ACS Appl. Mater. Interfaces*, 2016, **8**, 30294-30303.
216. A. Rana and S. Biswas, *Inorg. Chem. Front.*, 2023, **10**, 2742-2753.
217. S. Halder, J. Mondal, J. O. -Castro, A. Frontera and P. Roy, *Dalton Trans.*, 2017, **46**, 1943-1950.
218. E. Moradi, R. Rahimi and V. Safarifard, *J. Solid State Chem.*, 2020, **286**, 121277-121286.
219. P.-P. Hu, N. Liu, K.-Y. Wu, L.-Y. Zhai, B.-P. Xie, B. Sun, W.-J. Duan, W.-H. Zhang and J.-X. Chen, *Inorg. Chem.*, 2018, **57**, 8382–8389.
220. P. Samant, A. V. Desai, S. Sharma, P. Chandra and S. K. Ghosh, *Inorg. Chem.*, 2018, **57**, 2360−2364.
221. T. Xia, T. Song, G. Zhang, Y. Cui, Y. Yang, Z. Wang and G. Qian, *Chem. Eur. J.*, 2016, **22**, 18429-18434.
222. X.-Y. Xu and B. Yan, *J. Mater. Chem. C*, 2016, **4**, 1543-1549.
223. N.-H. Huang, R.-T. Li, C. Fan, K.-Y. Wu, Z. Zhang and J.-X. Chen, *J. Inorg. Biochem.*, 2019, **197**, 110690-110697.
224. A. Radwan, I. M. E. -Sewify, A. Shahat, H. M. E. Azzazy, M. M. H. Khalil and M. F. E. -Shahat, *ACS Sustain. Chem. Eng.*, 2020, **8**, 15097–15107.

225. N.-H. Huang, Y. Liu, R.-T. Li, J. Chen, P.-P. Hu, D. J. Young, J.-X. Chen and W.-H. Zhang, *Analyst*, 2020, **145**, 2779-2788.
226. P. Wu, Y. Liu, Y. Liu, J. Wang, Y. Li, W. Liu and J. Wang, *Inorg. Chem.*, 2015, **54**, 11046−11048.
227. X. Wu, L. K. Macreadie and P. A. Gale, *Coord. Chem. Rev.*, 2021, **432**, 213708.
228. K. A. Walters, W. Bialik and K. R. BRAIN, *Int. J. Cosmet. Sci.*, 1993, **15**, 260-271.
229. G. O. Reznik, P. Vishwanath, M. A. Pynn, J. M. Sitnik, J. J. Todd, J. Wu, Y. Jiang, B. G. Keenan, A. B. Castle and R. F. Haskell, *Appl. Microbiol. Biotechnol.*, 2010, **86**, 1387-1397.
230. S. Ghosh, J. Krishnan, V. Karthik, A. Dhakshinamoorthy and S. Biswas, *Inorg. Chem.*, 2023.
231. Y. Lou, L. Liu, H. Yao, X. Hu, J. Su, K. Xu, R. Luo, X. Yang, L. He and X. Lu, *Eur. J. Pharm. Sci.* , 2021, **157**, 105631.
232. S. Saadat, D. Rawtani and C. M. Hussain, *Sci. Total Environ.*, 2020, **728**, 138870.
233. H.-B. Zhu, Y. Shen, Z.-Z. Fu, Y.-Y. Yu, Y.-F. Jiang and Y. Zhao, *Inorg. Chem. Commun.*, 2019, **103**, 21-24.
234. B.-X. Dong, Y.-M. Pan, W.-L. Liu and Y.-L. Teng, *Cryst. Growth Des.*, 2018, **18**, 431-440.
235. H. He, Y.-Q. Xue, S.-Q. Wang, Q.-Q. Zhu, J. Chen, C.-P. Li and M. Du, *Inorg. Chem.*, 2018, **57**, 15062-15068.
236. M. Yu, X. Yao, X. Wang, Y. Li and G. Li, *Polymers*, 2019, **11**, 99.
237. L. Wang, W. Xu, W. Y. Li, M. Xie and Y. Q. Zheng, *Chem. Asian J.*, 2019, **14**, 4246-4254.
238. J. Xiong, L. Yang, L. X. Gao, P. P. Zhu, Q. Chen and K. J. Tan, *Anal. Bioanal. Chem.*, 2019, **411**, 5963-5973.
239. X. Wang, K. Batra, G. Clavier, G. Maurin, B. Ding, A. Tissot and C. Serre, *Chem. Eur. J.*, 2023, **29**, e202203136.
240. Q. Zhang, M. Lei, F. Kong and Y. Yang, *Chem. Commun.*, 2018, **54**, 10901-10904.
241. B. Chu, C. Lan, J.-H. Yin, M. Liu, L. Meng and N. Xu, *Spectrochim. Acta A Mol. Biomol.*, 2022, **283**, 121752.
242. Y. Li, M. Sun, Y. Yang, H. Meng, Q. Wang, C. Li and G. Li, *J. Mater. Chem. C*, 2021, **9**, 8683-8693.
243. B. R. A.-Hashimi, K. M. Omer, H. S. Rahman and H. H. Othman, *Spectrochimica Acta Part A: Molecular and Biomol. Spectra.*, 2021, **244**, 118835-118834.
244. Q. Chu, B. Zhang, H. Zhou, B. Liu, L. Hou and Y.-Y. Wang, *Inorg. Chem.*, 2020, **59**, 2853–2860.
245. B.-X. Dong, Y.-M. Pan, W.-L. Liu and Y.-L. Teng, *Cryst. Growth Des.*, 2018, **18**, 431−440.
246. Y.-S. Lu, W.-Y. Pan, T.-C. Hung and Y.-T. Hsieh, *Langmuir*, 2020, **36**, 11358−11365.
247. J. Zhang, L. Gao, Y. Wang, L. Zhai, X. Niu and T. Hu, *CrystEngComm*, 2019, **21**, 7286–7292.
248. M. Roushani and Z. Rahmati, *J. Iran. Chem. Soc.*, 2019, **16**, 999–1006.
249. Z. Liu and Y. Liu, *ACS Publications*, 2021, 1-31.
250. Y. Du, X. Li, X. Lv and Q. Jia, *ACS Appl. Mater. Interfaces*, 2017, **9**, 30925-30932.

251. Q. Du, P. Wu, P. Dramou, R. Chen and H. He, *New J. Chem.*, 2019, **43**, 1291-1298.
252. W. Morris, W. E. Briley, E. Auyeung, M. D. Cabezas and C. A. Mirkin, *J. Am. Chem. Soc.*, 2014, **136**, 7261-7264.
253. X. Zhu, H. Zheng, X. Wei, Z. Lin, L. Guo, B. Qiu and G. Chen, *Chem. Commun.*, 2013, **49**, 1276-1278.
254. R. Mejia-Ariza, J. Rosselli, C. Breukers, A. Manicardi, L. W. Terstappen, R. Corradini and J. Huskens, *Chem. Eur. J.*, 2017, **23**, 4180-4186.
255. B.-P. Xie, G.-H. Qiu, P.-P. Hu, Z. Liang, Y.-M. Liang, B. Sun, L.-P. Bai, Z.-H. Jiang and J.-X. Chen, *Sens. Actuators B: Chem.*, 2018, **254**, 1133-1140.
256. Y. Cui, F. Chen and X.-B. Yin, *Biosens. Bioelectron.*, 2019, **135**, 208-215.
257. P. Chandrasekhar, A. Mukhopadhyay, G. Savitha and J. N. Moorthy, *Chem. Sci.*, 2016, **7**, 3085-3091.
258. S. Nandi and S. Biswas, *Dalton Trans.*, 2019, **48**, 9266-9275.
259. F. Moghzi, J. Soleimannejad, E. C. Sañudo and J. Janczak, *ACS Appl. Mater. Interfaces*, 2020, **12**, 44499-44507.
260. S. Ghosh, N. Nagarjun, S. Nandi, A. Dhakshinamoorthy and S. Biswas, *J. Mater. Chem. C*, 2022, **10**, 6717-6727.
261. Y. Zhang and B. Yan, *J. Mater. Chem. C*, 2022, **10**, 9326-9333.
262. L. Song, F. Tian and Z. Liu, *J. Solid State Chem.*, 2022, **312**, 123231.
263. J. Tian, Q. Liu, J. Shi, J. Hu, A. M. Asiri, X. Sun and Y. He, *Biosens. Bioelectron.*, 2015, **71**, 1-6.
264. J. Li, J. Xia, F. Zhang, Z. Wang and Q. Liu, *J. Chin. Chem. Soc.*, 2018, **65**, 743-749.
265. Y. Pan, S. Zhan and F. Xia, *Anal. Biochem.*, 2018, **546**, 5-9.
266. W. Li, S. Lv, Y. Wang, L. Zhang and X. Cui, *Sens. Actuators B Chem.*, 2019, **281**, 652-658.
267. N. Chauhan, S. Tiwari, T. Narayan and U. Jain, *Appl. Surf. Sci.*, 2019, **474**, 154-160.
268. A. Rana, S. Ghosh and S. Biswas, *Inorg. Chem. Front.*, 2023.
269. S. Ghosh, A. Rana, S. Kumar, C. Gogoi, S. Mukherjee, U. Manna and S. Biswas, *Mater. Chem. Front.*, 2022, **6**, 2051-2060.
270. H. Saini, E. Otyepková, A. Schneemann, R. Zbořil, M. Otyepka, R. A. Fischer and K. Jayaramulu, *J. Mater. Chem. A*, 2022, **10**, 2751-2785.
271. S. Roy, V. M. Suresh and T. K. Maji, *Chem. Sci.*, 2016, **7**, 2251-2256.
272. S. Mukherjee, A. M. Kansara, D. Saha, R. Gonnade, D. Mullangi, B. Manna, A. V. Desai, S. H. Thorat, P. S. Singh and A. Mukherjee, *Chem. Eur. J.*, 2016, **22**, 10937-10943.
273. J. Du, L. Chen, X. Zeng, S. Yu, W. Zhou, L. Tan, L. Dong, C. Zhou and J. Cheng, *ACS Appl. Mater. Interfaces*, 2020, **12**, 28576-28585.
274. N. X. Zhu, Z. W. Wei, C. X. Chen, D. Wang, C. C. Cao, Q. F. Qiu, J. J. Jiang, H. P. Wang and C. Y. Su, *Angew. Chem. Int. Ed.*, 2019, **131**, 17189-17196.
275. K. Jayaramulu, K. K. R. Datta, C. Rösler, M. Petr, M. Otyepka, R. Zboril and R. A. Fischer, *Angew. Chem., Int. Ed.*, 2016, **55**, 1178-1182.
276. K. Jayaramulu, F. Geyer, M. Petr, R. Zboril, D. Vollmer and R. A. Fischer, *Adv. Mater.*, 2017, **29**, 1605307.

277. J. Gu, H. Fan, C. Li, J. Caro and H. Meng, *Angew. Chem. Int. Ed.*, 2019, **131**, 5351-5355.
278. Y. Pan, T. Zhu, Q. Xia, X. Yu and Y. Wang, *J. Environ. Chem. Eng.*, 2021, **9**, 104977.
279. S. Wang, Z. Kang, B. Xu, L. Fan, G. Li, L. Wen, X. Xin, Z. Xiao, J. Pang and X. Du, *Inorg. Chem. Commun.*, 2017, **82**, 64-67.
280. H. Li, P. Mu, J. Li and Q. Wang, *J. Mater. Chem. A*, 2021, **9**, 4167-4175.
281. S. He, Y. Zhan, J. Hu, G. Zhang, S. Zhao, Q. Feng and W. Yang, *Composites Part B: Eng.*, 2020, **197**, 108188.
282. Y. Cai, D. Chen, N. Li, Q. Xu, H. Li, J. He and J. Lu, *J. Membr. Sci.*, 2017, **543**, 10-17.
283. R. Qu, W. Zhang, N. Liu, Q. Zhang, Y. Liu, X. Li, Y. Wei and L. Feng, *ACS Sustain. Chem. Eng.*, 2018, **6**, 8019-8028.
284. H. You, G. Y. Shangkum, P. Chammingkwan and T. Taniike, *Colloids Surf. A*, 2021, **614**, 126204.

Chapter 2

A Functionalized MOF for Selective Fluorometric Detection of Sodium Dodecyl Sulphate and Vitamin B_{12} Using MOF@Cotton Composite

This chapter contains the synthesis and characterization of 2,5-diaminoterephthalic acid (H_2BDC-$(NH)_2$) linker containing porous (S_{BET} = 504 $m^2\ g^{-1}$) zirconium(IV)-based metal-organic framework (MOF) which serves as a fluorophore for sodium dodecyl sulphate (SDS) surfactant and vitamin B_{12}. This is the first ever reported MOF-based dual optical sensor of SDS and vitamin B_{12}. Along with the lowest ever reported LOD values (LOD for SDS = 108 nM and LOD for vitamin B_{12} = 45.3 nM), the sensor displayed short response time for SDS (50 s) and vitamin B_{12} (5 s) detection. The MOF was able to detect SDS in various real water samples and vitamin B_{12} in various bio-fluids (human urine and serum) and pH media. A MOF-coated, reusable cotton composite was fabricated which displayed a visible color change under UV-light even after treating it with a nanomolar concentration of both the analytes.

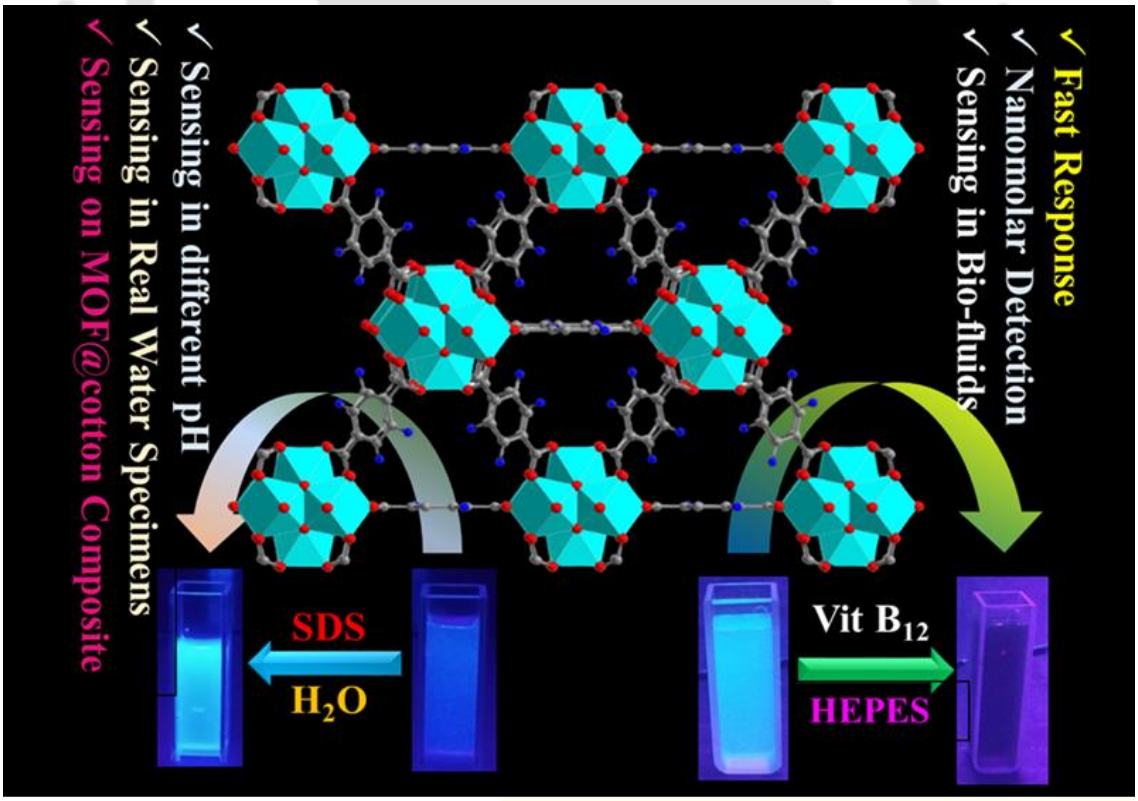

Inorganic Chemistry

S. Ghosh, J. Krishnan, V. Karthik, A. Dhakshinamoorthy, S. Biswas, Inorg. Chem., 2023, 62, 8605-8614.

2.1 Introduction

Metal-organic frameworks (MOFs) are a class of crystalline, porous coordination polymers made up of an vast number of nodes (metal ions) which are interconnected by organic linkers.[1] In these crystalline porous materials, molecular building blocks are joined by coordinative bonds.[1] The electronic communication between the metal ions and the π-conjugated polytopic organic linker makes MOF fluorescence active.[2] Such fluorescent MOFs become useful and well-established senor materials in the past few years for the sensing of various metal ions, anions, bio-active molecules, toxic organics and gas molecules.[3-5] The heterogeneous nature and large surface area of the MOFs favor the transformation of various organic starting materials into their desired product.[6, 7] The presence of a definite pore facilitated the selective formation of the anticipated product.[8, 9]

Surfactants are organic molecules that contain two components, i.e., hydrophilic (polar) and hydrophobic (non-polar) parts.[10] These are used all over the world as industrial cleaners, detergents, emulsifiers in cosmetics, etc.[10, 11] Around 15 million tons of surfactants are produced worldwide every year because of the excessive demand for surfactants.[12] Among the various types of surfactants, anionic surfactants (such as sodium dodecyl sulphate or SDS) are the most frequently used.[13] The overuse of these surfactants results in the release of these materials into the environment, which directly affects the health of aquatic animals and indirectly human beings. Long-term exposure to surfactants can irritate and harm the skin because they can penetrate the lipid barrier of the skin and other cells.[14] Surfactants can enter the gills, kidneys, blood, gallbladder, pancreas and liver when their concentration in the water is very high, which can hamper the functions of these organs.[15]

Cyanocobalamin (vitamin B_{12}) is a very important bio-molecule that plays a crucial role in metabolic cycles.[16] It helps to transfer a -CH_3 group from 5-methyltetrahydrofolate to homocysteine (Hcy). During this process, tetrahydrofolate is generated which is important in the DNA synthesis of intestinal wall cells and red blood cells.[16] Tetrahydrofolate level drops and Hcy level rises when this mechanism is compromised. Elevated Hcy levels can be harmful to cognitive health.[16, 17] Vitamin B_{12} participates in the conversion reaction of methylmalonyl-coenzyme A to succinyl-coenzyme A which is a crucial step in the extraction of energy from fats and proteins.[17, 18] In the blood serum inside a healthy human body, the concentration of vitamin B_{12} is 200-900 ng/mL.[16] Lower concentration of vitamin B_{12} can cause anemia, paleness, fatigue, weakness, dizziness and shortness of breath. A severe deficiency of vitamin B_{12} can damage nerves, also cause sensation in the hands and feet, loss of reflexes, muscle weakness, difficulty in walking, dementia and confusion.[16, 18] However, higher concentrations of vitamin B_{12} can also cause some life-threatening diseases. Hematologic disorder, leukemia, hypereosinophilic syndrome and polycythemia vera can also result in higher concentrations of cobalamin.[16, 18]

Hence, we need to develop efficient detection methods for hazardous surfactants and important bio-molecules (e.g. vitamin B_{12}). There are several techniques for the determination of concentrations of these targeted analytes i.e. high-performance liquid chromatography, light scattering detection, mass spectrometry, charged aerosol detection and titration, etc.[19-21] But,

the majority of used techniques demand complicated and expensive instrumental support and professional technical experts for the preparation of the sample.[19, 22] Selection of sensing solvents, accuracy of measurement and high limit of detection (LOD) are the other drawbacks of most the available sensors of SDS and vitamin B_{12}.[19, 22] In contrast, the equipment used in fluorescence-based detection is very simple, user-friendly, less expensive and less time-consuming and accurate.[23, 24] The aforementioned advantages made luminescent-based sensing a widely accepted way of sensing of various analytes.

Herein, we strategically architected a diamino-anchored Zr-based MOF (**1′**) for the selective sensing of the most widely used anionic surfactant such as SDS. Anionic surfactant SDS contains a free $-SO_3^-$ group. Therefore, electrostatic interactions are possible between the $-SO_3^-$ functional group of SDS and $-NH_2$ functional groups of the linker of **1′**. Such interaction may result in the increase or decrease of the fluorescence emission output of the fluorophore. In practice, the increase in fluorescence emission of **1′** was observed in the presence of SDS. Previous literature suggested that the absorption maxima of vitamin B_{12} are centered at 361 and 550 nm,[25] which is within the range of the emission spectrum of **1′**. Therefore, the energy transfer is possible between the MOF and vitamin B_{12}. Besides the lowest ever reported LOD value, the reusable probe displayed excellent fluorescence enhancement (~18.9 fold) within 50 s of the addition of SDS solution. This sensor can also sense the presence of SDS in various real water samples. In case of vitamin B_{12}, >99% quenching in fluorescence intensity was observed within 5 s of the addition of vitamin B_{12}. The sensor displayed almost equal sensing efficiency in various bio-fluids (human serum and urine) and a wide range of pH media. Moreover, inexpensive and portable MOF@cotton composites were developed which displayed the sensing of both the targeted analytes up to nanomolar level under UV light.

2.2 Experimental Section

2.2.1 Synthesis and Characterization Procedure of 2,5-Diaminoterephthalic Acid Linker

The 2,5-diaminoterephthalic acid linker was synthesized according to the previously reported procedure (Scheme 2.1).[26] The purity of the linker was again confirmed by ^{1}HNMR, ^{13}C NMR and mass spectrometric analysis. ^{1}H NMR (400 MHz, DMSO-d_6): δ = 7.24 (s, 2H) ppm ^{13}C NMR (100 MHz, DMSO-d_6): δ = 169.24, 140.47, 119.18, 117.73 ppm. ESI-MS (m/z): 196.0566 for $(M-H)^+$ ion (M = mass of 2,5-diaminoterephthalic acid linker). In Figures 2.1-2.3, the NMR and mass spectra of the synthesized linker are shown.

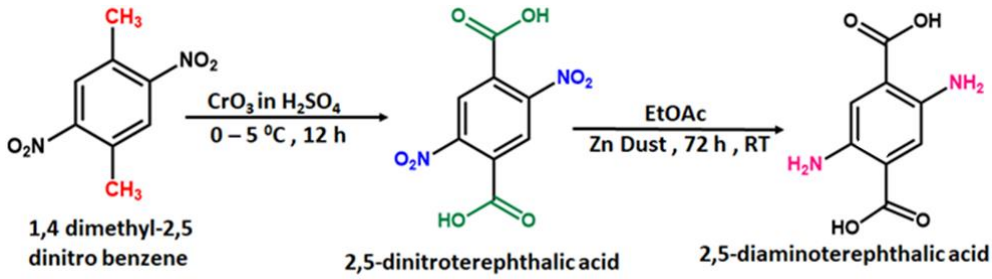

Scheme 2.1 Reaction scheme for the preparation of 2,5-diaminoterephthalic acid linker.

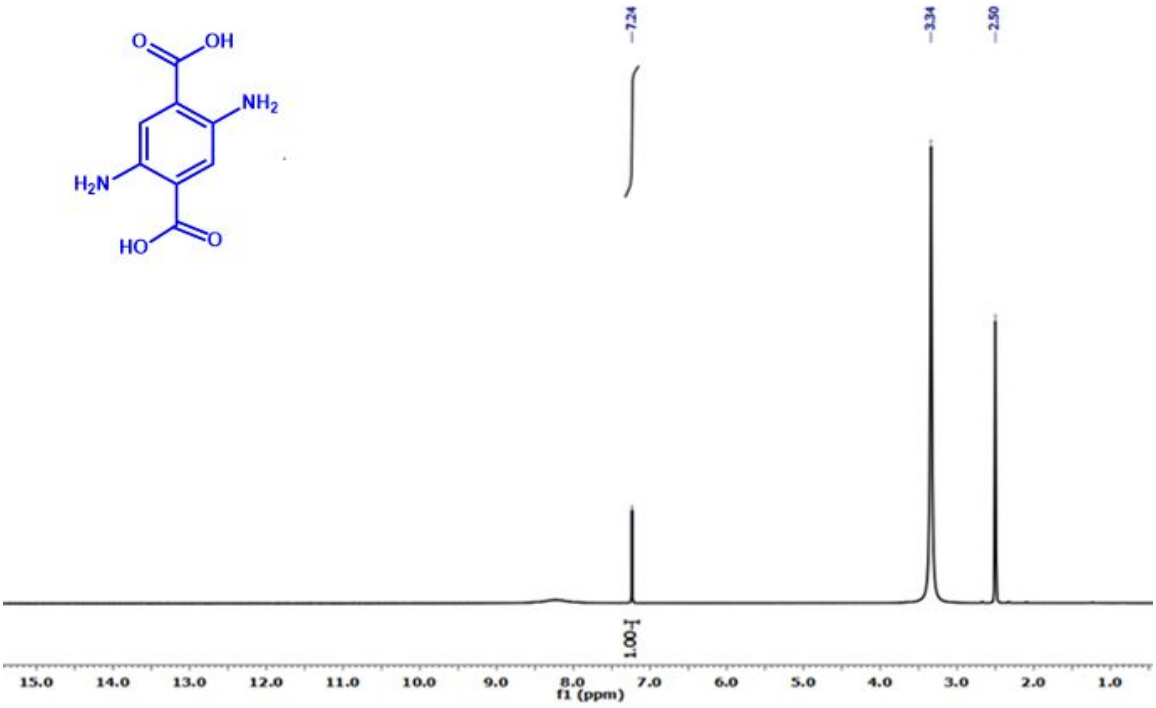

Figure 2.1 ^{1}H NMR spectrum of 2,5-diaminoterephthalic acid linker in DMSO-d_6.

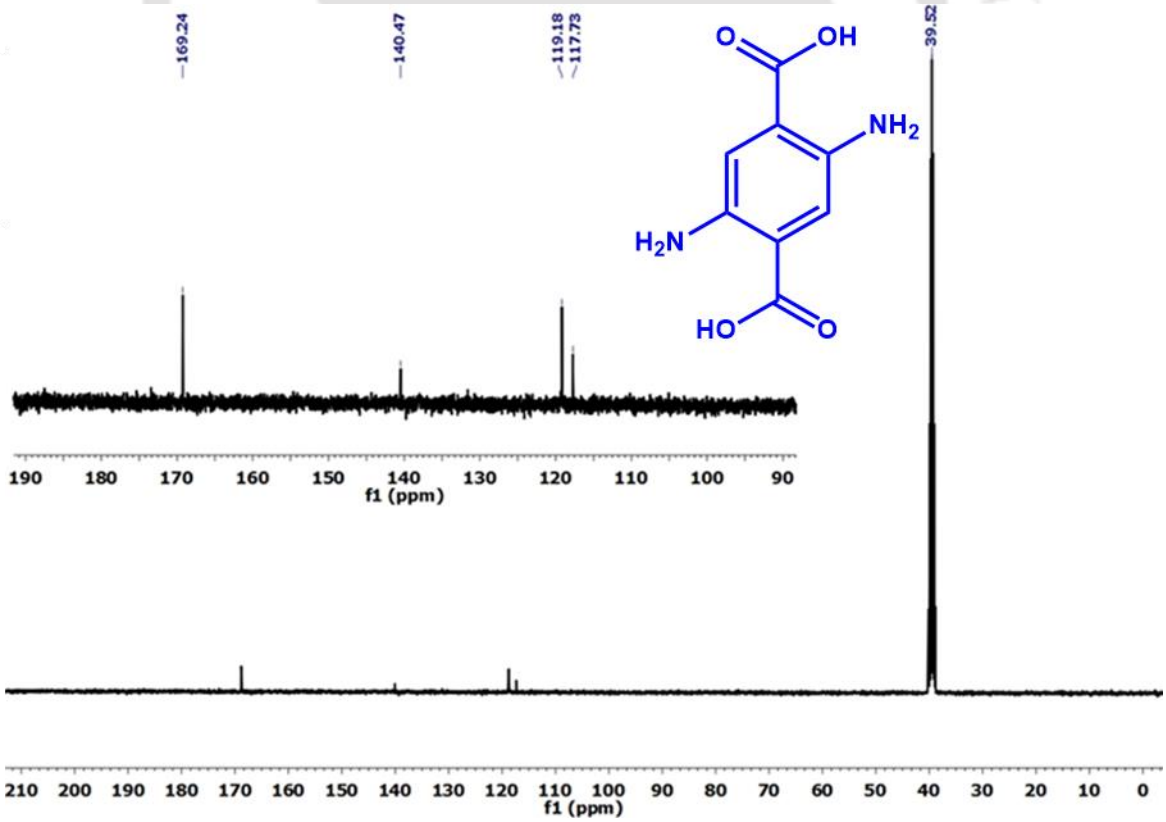

Figure 2.2 ^{13}C NMR spectrum of 2,5-diaminoterephthalic acid linker in DMSO-d_6.

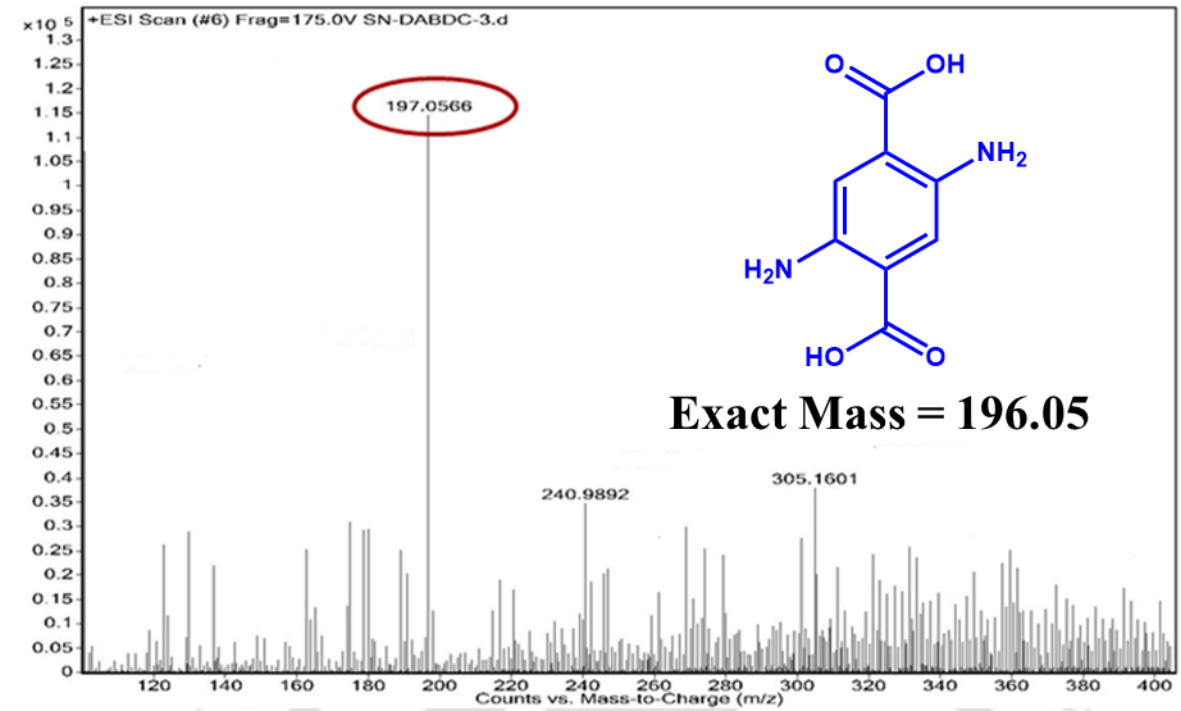

Figure 2.3 ESI-MS spectrum of 2,5-diaminoterephthalic acid linker measured in methanol. The spectrum shows m/z peak at 197.0566, which corresponds to $(M-H)^+$ ion (M = mass of 2,5-diaminoterephthalic acid linker).

2.2.2 Synthesis of $[Zr_6O_4(OH)_4(C_8H_6N_2O_4)_6]\cdot 7H_2O\cdot 2DMF$ (1)

The $H_2BDC\text{-}(NH_2)_2$ linker containing Zr(IV) based UiO-66 MOF was already synthesized in some of the previously reported literature.[27, 28] Yin *et al.* recently synthesized the MOF using HCl as an additive in a mixed solvent of DMF and water after heating $ZrCl_4$ salt and linker at a temperature of 100 °C for 48 h.[27] A mixed-linker MOF using $H_2BDC(NH_2)_2$ and $H_2BDC(NH_2)$ linkers was synthesized by Li *et al. in* DMF solvent by using $ZrCl_4$ salt.[28] Xu et al. also synthesized the same MOF using $ZrCl_4$ salt in DMF medium by heating the homogeneous mixture of metal salt, linker and acetic acid modulator at 80 ℃ for 12 h.[29] Herein, we used an easy and straightforward procedure for the synthesis of the MOF. For the synthesis of the MOF, in a Pyrex tube, 24 mg of $ZrCl_4$ (0.1 mmol), 20 mg of $H_2BDC(NH_2)_2$ linker (0.1 mmol), 3 mL of *N*,*N*-dimethyl formamide (DMF) and 388 µL (3 mmol) of formic acid were poured. After that, the tube was sonicated for 15 min to homogenize all the reacting components. After 15 min of sonication, the Pyrex tube was placed on a pre-heated heating block at 150 °C and it was kept at 150 °C for 24 h. After 24 h, the tube was allowed to come to the ambient temperature. When it came to room temperature, the precipitate was filtered off and washed three times with acetone. Finally, the compound was dried for 8 h at a temperature of 80 °C. Yield of **1** was 24 mg (0.01 mmol, 67% with reference to metal salt). Anal. calcd. for $C_{54}H_{68}N_{14}O_{41}Zr_6$ (2108 g mol^{-1}): C, 30.74; N, 9.30; H, 3.22. Found C, 30.58; N, 9.16; H, 3.12.%. IR (cm^{-1}): 3462 (br), 3200 (br), 1654 (s), 1594 (vs), 1526 (s), 1437 (vs), 1364 (s), 1275 (w), 1250 (w), 1110 (w), 910 (w), 790 (s), 654 (s).

2.2.3 Activation Procedure of As-synthesized 1

To eliminate the DMF molecules from the pore of **1**, 50 mg of **1** was first stirred for 6 h in 100 mL of methanol. The recovered material was then filtered and dried for 12 h at 60 °C in an air oven. Finally, the low boiling MeOH solvents were removed by heating the compound for 12 h under vacuum at 100 °C using an oil bath. After all the above processes, the thermally activated **1′** was achieved.

2.2.4 Preparation of MOF (1′) Suspension for the Fluorescence Sensing Experiments

The probe **1′** (3 mg) was taken in a 5 mL glass vial containing 3 mL deionized water/HEPES buffer. Then, the suspension was sonicated for 15 min and kept it for overnight to make the suspension stable. During the fluorescence experiment, 200 µL of above-mentioned suspension of **1′** was added to 3000 µL of deionized water/HEPES buffer in a quartz cuvette. All the fluorescence spectra were collected in the range of 380-600 nm by exciting the suspension at 365 nm for SDS sensing and in the range of 350-600 nm (λ_{ex} = 335 nm) for vitamin B_{12} sensing. For competitive experiments, the solutions of the different competitive analytes (concentration = 10 mM for SDS sensing and 5 mM for vitamin B_{12} sensing) were added to the suspension of **1′** and spectra were collected in the aforementioned ranges.

2.2.5 Sensing of Vitamin B_{12} in Human Blood Serum Samples

10 mL of blood sample was collected from the right arm vein of a healthy person (blood group A^+) and the blood plasma was separated by centrifuging the sample at 10,000 rpm for 15 min. The light-yellow blood serum was collected in a Falcon tube and stored at -20 °C in a refrigerator. For fluorescence detection experiments, aliquots of different concentrations of vitamin B_{12} spiked into the human blood serum sample, which contained HEPES buffer suspension of the MOF.

2.2.6 Sensing of Vitamin B_{12} in Human Urine Sample

10 mL of the first morning urine sample from a healthy person was taken and 500 mL of HNO_3 was added to the sample to kill any interfering living things. After that, the sample was centrifuged at 8000 rpm for 10 min. For the sensing experiments, the supernatants of the vitamin B_{12}-spiked urine solution were taken. Different vitamin B_{12} aliquots were added into urine samples containing HEPES buffer suspensions of the probe and fluorescence spectra were recorded.

2.3 Results and Discussion

2.3.1 Structural Characterization

The reaction between $ZrCl_4$ and H_2BDC-$(NH_2)_2$ linker molecule resulted in the formation of UiO-66 framework. The measured peak locations and intensities in the PXRD pattern of **1** were similar to the simulated PXRD pattern (Figure 2.4). The closeness between the measured and simulated PXRD data was further confirmed by the Pawley refinement (Figure 2.5a) and indexing of the slow scan PXRD data of **1** (Table 2.1). The framework contains $[Zr_6O_4(OH)_4]^{12+}$ secondary building units (SBUs) and the core Zr(IV) ions are coordinated with

four μ_3-OH and four μ_3-O sites. Six $[BDC\text{-}(NH_2)_2]^{2-}$ linkers are employed in the framework to join the SBUs resulting in **1** (Figure 2.5b-d). The framework structure has two different types of structural voids: larger size octahedral voids and smaller size tetrahedral voids. The closeness of PXRD patterns (Figure 2.4) of **1** and **1′** confirms the integrity of the framework after the thermal activation process.

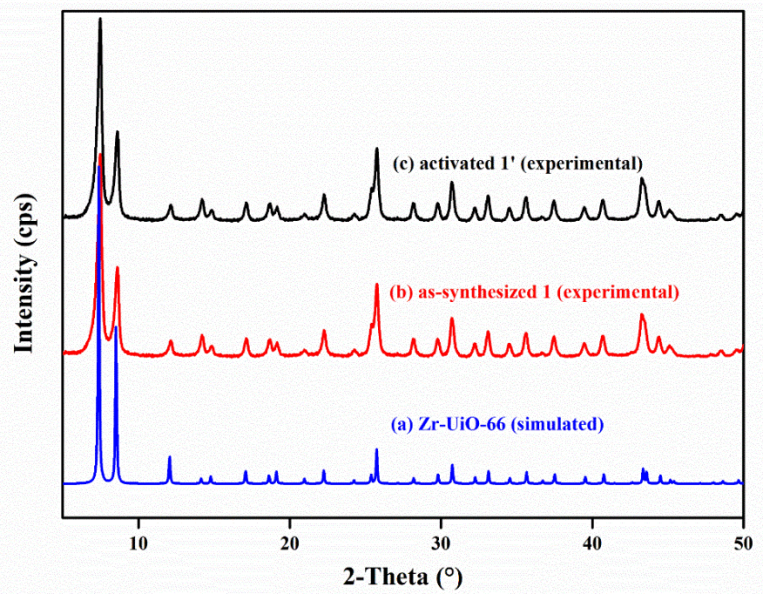

Figure 2.4 PXRD patterns of (a) simulated Zr-UiO-66 (blue), (b) as-synthesized **1** (red) and (c) activated **1′** (black).

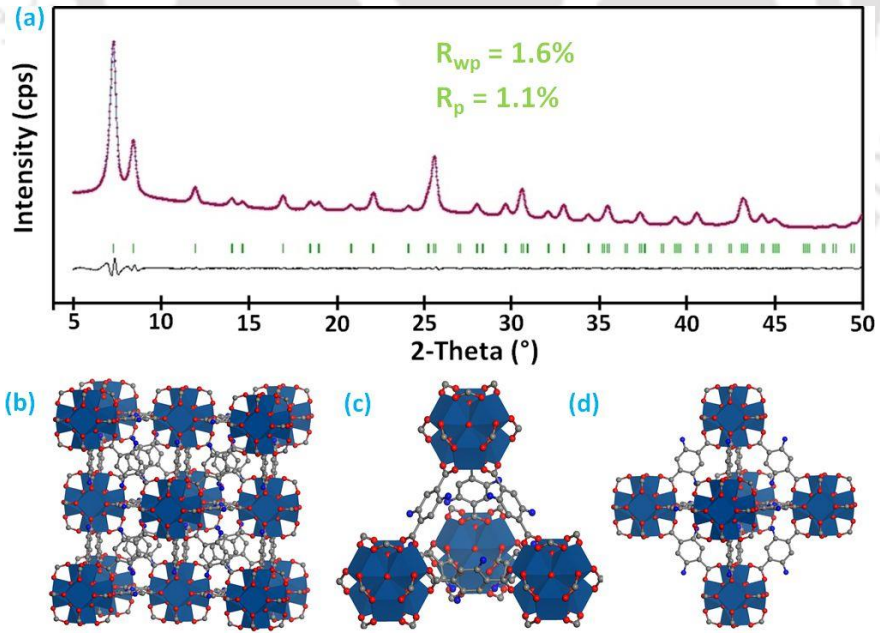

Figure 2.5 Fitted Pawley plot of the experimental PXRD data of **1** (a), cubic structure of **1** (b) and its tetrahedral (c) and octahedral (d) cages.

Table 2.1 Unit cell parameters of **1′** obtained by indexing its PXRD data. The obtained values have been compared with parent UiO-66 MOF.

Compound Name	**1′**	UiO-66[30]
crystal system	cubic	cubic
a = b = c (Å)	20.755 (22)	20.890 (2)
V (Å^3)	8940.6 (23)	8870.03 (2)

2.3.2 Morphology and EDX Analysis

The homogenous distribution of particles in the FE-SEM images of **1′** (Figure 2.6) validated the phase purity and crystalline nature of the activated MOF (**1′**). The EDX spectrum of **1′** (Figure 2.7) ensured the presence of the desired elements (Zr, C, N and O) in the framework.

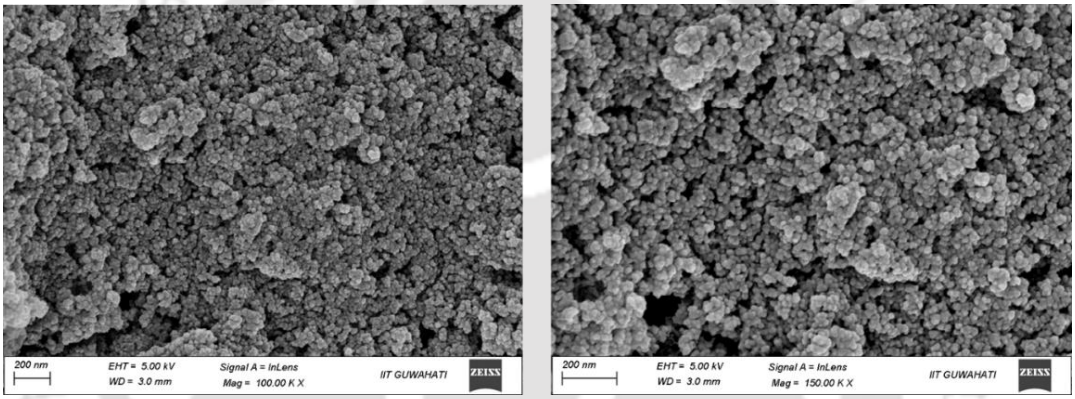

Figure 2.6 FE-SEM images of as-synthesized **1′**.

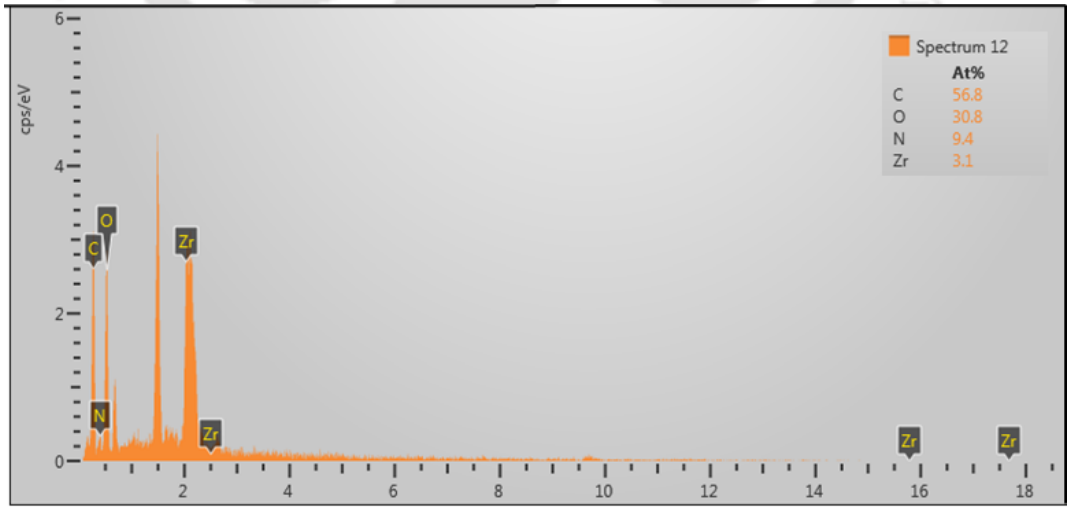

Figure 2.7 EDX spectrum of **1′**.

2.3.3 IR Spectroscopy

We used IR spectroscopy (Figure 2.8) to confirm the existence of different functional groups and the complete elimination of DMF (solvent) molecules from the pores of the framework structure. Both **1** and **1′** displayed two distinct absorption bands at 1586 and 1440 cm^{-1}, which originated from the Zr-coordinated asymmetric and symmetric stretching of the carboxylate groups of the linker molecules. In the linker, these peaks were located at 1591 and 1492 cm^{-1}, respectively. The shift of asymmetric and symmetric stretching peaks in MOF, ensures the formation of coordination bonds between Zr(IV) and the carboxylate groups of the linker. The absorption band around 1658 cm^{-1} was present in **1**, which was due to the carbonyl stretching vibration of DMF molecules present inside the pore of as-synthesized MOF. Such peak at 1658 cm^{-1} was not observed in **1′**, which indicated that all guest DMF molecules had been removed from the pore of **1** after thermal activation.

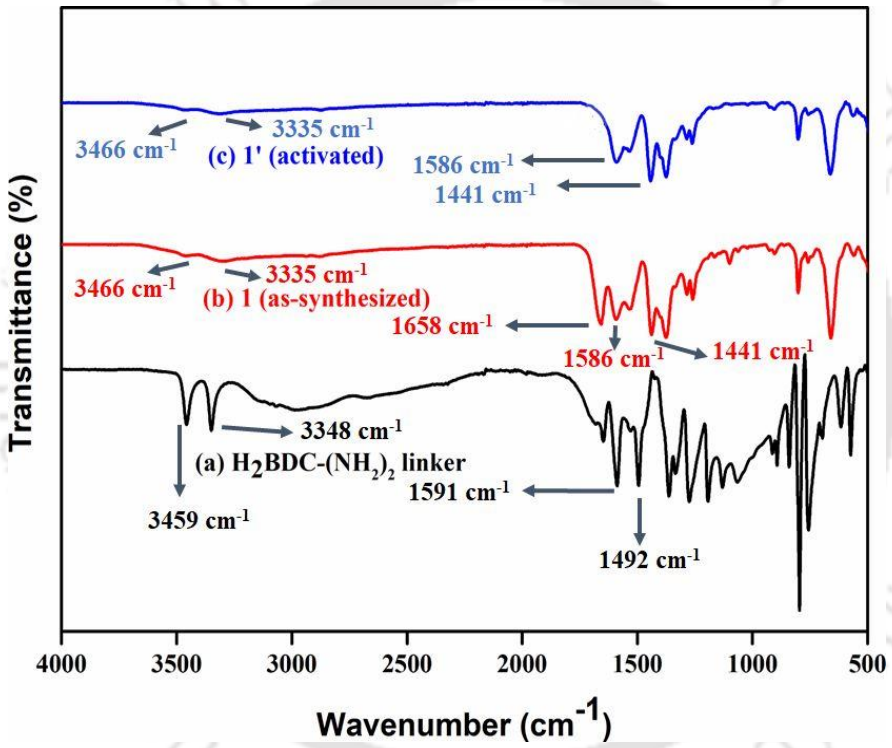

Figure 2.8 ATR-IR spectra of (a) 2,5-diaminoterephthalic acid ($H_2BDC-(NH_2)_2$) linker (b) **1** (as-synthesized) (c) **1′** (activated).

2.3.4 Chemical Stability

To determine the chemical stability of **1′** in the sensing media (H_2O and HEPES), in various organic solvents and different pH, compound **1′** was stirred in the sensing media (H_2O and HEPES), in various organic solvents (methanol, ethanol and ethyl acetate) and different pH solutions (pH = 2-12) for 6 h at room temperature. After that, the MOF materials were recovered by filtration and dried at temperature of 80 °C. Then, the PXRD analysis was performed using the recovered MOF materials (Figure 2.9-2.10). The PXRD pattern of the recovered MOF materials remained the same as that of fresh **1′** even after stirring in the different solvents. Moreover, the crystallinity of the MOF was completely lost after stirring it

at pH = 12, which implies the MOF is unstable at highly basic pH. This observation proved the integrity of the framework structure after stirring in the aforementioned solvents, which opens the scope of using **1′** as a sensor in a wide range of solvent media.

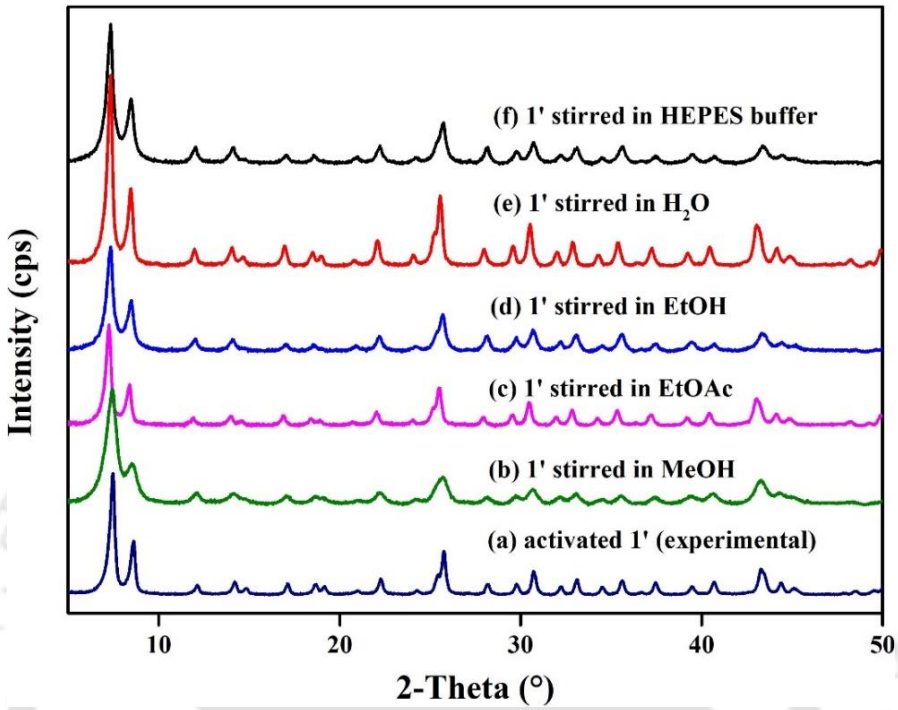

Figure 2.9 PXRD patterns of **1′** in different forms: (a) activated **1′**, after stirred with (b) MeOH, (c) EtOAc (d) EtOH, (e) H_2O and (f) HEPES buffer (pH =7.4).

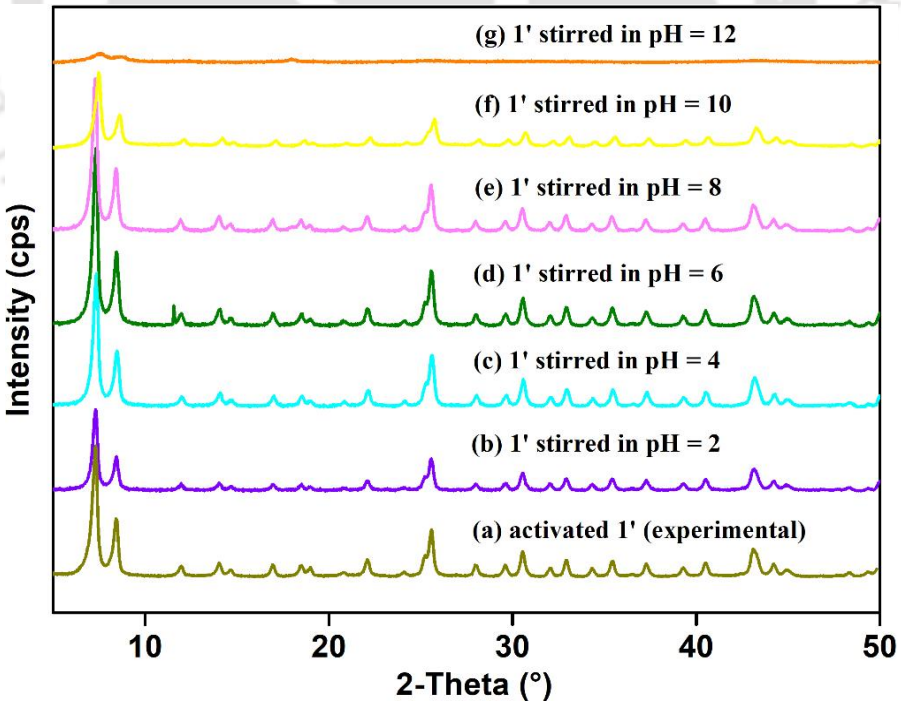

Figure 2.10 PXRD patterns of **1′** in different forms: (a) activated **1′**, after stirred in (b) pH = 2, (c) pH = 4, (d) pH = 6, (e) pH = 8, (f) pH = 10 and (g) pH = 12.

2.3.5 Thermal Stability

Thermal stability of both **1** and **1′** was determined using thermogravimetric analysis. Both **1** and **1′** displayed thermal stability up to 230 °C under N_2 atmosphere (Figure 2.11). Three sequential weight losses were observed for **1**. An initial weight loss of 5.7% was observed in the temperature range of 35-130 °C, which was due to the loss of 7 H_2O molecules per formula unit (cal.: 5.7 wt.%). In the middle, within the temperature range of 130-230 °C, the weight loss of 6.8% corresponds to the removal of 2 DMF molecules (per formula unit) from **1** (cal.: 6.8 wt.%). Finally, the framework structure decomposed after reaching the temperature of 230 °C. TGA analysis of **1′** displays two steps of weight loss. The initial weight loss is due to the removal of water molecules absorbed during the storage of **1′**. After 230 °C, the final weight loss was observed due to the disintegration of the framework structure. Therefore, both **1** and **1′** have thermal stability up to 230 °C.

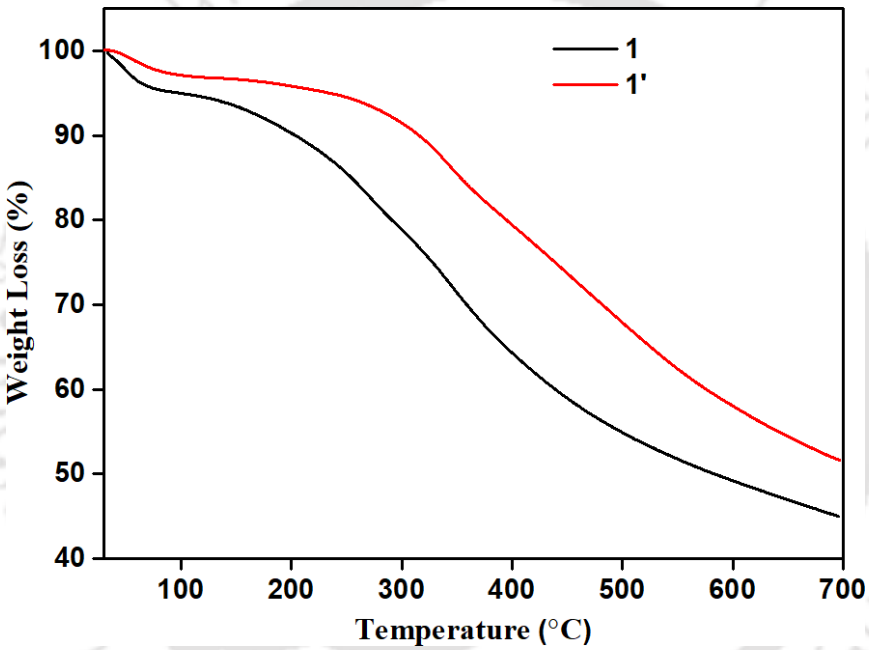

Figure 2.11 Thermogravimetric analysis curves of as-synthesized **1** (black) and thermally activated **1′** (red) recorded under N_2 atmosphere in the temperature range of 25-700 °C with a heating rate of 4 °C min^{-1}.

2.3.6 Nitrogen Sorption Analysis

N_2 sorption study was performed at a temperature of -196 °C to determine the surface area (BET) and pore volume of **1′** (Figure 2.12). The measured N_2 surface area of the MOF is 504 m^2g^{-1} with a pore volume of 0.6 cm^3 g^{-1} (measured at p/p_0 = 0.5). The pore-size distribution plot displayed that most of the micropores of **1′** are concentrated at 8.04 Å (Figure 2.13).

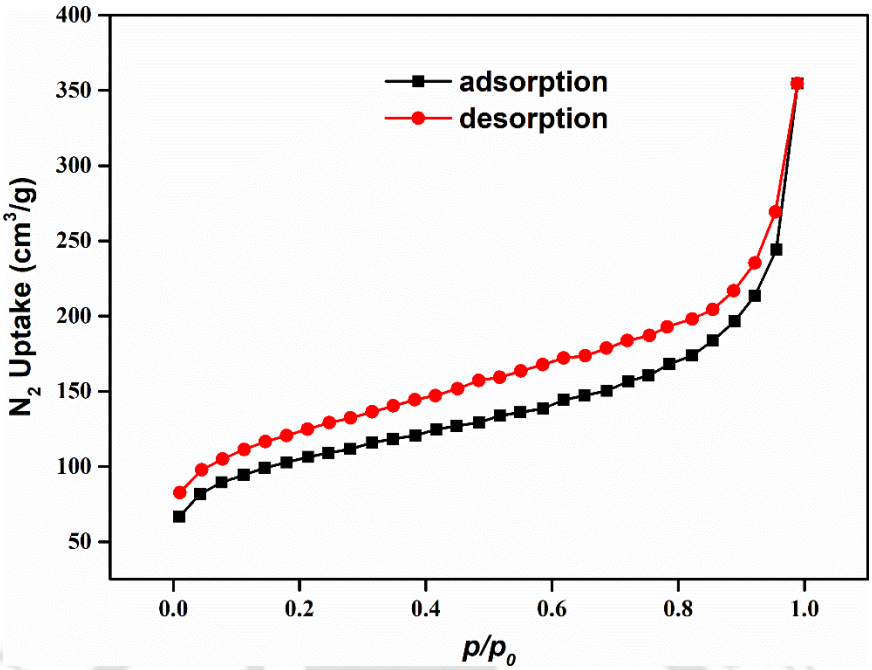

Figure 2.12 N_2 adsorption (black squares) and desorption (red circles) isotherms of thermally activated **1′** recorded at –196 °C.

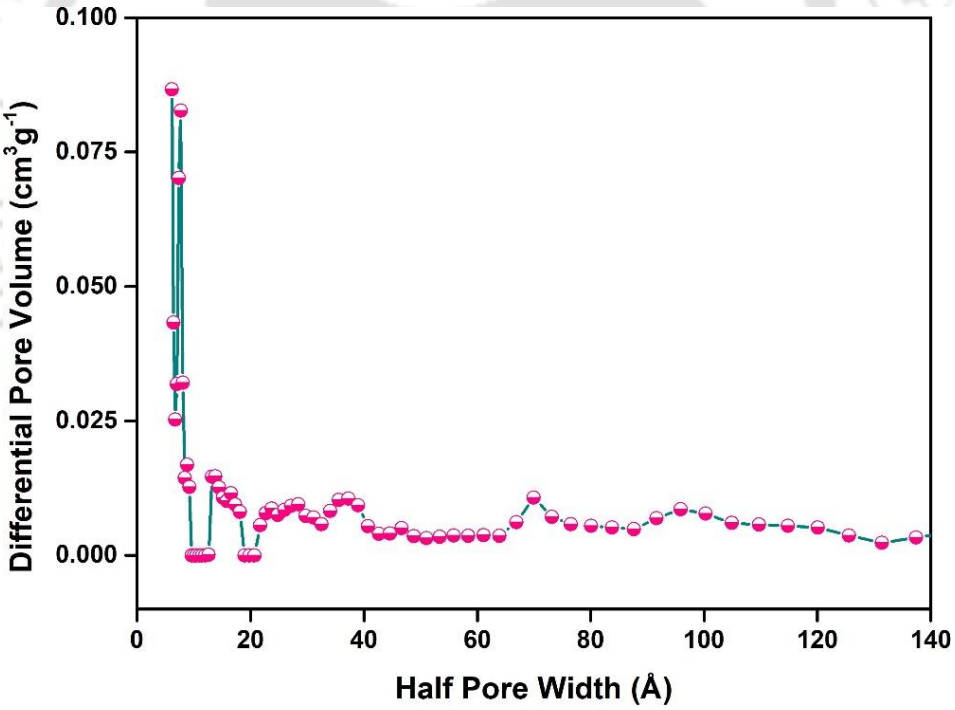

Figure 2.13 Density functional theory pore-size distribution of compound **1′** as determined from its N_2 adsorption isotherms at -196 °C.

2.3.7 Fluorescence Response Towards SDS

With the continuous development of modern civilization, the use of various surfactants gradually increases. Surfactants play a crucial role as wetting, cleaning, emulsifying, dispersing, foaming and anti-foaming agents in various practical applications, including fabric

softeners, detergents, motor oils, soaps, emulsions, paints, inks, adhesives, anti-fogs, snowboard waxes, ski waxes, deinking of recycled papers, etc.[31] Due to the excessive use and toxic nature of the surfactants, determining the presence of surfactants in environmental water bodies is highly necessary.

The high physicochemical stability, non-toxic nature and presence of $–NH_2$ functionality in **1′** inspired us to verify the fluorogenic sensing ability of **1′** towards the SDS in H_2O. The MOF material was excited with a light of 365 nm wavelength and a weak fluorescence emission with an emission maximum of 483 nm was observed (Figure 2.14). After the addition of 350 µL of 10 mM aqueous solution of SDS solution, an enhancement of photoluminescence of 18.9 fold was noticed (Figure 2.15).

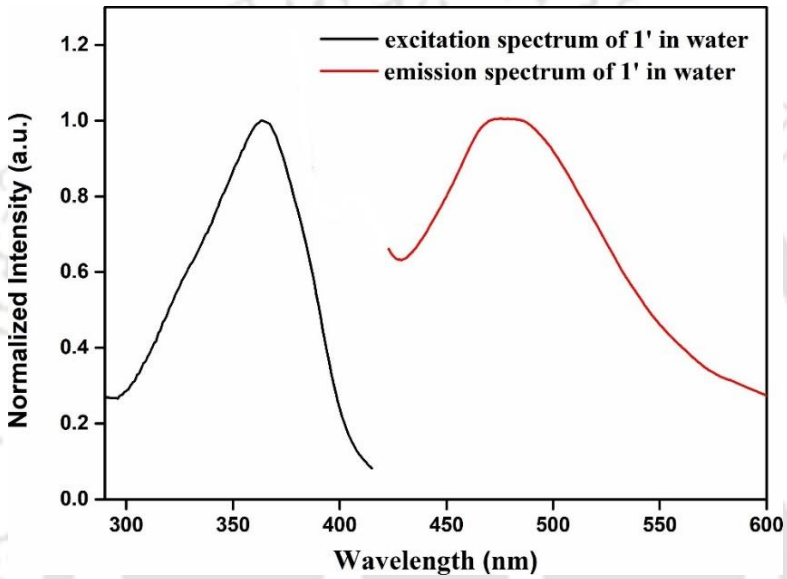

Figure 2.14 Excitation (black) and emission (red) spectra of **1′** in water.

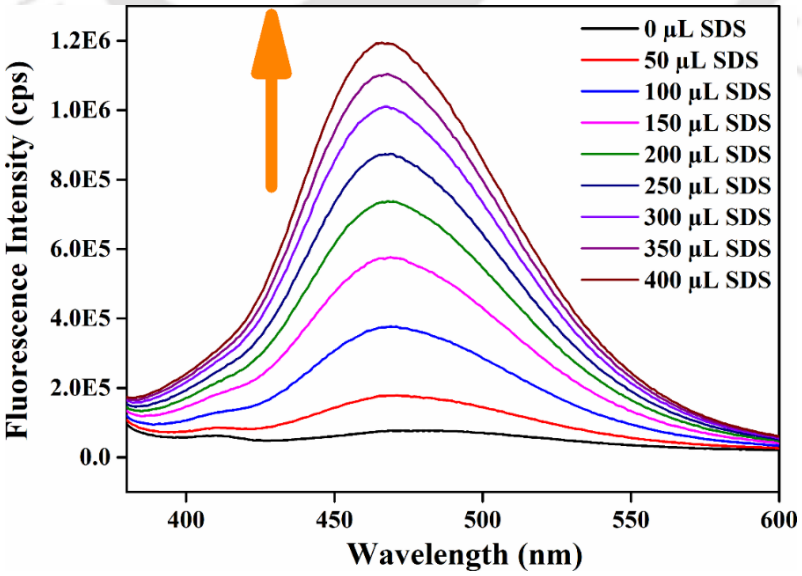

Figure 2.15 Turn-on in the fluorescence spectrum of **1′** with step-wise addition (0 to 400 µL) of 10 mM SDS solution.

In search of the response time of the probe, we added 350 µL of SDS solution at a time in the MOF suspension and continuously collected the emission spectra with an interval of 5 s. After 50 s, the increment of emission response was diminished. Hence, 50 s was considered as saturation time (Figure 2.16a-b).

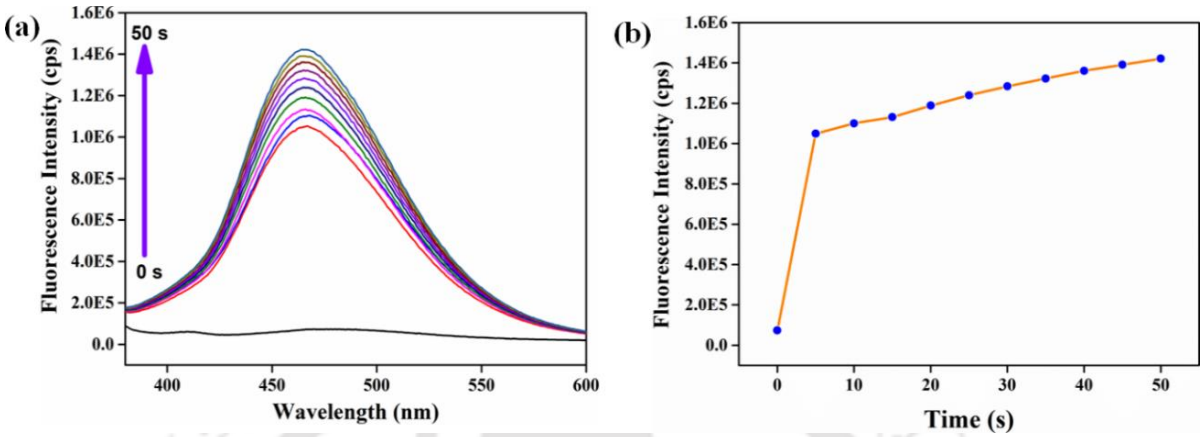

Figure 2.16 (a) Quenching in the fluorescence spectrum of **1′** in water as a function of time after the addition of 400 µL of 10 mM SDS solution. (b) Time-dependent saturation plot (luminescence colour change of **1′** under UV-lamp after injection of SDS displayed in inset of the figure 2.16b).

A sensor of SDS should be selective even in the presence of other competitors. To verify the same, we determined the selectivity of the probe in the presence of other competitors (urea, CTAB, tween-80, triton-100, NO_3^-, Ca^{2+}, Na^+, Zn^{2+}, NH_4^+, I^-, K^+, Cl^-, Co^{2+}, Br^-, Mg^{2+} and Al^{3+}). Figures 2.17-2.18 clearly evidence the selectivity of the MOF for the sensing of SDS. To ensure the reproducibility and originality of all the measurements, statistical analysis of all the measurements were performed and errors after three individual measurements were determined. The accuracy and precision of sensing in intra-day (Table 2.2) and inter-day (on three different days) were also determined.

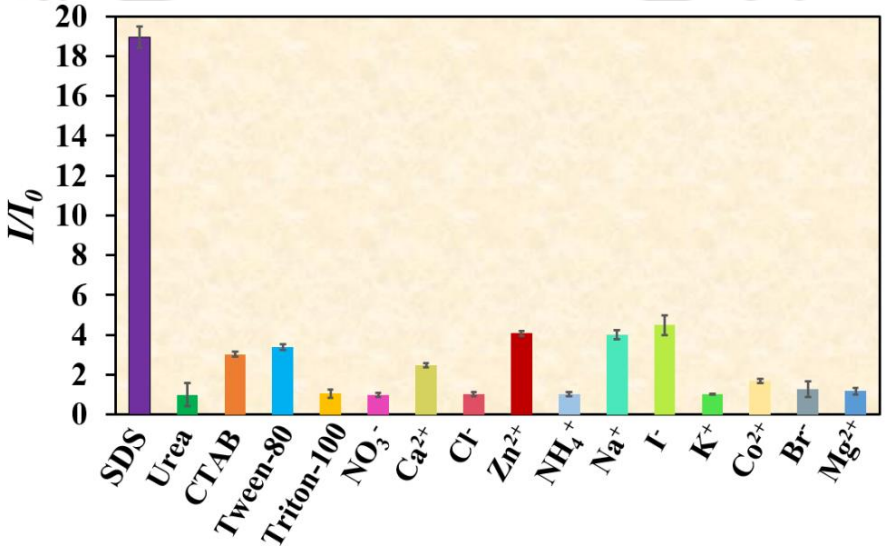

Figure 2.17 Selectivity test of **1′** for the sensing of SDS.

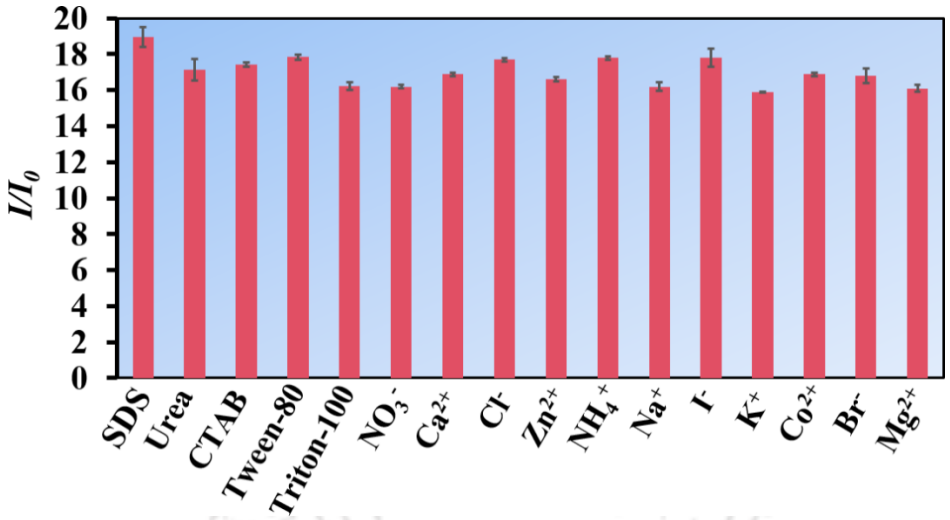

Figure 2.18 Selectivity test for the sensing of SDS in the presence of other competitors (error bars represent the standard deviations of three individual measurements).

Table 2.2 Evaluation of intra-day, inter-day accuracy and precision study of change in fluorescence intensity of **1′** after incremental addition of 10 mM aqueous solution of SDS.

Parameter	Amount of SDS Added (μL)	Fluorescence Intensity (cps) at λ_{max} = 483 nm			Average PL Intensity (cps)	SD	RE%
repeatability	0	63785.4	63260.8	63401.9	63482.7	271.5	0.004
intra-day	50	171477.6	170242.5	168969.3	170229.8	1254.2	0.007
precision	100	358518.4	357020.7	358102.3	357880.5	773.1	0.001
	150	576539.7	574396.3	574787.6	575241.2	1141.5	0.003
	200	735926.9	736439.4	734860.0	735742.1	805.8	0.002
	250	874541	875929.5	875918.6	875463.0	798.5	0.001
	300	1196550	1196980	1195840	1196457	575.7	0.007
	350	1198180	1199400	1197350	1198310	1031.2	0.001
reproducibility	0	70049.03	70061.7	63401.93	72170.89	7610.2	0.031
inter-day	50	169921.7	165487.6	168969.3	168126.2	2334.2	0.011
precision	100	356638.3	353672.9	358102.3	356137.8	2256.7	0.004
	150	571330.7	567742.3	574787.6	571286.9	3522.9	0.001
	200	728285.4	724655.7	734860	729267	5172.5	0.002
	250	862681.8	864084.2	875918.6	867561.6	7271.3	0.001
	300	1199450	1192240	1195840	1195843	3605.0	0.018
	350	1312950	1303990	1297350	1304763	7828.7	0.001

To calculate the limit of detection (LOD) value of the probe for SDS sensing, six fluorescence spectra of the MOF suspension were collected. After that, fluorescence emission spectra were recorded with the incremental addition of low concentration of SDS to the MOF suspension. A linear plot was obtained after plotting the intensity value against the concentrations of SDS (Figure 2.19). By using the $3\sigma/k$ equation, the assessed LOD and LOQ values from this experiment were 107.8 ± 12.4 and 357 ± 43.2 nM, respectively. Rigorous statistical details of three individual measurements are summarised in Table 2.3. The obtained LOD value is the lowest ever among all the reported sensors of SDS (Table 2.4).

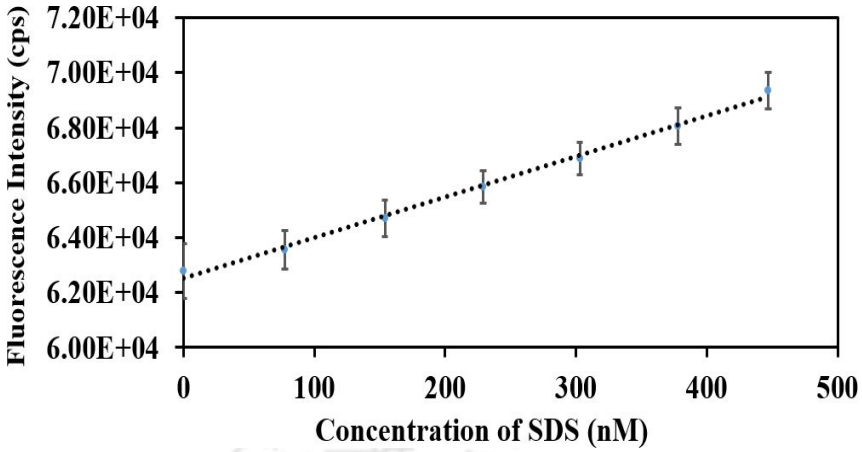

Figure 2.19 Change in the fluorescence emission intensity of **1′** in H_2O as a function of concentration of SDS.

Table 2.3 Statistical details of different analytical parameters for the sensing of SDS by **1′.**

Concentration Range (nM)	Slopes	Intercepts	Correlation Coefficient (R^2)	$S_{y/x}$ [a]	LOD[b] (nM)	LOQ[c] (nM)	Regression Equation
0-447	1222.1	61526.6	0.992	49500.2	121.5	405.0	1222.1x + 61526.6
	1447.5	61601.8	0.993	50635.1	104.9	346.2	1447.5x + 61601.8
	1522.0	62696.4	0.998	49346.8	97.2	320.8	1522.0x + 62696.4
Average	1397.2	61941.6	0.994	49827.4	107.8	357.3	1397.2x + 61941.6
SD	156.1	654.7	0.003	703.7	12.4	43.2	(1397.2 ± 156.1)x + (61941.6 ± 654.7)

[a] Standard deviation of the residuals, [b] Limit of detection, [c] Limit of quantification

Table 2.4 Comparison of the present probe (**1′**) with some previous probes of SDS.

Sl. No.	Sensor Material	Type of Material	Sensing Medium	Detection Limit (nM)	Response Time (s)	Detection Method	Ref.
1	Poly-diacetylenes (PDAs)	polymers	HEPES buffer	2000	30	colorimetric	21
2	quaternary alkylammonium compounds (QAC)	(i) QAC1-TPB (ii) QAC2-TPB (iii) QAC3-TPB (iv) QAC4-TPB (v) QAC4-TPB	-	(i) 750 (ii) 1500 (iii) 2000 (iv) 2500 (v) 2500	(i) 8 (ii) 8 (iii) 8 (iv) 8 (v) 12	electro-chemical	22
3	TA-DS	ion-exchange complex	-	1400	-	potentiometric	32
4	DMI-TPB	ion-exchange complexes	-	320	-	potentiometric	33
5	HTA-TPB	organic ion pair	water	200	seconds	potentiometric	34
6	CTA-DS	PVC membrane	water	300	25	potentiometric	35

7	DDA-TPB	polymer	water	250	6-8	potentiometric	36
8	MWCNTs with TODA-TPB	carbon nanotube	water	(i) 150 (ii) 200	8-12	potentiometric	37
9	**1′**	MOF	Water	107.8	50	fluorescence	this work

The excited state lifetimes of the sensor were measured before and after the injection of SDS solution. The obtained lifetimes were 9.8 and 11.9 ns, respectively (Table 2.5). The decay profile (Figure 2.20) shows that after the addition of SDS solution, weakly fluorescent **1′** readily become strong fluorescent.

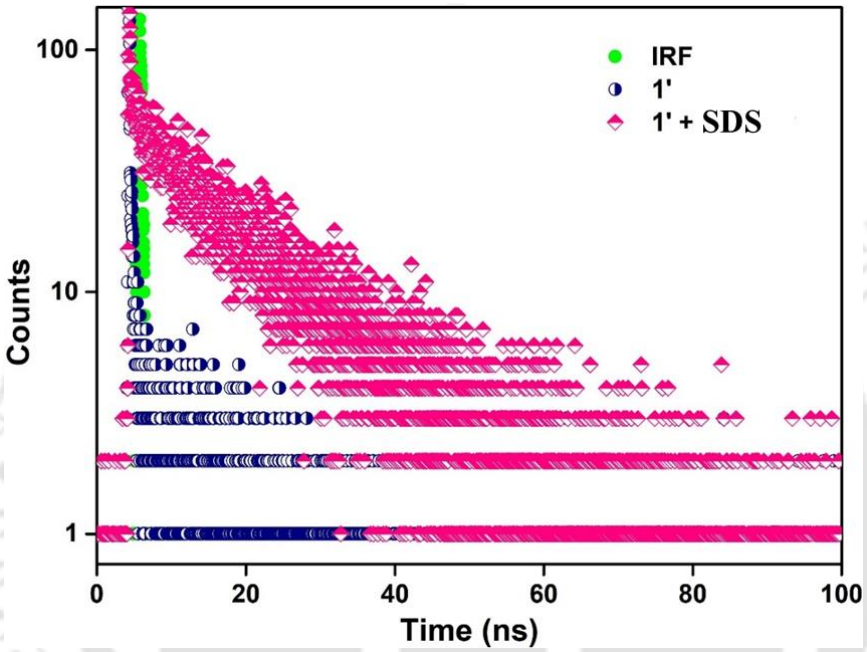

Figure 2.20 Lifetime decay profile of **1′** in the absence and presence of SDS solution (λ_{ex} = 360 nm, monitored at 375 nm).

Table 2.5 Fluorescence lifetimes of **1′** before and after the addition of SDS solution (λ_{ex} = 375 nm, pulsed diode laser).

Volume of SDS solution added (μL)	f_1	f_2	τ_1 (ns)	τ_2 (ns)	$<\tau>$* (ns)	χ^2
0	0.0004	0.9996	17.28	9.864	9.8	1.053
350	0.0115	0.8875	0.052	13.428	11.9	1.005

* $<\tau> = f_1\tau_1 + f_1\tau_2$

To examine the reusability, we performed a reusability test for **1′**. We centrifuged the suspension (obtained after each step of sensing) to recover the MOF material. After removing the liquid part, the solid part was collected and thoroughly cleaned with water to remove any remaining SDS that had been absorbed. After that, the recovered solid was again activated before being used in the following cycles of sensing. Figure 2.21 shows that **1′** can sense SDS

up to five cycles with almost comparable sensitivity. The probe's high efficiency along with excellent reusability guarantees that it is well suited for use in practical sensing applications.

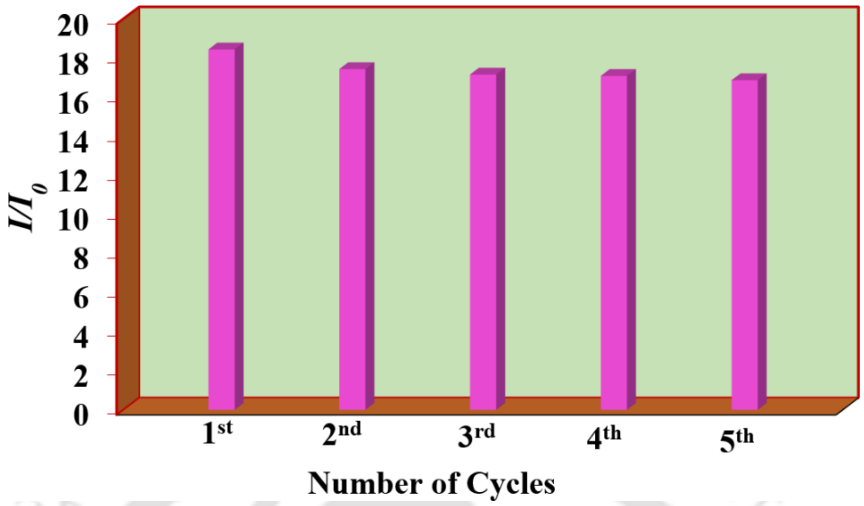

Figure 2.21 Reusability of **1′**for the sensing of SDS in aqueous medium.

SDS is mainly available in environmental water bodies (river water, lake water, or tap water). Thus, we extended our sensing experiment to real water specimens to verify the broad applicability of the newly developed sensor. In this context, suspensions of **1′** were prepared in the aforementioned water media and similar titration experiments were performed using different concentrations of SDS solutions. Figure 2.22 clearly shows the sensing ability of the probe for the various concentrations (2.5, 5 and 10 mM) of SDS solutions in real-water specimens. The concentrations of SDS in real water samples were also measured after varying the concentration of SDS (2.5-10 mM). The measured concentrations were similar to the spiked concentrations of SDS and the obtained recovery percentages were ~100% (Table 2.6). Such fruitful results signify the broad scope and real-world applicability of the probe for SDS sensing.

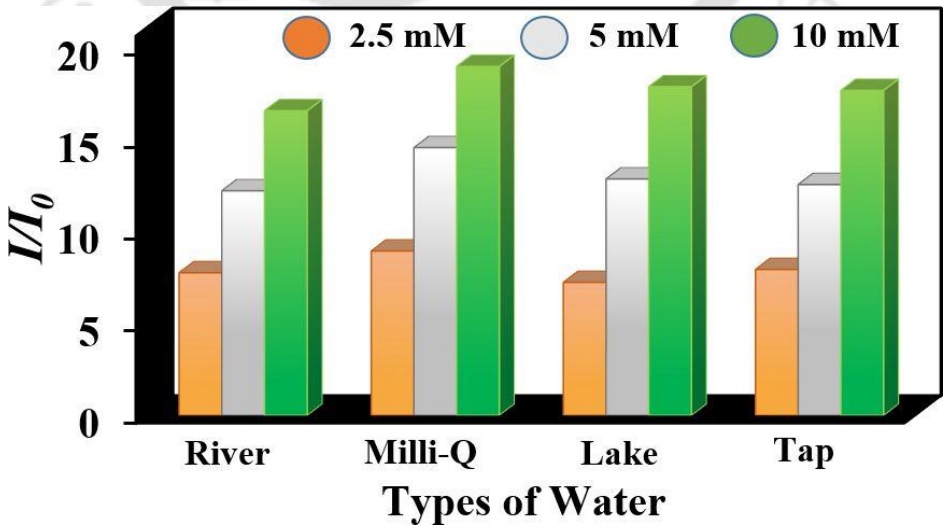

Figure 2.22 Sensing of SDS in various real water specimens.

Table 2.6 Comparison between the spiked and observed concentrations and recovery of SDS in different real water specimens.

Type of Water	Spiked Conc. of SDS (mM)	Observed Conc. of SDS (mM)	Recovery (%)
milli-Q water	(i) 1076.9 (ii) 538.5 (iii) 269.3	(i) 1069 (ii) 545 (iii) 280	(i) 99.2 (ii) 101.2 (iii) 103.9
lake water	(i) 1076.9 (ii) 538.5 (iii) 269.3	(i) 1071 (ii) 525 (iii) 280	(i) 99.2 (ii) 97.4 (iii) 103.9
tap water	(i) 1076.9 (ii) 538.5 (iii) 269.3	(i) 1067 (ii) 528 (iii) 281	(i) 99.0 (ii) 98.0 (iii) 104.3
river water	(i) 1076.9 (ii) 538.5 (iii) 269.3	(i) 1081 (ii) 541 (iii) 275	(i) 100.4 (ii) 100.5 (iii) 102.1

2.3.8 Mechanism of SDS Sensing

In search of the probable reason behind the turn-on response after injection of SDS solution in the aqueous solution of **1′**, firstly, we confirmed the structural integrity of the framework during the sensing event by PXRD and FE-SEM analysis (Figures 2.23-2.24). The recyclable nature of the probe also indicates towards non-reaction-based sensing mechanism. We also performed the sensing experiments by using non-functionalized UiO-66 and UiO-66-NH_2 MOFs to examine the role of diamine functionalization. Figure 2.25 displays that the fold increments of the probe gradually increase with the increase of the number of $–NH_2$ groups. The observation clearly evidences that the $–NH_2$ groups in the linker molecules are solely responsible for this switch-on response.

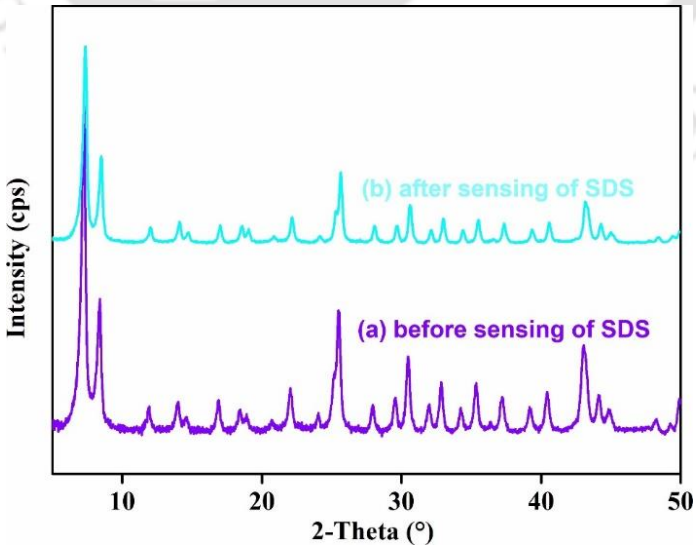

Figure 2.23 PXRD patterns of **1′** before (a) and after (b) treatment with SDS in water.

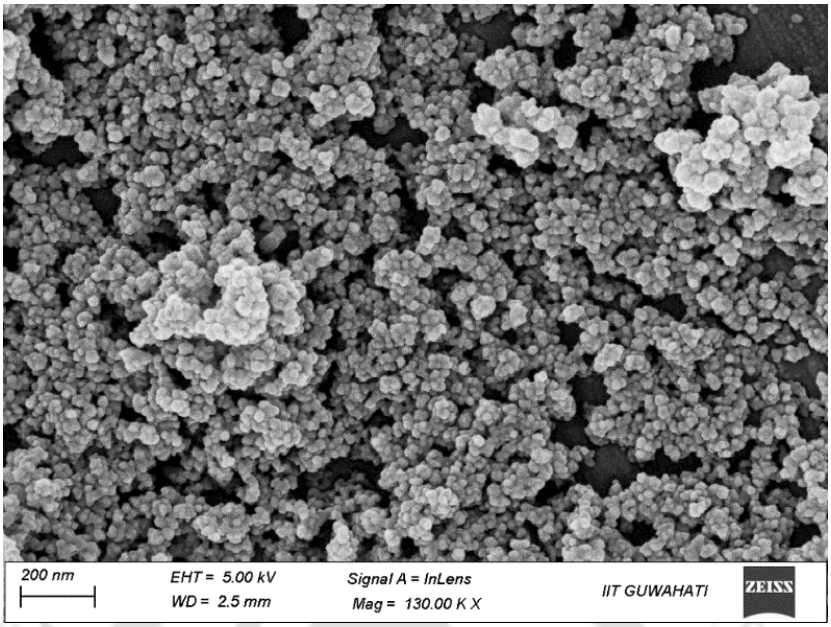

Figure 2.24 FE-SEM images of **1′** after SDS sensing experiment.

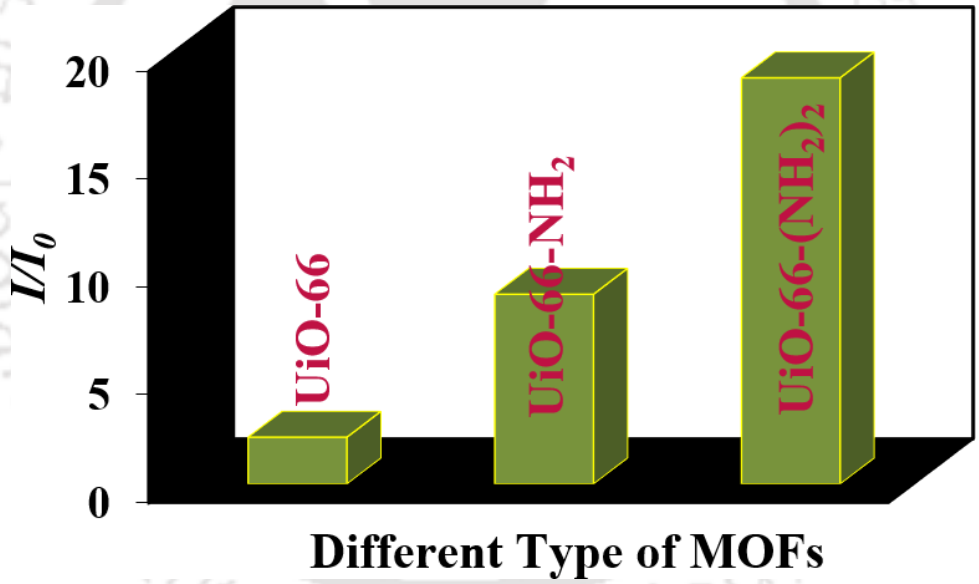

Figure 2.25 Sensing performances of different MOFs towards SDS in aqueous medium.

The sensor **1′** is highly selective towards the sensing of SDS which made us curious to investigate the nature of interaction between the probe and the $–SO_3^-$ group of SDS. Yin *et al.* reported that the $–NH_2$ functional group of MOF can be present in protonated ($-NH_3^+$) form in the aqueous medium.[38] The presence of $–NH_2$ groups in protonated form was proved by measuring the fluorescence intensity of the MOF in EtOH-H_2O mixture. It was observed that **1′** displays high fluorescence intensity in EtOH medium but the intensity gradually decreased with the increase in concentration of H_2O (Figure 2.26). This experiment concludes that $–NH_2$ groups of the linker are present in protonated ($-NH_3^+$) form in aqueous medium.

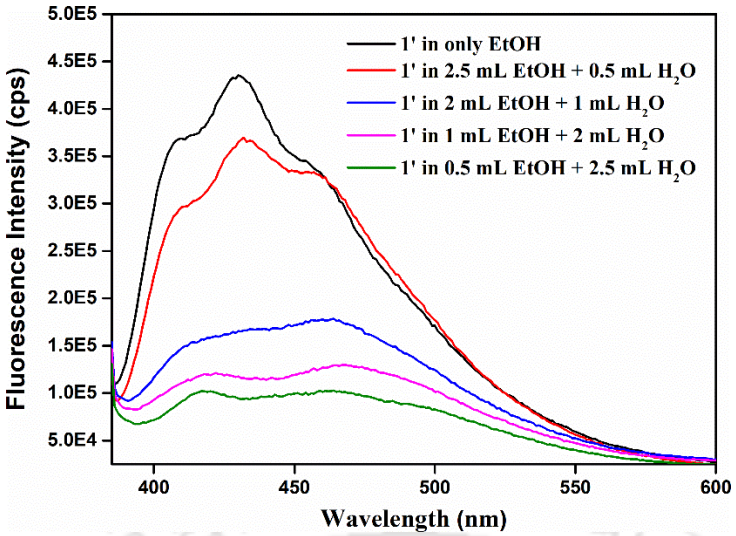

Figure 2.26 Change in fluorescence intensity of **1′** in different ratio of EtOH and H_2O.

The prior literature suggests that the dipolar interactions between the $–NH_3^+$ and $–SO_3^-$ groups are possible in aqueous medium.[39] Zeta potential measurement is an effective method for proving electrostatic interactions. In literature, numerous electrostatic interactions-related sensing processes have been demonstrated by comparing the value of the zeta potential before and after the addition of the targeted sensing analyte.[40] Here, **1′** displays zeta potential values of +33.3 and -32.1 mV, respectively, before and after the addition of SDS (Figure 2.27). The presence of electrostatic interactions between **1′** and SDS was once more corroborated by this change in zeta potential value.

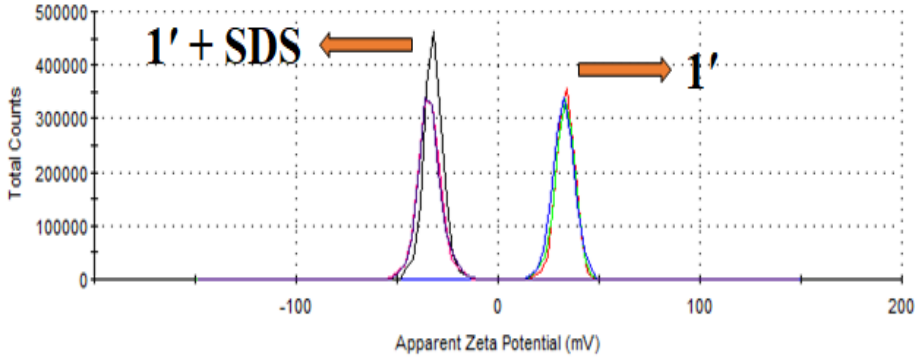

Figure 2.27 Change in Zeta potential value of **1′** before and after addition of SDS in aqueous medium.

According to the previous literature, the electrostatic interaction can deteriorate in the presence of salt solution (like NaCl).[41, 42] Figure 2.28 evidences that the increment in emission response after addition of SDS solution gradually decreases with the increase of concentration of NaCl (0-50 mM) in the sensing medium. The observed increment in emission response was ~18.9 folds after SDS addition in absence of any external electrolyte. But, with the increase in the concentration of NaCl in the sensing medium from 5 to 50 mM, the switch-on in emission response steadily decreased from 11 to 5.5 folds. This finding confirmed the existence of

electrostatic interactions between **1′** and SDS, which were hampered up by the presence of NaCl solution.

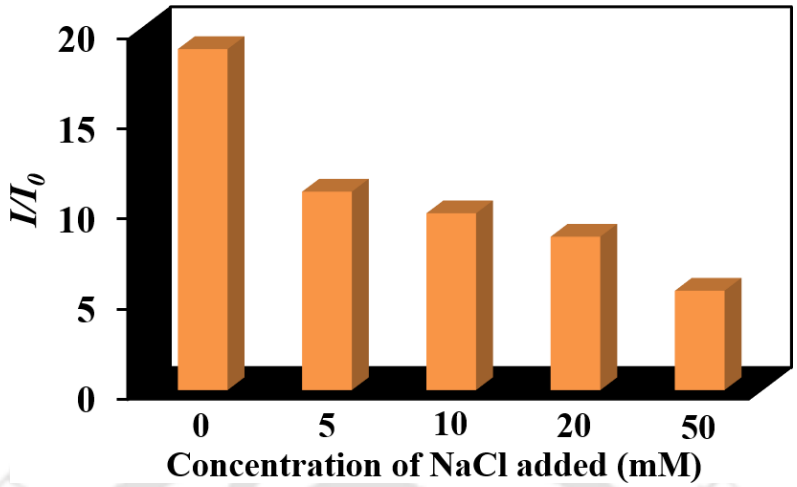

Figure 2.28 Change in fold increments of **1′** with the increasing concentration of NaCl in the sensing medium.

Electrostatic interactions are exothermic in nature.[39] To verify the same, we also performed the isothermal titration calorimetry experiment. The experiment indicates the formation of complex between SDS and the $H_2BDC\text{-}(NH_2)_2$ linker with a molar ratio of 2:1 (Figure 2.29). The exothermic nature of complexation and the decrease in entropy of binding (ΔS) after the addition of SDS solution again supported the electrostatic interaction mechanism (Table 2.7).

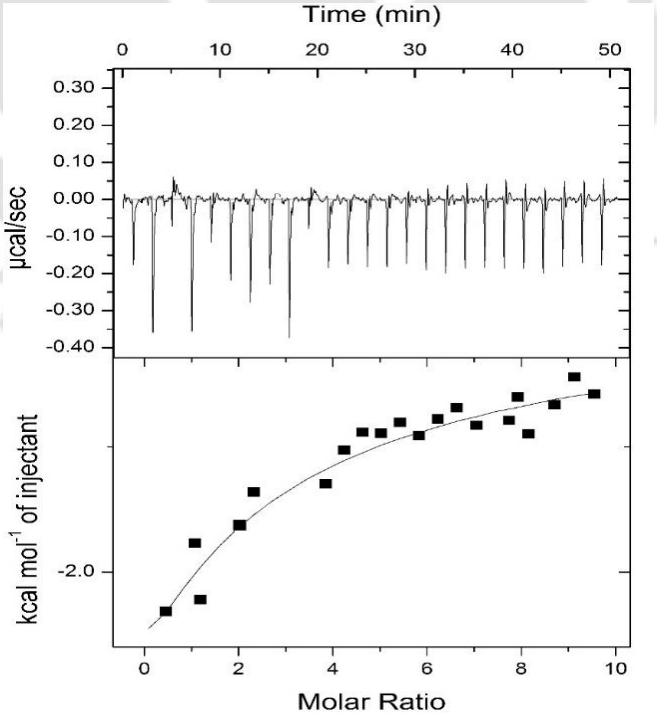

Figure 2.29 Isothermal titration calorimetry (ITC) of $H_2BDC\text{-}(NH_2)_2$ linker upon gradual addition of SDS solution.

Table 2.7 ITC thermogram enthalpy and entropy values in each step upon gradual addition of SDS solution.

Binding Constant (K_i) in M^{-1}	Enthalpy Change (ΔH) in $calmol^{-1}$	Entropy Change (ΔS) in $calmol^{-1}deg^{-1}$
$3.96E^4 \pm 6.0\ E^4$	$-5594 \pm 4.65\ E^3$	- 2.58
$3.15\ E^3 \pm 2.3\ E^3$	$-2.223\ E^4 \pm 1.16\ E^4$	+ 57.3

The sensing experiment was also executed in the pH range of 2-12. Figure 2.30 suggests that the increment in fluorescence intensity gradually decreases with the increase of pH value. Such observation further supported the electrostatic interaction mechanism. With the increase in pH of the medium, the $–NH_3^+$ groups present in the medium were converted to $–NH_2$. Therefore, the electrostatic interactions between $–NH_3^+$ and $–SO_3^-$ groups decreased and the corresponding turn-on response decreased.

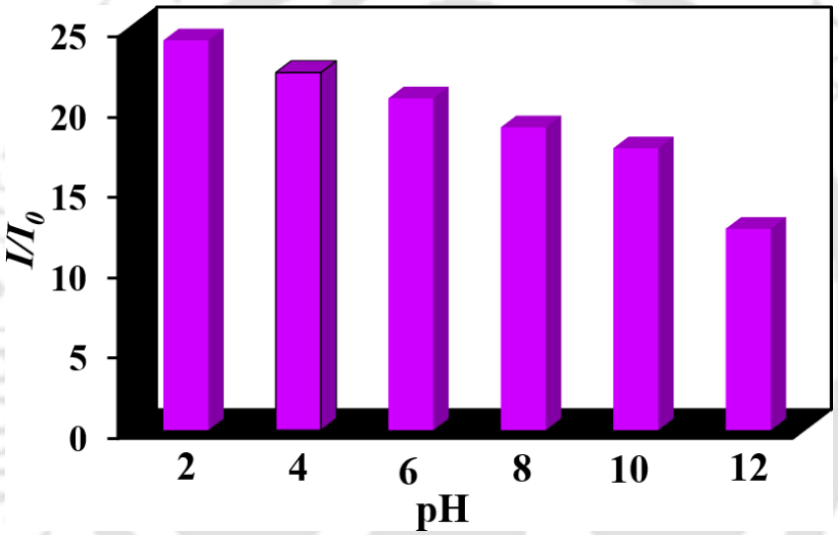

Figure 2.30 Change in fold increments of **1′** with the increase of pH of the sensing medium.

Finally, the most conclusive evidence of the presence of electrostatic interaction was proved by XPS analysis of the fresh and SDS-treated MOF samples. Figures 2.31-2.35 show that the binding energies of C (1s), Zr (3d) and O (1s) did not change before and after the treatment of SDS. A clear shift of the binding energy of N 1s orbital (from 400.00 eV to 399.78 eV) was observed for the SDS treated MOF. The shift of binding energy of N 1s orbital strongly supported the presence of electrostatic interactions between SDS and the **1′** (Scheme 2.2). Because of this interaction, charge transfer occurs from the $–SO_3^-$ group of SDS to the electron withdrawing ($-NH_3^+$) functional groups of **1′**, which results in 'turn-on' response.

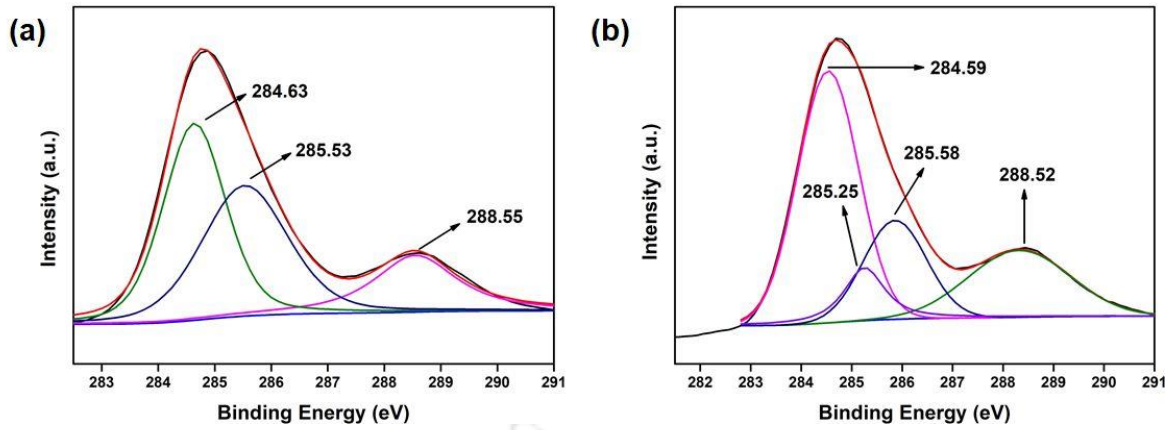

Figure 2.31 Fitted XPS spectra of C (1s) before (a) and after (b) treatment of **1′** with SDS.

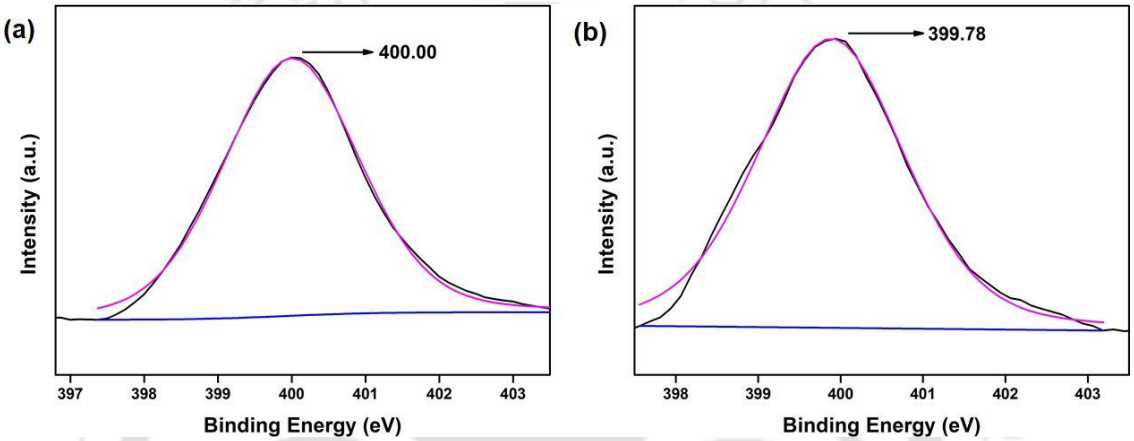

Figure 2.32 Fitted XPS spectra of N (1s) before (a) and after (b) treatment of **1′** with SDS.

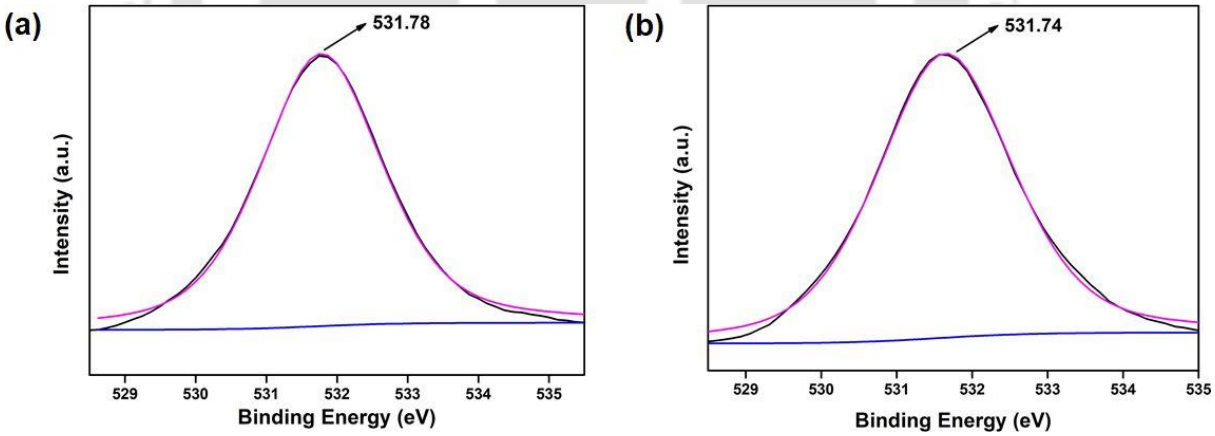

Figure 2.33 Fitted XPS spectra of O (1s) before (a) and after (b) treatment of **1′** with SDS.

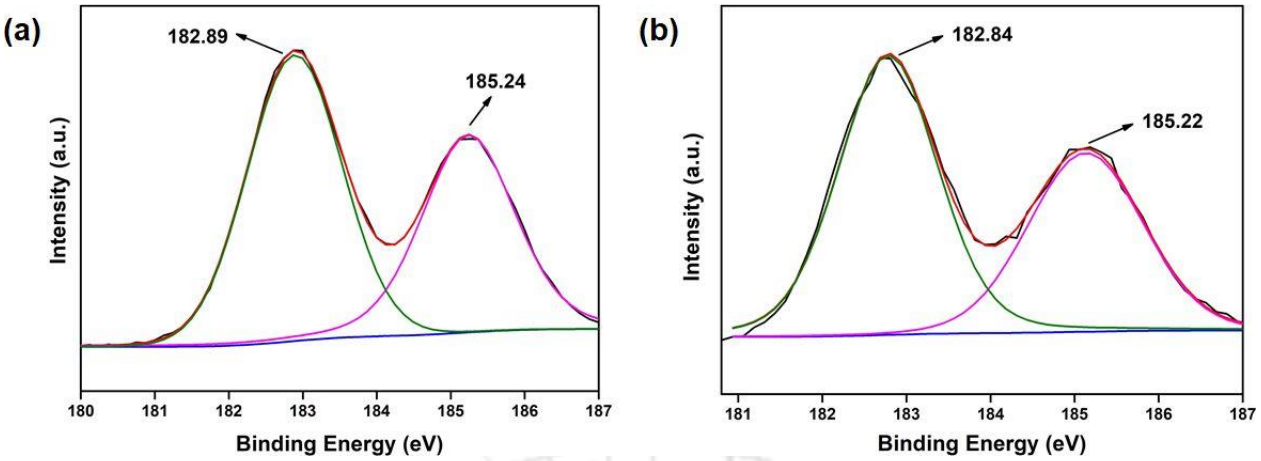

Figure 2.34 Fitted XPS spectra of Zr (3d) before (a) and after (b) treatment of **1′** with SDS.

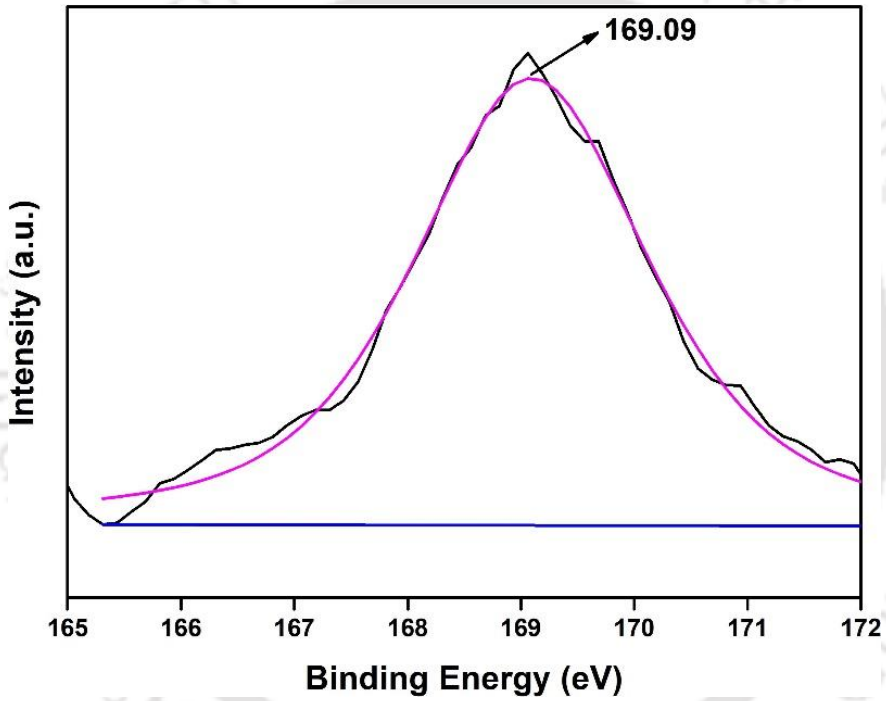

Figure 2.35 Fitted XPS spectrum of S (2p) after treatment of **1′** with SDS.

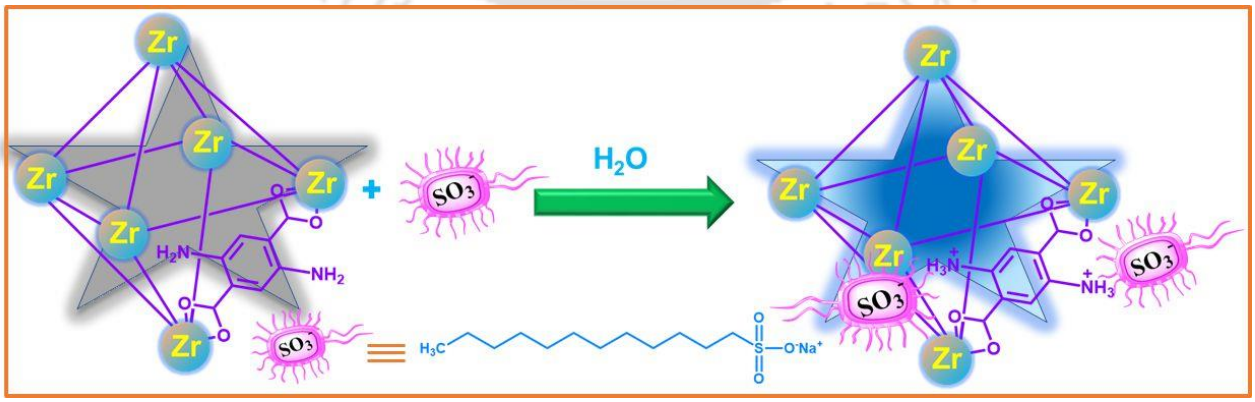

Scheme 2.2 Schematic representation of SDS sensing.

2.3.9 Sensing of Vitamin B_{12} in HEPES Buffer

Both higher and lower concentrations of vitamin B_{12} in the human body cause several disorders.[16] Therefore, it is very important to determine the exact concentration of vitamin B_{12} in various body fluids. Previous literature reports suggested that vitamin B_{12} has three absorption maxima at 278, 361 and 550 nm. Out of them, the maxima at 361 nm and 550 nm are within the emission range of **1′** (in HEPES buffer) (Figure 2.36). This fact made us interested to check the emission response of **1′** in presence of vitamin B_{12}. In practice, >99% quenching in fluorescence was observed after 5 s of addition of 300 µL of 5 mM solution of vitamin B_{12} (Figures 2.37-2.38).

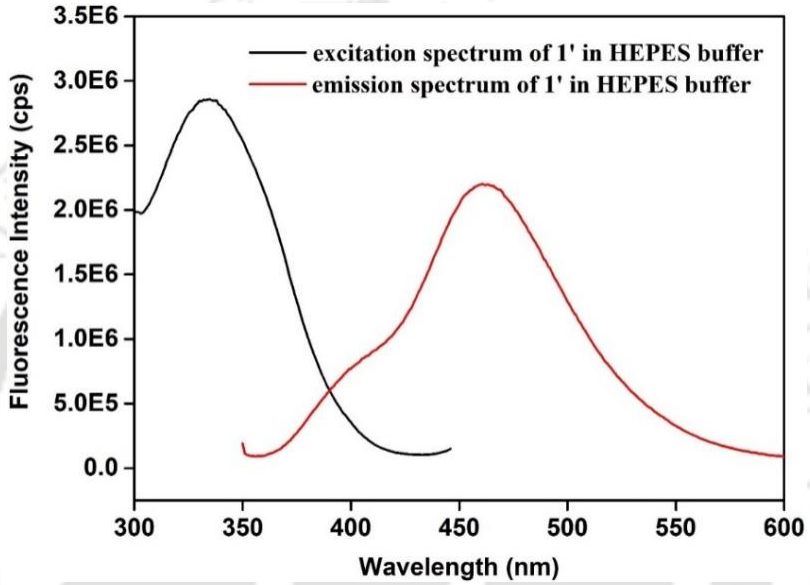

Figure 2.36 Excitation (black) and emission (red) spectra of **1′** in HEPES buffer.

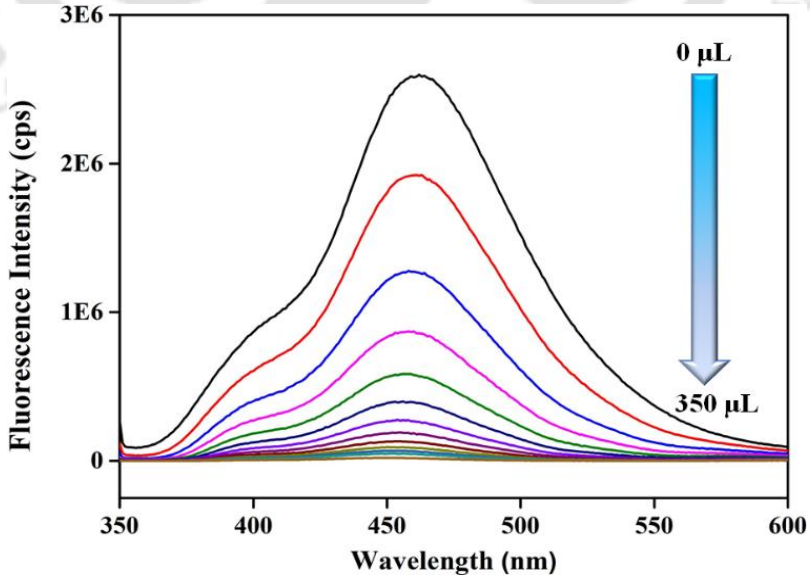

Figure 2.37 Quenching in the fluorescence spectrum of **1′** in HEPES buffer with step-wise addition (0 to 350 µL) of 5 mM vitamin B_{12} solution.

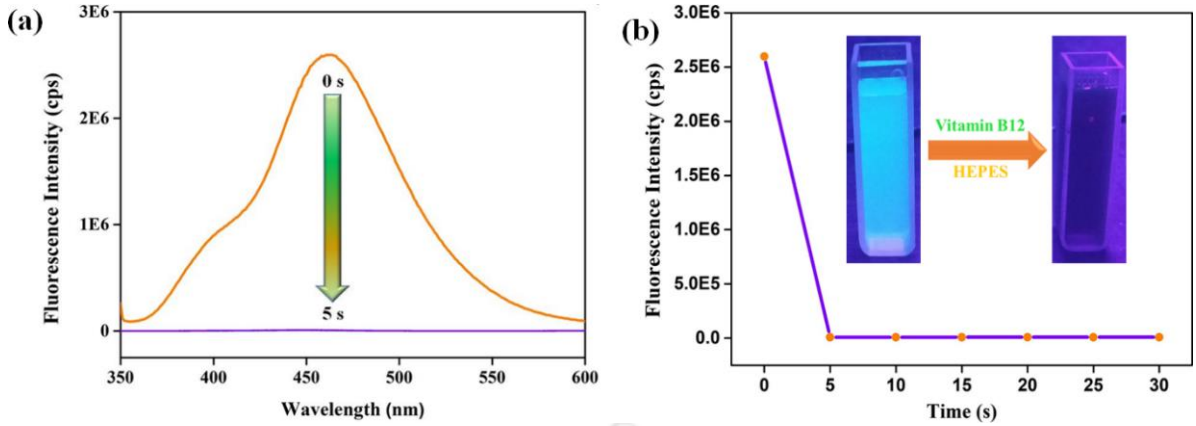

Figure 2.38 (a) Quenching in the fluorescence spectrum of **1′** in HEPES buffer as a function of time after addition of 350 µL of 5 mM vitamin B_{12} solution. (b) Time dependent saturation plot (luminescence colour change of **1′** under UV-lamp after injection of vitamin B_{12} displayed in inset figure of 2.36b).

Such rapid and significant decrease in emission intensity of **1′** motivated us to check the selectivity of the sensing in presence of other commonly available bio-molecules and metal ions in human serum and urine. The aim of this study was to prove the potential applicability of the probe for selective sensing and measuring the concentration of vitamin B_{12} in various bio-fluids. Figures 2.39-2.40 clearly signify the selectivity of the sensor in presence of all the used competitive analytes and other vitamins. Selectivity remained intact even in presence of other 'B' vitamins (Figure 2.41). Recyclability test has shown that the probe was recyclable up to five cycles of sensing without loss of its efficiency (Figure 2.42).

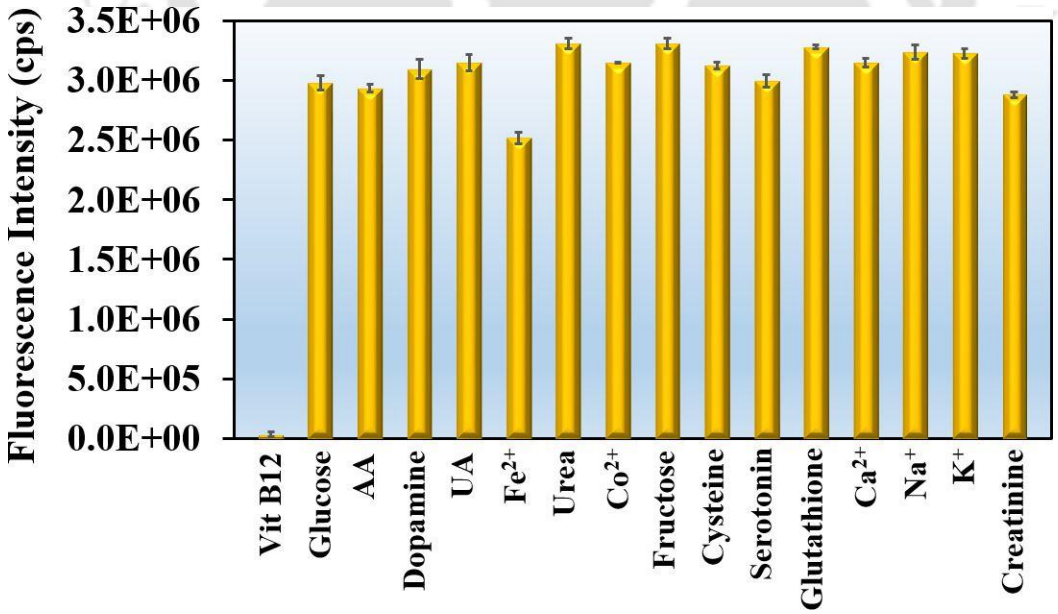

Figure 2.39 Selectivity test of **1′** for the sensing of vitamin B_{12}.

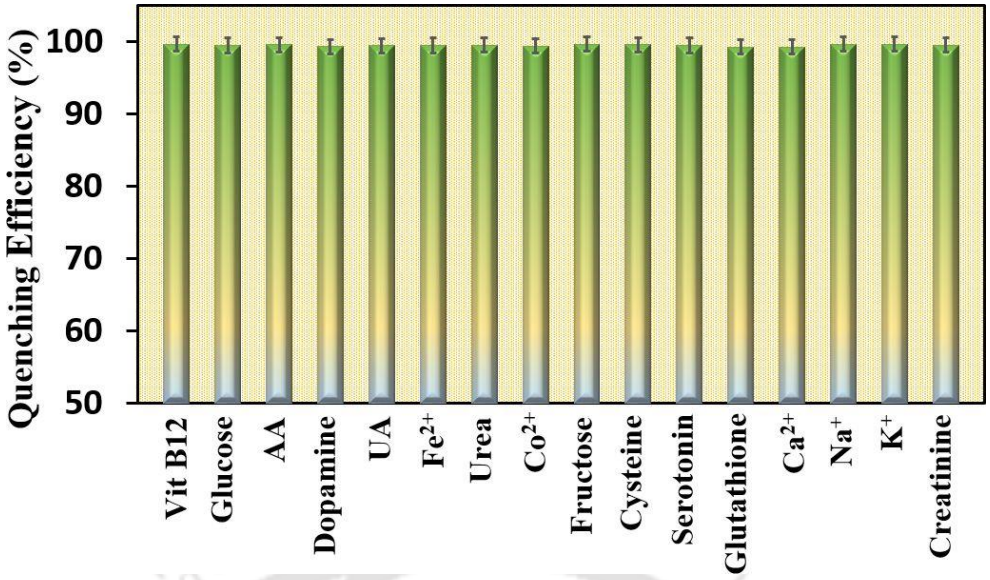

Figure 2.40 Selectivity test for the sensing of vitamin B_{12} in the presence of other competitors (error bars represent the standard deviations of three individual measurements).

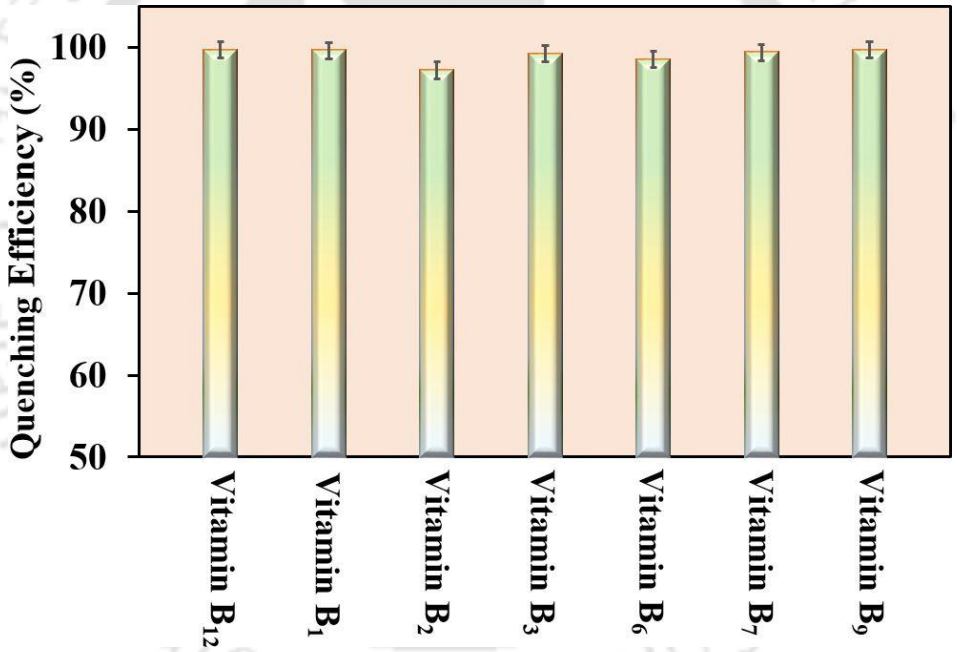

Figure 2.41 Quenching efficiencies of **1′** after adding 300 µL of 5 mM vitamin B_{12} solution in presence of 300 µL 5 mM different vitamin B solutions in HEPES buffer medium (λ_{ex} = 335 nm, λ_{em} = 462 nm).

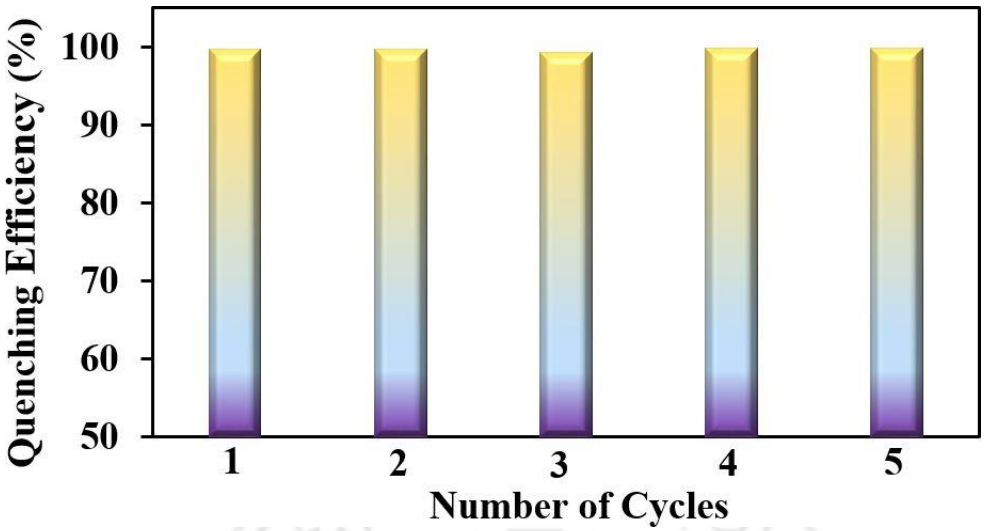

Figure 2.42 Recyclability test of **1′** towards the sensing of vitamin B_{12} in HEPES buffer medium.

The LOD and LOQ values were determined following the same procedure used in case of SDS sensing (Figure 2.43 and Table 2.8). The obtained LOD and LOQ of the MOF for the sensing of vitamin B_{12} were 45.3 ± 4.2 and 150.9 ± 13.9 nM, respectively which are much lower than the previously reported sensors of vitamin B_{12} (Table 2.9). All the measurements were statistically analyzed and errors after three distinct measurements were identified to assure the reproducibility and originality of each measurement. Intra-day (Table 2.10) and inter-day (Table 2.10) accuracy and precision of the sensing experiments were also examined.

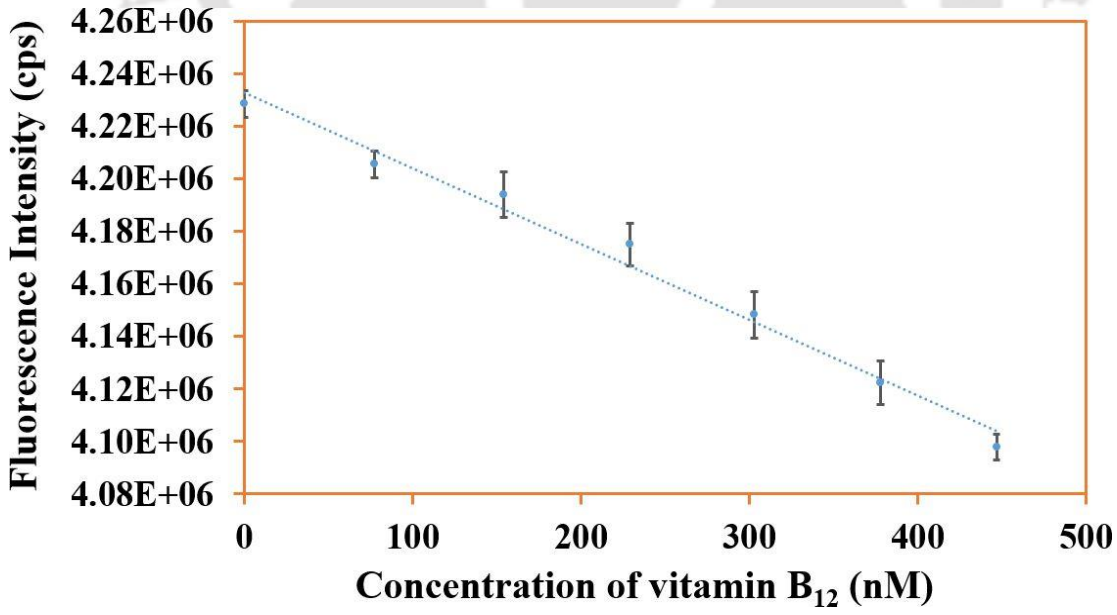

Figure 2.43 Change in the fluorescence emission intensity of **1′** in HEPES as a function of concentration of vitamin B_{12}.

Table 2.8 Statistical details of different analytical parameters for the sensing of vitamin B_{12} by **1′.**

Concentration Range (nM)	Slope	Intercept	Correlation Coefficient (R^2)	$S_{y/x}$ [a]	LOD[b] (nM)	LOQ[c] (nM)	Regression Equation
0-480	-256.3	4228913	0.994	3818.9	42.5	141.7	-256.3x + 4228913
	-263.9	4236470	0.995	4499.7	50.0	166.9	-263.9x + 4236470
	-345.1	4233025	0.999	3884.3	43.2	144.1	-345.1x + 4233025
Average	-288.4	4232803	0.996	4067.7	45.3	150.9	-288.4x + 4232803
SD	49.2	3783.4	0.002	375.7	4.2	13.9	(-288.4±49.2)x + (4232803 ± 3783.4)

[a] Standard deviation of the residuals, [b] Limit of detection, [c] Limit of quantification

Table 2.9 Comparison of the present probe (**1′**) with some previous probes of vitamin B_{12}.

Sl. No.	Sensor Material	Type of Material	Sensing Medium	Detection Limit (nM)	Response Time (s)	Detection Method	Ref.
1	bovine serum albumin (BSA) and thiosalicylic acid capped AuAgNCs	nanocluster	water	71	-	fluorescence	43
2	BSA capped AuNCs	nanocluster	PBS	73.8	-	fluorescence	44
3	citric acid and safranine T derived carbon dots	carbon dots	water	60.78	30	fluorescence	45
4	saccharomycetes and ethanediamine deived carbon dots	carbon dots	PBS	2190	30	fluorescence	46
5	citric acid derived carbon dots	carbon dots	water	100	-	fluorescence	47
6	LYS-AgNCs	silver nanoclusters	water	48	-	fluorescence	48
7	$[Zr_6O_4(OH)_4(C_8H_6N_2O_4)_6]$ (**1′**)	MOF	HEPES	45.3	< 5	fluorescence	this work

Table 2.10 Evaluation of intra-day, inter-day accuracy and precision study of change in fluorescence intensity of **1′** after incremental addition of 5 mM aqueous solution of vitamin B_{12}.

Parameter	Amount of Vitamin B_{12} Added (μL)	Fluorescence Intensity (cps) at λ_{max} = 462 nm			Average PL Intensity (cps)	SD	RE%
	0	2783690	2783590	2770060	2779113	7840.6	0.164
	50	1265190	1258260	1263380	1262277	3594.3	0.230

repeatability	100	567723.1	568339.4	560848.5	565637	4158.4	0.367
intra-day	150	262734.5	256101.2	257137.2	258657.6	3568.5	1.552
precision	200	123803.4	122938.0	120256.3	122332.6	1849.4	1.880
	250	62376.5	60596.3	60779.9	61284.29	946.8	1.751
	300	17609.3	17219.4	16860.9	17229.9	374.3	2.155
reproducibility	0	2584920	2783690	2591480	2653363	112913.9	4.681
inter-day	50	1246480	1265190	1238860	1250177	13548.6	1.186
precision	100	561666	567723	552425	560605	7703.5	1.253
	150	253756.2	262734.5	246847.8	254446.1	7965.8	3.155
	200	118667.4	123803.4	115711.7	119394.2	4094.5	3.562
	250	59860.0	62376.5	57820.6	60019.0	2282.1	3.779
	300	17048.6	17609.3	15624.4	1195843	1023.2	4.818

Drawing the S-V plot and determining of S-V constant is necessary to understand the precise mechanism causing the quenching of fluorescence intensity after the addition of vitamin B_{12} to the suspension of **1′** (Figure 2.44). The K_{sv} value of this quenching procedure was calculated using the mathematical formula: $I_0/I = K_{sv}[Q] + 1$. The intensities of the MOF suspension before and following the treatment of various analytes are represented in the formula by I_0 and I, respectively. [Q] specifies the concentrations (in molar) of specific analytes. The measured K_{sv} value for sensing vitamin B_{12} was 5.3×10^4 M^{-1} (Figure 2.45), which is higher than the majority of vitamin B_{12} sensors that have previously been reported.

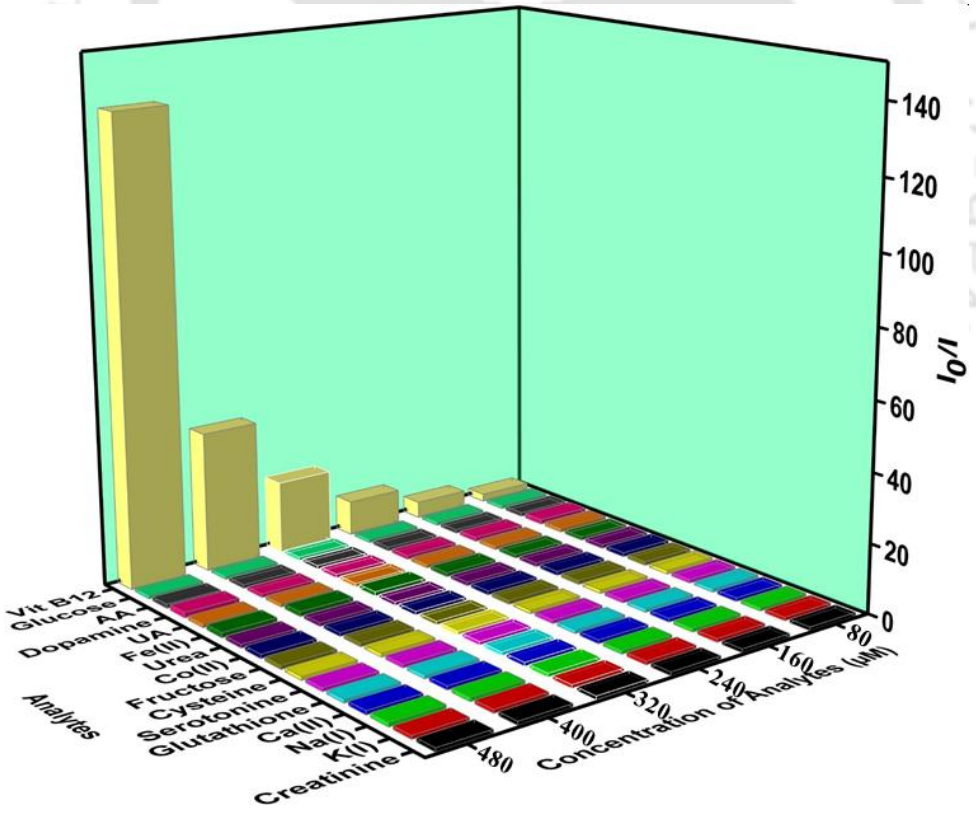

Figure 2.44 S-V plots for the decrease in luminescence intensities of **1′** with gradual addition of various analytes in case of vitamin B_{12} sensing.

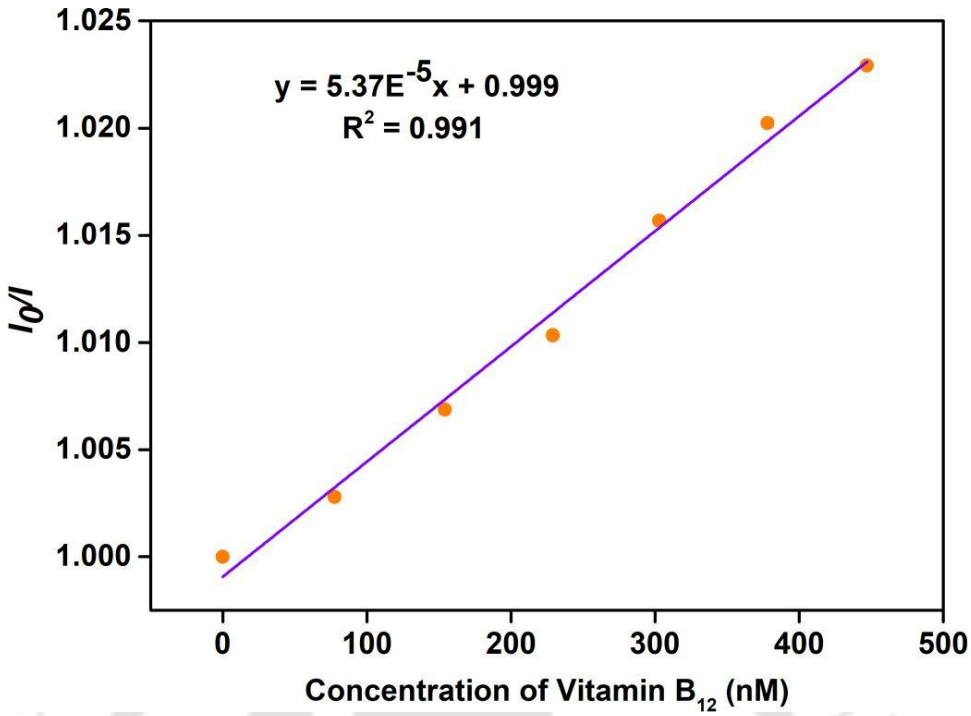

Figure 2.45 Stern-Volmer plot for the fluorescence emission quenching of **1′** in presence of vitamin B_{12} sensing.

2.3.10 Sensing of Targeted Analytes in MOF@cotton Composite

Reusability of the probe towards both sensing encouraged us for the preparation of MOF@cotton composite for on-site detection of SDS and vitamin B_{12}. In the previously reported literature, sensor-coated filter paper strip technology was utilized for the on-site sensing of targeted analytes.[5, 9] The use of paper strips has various downsides. Paper strips are often not reusable because they are readily brittle in the presence of solvents. Thus, these are not user-friendly for a recyclable sensor. A cotton composite is durable, hygienic, and reusable. As a result, we developed MOF@cotton composites and tested their capacity to detect SDS and vitamin B_{12}. For this experiment, two little pieces of cotton fabric were evenly covered with the MOF suspension and they were dried in a 60 °C oven. The successful fabrication of the MOF particles on the cotton fabric was confirmed by PXRD and ATR-IR measurements (Figures 2.46-2.47). Thereafter, one composite was treated with SDS solution and after treatment, both SDS-treated and fresh composites were placed under UV light. Under UV light, the SDS-treated composite displayed strong blue colour fluorescence, but the untreated composite was less fluorescent (Figure 2.48). Similar test was performed in case of vitamin B_{12} but opposite trend was noticed for the fluorescence change of the composite. We also determined the LOD of SDS and vitamin B_{12} detection using the cotton composite by treating the composite with different concentrations of analyte solutions. The results revealed nanomolar level detection ability of the composite for both analytes (Figure 2.48).

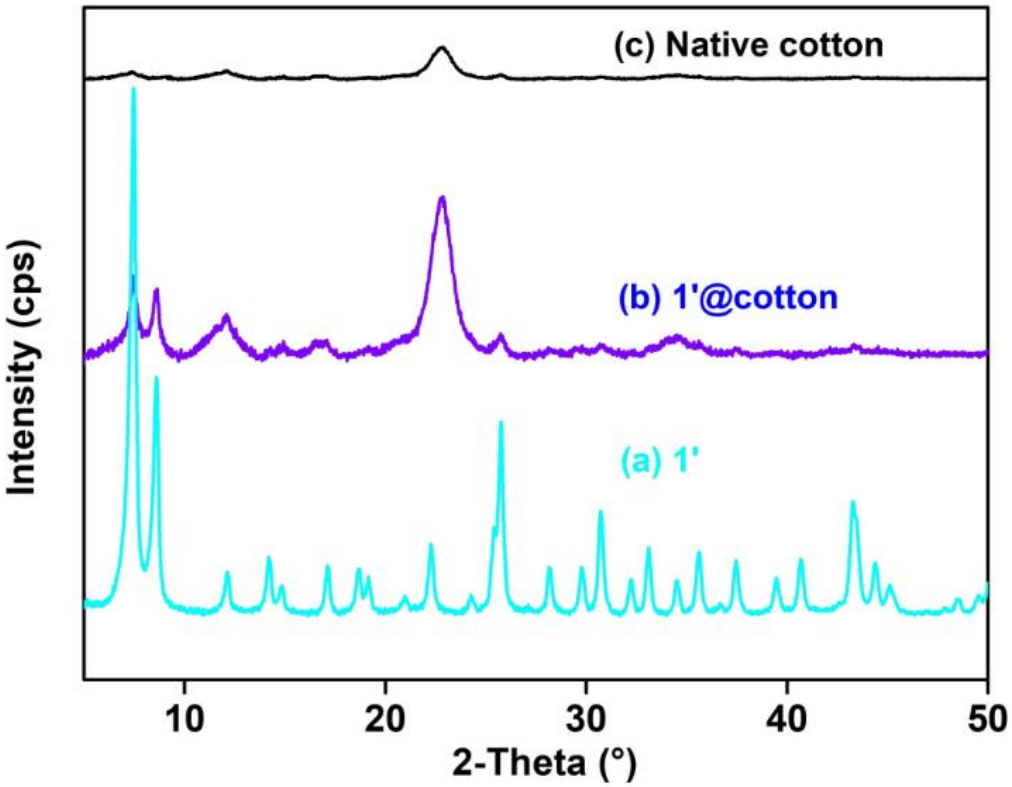

Figure 2.46 PXRD patterns of compound (a) **1′**, (b) **1′@cotton** composite and (c) native cotton**.**

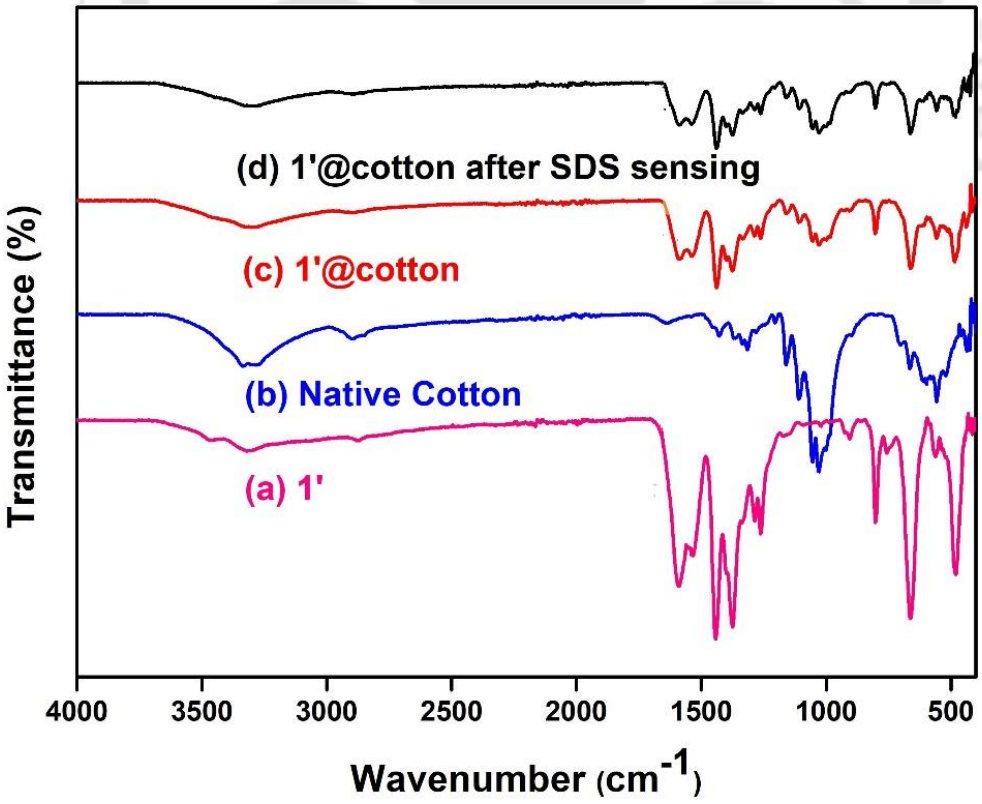

Figure 2.47 ATR-IR spectra of compound (a) **1′**, (b) native cotton, (c) **1′@cotton** composite.

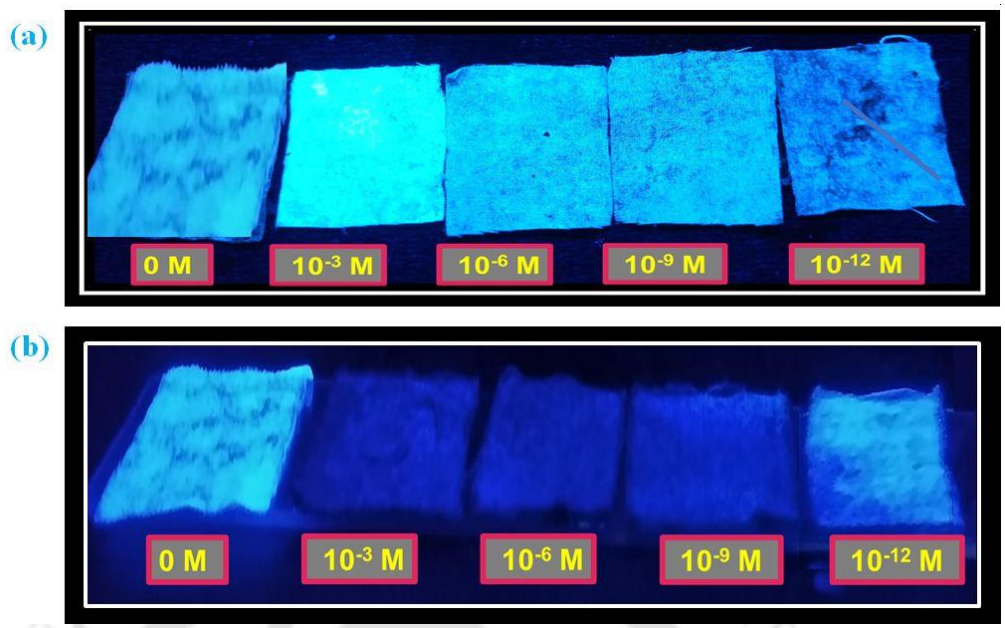

Figure 2.48 Images of **1′@cotton** composites under UV lamp after treatment with (a) SDS (b) vitamin B_{12} solutions having different concentrations.

2.3.11 Sensing of Vitamin B_{12} in Human Bio-Fluids and Various pH Media

The lowest vitamin B_{12} concentrations of a healthy human's serum and urine are 200-900 ng/mL and 160-950 ng/mL, respectively.[16] The sensing ability of **1′** is up to 45.3 nM which is lower than the concentration of vitamin B_{12} present in human bio-fluids. This fact inspired us to check the sensing ability of the probe toward vitamin B_{12} in human serum and urine samples (Figures 2.49-2.50). The fluorescence intensity of the probe decreased by >99% after the treatment of vitamin B_{12}-infused serum and urine samples (in both cases) in HEPES buffer. The obtained concentrations of vitamin B_{12} were compared with the spiked concentrations of vitamin B_{12} and recovery percentages were calculated which were ~100% for all the measurements (Tables 2.11-2.12). Figure 2.51 displays the sensing ability of the probe in different pH media. The probe can sense vitamin B_{12} up to pH 10. At highly basic pH, the MOF lost its sensing efficiency due to loss of its structural integrity. These findings imply that the MOF is capable of sensing vitamin B_{12} in human urine and serum samples. The material can thus be used as a diagnostic tool to identify several disorders linked to aberrant vitamin B_{12} levels in body fluids.

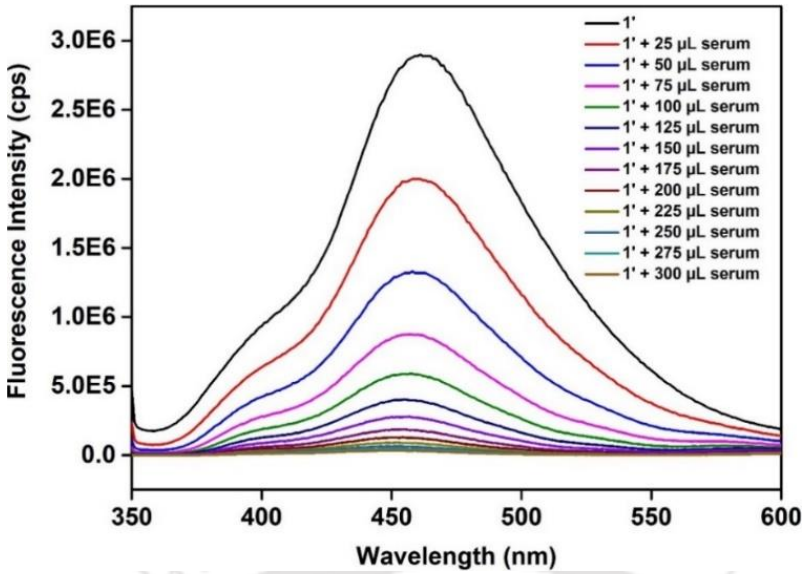

Figure 2.49 Turn-off in fluorescence emission intensity of the suspension of **1′** in HEPES buffer medium after addition of 5 mM of different volumes of vitamin B_{12}-spiked serum solution.

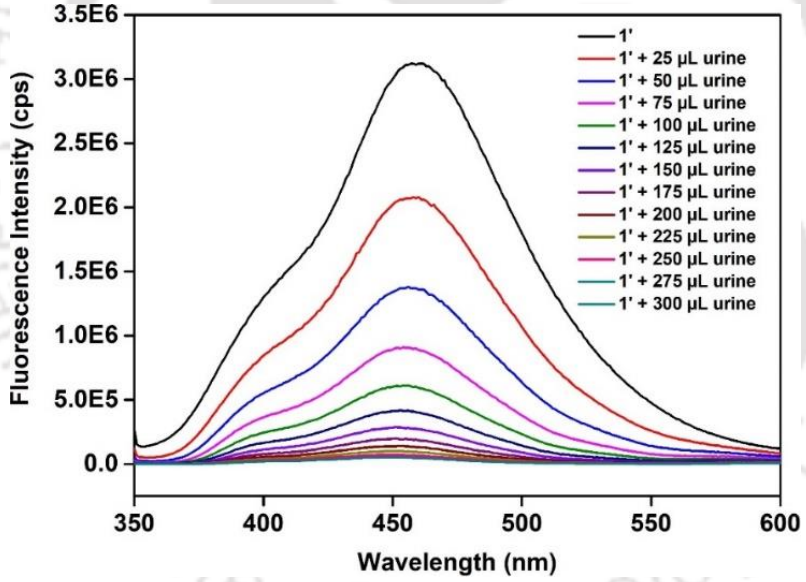

Figure 2.50 Turn-off in fluorescence emission intensity of the suspension of **1′** in HEPES buffer medium after addition of 5 mM different volumes of vitamin B_{12}-spiked urine solution.

Table 2.11 Detection of vitamin B_{12} in human serum samples.

Vitamin B_{12} Spiked (mol L^{-1})	Vitamin B_{12} Found (mol L^{-1})	Recovery (%)	RSD (%) (n=3)
1.54×10^{-4}	1.52×10^{-4}	98.7	1.52
3.03×10^{-4}	3.05×10^{-4}	100.6	0.56
4.47×10^{-4}	4.44×10^{-4}	99.3	2.51
5.88×10^{-4}	5.84×10^{-4}	99.3	2.20
7.24×10^{-4}	7.15×10^{-4}	98.7	1.05
8.57×10^{-4}	8.60×10^{-4}	100.3	0.59

Table 2.12 Detection of vitamin B_{12} in human urine samples.

Vitamin B_{12} spiked (mol L^{-1})	Vitamin B_{12} found (mol L^{-1})	Recovery (%)	RSD (%) (n = 3)
1.54×10^{-4}	1.48×10^{-4}	96.1	0.48
3.03×10^{-4}	3.04×10^{-4}	100.3	2.39
4.47×10^{-4}	4.48×10^{-4}	100.2	1.59
5.88×10^{-4}	5.89×10^{-4}	100.1	1.75
7.24×10^{-4}	7.26×10^{-4}	100.2	1.95
8.57×10^{-4}	8.55×10^{-4}	99.7	2.68

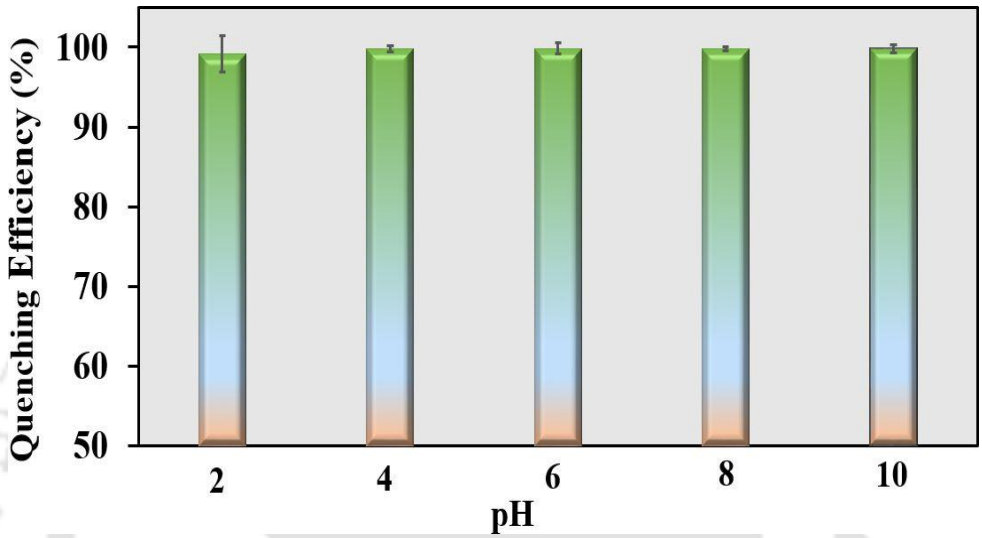

Figure 2.51 Quenching efficiencies of **1′** after adding 300 µL of 5 mM vitamin B_{12} solution in different pH solutions (λ_{ex} = 335 nm, λ_{em} = 462 nm).

2.3.12 Mechanism of Vitamin B_{12} Sensing

The integrity of the framework of the MOF after five conjugative cycles of vitamin B_{12} sensing (Figures 2.52-2.53) and reusability of the sensor with almost equal efficiency (Figure 2.54) confirmed that the mechanism is not reaction based. As previously mentioned, the absorbance maxima of vitamin B_{12} lie within the emission range of **1′** which inspired us to consider energy transfer mechanistic processes.[25] There are a few fundamental events documented in the literature (molecular collisions, excited-state reaction, ground-state complexation, inner filter effect (IFE) and excited-state energy transfer process) which can be responsible for the non-reaction-based energy transfer process.[49] All these events can be divided into two categories of quenching processes: static and dynamic quenching processes. The main causes of dynamic quenching are the diffusion of quencher molecules into the fluorophore's excited state and collisions between the fluorophore and the quencher molecules. On the other hand, static quenching may happen when the fluorophore and the quencher molecules are tightly bound together.[49]

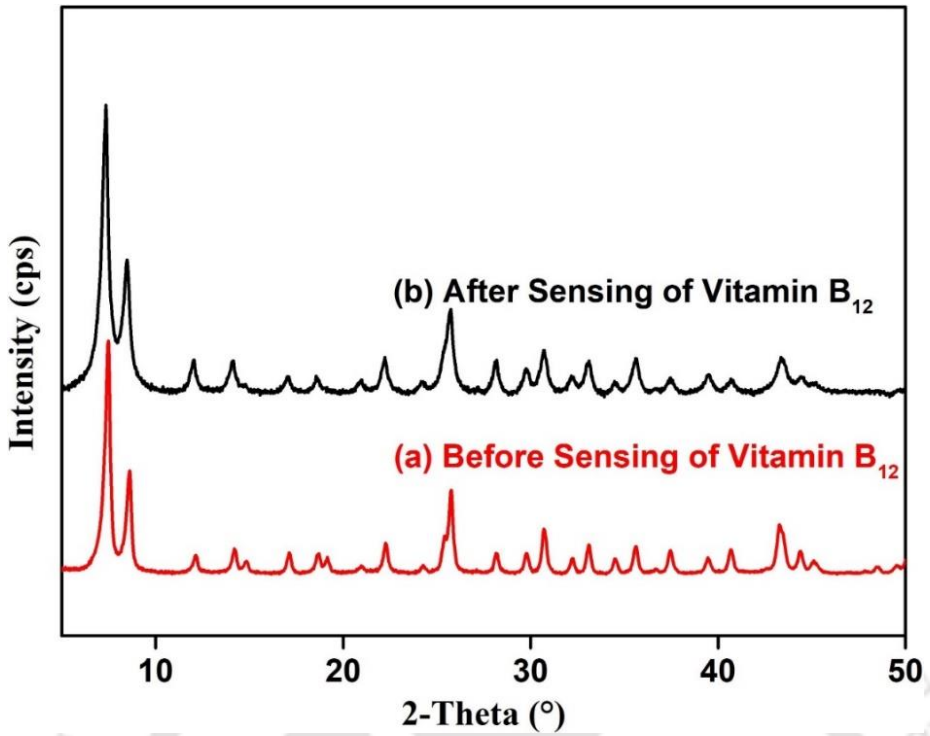

Figure 2.52 PXRD patterns of compound **1′** before (a) and after (b) treatment with vitamin B_{12} in HEPES buffer medium.

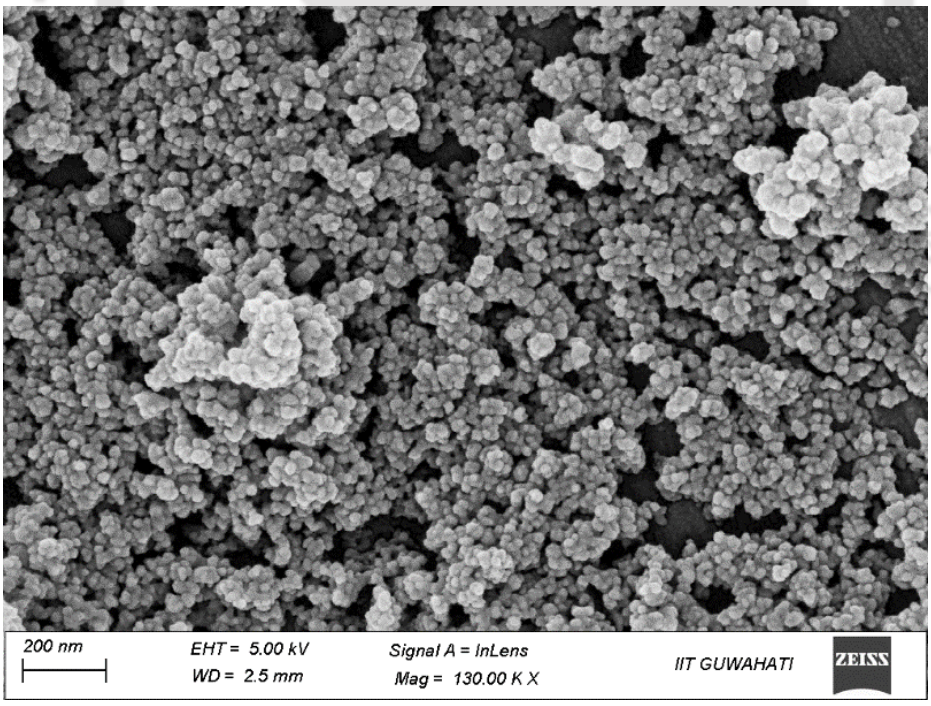

Figure 2.53 FESEM of **1′** after vitamin B_{12} sensing in HEPES buffer medium.

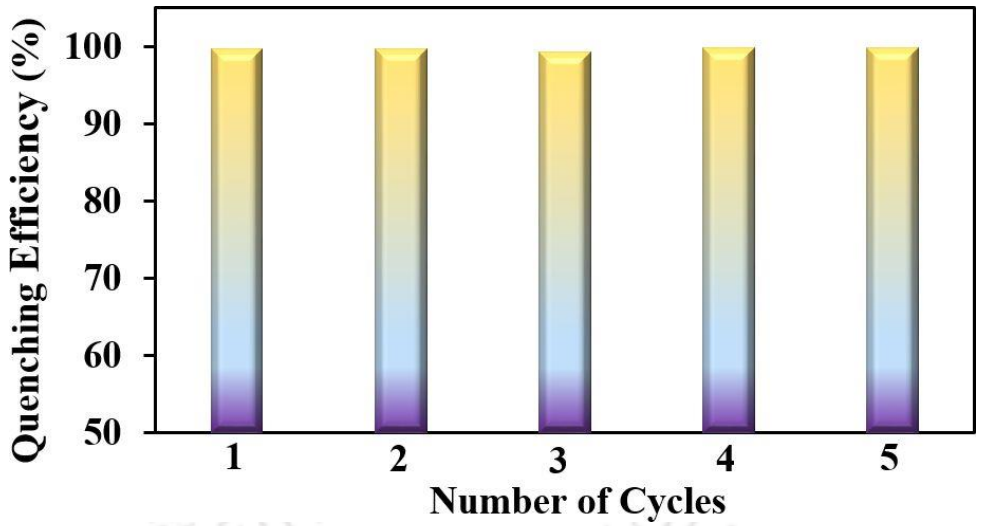

Figure 2.54 Recyclability test of **1′** towards the sensing of vitamin B_{12} in HEPES buffer medium.

The type of quenching can be confirmed by the measurement of the fluorescence lifetime of the sensor before and after the addition of the targeted analyte. Static quenching occurs when the fluorescence lifetime of the excited state fluorophore does not change even after the addition of a quencher molecule. But, the process is dynamic if the fluorescence lifetime diminishes. Herein, the lifetime changed from 12.9 ns to 7.7 ns after the addition of vitamin B_{12} solution to the suspension of MOF (Figure 2.55 and Table 2.13), which confirmed the dynamic nature of quenching. Dynamic quenching canceled out the possibilities of static quenching and IFE.

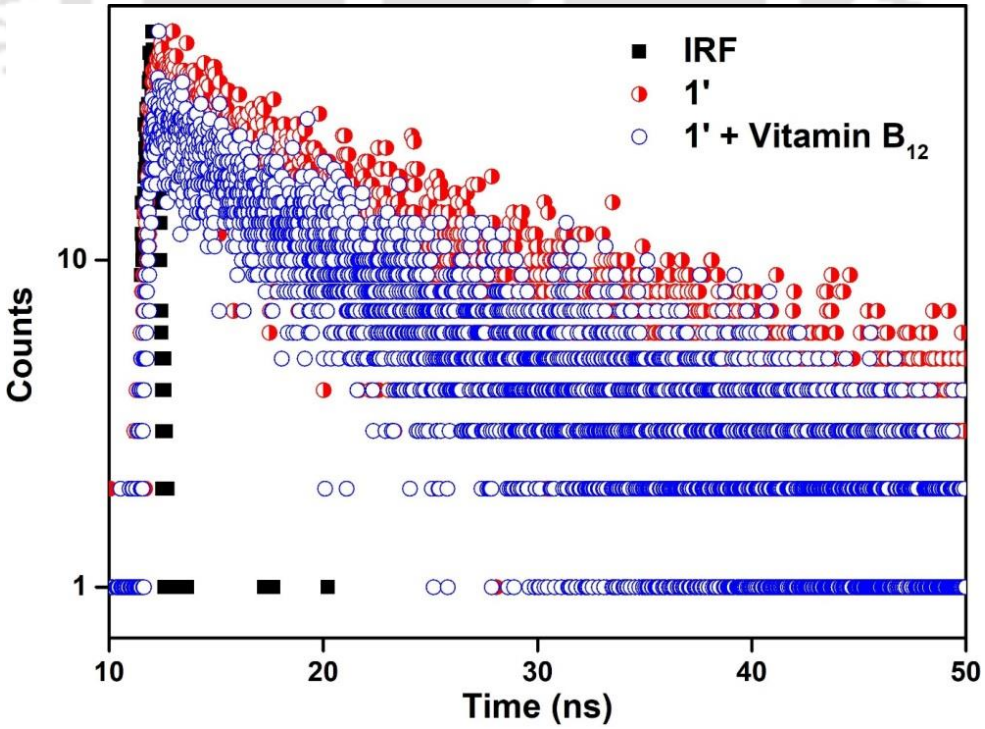

Figure 2.55 Lifetime decay profile of **1′** in absence and presence of vitamin B_{12} solution (λ_{ex} = 335 nm, monitored at 336 nm). Here, IRF = instrument response function.

Table 2.13 Fluorescence lifetimes of **1′** before and after the addition of vitamin B_{12} solution (λ_{ex} = 336 nm, pulsed diode laser).

Volume of Vitamin B_{12} Solution Added (µL)	a_1	a_2	τ_1 (ns)	τ_2 (ns)	$<\tau>$*(ns)	χ^2
0	0.17	0.83	3.28	14.87	12.9	1.047
300	0.04	0.96	0.58	8.01	7.7	1.004

* $<\tau> = a_1\tau_1 + a_2\tau_2$

We collected the UV-Vis spectra of all the used analytes and overlaid the normalized absorption spectra with the emission spectrum of **1′** to examine the cause of the quenching process in detail. Only the absorption spectrum of vitamin B_{12} and the emission spectrum of **1′** clearly showed the greatest overlap in Figure 2.56. No overlap was visible for any of the other used analytes. Such overlap ensured the resonance energy transfer from **1′** to vitamin B_{12}, which is the most possible mechanism behind this selective quenching of fluorescence of **1′** in the presence of vitamin B_{12}. The mechanism outlined above was used in many of the quenching-based sensing procedures reported in the literature.[2, 49, 50]

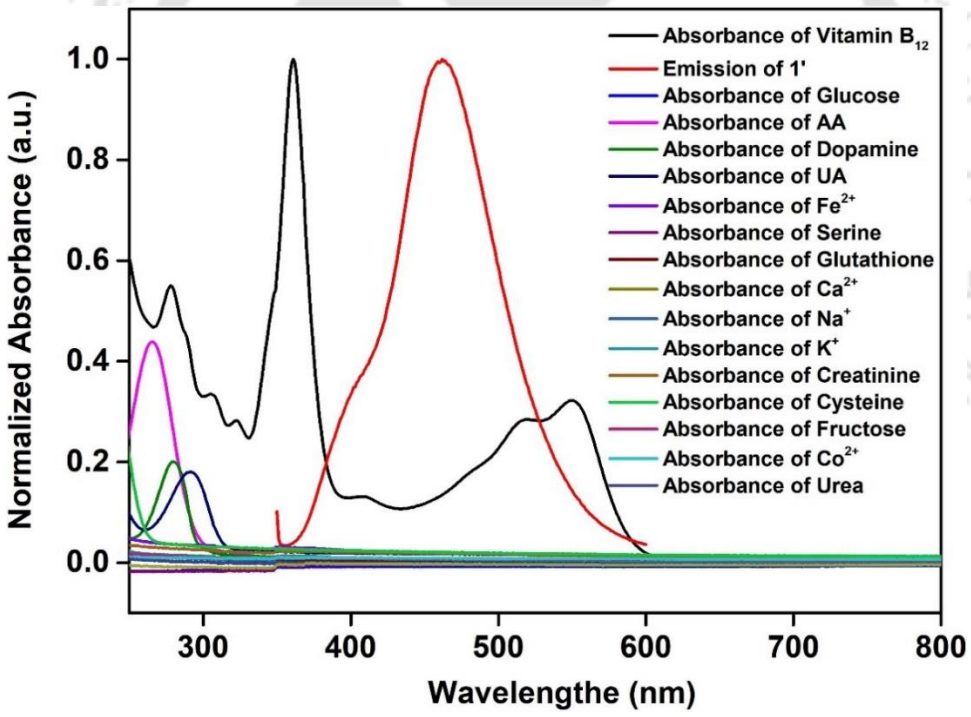

Figure 2.56 Spectral overlap between emission spectrum of **1′** and absorption spectra of the vitamin B_{12} and other analytes.

2.4 Conclusions

This study contains the details of synthesis and analytical characterization of an aqua-stable MOF and its application for the sensing of SDS surfactant and vitamin B_{12}. The presented MOF is the first ever reported MOF-based sensor of SDS and vitamin B_{12}. The lowest ever reported LOD values of 108 and 45.3 nM for SDS and vitamin B_{12}, respectively, quick response time,

excellent selectivity and reusability are the special characteristics of the sensor. For the practical application of the sensor, the sensing ability of the MOF was examined in various real-water specimens and biofluids. MOF@cotton composites were fabricated for the on-field detection of both the targeted analytes. Visible changes in color of the composites were observed even after treatment with nanomolar concentrations of the analytes solutions. The electrostatic interactions between the $–NH_2$ groups present in the linker and the $–SO_3^-$ group of the SDS were responsible for the selective turn-on sensing of SDS. For vitamin B_{12}, the FRET from the probe to vitamin B_{12} quenched the fluorescence of the MOF.

2.5 References

1. S. R. Batten, N. R. Champness, X.-M. Chen, J. Garcia-Martinez, S. Kitagawa, L. Öhrström, M. O'Keeffe, M. P. Suh and J. Reedijk, *Pure Appl. Chem.*, 2013, **85**, 1715-1724.
2. J.-X. Wang, J. Yin, O. Shekhah, O. M. Bakr, M. Eddaoudi and O. F. Mohammed, *ACS Appl. Mater. Interfaces*, 2022, **14**, 9970-9986.
3. W. P. Lustig, S. Mukherjee, N. D. Rudd, A. V. Desai, J. Li and S. K. Ghosh, *Chem. Soc. Rev.*, 2017, **46**, 3242-3285.
4. M. Singh, S. Senthilkumar, S. Rajput and S. Neogi, *Inorg. Chem.*, 2020, **59**, 3012-3025.
5. S. Mukherjee, S. Ghosh and S. Biswas, *Inorg. Chem. Front.*, 2022, **9**, 6288-6298.
6. M. C. Das, H. Xu, Z. Wang, G. Srinivas, W. Zhou, Y.-F. Yue, V. N. Nesterov, G. Qian and B. Chen, *Chem. Commun.*, 2011, **47**, 11715-11717.
7. D. Markad and S. K. Mandal, *Dalton trans.*, 2018, **47**, 5928-5932.
8. S. Ghosh, J. Krishnan, V. Karthik, A. Rana, A. Dhakshinamoorthy and S. Biswas, *Mol. Catal.*, 2022, **533**, 112748.
9. S. Ghosh, N. Nagarjun, S. Nandi, A. Dhakshinamoorthy and S. Biswas, *J. Mater. Chem. C*, 2022, **10**, 6717-6727.
10. M. U. H. Shah, A. V. B. Reddy and M. Moniruzzaman, *Elsevier*, 2022, pp. 257-268.
11. F. Raeisi, S. M. Mousavi, S. A. Hashemi, L. Malekpour, S. Bahrani, C. W. Lai, W.-H. Chiang, A. Babapoor, S. Mazraedoost and H. Esmaeili, *Elsevier*, 2021, pp. 399-422.
12. K. Kosswig, *A25, VCH, Verlegsellshaft*, 1994, 783-790.
13. M. d. C. Hernández-Soriano, A. Peña and M. D. Mingorance, *J. Environ. Qual.*, 2010, **39**, 1298-1305.
14. K. A. Walters, W. Bialik and K. R. BRAIN, *Int. J. Cosmet. Sci.*, 1993, **15**, 260-271.
15. G. O. Reznik, P. Vishwanath, M. A. Pynn, J. M. Sitnik, J. J. Todd, J. Wu, Y. Jiang, B. G. Keenan, A. B. Castle and R. F. Haskell, *Appl. Microbiol. Biotechnol.*, 2010, **86**, 1387-1397.
16. G. Tsiminis, E. P. Schartner, J. L. Brooks and M. R. Hutchinson, *Appl. Spectrosc. Rev.*, 2017, **52**, 439-455.
17. C. W. Wong, *Elsevier*, 2017, pp. 159-166.
18. S. Hanna, L. Lachover and R. Rajarethinam, *J. Clin. Psychiatry*, 2009, **11**, 269.
19. M. Ahel and W. Giger, *Anal. Chem.*, 1985, **57**, 2584-2590.
20. Y. Mengerink, H. De Man and S. Van Der Wal, *J. Chromatogr. A*, 1991, **552**, 593-604.

21. X. Chen, S. Kang, M. J. Kim, J. Kim, Y. S. Kim, H. Kim, B. Chi, S. J. Kim, J. Y. Lee and J. Yoon, *Angew. Chem. Int. Ed.*, 2010, **49**, 1422-1425.
22. M. Samardžić, M. Budetić, A. Széchenyi, D. Marković, P. Živković, B. Šarkanj and M. Jozanović, *Sens. Actuators B Chem.*, 2021, **343**, 130103.
23. H. Wang, S. I. Vagin, B. Rieger and A. Meldrum, *ACS Appl. Mater. Interfaces*, 2020, **12**, 20507-20513.
24. N. Vasimalai, M. a. T. Fernández-Argüelles and B. a. Espiña, *ACS Appl. Mater. Interfaces*, 2018, **10**, 1634-1645.
25. J. Wang, J. Wei, S. Su and J. Qiu, *New J. Chem.*, 2015, **39**, 501-507.
26. J. Quinn, E. Jin and Y. Li, *Tetrahedron Lett.*, 2015, **56**, 2280-2282.
27. R.-D. Ding, Y.-L. Li, F. Leng, M.-J. Jia, J.-H. Yu, X.-F. Hao and J.-Q. Xu, *ACS Appl. Nano Mater.*, 2021, **4**, 9790-9798.
28. Y. Li, M. Hu, X. Huang, M. Wang, L. He, Y. Song, Q. Jia, N. Zhou, Z. Zhang and M. Du, *Sens. Actuators B Chem.*, 2020, **306**, 127608.
29. X. Xu, G. Hua, Y. Chen, Y. Zhang, Z. Zhang, W. Yang, F. Liu and A. Li, *Sep. Purif. Technol.*, 2023, **311**, 123223.
30. V. Bon, I. Senkovska, M. S. Weiss and S. Kaskel, *CrystEngComm*, 2013, **15**, 9572-9577.
31. M. A. Bunge, E. Pasciak, J. Choi, L. Haverhals, W. M. Reichert and T. G. Glover, *Ind. Eng. Chem. Res.*, 2020, **59**, 19285-19298.
32. M. Sak-Bosnar, R. Matesic-Puac, D. Madunic-Cacic and Z. Grabaric, *Tenside Surf. Det.*, 2006, **43**, 82-87.
33. D. Madunić-Čačić, M. Sak-Bosnar, R. A. Matešić-Puač and Z. Grabarić, *Sens. Lett.*, 2008, **6**, 339-346.
34. D. Madunić, M. Sak-Bosnar and R. Matešić-Puač, *Int. J. Electrochem. Sci.*, 2011, **6**, 240-253.
35. G. A. Mostafa, *J. Environ. Anal. Chem.*, 2008, **88**, 435-446.
36. M. Samardžić, O. Galović, M. Hajduković and M. Sak-Bosnar, *Talanta*, 2017, **162**, 316-323.
37. S. Petrušić, M. Samardžić, A. Széchenyi and M. Sak-Bosnar, *Croat. Chem. Acta*, 2017, **90**, 241-250.
38. H.-Q. Yin, J.-C. Yang and X.-B. Yin, *Anal. Chem.*, 2017, **89**, 13434-13440.
39. G. Skvarnavičius, D. Dvareckas, D. Matulis and V. Petrauskas, *ACS Omega*, 2019, **4**, 17527-17535.
40. L.-L. Liu, Y.-Z. Yu, X.-J. Zhao, Y.-R. Wang, F.-Y. Cheng, M.-K. Zhang, J.-J. Shu and L. Liu, *Dalton trans.*, 2018, **47**, 7787-7794.
41. A. Das, S. Ghosh, L. Bourda, S. Mostakim, K. Banerjee, K. Van Hecke and S. Biswas, *CrystEngComm*, 2022, **24**, 4723-4730.
42. R. Dalapati and S. Biswas, *Inorg. Chem.*, 2019, **58**, 5654-5663.
43. Y. Hu, W. Yu, Y. Liao, X. Jiang and Z. Cheng, *Spectrochim. Acta A Mol.*, 2021, **263**, 120194.
44. F. Samari, B. Hemmateenejad, Z. Rezaei and M. Shamsipur, *Anal. Methods*, 2012, **4**, 4155-4160.

45. W. He, W. Weng, X. Sun, Y. Pan, X. Chen, B. Liu and J. Shen, *ACS Appl. Nano Mater.*, 2020, **3**, 7420-7427.
46. Y. Yu, C. Li, C. Chen, H. Huang, C. Liang, Y. Lou, X.-B. Chen, Z. Shi and S. Feng, *Talanta*, 2019, **195**, 117-126.
47. L. Ding, H. Yang, S. Ge and J. Yu, *Spectrochim. Acta A Mol.*, 2018, **193**, 305-309.
48. P. Sarkar, M. Saha, N. Nandi, D. K. Sahu and K. Sahu, *ACS Appl. Nano Mater.*, 2022.
49. S. Ghosh, F. Steinke, A. Rana and S. Biswas, *Inorg. Chem. Front.*, 2022, **9**, 859-869.
50. S. Mukherjee, K. Sarkar and S. Biswas, *Dalton Trans.*, **52**, 5597-5605.

Chapter 3

A Fluorescent Zirconium Organic Framework Displaying Rapid and Nanomolar Level Detection of Hg(II) and Nitroantibiotics

*This chapter represents the solvothermal synthesis and analytical characterization of a new Zr-based highly porous (surface area = 1228 m^2g^{-1}) MOF material containing benzo[1,2-b:4,5-b']dithiophene-2,6-dicarboxylic acid linker molecule (named as **2**). The thermally activated compound (**2'**) exhibited excellent detectability and recyclability towards Hg^{2+} in H_2O medium and various nitro-antibiotics (nitrofurazone and nitrofurantoin) in MeOH. Besides ultra-fast response (1 min for all analytes), very low limits of detection (LODs) were observed for the sensing of all the targeted analytes (LOD for Hg^{2+}, nitrofurazone and nitrofurantoin were 5, 156.7 and 96.3 nM, respectively). Moreover, a paper strip-based sensing technique was developed for all three analytes.*

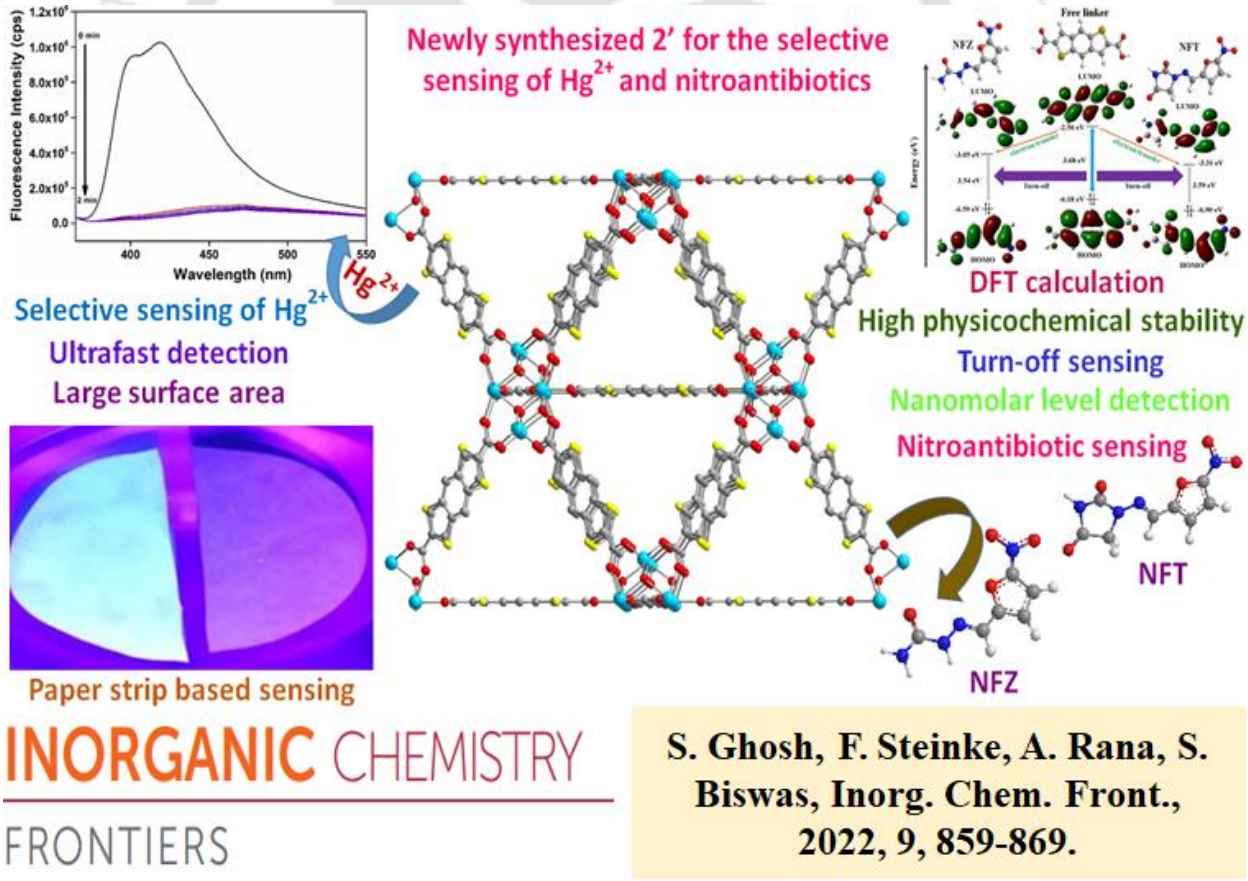

INORGANIC CHEMISTRY FRONTIERS

S. Ghosh, F. Steinke, A. Rana, S. Biswas, Inorg. Chem. Front., 2022, 9, 859-869.

3.1 Introduction

Mercury (Hg) is a highly toxic, non-biodegradable and soft heavy metal.[1] In the year of 1956, Japan's Minamata disease already displayed the horrible toxic effect of Hg.[2] In the environment, Hg is mainly present in its inorganic salt form. However, the inorganic form of Hg^{2+} can easily be converted into its more toxic form methylmercury (CH_3Hg^+) by fish and microorganisms.[3] Due to the soft and lipophilic nature of CH_3Hg^+, it can easily be absorbed by the human body.[3] This toxic heavy metal (Hg) mainly enters into the human body via aquatic organisms. A trace amount of mercury can easily bind with the soft sulphur containing amino acid molecules of living organisms and collapse the immune and central nervous systems.[4, 5] Absorption of higher concentration of Hg can cause cancer, heart troubles, respiratory failure, motion disorder, temporary blindness, kidney failure, intelligence loss, nephrotic syndrome, etc.[6] In spite of the huge number of toxic effects of Hg, the ongoing development of various industries, numerous natural phenomena like a volcanic eruption and human activities (e.g. burning of coal, waste incineration, combustion of fossil fuels, etc.) increase Hg pollution.[7] Therefore, environmental pollution because of Hg has become a highly concerned global issue which requires to be resolved urgently.

In modern days, different types of pharmaceutical antibiotics are being used all over the world for the purpose of human therapy and the farming industry.[8] In the year of 1928, the first antibiotic penicillin was discovered.[9] Thereafter, in the last 90 years, a variety of antibiotics were developed to get rid of different bacterial diseases.[10, 11] However, the excessive use and arbitrary disposal of poorly metabolized antibiotics create a lot of problems for the environment and also for the living beings.[12, 13] Long term intake of antibiotics may develop the antibiotic-resistant genes in living organisms which have serious effects on ecosystem.[13, 14] Residues of pharmaceutical antibiotics and their various transformed products may cause different adverse effects like chronic and acute toxicity and microorganism antibiotic resistance.[15] Nitrofurazone (NFZ) and nitrofurantoin (NFT) are two very common antibiotics that are mainly used for the remedy of skin infections, and urinary tract and kidney infections, respectively.[16, 17] Exposure to these antibiotics for a long-time may cause several side effects, such as nausea, vomiting, headache, loss of appetite and dizziness.[18, 19] Thereafter, it is necessary to develop a suitable method to prevent the environmental pollutions which are caused by these antibiotics.

One of the most common ways to protect the environment and living beings from the toxic effects of heavy metal ion (Hg) and various antibiotics (NFZ and NFT) is to know their presence in the environmental samples (soil and water). The fluorometric method of sensing is one of the most user-friendly, easily accessible, rapidly responsive, low cost and reliable methods of sensing.[20] Such features have made the fluorescent-based method of sensing more popular in the scientific community as compared to other conventional techniques of sensing like HPLC, capillary electrophoresis, LC-MS, atomic emission, and absorption spectroscopy, etc.[21] Choice of appropriate sensor molecules (fluorophores) can permit the easy sensing of the targeted analytes.

Fluorescent MOFs contain linkers as fluorophores, which are able to sense various metal ions, anions, biologically signalling molecules, various toxic gas molecules, antibiotics, etc. in the past few years.[22-25] Rapid development of various MOF-based sensors took place in recent

times because of their high physicochemical stability, porous nature and tenable nature of functional groups (as required) even after their synthesis.[24, 26] Wide choice of solvent molecules for the sensing purpose and stability in H_2O medium have made MOF materials as suitable sensing probes for various analytes.[27]

Various sulfur-containing organic linker molecules and MOFs are reported in the literature which was used for the sensing of Hg^{2+}. For the sensing of various nitro-group-containing antibiotics, an electron-rich probe can be used.[26, 27] The interaction between the soft sulfur atom with soft Hg^{2+} ion and intermolecular energy transfer are the probable reasons behind the sensing of Hg^{2+} ion and nitro-group containing antibiotics in most of the reported probes.[28-30]

Thereby, we strategically synthesized a Zr-based UiO-66 MOF material using benzo[1,2-b:4,5-b']dithiophene-2,6-dicarboxylic acid linker (**L1**). Our aim was to utilize such a linker for the sensing of Hg^{2+} and various nitro-group-containing antibiotics. In reality, the thermally activated MOF material displayed outstanding selectivity towards the sensing of Hg^{2+} and nitro-group-containing antibiotics (NFZ and NFT) (Scheme 3.1). Rapid responses were observed in both the cases of sensing (for Hg^{2+} = 1 min; for NFZ = 1 min and for NFT = 1 min). In addition to the fast and selective response, this MOF material also exhibited extraordinarily low LODs for all the targeted analytes (LOD for Hg^{2+} = 5 nM; for NFZ and NFT = 156.7 and 96.3 nM). Together with the solvent phase, this newly synthesized MOF material can also sense the targeted analytes in a paper strip coated with MOF.

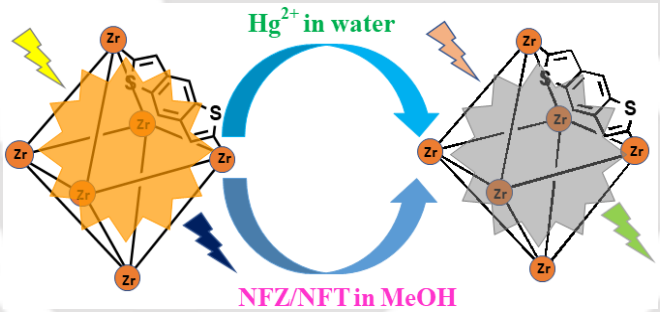

Scheme 3.1. Fluorogenic switch-off sensing of Hg^{2+} and NFT/NFZ by **2′.**

3.2 Experimental Section

3.2.1 Synthesis and Characterization Procedure of Benzo[1,2-b:4,5-b']Dithiophene-2,6-Dicarboxylic Acid Linker

The linker was synthesized using a two-step synthesis procedure (Scheme 3.2). The diethyl benzo[1,2-b:4,5-b']dithiophene-2,6-dicarboxylate was synthesized according to the previously reported literature procedure.[31] Then, 850 mg (2.77 mmol) of the obtained ester product was dissolved in a mixture of 10 mL of THF, 10 mL of EtOH and 10 mL of 1(M) LiOH. After that, the mixture was refluxed for 3 h at 80 °C. After 3 h, these solvents were evaporated under vacuum. Thereafter, the remaining liquid part was acidified with 3 (M) HCl solution. At last, the obtained solid precipitate was filtered, washed with 10 mL of water and then dried in an oven at 80 °C for 12 h. Yield: 565 mg (2.03 mmol, 73%). ^{1}H NMR (400 MHz, DMSO-d_6): δ

= 8.68 (s, 2H), 8.17 (s, 2H) ppm ^{13}C NMR (100 MHz, DMSO-d_6): δ = 163.50, 138.51, 138.38, 136.75, 129.68, 120.05 ppm. ESI-MS (m/z): 276.0665 for $(M-H)^-$ ion (M = mass of benzo[1,2-b:4,5-b']dithiophene-2,6-dicarboxylic acid linker). In Figures 3.1-3.3, the NMR and mass spectra of the synthesized benzo[1,2-b:4,5-b']dithiophene-2,6-dicarboxylic acid linker are shown.

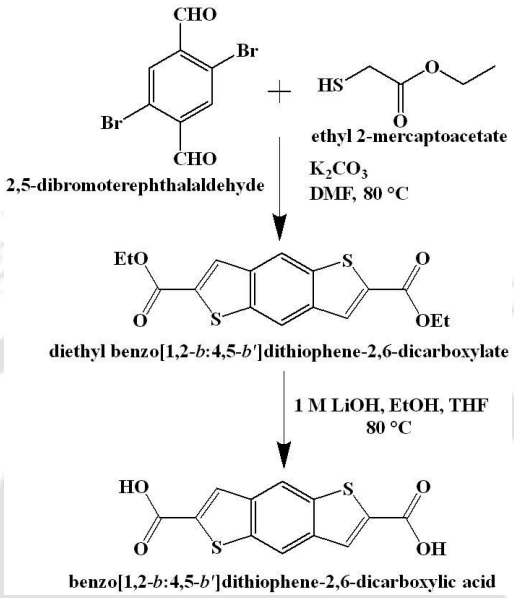

Scheme 3.2 Reaction scheme for the preparation of benzo[1,2-b:4,5-b']dithiophene-2,6-dicarboxylic acid linker.

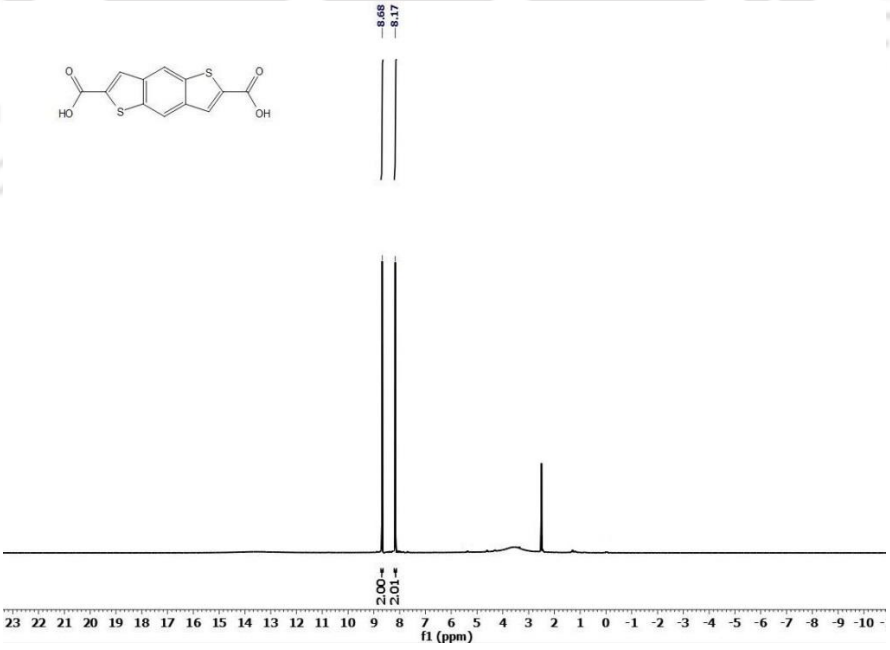

Figure 3.1 ^{1}H NMR spectrum of benzo[1,2-b:4,5-b']dithiophene-2,6-dicarboxylic acid linker in DMSO-d_6.

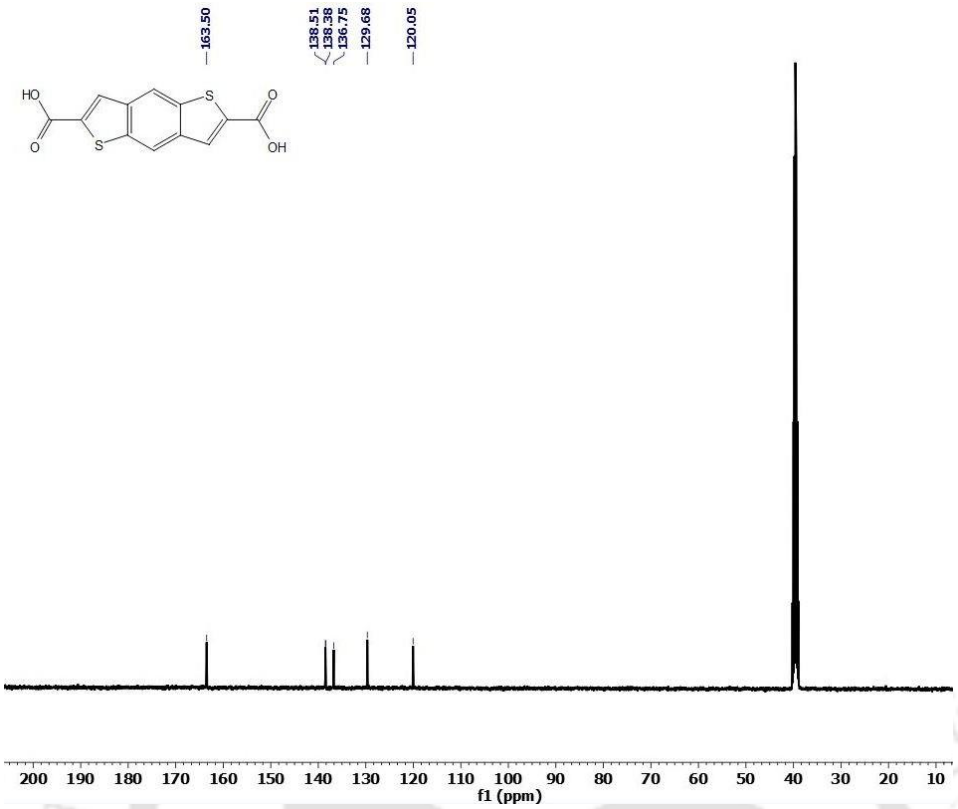

Figure 3.2 ^{13}C NMR spectrum of benzo[1,2-b:4,5-b']dithiophene-2,6-dicarboxylic acid linker in DMSO-d_6.

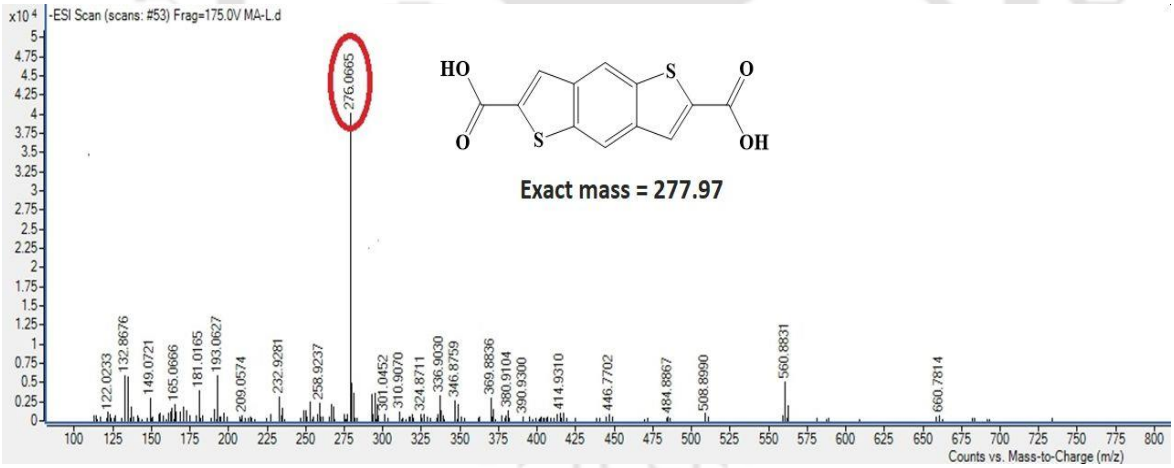

Figure 3.3 ESI-MS spectrum of benzo[1,2-b:4,5-b']dithiophene-2,6-dicarboxylic acid linker measured in methanol. The spectrum shows m/z peak at 276.0665, which corresponds to $(M-H)^-$ ion (M = mass of benzo[1,2-b:4,5-b']dithiophene-2,6-dicarboxylic acid linker).

3.2.2 Synthesis of $[Zr_6O_4(OH)_4(C_{12}H_4S_2)_6]\cdot 5H_2O\cdot 4DMF$ (2)

A mixture of benzo[1,2-b:4,5-b']dithiophene-2,6-dicarboxylic acid linker molecule (20 mg, 0.07 mmol), $ZrCl_4$ metal salt (17 mg, 0.07 mmol), trifluoroacetic acid (166 µL, 2.1 mmol) and 3 mL DMF was sonicated for 30 min after pouring all the components in a Pyrex tube. Here, the linker molecule, $ZrCl_4$ and trifluoroacetic acid modulator were taken in a molar ratio of 1:1:30. After complete dissolution of all the components by sonication, the mixture was

positioned on a pre-heated heating block at 150 °C for 1 day. After completion of 1 day, a yellow colour solid precipitate (**2**) was collected via filtration. The obtained solid was washed with acetone (3 × 2 mL) and placed in an 80 °C air oven for 6 h. Yield: 25 mg (0.01 mmol, 77% related to Zr salt). Anal. calcd. for $C_{84}H_{66}N_4O_{41}S_{12}Zr_6$ (2710 g mol^{-1}): C, 29.38; H, 1.92; N, 1.63. Found C, 29.25; H, 1.73; N, 1.46%. FT-IR (cm^{-1}): 3387 (br), 2846 (w), 2550 (w), 1654 (s), 1542 (vs),1445 (s), 1402 (vs), 1358 (s), 1310 (s), 1253 (w), 1162 (s), 1075 (m), 886 (m), 773 (s), 660 (s), 602 (m), 442 (s).

3.2.3 Activation of Compound 2

In as-prepared compound (**2**), some DMF molecules are encapsulated inside the pore. To remove the DMF molecules, at first, 50 mg of **2** was stirred in 100 mL of methanol (MeOH) for 1 day. Then, the recovered material was collected by filtration and completely dried in an oven of 60 °C for 1 day. Finally, the low boiling MeOH solvents (encapsulated inside the pore of **2** during solvent exchange) were removed by heating the compound in a 100 °C oil-bath for 1 day under vacuum. Thus, we obtained the thermally activated compound **2′**.

3.2.4 Preparation of MOF (2′) Suspension for the Fluorescence Sensing Experiments

The probe **2′** (2 mg) was taken in a 5 mL glass vial and 3 mL Milli-Q water/ MeOH was added to it to make a homogeneous suspension. Then, the suspension was sonicated for 30 min and kept it for overnight to make the suspension stable. During the fluorescence titration experiments, we used 100 µL of above-mentioned suspension of **2′** and 3000 µL of Milli-Q water/MeOH was added to it in a quartz cuvette. All the fluorescence spectra were collected by exciting the suspension at 310 nm (for aqueous suspension) and 370 nm (for methanolic suspension), within the range of 350-550 nm for Hg^{2+} sensing and 390-550 nm for antibiotics (NFZ and NFT) sensing. The solutions of the different competitive analytes of Hg^{2+} and nitro-antibiotics (NFZ and NFT) (concentration = 10 mM) were added in an incremental manner to **2′** suspension.

3.3 Results and Discussion

3.3.1 Infrared (IR) Spectroscopy

To ensure the presence of various functional groups and the whole removal of DMF (solvent) molecules from the pore of the framework structure, we took the support of FT-IR spectroscopy (Figure 3.4). Two sharp absorption bands at 1542 and 1402 cm^{-1} were observed both in case of **2** and **2′** which were originated from the Zr-coordinated asymmetric and symmetric stretching of carboxylate groups of the linker molecules. A weak absorption band near 1654 cm^{-1} was observed for compound **2**, which denotes the carbonyl stretching vibration of DMF molecules. Such an absorption frequency was not observed in the case of **2′**. This confirmed the whole removal of guest DMF molecules from the pore of the framework structure of **2**.

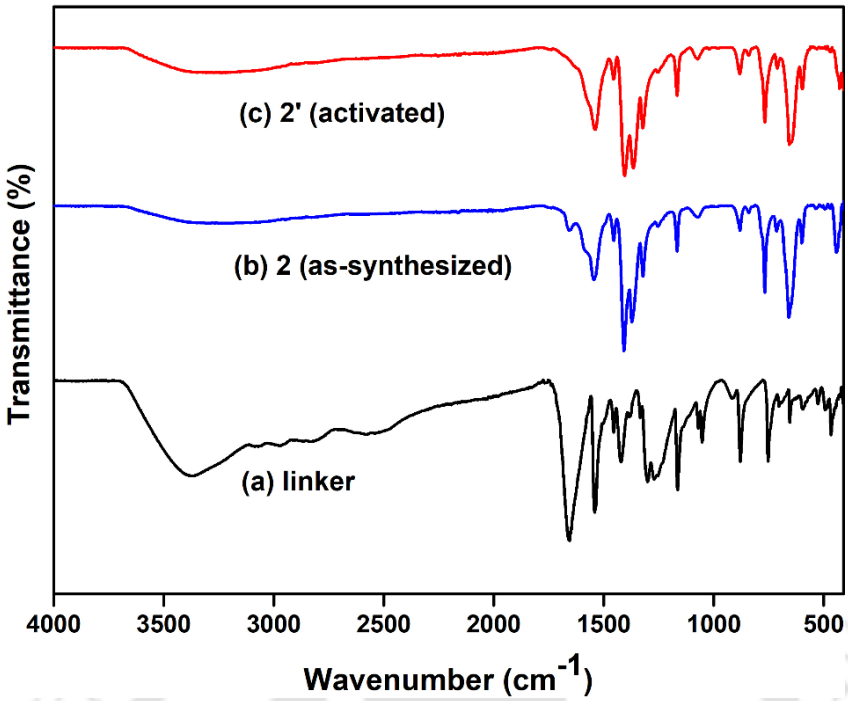

Figure 3.4 FT-IR spectra of (a) linker, (b) as-synthesized **2** and (c) activated **2′**.

3.3.2 Rietveld Refinement

At first, a starting model for the Rietveld refinement based on the UiO-66 structure[32] was built in Materials Studio[33] and geometrically optimized by applying force-field calculations. For the refinement using Topas Academics,[34] the bond lengths of the Zr-O-bonds of the hexanuclear cluster were restrained. For the C-C-, C-S- and C-O-bonds of the linker, a set of distance and angle restraints were used. Since the linker is placed on a mirror plane, the atoms S1 and C3 were refined almost on top of each other, but with an occupancy of 0.5, respectively. No indication for a preferred orientation of the linker molecule was found. The final parameters obtained from the Rietveld refinement are summarized in Table 3.1. The Rietveld plot is displayed in Figure 3.5 and the details of bond lengths in the structure of **2** are shown in Table 3.1.

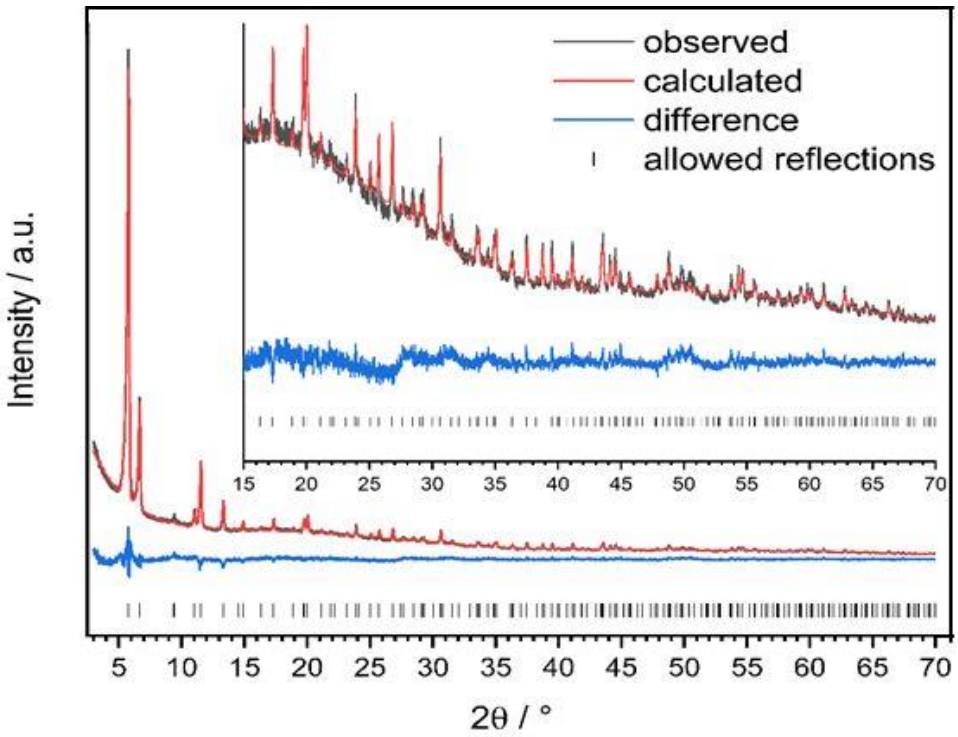

Figure 3.5 Rietveld plot for the structural refinement of **2**.

Table 3.1 Lattice parameter and crystallographic data obtained from the Rietveld refinement of **2**.

Compound	**2**
space group	$Fm\bar{3}m$
$a = b = c$ [Å]	26.5967(11)
R_{wp} [%]	4.95
R_{Bragg} [%]	2.62
GoF	1.02

3.3.3 Analysis of Structure

At first, PXRD analysis with both **2** and **2′** was performed (Figure 3.6). The obtained PXRD data of **2** was indexed. This resulted in a cubic space group ($Fm\bar{3}m$, no. 225). By utilizing the obtained lattice parameters from refinement (Table 3.1) and the crystal structure of UiO-66, a model for the structure of **2** was constructed. The modeled crystal structure of **2** was refined utilizing the Rietveld method utilizing the PXRD data of the compound. To our satisfaction, the refinement results indicated that the structure of **2** (Figure 3.5) owns a similar framework structure as UiO-66.[32] Similar to the pristine UiO-66 framework, **2** also has octahedral and tetrahedral structural voids. Here, all the Zr-atoms are present in a square antiprismatic coordination environment. Such similarities in both the structures imply that the incorporation of benzo[1,2-b:4,5-b']dithiophene-2,6-dicarboxylic acid linker molecule in place of un-functionalized terephthalic acid linker molecule does not make any change in the framework structure (Figure 3.7). The activated compound (**2′**) also displayed a similar PXRD pattern as

that of **2′**. That means the framework of **2** remains unaltered even after thermal activation (Figure 3.6).

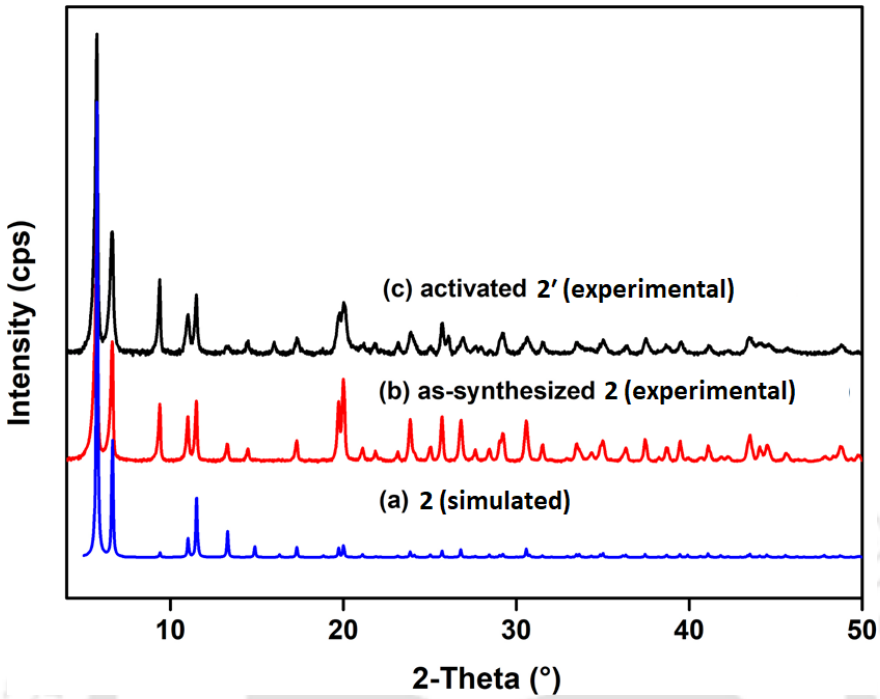

Figure 3.6 PXRD patterns of (a) **2** (simulated), (b) as-synthesized **2** (red) and (c) activated **2′** (black).

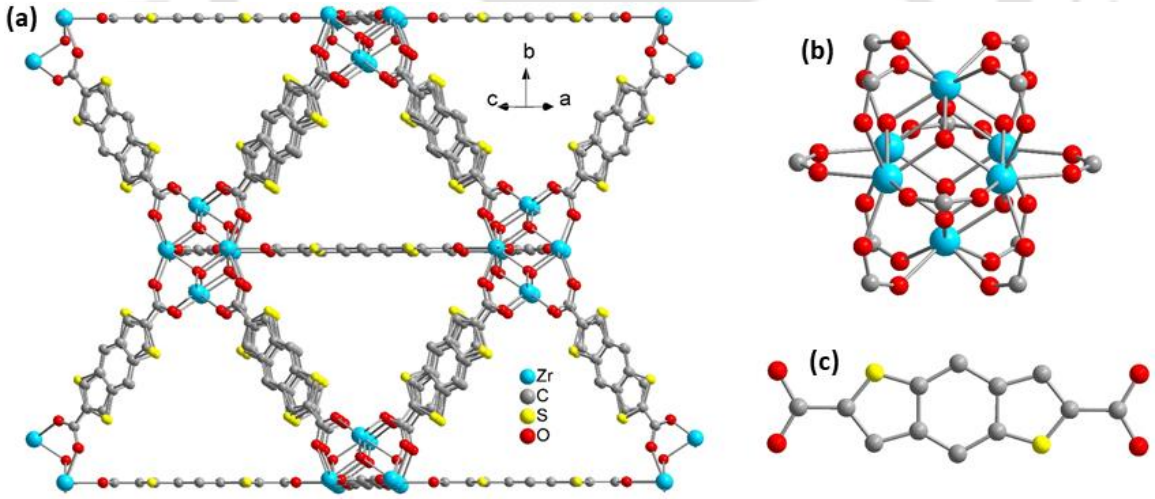

Figure 3.7 Structure of compound **2** (a), its SBU (b) and corresponding linker (c).

3.3.4 FE-SEM and EDX Analysis

A homogeneous crystalline phase consisting of cubic-shaped crystals of **2′** was visualized from the FE-SEM images (Figure 3.8). The presence of C, S, O and Zr atoms in the MOF was confirmed by the EDX analysis (Figure 3.9).

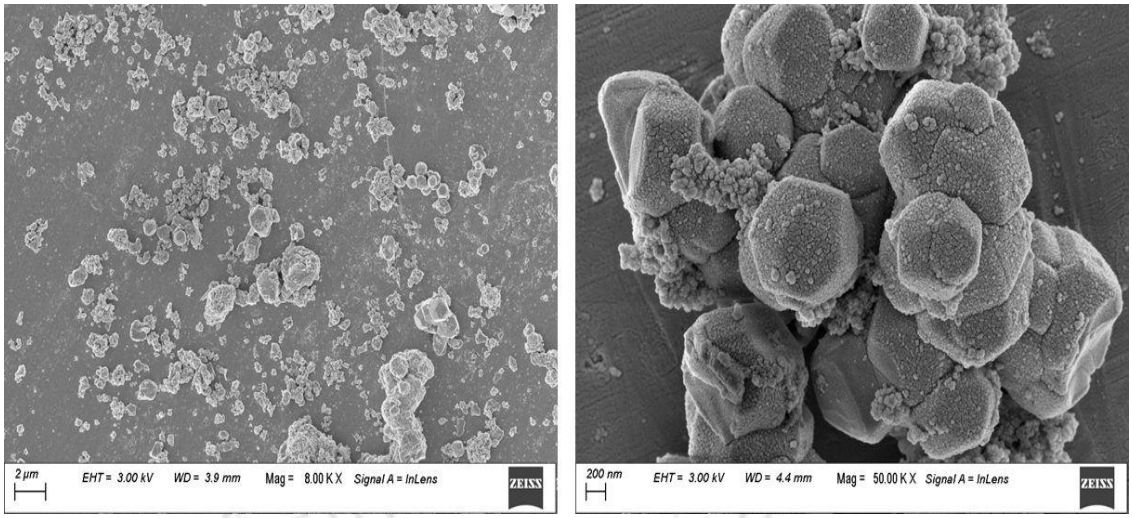

Figure 3.8 FE-SEM images of **2**.

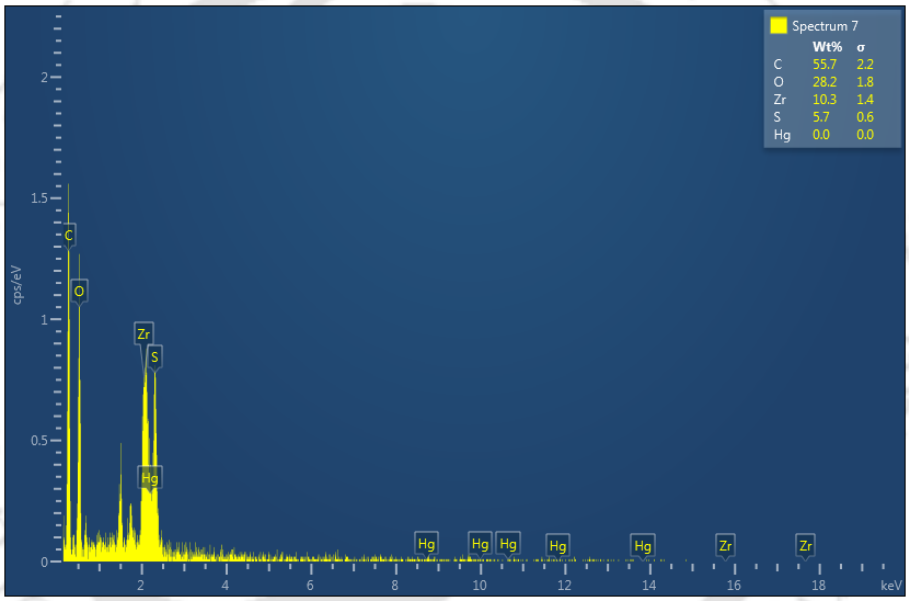

Figure 3.9 EDX spectrum of **2′**.

3.3.5 Thermal Stability

Thermogravimetric analysis (TGA) of both **2** and **2′** was conducted to know the thermal stabilities of this newly synthesized MOF material in as-synthesized (**2**) and activated forms (**2′**). Figure 3.10 displays that both **2** and **2′** are thermally stable up to the temperature of 415 °C. For the as-synthesized compound (**2**), three consecutive losses of weights took place. The first loss of weight (3.4%) in between the temperature of 25-115 °C can be attributed to loss of 5 H_2O molecules per formula unit (cal.: 3.4 wt.%). Escaping of 4 DMF molecules (per formula unit) from the pore of the framework is the reason behind the weight loss of 10.1% within the temperature range of 115-415 °C (cal.: 10.1 wt.%). After the temperature of 415 °C, decomposition of the framework structure took place. In case of **2′,** the only weight loss was observed at temperatures above 415 °C due to decomposition of the framework structure. Hence, it can be concluded that both **2** and **2′** have similar thermal stability as that of the other reported UiO-66 family of Zr-MOFs.[35, 36]

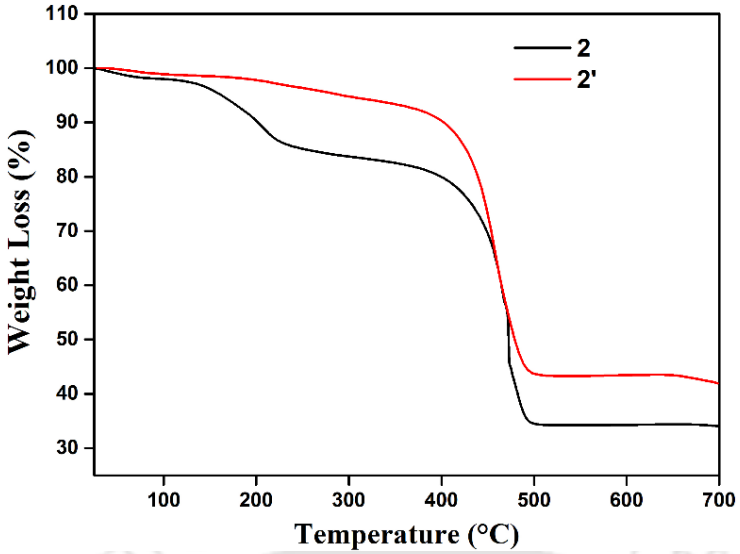

Figure 3.10 Thermogravimetric analysis curves of as-synthesized **2** (black) and thermally activated **2′** (red) recorded under air atmosphere in the temperature range of 25-700 °C with a heating rate of 5 °C min^{-1}.

3.3.6 Chemical Stability

Chemical stability of **2′** in different solvents (H_2O, MeOH, CH_2Cl_2, acetone, hexane and DMF) was investigated (Figure 3.11). For this investigation, at first, 15 mg of **2′** was stirred in 20 mL of different solvents for 6 h at room temperature. Afterwards, the material was collected by filtration and PXRD analysis was performed after drying the recovered material at 60 °C inside an oven. The unperturbed nature of the PXRD patterns confirms the stability of **2′** in various solvents. The robust nature of the material in the sensing media (H_2O and MeOH) fulfills the criteria of a smart sensor molecule. Therefore, the chemical stability of **2′** is comparable to other reported UiO-66 type of Zr-MOFs.[35, 37]

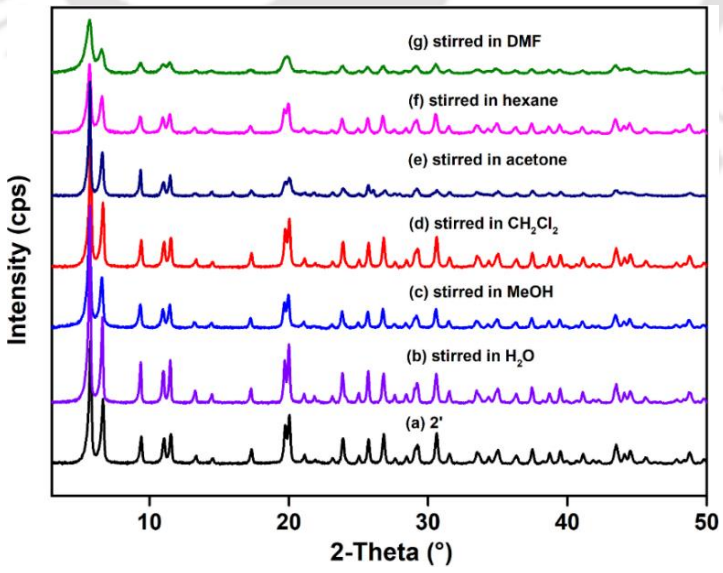

Figure 3.11 PXRD patterns of **2′** in different forms: (a) activated (**2′**), after stirred with (b) H_2O (c) MeOH (d) CH_2Cl_2 (e) acetone (f) hexane and (g) DMF for 6 h.

3.3.7 N_2 Sorption Analysis

For the determination of surface area (BET) and pore volume of **2′,** the N_2 sorption analysis was performed at a temperature of -196 °C (Figure 3.12). The N_2 sorption study and density functional theory pore-size distribution plot confirm the microporous nature of the framework. The obtained surface area of **2′** was 1228 m^2 g^{-1} with a pore volume of 0.6 cm^3 g^{-1} (measured at p/p_0 = 0.5). The average pore radius was 10.8 Å (Figure 3.13). Therefore, it is worthy to state that the BET surface area of **2′** is comparable to the other literature reported Zr-based UiO-66 type of materials.[36, 38]

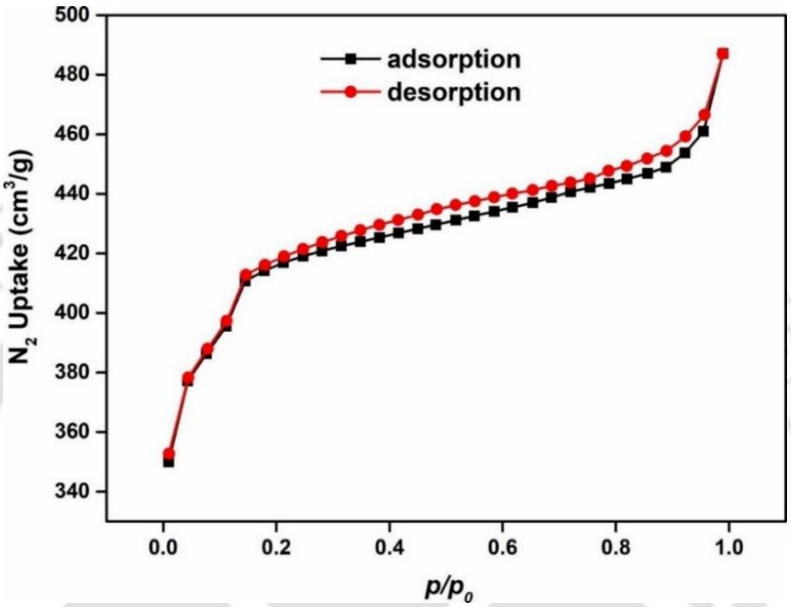

Figure 3.12 N_2 adsorption (black squares) and desorption (red circles) isotherms of thermally activated **2′** recorded at –196 °C.

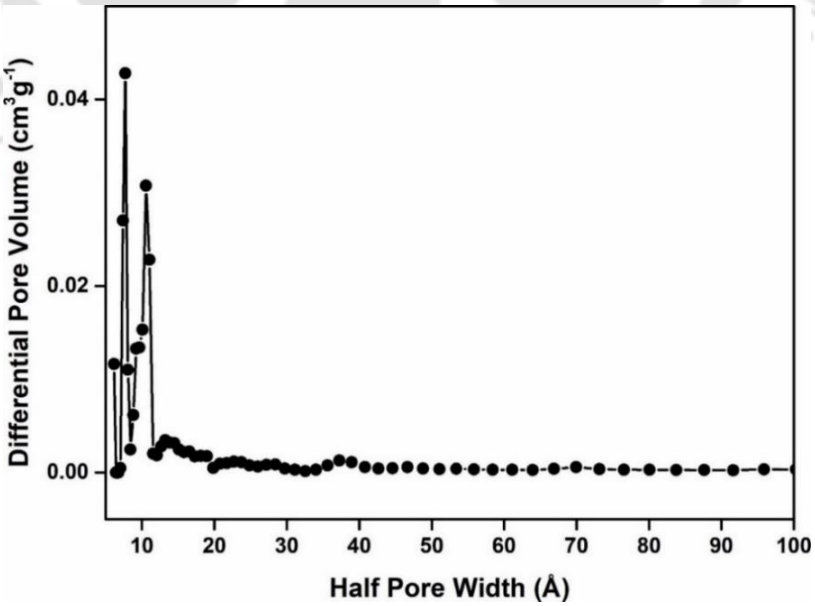

Figure 3.13 Density functional theory pore-size distribution of compound **2′** as determined from its N_2 adsorption isotherms at -196 °C.

3.3.8 Fluorescence Sensing of Hg^{2+} in Water

To examine the sensing capability of **2′** for the sensing of Hg^{2+} in universal solvent (H_2O), at first, we conducted the fluorescence titration experiment with the aqueous suspension of **2′** (100 µL) (taken in a 3 mL cuvette containing 2900 µL of H_2O) by adding an incremental volume of 25 µL of aqueous solution (10 mM) of Hg^{2+}. Initially, **2′** displayed very high luminescence emission intensity but with the incremental addition of Hg^{2+} solution, the emission intensity gradually decreased and finally became saturated after the addition of 75 µL of 10 mM aqueous solution of Hg^{2+} (λ_{ex} = 320 nm, λ_{em} = 420 nm) (Figure 3.14). Around 92% decrease in fluorescence intensity was observed after the addition of 75 µL of 10 mM solution of Hg^{2+} (Figure 3.15).

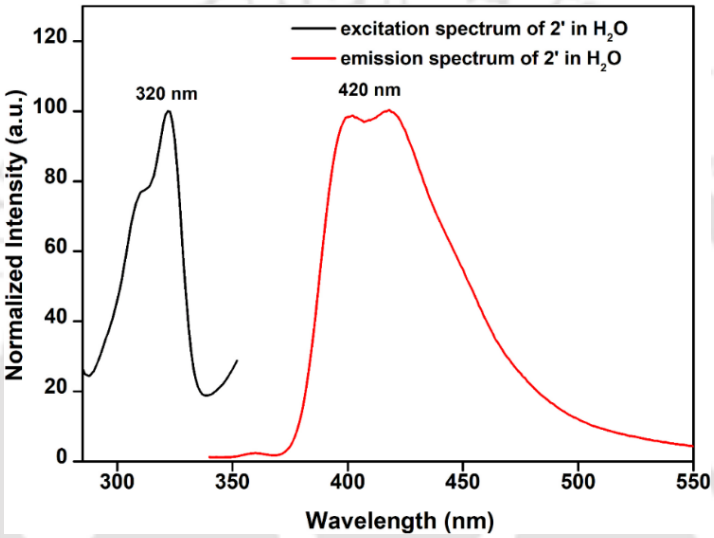

Figure 3.14 Excitation (black) and emission (red) spectra of **2′** in water.

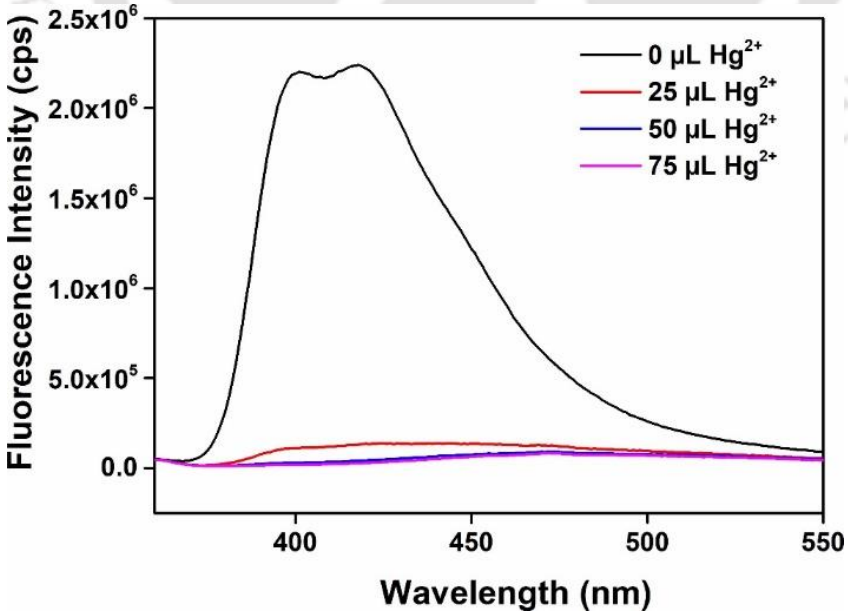

Figure 3.15 Decrease in emission intensity of **2′** with the incremental addition of 10 mM aqueous solution of Hg^{2+} (from 0 µL to 75 µL) (λ_{ex} = 320 nm and λ_{em} = 420 nm).

A time-dependent luminescent study was conducted to deduce the response time of **2′** for the sensing of Hg^{2+} (Figure 3.16a). We know that the sensors with lower response times are more applicable for the real-life sensing purposes. At first, 100 µL of aqueous suspension of **2′** was taken in a cuvette containing 2900 µL of water. It was followed by the inclusion of 75 µL of 10 mM aqueous Hg^{2+} to that mixture and fluorescence spectra were recorded with a regular time interval of 1 min. It was observed that the emission spectrum rapidly became saturated after 1 min of the addition of Hg^{2+} (Figure 3.16b). Therefore, this probe will be highly applicable for the real-life detection of Hg^{2+} because of its very low response time (1 min).

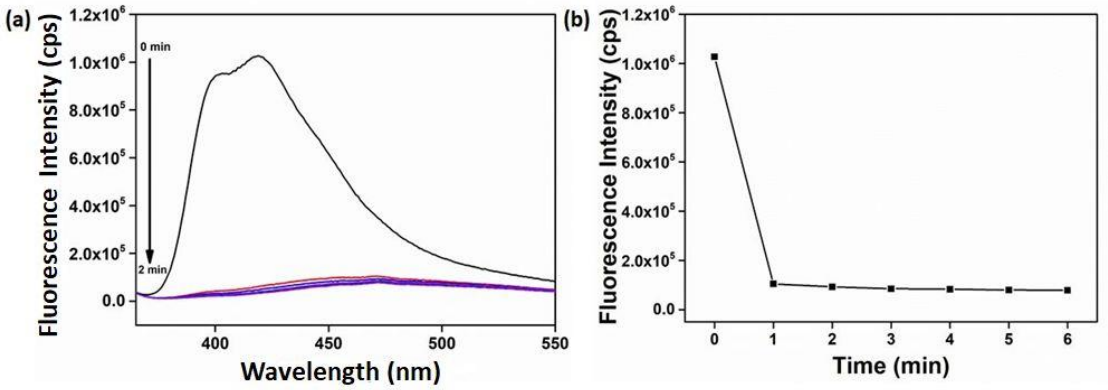

Figure 3.16 (a) Switch-off in luminescent intensity of **2′** with the increase in time after adding 75 µL of 10 mM of Hg^{2+} solution (λ_{ex} = 320 nm, λ_{em} = 420 nm). (b) Change of luminescent emission intensity with the increase in time.

A reliable sensor material should sense the targeted analyte only. To verify these criteria, we conducted similar sensing experiments using the other competitive metal ions (Fe^{2+}, Cu^{2+}, Al^{3+}, K^{+}, Ni^{2+}, Cd^{2+}, Na^{+}, Mn^{2+}, Cr^{3+}, Zn^{2+}, Co^{2+}, Pb^{2+}, Pd^{2+} and Pt^{2+}) of Hg^{2+}. Figure 3.17 displays that no other competitive metal ion can effectively quench the fluorescence emission intensity of **2′**. Thus, we can conclude that **2′** is highly selective in sensing of Hg^{2+} in H_2O.

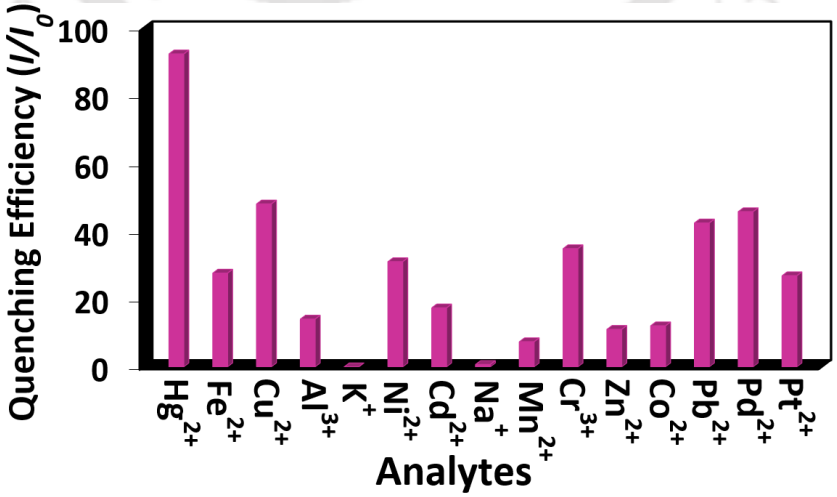

Figure 3.17 Turn-off in emission intensity of **2′** after inclusion (75 µL) of 10 mM of Hg^{2+} solution and 75 µL (10 mM) solutions of competitor metal ions (λ_{ex} = 320 nm, λ_{em} = 420 nm).

In actual situations, more than one competitive analyte can be present together. A smart sensor should have the quality to sense the targeted analyte even in the presence of other competitive analytes. To corroborate this phenomenon, at first, we treated the aqueous suspension of **2′** with 75 µL of 10 mM other competitive analytes. Thereafter, the suspensions were further treated with 75 µL of 10 mM aqueous solution of Hg^{2+}. From the Figure 3.18, it can be evidenced that the fluorescence intensities of **2′** were not effectively quenched in presence of other competitive analytes. But, a rapid decrease in fluorescence intensities was observed after the addition of Hg^{2+} solution. This proved the selective nature of **2′** even in the presence of other competitive analytes.

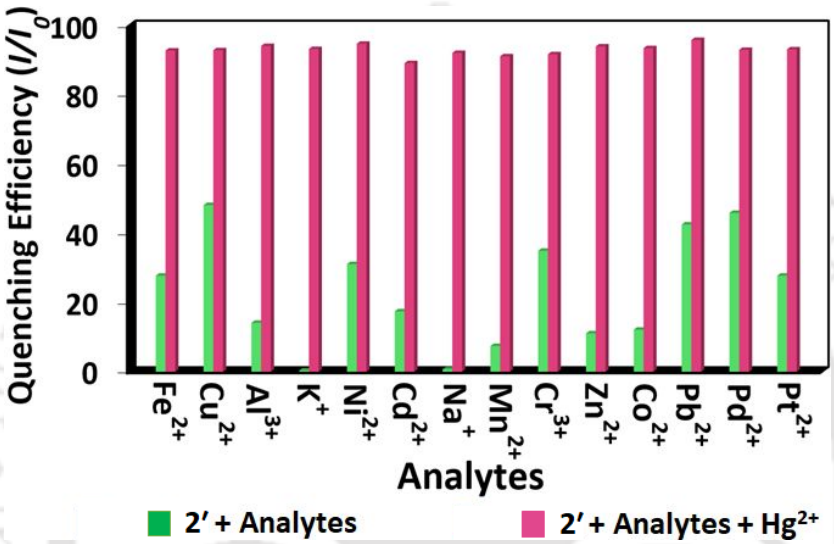

Figure 3.18 Change in emission response of **2′** after the inclusion of 75 µL of 10 mM Hg^{2+} in the co-existence of 75 µL of 10 mM solutions (in H_2O) of various competitor metal ions of Hg^{2+} (λ_{ex} = 320 nm, λ_{em} = 420 nm).

Stern-Volmer (S-V) plot in different concentrations of various analytes provides us valuable information on the nature of quenching. Here, sensing of Hg^{2+} takes place through the quenching pathway. Therefore, it is obvious to draw a S-V plot to know the mechanism behind the quenching of fluorescence intensity (Figure 3.19). Here, the K_{sv} value (K_{sv} = S-V quenching constant) was calculated by using the following mathematical equation: $I_0/I = K_{sv}[Q] + 1$.

In the equation, I_0 and I denote the fluorescence intensities of **2′** in the absence and attendance of different analytes, respectively. [Q] represents the concentrations (in molar) of different analytes. The obtained value of K_{sv} for the sensing of Hg^{2+} was 3.54×10^5 M^{-1} (Figure 3.20), which is much higher than most of the other reported MOF-based sensors of Hg^{2+}.[39, 40]

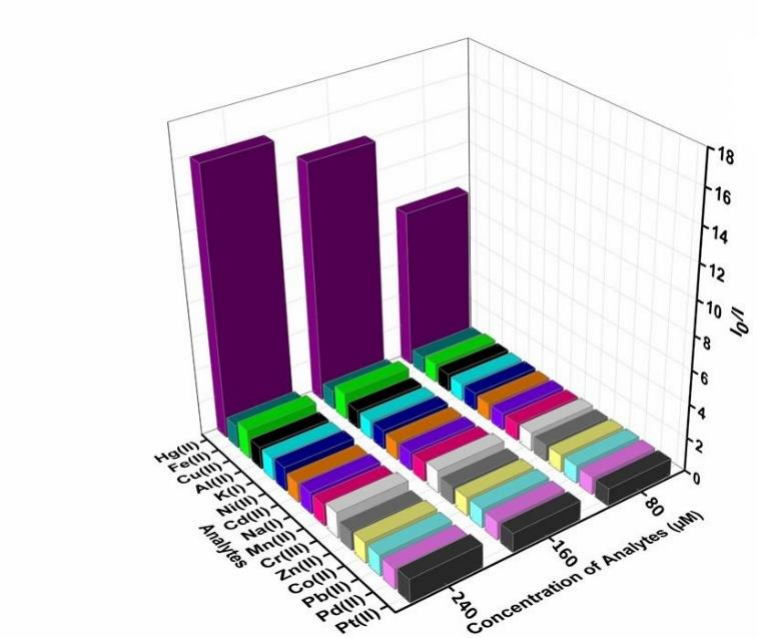

Figure 3.19 S-V plots for the decrease in luminescence intensities of **2′** with the gradual addition of various analytes in the case of Hg^{2+} sensing.

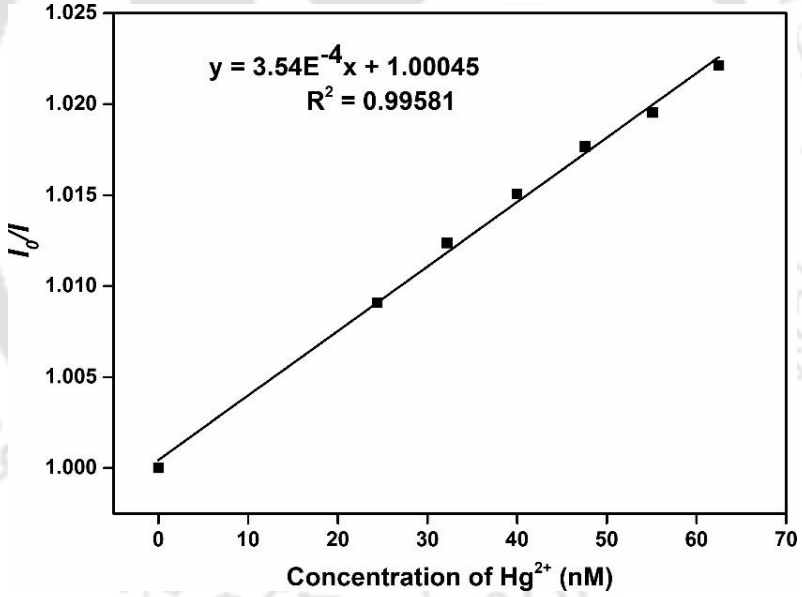

Figure 3.20 Stern-Volmer plot for the fluorescence emission quenching of **2′** in presence of Hg^{2+} solution.

The limit of detection value denotes the quality of a sensing probe. To obtain the LOD value for the sensing Hg^{2+}, at first, the standard deviation (σ) of the luminescence intensities of the suspension of **2′** (in the absence of any analyte) was calculated. Afterward, a series of fluorometric titration experiments were carried out after gradually diluting the concentration of Hg^{2+}. A straight line with a negative slope (k) was obtained after plotting the concentrations against the fluorescence emission intensities (Figure 3.21). Finally, the LOD value was calculated using the formula: $3\sigma/k$. Here, the obtained LOD value (5 nM) is lower than most of the reported MOF-based chemosensors of Hg^{2+} (Table 3.2).

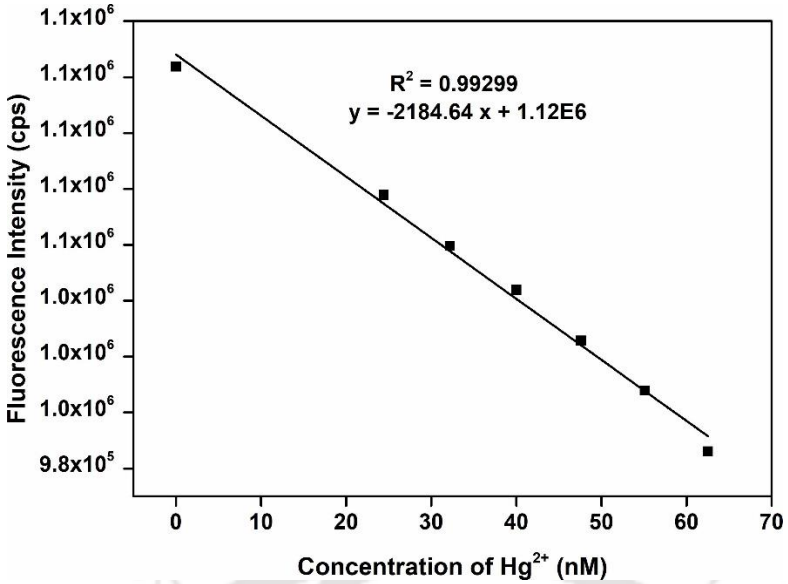

Figure 3.21 Change in the fluorescence intensity of **2′** in water as a function of concentration of Hg^{2+}.

Table 3.2 Comparison of the response time, detection limit and sensing media used for the reported chemosensors of Hg^{2+} in the literature.

Sl. No.	Sensor Material	Type of Material	Sensing Medium	Detection Limit (nM)	Response Time (min)	Detection Method	Ref.
1	thiosemicarbazone	organic-molecule	0.01 M acetic acid/sodium acetate buffer	770	-	fluorescence	41
2	GT capped AgNPs	nano-particles	water	0.037	0-60	fluorescence	42
3	azo Crown ether	organic molecule	methanol	13900	-	fluorescence	43
4	silver nano-particles	nano-particles	water	850	30	colorimetric	44
5	rhodamine 6G	Rh-complex	THF: water (8:2, pH = 7)	30.37	-	fluorescence	45
6	tetraphenyl ethylene based AIE probe	organic molecule	water	63	-	fluorescence	46
7	squaraine based fluorescent probe	organic molecule	ethanol: water (20:80, v/v)	21.9	3	fluorescence	47
8	rhodamine appended terphenyl	organic molecule	THF	500	30	fluorescence	48
9	ruthenium complex	metal complex	ethanol	100	-	fluorescence	49
10	double naphthalene Schiff base	organic compound	DMSO	55.9	80	fluorescence	50
11	gold nano-particles	nano-particles	water	50	0.16	potentiometric	51
12	gold nano-particles	nano-particles	water	50	40	colorimetric	52
13	poly (vinyl chloride)	polymer	tris buffer	20	10	potentiometric	53
14	polyaniline-naflon nano-structure	nano-particles	PBS buffer	50	1.47-2.1	amperometry	54
15	thiol functionalized reduced GO	nano-particles	water	20	180	electro-chemical	55

16	2-hydroxy benzothiazole modified rhodol	organic compound	THF: HEPES (4:6, v/v)	270	-	fluorescence	56
17	nitrogen-doped carbon quantum dots	quantum dots	water	230	15	fluorescence	57
18	$[Ni(3\text{-}bpd)_2(NCS)_2]_n$	MOF	water	-	120	fluorescence	58
19	[PCN-221]	MOF	water	10	1	fluorescence	59
20	[Cu(Dcbb)(Bpe)].Cl	MOF	HEPES buffer	3.2 and 3.3	30	fluorescence	60
21	UiO-66@ Butyne	MOF	water	10.9	3	fluorescence	61
22	$Ln(TATAB)\cdot(DMF)_4(H_2O)(MeOH)_{0.5}$	MOF	water	4.4	-	fluorescence	62
23	Eu^{3+}/CDs@MOF-253	MOF	water	47.88	3	fluorescence	63
24	$[Cu(Cdcbp)(H_2O)_2\cdot 2H_2O]_n$	MOF	water	(2.3 ± 0.8)	2	fluorescence	64
25	Al-MOF (TAM)	MOF	water	2.94	0.5	fluorescence	65
26	$[Cu(Cbdcp)(Dps)(H_2O)_3]\cdot 6H_2O_n$	MOF	HEPES buffer	2.6	10	fluorescence	66
27	Cd−EDDA	MOF	water	2	0.25	fluorescence	39
28	tetrahydrodibenzo phenanthridine derivatives	organic compound	DMSO : THF = 1 : 1	0.91 and 0.041	-	fluorescence	28
29	$[Zn(L)(BBI).(H_2O)_2]$ $[Cd(L)(TPOM)0_{.75}]_xS$	MOF	water	-	-	fluorescence	67
30	$Zr_6O_4(OH)_4(C_{12}H_4S_2)_6$ (**2′**)	MOF	water	5	1	fluorescence	this work

Recyclability tests up to five cycles were conducted using the probe **2′**. The MOF material was recovered after each cycle by centrifugation. Then, the material was filtered, dried and used for next cycle of sensing. Figure 3.22 displays that the material can sense with almost equal efficiency up to five cycles. High reusability with equal efficiency ensures that the probe is highly applicable for the real-life sensing purpose.

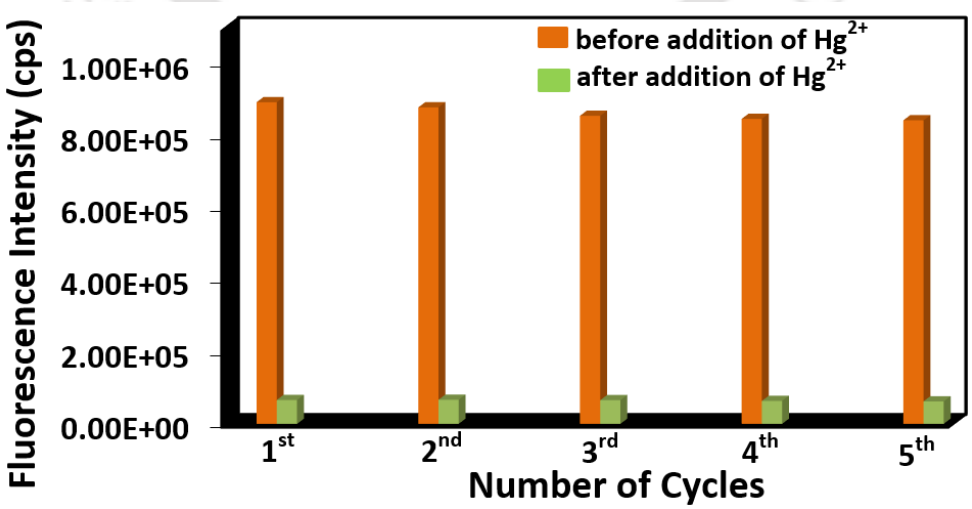

Figure 3.22 Recyclability plot of **2′** towards the sensing of Hg^{2+} in water.

3.3.9 Mechanistic Investigation for Hg^{2+} Sensing

Recyclability performance up to five cycle (Figure 3.22) and integrity of the framework structure of **2′** after Hg^{2+} sensing (Figure 3.23) ensure that the sensing mechanism is not reaction-based. Many sulphur containing sensor molecules of Hg^{2+} are available in literature where the interaction between the soft sulphur (S) atoms with the soft Hg^{2+} was the reason behind the quenching of fluorescence emission intensities of the sensors.[68] We also expected here that the interaction between the sulphur atoms of the thiophene rings (present in the linker molecule) and Hg^{2+} may be the reason behind the quenching process.

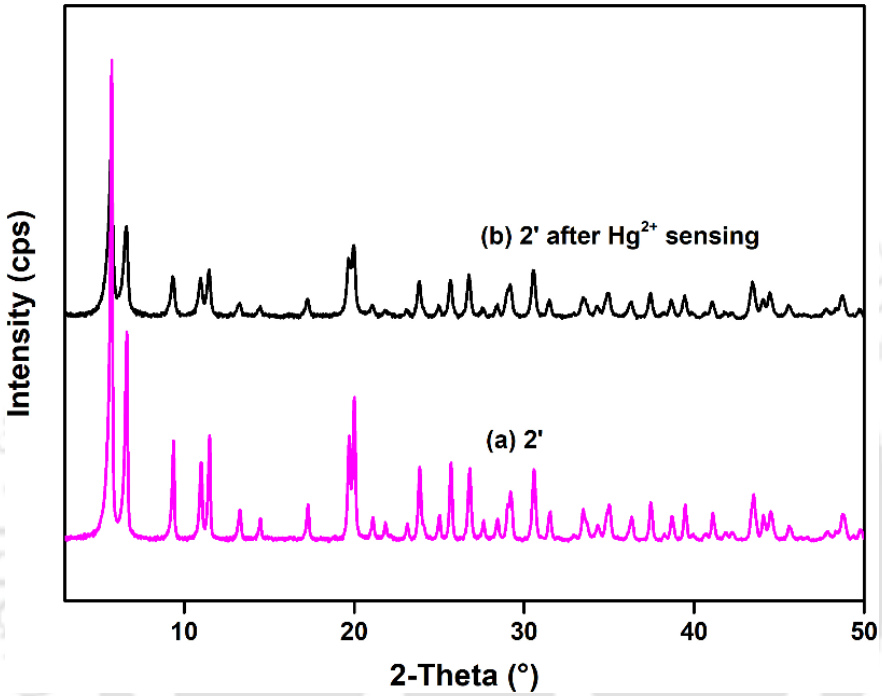

Figure 3.23 PXRD patterns of compound **2′** before (a) and after (b) treatment with Hg^{2+} in aqueous medium.

To explore the actual reason for quenching, we have performed the luminescence lifetime measurements (Figure 3.24 and Table 3.3). Insignificant change in fluorescence lifetime (2.08 and 2.07 ns) before and after the addition of Hg^{2+} confirms the static nature of the quenching process.[69] Static nature of quenching ruled out the possibility of resonance energy transfer from **2′** to Hg^{2+}. Therefore, the coordinative interaction between soft sulfur atoms of **2′** and Hg^{2+} ($S\cdots Hg^{2+}$ interaction)[70] may be the reason behind the quenching process. This kind of interaction was reported in many of the sensing/absorption processes of Hg^{2+} in literature.[28, 71]

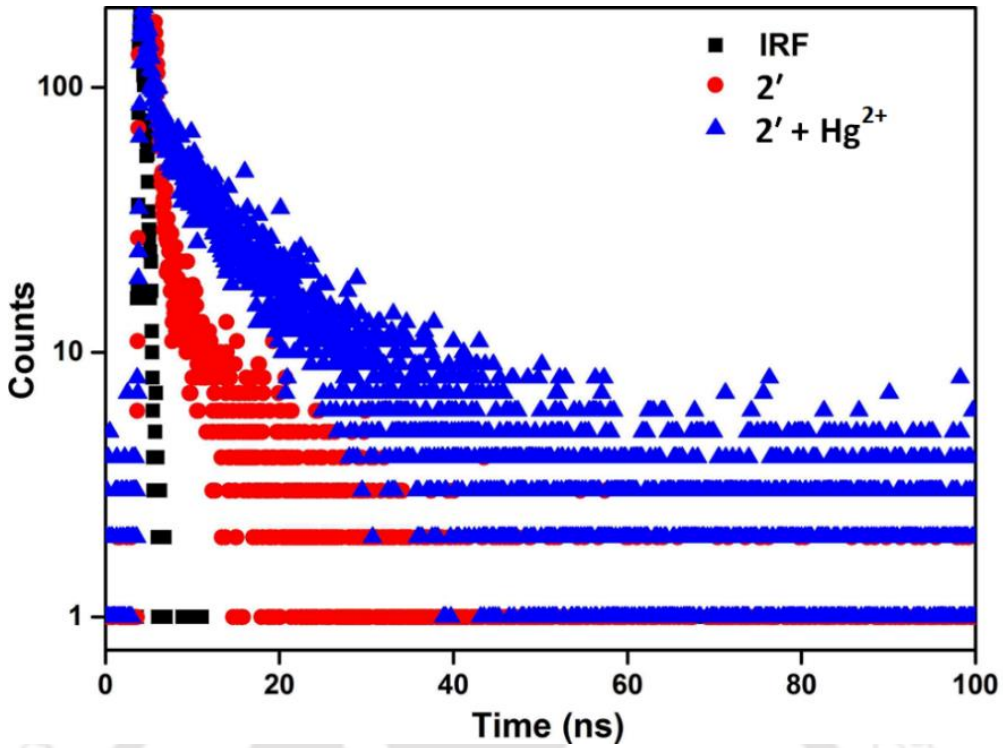

Figure 3.24 Lifetime decay profile of **2′** in the absence and presence of Hg^{2+} solution (λ_{ex} = 320 nm, monitored at 308 nm). Here, IRF = instrument response function.

Table 3.3 Fluorescence lifetimes of **2′** before and after the addition of Hg^{2+} solution (λ_{ex} = 320 nm, pulsed diode laser).

Volume of NFT Solution Added (μL)	a_1	a_2	τ_1 (ns)	τ_2 (ns)	$<\tau>$*(ns)
0	0.82	0.18	0.61	8.81	2.08
100	0.78	0.22	0.58	7.39	2.07

* $<\tau> = a_1\tau_1 + a_2\tau_2$

Furthermore, we took the supports of UV-Vis, EDX and XPS analysis to validate the probable interaction between the S atoms (of the linker) and Hg^{2+}. EDX analysis of the recovered material obtained after sensing displayed the presence of Hg^{2+} (3.1 wt%) (Figure 3.25). This implies that some complexation took place between Hg^{2+} and S atoms of the linker molecule. But, the retention of PXRD profile indicates that the interactions between Hg^{2+} and the S atoms of the thiophene rings are not sufficiently strong to break down the crystalline nature of **2′**. Furthermore, the possible interaction between soft S atoms of **2′** and Hg^{2+} was examined by the UV-Vis spectroscopy (Figure 3.26). Before the addition of Hg^{2+}, **2′** displayed absorption peaks at 374 and 255 nm and a shoulder peak at 362 nm. But, after the inclusion of Hg^{2+}, the peak at 374 nm vanished and a new absorption peak at 344 nm appeared along with two small peaks at 381 and 403 nm. The peak at 255 nm remained at the same position. These changes in the UV-Vis spectra strongly support the interaction between the soft S atoms and Hg^{2+}.[72, 73]

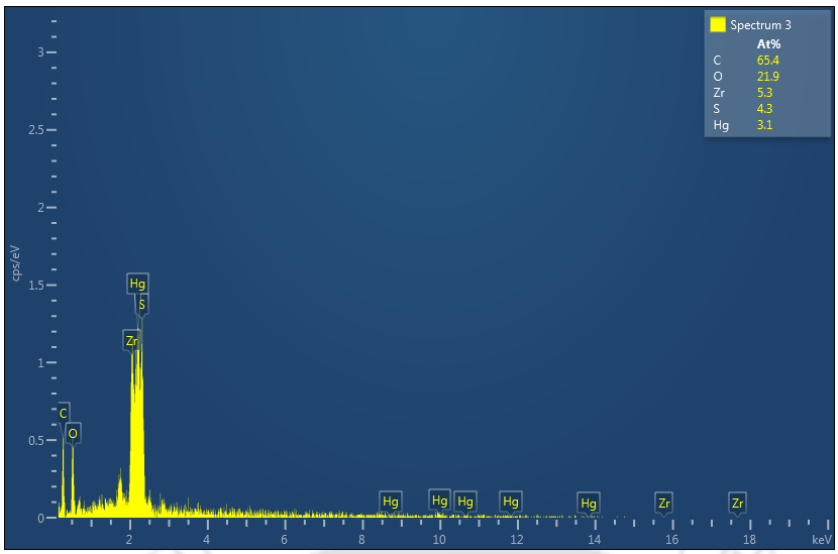

Figure 3.25 EDX spectrum of **2′** after treatment with 10 mM Hg^{2+} solution under sensing conditions.

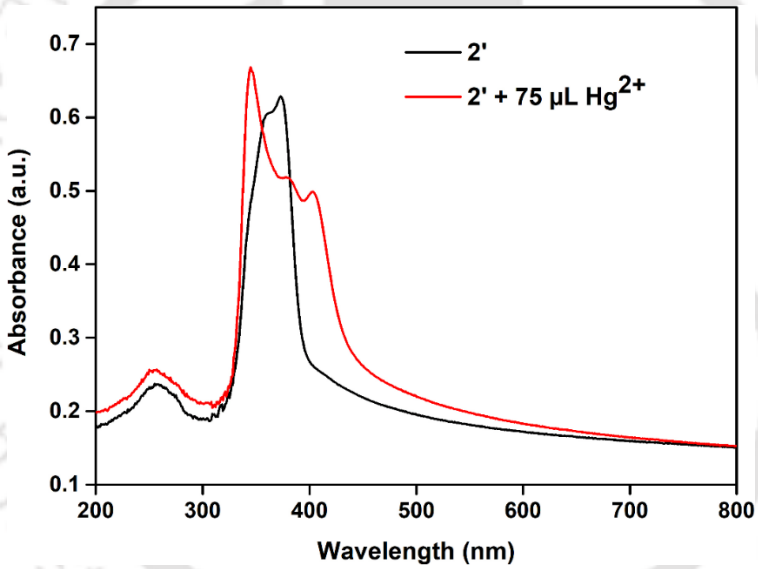

Figure 3.26 UV-Vis spectra of compound **2′** in absence (black) and presence (red) of solution (75 µL, 10 mM).

To confirm the specific interaction between S and Hg^{2+}, we performed XPS analysis. The XPS spectra of **2′** before and after the treatment of Hg^{2+} were analysed (Figures 3.27-3.31). The XPS signature of the 4f orbital of Hg^{2+} showed sharp peaks at 101.38 and 105.41 eV. This confirmed the presence of Hg^{2+} in the recovered material obtained after the sensing event. Furthermore, the XPS spectra of the fresh and Hg^{2+} treated **2′** for Zr 3d, O 1s and C 1s orbitals were similar. However, an obvious change in the XPS spectrum of S 2p orbital of the fresh and used **2′** confirmed the interaction between the S atoms of thiophene rings and Hg^{2+}. The peaks at 163.82, 164.88, 168.78 and 169.91 eV for the fresh sample correspond to the 2p orbital of S atoms, which were shifted to the lower energy region (163.15, 164.22, 168.07 and 169.22 eV) after the treatment of Hg^{2+}. All the above experimental results strongly support that the

coordinative interactions between the S atoms of **2′** to Hg^{2+} were the reasons behind the fluorescence quenching of **2′**.

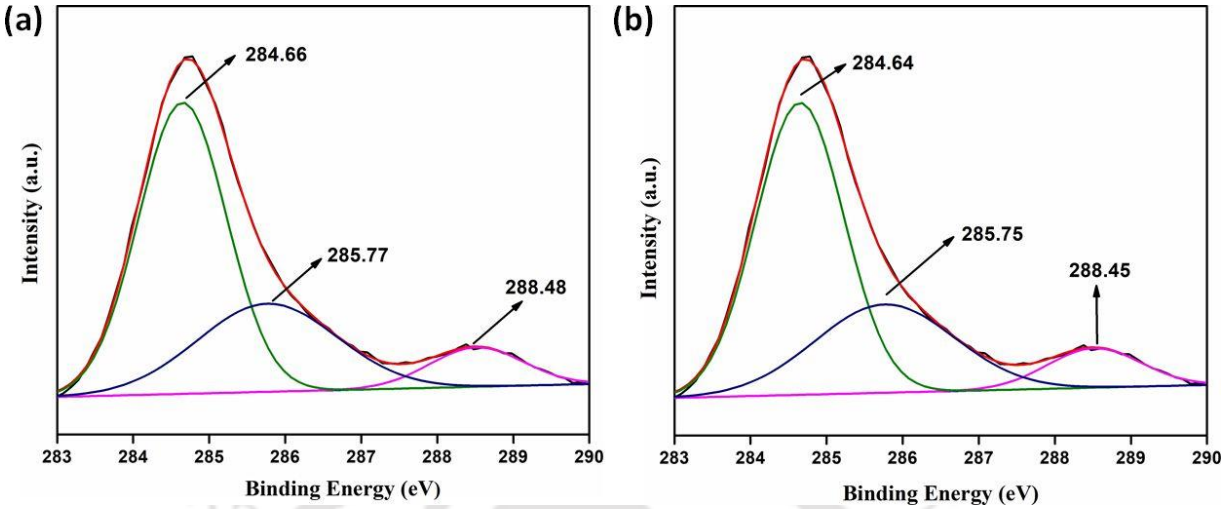

Figure 3.27 Fitted XPS spectra of C (1s) before (a) and after (b) treatment of **2′** with Hg^{2+}.

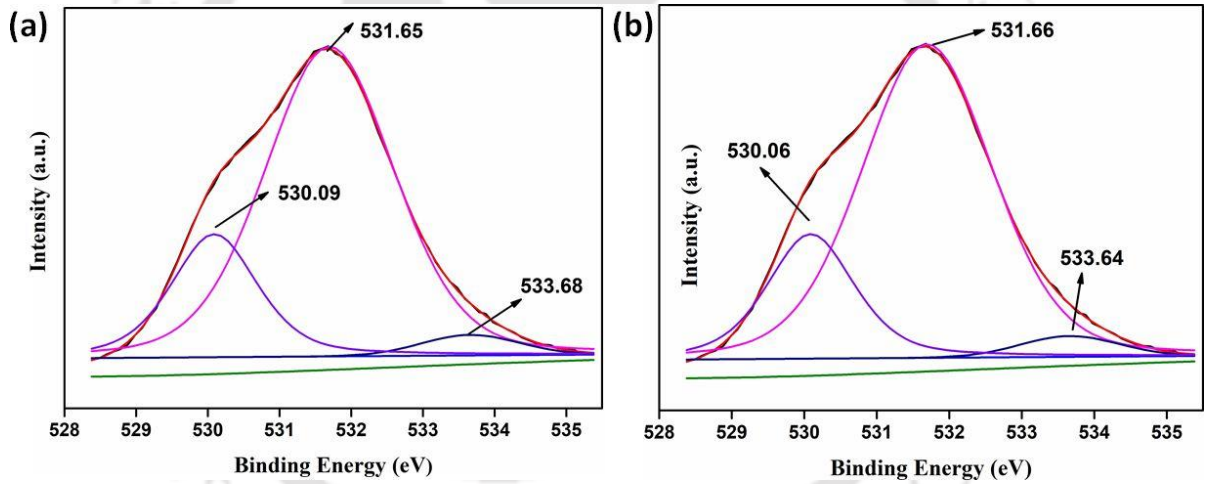

Figure 3.28 Fitted XPS spectra of O (1s) before (a) and after (b) treatment of **2′** with Hg^{2+}.

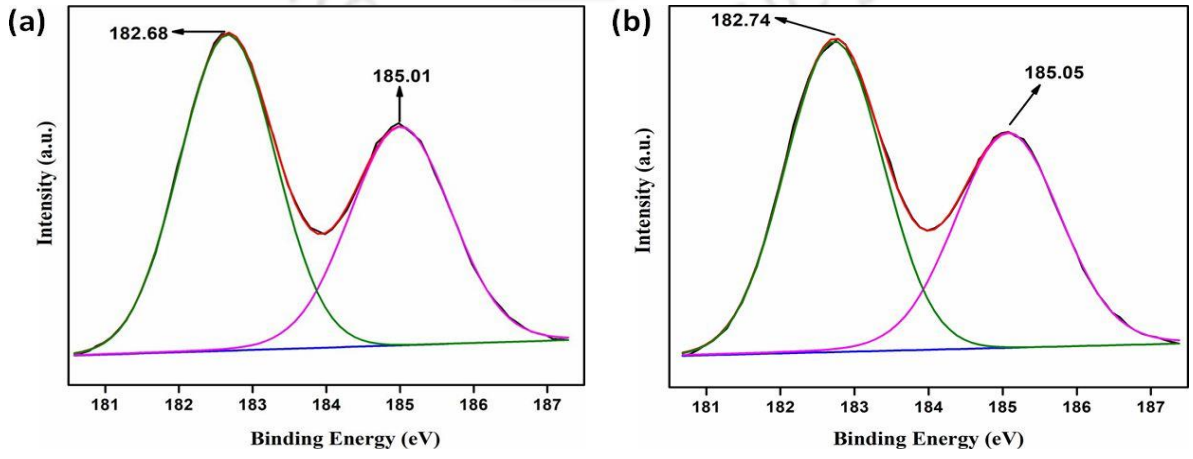

Figure 3.29 Fitted XPS spectra of Zr (3d) before (a) and after (b) treatment of **2′** with Hg^{2+}

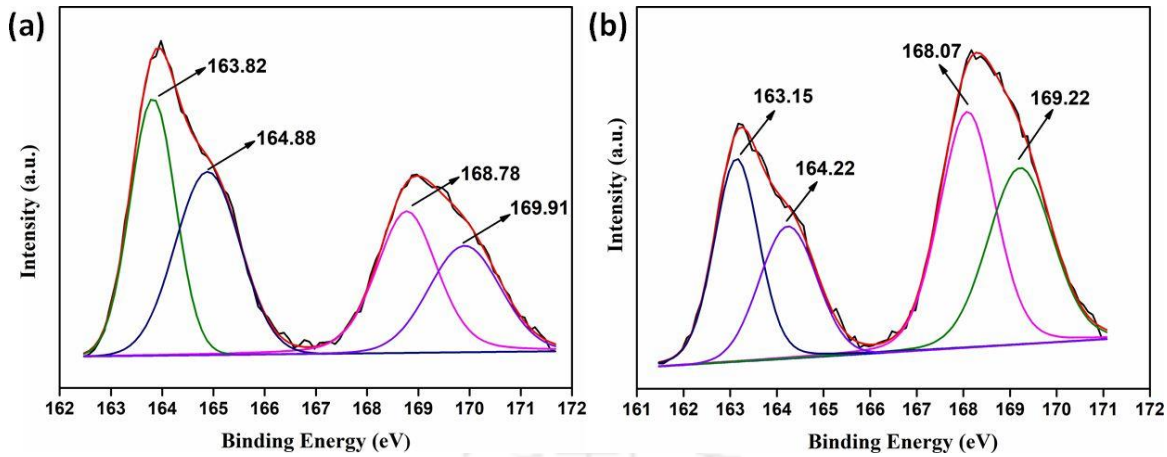

Figure 3.30 Fitted XPS spectra of S (2p) before (a) and after (b) treatment of **2′** with Hg^{2+}.

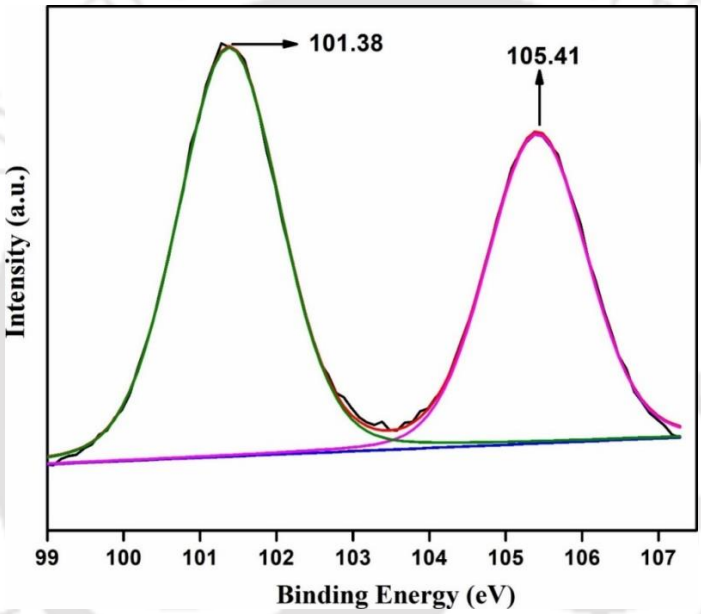

Figure 3.31 Fitted XPS spectrum of Hg (4f) after treatment of **2′** with Hg^{2+}.

3.3.10 Fluorescence Sensing of Antibiotics (NFZ and NFT) in MeOH

In modern days, different types of pharmaceutical antibiotics are being used all over the world for the purpose of human therapy and farming industry.[8] In the year of 1928, the first antibiotic penicillin was discovered.[9] Thereafter in the last 90 years, a variety of antibiotics were developed to get rid of different bacterial diseases.[10, 11] However, the excessive use and arbitrary disposal of the poorly metabolized antibiotics create lot of problems for the environment and also for the living beings.[12, 13] Long term intake of antibiotics may develop the antibiotic resistant genes in living organisms which have serious effects on ecosystem.[13, 14] Residues of pharmaceutical antibiotics and their various transformed products may cause different adverse effects like chronic and acute toxicity and microorganism antibiotic resistance.[15] Nitrofurazone (NFZ) and nitrofurantoin (NFT) are two very common antibiotics which are mainly used for the remedy of skin infections, and urinary tract and kidney infections, respectively.[16, 17] Exposure to these antibiotics for long-time may cause several side

effects, such as nausea, vomiting, headache, loss of appetite and dizziness.[18, 19] Thereafter, it is necessary to develop a suitable method to prevent the environmental pollutions which are caused by these antibiotics.

To verify the efficiency of **2′** for the sensing of antibiotics, firstly, we measured the emission intensity of **2′** (100 µL MOF in 2900 µL MeOH) after exciting the MOF suspension at 370 nm. Strong emission intensity with an emission maximum at 442 nm was observed before the addition of NFZ and NFT antibiotic solutions. But, the emission intensities of **2′** gradually decreased after each incremental accumulation of 10 mM of NFZ and NFT antibiotic solutions. The diminution of emission intensities became saturated after the addition of 100 µL of 10 mM methanolic solution of NFZ and NFT antibiotics (Figure 3.32).

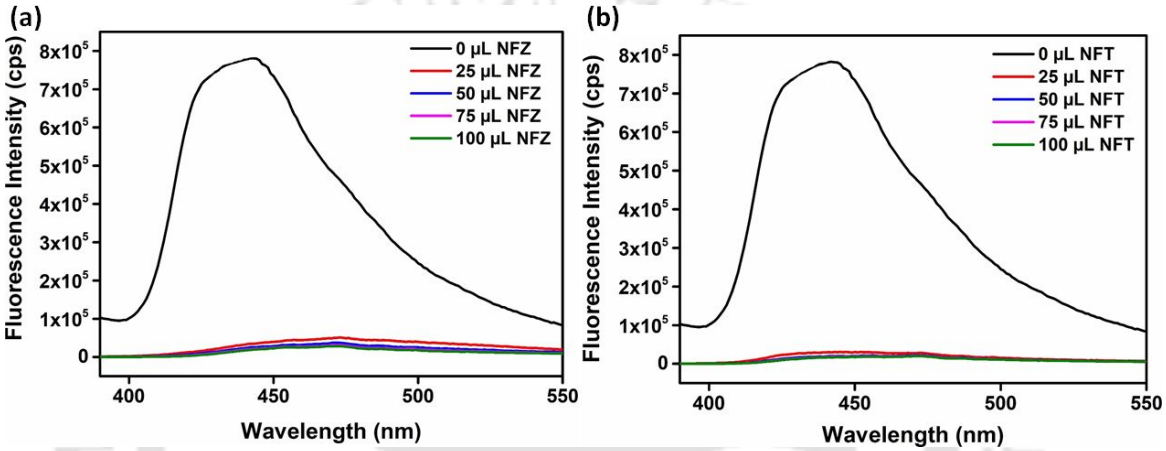

Figure 3.32 Quenching in luminescence intensity of **2′** with the gradual addition of 10 mM aqueous solution of NFZ and NFT (from 0 µL to 100 µL) (λ_{ex} = 370 nm and λ_{em} = 442 nm).

Detection time for these antibiotic by the probe was measured after addition of 100 µL of methanolic solution of NFZ and NFT antibiotics into a cuvette filled with the mixture of 100 µL MOF in 2900 µL MeOH. The reduction in fluorescence intensity became saturated after 1 min of the addition of NFZ and NFT antibiotics (Figure 3.33). The experiment evidenced that the response time of the probe towards antibiotics is less than 1 min.

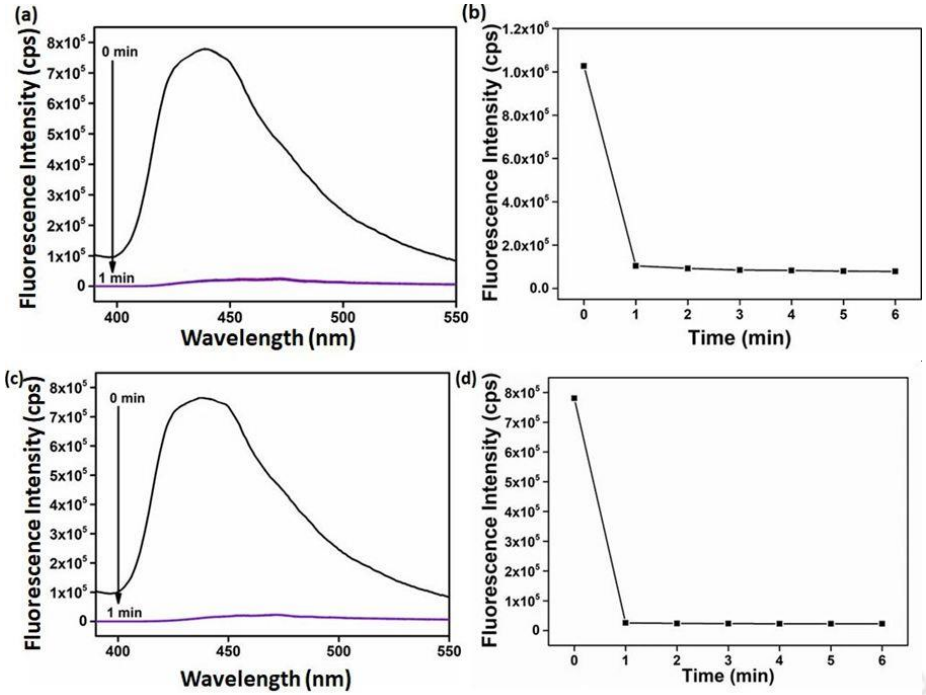

Figure 3.33 Switch-off in luminescence intensity of **2′** with respect to time after the inclusion of 100 µL of 10 mM of (a) NFZ and (c) NFT solutions in MeOH. Variation of fluorescence intensity with time for (b) NFZ and (d) NFT (λ_{ex} = 370 nm, λ_{em} = 442 nm).

The selective sensing efficiency was verified after addition of 100 µL of 10 mM of the other antibiotic solutions to the suspension of 100 µL of MOF in 2900 µL MeOH. From Figure 3.34, it can be concluded that other antibiotics (except NFZ) did not effectively quench the fluorescence intensity of **2′**. Analogous experiments using 100 µL of 10 mM methanolic solution of antibiotics were performed in case of NFT. Similar result was also obtained in case of NFT. All these results imply that MOF is highly selective for the sensing of NFZ and NFT.

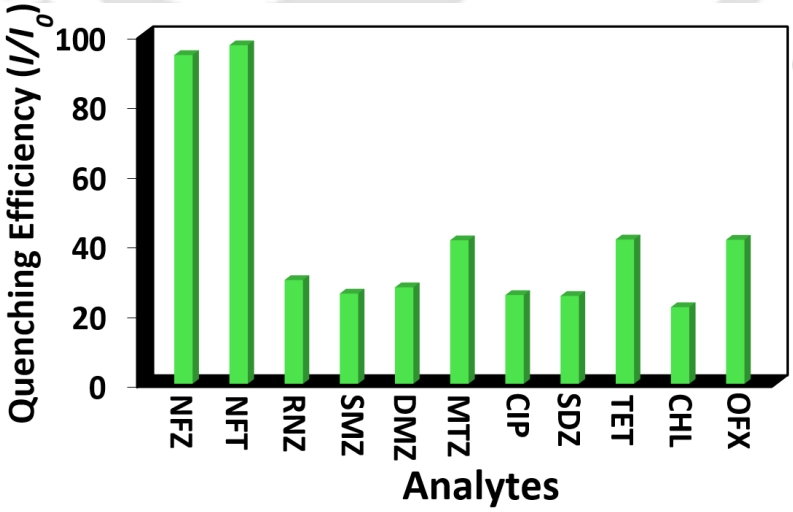

Figure 3.34 Switch-off in luminescence intensity of **2′** after inclusion (100 µL) of 10 mM of NFZ and NFT solutions and 100 µL of 10 mM solutions (in MeOH) of other competitor antibiotics (λ_{ex} = 370 nm, λ_{em} = 442 nm).

The selectivity of luminescence response of **2′** towards NFZ and NFT even in presence of other competitive analytes (metronidazole (MTZ), chloramphenicol (CHL), ofloxacin (OFX), ciprofloxacin (CIP), tetracycline (TET), dimetridozole (DMZ), sulfamethazine (SMZ), ronidazole (RNZ) and sulfadiazine (SDZ)) were also verified. For this study, at first, the MOF material was treated with 100 µL of other competitive antibiotics. After that, the material was further treated with 100 µL (10 mM) MeOH solution of NFZ (identical experiments were also carried out in case of NFT antibiotic after taking 100 µL of 10 mM of NFT solution). From Figure 3.35, it is clear that NFT and NFZ can quench the emission intensity of **2′** with equal efficiency even in attendance of its other congeners. Therefore, we can deduce that **2′** is highly suitable for the selective sensing of NFZ and NFT in MeOH.

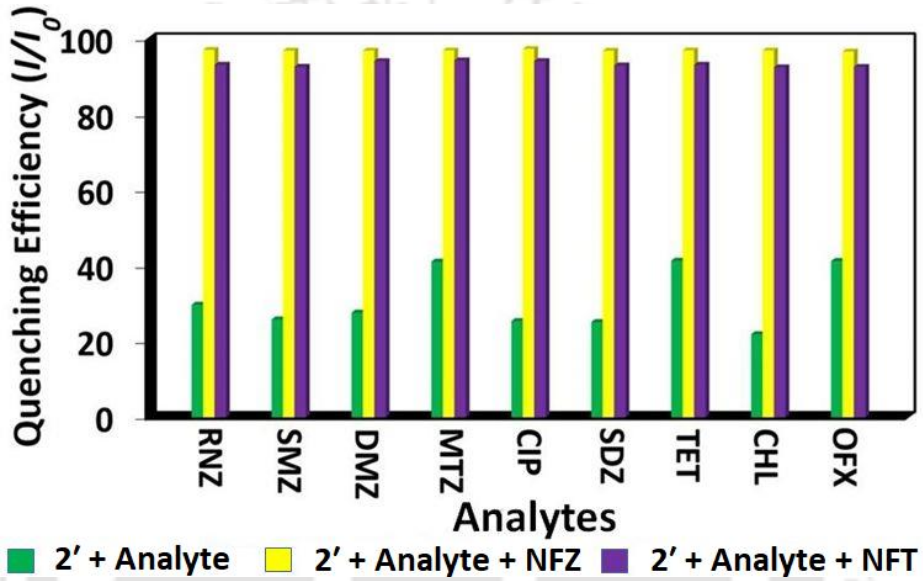

Figure 3.35 Switch-off in fluorescence emission intensity of **2′** after addition (100 µL) of 10 mM of NFZ and NFT solutions in the presence of 100 µL of 10 mM solutions (in MeOH) of other competitor antibiotics (λ_{ex} = 370 nm, λ_{em} = 442 nm).

To realize the actual mechanism behind the quenching of fluorescence intensity in the presence of NFZ and NFT, we analysed the S-V plots (Figure 3.36). The K_{sv} values were determined using the following formula: $I_0/I = K_{sv}[Q] + 1$

The K_{sv} value of 1.42×10^5 M^{-1} and 4.3×10^5 M^{-1} for NFZ and NFT are superior to most of the other reported chemosensors of nitro-antibiotics (Figure 3.37-3.38).[30, 74, 75] Initially, at lower concentration of nitro-antibiotics, the S-V plots were linear in nature. But, at higher concentrations of nitro-antibiotics, they deviate from their linearity. Thereby, the energy transfer process or self-absorption may be the reason behind these quenching processes.

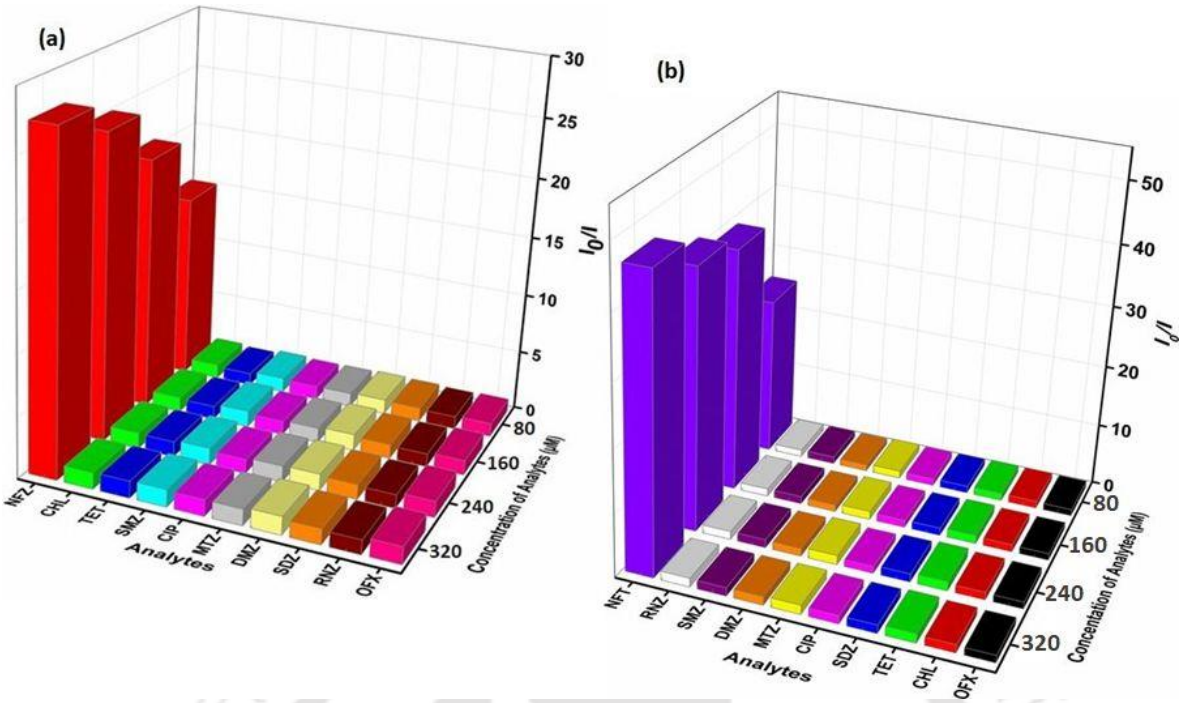

Figure 3.36 S-V plots for the decrease in luminescence intensities of **2′** with the gradual addition of various antibiotics in case of (a) NFZ and (b) NFT sensing.

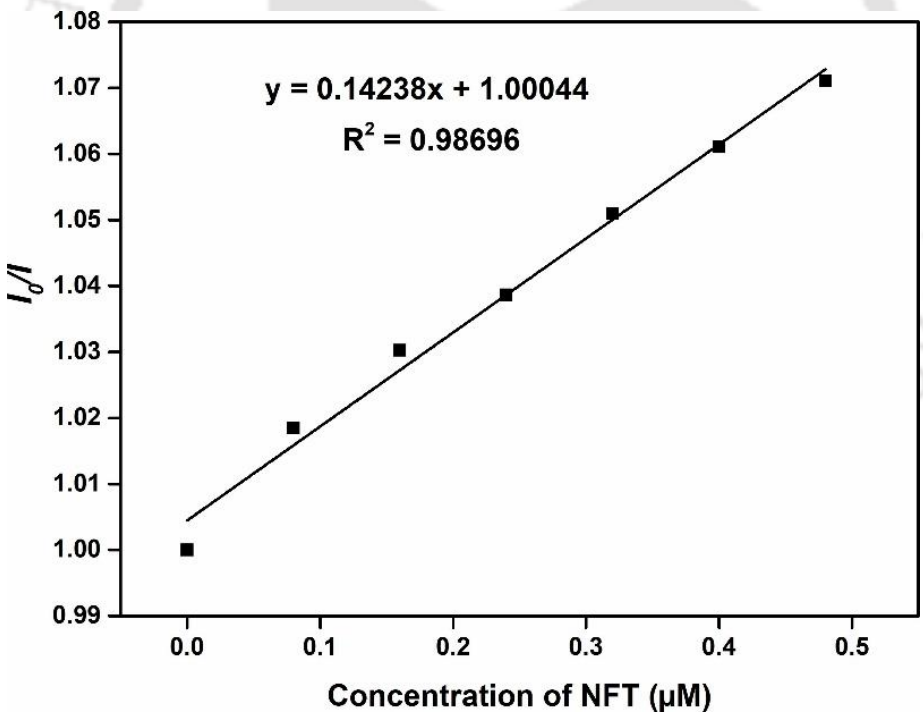

Figure 3.37 Stern-Volmer plot for the fluorescence emission quenching of **2′** in presence of NFZ solution.

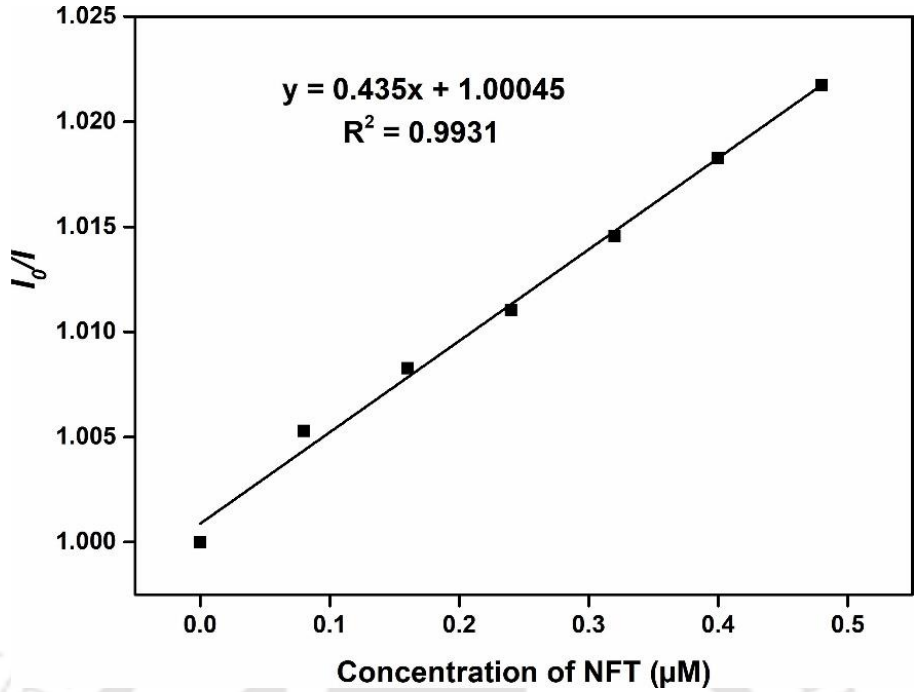

Figure 3.38 Stern-Volmer plot for the fluorescence emission quenching of **2′** in presence of NFT solution.

Similar to Hg^{2+} sensing, here also LOD values for the detection of NFZ and NFT were calculated (Figures 3.39-3.40) using the 3σ/k rule. The final obtained values of LODs are 156.7 nM and 96.3 nM for NFZ and NFT, respectively. The obtained LOD values are much lower than most of the reported chemosensors of NFZ and NFT (Table 3.4).

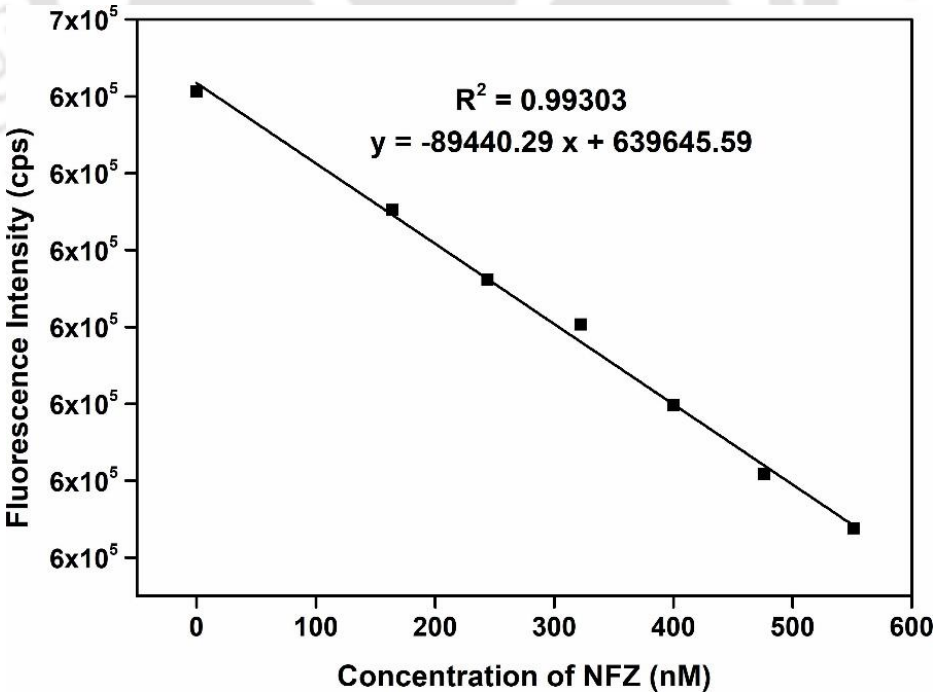

Figure 3.39 Change in the fluorescence intensity of **2′** in MeOH as a function of concentration of NFZ.

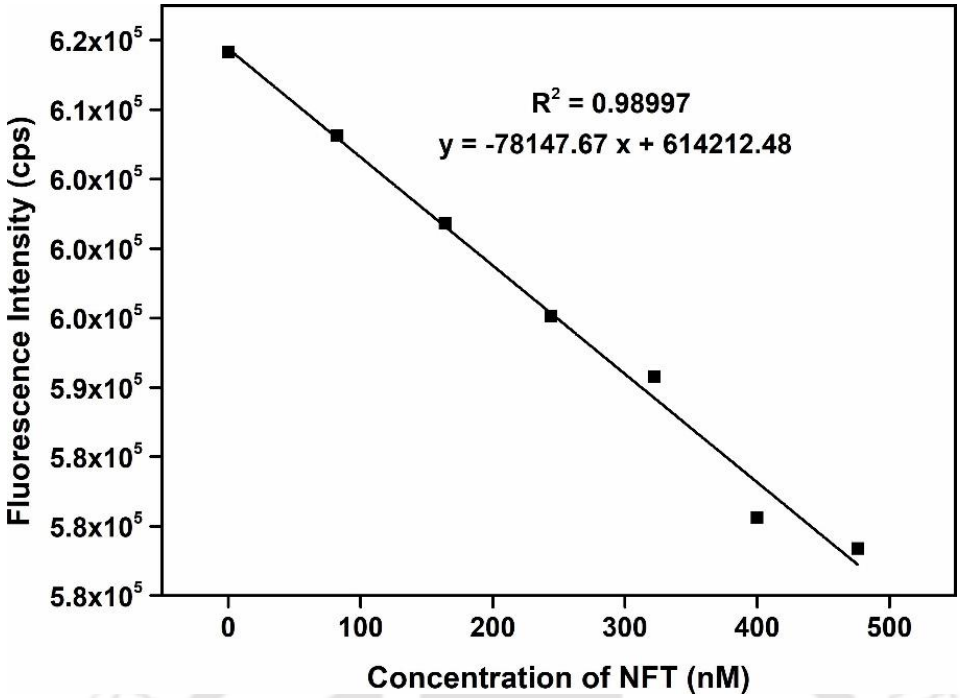

Figure 3.40 Change in the fluorescence intensity of **2′** in MeOH as a function of concentration of NFT.

Table 3.4 Comparison of the response time, detection limit and sensing media used for the reported chemosensors of NFT and NFZ in the literature.

Sl. No.	Sensor Material	Type of Material	Name of Antibiotic	Sensing Medium	Detection Limit (nM)	Response Time (min)	Detection Method	Ref.
1	HNU-52	MOF	NFT NFZ	DMF	920 720	1	fluorescence	76
2	$[Zn(TTPBA\text{-}4)_{0.5}(TPA)]\cdot H_2O\cdot 0.5DMF$	MOF	NFT NFZ	DMAc	-	-	fluorescence	30
3	Cr-MIL-101/A	MOF	NFT	-	3	10	electro-chemical	77
4	CNDs	nano-particles	NFT	-	1400	-	fluorescence	78
5	Gold nimrods	nanorods	NFT	-	6510	60	voltammetry	79
6	MIPs	polymers	NFT	acetonitrile + 0.2% dimethyl sulfoxide	5000	-	voltammetry	80
7	$(Me_2NH_2)_{1.5}\cdot[In_{1.5}(FBDC)(BDC)]_{2.5}\cdot NMF\cdot CH_3CN$	MOF	NFT	water	1900	60	fluorescence	81
8	$[Cd_3(DBPT)_2(H_2O)_4]\cdot 5H_2O$		NFT	methanol	5000	-	fluorescence	82

9	Ag-SDS electrode	nano-particles	NFZ	ternary choline chloride-urea-glycerol	370	-	voltammetry	83
10	rGO/Fe_3O_4NR	nanorod	NFT	water	1.14	-	electro-chemical sensor	84
11	TiO_2-rGO NC	nano-particles	NFT	water	2.28	20	voltammetry	85
12	$Tb(TCPB)_{0.5}$ DMF		NFZ NFT	water	55000 120000	120	fluorescence	86
13	MIP film	polymer	NFT	real serum samples	0.3	30	electrochemical sensor	87
14	LMNS	nano-spheres	NFT	water	72	20	voltammetry	88
15	$[Cd_3(TDCPB)\cdot 2DMAc]\cdot DMAc\cdot 4H_2O$	MOF	NFT NFZ	DMAc	60000	1.25	fluorescence	89
16	**4**⊃DEASM	MOF	NFZ	water	208	-	fluorescence	90
17	$[Zr_6O_4(OH)_4(C_{12}H_4S_2)_6]$ (**2′**)	MOF	NFT NFZ	MeOH	96.3 156.7	1	fluorescence	this work

Reusability performance for the sensing of NFZ and NFT up to five cycles was explored (Figures 3.41-3.42). A similar experimental procedure as applied in the case of Hg^{2+} sensing was followed. It is worth noting that, the material is highly recyclable for the sensing of the selected nitro-antibiotics. High recyclable performance without loss of its sensing efficiency increases its practical application possibilities.

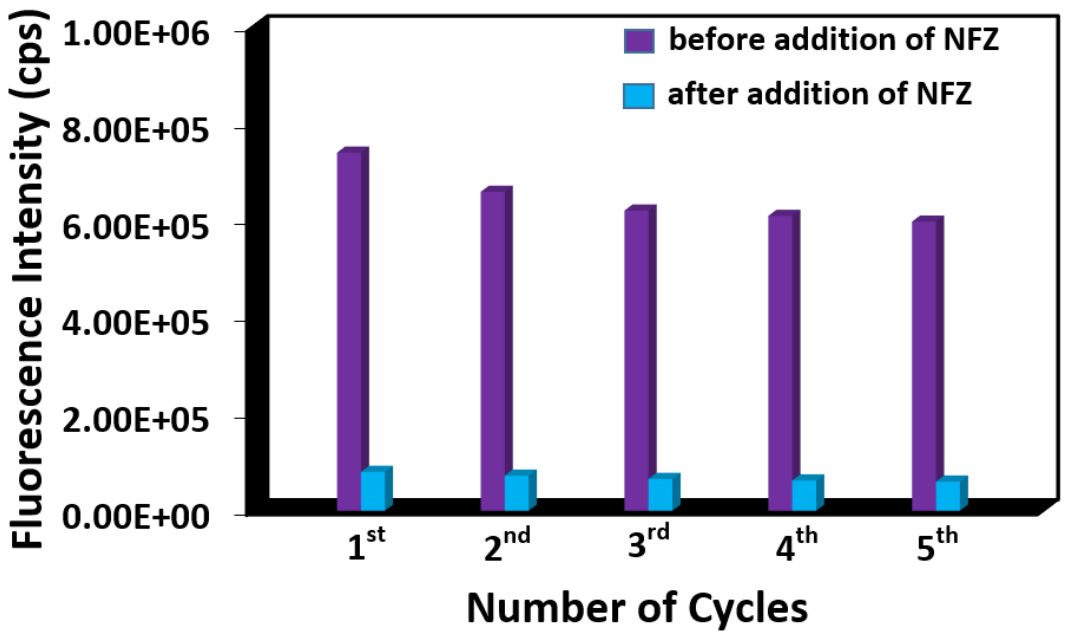

Figure 3.41 Recyclability plot of **2′** towards the sensing of NFZ in MeOH.

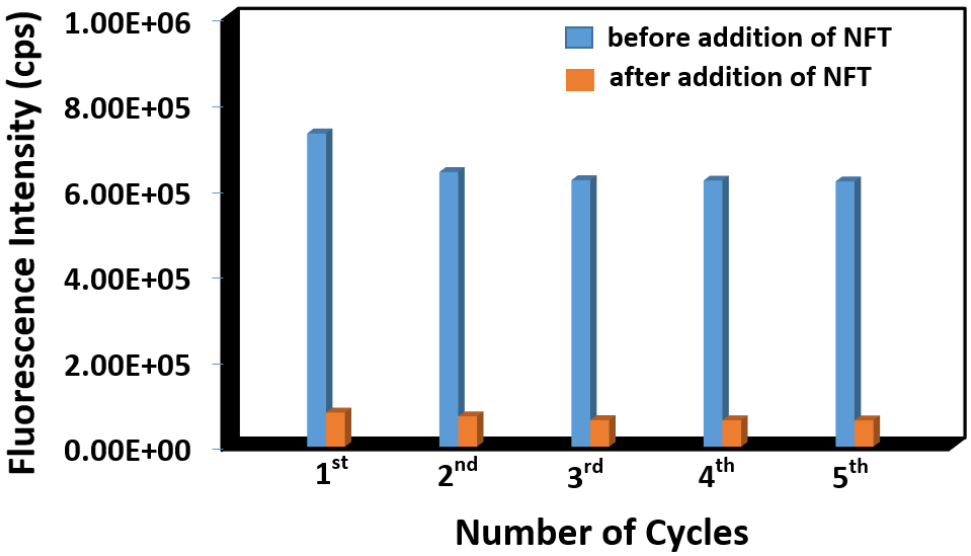

Figure 3.42 Recyclability plot of **2′** towards the sensing of NFT in MeOH.

3.3.11 Mechanistic Investigation for NFZ and NFT Sensing

Reusability of **2′** for the sensing of NFZ and NFT up to five conjugative cycles (Figures 3.41-3.42) and retention of PXRD profile of **2′** after sensing (Figure 3.43) confirmed that the mechanism behind quenching is not reaction based.

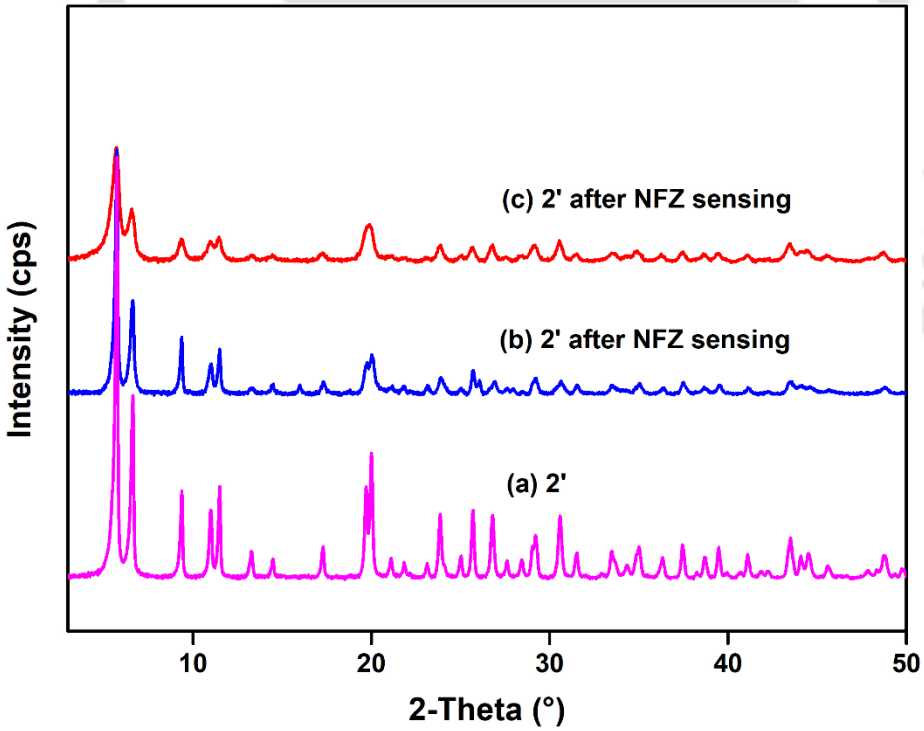

Figure 3.43 PXRD patterns of compound **2′** before (a) and after (b) treatment with Hg^{2+} in aqueous medium, (c) after treatment with NFZ and (d) after treatment with NFT in MeOH.

There are some basic phenomena like collision between molecules, ground state complexation, energy transfer process, inner filter effect (IFE) and excited-state reaction which are reported in the literature reasons behind quenching processes.[91] All the above processes can

be classified into two different types of quenching processes. These are static and dynamic quenching processes. The diffusion of quencher molecules to the excited state of the fluorophore and the collision between the fluorophore and the quencher molecules are the main reasons behind the dynamic quenching. On the other hand, the close association between the fluorophore and the quencher molecules may result in static quenching.[70]

A time-resolved fluorescence study can corroborate the nature of quenching. If the fluorescence lifetime of the excited state fluorophore remains constant even after the addition of a quencher molecule, the process is static quenching. But, if the fluorescence lifetime decreases, the process is dynamic quenching.[69]

Here, after the addition of nitro-antibiotics, the fluorescence lifetime of the fluorophore was reduced from 1.68 ns to 1.28 and 1.38 ns for NFZ and NFT, respectively (Figures 3.44-3.45 and Table 3.5-3.6). It confirmed the dynamic nature of quenching. Hence, the possibilities of IFE and static quenching are completely ruled out.

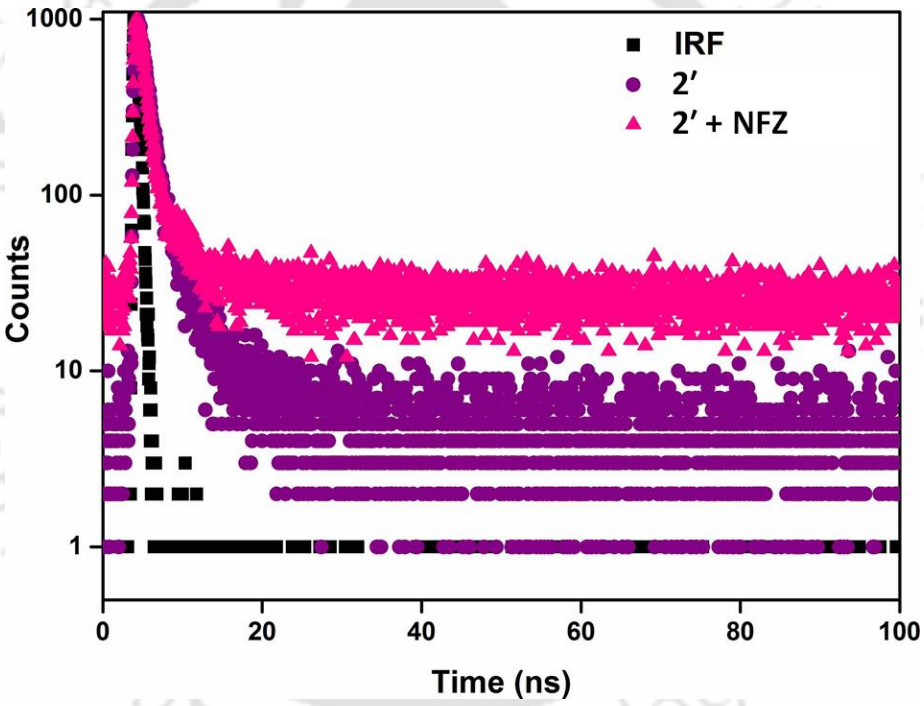

Figure 3.44 Lifetime decay profile of **2′** in the absence and presence of NFZ solution (λ_{ex} = 320 nm, monitored at 308 nm). Here, IRF = instrument response function.

Table 3.5 Fluorescence lifetimes of **2′** before and after the addition of NFZ solution (λ_{ex} = 308 nm, pulsed diode laser).

Volume of NFZ Solution Added (μL)	a_1	a_2	τ_1 (ns)	τ_2 (ns)	$<\tau>$*(ns)
0	0.73	0.27	0.94	3.67	1.68
100	0.76	0.24	0.70	3.12	1.28

* $<\tau> = a_1\tau_1 + a_2\tau_2$

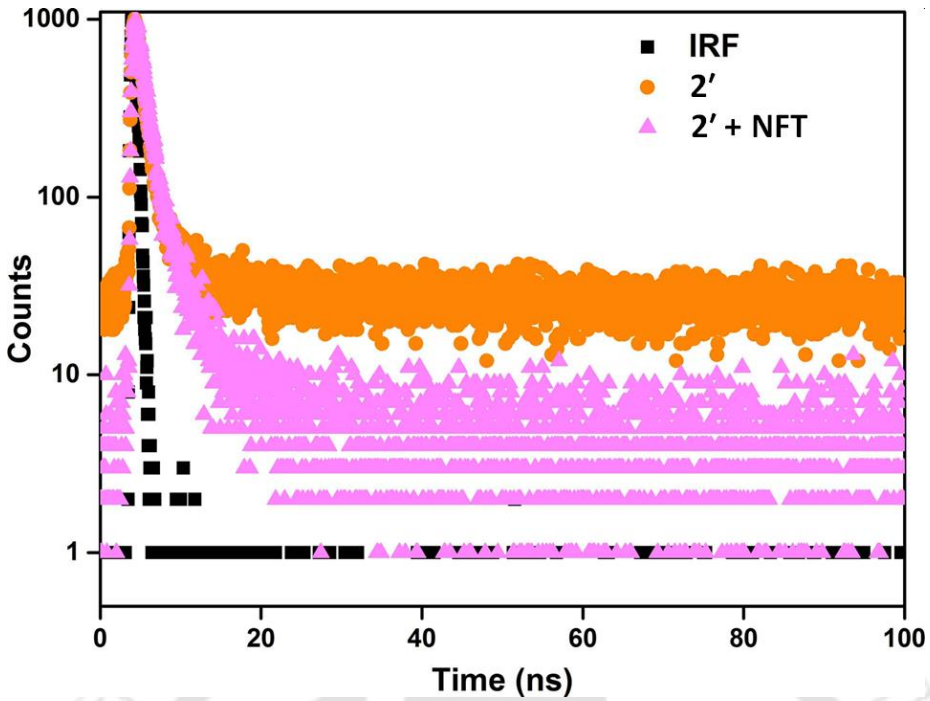

Figure 3.45 Lifetime decay profile of **2′** in absence and presence of NFT solution (λ_{ex} = 320 nm, monitored at 308 nm). Here, IRF = instrument response function.

Table 3.6 Fluorescence lifetimes of **2′** before and after the addition of NFT solution (λ_{ex} = 308 nm, pulsed diode laser).

Volume of NFT Solution Added (μL)	a_1	a_2	τ_1 (ns)	τ_2 (ns)	$<\tau>$* (ns)
0	0.73	0.27	0.94	3.67	1.68
100	0.72	0.28	0.58	3.47	1.38

* $<\tau> = a_1\tau_1 + a_2\tau_2$

For examination of the reason behind the quenching process in detail, we collected the UV-Vis spectra of all the antibiotics and the normalized absorption spectra overlapped with the emission spectrum of **2′**. From Figure 3.46, it is obvious that the maximum overlap took place between the absorption spectra of nitro-antibiotics and the emission spectra of **2′**, whereas, all the other antibiotics did not show any overlap. This satisfactory overlap resulted in the resonance energy transfer from **2′** to the nitro-antibiotics. This is the possible reason behind the quenching in fluorescence intensity which was further supported by the decrease in fluorescence lifetime value. It is worthily to note that the above-discussed mechanism was followed in many of the literature-reported sensing processes of nitro-antibiotics.[30, 92, 93]

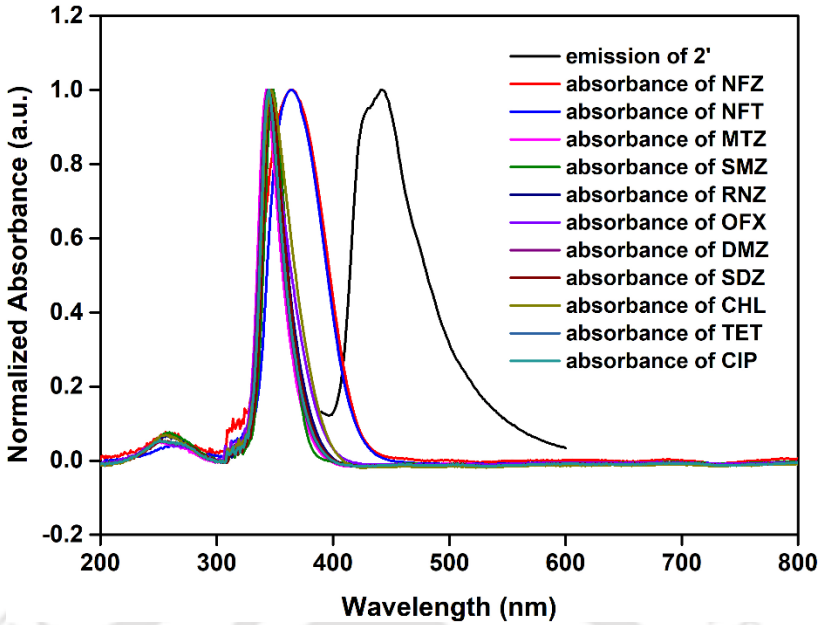

Figure 3.46 Spectral overlap between the emission spectrum of **2′** and absorption spectra of antibiotics.

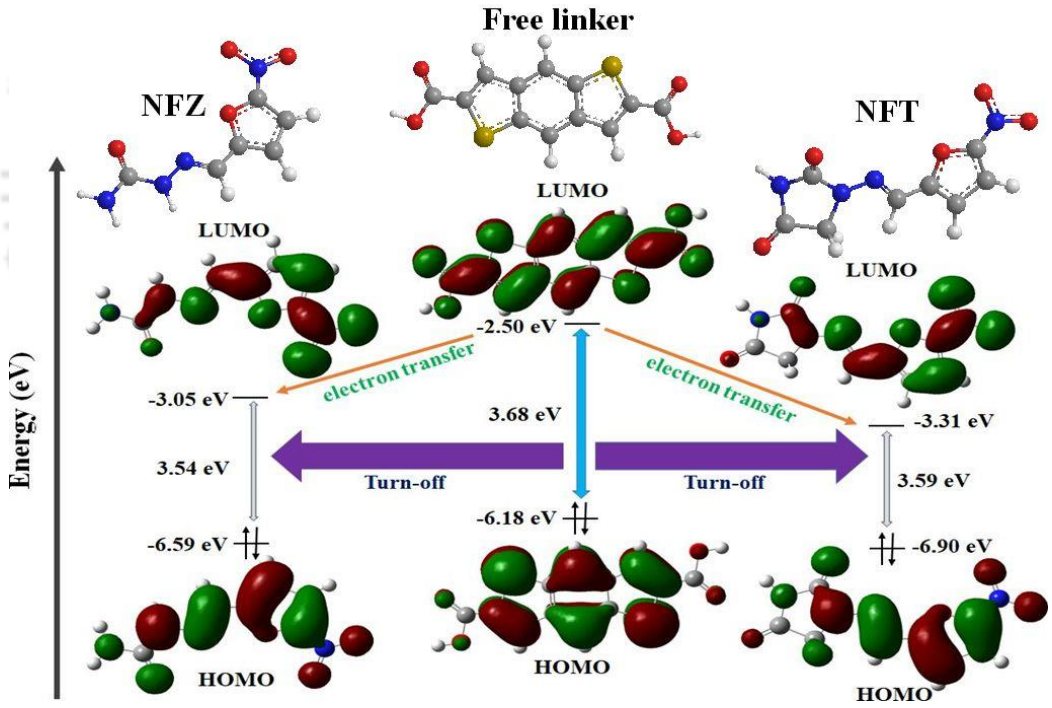

Figure 3.47 HOMO-LUMO energy levels of the linker, NFZ and NFT obtained from the DFT calculations using Gaussian 09 software.

The dynamic nature of quenching also inspired us to verify the possibility of photo-induced electron transfer (PET) between the electron-rich, donor MOF to electron-deficient nitro-antibiotics (NFZ and NFT), we executed the DFT calculations using Gaussian 09 software. The functional, B3LYP and Pople diffuse basis set 6-31G were utilized for all the calculations. The aim of these calculations was to know the exact location of the HOMOs and LUMOs of the linker molecule and the targeted sensing analytes. For an ideal electron transfer process, the

LUMOs of the electron-lacking analytes should stay in a lower energy level than the conduction band of the electron-rich probes. After DFT calculation with the linker molecule and nitro-antibiotics, we observed that the energy of the LUMO of the linker (-2.50 eV) is higher than the LUMO of the nitro-antibiotics (NFZ: -3.05 and NFT: -3.31 eV) (Figure 3.47). Such alignment of energy levels facilitated the PET process. These theoretical observations and aforementioned experimental evidence concluded that both FRET and PET are responsible for the observed change in fluorescence of the MOF in the presence of targeted antibiotics. Moreover, the possible interaction sites between the MOF (**2′**) and nitroantibiotics were investigated via an electrostatic potential (ESP) diagram of the linker of the MOF and nitroantibiotics, which revealed that the electron-rich sites of the linker majorly interacted with the electron deficient -NO_2 group containing sites of the anti-biotics.

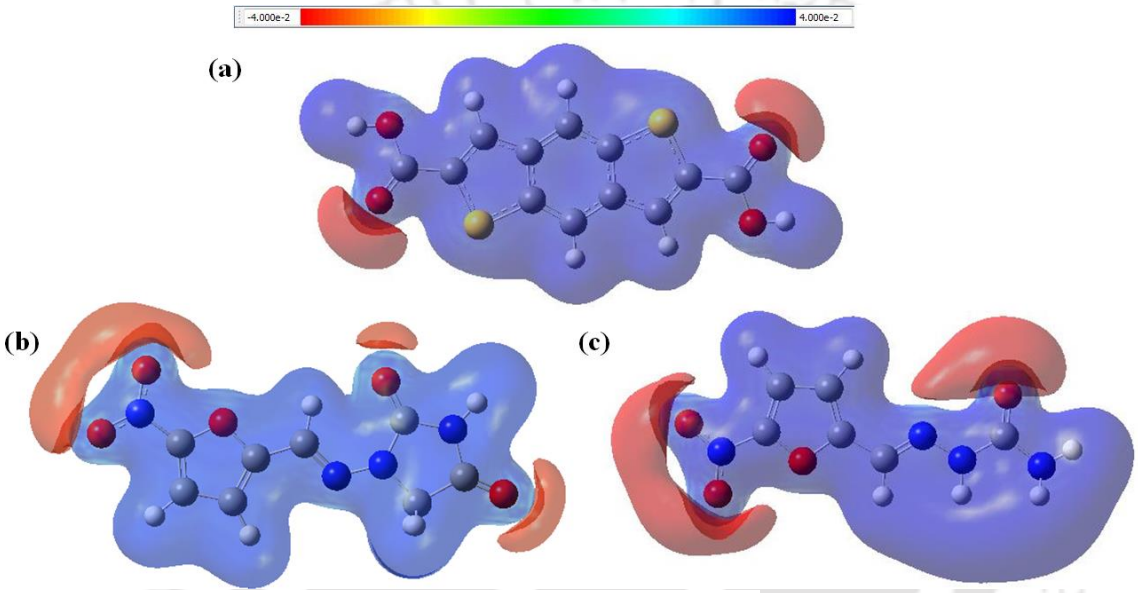

Figure 3.48 ESP surfaces of (a) linker, (b) NFT and (c) NFZ.

3.3.12 Sensing of Hg^{2+} and Nitro-antibiotics in Paper Strips

In recent times, the use of sensor-coated, cheap paper strips has rapidly increased for the in-field monitoring of toxic analytes. Here, we also verified the ability of our newly synthesized **2′** to sense our targeted analytes in a paper strip coated with **2′**. For this experiment, two filter paper strips were taken and both of them were homogeneously coated with **2′**. Then, **2′** coated paper strips were dried and treated with Hg^{2+} solution. After the treatment with Hg^{2+}, both of the filter papers were placed under UV light. A strong blue fluorescence was observed in the case of the untreated paper strip but no fluorescence was observed for the Hg^{2+} treated paper strip (Figure 3.49). This result implies that **2′** can sense Hg^{2+} in a paper strip. Analogous experiments were carried out in the case of both the nitro-antibiotics and similar observations were obtained in the case of both the antibiotics (Figure 3.50). Therefore, it can be concluded that real-time monitoring of Hg^{2+} and nitro-antibiotics is possible using **2′** coated paper strips.

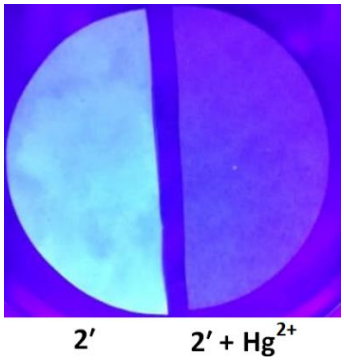

Figure 3.49 Images of **2′**-coated paper strips under UV lamp after and before the treatment of 10 mM aqueous Hg^{2+} solution.

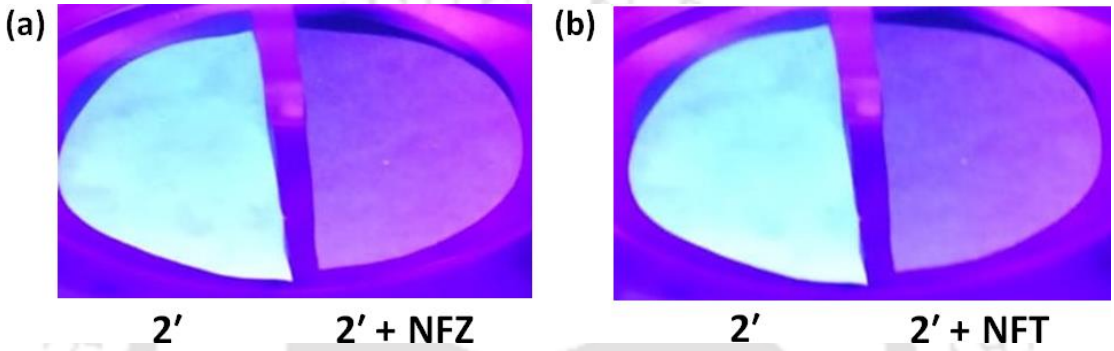

Figure 3.50 Images of **2′**-coated paper strips under UV lamp after and before the treatment of 10 mM methanolic(a) NFZ & (b) NFT solution.

3.4 Conclusions

A Zr(IV)-metal-based UiO-66 type MOF was successfully synthesized using benzo[1,2-b:4,5-b']dithiophene-2,6-dicarboxylic acid linker molecule. After single-step solvothermal synthesis, the material was characterized with the help of various instrumental supports (PXRD, elemental analysis, EDX, FE-SEM and IR analysis). Both **2** and **2′** displayed outstanding thermal stability up to the temperature of 415 °C. Excellent chemical stability of this porous material (surface area = 1228 m^2g^{-1}) in various solvents (H_2O, MeOH, CH_2Cl_2, acetone, hexane and DMF) was observed. The thermally activated compound showed a super selective nature of sensing towards Hg^{2+} in H_2O, and NFZ and NFT in MeOH medium. Along with ultra-fast response (1 min for all analytes), nanomolar level detection capability (LOD: Hg^{2+} = 5 nM, NFZ = 156.7 nM and NFT = 96.3 nM) was observed in all the cases of sensing. A real-time paper strip method of sensing technique was also developed for all the sensing targets. In-depth investigations were carried out to establish the mechanisms for all the cases of sensing with the help of analytical and spectroscopic methods as well as molecular simulations.

3.5 References

1. B. L. Rivas, S. Villegas, B. Ruf and I. M. Peric, *J. Chil. Chem. Soc*, 2007, **52**, 1164-1168.
2. Environmental Health Department, Minimata Disease: The History and Measures, Ministry of the Environment, Government of Japan, Tokyo, Japan, 2002.
3. F. Ma, M. Sun, C. Yuan, J. Yao and S. Wang, *APCBEE Procedia*, 2014, **10**, 12-15.

4. C. C. Bridges, B. F. Krasnikov, L. Joshee, J. T. Pinto, A. Hallen, J. Li, R. K. Zalups and A. J. L. Cooperb, *Arch. Biochem. Biophys.*, 2012, **517**, 20-29.
5. T. Rush, X. Liu and D. Lobner, *Neuroreport*, 2012, **23**, 216-219.
6. R. K. B. Barvin, P. Prakash, V. Ganesh and B. Jeyaprabha, *Int. J. Environ. Res. Public Health.*, 2019, **13**, 1015–1023
7. C. T. Driscoll, R. P. Mason, H. M. Chan, D. J. Jacob and N. Pirrone, *Environ. Sci. Technol.*, 2013, **47**, 4967–4983.
8. S. Flasche and K. E. Atkins, *J. Infect. Dis.*, 2018, **218**, 1351–1353.
9. R. Gaynes, *Emerg Infect Dis.*, 2017, **5**, 849–853.
10. T. P. V. Boeckel, S. Gandra, A. Ashok, Q. Caudron, B. T. Grenfell, S. A. Levin and R. Laxminarayan, *Lancet. Infect. Dis.*, 2014, **14**, 742-750.
11. B. Sloan and N. Scheinfeld, *Expert Opin. Drug Saf.*, 2008, **7**, 571–577.
12. A. K. Mittal, R. Bhardwaj, P. Mishra and S. K. Rajput, *Biotech. J.*, 2020, **14**, 107-112.
13. C. Llor and L. Bjerrum, *Ther. Adv. Drug. Saf.*, 2014, **5**, 229–241.
14. A. B. A. Boxall, D. W. Kolpin, B. Halling-Sørensen and J. Tolls, *Environ. Sci. Technol.*, 2003, **37**, 286-294.
15. O. O. Komolafe, *Malawi Med. J.*, 2003, **15**, 63–67.
16. B. J. Gardiner, A. J. Stewardson, I. J. Abbott and A. Y. Peleg, *Aust. Prescr.*, 2019, **42**, 14–19.
17. A. Ryan, E. Kapla, N. Laurieri, E. Lowe and E. Sim, *Sci. Rep.*, 2011, **63**, 1-5.
18. L. L. Rego, C. S. Glazer and P. E. Zimmern, *Urol. Sci.*, 2016, **27**, 193-198.
19. S. G. Bilgili, G. O. -Yavuz, I. H. Yavuz, M. A. Bilgili and A. S. Karadag, *Postepy Dermatol. Alergol.*, 2019, **36**, 398–402.
20. Y.-H. Shin, M. T. G. -Wing and J.-W. Choi, *J. Electrochem. Soc.*, 2021, **168**, 017502.
21. N. Kwon, Y. Hu and J. Yoon, *ACS Omega*, 2018, **3**, 13731–13751.
22. C. Gogoi, A. Kumar and M. SK, *Microporous Mesoporous Mater.*, 2021, **311**, 110725-110732.
23. S. Nandi and S. Biswas, *Dalton Trans.*, 2020, **49**, 17612-17620.
24. R. Dalapati, S. Nandi and S. Biswas, *Dalton Trans.*, 2020, **49**, 8684-8692.
25. V. Trannoy, N. Guillou, C. Livage, C. R.-Marchal, M. Haouas, A. Leaustic, C. Allain, G. Clavier, P. Yu and T. Devic, *Inorg. Chem.*, 2019, **58**, 6918–6926.
26. S. Nandi and S. Biswas, *Microporous Mesoporous Mater.*, 2020, **299**, 110116-110124.
27. R. Dalapati and S. Biswas, *Chem. Asian J.*, 2019, **14**, 2822-2830.
28. M. Ponram, U. Balijapalli, B. Sambath, S. K. Iyer, V. B, R. Cingarama and K. N. Sundaramurthy, *New J. Chem.*, 2018, **42**, 8530--8536.
29. J.-M. Li, R. Li and X. Li, *CrystEngComm*, 2018, **20**, 4962–4972.
30. H. He, Q.-Q. Zhu, M.-T. Guo, Q.-S. Zhou, J. Chen, C. -P. Li and M. Du, *Cryst. Growth Des.*, 2019, **19**, 5228−5236.
31. Q. Tao, T. Liu, L. Duan, Y. Cai, W. Xiong, P. Wang, H. Tan, G. Lei, Y. Pei, W. Zhu, R. Yang and Y. Sun, *J. Mater. Chem. A*, 2016, **4**, 18792-18803.
32. J. H. Cavka, S. Jakobsen, U. Olsbye, N. Guillou, C. Lamberti, S. Bordiga and K. P. Lillerud, *J. Am. Chem. Soc.*, 2008, **42**, 13850–13851.
33. Accelrys Incorporated. Materials Studios; San Diego, 2009.
34. A. A. Coelho, *J. Appl. Cryst.*, 2018, **51**, 210-218.

35. A. Das, N. Anbu, M. SK, A. Dhakshinamoorthy and S. Biswas, *ChemCatChem*, 2020, **12**, 1789-1798.
36. A. Das, N. Anbu, H. Reinsch, A. Dhakshinamoorthy and S. Biswas, *Inorg. Chem.*, 2019, **58**, 16581-16591.
37. R. Dalapati, S. Nandi, C. Gogoi, A. Shome and S. Biswas, *ACS Appl. Mater. Interfaces*, 2021, **13**, 8563–8573.
38. D. Zou and D. Liu, *Mater. Today Chem.*, 2019, **12**, 139-165.
39. P. Wu, Y. Liu, Y. Liu, J. Wang, Y. Li, W. Liu and J. Wang, *Inorg. Chem.*, 2015, **54**, 11046−11048.
40. Y. Zhao, X. Xu, L. Qiu, X. Kang, L. Wen and B. Zhang, *ACS Appl. Mater. Interfaces*, 2017, **9**, 15164–15175.
41. Y. Yu, L.-R. Lin, K.-B. Yang, X. Zhong, R.-B. Huang and L.-S. Zheng, *Talanta*, 2006, **69**, 103-106.
42. P. G. Mahajan, N. C. Dige, B. D. Vanjare, A. R. Phull, S. J. Kim and K. H. Lee, *J. Lumin.*, 2019, **206**, 624–633.
43. Y. C. Hsieh, J. L. Chir, H. H. Wu, P. S. Chang and A. T. Wu, *Carbohydr. Res.*, 2009, **344**, 2236–2239.
44. M. L. Firdaus, I. Fitriani, S. Wyantuti, Y. W. Hartati, R. Khaydarov, J. A. Mcalister, H. Obata and T. Gamo, *Anal. Sci.*, 2017, **33**, 831–837.
45. B. D. Vanjare, P. G. Mahajan, H.-I. Ryoozz, N. C. Dige, N. G. Choi, Y. Han, S. J. Kim, C.-H. Kim and K. H. Lee, *Sens. Actuators B Chem.*, 2021, **330**, 129308-129322.
46. V. Bhalla, R. Tejpal and M. Kumar, *Sensors Actuators, B Chem.*, 2010, **151**, 180–185.
47. B. Yuan, D. X. Wang, L. N. Zhu, Y. L. Lan, M. Cheng, L. M. Zhang, J. Q. Chu, X. Z. Li and D. M. Kong, *Chem. Sci.*, 2019, **10**, 4220–4226.
48. S. Y. Lin, H. J. Zhu, W. J. Xu, G. M. Wang and N. Y. Fu, *Chin. Chem. Lett.*, 2014, **25**, 1291–1295.
49. J. S. Do, K. H. Lin and R. Ohara, *J. Taiwan Inst. Chem. Eng.*, 2011, **42**, 662–668.
50. T. B. Wei, G. Y. Gao, W. J. Qu, B. B. Shi, Q. Lin, H. Yao and Y. M. Zhang, *Sensors Actuators, B Chem.*, 2014, **199**, 142–147.
51. Y. Yang, Z. Wang, M. Yang, M. Guo, Z. Wu and G. Shen, *Sensors Actuators, B Chem.*, 2006, **114**, 1–8.
52. G. H. Chen, W. Y. Chen, Y. C. Yen, C. W. Wang, H. T. Chang and C. F. Chen, *Anal. Chem.*, 2014, **86**, 6843–6849.
53. T. K. V. Krawczyk, M. Moszczynska and M. Trojanowicz, *Biosens. Bioelectron.*, 2000, **15**, 681–691.
54. J. S. Do, K. H. Lin and R. Ohara, *J. Taiwan. Inst. Chem. Eng.*, 2011, **42**, 662–668.
55. N. R. Devi, M. Sasidharan and A. K. Sundramoorthy, *J. Electrochem. Soc.*, 2018, **165**, B3046–B3053.
56. S. Chen, W. Wang, M. Yan, Q. Tu, S. W. Chen, T. Li, M. S. Yuan and J. Wang, *Sensors Actuators, B Chem.*, 2018, **255**, 2086–2094.
57. R. Zhang and W. Chen, *Biosens. Bioelectron.*, 2013, **55**, 83–90.
58. S. Halder, J. Mondal, J. O. -Castro, A. Frontera and P. Roy, *Dalton Trans.*, 2017, **46**, 1943-1950.

59. E. Moradi, R. Rahimi and V. Safarifard, *J. Solid State Chem.*, 2020, **286**, 121277-121286.
60. P.-P. Hu, N. Liu, K.-Y. Wu, L.-Y. Zhai, B.-P. Xie, B. Sun, W.-J. Duan, W.-H. Zhang and J.-X. Chen, *Inorg. Chem.*, 2018, **57**, 8382–8389.
61. P. Samant, A. V. Desai, S. Sharma, P. Chandra and S. K. Ghosh, *Inorg. Chem.*, 2018, **57**, 2360−2364.
62. T. Xia, T. Song, G. Zhang, Y. Cui, Y. Yang, Z. Wang and G. Qian, *Chem. Eur. J.*, 2016, **22**, 18429-18434.
63. X.-Y. Xu and B. Yan, *J. Mater. Chem. C*, 2016, **4**, 1543-1549.
64. N.-H. Huang, R.-T. Li, C. Fan, K.-Y. Wu, Z. Zhang and J.-X. Chen, *J. Inorg. Biochem.*, 2019, **197**, 110690-110697.
65. A. Radwan, I. M. E. -Sewify, A. Shahat, H. M. E. Azzazy, M. M. H. Khalil and M. F. E. -Shahat, *ACS Sustain. Chem. Eng.*, 2020, **8**, 15097–15107.
66. N.-H. Huang, Y. Liu, R.-T. Li, J. Chen, P.-P. Hu, D. J. Young, J.-X. Chen and W.-H. Zhang, *Analyst*, 2020, **145**, 2779-2788.
67. Y. Zhao, X. Xu, L. Qiu, X. Kang, L. Wen and B. Zhang, *ACS Appl. Mater. Interfaces*, 2017, **9**, 15164−15175.
68. S. Bayindir, *J. Photochem. Photobiol. A* 2019, **372**, 235–244.
69. Y. Li, K. Liu, W.-J. Li, A. Guo, F.-Y. Zhao, H. Liu and W.-J. Ruan, *J. Phys. Chem. C*, 2015, **119**, 28544–28550.
70. H. Sohn, M. J. Sailor, D. Magde and W. C. Trogler, *J. Am. Chem. Soc.*, 2003, **125**, 3821–3830.
71. G. R. You, S. Y. Lee, J. J. Lee, Y. S. Kim and C. Kim, *RSC Adv.*, 2016, **6**, 4212–4220.
72. Q. Mei, Y. Shi, Q. Huaa and B. Tong, *RSC Adv.*, 2015, **5**, 74924–77493.
73. A. Singh, S. Kaur, N. Singh and N. Kaur, *Org. Biomol. Chem.*, 2014, **12**, 2302–2309.
74. K. Xing, R. Fan, X. Du, X. Zheng, X. Zhou, S. Gai, P. Wang and Y. Yang, *Sensors Actuators, B Chem.*, 2019, **288**, 307–315.
75. Q.-Q. Zhu, Q.-S. Zhou, H.-W. Zhang, W.-W. Zhang, D.-Q. Lu, M.-T. Guo, Y. Yuan, F. Sun and H. He, *Inorg. Chem.*, 2020, **59**, 1323-1331.
76. Y. Yang, G. Ren, W. Yang, X. Qin, D. Gu, Z. Liang, D.-Y. Guo and Q. Pan, *Polyhedron*, 2021, **194**, 114923-114928.
77. J. Cheng, Y. Li, J. Zhong, Z. Lu, G. Wang, M. Sun, Y. Jiang, P. Zou, X. Wang, Q. Zhao, Y. Wang and H. Rao, *Chem. Eng. Sci.*, 2020, **318**, 125664-126671.
78. B. R. A.-Hashimi, K. M. Omer, H. S. Rahman and H. H. Othman, *Spectrochim. Acta - A: Mol. Biomol. Spectrosc.*, 2021, **244**, 118835-118834.
79. A. Rahi, N. Sattarahmady, R. D. Vais and H. Heli, *Sensors Actuators, B Chem.*, 2015, **210**, 96–102.
80. U. Athikomrattanakul, N. G. -Eichelmann and F. W. Scheller, *Anal. Chem.*, 2011, **83**, 7704–7711.
81. Q. Chu, B. Zhang, H. Zhou, B. Liu, L. Hou and Y.-Y. Wang, *Inorg. Chem.*, 2020, **59**, 2853–2860.
82. B.-X. Dong, Y.-M. Pan, W.-L. Liu and Y.-L. Teng, *Cryst. Growth Des.*, 2018, **18**, 431−440.
83. Y.-S. Lu, W.-Y. Pan, T.-C. Hung and Y.-T. Hsieh, *Langmuir*, 2020, **36**, 11358−11365.

84. B. He and J. Li, *Anal. Methods*, 2019, **11**, 1427–1435.
85. T.-W. Chen, E. Tamilalagan, D. A. A. Farraj, S.-M. Chen, A. Muthumariappan, S. Maheshwaran and M. S. Elshikh, *Nanotechnology*, 2020, **31**, 445502-445511.
86. J. Zhang, L. Gao, Y. Wang, L. Zhai, X. Niu and T. Hu, *CrystEngComm*, 2019, **21**, 7286–7292.
87. M. Roushani and Z. Rahmati, *J. Iran. Chem. Soc.*, 2019, **16**, 999–1006.
88. B. Karuppaiah, R. Ramachandran, S.-M. Chen, S. W. -Ling and J. Y. Wan, *New J. Chem.*, 2020, **44**, 46--54.
89. Q.-Q. Zhu, Q.-S. Zhou, H.-W. Zhang, W.-W. Zhang, D.-Q. Lu, M.-T. Guo, Y. Yuan, F. Sun and H. He, *Inorg. Chem.*, *59*, 2020, 1323-1331.
90. K. Xing, R. Fan, X. Du, X. Zheng, X. Zhou, S. Gai, P. Wang and Y. Yang, *Sensors Actuators, B Chem.*, 2019, **288**, 307–315.
91. S. Nandi, A. Mondal, H. Reinsch and S. Biswasa, *Inorg. Chim. Acta*, 2019, **497**, 119078-119087.
92. H.-B. Zhu and Z.-Y. Sun, *Inorg. Chem. Commun.*, 2018, **96**, 202–205.
93. F. Zhang, H. Yao, T. Chu, G. Zhang, Y. Wang and Y. Yang, *Chem. Eur. J.*, 2017, **23**, 10293-10300.

Chapter 4

MOF-Fabric Composites Based on a Multi-Functional MOF as Luminescent Sensor for a Neurotransmitter and an Anti-Cancer Drug

This chapter represents the synthesis and characterization of an aqua-stable, biocompatible, thiourea functionalized Zr(IV) metal-organic framework (MOF) for selective and rapid sensing of adrenaline and 6-MP with ultra-low limit of detection (LOD for adrenaline = 1.9 nM, LOD for 6-MP = 0.028 nM). It is the first MOF-based fluorescent sensor of both the targeted analytes. The sensor not only can detect adrenaline in HEPES buffer medium but also in different bio-fluids (e.g. human urine and blood serum) and pH media. It also exhibited 6-MP sensing ability in aqueous medium and in various wastewater specimens and in pH solutions. For the quick and on-site detection of this neuro-messenger (adrenaline) and the drug (6-MP), cost-effective sensor-coated cotton fabric composites were fabricated. The recyclable MOF@cotton fabric composite is capable to detect both the analytes up to the nanomolar level by the naked eye under UV-light.

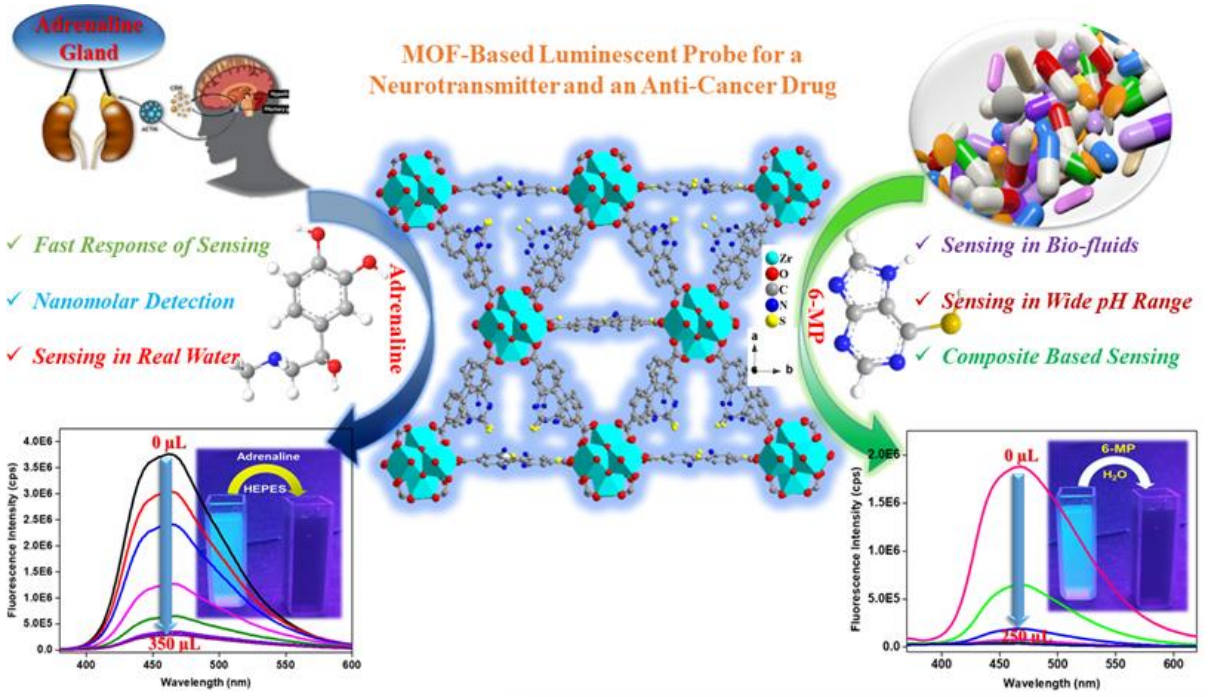

ACS APPLIED MATERIALS & INTERFACES

S. Ghosh, J. Krishnan, S. Hossain, A. Dhakshinamoorthy, S. Biswas, ACS Appl. Mater. Interfaces, 2023, 15, 26843-26851.

4.1 Introduction

In the central nervous system of mammalians, adrenaline plays a significant role as a chemical messenger.[1] It is present in the biological body fluids and nerve tissues as an organic molecule.[2] In the endogenous plasma of an adult, the adrenaline concentration should be less than 25-50 ng/L.[3] In human body, adrenaline promotes the elevation of blood sugar, glycogenolysis, heart-beat and lipolysis.[4] It also has a significant impact on reducing osteoarthritis pain and the development of cartilaginous arthrosis.[5] An adrenaline rush in the body can cause rapid heart rate, rapid breathing, sweating heightened senses, feeling jittery, decreased ability to feel pain and dilated pupils etc.[1, 5] In the body fluids of patients with Parkinson's disease, the adrenaline concentration is found to be much lower than the actual concentration.[6] Therefore, the determination of adrenaline concentration in various body fluids is highly necessary.

Leukaemia is a type of cancer that affects the blood-forming tissues of the human body, lymphatic system and bone marrow.[7] According to a report, globally, 2.3 million people had leukaemia in 2015 and it was responsible for 353,500 fatalities. Moreover, 352,000 newly affected people were found in 2012 and the number is increasing day by day.[8] One of the common treatments for leukaemia is chemotherapy.[9] 6-MP is a widely used drug for acute lymphoblastic leukaemia.[10] The proliferation of cancer cells is hampered by 6-MP, which ultimately results in their demise. This medication may also have an impact on the proliferation of normal cells. Other harmful effects i.e. loss of appetite, lower back pain, painful urination, unusual bleeding, clay-colored stools, yellow eyes or skin and problems in breathing etc. can also occur by the regular intake of 6-MP.[11] There was a higher rate of abortion in women receiving mercaptopurine during the first trimester of pregnancy.[12] Moreover, there is a chance that the medicine will cause people to develop cancer.[12] The excessive usage and careless disposal of 6-MP increase its concentration in wastewater. The rise in concentration of 6-MP and its metabolites is also harmful to aquatic plants and animals. Drug-resistant genes can also arise in living creatures as a result of prolonged exposure to such drugs through wastewater, which would be harmful to the ecosystem. Hence, there is urgency of measuring the concentration of 6-MP in wastewater specimens.

To date, the quantitative determination of adrenaline and 6-MP has been reported using a variety of techniques, including electrochemical, liquid chromatography, capillary electrophoresis and chemiluminescence, etc.[12-14] However, the majority of these approaches are constrained by their laborious operation, high cost and even reliance on pre-treatment.[14-16] On the other hand, fluorescence-based detection methods are widely used because they satisfy key requirements for practical sensors, including high selectivity, sensitivity, short response time, real-time sensing capability and cost-effectiveness.[17, 18]

Fluorescence sensing requires a fluorescent probe. Heterogeneous MOFs are fluorescence active because of the electronic interaction between the metal ions and the π-conjugated polytopic organic linkers.[19] In recent years, these fluorescent MOFs were used as effective and reliable sensor materials for the detection of diverse cations, anions, hazardous organics, bioactive chemicals and vapour/gas molecules.[20, 21] The heterogeneity and definite pore size of the MOFs make them suitable for the conversion of different organic starting ingredients into the required products.[22, 23]

Herein, a thiourea functionalized Zr-based MOF (**3′**) has been strategically engineered for the selective detection of adrenaline and 6-MP. According to earlier research, the absorption maxima of adrenaline and 6-MP are centered at 446 and 325 nm, respectively which are within the excitation/emission spectrum of **3′**.[24, 25] Consequently, there is a possibility of energy transfer between the MOF and adrenaline which can enhance or quench the emission of the probe. Indeed, the quenching in photoluminescence of the MOF was observed after the addition of adrenaline and 6-MP solutions to the MOF suspension. This reusable sensor showed excellent fluorescence quenching within 5 s after the addition of both the targeted analytes and the observed LOD values are lower than the majority of the previously reported sensors of adrenaline and 6-MP (Table 4.1 and 4.8). This sensor can detect adrenaline in different bio-fluids (human urine and serum) and pH media and 6-MP in various real water. Additionally, a sensor-coated, medical-friendly, cheap and transportable MOF@cotton composite was developed for the sensing of adrenaline and 6-MP up to nanomolar level under UV light.

4.2 Experimental Section

4.2.1 Synthesis and Characterization of 6-Thioxo-6,7-Dihydro-5H-Dibenzo[d,f][1,3]Diazepine-3,9-Dicarboxylic Acid (H_2L)

For the synthesis of H_2L linker, 1 g (3.3 mmol) of dimethyl 2,2′-diamino-[1,3′-biphenyl]-4,4′-dicarboxylate was taken in a 100 mL round bottom flux containing 25 mL of pyridine and it was solubilized by sonication. Then, 5 mL (52.1 mmol) of CS_2 was added to the aforementioned solution and it was kept at 85 °C for 12 h. After 12 h, light yellow solid was filtered and washed with excess water and kept at 60 °C for 4 h. Yield: 900 mg (79%)

The obtained ester in the first step was hydrolysed in the second step. For that, the product was dissolved in a mixture of 10 mL of THF, 10 of mL MeOH and 10 mL of 1(M) LiOH. Then, the mixture was refluxed for 3 h at 80 °C. After 3 h, these solvents were evaporated under vacuum. Then, the remaining liquid part was acidified with 3 M HCl solution (Scheme 4.1). At last, the obtained solid precipitate was filtered, washed with 10 mL of water and then dried in an oven at 80 °C for 12 h. Yield: 750 mg (2.38 mmol, 91%). ^{1}H NMR (500 MHz, DMSO-d_6): δ = 10.31 (s, 1H), 7.75 (m, 2H), 7.58 (d, 2H) ppm. ^{13}C NMR (125 MHz, DMSO-d_6): δ = 194.31, 166.84, 141.41, 133.82, 132.18, 130.45, 126.55, 122.96 ppm. ESI-MS (m/z): 313.0415 for $(M-H)^-$ ion (M = mass of H_2L linker). In Figures 4.1-4.3, the NMR and mass spectra of the H_2L linker are shown.

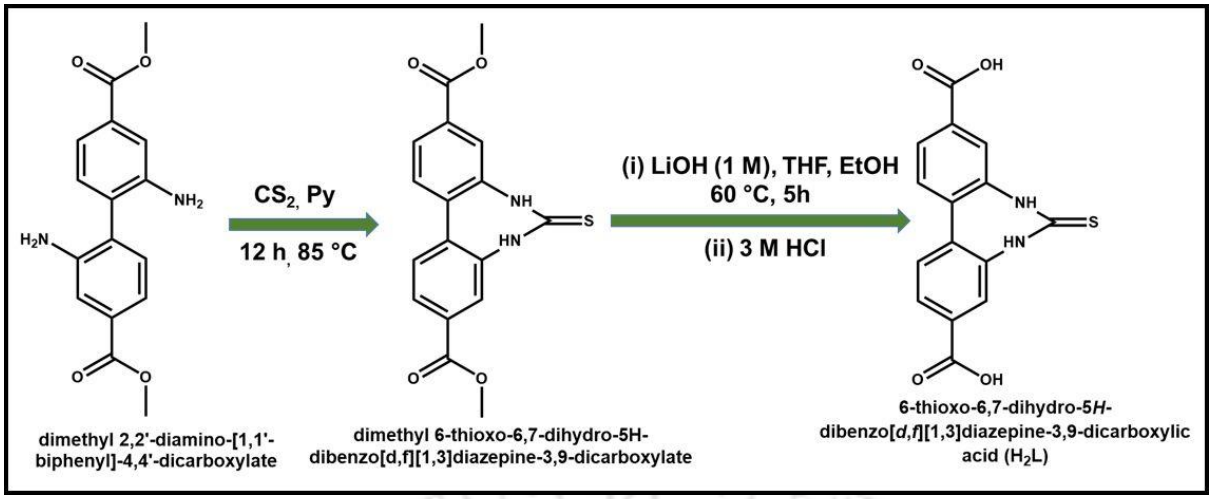

Scheme 4.1. Reaction scheme for the preparation of H_2L linker.

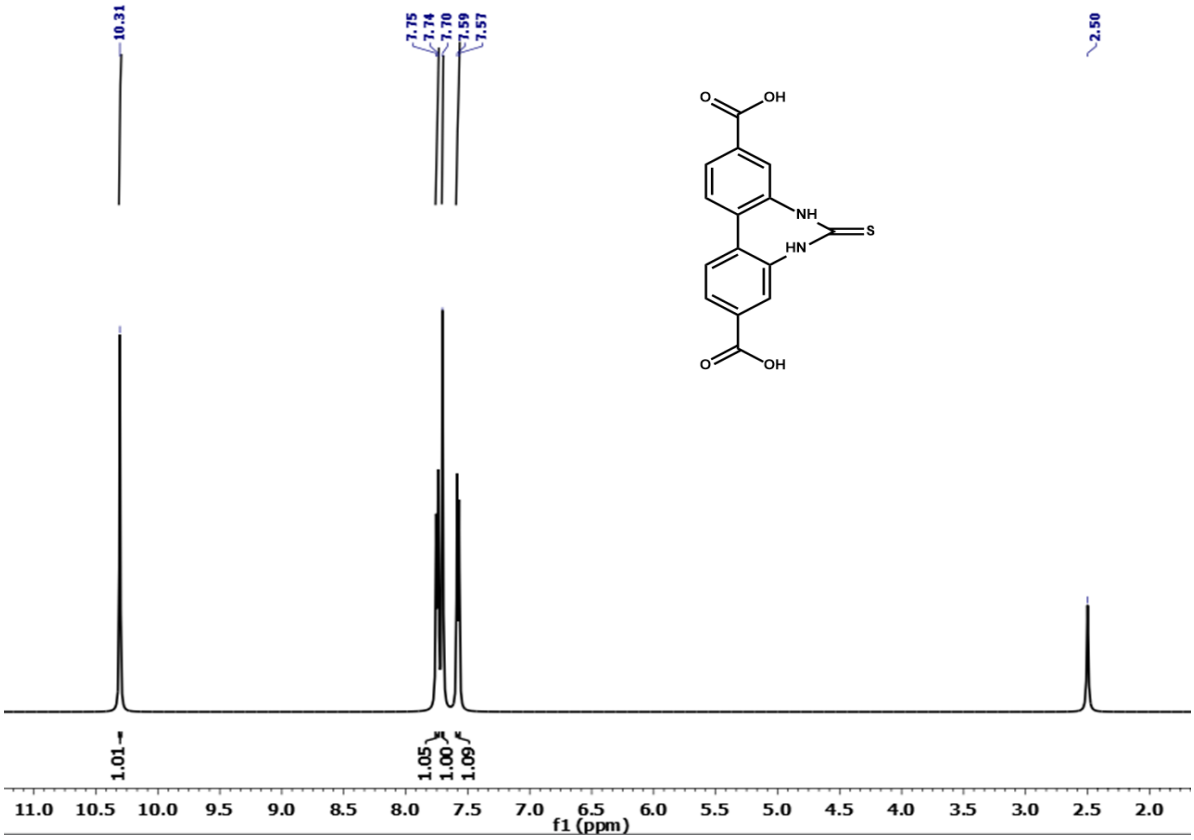

Figure 4.1 ^{1}H NMR spectrum of H_2L linker in DMSO-d_6.

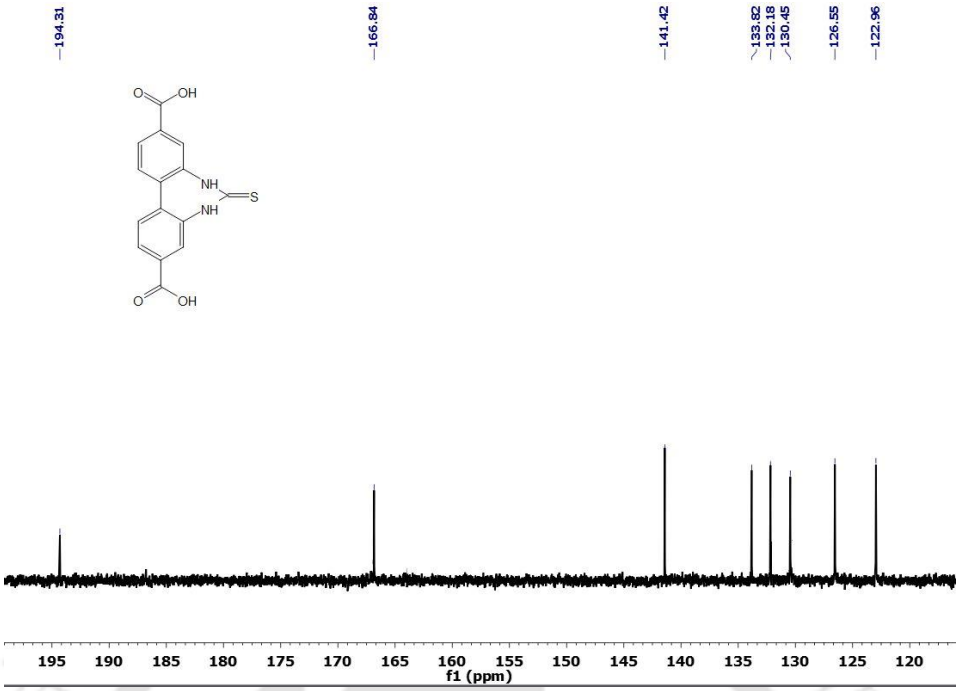

Figure 4.2 ^{13}C NMR spectrum of H_2L linker in DMSO-d_6.

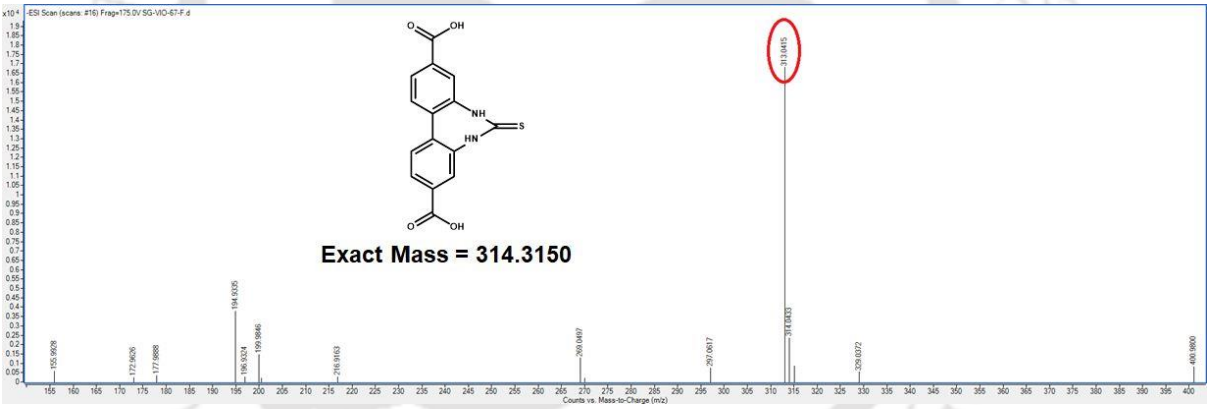

Figure 4.3 ESI-MS spectrum of H_2L acid linker measured in methanol. The spectrum shows m/z peak at 313.0415, which corresponds to $(M-H)^-$ ion (M = mass of the H_2L linker).

4.2.2 Synthesis and Activation Procedure of $[Zr_6O_4(OH)_4(C_{15}H_8N_2O_4S)_6]\cdot 4.5H_2O\cdot 4DMF$ (3)

Conventional solvothermal procedure was applied for the synthesis of **3**. After trying different reactions with different Zr-salts ($ZrOCl_2\cdot 8H_2O$, $ZrCl_4$, and $ZrN_2O_7\cdot xH_2O$), different acid modulators (trifluoroacetic acid (TFA), acetic acid, formic acid and benzoic acid) and different solvents (DMF, DEF and DMA) in wide temperature range (80-150 °C), most crystalline **3** was obtained when we heated the Pyrex tube containing 15 mg (0.06 mmol) of $ZrCl_4$ metal salt with 20 mg (0.06 mmol) of H_2L linker in presence of 150 µL (1.9 mmol) of TFA modulator in DMF solvent at 150 °C for 24 h. After the filtration and washing with acetone, light yellow colour MOF solid was obtained. Its crystalline nature was characterized by PXRD, ART-IR, FE-SEM, EDX and elemental analysis. Yield of **3** was 27 mg (0.007 mmol, 70% with reference

to metal salt). Anal. calcd. for $C_{102}H_{89}N_{16}O_{40}S_6Zr_6$ (2917 g mol^{-1}): C, 41.96; N, 7.68; H, 3.05. Found C, 41.89; N, 7.62; H, 3.01.%. ART-IR (cm^{-1}): 1657 (vs), 1604 (w),1543 (s), 1412 (vs), 1202 (w), 1156 (w), 1092 (w), 773 (s), 662 (s).

During the process of synthesis, some solvent (DMF) molecules may be encapsulated inside the pore of the framework. But for the gas sorption, sensing or catalysis application, the pore should be completely vacant. For that, solvent molecules present in the pore of **3** were first removed by stirring 100 mg of **3** in 20 mL of DCM for 12 h. After that, the solvent-exchanged MOF material was filtered and dried in an air oven for 8 h at 70 °C. Finally, by heating the compound for 6 h under vacuum in oil bath at 100 °C, in this way, the low boiling DCM solvents were evacuated from the pore of **3**. After using the aforementioned procedures, we obtained the activated form of **3** (named **3′**).

4.2.3 Preparation of MOF (3′) Suspension for Fluorescence Sensing Experiments

The probe **3′** (3 mg) was taken in a 5 mL glass vial containing 3 mL HEPES buffer for adrenaline sensing and 3 mL H_2O for 6-MP sensing. Then, the suspension was sonicated for 15 min and kept it for overnight to make the suspension stable. During the fluorescence experiment, 100 µL of the above-mentioned suspension of **3′** was added to 3000 µL of deionized water in a quartz cuvette. Solution of 6-MP was prepared in a mixture of H_2O and DMSO with a volume ratio of 8:2. All the fluorescence spectra were collected in the range of 380-600 nm by exciting the suspension at 365 nm. For competitive experiments, the solutions of the different competitive analytes (concentration = 10 mM) were added to the suspension of **3′** and spectra were collected in the same range.

4.2.4 Sensing of Adrenaline in Human Blood Serum Samples

10 mL of blood sample was collected from the right arm vein of a healthy person (blood group A^+) and the blood plasma was separated by centrifuging the sample at 10,000 rpm for 15 min. The light yellow blood serum was collected in a Falcon tube and stored at -20 °C in a refrigerator. For fluorescence detection experiments, aliquots of different concentrations of adrenaline were spiked into the human blood serum sample, which contained HEPES buffer suspension of the MOF.

4.2.5 Sensing of Adrenaline in Human Urine Samples

10 mL of the first morning urine sample from a healthy person was taken and 500 mL of HNO_3 was added to the sample to kill any interfering living things. For 10 min, the sample was centrifuged at 8000 rpm. For the experiments, the supernatants were taken. Different adrenaline aliquots were added into urine samples containing HEPES buffer suspensions of the probe as part of fluorescence detection tests.

4.2.6 Calculation of Corrected Fluorescence Intensity

The corrected fluorescence intensity is calculated using equation (1)

$$\frac{F_{corrected}}{F_{observed}} = \frac{2.3dA_{ex}}{1-10^{-dA_{ex}}} 10^{gA_{em}} \frac{2.3sA_{em}}{1-10^{-sA_{em}}} \quad \ldots\ldots\ldots\ldots\ldots\ldots\ldots (1)$$

where $F_{observed}$ is the maximum fluorescence intensity; $F_{corrected}$ is the corrected fluorescence intensity, which is the fluorescence intensity obtained after removing the IFE; A_{ex} and A_{em} represent the absorbance at the excitation wavelength of **3′** (λ_{ex} = 330 nm) and maximum emission wavelength (λ_{em} = 468 nm), respectively; 'd' is the width of the quartz cell (d =1.00 cm); 'g' is the distance between the edges of the cuvette and the excitation beam (0.40 cm in this case); s is the thickness of excitation light (s = 0.10 cm).

4.3 Results and Discussion

4.3.1 Structural Details of 3

Previously reported literature suggested that the coordination bond formation between the metal ions of the same oxidation state in presence of identical coordination environments and coordinating groups result in the formation of MOFs with similar topologies. The functionalization of the organic linker does not generally affect the coordination geometry. Many literature reports suggested that in presence of biphenyl dicarboxylic acid and Zr(IV)-metal salt, UiO-67 type of MOFs are formed.[26] Because of the same reason, we also expected the creation of an isostructural framework as a result of the coordination bond formation between the Zr^{4+} ion and the carboxylate groups of the linker molecule. The experimental PXRD patterns and intensities of the newly synthesized MOF are also remarkably comparable to the theoretical PXRD pattern (Figure 4.4). The modest values of R_{wp} and R_p obtained after Pawley refinement of the PXRD pattern of **3** further supported the similarity of the MOF's PXRD data with the simulated PXRD pattern (Figure 4.5a). All the above results suggested the newly synthesized (**3**) also has $[Zr_6O_4(OH)_4]^{12+}$ SBUs (secondary building units) and the Zr^{4+} ions are coordinated with four μ_3-O and μ_3-OH four sites. The SBUs were joined by six $(BPDC\text{-}CS)^{2-}$ linkers in the framework. These building pattern results in the construction of a cubic framework structure with two types of internal voids e.g. larger sized (octahedral shaped) and smaller sized (tetrahedral shaped) voids. These two voids are interconnected by triangular windows (Figures 4.5c-d). The experimentally obtained PXRD patterns remained unaltered after the thermal activation process which suggested that the framework preserved its crystalline nature after the activation process. The uniform distribution of octahedral particles in the FE-SEM images of **3′** (Figure 4.5d) further confirmed the crystalline structure and phase purity of **3′**. The confirmation of the presence of required elements (Zr, O, C, S and N) was obtained from the EDX spectrum of **3′** (Figure 4.6).

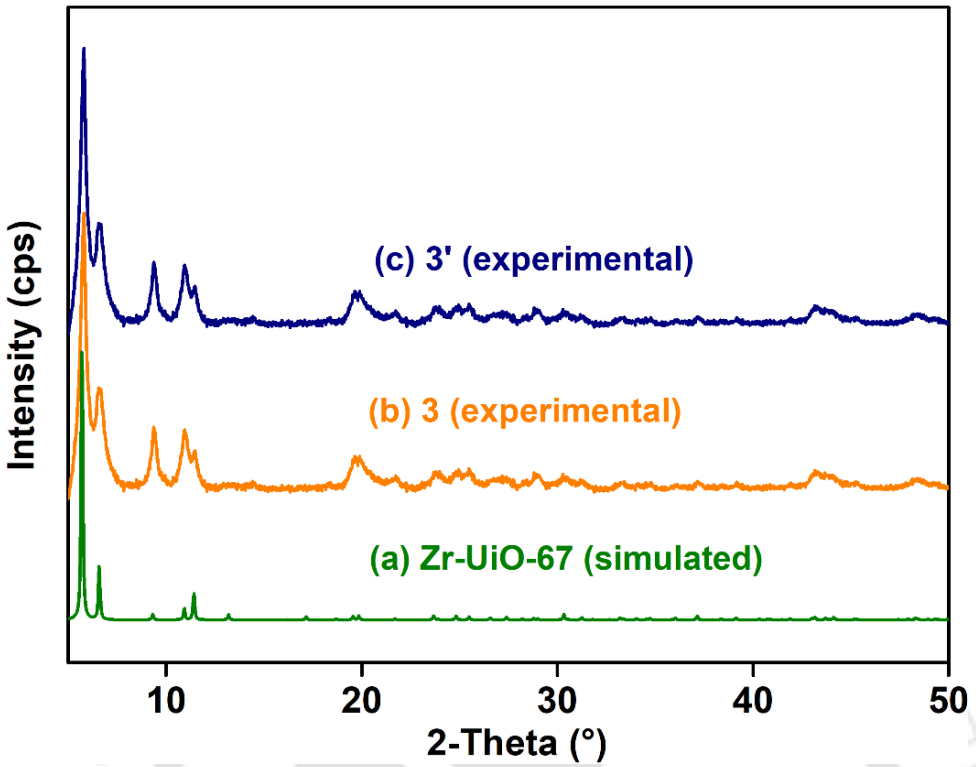

Figure 4.4 PXRD patterns of (a) simulated Zr-UiO-67 (green), (b) **3** (orange) and (c) **3′** (navy blue).

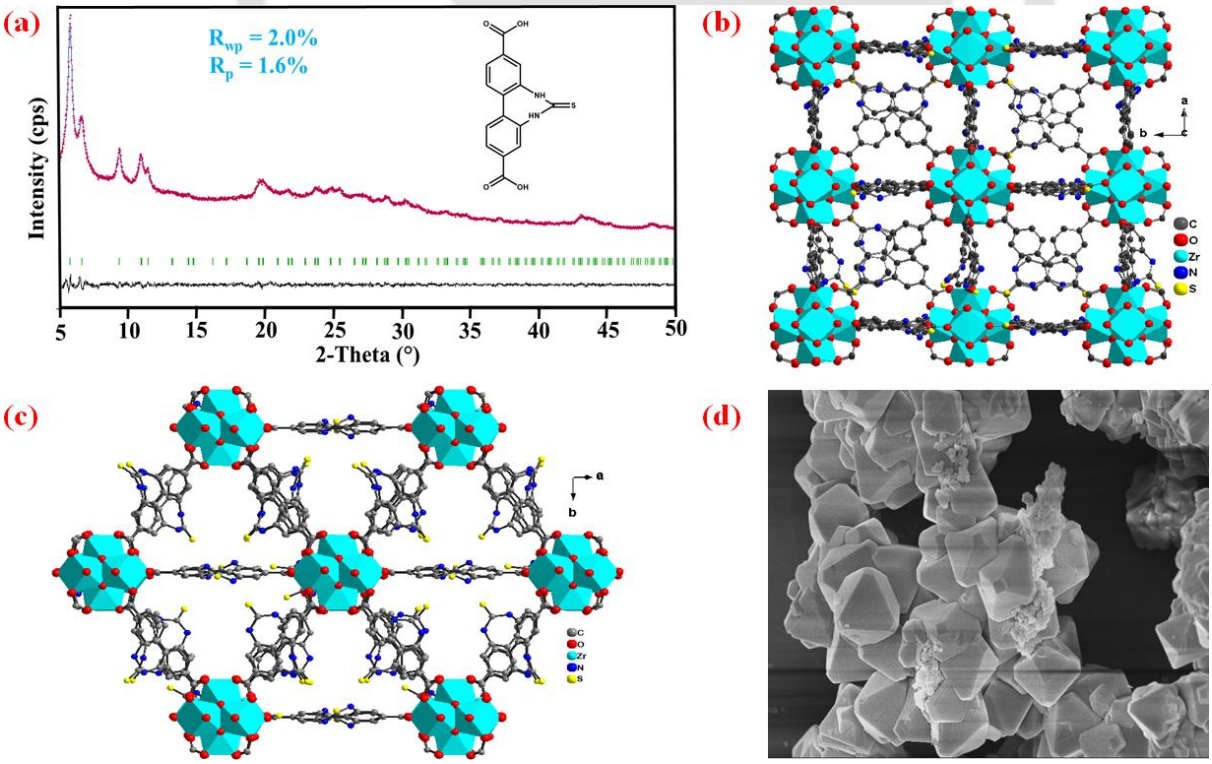

Figure 4.5 (a) Pawley refinement plot of the PXRD of **3**, (b and c) structure of **3** and (d) FE-SEM image of **3**.

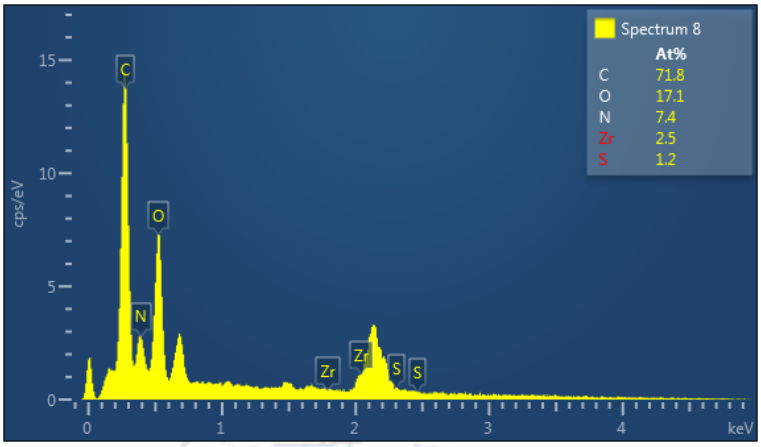

Figure 4.6 EDX spectrum of **3′**.

4.3.2 Functional Groups Analysis

ATR-IR is a powerful and reliable technique to validate the existence of various functional groups and the full removal of DMF (solvent) molecules from the pore of the as-prepared framework structure. To verify the same, we performed ART-IR analysis of both **3** and **3′**. Figure 4.7 shows that both **3** and **3′** have two separate absorption bands at 1604 and 1543 cm^{-1}, which originate from the asymmetric and symmetric stretching vibration of the Zr-coordinated carboxylate groups of the linker molecule. Another common peak (located at 1412 cm^{-1}) was observed in both the IR spectra (**3** and **3′**) which is due to the –C=S group present in the linker. The presence of the absorption band at 1657 cm^{-1} in **3** is caused by the carbonyl stretching vibration of DMF molecules which were encapsulated inside the pore of the as-prepared MOF. The absence of such signal at 1657 cm^{-1} in the ATR-IR spectra of **3′** confirmed the complete removal of all the guest DMF molecules from the pore of **3**.

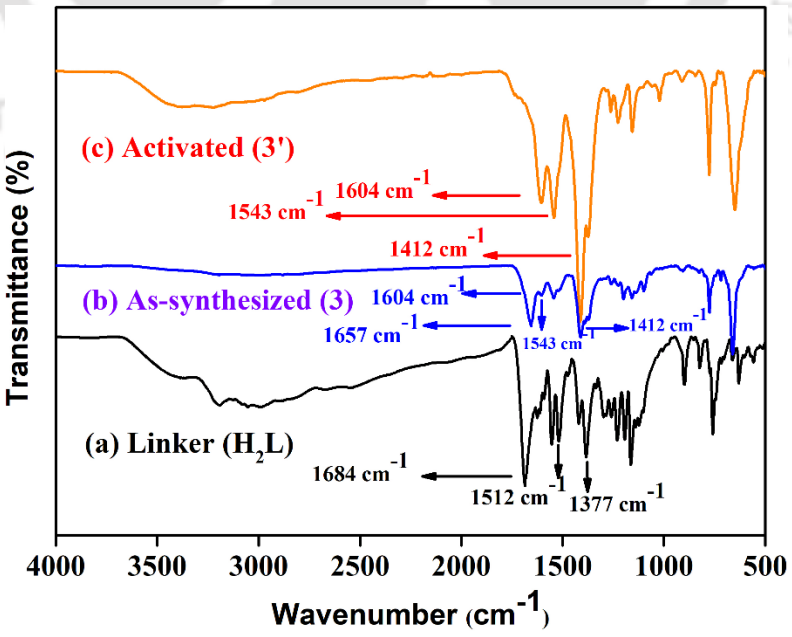

Figure 4.7 ATR-IR spectra of (a) H_2L linker, (b) **3** (as-synthesized) and (c) **3′** (activated).

4.3.3 Physicochemical Stability of 3′

For the broad-scope applications of a sensor, the sensor should be stable in the sensing medium. To verify the same, the stability of **3′** was measured in the sensing media (HEPES buffer) by collecting the PXRD of the recovered MOF powder after stirring in HEPES buffer at room temperature. We also measured the stability of **3′** in different other solvents (methanol, ethanol, ethyl acetate, water and chloroform) following the same procedure (used in the case of HEPES buffer). Figure 4.8 evidences the stability of the framework structure in the aforementioned solvents at room temperature for 6 h. The integrity of **3′** in wide range of solvents unlocks the scope of applications of **3′** in the above-mentioned solvents.

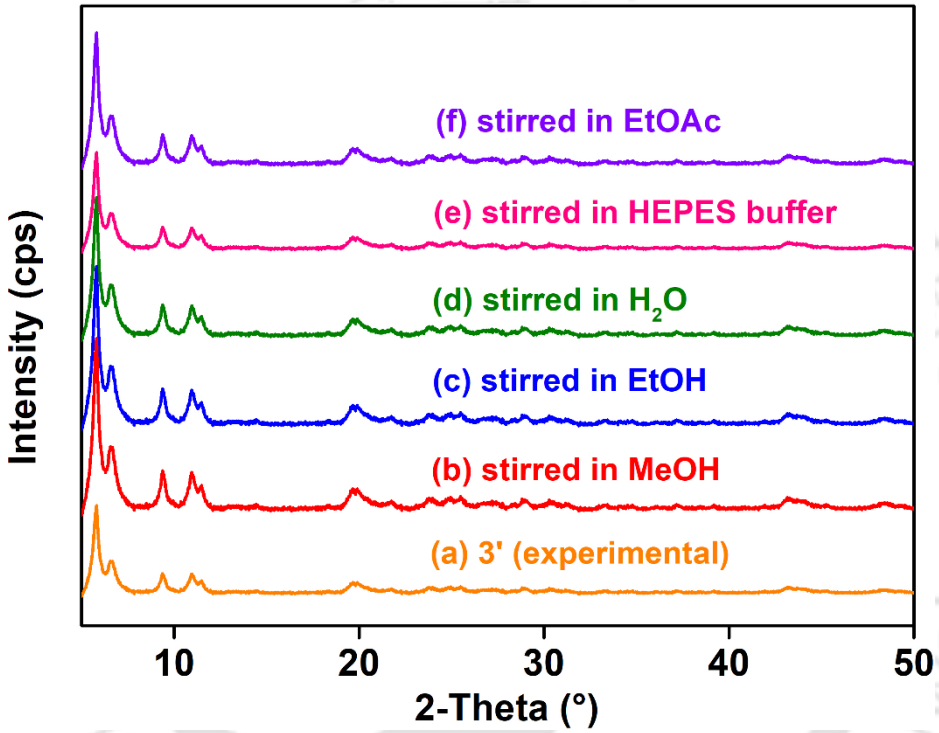

Figure 4.8 PXRD patterns of **3′** in different forms: (a) activated **3′**, after stirred with (b) MeOH, (c) EtOH, (d) H_2O, (e) HEPES buffer (pH = 7.4) and (f) EtOAc for 6 h at room temperature.

The thermal tolerance of both **3** and **3′** was determined by performing the TGA analysis of both samples under air atmosphere with a heating rate of 5 °C/min. Analysis showed that both **3** and **3′** are stable up to temperature of 400 °C (Figure 4.9). TGA curve of **3** displayed three sequential losses of its weight. The first weight loss of 2.7% due to the loss of 4.5 H_2O molecules (per formula unit) was observed between 25-130 °C. In the middle (between 130 and 220 °C), the escape of 4 DMF molecules (per formula unit) resulted in a weight loss of 10.6% (cal.: 10.7 wt%). After reaching the temperature 400 °C, the framework structure began to disintegrate which caused the final weight loss of the compound. The only weight loss due to the cleavage of the coordination bonds between the metal ion and the 'O' atoms of the carboxylates of the linker for **3′** was observed after the temperature of 400 °C. The thermal stability of the MOF was again confirmed by the variable temperature PXRD measurement which also suggested the similar thermal stability of the MOF as that of the TG analysis (Figure

4.10). Therefore, the thermal tolerance of **3** and **3′** are comparable to the other Zr-based MOFs.[27, 28]

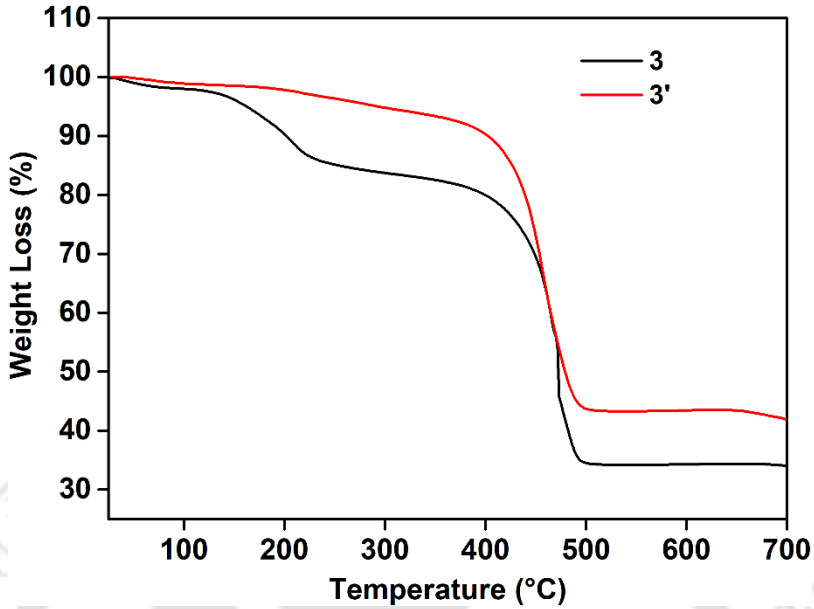

Figure 4.9 Thermogravimetric analysis curves of as-synthesized **3** (black) and thermally activated **3′** (red) recorded under air atmosphere in the temperature range of 25-700 °C with a heating rate of 5 °C min^{-1}.

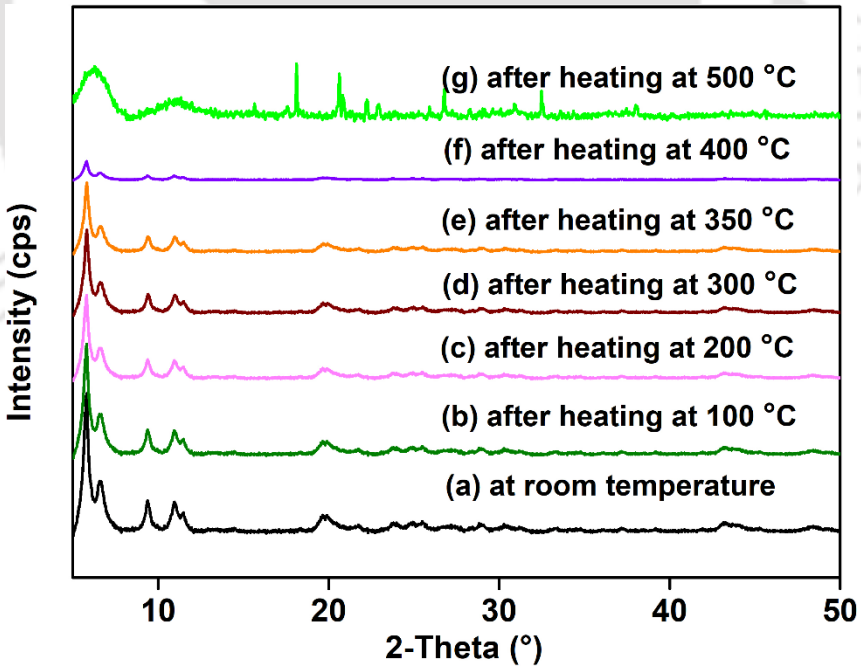

Figure 4.10 PXRD patterns of **3′** at different temperatures.

4.3.4 Sorption Study

Porosity is one of the most interesting features of a MOF. The definite pore size of a MOF permits to passage of only the reactants (during catalysis) which have less size than the pore of the MOF. The construction of MOFs with definite pores favors the formation of desired

products only (for catalysis) and selective sensing of a particular analyte. Therefore, to determine the surface area and pore volume of **3′**, we measured the BET surface area at -196 °C. Type-I N_2 sorption isotherms with BET surface area of 1265 m^2/g confirmed the microporous nature of the MOF (Figure 4.11). The pore-size distribution plot (Figure 4.12) displayed that most of the micropores of the MOF are concentrated at 8.0 Å.

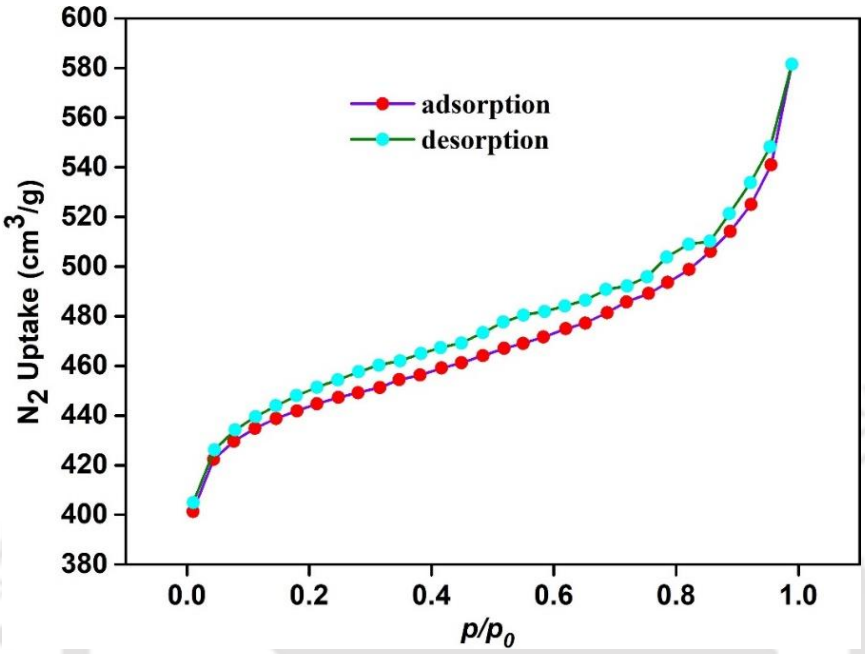

Figure 4.11 N_2 adsorption (orange circles) and desorption (cyan circles) isotherms of thermally activated **3′** recorded at –196 °C.

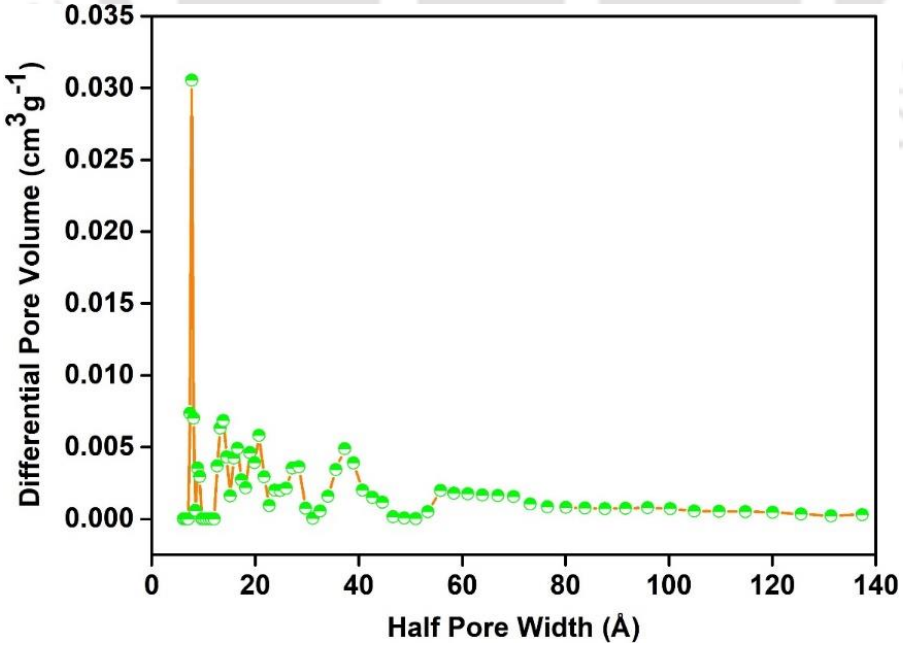

Figure 4.12 Density functional theory pore-size distribution of **3′** as determined from its N_2 adsorption isotherms at -196 °C.

4.3.5 Selective Sensing of Adrenaline by 3′

Adrenaline is an important mammal hormone that regulates various biological processes.[2] Thus, it is necessary to detect the exact concentration of adrenaline in different bio-fluids to diagnose several disorders which are caused by the abnormal secretion of adrenaline in the human body. In the literature, very few adrenaline sensors are described (Table 4.1). The majority of them are toxic to the human body as most of them are tiny organic molecules.[15] Additionally, the reported sensors respond to adrenaline slowly, their sensing media are not bio-friendly and some probes lack selectivity towards adrenaline.[5, 15, 29] Considering these drawbacks of reported sensors and demands of the modern-day pharmaceutical industries, herein, we developed a selective, fast and sensitive MOF-based sensor of adrenaline in bio-compatible HEPES buffer medium. The sensor displayed an excellent fluorescence response (λ_{em} = 462 nm) when it was excited with a light of 330 nm (Figure 4.13). The fluorescence intensity was immediately (within 5 s) quenched by the addition of 300 µL of 5 mM solution of adrenaline (Figure 4.14). Moreover, no further decrease in emission response was observed with time and further increase of the concentration of adrenaline (Figure 4.15a-b).

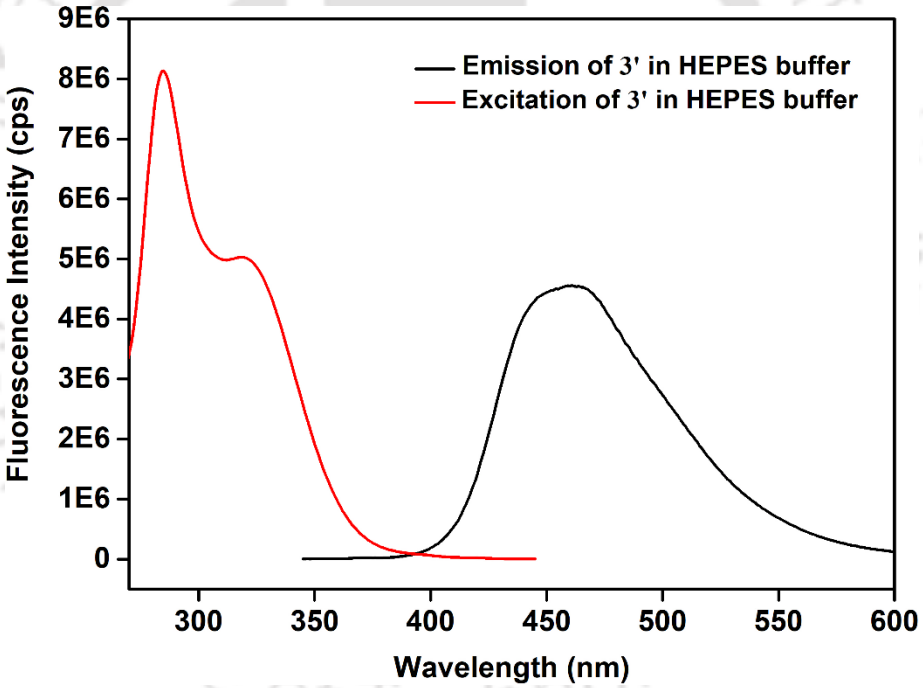

Figure 4.13 Excitation (red) and emission (black) spectra of **3′** in HEPES buffer.

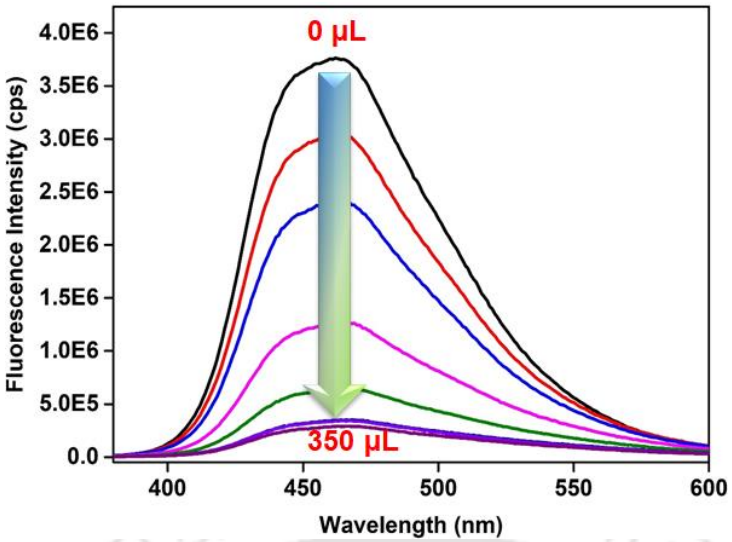

Figure 4.14 Switch-off in the fluorescence intensity of **3′** with incremental addition (0 to 350 µL) of 5 mM adrenaline solution.

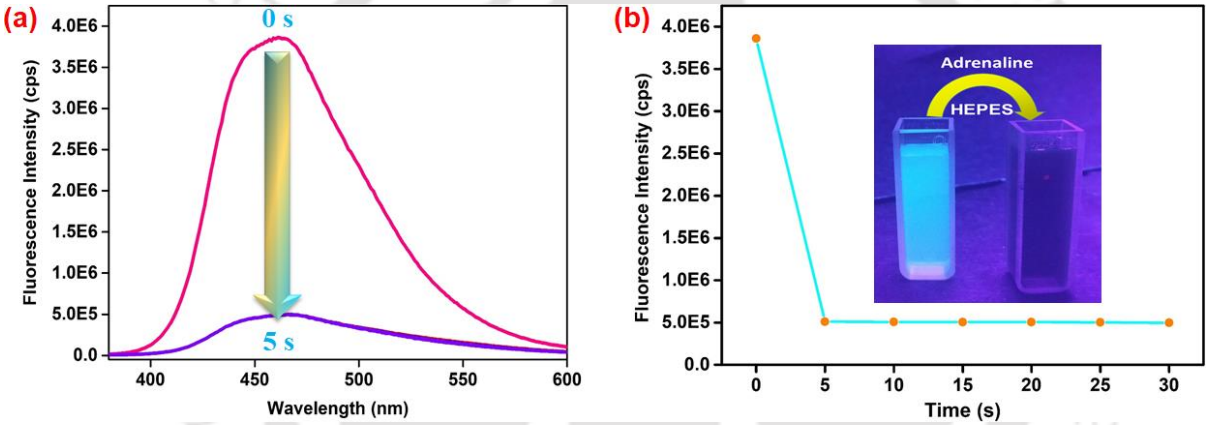

Figure 4.15 (a) Change in luminescence intensity of **3′** with respect to time. (b) Time-dependent saturation plot of fluorescence intensity of **3′** (change in fluorescence under UV-light is shown in the inset of Figure 4.15b).

Table 4.1 Comparison of the detection performance of the present probe (**3′**) with various previously reported probes for adrenaline.

Sl. No.	Sensor Material	Type of Material	Sensing Medium	LOD (nM)	Response Time (s)	Sensing Method	Ref.
1	carbon nanotube paste electrode	carbon nanotube	pH 6.5	31	-	cyclic voltammetry	15
2	4-amino-3-hydrazino-5-mercapto-1,2,4-triazol	gold nano-particles	DMSO-d_6	1.0	1200	colorimetric	30
3	laccase and PQQ-dependent glucose dehydrogenase	polymer matrix	water	0.2	<120	electrochemistry	31
4	modified carbon quantum dots	quantum dots	water	10	300	fluorescence	32
5	tyrosinase/SiC/chitosan modified electrode	glassy carbon electrode	water	0.5	250	electrochemi luminescence	33
6	$CuInS_2$ quantum dots	quantum dots	water	3.6	1800	fluorescence	29

7	rGO-AuNPs electrode	Nano-particles	water	450	900	electrochemistry	34
8	Ceramic-based miniature	polymer	water	2300	-	low temp. cofired ceramics technology	14
9	$[Zr_6O_4(OH)_4(C_{15}H_8N_2O_4S)_6]$ (**3′**)	MOF	HEPES	1.9	< 5	fluorescence	this work

To verify the selectivity of the sensor, a similar series of sensing experiments were carried out by adding 300 µL of analyte solutions to the MOF suspension. It is important to note that none of the competitive analytes showed considerable quenching in the fluorescence intensity of the MOF (Figure 4.16). Such a finding demonstrates the selectivity of the MOF for adrenaline over other interfering bio-molecules and biologically active metal ions. The selectivity of the sensor even in the coexistence of other competitive analytes was verified by treating the MOF suspension with a competitive analyte followed by the addition of the solution of adrenaline. Figures 4.17 signify the selectivity of the MOF towards adrenaline even in the coexistence of other possible biomolecules that can be present in various bio-fluids. To quantify the reproducibility and accuracy of the measurements, the standard deviations of three individual measurements were recorded, and inter as well as intra-day precisions were calculated (Table 4.2).

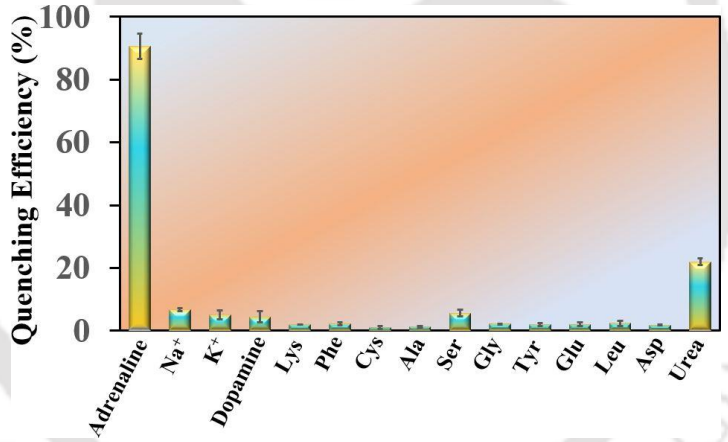

Figure 4.16 Selectivity of **3′** towards adrenaline.

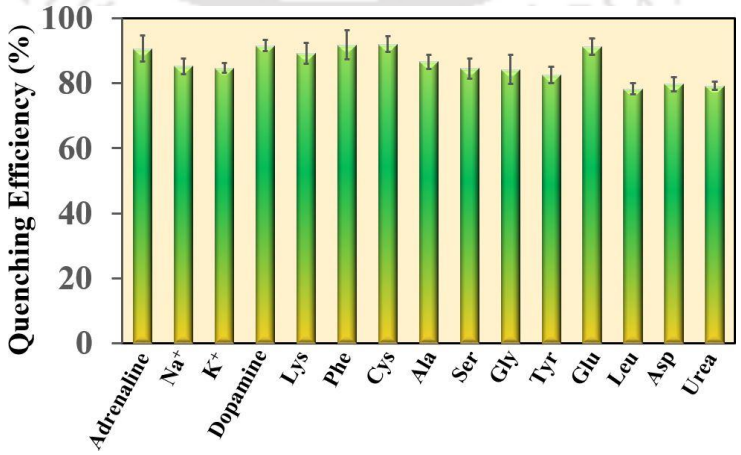

Figure 4.17 Selectivity of **3′** towards adrenaline sensing in the existence of other competitors (error bars signify the standard deviations of three individual measurements).

Table 4.2 Evaluation of intra-day, inter-day accuracy and precision study of change in fluorescence intensity of ***3′*** after incremental addition of 5 mM aqueous solution of adrenaline.

Parameter	Amount of Adrenaline Added (μL)	Fluorescence Intensity (cps) at λ_{max} = 483 nm			Average PL Intensity (cps)	SD	RE%
repeatability intra-day precision	0	3764730	3756500	3749240	375682	7750.0	0.210
	50	3038290	3046930	3043740	3042987	4368.	0.154
	100	2407820	2416740	2411540	2412033	4480.4	0.175
	150	1262750	1274670	1261310	1266243	7333.1	0.276
	200	643679.7	642749.2	645475.	643968.1	1385.8	0.044
	250	345860.3	346994.6	349820.2	347558.4	2039.2	0.491
	300	340835.4	340416.6	342929.5	341393.9	1346.2	0.163
reproducibility inter-day precision	0	3764730	3751030	3759740	3758500	6933.6	0.165
	50	3038290	3035850	3023560	3032567	7894.8	0.188
	100	2407820	2407580	2403230	2406210	2583.5	0.066
	150	1262750	1269610	1271190	1267850	4486.8	0.404
	200	643679.7	648971.6	647893.4	646848.2	2796.4	0.492
	250	345860.3	347132.9	351267.9	348087	2827.2	0.644
	300	340835.4	342363.9	339359.2	340852.9	1502.443	0.005

Adrenaline levels in circulating plasma for a healthy person can typically vary from 25 to 50 pg/mL.[3] Therefore, the sensor material should have the ability to detect adrenaline at concentration lower than the typical concentration of adrenaline present in different bio-fluids. Thus, the determination of the limit of detection (LOD) is very crucial. For that measurement, firstly, we determined the standard deviation (σ) of the emission maxima of the probe. After that, dilute solution of adrenaline was gradually injected into the suspension of the MOF in HEPES buffer medium. Finally, the LOD and LOQ values were calculated using the mathematical equation LOD = 3σ /m and LOQ = 10σ /m, respectively which were 1.9 ± 0.3 and 6.6 ± 0.1 nM, respectively (in the used formula 'm' is the slope of the linear fit that was achieved after plotting the fluorescence intensity versus adrenaline concentration) (Figure 4.18). Interestingly, the obtained LOD value is much lower than most of the published chemosensors of adrenaline (Table 4.1). The standard deviations of three individual measurements and details of statistical analysis are summarised in Table 4.3. The measured fluorescence lifetimes of the sensor before and after the treatment of adrenaline solution were 12.9 and 11.8 ns, respectively (Figure 4.19 and Table 4.4).

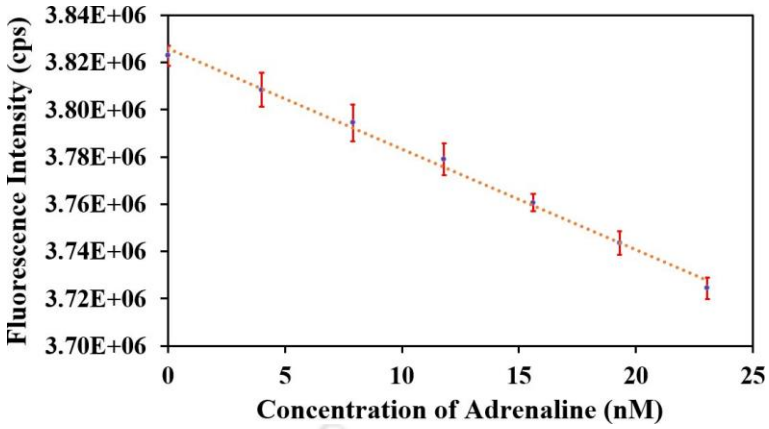

Figure 4.18 Change in the fluorescence emission intensity of **3′** in HEPES buffer as a function of concentration of adrenaline.

Table 4.3 Statistical details of different analytical parameters for the sensing of adrenaline by **3′.**

Concentration Range (nM)	Slopes	Intercepts	Correlation Coefficient (R^2)	$S_{y/x}$ [a]	LOD[b] (nM)	LOQ[c] (nM)	Regression Equation
0-24	-4441.9	3827423	0.998	2914.1	1.96	6.56	-4441.9x + 3827423
	-4072.9	3820081	0.995	2658.5	1.95	6.52	-4072.9x + 3820081
	-4303.0	3830667	0.997	2921.8	2.03	6.79	-4303.0x + 3830667
Average	-4272.6	3826057	0.996	2831.5	1.98	6.62	-4272.6x + 3826057
SD	186.4	5423.5	0.002	149.8	0.03	0.14	(-4272.6 ± 186.4)x + (3826057 ± 5423.5)

[a] Standard deviation of the residuals, [b] Limit of detection, [c] Limit of quantification

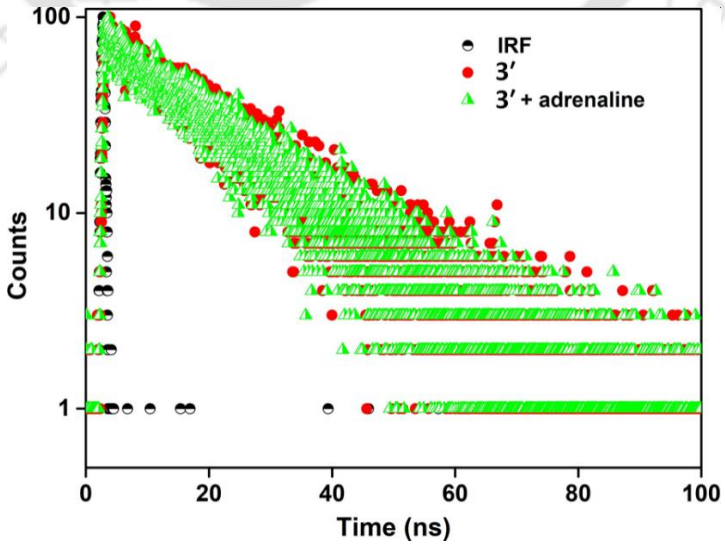

Figure 4.19 Lifetime decay profile of **3′** in the absence and presence of adrenaline solution (λ_{ex} = 330 nm, monitored at 336 nm).

Table 4.4 Fluorescence lifetimes of **3′** before and after the addition of adrenaline solution (λ_{ex} = 336 nm, pulsed diode laser).

Volume of Adrenaline Solution Added (μL)	f_1	f_2	τ_1 (ns)	τ_2 (ns)	$<\tau>^*$(ns)	χ^2
0	0.149	0.851	2.88	14.70	12.94	1.009
300	0.151	0.848	2.99	13.43	11.85	1.006

* $<\tau> = f_1\tau_1 + f_1\tau_2$

The reusability test of the sensor was executed up to five cycles. For this experiment, the sensor material was collected, cleaned and activated before each cycle of sensing. Figure 4.20 displays that the quenching efficiencies of the material were not lost even after five cycles of sensing.

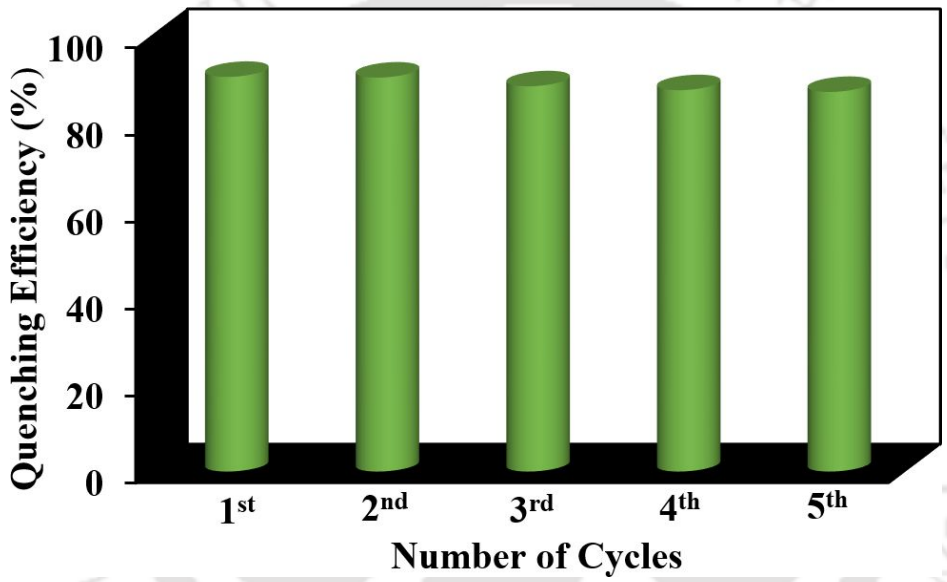

Figure 4.20 Reusability of **3′** for the sensing of adrenaline in HEPES buffer.

The Stern-Volmer (S-V) plot in different concentrations of various analytes provides us with crucial information about the nature of the quenching process. The Stern-Volmer quenching constant (K_{sv}) informs us about the selectivity of the sensor towards the quencher. The *Ksv* value of this quenching process was determined using the mathematical formula $K_{sv}[Q] + 1 = I_0/I$ (Figure 4.21-4.22). The intensities of **3′** before and following the treatment of various analytes are represented in the formula by I_0 and I, respectively and [Q] specifies the adrenaline concentration (in molar). The calculated K_{sv} value for this measurement was 1.15×10^6 M^{-1}, which is much higher than most of the other adrenaline sensors (Figure 4.22).[29, 32]

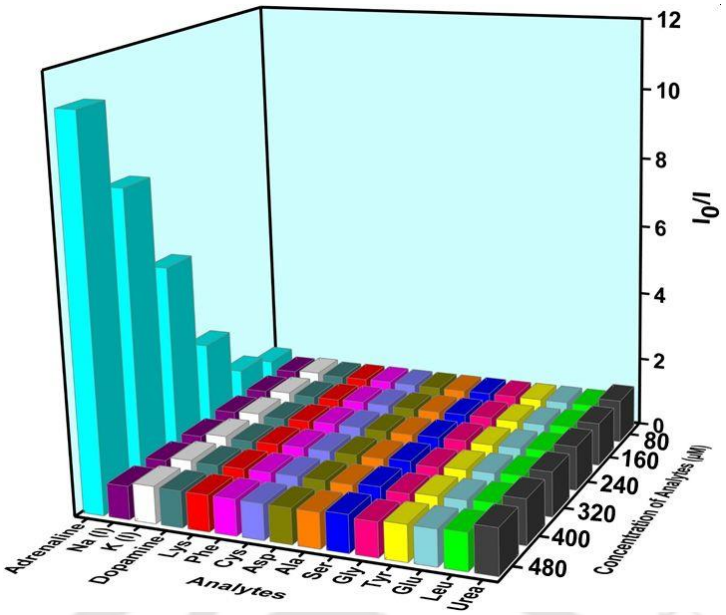

Figure 4.21 Stern-Volmer plots for the decrease in luminescence intensities of **3′** with gradual addition of various analytes in case of adrenaline sensing.

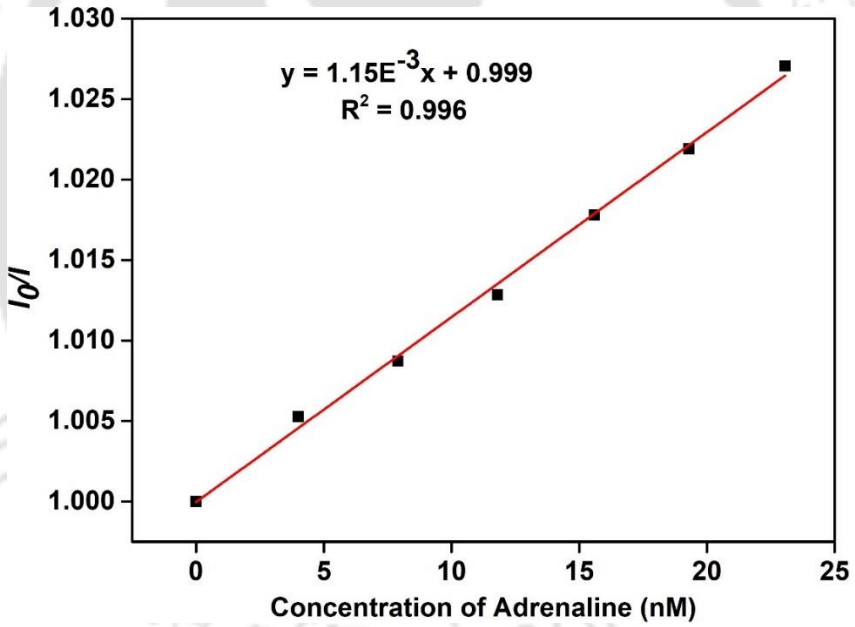

Figure 4.22 Stern-Volmer plot for the fluorescence emission quenching of **3′** in presence of adrenaline.

4.3.6 Sensing of Adrenaline in Different pH Media and Human Bio-fluids

The excellent stability of the probe, selectivity, reusability and low LOD value encouraged us to know the sensing efficiencies of the probe in different pH solutions and human bio-fluids. The sensor's ability to detect adrenaline in various pH solutions is shown in Figure 4.23. Up to pH 10, the probe can detect adrenaline but when the pH was too basic (pH =12), the MOF lost its sensing ability due to the loss of its structural integrity. The sensitivity of the MOF to recognize adrenaline in human serum and urine was also verified and the concentrations of adrenaline present in the bio-fluids were also measured (Tables 4.5-4.6). Figures 4.24-4.25

display the sensing ability of the MOF in the above-mentioned media. After the addition of 350 µL of 5 mM adrenaline-spiked serum and urine samples, there was 60% decrease in fluorescence intensities in the case of serum and urine samples, respectively. The found concentrations of adrenaline and recovery percentages were compared with the spiked concentrations and the obtained recovery percentages were all close to 100% (Tables 4.5-4.6). All these findings imply that the probe can be applied for the critical measurement of concentrations in pharmaceutical industries.

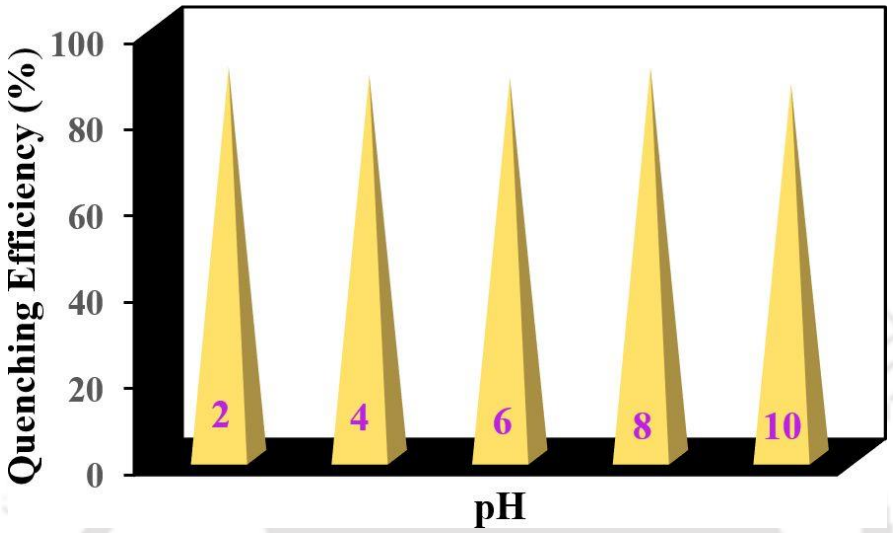

Figure 4.23 Quenching efficiencies of the suspension of **3′** after addition of 300 µL of 5 mM adrenaline solution in different pH media.

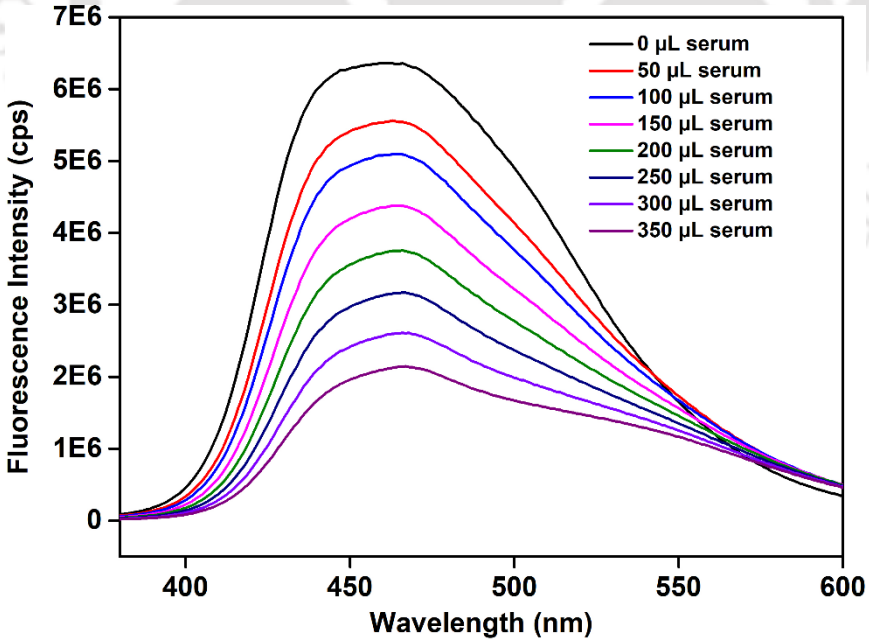

Figure 4.24 Turn-off in fluorescence emission intensity of the suspension of **3′** in HEPES buffer medium after addition of 5 mM of different volumes of adrenaline-spiked serum solution.

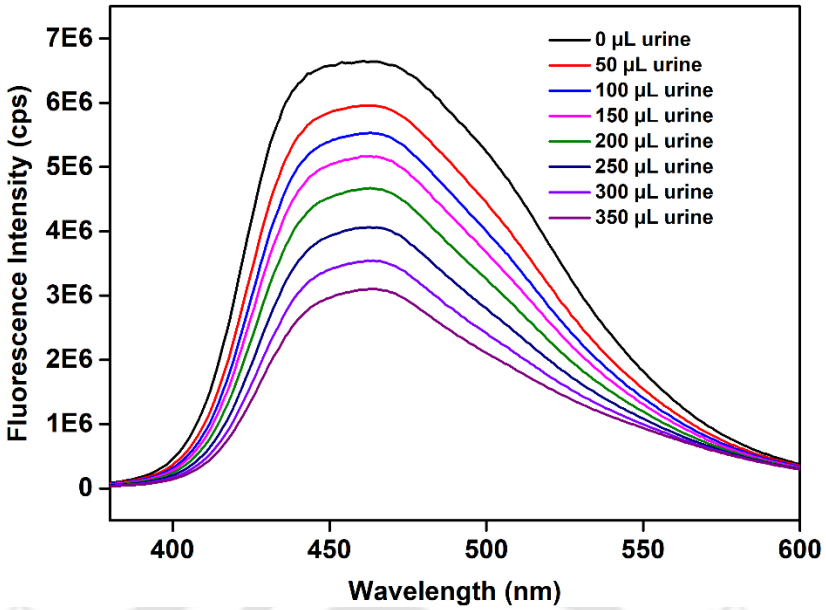

Figure 4.25 Turn-off in fluorescence emission intensity of the suspension of **3′** in HEPES buffer medium after addition of 5 mM of different volumes of adrenaline-spiked urine solution.

Table 4.5 Fluorometric detection of adrenaline in human serum samples by using **3′**.

Adrenaline Spiked (mol L^{-1})	Adrenaline Found (mol L^{-1})	Recovery (%)	RSD (%) (n=3)
8.0×10^{-5}	7.79×10^{-5}	97.3	1.42
2.36×10^{-4}	2.28×10^{-4}	96.6	3.06
3.87×10^{-4}	3.89×10^{-4}	100.5	0.51

Table 4.6 Fluorometric detection of adrenaline in human urine samples by using **3′**.

Adrenaline Spiked (mol L^{-1})	Adrenaline Found (mol L^{-1})	Recovery (%)	RSD (%) (n=3)
8.0×10^{-5}	7.93×10^{-5}	99.1	1.28
2.36×10^{-4}	2.31×10^{-4}	97.9	1.09
3.87×10^{-4}	3.86×10^{-4}	99.7	1.85

4.3.7 Sensing of 6-MP by 3′

Excessive use and arbitrary disposal of the anti-cancer drug (6-MP) increases the concentration of this drug and its metabolized, harmful side products in the environmental water bodies which has become a threat to aquatic plants and animals and also to the higher-class animals. Therefore, the detection and measurement of the concentration of this drug in domestic wastewater are highly necessary. Realizing this urgency, herein, we used **3′** as a sensor of 6-MP in aqueous medium. Initially, the MOF showed high fluorescence intensity in water but it was completely quenched within 5 s of the addition of 200 µL (5 mM) of aqueous solution of 6-MP (Figures 4.26-4.27).

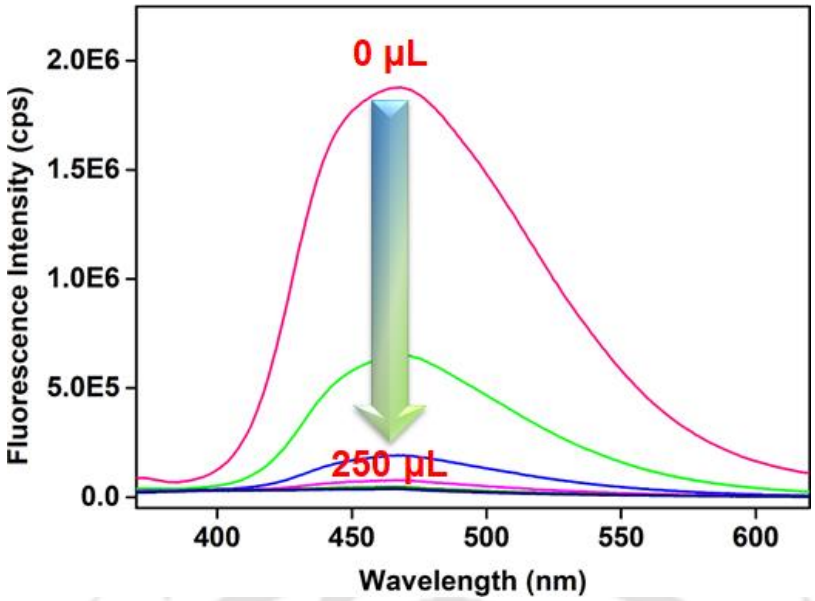

Figure 4.26 Quenching in the fluorescence intensity of **3′** with incremental addition (0 to 250 µL) of 5 mM 6-MP solution.

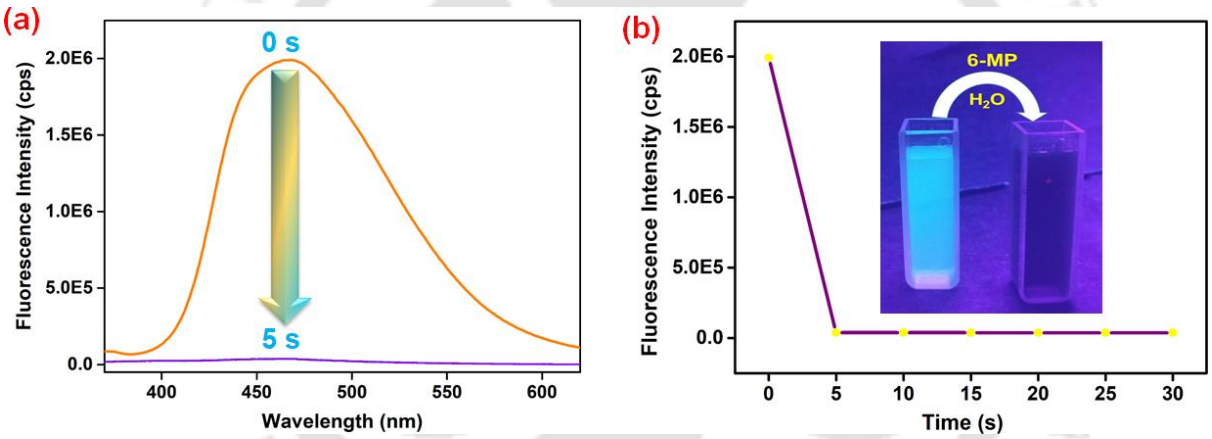

Figure 4.27 Quenching in luminescence intensity of **3′** with respect to time (change in fluorescence under UV-light is shown in the inset of Figure 4.27b).

The selectivity of the probe towards 6-MP was determined in absence and presence of other potential competitors normally present in wastewater specimens. Figures 4.28-4.29 display that none of the competitors interferes in this sensing event. Following the aforementioned procedure, the LOD and LOQ values of the probe for the sensing of 6-MP were calculated. The obtained LOD and LOQ values were 28 ± 1 and 94 ± 2 pM, respectively (Figure 4.30 and Table 4.7). The obtained LOD value is the lowest ever of all the other reported sensors of 6-MP (Table 4.8). Lower value of LOD implies the high selectivity of the probe towards 6-MP. Such selectivity was further confirmed by the high value of Stern-Volmer quenching constant (K_{sv}) (Figures 4.31-4.32). The obtained K_{sv} value was 2.6×10^5 M^{-1}. The Stern-Volmer 3D plot displays that at lower concentration of 6-MP, it maintained its linearity but it adapted curvature at higher concentration of analyte.

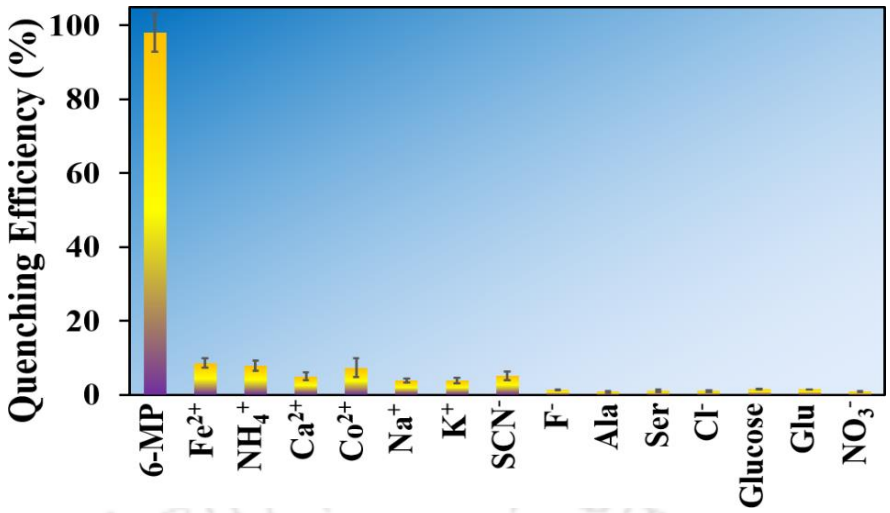

Figure 4.28 Selectivity of **3′** towards the sensing of 6-MP.

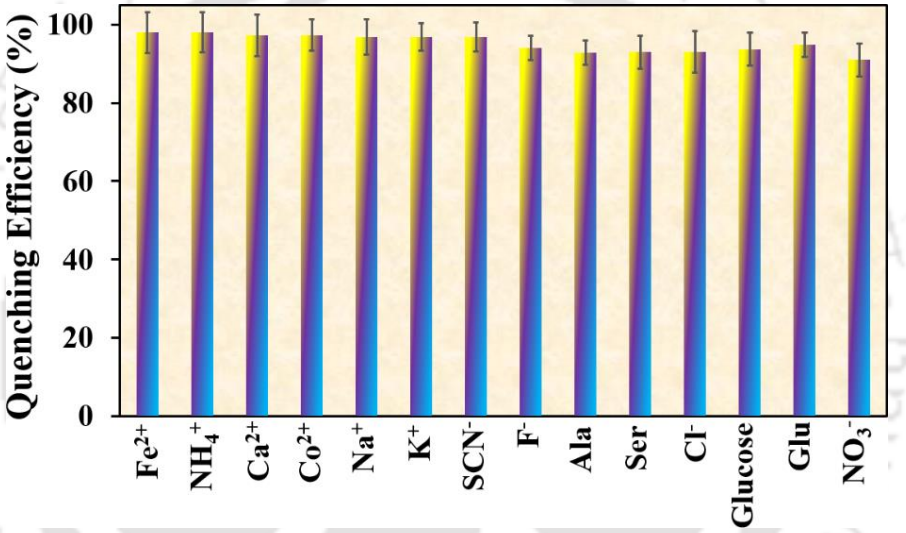

Figure 4.29 Selectivity of **3′** towards the sensing of 6-MP in the existence of other competitors (error bars signify the standard deviations of three individual measurements).

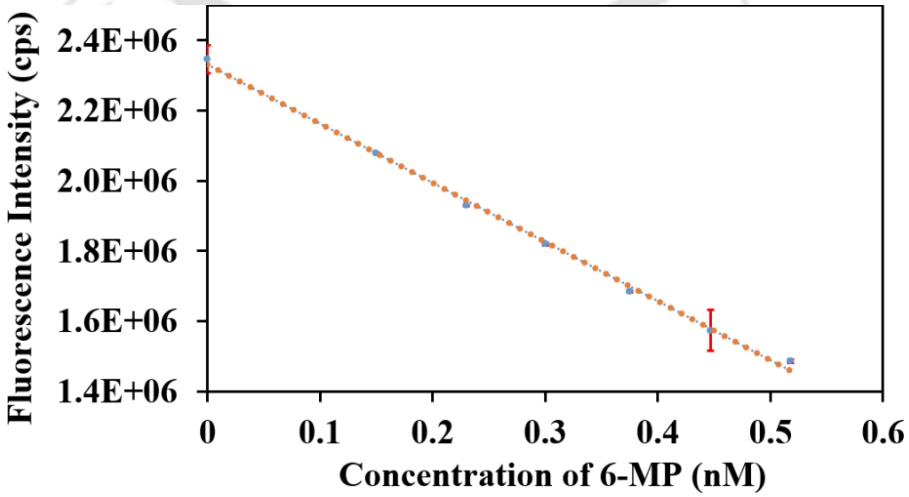

Figure 4.30 Change in the fluorescence emission intensity of **3′** in aqueous medium as a function of concentration of 6-MP.

Table 4.7 Statistical details of different analytical parameters for the sensing of 6-MP by **3′**.

Concentration Range (nM)	Slopes	Intercepts	Correlation Coefficient (R^2)	$S_{y/x}$ [a]	LOD[b] (nM)	LOQ[c] (nM)	Regression Equation
0-0.52	-1686851	2340527	0.995	15449.1	0.027	0.092	-1686851x +2340527
	-1769212	2351571	0.998	16810.3	0.028	0.095	-1769212x + 2351571
	-1590715	2301175	0.997	15149.9	0.029	0.096	-1590715x + 2301175
Average	-1682259	2331091	0.996	15803.1	0.028	0.094	-1682259x + 2331091
SD	89337.2	26490	0.002	885.0	0.001	0.002	(-1682259 ± 89337.2)x + 2331091 ± 26490)

[a] Standard deviation of the residuals, [b] Limit of detection, [c] Limit of quantification

Table 4.8 Comparison of the detection performance of present probe (**3′**) with various previously reported probes for 6-MP.

Sl. No.	Sensor Material	Type of Material	Sensing Medium	LOD (nM)	Response Time (s)	Sensing Method	Ref.
1	carbon nanotubes-TiO_2	carbon nanotube	pH = 9	65	-	cyclic voltammetry	12
2	$Co(phen)_3]^{3+}$/MWNT modified graphite electrode	graphite electrode	tris buffer	16000	1800	cyclic voltammetry	35
3	molecular imprinted polymer	polymer matrix	methanol /water	20	2400	fluorescence	36
4	6-TGN	organic compound	water	6	780	HPLC	37
5	silver nanoparticles	nanoparticles	water	10	-	colorimetry	38
6	carbon dots and gold nanoclusters	carbon dots and nanoclusters	water	54	600	fluorescence	39
7	MoS_2 quantum dots	quantum dots	water	290	2400	fluorescence	40
8	carbon dots	nanoparticles	water	10	-	fluorescence	41
9	CdTe quantum dots	quantum dots	water	8	-	fluorescence	42
10	$[Zr_6O_4(OH)_4(C_{15}H_8N_2O_4S)_6]$ (**3′**)	MOF	water	0.028	< 5	fluorescence	this work

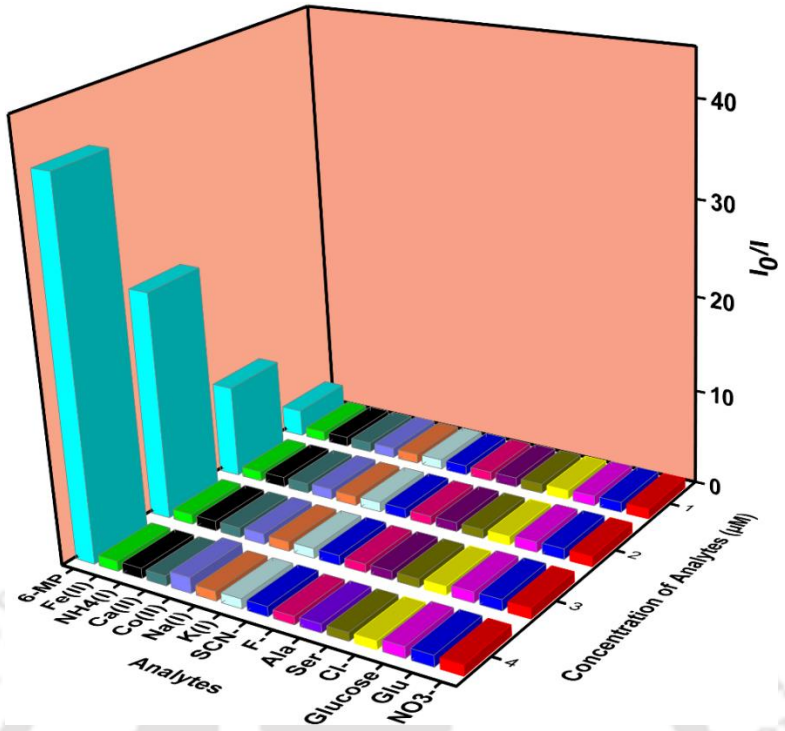

Figure 4.31 Stern-Volmer plots for the decrease in luminescence intensities of **3′** with gradual addition of various analytes in case of 6-MP sensing.

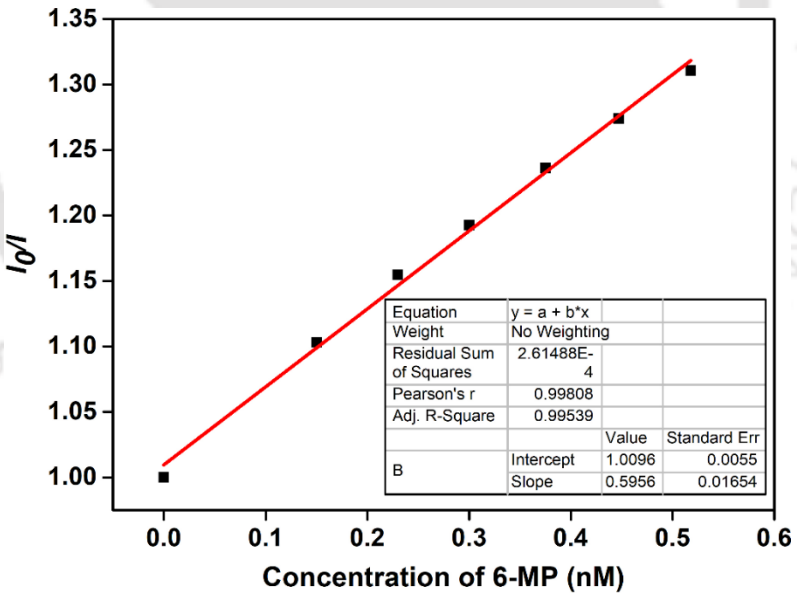

Figure 4.32 Stern-Volmer plot for the fluorescence emission quenching of **3′** in presence of 6-MP.

The fluorescence lifetimes of the MOF were measured before and after the treatment of 6-MP which were 9.5 and 8.9 ns, respectively (Figure 4.33, Table 4.9). The reusability test has shown that the MOF can be reused up to five cycles (Figure 4.34). The loss of quenching efficiency after five cycles of sensing was ~5%. The standard deviations of three different measurements

were collected and inter-day and intra-day precisions were calculated to quantify the measurement's repeatability and accuracy (Table 4.10).

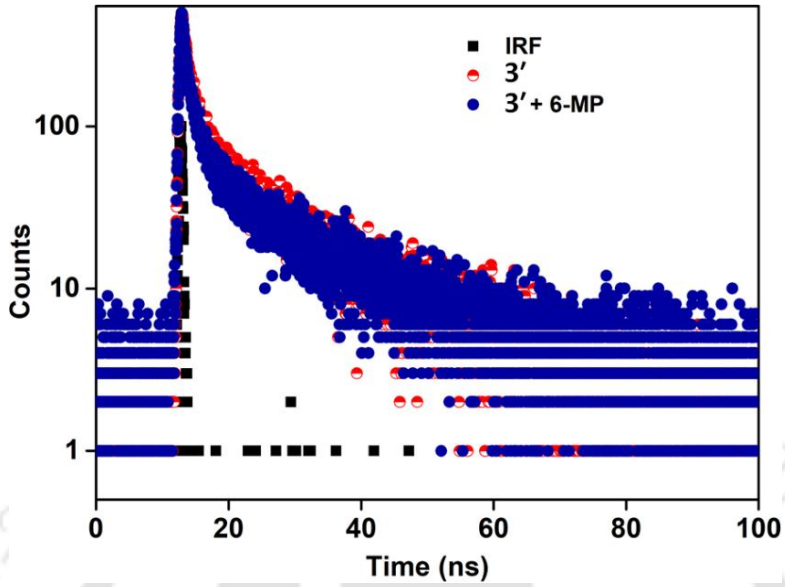

Figure 4.33 Lifetime decay profile of **3′** in absence and presence of 6-MP solution (λ_{ex} = 330 nm, monitored at 336 nm).

Table 4.9 Fluorescence lifetimes of **3′** before and after the addition of 6-MP solution (λ_{ex} = 336 nm, pulsed diode laser).

Volume of 6-MP Solution Added(μL)	f_1	f_2	f_3	τ_1 (ns)	τ_2 (ns)	τ_3 (ns)	$<\tau>$*(ns)	χ^2
0	0.26	0.23	0.49	0.74	3.29	17.57	9.55	1.10
200	0.21	0.25	0.52	0.49	2.25	15.95	8.95	1.08

* $<\tau> = f_1\tau_1 + f_2\tau_2 + f_3\tau_3$

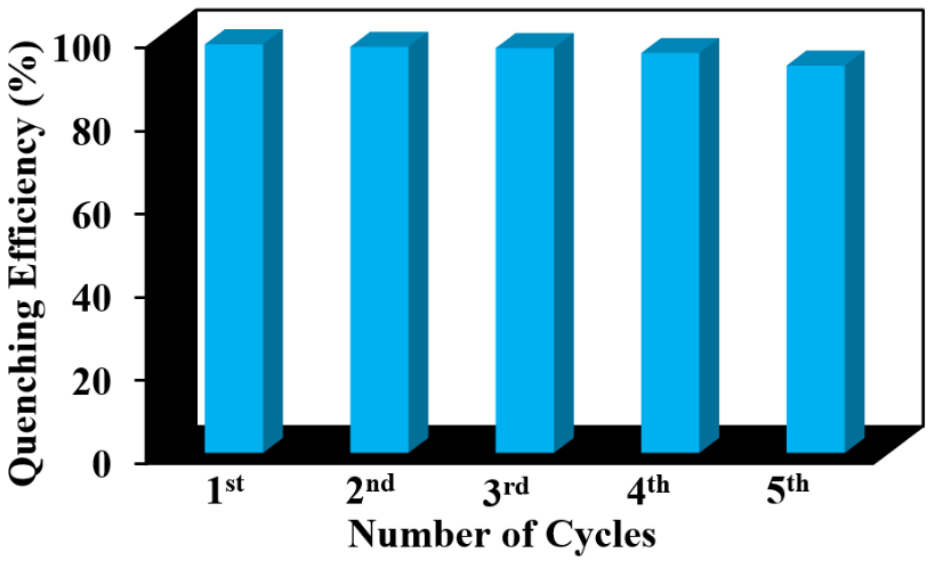

Figure 4.34 Reusability of **3′** for the sensing of 6-MP in H_2O.

Table 4.10 Evaluation of intra-day, inter-day accuracy and precision study of change in fluorescence intensity of **3′** after incremental addition of 5 mM aqueous solution of 6-MP.

Parameter	Amount of 6-MP Added (µL)	Fluorescence Intensity (cps) at λ_{max} = 468 nm			Average PL Intensity (cps)	SD	RE%
repeatability intra-day precision	0	1875790	1876880	1878370	1877013.3	1295.2	0.065
	50	647623.9	650832.8	651355.2	649937.3	2020.4	0.356
	100	191162.8	191431.1	190264.7	190952.9	610.8	0.109
	150	77899.0	77583.5	77435.4	77639.3	236.8	0.335
	200	47098.5	46705.3	46462.5	46755.4	320.9	0.734
reproducibility inter-day precision	0	1874970	1874060	1869160	1872730	3125.0	0.119
	50	651112.1	650962.4	648790.3	650288.3	1299.4	0.126
	100	191391.4	190312.9	189683	190462.4	863.9	0.487
	150	77288.6	76488.1	76536.2	76770.9	448.9	0.674
	200	46428.5	45910.0	45091.8	45091.1	673.9	1.349

4.3.8 Sensing of 6-MP in Various Waste Water Samples and pH Media

The main aim of this experiment is to detect and calculate the concentration of 6-MP in various waste water samples. Therefore, we expanded our sensing experiment to various real water samples (lake water, river water and tap water) to confirm the wide sensing ability of this newly developed sensor (Figure 4.35). For this experiment, suspensions of **3′** were made in the aforementioned water media and 200 µL of the different concentration solutions (5, 2.5 and 1 mM) of 6-MP were injected into the MOF-containing real water media. It was observed that with the continuous decrease in the concentration of 6-MP, the quenching efficiency of the MOF gradually decreases. The resulting recovery percentages were ~100%, and the measured concentrations were comparable to the spiked concentrations of 6-MP (Table 4.11). Figure 4.36 displays that the sensing efficiency remained similar in the pH range of 2-10 but it decreased at pH = 12. The disintegration of the framework structure of the MOF at highly alkaline pH may be the reason for such limitation. Such positive outcomes demonstrated the probe's broad scope and real-world applicability for 6-MP sensing.

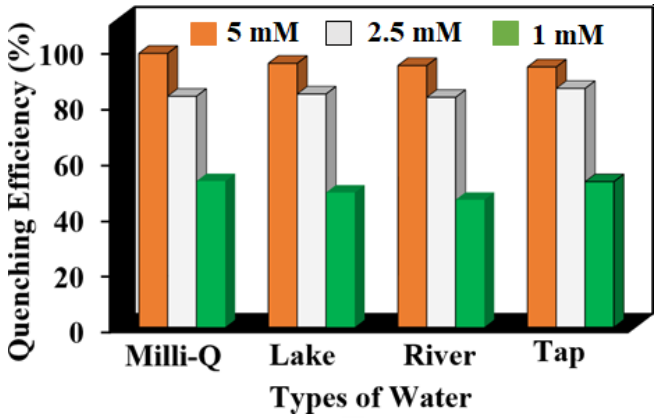

Figure 4.35 Quenching efficiencies of the suspension of **3′** after addition of 200 µL of 5, 2.5 and 1 mM 6-MP solution in different water specimens.

Table 4.11 Comparison between the spiked and observed concentrations and recovery of 6-MP in different real water specimens.

Type of Water	Spiked Conc. of 6-MP (mM)	Observed Conc. of 6-MP (mM)	Recovery (%)
milli-Q water	(i) 0.294 (ii) 0.147 (iii) 0.058	(i) 0.292 (ii) 0.143 (iii) 0.060	(i) 99.3 (ii) 97.3 (iii) 103.4
lake water	(i) 0.294 (ii) 0.147 (iii) 0.058	(i) 0.289 (ii) 0.140 (iii) 0.063	(i) 98.3 (ii) 95.2 (iii) 108.6
tap water	(i) 0.294 (ii) 0.147 (iii) 0.058	(i) 0.295 (ii) 0.157 (iii) 0.054	(i) 100.3 (ii) 106.8 (iii) 93.1
river water	(i) 0.294 (ii) 0.147 (iii) 0.058	(i) 0.285 (ii) 0.135 (iii) 0.065	(i) 96.9 (ii) 91.8 (iii) 112.0

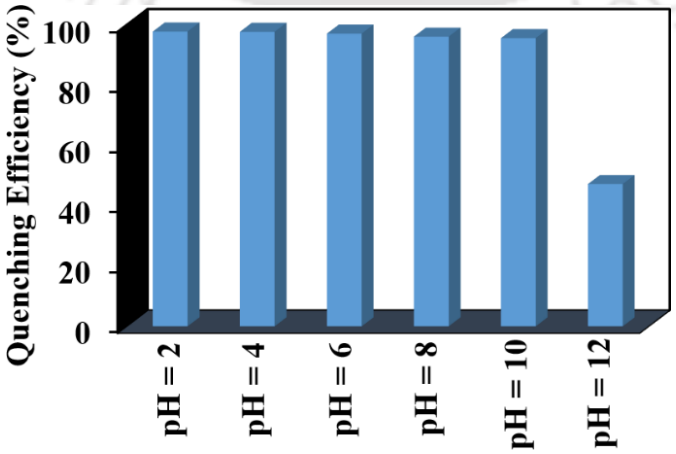

Figure 4.36 Quenching efficiencies of the suspension of **3′** after addition of 200 µL of 5 mM 6-MP solution in different pH media.

4.3.9 Sensing of Adrenaline and 6-MP in MOF@cotton Fabric Composites

Reusability up to five cycles with minimum loss of efficiency, high selectivity and nanomolar level detection ability inspired us to develop inexpensive, handy MOF@cotton fabric composites for the on-site sensing of adrenaline and 6-MP. Sensor-coated filter paper strip technology was used in many of the previously published literature to detect specified analytes.[43, 44] There are several drawbacks to use paper strips. Because they are easily fragile in the presence of solvents, paper strips are frequently not reusable. These make them unusable for a recyclable sensor. A cotton fabric composite is reusable, long-lasting and sanitary which are necessary for sensing of bio-molecules (such as adrenaline) using a recyclable sensor like **3′**. For this experiment, five tiny pieces (1 × 1 cm^2) of cotton fabric were uniformly covered with the MOF suspension and they were then dried in an 80 °C oven. The immobilization of MOF particles on the fabric surface was proved by the PXRD, ATR-IR and FE-SEM analysis of the MOF@cotton composites (Figures 4.37-4.39). Together with the characteristic peaks of the MOF, the PXRD profile of **3′**@cotton showed three peaks at 14.8°, 16.5° and 22.8° which correspond to the peak of cotton fabric. The IR spectrum of **3′**@cotton showed cotton's peak at 3338, 3278, 1154, 1104 and 1017 cm^{-1}. The presence of MOF particles on the surface of the cotton fabric was further confirmed by the FE-SEM images of **3′**@cotton. After that, fabric composites were treated with different concentrations of adrenaline and 6-MP solutions. Figure 4.40 clearly shows the visible change in fluorescence intensities of the composites with the change in concentrations of the analytes solutions. The decrease in fluorescence intensity was observed up to nanomolar concentration of analytes (Figure 4.40). All these findings imply the naked eye detection ability of the composites of both the analytes up to nanomolar level concentration.

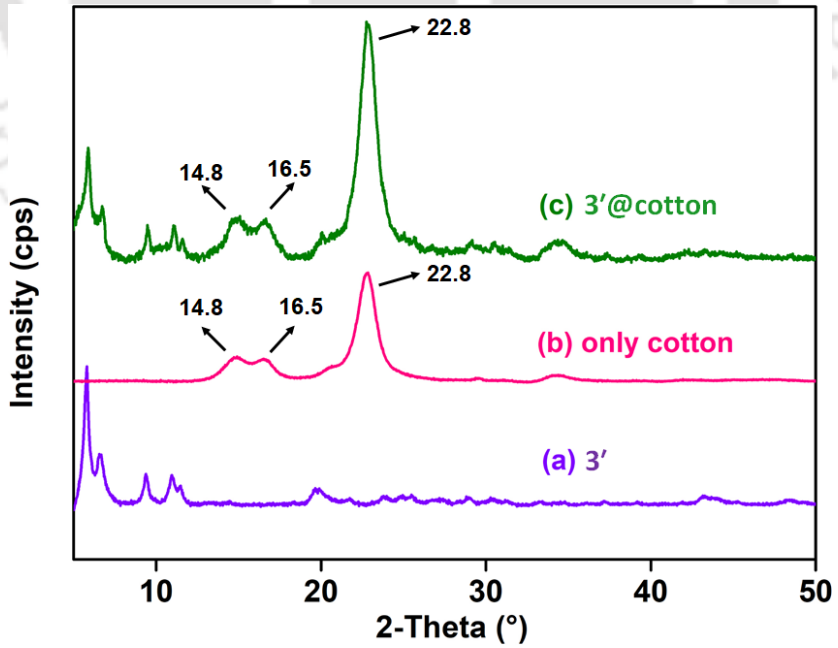

Figure 4.37 PXRD patterns of (a) compound **3′**, (b) native cotton, and (c) **3′**@cotton composite.

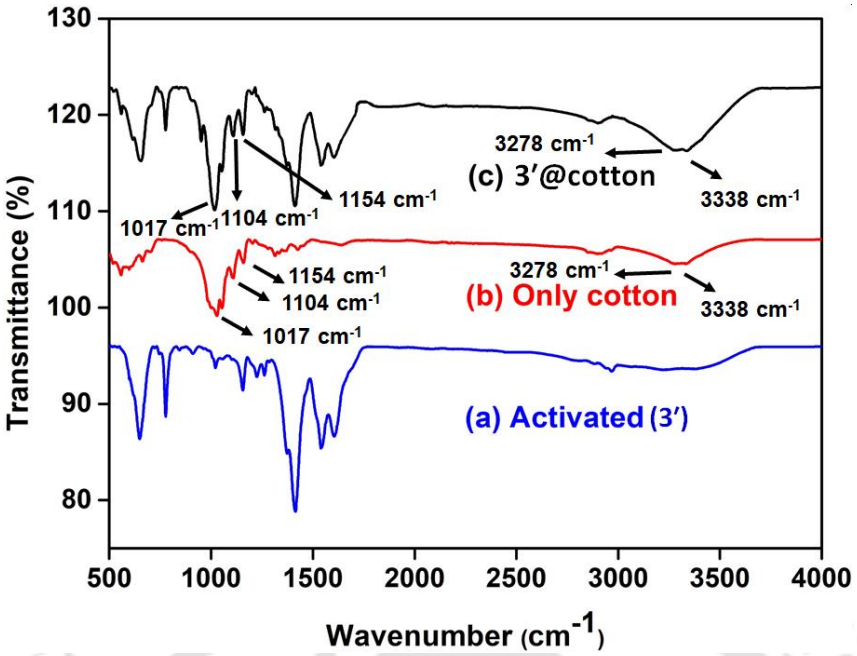

Figure 4.38 ATR-IR spectra of (a) compound **3′**, (b) only cotton, and (c) **3′**@cotton composite**.**

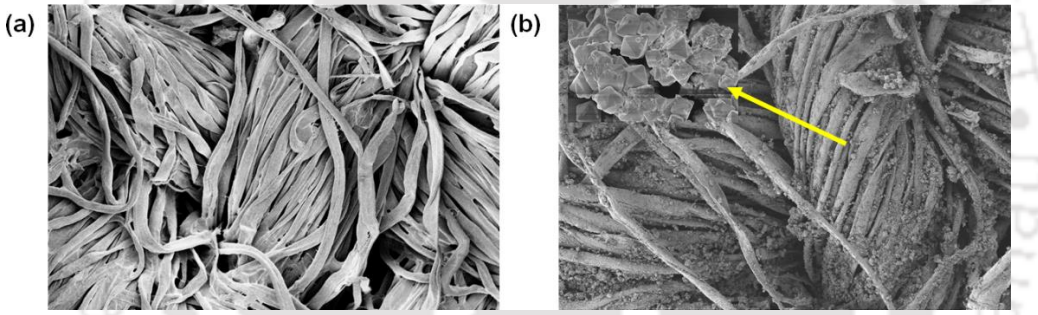

Figure 4.39 FE-SEM images of (a) native cotton fabric and (b) **3′**@cotton composite.

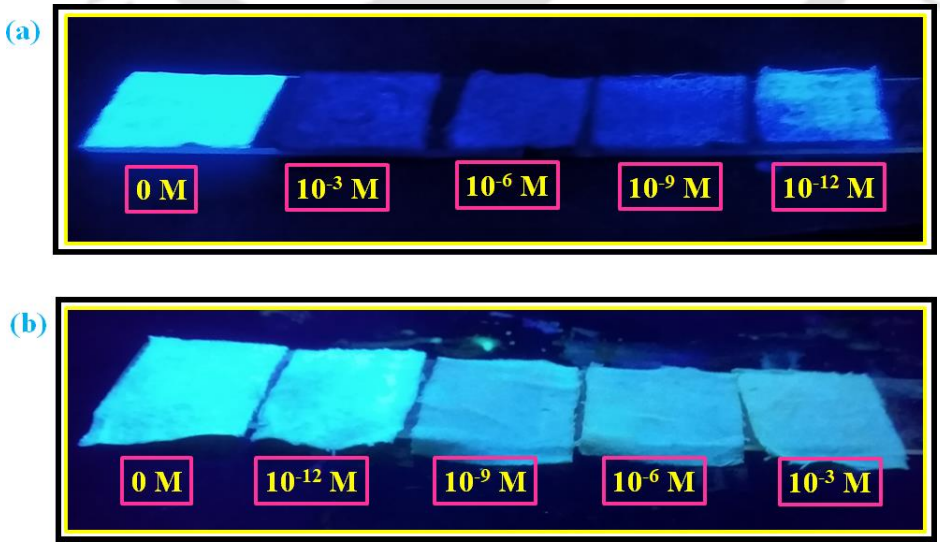

Figure 4.40 Sensing of different concentrations of (a) adrenaline and (b) 6-MP in a MOF@cotton composite.

4.3.10 Possible Mechanisms of Sensing

The possible reasons behind the sensing of adrenaline and 6-MP by **3′** were investigated with the support of various analytical instruments. Firstly, we confirmed the structural integrity of the MOF by measuring the PXRD patterns, and FE-SEM images of the recovered sample after the sensing experiments (Figures 4.41-4.42). The recyclability of the sensor up to five cycles with minimum loss of its efficiencies confirmed that the structure of the MOF remained unperturbed during the sensing events (Figure 4.20 and 4.34). The BET surface area of the MOF was also measured after both sensing experiments. The obtained BET surfaces of the recovered MOF after the adrenaline and 6-MP sensing were 1223 and 1235 m^2/g, respectively (Figure 4.43). These surface area values are very close to the un-treated MOF. The obtained surface area of the analytes treated MOF supported the reversibility and reusability of the material. The aforementioned findings forced us to think about non-reaction-based mechanistic processes.

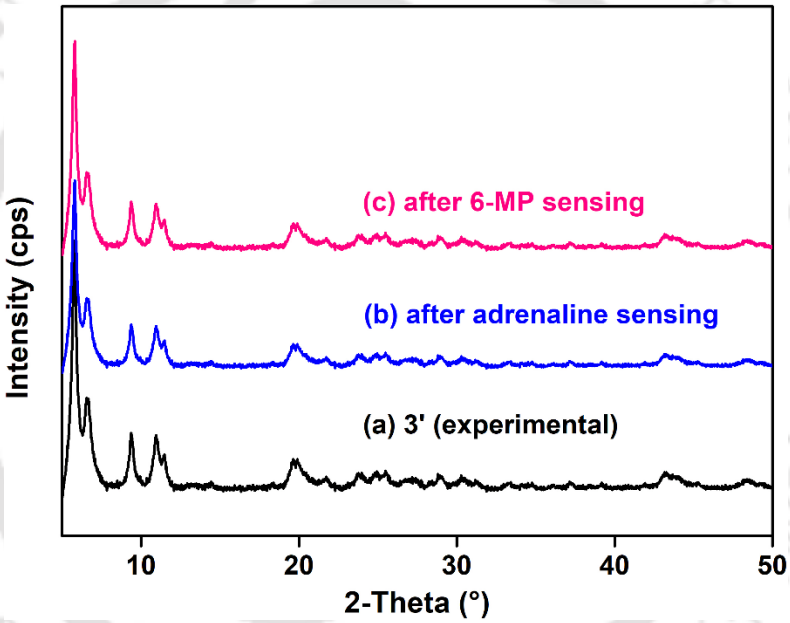

Figure 4.41 PXRD patterns of (a) activated **3′** and **3′** after (b) adrenaline sensing and (c) 6-MP sensing.

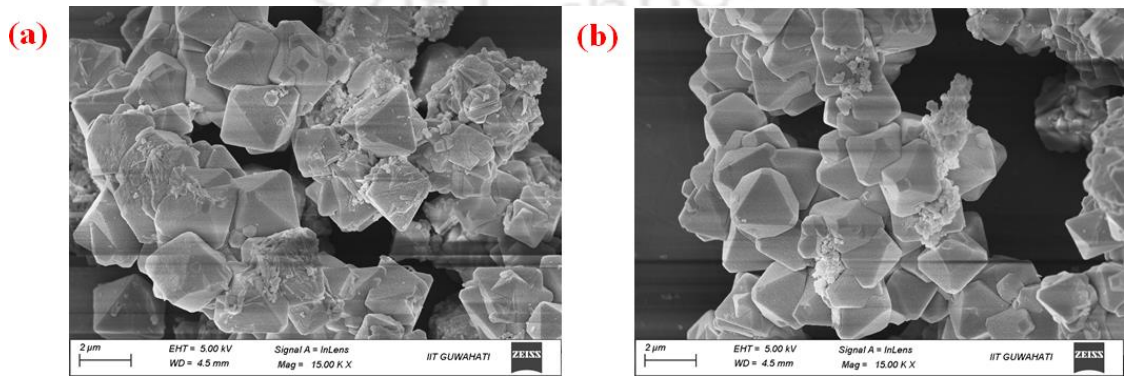

Figure 4.42 FE-SEM images of **3′** after sensing of (a) adrenaline and (b) 6-MP.

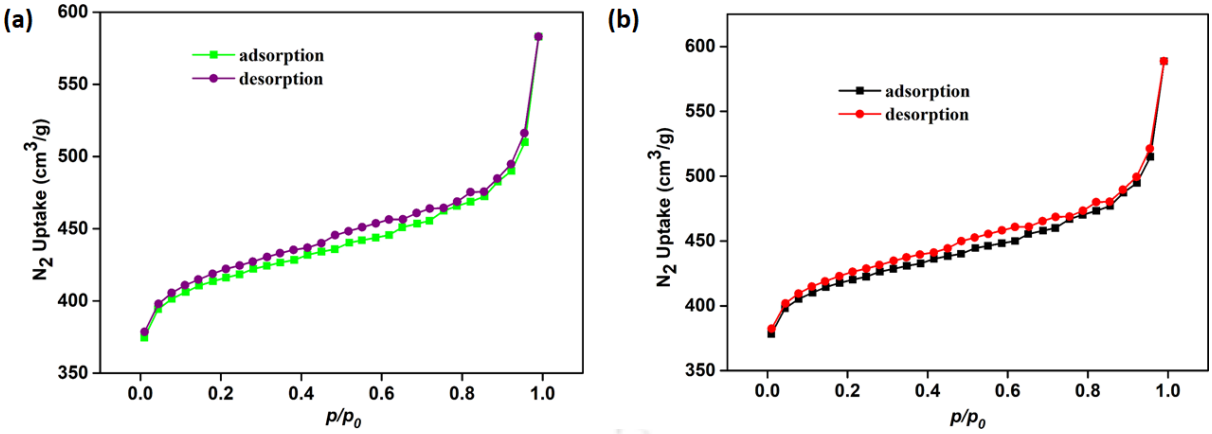

Figure 4.43 N_2 adsorption and desorption isotherms of thermally activated **3′** after sensing of (a) adrenaline and (b) 6-MP recorded at -196 °C.

There are several phenomena (e.g. Förster resonance energy transfer (FRET), inner-filter effect (IFE) and ground-state complexation) reported in the literature which can cause of quenching of the fluorescence intensity of a fluorophore.[45] The above-mentioned events can be categorized into two parts: static and dynamic quenching.[45, 46] Excited state collisions between the quencher and the fluorophore can cause dynamic quenching and if they are tightly bound, then static quenching occurs.[46] These two quenching processes can be differentiated by measuring the fluorescence lifetimes of the fresh and analyte-treated fluorophores. If the fluorescence lifetimes of the fresh and quencher-treated samples remain the same, then the quenching process is static and if the lifetime gets decreased, then it is dynamic in nature.[46, 47]

Table 4.4 shows that the average fluorescence lifetime in case of adrenaline sensing was changed from 12.9 to 11.8 ns after the addition of adrenaline. The considerable change in fluorescence lifetime after the addition of adrenaline suggests the possibility of dynamic quenching mechanism. The ground state complex formation possibility was investigated in detail by measuring the ATR-IR and solid state UV-Vis spectra of the fresh and adrenaline-treated MOF samples (Figures 4.44-4.45). No significant changes were observed in the adrenaline-treated IR and UV-Vis spectra which eliminates the possibility of ground state complex formation.

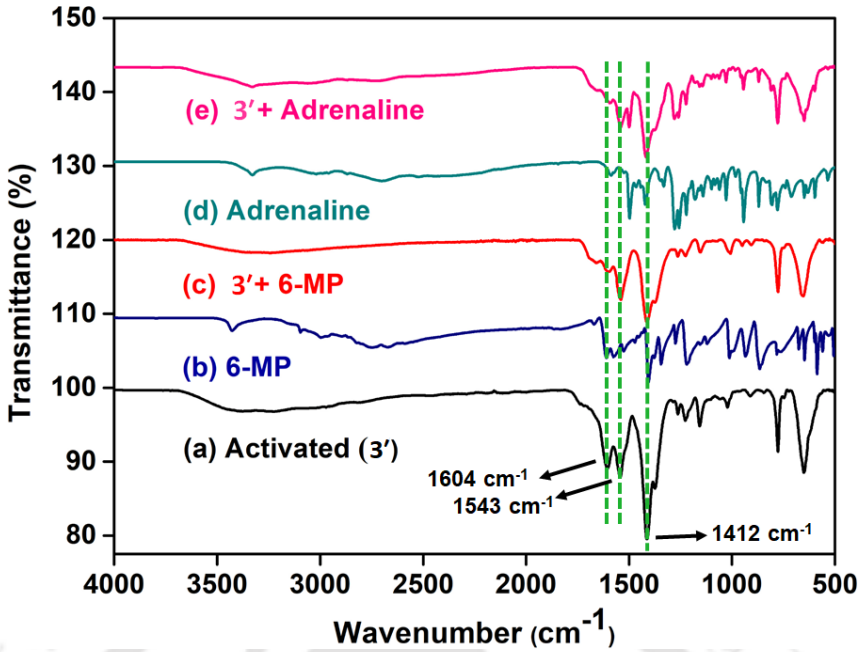

Figure 4.44 ATR-IR spectra of (a) compound **3′**, (b) 6-MP, (c) **3′** + 6-MP, (d) adrenaline and (e) **3′** + adrenaline**.**

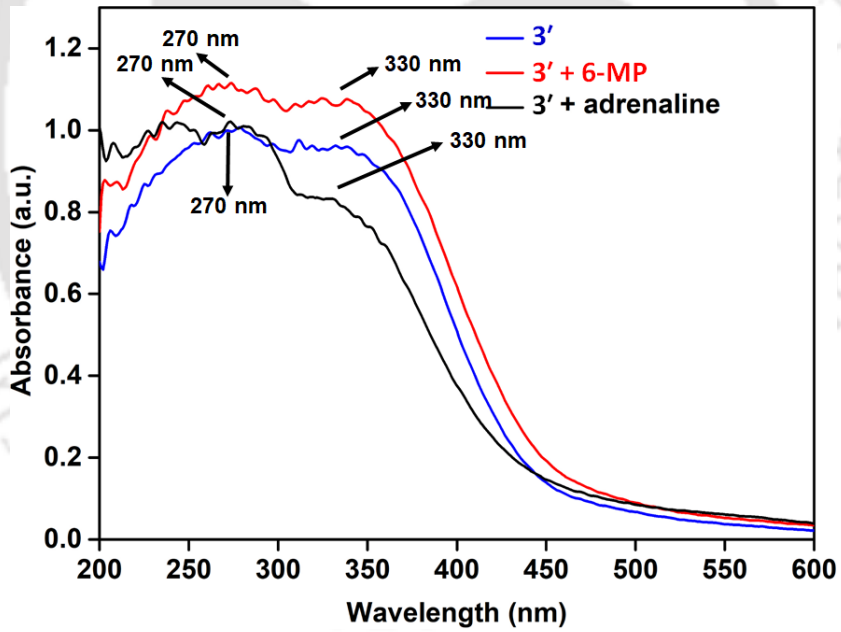

Figure 4.45 Solid state UV-Vis spectra of **3′** (blue), **3′** + 6-MP (red) and **3′** + adrenaline**.**

Here, the contribution of inner filter effect (IFE) for quenching of fluorescence can't be ignored as the absorption maxima of adrenaline (λ_{abs} of adrenaline = 346 nm) is very close to the excitation wavelength of the MOF (λ_{ex} = 330 nm). After the addition of adrenaline, there is a possibility of absorption of a part of the excitation beam of light by adrenaline which can interrupt the complete excitation of the probe which eventually results in the less emission signal output of the probe. It is reported in the literature that the IFE can be eliminated by

shifting the excitation wavelength of the probe to the higher wavelength region from the absorption maxima of the analyte (the presence of which is responsible for IFE).[48, 49]

Hence, we conducted the aforementioned experiment for adrenaline sensing to verify the possibility of IFE. For this experiment, the MOF material was excited at 370 nm and corresponding emission results were collected after gradual increment of the concentration of adrenaline. The quenching efficiency remained similar even after shifting the excitation wavelength, which implies that the IFE is not responsible for the quenching (Figure 4.46).

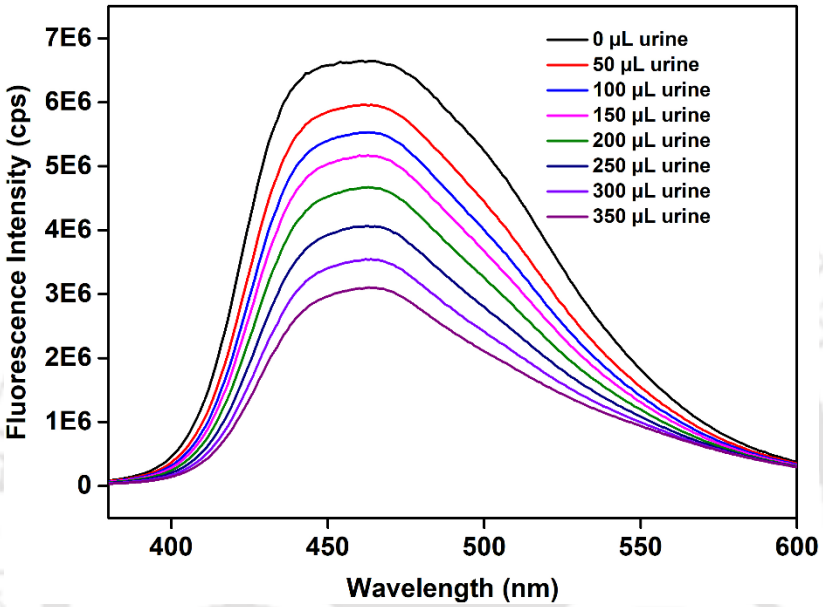

Figure 4.46 Change in the fluorescence intensity of **3′** with incremental addition (0 to 350 µL) of 5 mM adrenaline solution (λ_{ex} = 370 nm).

Here, the fluorescence lifetime of the probe significantly decreased after the addition of adrenaline. Therefore, photoinduced electron transfer (PET) from electron-rich MOF to adrenaline can be also possible. To verify the same, the HOMO and LUMO energy of the linker of MOF and adrenaline were theoretically calculated using DFT method. The functional B3LYP and Pople diffuse basis set 6-31G+ (d, p) were utilized for all the calculations. The LUMO of adrenaline has higher energy than the LUMO of the linker (Figure 4.50). Therefore, electron transfer from linker LUMO to adrenaline LUMO is not possible which rules out the possibility of PET.

The absorption spectrum of adrenaline strongly overlapped with the emission spectrum of the MOF and a considerable change in the lifetime of the MOF after the addition of adrenaline (Figure 4.47) was observed. All the results indicate that FRET is the most probable reason behind this quenching.

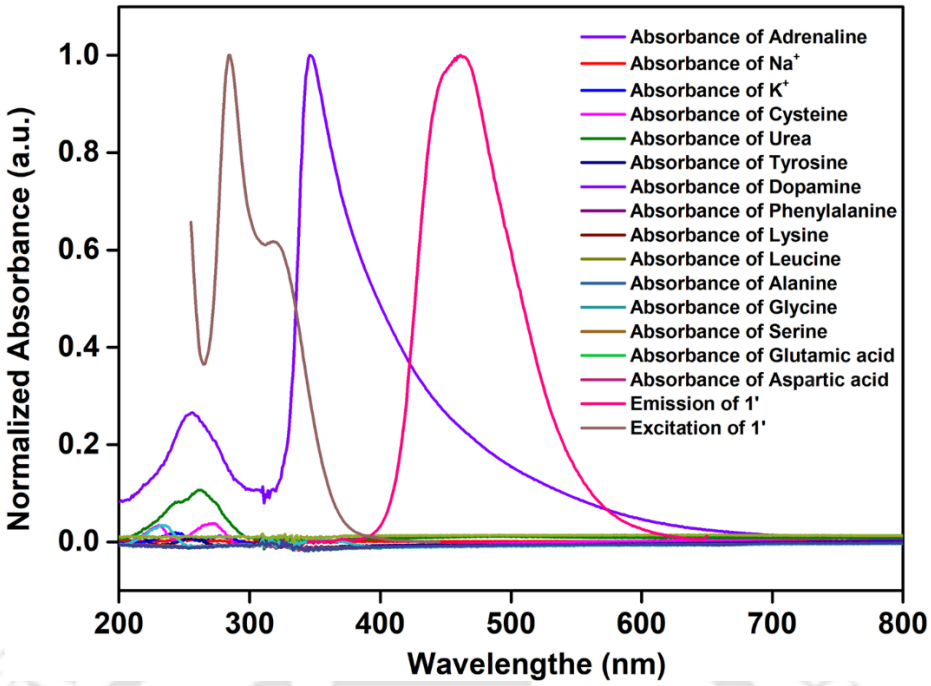

Figure 4.47 Spectral overlap between excitation/emission spectrum of **3′** and absorption spectra of adrenaline and other analytes.

In case of 6-MP sensing, 98% quenching in fluorescence intensity was observed when the MOF was excited at 330 nm but on exciting at 370 nm, the observed quenching efficiency was only 8% (Figure 4.48). Therefore, the possibility of IFE can't be ignored. The possibility of FRET can be eliminated as there was no overlap between the absorption spectrum of 6-MP and the emission spectrum of the adrenaline (Figure 4.49).

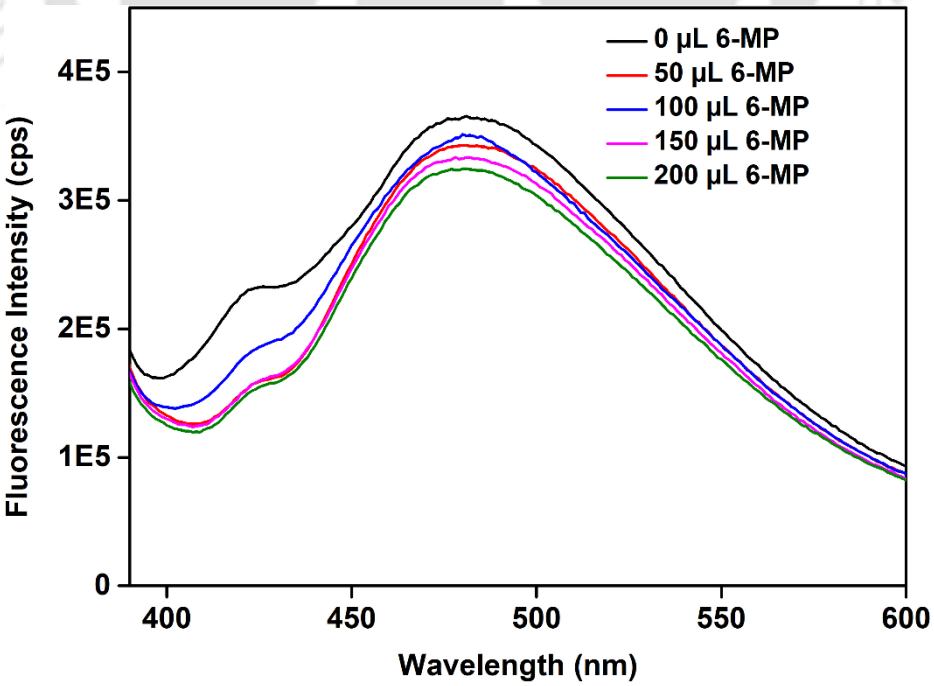

Figure 4.48 Change in the fluorescence intensity of **3′** with incremental addition (0 to 350 µL) of 5 mM adrenaline solution (λ_{ex} = 370 nm).

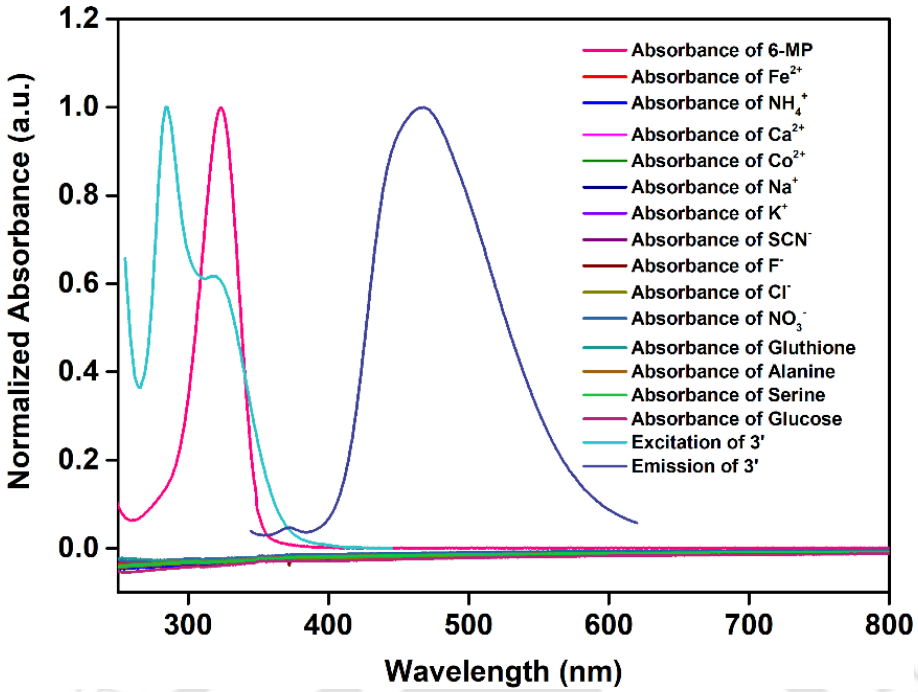

Figure 4.49 Spectral overlap between excitation/emission spectrum of **3′** and absorption spectra of 6-MP and other analytes.

Similar to the adrenaline sensing, no significant changes were observed in the 6-MP treated IR and UV-Vis spectra which eliminates the possibility of ground state complex formation (Figure 4.44-4.45).

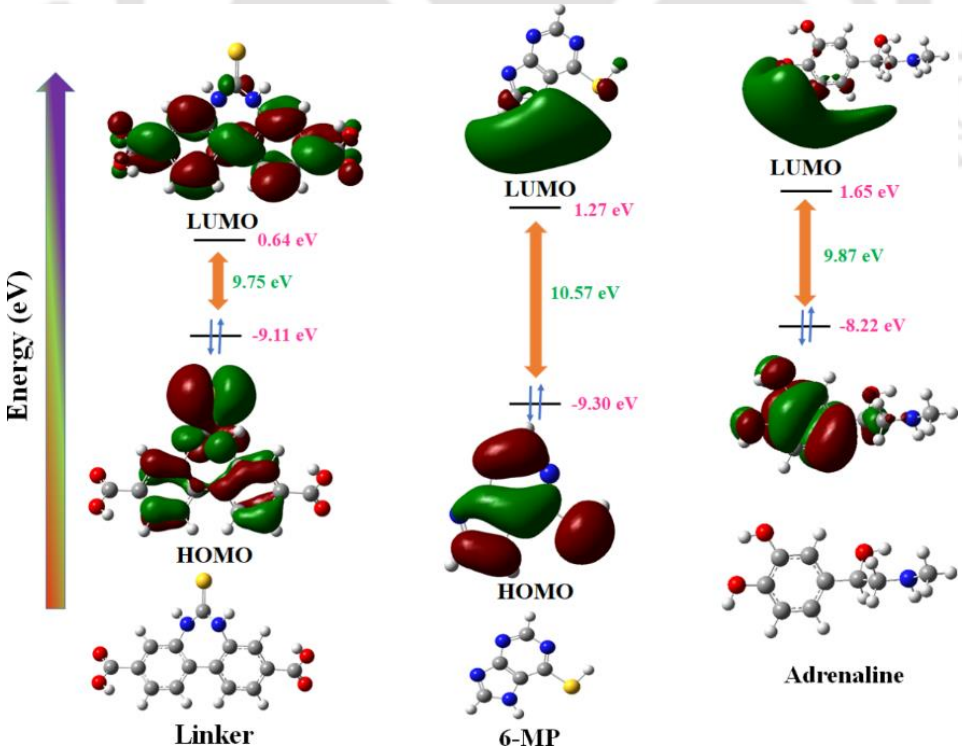

Figure 4.50 HOMO and LUMO energy levels of the free linker of the MOF, 6-MP and adrenaline.

To examine the possibility of PET, we calculated the HOMO and LUMO energies of the 6-MP. The same function and basis set (used in the case of adrenaline) were utilized for these calculations. The obtained energy values are summarized in Figure 4.50, which suggested that the LUMO of 6-MP has much higher energy than that of the linker, which excluded the possibility of PET.

To further support the IFE mechanism, the correction factors for fluorescence intensity were calculated as described in the experimental part of this chapter. The observed and corrected (after the subtraction of IFE contribution) fluorescence intensities and their ratios for different concentrations of 6-MP were calculated (Table 4.12). The quenching efficiency ($E = 1-F/F_0$) for observed and corrected fluorescence intensities obtained after the removal of IFE was also plotted against the different concentrations of 6-MP (Figure 4.51). The huge difference between observed and corrected quenching efficiencies strongly suggested that the IFE contribution is required to explain the observed quenching efficiency in the presence of 6-MP. Although IFE was once thought to be a flaw in fluorescence measurement, it has now been considered to be a non-irradiative energy transformation model in the spectroscopic technique and has been utilized in the creation of numerous photoluminescent-based detection systems.[45, 50-52] Moreover, this sensing mechanism has been reported in many of the previously reported literature for 6-MP and other analytes sensing.[45, 53-55]

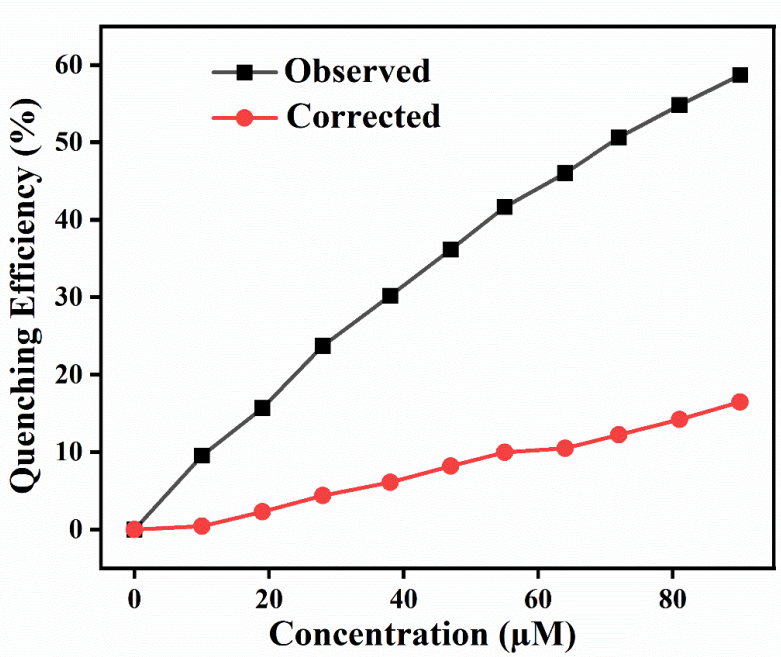

Figure 4.51 Quenching efficiency of observed (black curve) and corrected (red curve) measurements for **3′** after addition of 6-MP having different concentrations. Corrected quenching efficiency refers to the quenching efficiency when IFE contribution is not considered.

Table 4.12 IFE correction table for 6-MP.

[6-MP] (μM)	A_{ex}	A_{em}	Correction Factor (CF)	$F_{observed}$	$F_{corrected}$	$F_{corrected(0)}/F_{corrected}$
0	0.07126	0.02825	1.11168	974923	1083807	1
10	0.14967	0.03866	1.22381	881994	1079400	1.00408
19	0.19232	0.04475	1.28856	822037	1059247	1.02318
28	0.26466	0.04731	1.39364	743663	1036400	1.04574
38	0.32981	0.05181	1.49575	680478	1017825	1.06482
47	0.39206	0.05728	1.59931	622326	995297	1.08892
55	0.45977	0.06222	1.71531	568948	975926	1.11054
64	0.53043	0.06838	1.84332	526249	970048	1.11727
72	0.60088	0.07463	1.97665	481248	951260	1.13933
81	0.67019	0.07974	2.11102	440516	929941	1.16546
90	0.73722	0.08585	2.24813	402821	905594	1.19679

4.4 Conclusion

This chapter describes the synthesis, analytical characterization, and use of a water-stable MOF for the detection of adrenaline in a bio-friendly HEPES buffer medium and 6-MP in various waste water specimens. The presented MOF is the first MOF-based luminescent sensor of adrenaline and 6-MP. The unique features of the sensor include a quick response time, good selectivity and recyclability. The sensor's LOD values for the sensing of adrenaline and 6-MP are much lower than most the other sensors of adrenaline. The sensing capacity of the MOF was investigated in different bio-fluids, wastewaters and pH media. For the on-field sensing of adrenaline, MOF@cotton fabric composite was fabricated which displayed nanomolar level sensing capability towards both the targeted analytes under UV light. Reproducibility, inter and intra-day precision and error of every measurement were investigated in detail. Various instrumental outcomes indicated that FRET in presence of adrenaline and IFE in presence of 6-MP are the most possible reasons behind the quenching of fluorescence intensities of the MOF.

4.5 References

1. J. Bergquist, A. Ściubisz, A. Kaczor and J. Silberring, *J. Neurosci. Methods*, 2002, **113**, 1-13.
2. W. Cai, T. Lai, H. Du and J. Ye, *Sens. Actuators B Chem.*, 2014, **193**, 492-500.
3. J. Feher, *Hum Physiol.*, 2012, **9**, 820-827.
4. T. Tavana, M. A. Khalilzadeh, H. Karimi-Maleh, A. A. Ensafi, H. Beitollahi and D. Zareyee, *J. Mol. Liq.*, 2012, **168**, 69-74.
5. K. Phillips and D. J. Clauw, *Clin. Rheumatol.*, 2011, **25**, 141-154.

6. L. I. Silva, F. D. Ferreira, A. C. Freitas, T. A. Rocha-Santos and A. Duarte, *Talanta*, 2009, **80**, 853-857.
7. G. M. Zou, *J. Cell. Physiol.*, 2007, **213**, 440-444.
8. C. P. Wild, B. W. Stewart and C. Wild, *World Cancer Report 2014*, World Health Organization Geneva, Switzerland, 2014.
9. J. J. Hutter, *Pediatr Rev.*, 2010, **31**.
10. C. Mason and G. G. Krueger, *J. Am. Acad. Dermatol.*, 2001, **44**, 67-72.
11. *Journal*, 2016.
12. A. A. Ensafi and H. Karimi-Maleh, *Drug Test Anal.*, 2012, **4**, 970-977.
13. H. Ye, H. Xu, X. Xu, C. Zheng, X. Li, L. Wang, X. Liu and G. Chen, *Chem. Commun.*, 2013, **49**, 7070-7072.
14. S. Baluta, K. Malecha, A. Świst and J. Cabaj, *Sensors*, 2020, **20**, 1429.
15. M. Charithra and J. Manjunatha, *Mater. Chem. Phys.*, 2021, **262**, 124293.
16. N. Alam, S. Mondal, S. S. Hossain, S. Sahoo and D. Sarma, *ACS Appl. Energy Mater.*, 2023.
17. Y.-H. Shin, M. T. Gutierrez-Wing and J.-W. Choi, *J. Electrochem. Soc.*, 2021, **168**, 017502.
18. S. Mukherjee, S. Ghosh and S. Biswas, *Inorg. Chem. Front.*, 2022, **9**, 6288-6298.
19. X.-D. Zhu, K. Zhang, Y. Wang, W.-W. Long, R.-J. Sa, T.-F. Liu and J. Lü, *Inorg. Chem.*, 2018, **57**, 1060-1065.
20. S. Ghosh and S. Biswas, *Dalton Trans.*, 2021, **50**, 11631-11639.
21. L. E. Kreno, K. Leong, O. K. Farha, M. Allendorf, R. P. Van Duyne and J. T. Hupp, *Chem. Rev.*, 2012, **112**, 1105-1125.
22. S. Ghosh, J. Krishnan, V. Karthik, A. Rana, A. Dhakshinamoorthy and S. Biswas, *Mol. Catal.*, 2022, **533**, 112748.
23. D. Farrusseng, S. Aguado and C. Pinel, *Angew. Chem. Int. Ed.*, 2009, **48**, 7502-7513.
24. K. Polewski, *Biochim. Biophys. Acta Gen. Subj.*, 2000, **1523**, 56-64.
25. B. Saboorizadeh and R. Zare-Dorabei, *ACS Biomater. Sci. Eng.*, 2022, **8**, 3589-3595.
26. A. H. Vahabi, F. Norouzi, E. Sheibani and M. Rahimi-Nasrabadi, *Coord. Chem. Rev.*, 2021, **445**, 214050.
27. S. Øien-Ødegaard, B. Bouchevreau, K. Hylland, L. Wu, R. Blom, C. Grande, U. Olsbye, M. Tilset and K. P. Lillerud, *Inorg. Chem.*, 2016, **55**, 1986-1991.
28. S. Mukherjee, K. Sarkar and S. Biswas, *Dalton Trans.*, 2023.
29. Z. Liu and S. Liu, *Anal. Bioanal. Chem.*, 2018, **410**, 4145-4152.
30. Z. Chen, Y. Hu, Q. Yang, C. Wan, Y. Tan and H. Ma, *Sens. Actuators B Chem.*, 2015, **207**, 277-280.
31. J. Szeponik, B. Möller, D. Pfeiffer, F. Lisdat, U. Wollenberger, A. Makower and F. W. Scheller, *Biosens. Bioelectron.*, 1997, **12**, 947-952.
32. W. Wu, L. Ding, H. Lin, S. Yu, J. Huang and Z. Xia, 2018.
33. H. Ye, H. Xu, X. Xu, C. Zheng, X. Li, L. Wang, X. Liu and G. Chen, *Chem. Commun.*, 2013, **49**, 7070-7072.
34. H. Lu, Y. Huang, X. Zhu and W. R. Heineman, 2022.
35. B.-Y. Lu, H. Li, H. Deng, Z. Xu, W.-S. Li and H.-Y. Chen, *J. Electroanal. Chem.*, 2008, **621**, 97-102.

36. L. Wang and Z. Zhang, *Talanta*, 2008, **76**, 768-771.
37. A. F. Hawwa, J. S. Millership, P. S. Collier and J. C. McElnay, *J. Pharm. Biomed. Anal.*, 2009, **49**, 401-409.
38. J. Duan, Y. Li, Q. Hou, W. Lv, L. Dai and S. Ai, *Anal Sci.*, 2020, **36**, 515-517.
39. Y. Zhai, M. Huang, L. Jiang and H. Liao, *J. Sens. Technol.*, 2021, **11**, 39-53.
40. F. Zhang, H. Liu, Q. Liu and X. Su, *Microchim. Acta*, 2018, **185**, 1-8.
41. Y. Yuan, Y. Wang, S. Liu, Y. Li, R. Duan, H. Zhang and X. Hu, *RSC Adv.*, 2016, **6**, 52255-52263.
42. Z. Li, Y. Ni and S. Kokot, *Biosens. Bioelectron.*, 2015, **74**, 91-97.
43. S. Ghosh, N. Nagarjun, S. Nandi, A. Dhakshinamoorthy and S. Biswas, *J. Mater. Chem. C*, 2022, **10**, 6717-6727.
44. A. Rana, C. Gogoi, S. Ghosh, S. Nandi, S. Kumar, U. Manna and S. Biswas, *New J. Chem.*, 2021, **45**, 20193-20200.
45. N. Nandi, K. Choudhury, P. Sarkar, N. Barnwal and K. Sahu, *ACS Appl. Nano Mater.*, 2022, **5**, 17315-17324.
46. S. Nandi, A. Mondal, H. Reinsch and S. Biswas, *Inorg. Chim. Acta*, 2019, **497**, 119078.
47. S. Ghosh, F. Steinke, A. Rana and S. Biswas, *Inorg. Chem. Front.*, 2022, **9**, 859-869.
48. M. Kubista, R. Sjöback, S. Eriksson and B. Albinsson, *Analyst*, 1994, **119**, 417-419.
49. S. C. Chen, C. Y. Lin, T. L. Cheng and W. L. Tseng, *Adv. Funct. Mater.*, 2017, **27**, 1702452.
50. H. Liu, M. Li, Y. Xia and X. Ren, *ACS Appl. Mater. Interfaces*, 2017, **9**, 120-126.
51. J. Sun, J. Zhao, L. Wang, H. Li, F. Yang and X. Yang, *ACS Sensors*, 2018, **3**, 183-190.
52. H.-C. Chang and J.-a. A. Ho, *Anal. Chem.*, 2015, **87**, 10362-10367.
53. L. Han, S. G. Liu, J. Y. Liang, Y. J. Ju, N. B. Li and H. Q. Luo, *J. Hazard. Mater.*, 2019, **362**, 45-52.
54. M. Jin, Z.-L. Mou, R.-L. Zhang, S.-S. Liang and Z.-Q. Zhang, *Biosens. Bioelectron.*, 2017, **91**, 162-168.
55. A. Mousavi, R. Zare-Dorabei and S. H. Mosavi, *Anal. Methods*, 2020, **12**, 5397-5406.

Chapter 5

A Self-Cleaning Hydrophobic MOF Based Composite for Highly Efficient and Recyclable Separation of Oil from Water and Emulsion

*This chapter represents the synthesis, characterization and application of –CF_3 group containing hydrophobic MOF (**4'@CF_3**) which was synthesized by post-synthetic modification of the Zr- BDC-OH MOF (**4'**). The hydrophobic property of the MOF was used for the preparation of a robust hydrophobic composite (**4'@CF_3@melamine**) with melamine sponge. The water contact angle of **4'@CF_3@melamine** was found to be 145 ± 1°. The hydrophobic composite was utilized to separate oil-water mixtures and water-in-oil emulsions even under harsh aquatic environments. The oil-water and emulsion separations were carried out in an easy and fast way without the consumption of energy. The absorption capacity and separation efficiency of the composite for a wide variety of oils were found to be 27-37 g/g and 95-99%, respectively. The material showed high recyclability up to 50 cycles for oil-water separation and for 30 cycles for water-in-oil emulsion separation. In addition, the hydrophobic **polymer@4'@CF_3** coated glass substrate displayed excellent self-cleaning properties. Furthermore, inexpensive and facile gravity-driven filtration and against the gravity based separation techniques for different oils were developed by employing the composite.*

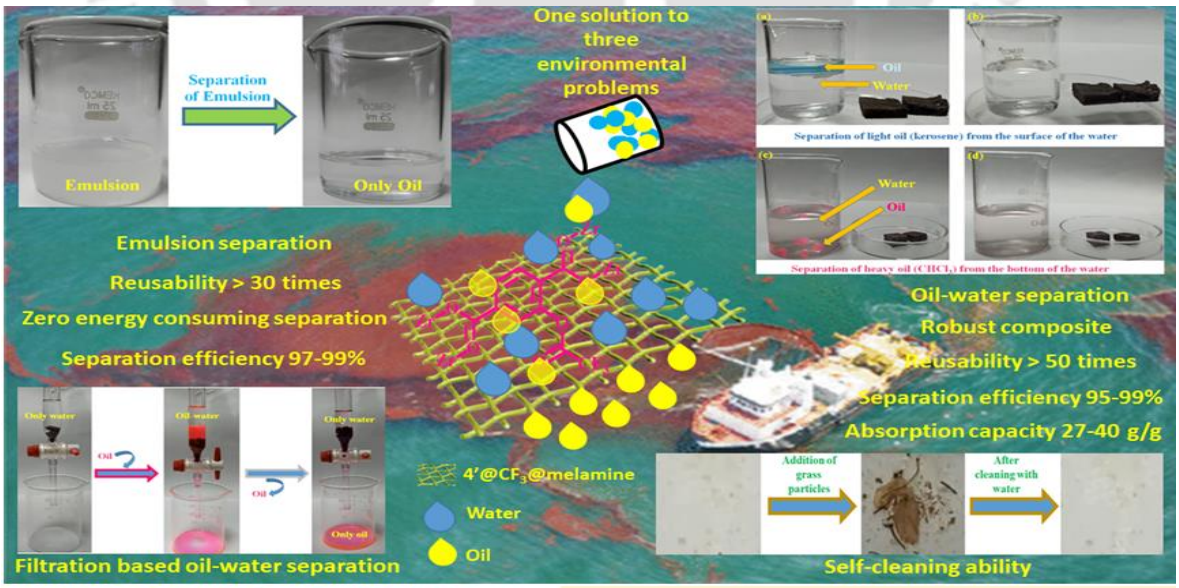

MATERIALS CHEMISTRY FRONTIERS

S. Ghosh, A. Rana, S. Kumar, C. Gogoi, S. Mukherjee, U. Manna, S. Biswas, Mater. Chem. Front., 2022, 6, 2051-2060.

5.1 Introduction

The pollution due to oil spill not only ends with water pollution but also affects the nearby land ecosystem and the humidity of air due to change in evaporation rate and the greenhouse gases released due to the burning of oil.[1] The vulnerability caused by 1991 Gulf war or Ixtoc I oil spills are yet in the mind of people.[2, 3] After every oil spillage, the oil forms a thin layer over water and causes sunlight blockage. The reduced amount of sunlight directly affects the producer of the aquatic food chain and as the producer is the first member of the food chain, the whole food chain is indirectly affected by the oil spills. The effect is not only inside the marine ecosystem. The highest vulnerability towards mammals of the seashore, fish nurseries and birds was due to the oil carried by the waves.[4] The poisonous and persistent part of oil injected into an organism could cause problems for another organism far away from oil-spill becoming his food.[5] The oil-layer present on the water's surface causes the accumulation of excreted gas inside the water body and inhibits the fresh air to enter into the water body. The exposure of polycyclic aromatic hydrocarbons of crude oil to the eggs of fishes causes teratogenic effect as well as premature hatching of eggs.[6] The oil carried by the waves to mangroves near the coastal area dramatically affects the mangrove ecosystem. The thin layer of oil absorbed onto the breathing surfaces of mangrove roots and stems causes the death of tiny plants and animals within a few days and mature plants hardly survive for six months.[7] The bio-accumulative and persistent part of crude oil is directly absorbed into the tissues of sea animals and later integrated into the human body by the consumption of seafood. Due to the above vulnerable environmental impacts, there is a requirement for an easy oil spill clean-up technique. The traditional methods of oil-spill cleanings like in-situ burning, bioremediation, manual labour, dispersant, etc., are not adequate. In-situ burning is not environmentally friendly because of the release of toxic gases.[8] In the bioremediation and dispersant method, the oil is not recovered, which is a loss from an economic point of view.[9] The use of manual labour requires much time and money. Therefore, the scientific community is searching for an eco-friendly, fast and economical way to settle this issue.

The dispersion of an immiscible liquid in another liquid is known as an emulsion. The emulsion formed by water dispersion in oil is the topic of interest for many scientists. The emulsion formation during crude oil extraction will cause problems if it is not appropriately treated. The presence of water will escalate the corrosion rate of pipes and equipment used during processing steps. The cost of transporting and pumping speed will increase due to the pressure drop in flowlines.[10] Therefore, people are searching for an easy solution to the separation of oil from oil-water emulsions.[11]

The adhesion of dust and contaminants to the surface of the glass, concrete walls, buildings, and even the surface of our garments causes various problems. The adhesion of pollutants and dust causes bacterial growth and foul-smelling. A new class of self-cleaning material was first reported by Heller et al. in 1995.[12] Afterwards, few materials with self-cleaning property were developed to deal with the above issue. Among them, very few numbers of hydrophobic MOFs were developed.[13, 14]

All the above-stated problems have an easy and single solution via hydrophobic-based composite materials. The composite being hydrophobic will attract the oil and repel the water.

The lipophilicity of hydrophobic composite will selectively attract the oil part of the oil-water mixture and the separation could be easily possible without consumption of external energy. When the hydrophobic composite comes into contact with oil-water mixture, it initially takes a little time to form a layer. Once there is oil on the composite surface, it will speed the process of demulsification on the principle of same attracts same. The hydrophobic coating on any surface causes the roll-over flow of water droplets, thereby removing all the dust or contaminants. There are many types of hydrophobic materials reported to date.[15, 16] Among them, very few are MOF-based. The MOF materials are chemically stable and can be functionalized very easily. The porous nature of MOFs made them famous in gas adsorption and storage, drug delivery and water harvesting purposes.[17-19] The wide range of functionality in the family of MOFs makes them unique in the field of sensing.[20] The porous and robust nature of MOFs attracted us to choose them for the above applications.

The Zr(IV) containing MOFs are highly stable. Therefore, we synthesized a Zr(IV) based MOF material with 2-hydroxyterepthalic acid (BDC-OH). The as-synthesized Zr-BDC-OH MOF was named as **4** and the activated form of this was named as **4′**. The activated MOF **4′** was post-synthetically modified to add one -$COCF_3$ group to the free -OH group of **4′**. The post-synthetic modification was achieved by a simple reaction between **4′** and trifluoroacetic anhydride to give hydrophobicity and the material was named as **4′@CF_3**. The powder form of **4′@CF_3** doesn't have the freestanding ability. Therefore, it was required to be anchored onto a substrate. Hence, we prepared a polydopamine (PDA) coated melamine sponge substrate. The PDA coating on the melamine sponge increased the number of free -OH and -NH_2 groups on the surface of the melamine substrate. Then, a PDMA-co-PMHS polymeric coating containing the hydrophobic MOF powder was applied to the modified melamine sponges to get a robust hydrophobic composite. The free -OH and -NH_2 groups of PDA coated sponge strongly bind with the oxophilic Zr(IV) ions of MOF to give a robust hydrophobic composite. The obtained hydrophobic composite was named **4′@CF_3@melamine**. The WCA of polymer-coated composite without MOF powder was found to be 106 ± 1°**,** whereas, for **4′@CF_3@melamine**, it was 145 ± 1°. The increased WCA value inferred that the hydrophobicity in the composite is because of **4′@CF_3** powder. The composite **4′@CF_3@melamine** was used for the separation of oil from oil-water mixture in very simple techniques (filtration-based separation, separation in opposite to gravity and by absorption-based separation). The robust nature of composite makes it sufficiently recyclable up to 50 cycles with only 10% decrease in efficiency after 50th cycle. The material was also applied for the separation of oils from water-in-oil emulsions (30 times recyclability) and it was also coated on a glass surface to use as a self-cleaning material.

5.2 Experimental Section

5.2.1 Synthesis of 2-Hydroxyterephthalic acid (H_2BDC-OH) Linker and Preparation of Zr-UiO-66-OH MOF (4)

The 2-hydroxyterephthalic acid (H_2BDC-OH) linker was prepared according to the reported procedure.[21] For the synthesis of hydroxyl (-OH) functionalized Zr-based UiO-66 MOF, we applied the previously reported solvothermal method of synthesis, reported by Katz et al.[22] In

brief, in a 25 mL Teflon autoclave, 250 mg (1.08 mmol) of $ZrCl_4$, 197 mg (1.08 mmol) of 2-hydroxyterephthalic acid was taken. After that, 5 mL of DMF and 2 mL of concentrated HCl were added to the previously mentioned solids. After homogeneous mixing of all the components for 15 min via sonication, the mixture was kept in a pre-heated hot air oven at 120 °C for 24 h. Then, the autoclave was gently allowed to come to room temperature and a white coloured product was collected after washing with acetone several times. Then, the white powder was dried in a 100 °C oven. The obtained yield of **1** was 28 mg (0.01 mmol, 76 %). ATR-IR (cm^{-1}): 3316 (br), 1574 (s), 1491 (vs), 1412 (vs), 1368 (sh), 1237 (vs), 1158 (w), 961 (w), 773 (vs), 716 (vs), 663 (vs), 572 (m), 488 (w).

5.2.2 Activation of 4

The as-prepared MOF may contain some unreacted starting materials and solvent molecules inside the pore of its framework. To remove such impurities, **4** was stirred in MeOH for 24 h and afterwards, it was recovered by filtration and dried. Then, the dry MOF was heated under a vacuum for another day. Thus, we obtained completely solvent-free, pure Zr-UiO-66-OH MOF called **4′**.

5.2.3 Post-synthetic Modification of 4′

To functionalize the free hydroxyl (-OH) groups of **4′** by $-COCF_3$ groups, 100 mg (0.06 mmol) of **4′** was placed in 20 mL of dry DCM inside a 50 mL round bottom flask. After the addition of 80 µL of trifluoroacetic anhydride, the reaction medium was stirred (0.6 mmol) for 12 h at an ambient condition (Scheme 5.1). After 12 h, the MOF material was filtered and washed with DCM for three times. Finally, it was allowed to dry at 60 °C for 4 h. ^{1}H NMR, ^{13}C NMR and ^{19}F NMR spectra after digestion of the modified MOF were collected to know the post-synthetic modification percentage (Figures 2.30-2.33). From the ^{1}H NMR integration, it was observed that around 67% of the parent MOF was converted to $-OCOCF_3$ functionalized Zr-UiO-66 MOF (Figure 31). Hereafter, this post-modified MOF will be called as **4′@CF$_3$**. ^{1}H NMR (400 MHz, DMSO-d_6): δ = 7.94 (d, 1H), 7.88 (d, 0.48H), 7.49 (m, 1.62H), 7.43 (m, 0.96H) ppm. ^{13}C NMR (100 MHz, DMSO-d_6): δ = 171.50, 167.81, 166.85, 162.87, 160.96, 159.42, 159.04, 158.67, 158.29, 137.32, 133.30, 131.18, 131.14, 129.70, 129.00, 119.99, 118.14, 117.24, 117.04, 114.17, 111.30 ppm. ^{19}F NMR (400 MHz, DMSO-d_6): -75.18 ppm. ESI-MS (m/z): 277.0665 for $(M-H)^-$ ion (M = mass of H_2BDC-$OCOCF_3$ linker) and m/z = 181.0165 corresponds to the mass of H_2BDC-OH linker (Figures 5.1-5.4). The appearance of a peak at 1202 cm^{-1} in the ATR-IR spectrum after post-synthetic modification was due to the C-F bond stretching (Figure 5.5).[23]

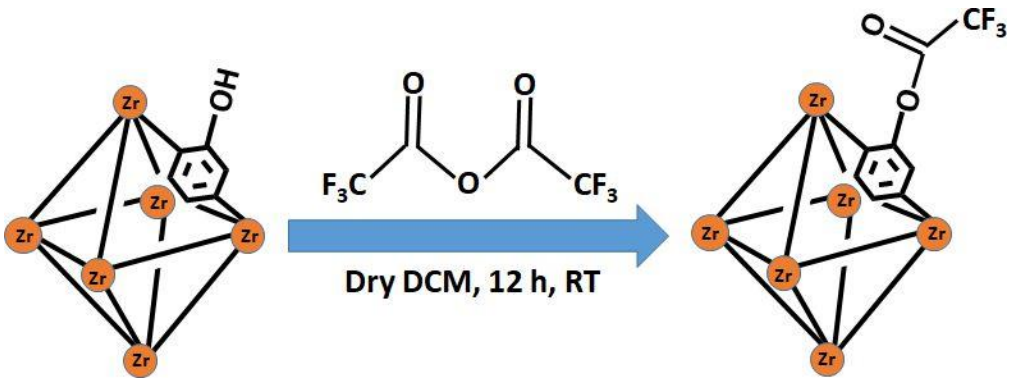

Scheme 5.1 Reaction scheme for the preparation of **4′@CF$_3$** MOF.

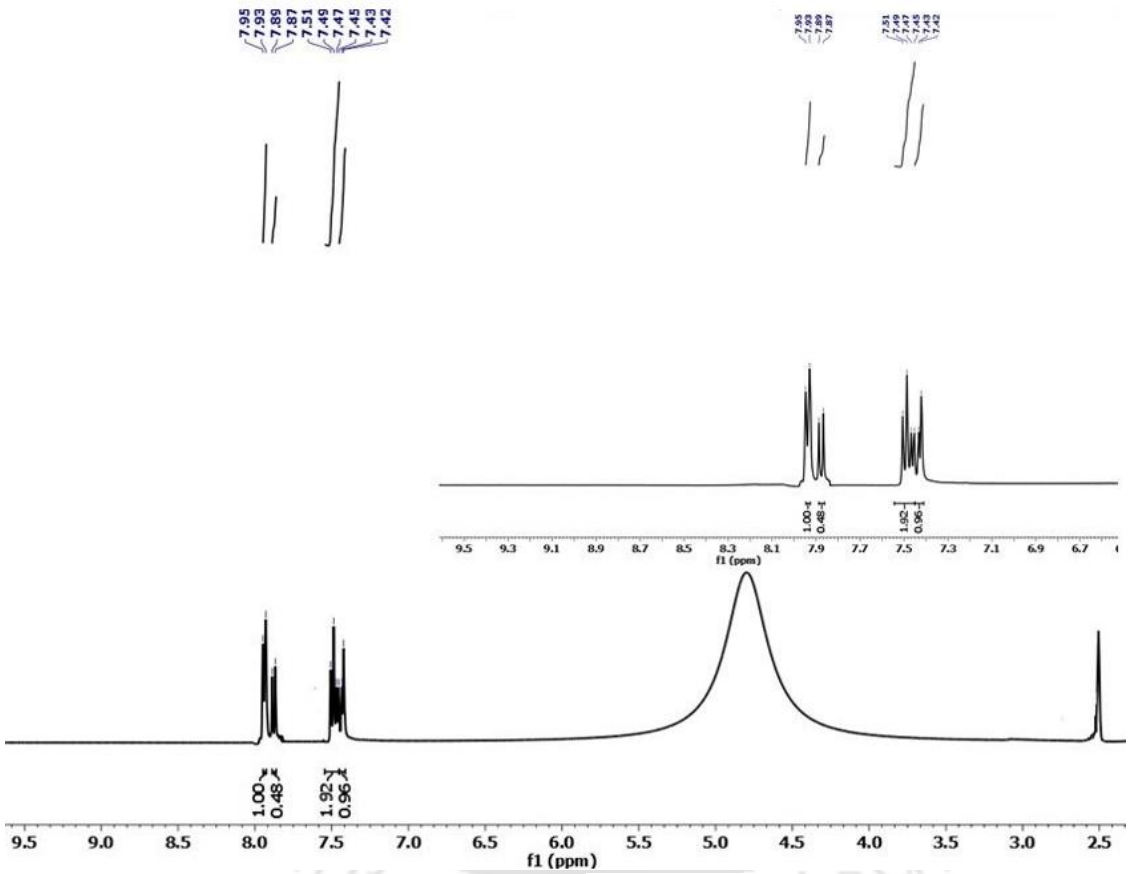

Figure 5.1 ^{1}H NMR spectrum of the digested **4′@CF$_3$** MOF in DMSO-d$_6$. The MOF was digested after adding two drops of 40% HF in DMSO-d$_6$ medium.

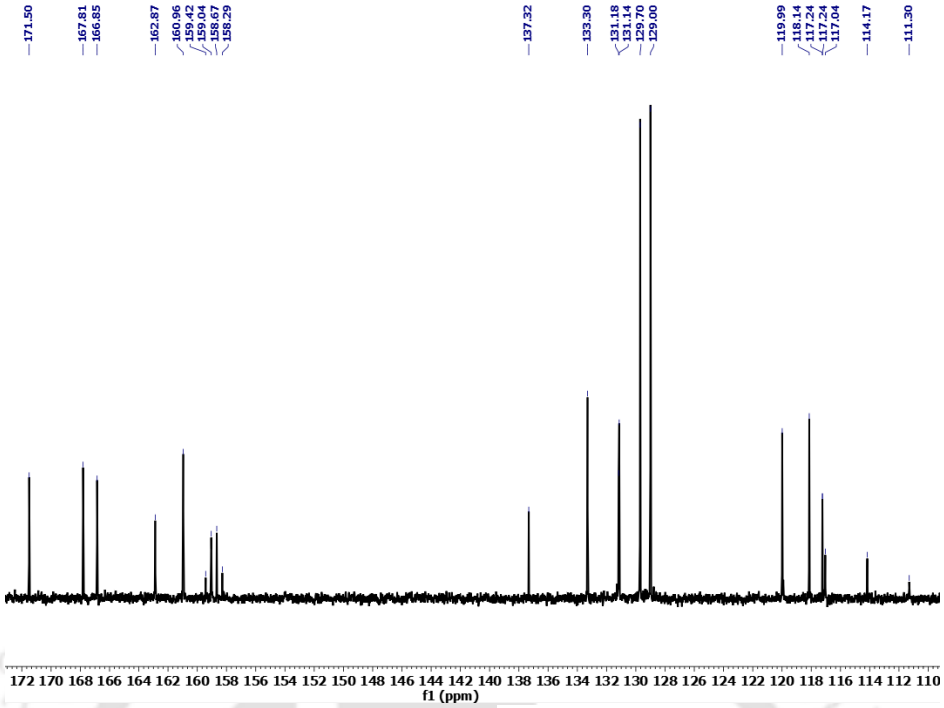

Figure 5.2 ^{13}C NMR spectrum of the digested **4′@CF_3** MOF in DMSO-d_6. The MOF was digested after adding two drops of 40% HF in DMSO-d_6 medium.

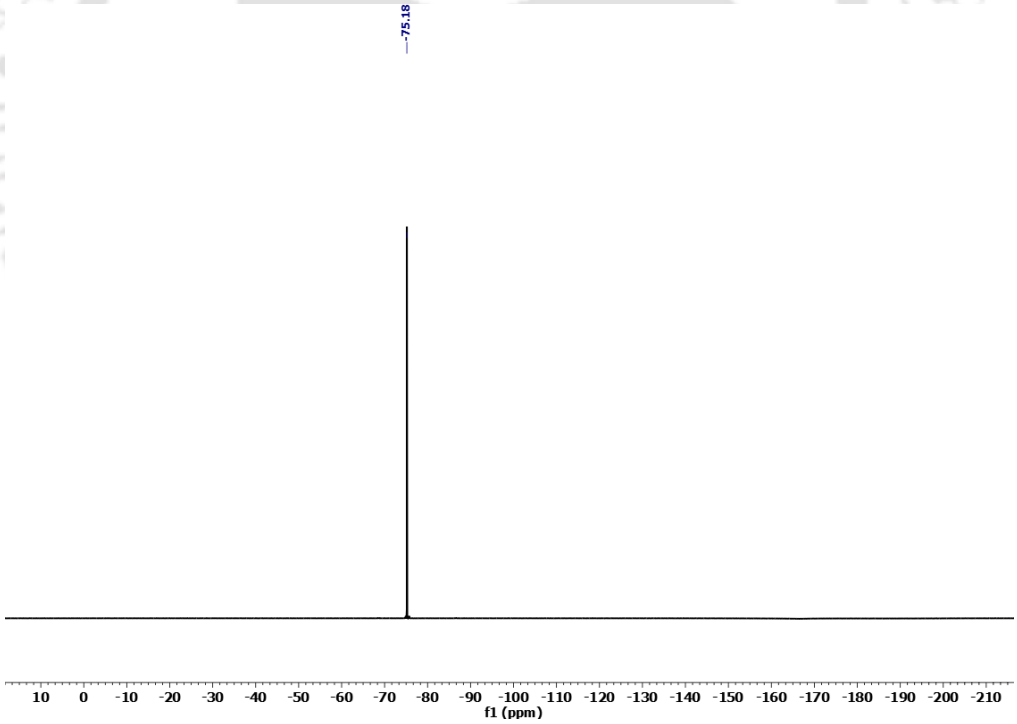

Figure 5.3 ^{19}F NMR spectrum of the digested **4′@CF_3** MOF in DMSO-d_6. The MOF was digested after adding two drops of 40% HF in DMSO-d_6 medium.

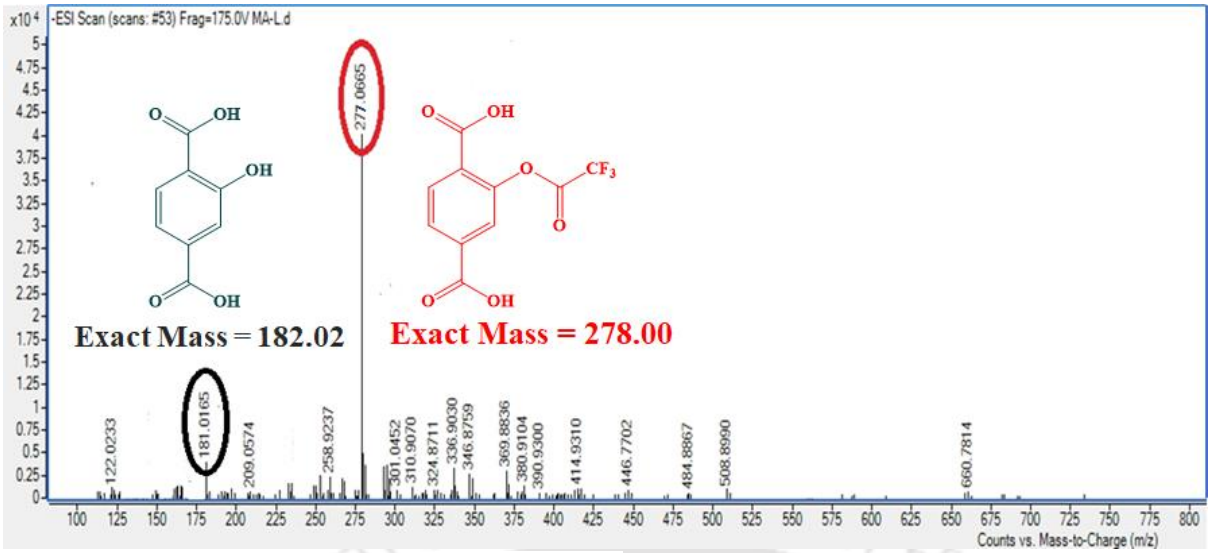

Figure 5.4 ESI-MS spectrum of **4′@CF₃** MOF measured in methanol. The spectrum shows m/z peak at 277.0665, which corresponds to $(M-H)^-$ ion (M = mass of $H_2BDC\text{-}OCOCF_3$ linker) and m/z peak at 181.0165 corresponds to $(M-H)^-$ ion (M = mass of $H_2BDC\text{-}OH$ linker).

5.2.4 Measurement of Absorption Capacities for Various Oils by 4′@CF₃@melamine Composite

For the oil absorption measurement, fully dry pre-weighed (~300-400 mg) **4′@CF₃@melamine** composite was placed in various heavy oils ($CHCl_3$, CH_2Cl_2 and CCl_4) and light oils (hexane, EtOAc, toluene, motor oil, gasoline and kerosene). The composites were kept in oil for 1 min to reach absorption equilibrium and then removed and weighed. All the experiments were performed at room temperature. Absorption capacities for various oils were calculated using the following formula:

Absorption capacity (g/g) = $(W_f\text{-}W_i)/W_i$

Where, W_i was the initial weight of **4′@CF₃@melamine** composite and W_f was the weight of oil-absorbed **4′@CF₃@melamine**. Six measurements were performed for each oil sample and the average value was plotted.

5.2.5 Absorption Based Separation of Oil and Water by 4′@CF₃@melamine Composite

A single piece of dry pre-weighed **4′@CF₃@melamine** composite (300-400 mg) was placed in several oil/water combinations containing 3 mL of oil and 40 mL of water to separate the light oils (hexane, EtOAc, toluene, motor oil, gasoline and kerosene) from the surface of the water. For heavy oils (CH_2Cl_2, $CHCl_3$ and CCl_4), a piece of **4′@CF₃@melamine** composite was brought into contact with the sediment oil for the separation of heavy oils from the oil/water combination from the bottom of the water. For each case, the **4′@CF₃@melamine** composite selectively soaked the oils when it came with the contact of oils and the separated oil was recovered by physically squeezing the material. All the tests were performed at room temperature. Separation efficiency (%) for various oils were calculated using the following formula:

Separation efficiency (%) = $V_f/V_i \times 100\%$

where V_i was the amount of oil used (mL) and V_f was the absorbed volume of water (mL). Six measurements were performed for each oil sample and average value was plotted.

5.2.6 Separation of Emulsions Using 4′@CF_3@melamine Composite

All the water-in-oil emulsions were prepared (water/toluene, water/$CHCl_3$, water/ kerosene and water/gasoline) by sonicating the water-oil mixtures for 60 min. To make the emulsion stable, 50 µL of surfactant **(**Triton X-100) was added to the oil-water mixture before sonication. Then, 4 mL (3.5 mL of oils + 0.5 mL of water) of different water-in-oil emulsions were allow to pass through a chromatographic column and the bottom of the column was packed by hydrophobic **4′@CF_3@melamine** composite. The time required for all the separation process were recorded.

Separation efficiency (%) for various water-in-oil emulsion were calculated using the following formula:

Separation efficiency (%) = $V_2/V_1 \times 100\%$

where V_1 was the amount of oil used (mL) for the preparation of the water in oil emulsion and V_2 was the obtained volume of oil (mL) after the separation experiment.

The flux for various emulsions was calculated using the formula: Flux = V/A × T (where V = volume of separated oil, A = area of the composite and T = time required for the separation of oil from water-in-oil emulsion).

5.3 Results and Discussion

5.3.1 Infrared (IR) Spectroscopy

To ensure the successful coordinative bond formation between the Zr(IV) ions and 2-hydroxyterephthalate linkers in **4′** and the incorporation of -$COCF_3$ group in **4′**, we measured the ATR-IR spectra of **4′** and **4′@CF_3** (Figure 5.5). In both the IR spectra, two sharp absorption peaks were observed at 1420 and 1573 cm^{-1}. These peaks were originated from the symmetric and asymmetric stretching vibrations of the Zr(IV)-bound carboxylate groups. A sharp peak at 1666 cm^{-1} was obtained for **4′@CF_3** due to the stretching vibration of the carbonyl group of trifluoroacetoxy functional group. The peak at 1202 cm^{-1} is due to the stretching of -C-F bond of -CF_3 group. Such peaks were absent in **4′**.[23] This evidenced the fruitful modification of –OH group of **4′** by trifluoroacetoxy functional group.

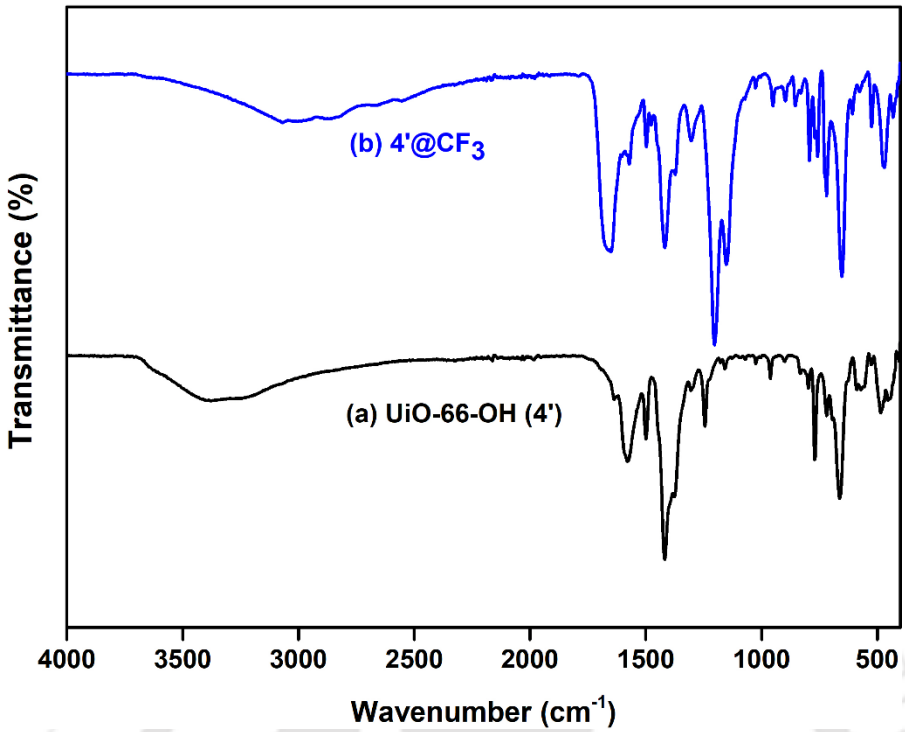

Figure 5.5 ATR-IR spectra of (a) UiO-66-OH (**4′**) and (b) **4′@CF₃** MOF.

5.3.2 Structural Overview

The obtained PXRD pattern of **4′** was also very similar to the PXRD pattern of the un-functionalized UiO-66 MOF material (Figure 5.6). We modified **4′** by reacting with trifluoroacetic anhydride in CH_2Cl_2 to obtain **4′@CF₃.** The PXRD patterns of **4′@CF₃** revealed that the peak positions and intensities of the modified MOF remained very similar to the parent MOF (**4′**). In **4′@CF₃,** the $[Zr_6O_4(OH)_4]^{12+}$ units are present as secondary building units (SBUs), where the central Zr(IV) ion is coordinated with four μ_3-OH and four μ_3-O sites.[24] The SBUs are interlinked with each other by six 2-(2,2,2-trifluoroacetoxy)terephthalate (TFBDC) linkers which give rise the final $[Zr_6O_4(OH)_4(TFBDC)_4(BDC\text{-}OH)_2]$ MOF material with UiO-66 structure. Similar to other UiO-n series of MOFs, there are two types of structural voids: larger size octahedral voids and smaller size tetrahedral voids are present in the framework structure.[25] These voids were interlinked by triangular windows. We carried out Pawley refinement (Figure 5.7) and indexing of the slow-scan PXRD pattern of **4′@CF₃**. The obtained R_{wp} and R_p values after Pawley refinement were 5.2% and 3.6% which suggested remarkable similarity between experimental and theoretical PXRD patterns. The unit cell parameters and unit cell volume (Table 5.1) were closely similar to the pristine UiO-66 MOF.

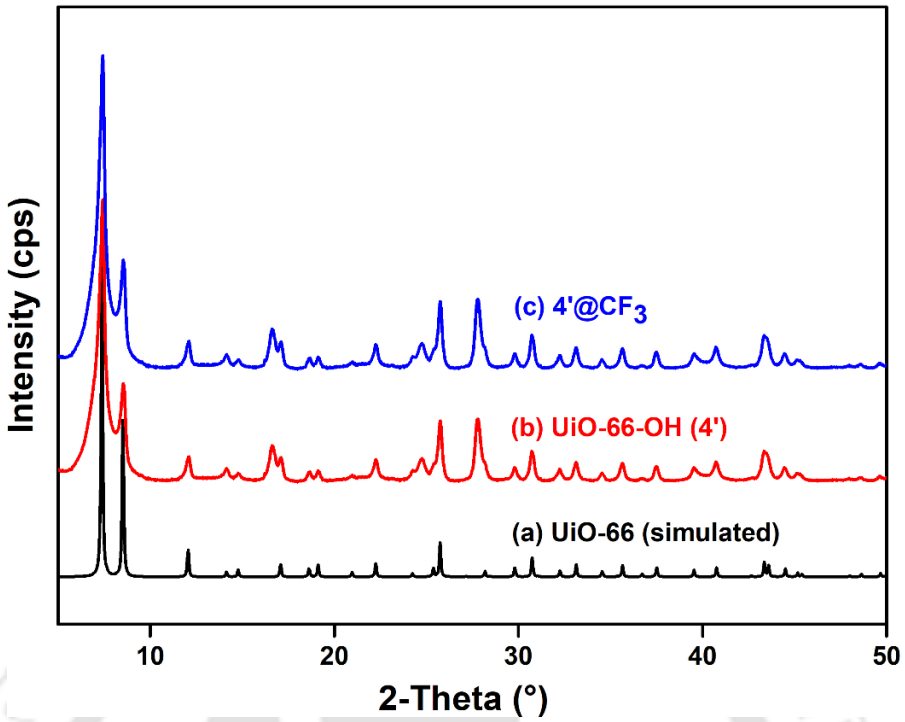

Figure 5.6 PXRD patterns of (a) Zr-UiO-66 (black), (b) activated Zr-UiO-66-OH (red) and (c) **4′@CF$_3$** (blue).

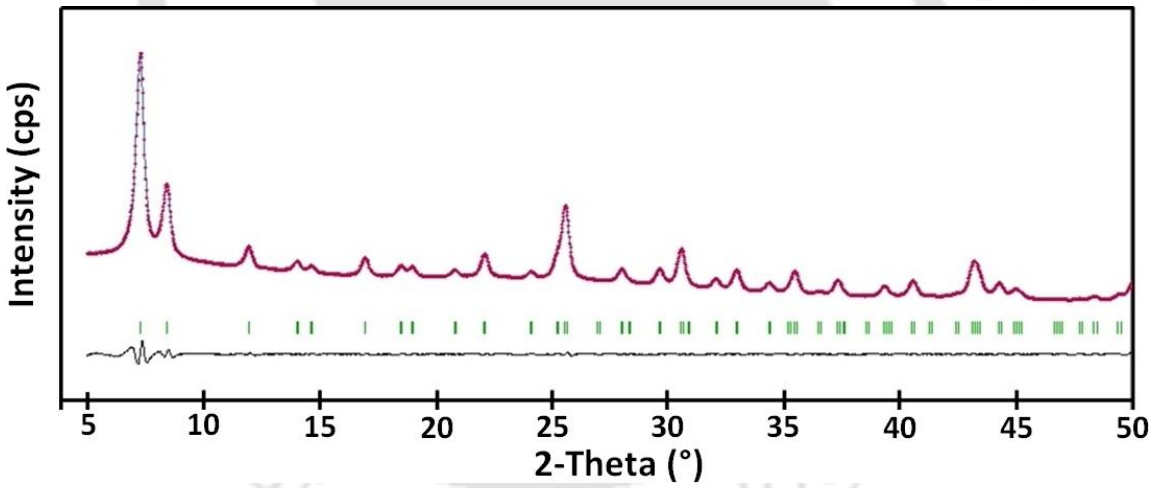

Figure 5.7 Pawley fit for the PXRD pattern of as-synthesized **4′@CF$_3$** (R_{wp} = 5.2%, R_p = 3.6%). Blue lines and red dots denote simulated and observed patterns, respectively.

Table 5.1 Unit cell parameters of **4′@CF$_3$** obtained by indexing its PXRD data. The obtained values have been compared with parent UiO-66 MOF.

Compound Name	**4′@CF$_3$**	UiO-66
crystal system	cubic	cubic
a = b = c (Å)	20.797(3)	20.790(3)
V (Å^3)	8994.6(25)	8985.9(9)

5.3.3 FE-SEM and EDX Analysis

The phase purity and crystalline nature of **4′** and **4′@CF₃** were again supported by the homogeneous distribution of octahedral shaped crystalline particles, as noticed from the FE-SEM images (Figure 5.8a-b). The EDX spectra and elemental mapping of **4′** and **4′@CF₃** proved the presence of Zr, C, O in **4′** and Zr, C, O and F in **4′@CF₃** (Figure 5.8c-d). The presence of F atoms in **4′@CF₃** proved the successful modification of the -OH groups of **4′** by –$COCF_3$ groups.

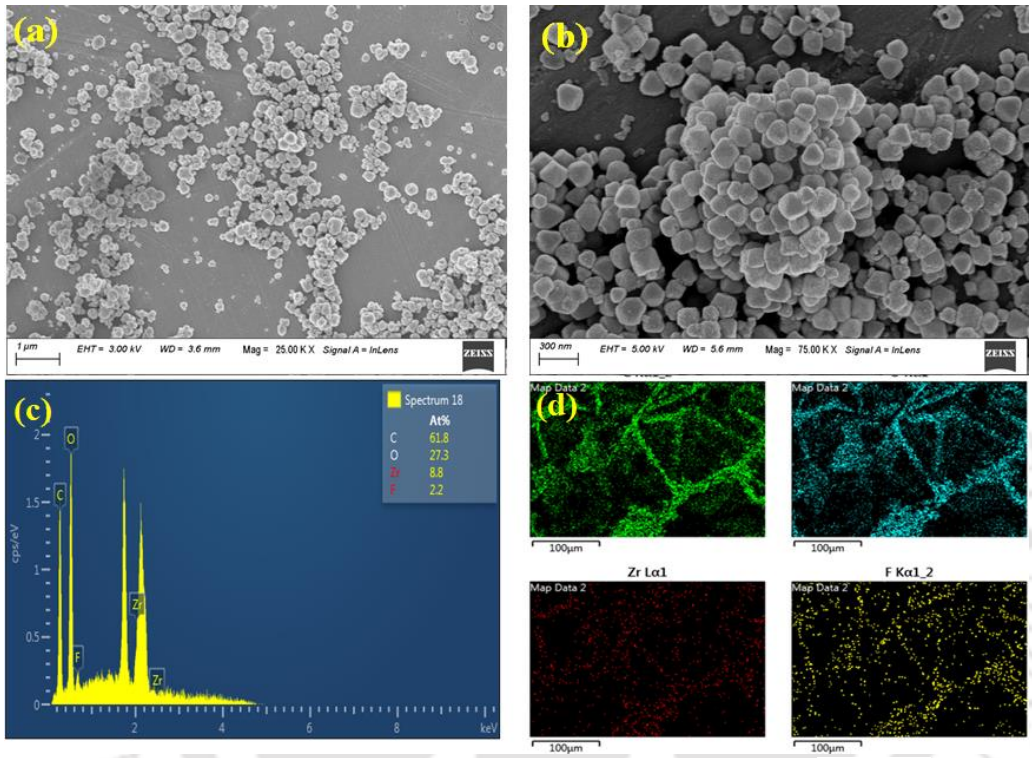

Figure 5.8 (a and b) FE-SEM, (c) EDX and (d) elemental mapping of **4′@CF₃**.

5.3.4 Surface Area Measurement

To measure the porosity and specific surface area of the pristine and post modified MOF materials, we conducted the BET surface area analysis of both **4′** and **4′@CF₃** at a temperature of -196 °C (Figure 5.9a-b). Type-I sorption isotherms were obtained for both **4′** and **4′@CF₃**. The obtained surface areas were 1002 and 631 m^2/g for **4′** and **4′@CF₃** with the micropore volumes of 0.58 and 0.35 cm^3/g, respectively. The obtained surface area of **4′@CF₃** was less than the surface area of **4′**. This is because of the functionalization of small -OH groups of by bulky -$OCOCF_3$ groups. The presence of bulky -$OCOCF_3$ groups decrease the availability of pore diameter in **4′@CF₃**, which restricts the free diffusion of N_2 gas molecules into the pore of **4′@CF₃**. The obtained surface area is similar to the other reported post modified UiO-66 MOFs.[26]

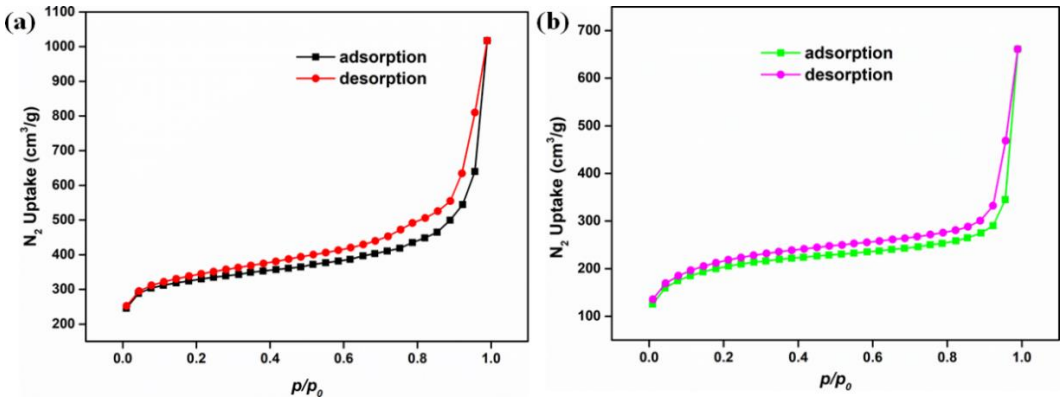

Figure 5.9 Nitrogen adsorption and desorption isotherms of (a) **4'** and (b) **4′@CF₃** recorded at -196 °C.

5.3.5. Thermogravimetric Analysis

Thermogravimetric analysis (TGA) of **4′** and **4′@CF₃** were carried out in the temperature range of 25-700 °C under air atmosphere to know the thermal stability of **4′** and **4′@CF₃** (Figure 5.10). From the TGA, two steps of weight losses were observed for **4′**. An initial weight loss of 11.9% (cal. 11.9%) was observed in the temperature range of 25-105 °C. This loss of weight is due to the removal of 13 water molecules absorbed from the atmosphere during the storage of the MOF for TG analysis. After the temperature of 420 °C, the second and final weight loss was observed. The thermal cleavage of the Zr(IV)-carboxylate coordinative bond and the decomposition of organic linker molecules are the reasons behind this weight loss. For **4′@CF₃,** the only weight loss started after the temperature of 200 °C. The removal of the thermally labile -$COCF_3$ group is responsible for the weight loss at low temperature (~200 °C). At high temperature, the connectivity between the metal ion and the carboxylate groups caused the final loss of weight. Therefore, from the TGA, it can be concluded that **4′@CF₃** has thermal stability up to the temperature of 200 °C, which is similar to the other available MOFs obtained after post-synthetic modification.[27]

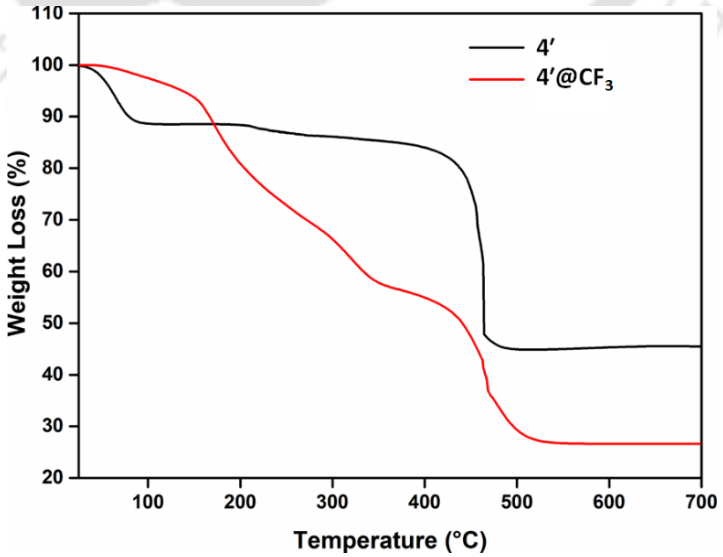

Figure 5.10 TGA curves of activated **4'** (black) and **4′@CF₃** (red) recorded in an air atmosphere in the temperature range of 25-700 °C at a heating rate of 10 °C min^{-1}.

5.3.6 Chemical Stability

For the real-world application purpose (e.g. oil-water separation), the material should be stable in respective oils and water media. To verify the same, **4′@CF$_3$** was stirred in various heavy (CH_2Cl_2, $CHCl_3$ and CCl_4) and light oil (toluene, ethyl acetate and hexane) media, acids (1 M HCl and 1 M AcOH), various water samples (pond, tap, sea and river waters) and different pH media (pH = 2 and pH = 12) for 24 h at room temperature. Afterwards, the recovered materials through filtration were dried and PXRD measurements were performed (Figure 5.11-5.13). It is worth to say that the PXRD profiles of the recovered MOFs after soaking in all the liquids mentioned above remained similar to the PXRD patterns of the fresh MOF. We also measured the WCA of all the recovered powdered samples, which remained identical to the measured WCA of the fresh MOF (Table 5.2). All the above experiments supported the stability of **4′@CF$_3$** and integrity of the -OCOCF$_3$ functional group in the MOF in the liquids mentioned above.

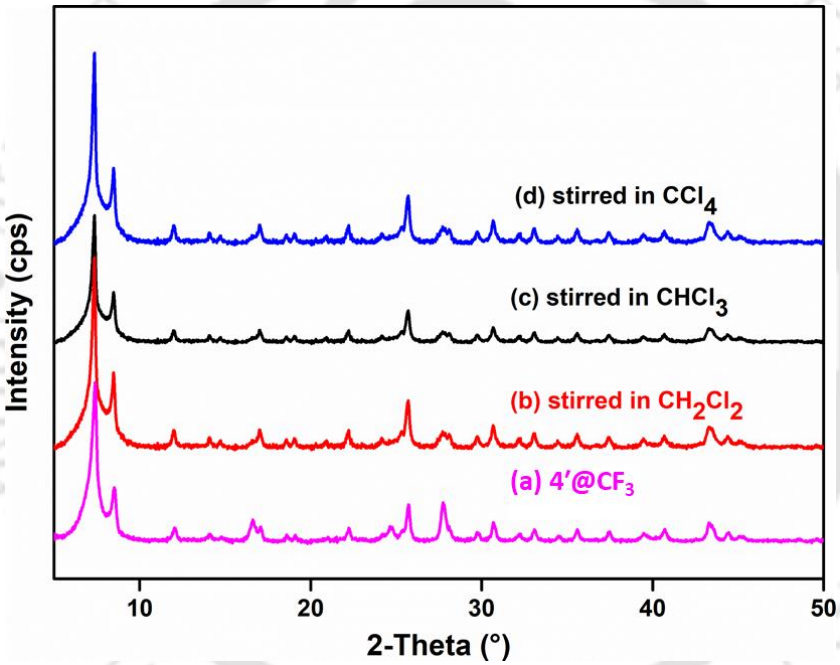

Figure 5.11 PXRD patterns of (a) **4′@CF$_3$**, **4′@CF$_3$** after stirring in (b) CH_2Cl_2, (c) $CHCl_3$ and (d) CCl_4.

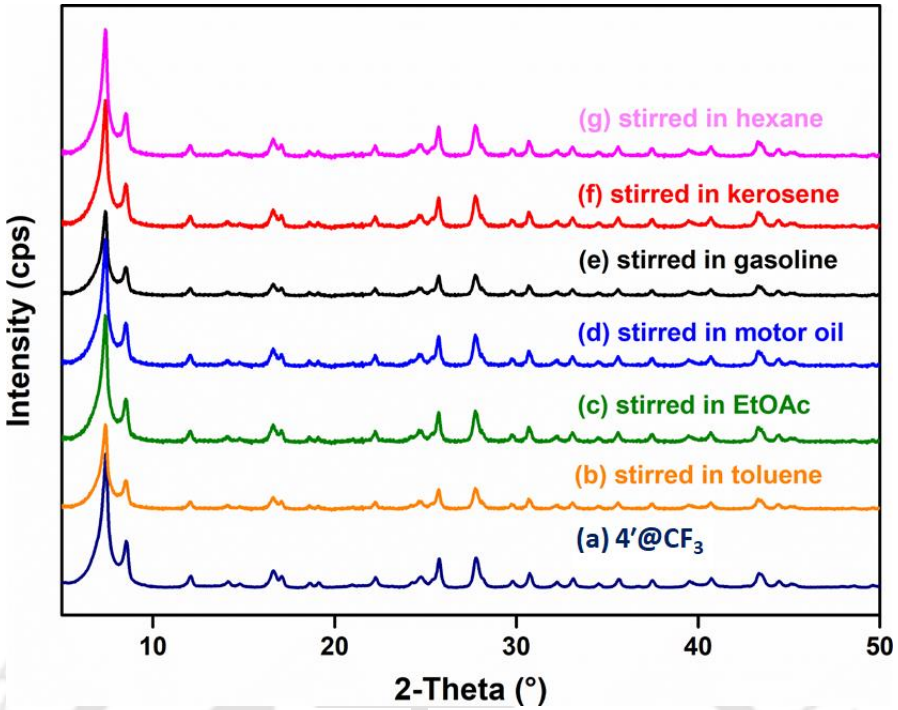

Figure 5.12 PXRD patterns of (a) **4′@CF₃**, **4′@CF₃** after stirring in (b) toluene, (c) EtOAc, (d) motor oil, (e) gasoline, (f) kerosene and (g) hexane for 24 h.

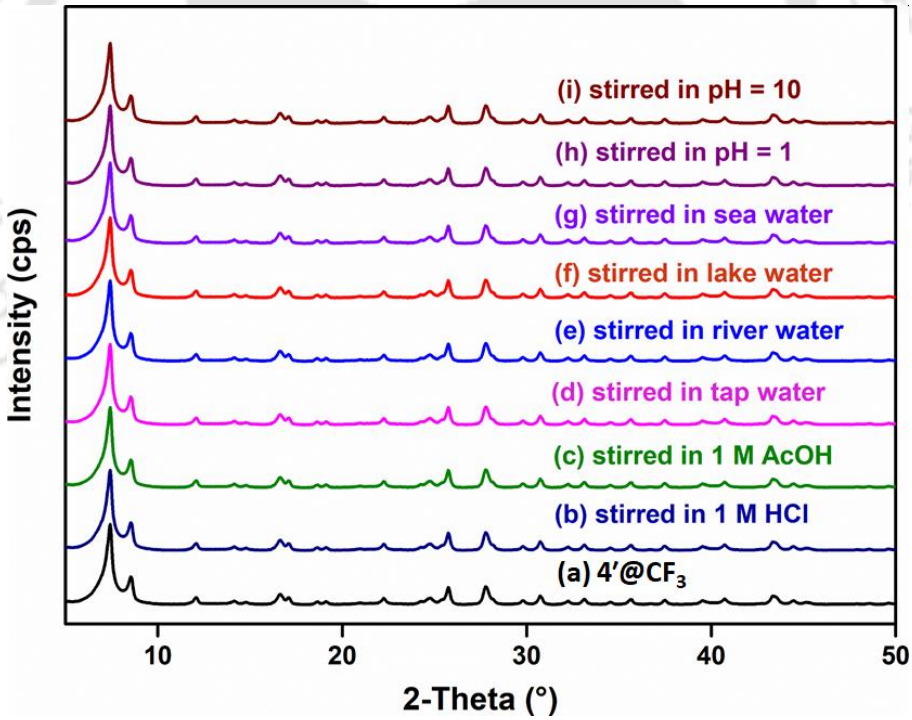

Figure 5.13 PXRD patterns of (a) **4′@CF₃**, **4′@CF₃** after stirring in (b) 1 M HCl, (c) 1 M AcOH, (d) tap water, (e) river water, (f) lake water, (g) sea water, (h) pH = 1 and (i) pH = 10 for 24 h.

Table 5.2 Water contact angle (WCA) of **4′@CF₃** after treatment with different types of water and oil specimens.

Sl No.	Liquids	Average WCA of **4′@CF₃** (°)
1	fresh **4′@CF₃**	146 ± 1.0
2	CCl_4	144 ± 1.2
3	$CHCl_3$	146 ± 1.5
4	CH_2Cl_2	143 ± 1.3
5	hexane	142 ± 1.2
6	kerosene	143 ± 1.1
7	gasoline	142 ± 1.3
8	motor oil	140 ± 1.6
9	EtOAc	141 ± 1.1
10	toluene	146 ± 1.2
11	pH =1	142 ± 1.6
12	pH = 10	146 ± 1.4
13	sea water	141 ± 1.0
14	lake water	143 ± 1.5
15	tap water	145 ± 1.3
16	river water	143 ± 1.2
17	1 M AcOH	142 ± 1.0
18	1 M HCl	144 ± 1.0

5.3.7 Hydrophobic Nature of 4′@CF₃

Our main aim of the modification of **4′** by -$COCF_3$ was to make the material hydrophobic. The incorporation of -CF_3 groups in **4′@CF₃** converted the hydrophilic **4′** to hydrophobic **4′@CF₃**. The post modified material displayed its self-floating ability when the **4′@CF₃** powder was placed on the surface of water. But, the **4′@CF₃** powder was readily immersed when it was put on the surface of hexane (Figure 5.14). A spherical droplet was immediately formed when 10 µL of water drop was carefully placed on the flat surface of **4′@CF₃** powder. All the above observations proved that after incorporation of -CF_3 group to **4′**, it became hydrophobic and lipophilic. The measurement of WCA further verified the hydrophobic nature of **4′@CF₃**. The MOF displayed an excellent average static contact angle of 146 ± 1° (Figure 5.15). Such contact angle value confirmed the water repealing nature of **4′@CF₃**.

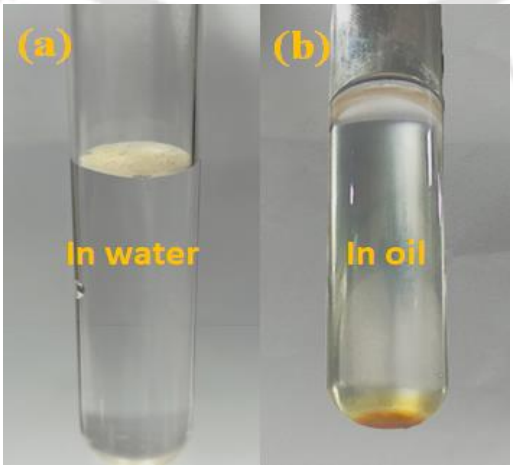

Figure 5.14 Self-floating ability of **4′@CF₃** in water (a) and oil (hexane) (b).

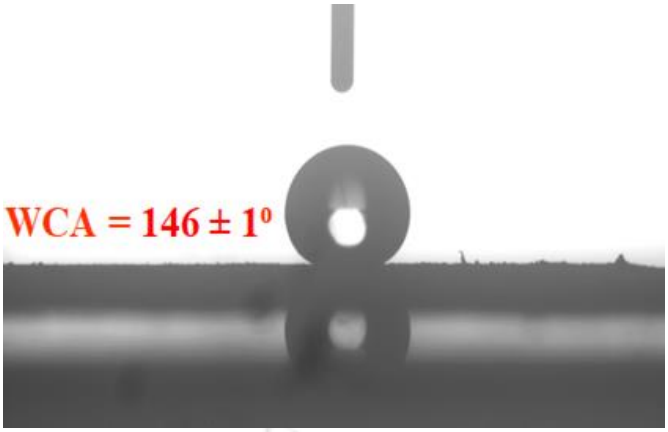

Figure 5.15 Water contact angle image of beaded water droplets on the surface of **4′@CF₃**.

5.3.8 Preparation of 4′@CF₃@melamine Composite

For the synthesis of the composites of **4′@CF₃** with the melamine sponge, at first, the commercially available melamine sponge was cut into small pieces (with a volume of 1 × 1 × 1 cm^3) and the sponges were sonicated with acetone for 15 min to remove the unwanted substrates present in the sponges. After that, the sponges were dried in a 50 °C oven for 2 h and a coating of PDA was made on the dry and clean sponges. For that, 80 mg of dopamine hydrochloride was added to a mixture of water and ethanol (volume ratio of water and ethanol was 1:1). Afterwards, 40 mL of 10 mM Tris-buffer solution was added to the previously maintained mixture and the final pH of the medium was adjusted to 8.5 by the addition of an aqueous solution of NaOH. Then, 10 small pieces of sponge (volume of 1 × 1 × 1 cm^3) were added to the mixture and they were allowed to stir for 24 h. After 24 h, black coloured PDA coated melamine sponges were obtained, which were washed with water and dried for 12 h in an 80 °C oven.

A cross-linked polymeric solution was obtained after mixing PDMS and PMHS in the presence of catalyst, dibutyltin dilaurate**.** For the preparation of the polymeric solution, PMHS and PDMS were dissolved in toluene with a volume ratio of 1:10 and 3% of dibutyltin dilaurate (with respect to total volume of the polymer) were totally mixed by sonication of the mixture for 45 min**.** After preparation of the cross-linked polymeric solution, it was diluted 25 times to its initial concentration. Thereafter, 1 g of **4′@CF₃** was added to 25 mL of the polymeric solution and the MOF was dispersed into the solution of the polymer through sonication for 1 h. Then, the mixture of MOF and polymer was heated for 1 h at 45 °C for maximum cross-polymerization. Next, ~5 mL of the mixture of MOF and polymer was homogeneously coated on a small piece of PDA coated sponge and it was fully dried at a temperature of 125 °C. The coating on a piece of sponge was repeated for four times. Thus, we achieved **4′@CF₃@melamine** composite (Scheme 5.2). Here, the cross-linked polymer was used as a binder of **4′@CF₃** to the polydopamine treated melamine sponge.

The loading percentage of **4′@CF₃** on the PDA coated melamine sponge was calculated using the following formula: loading percentage = $(W_f - W_i/W_i) \times 100\%$ where, W_i and W_f are the oven-dry weights of the polymer-coated melamine sponge and **4′@CF₃@melamine** composite, respectively. The obtained average loading percentage was ~36%.

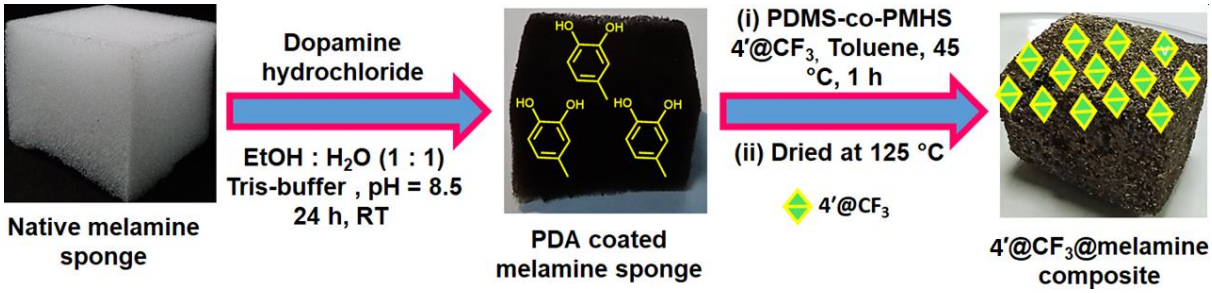

Scheme 5.2 Schematic representation for the preparation of **4′@CF₃@melamine** composite.

5.3.9 Characterization of 4′@CF₃@melamine Composite

After successful fabrication of **4′@CF₃@melamine** composites, the integration of the MOF powder on the melamine sponge was verified by the PXRD, ATR-IR, EDX, FE-SEM and BET analysis.

Digital image of **4′@CF₃@melamine** composite and polymer coated melamine sponge displayed the immobilization of **4′** powder on the melamine sponge (Figure 5.16). In the PXRD profile, the first two sharp characteristic peaks present in powder form of **4′@CF₃** were obtained at 2θ values of 7.4 and 8.5. These two characteristic peaks were not found for polymer coated sponge. The appearance of these crystalline peaks for **4′@CF₃@melamine** supported the presence of **4′@CF₃** MOF in the composite (Figure 5.17). Then, we took the support of ATR-IR spectroscopy to prove the immobilization of MOF on the melamine sponge. Two sharp bands at 1420 and 1570 cm^{-1} were observed in the IR spectra of **4′@CF₃@melamine**. These peaks arose from the symmetric and asymmetric stretching vibrations of carboxylate groups. Another sharp peak at 1666 cm^{-1} was observed in the IR spectra of **4′@CF₃@melamine**, which corresponds to the carbonyl stretching frequency of the trifluoroacetoxy functional group and the peak at 1202 cm^{-1} is due to the stretching of C-F bond of -CF_3 group (Figure 5.18). Such characteristic peaks were not obtained for polymer coated sponge. The existence of all the characteristic IR peaks of **4′@CF₃** confirmed the presence of **4′@CF₃** in the composite.

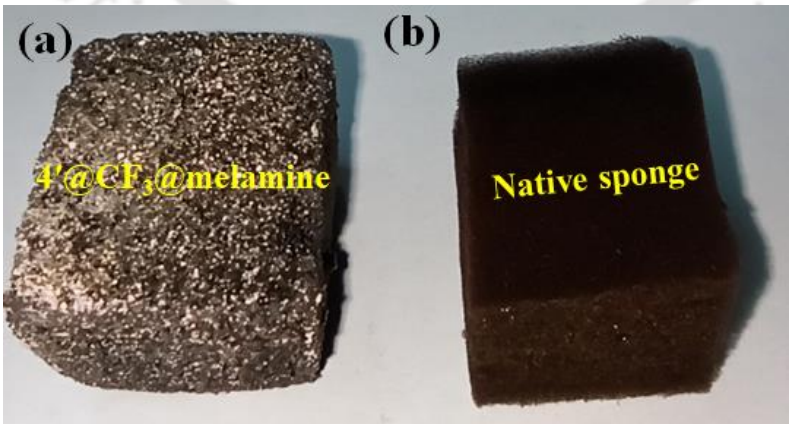

Figure 5.16 Digital images of (a) **4′@CF₃@melamine** composite and (b) polymer coated melamine sponge.

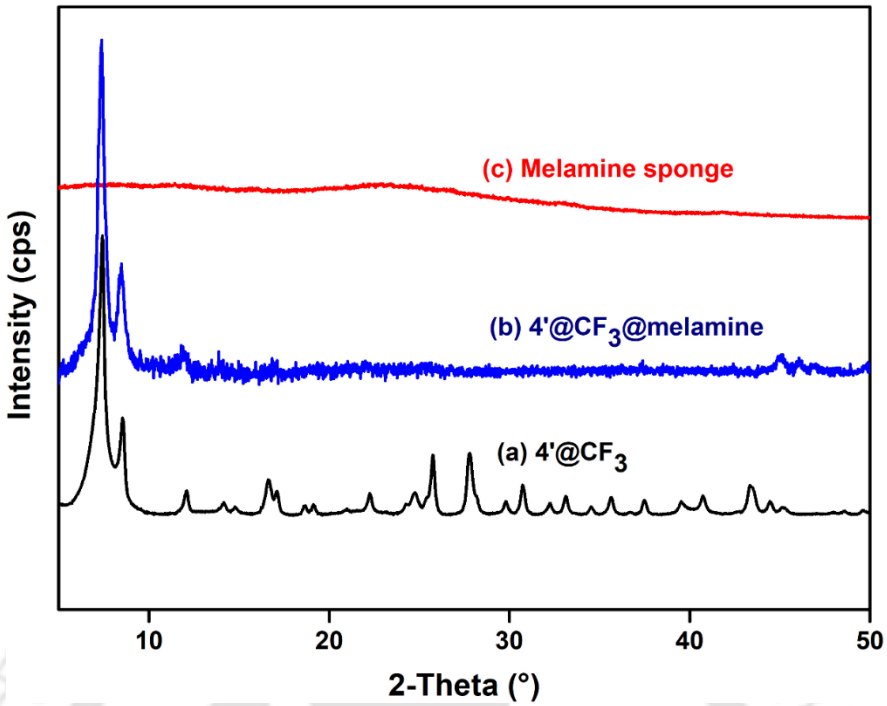

Figure 5.17 PXRD patterns of (a) **4′@CF₃**, (b) **4′@CF₃@melamine** composite and (c) only melamine sponge.

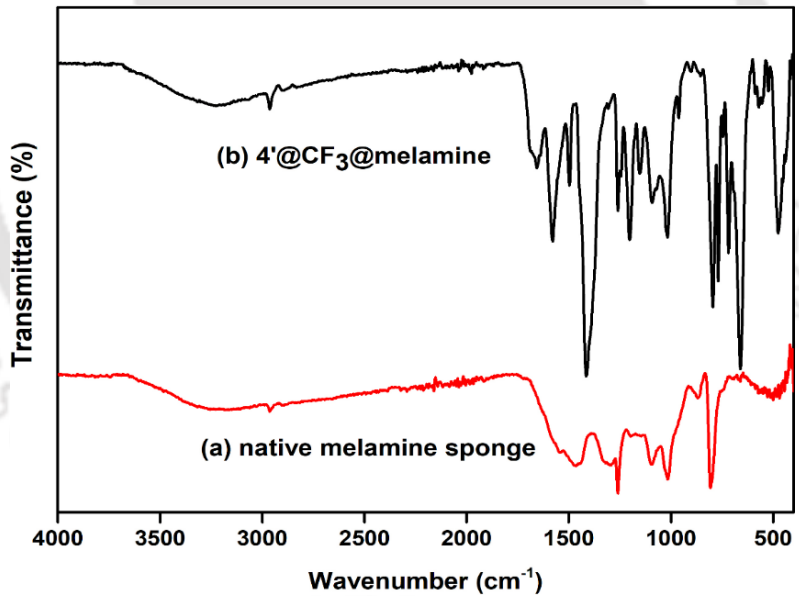

Figure 5.18 ATR-IR spectra of (a) native melamine sponge and (b) **4′@CF₃@melamine** composite.

We calculated the percentage of loading of **4′@CF₃** material in the composite by taking the weights of the composite after and before the integration of MOF powder on the sponge. The obtained percentage of loading was nearly 36%. The presence of Zr, C, O and F elements in the EDX spectra and elemental mapping of **4′@CF₃@melamine** composite further supported the successful loading of **4′@CF₃** on the melamine sponge **(**Figure 5.19-5.20). We also measured the BET surface area of the polymer coated and MOF loaded melamine sponges. The polymer coated sponge was non-porous, but surface area was 349 m^2/g for the surface-modified

sponge (Figure 5.21). Such an increase in surface area for the modified sponge evidenced the presence of a porous framework on the melamine sponge.

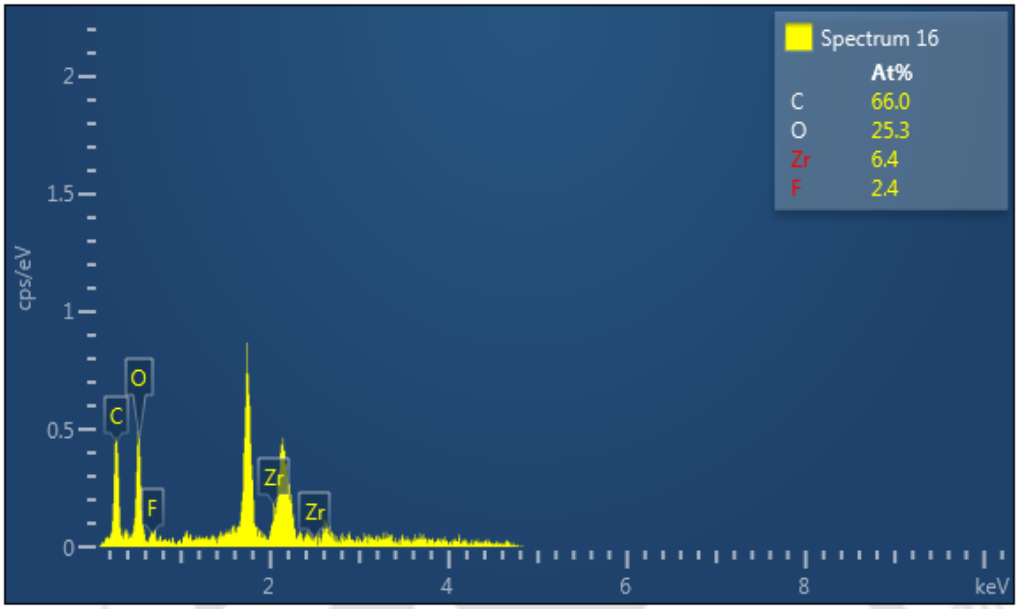

Figure 5.19 EDX spectrum of **4′@CF₃@melamine** composite.

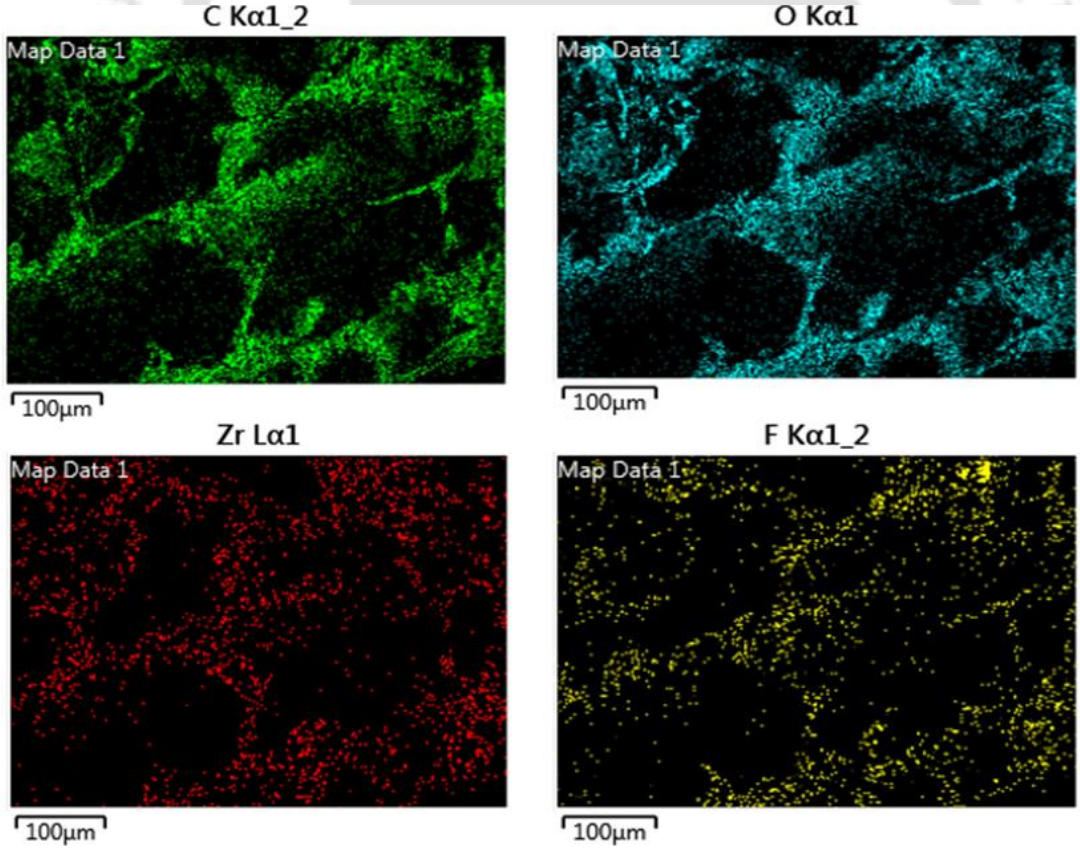

Figure 5.20 EDX elemental mapping of **4′@CF₃@melamine** composite.

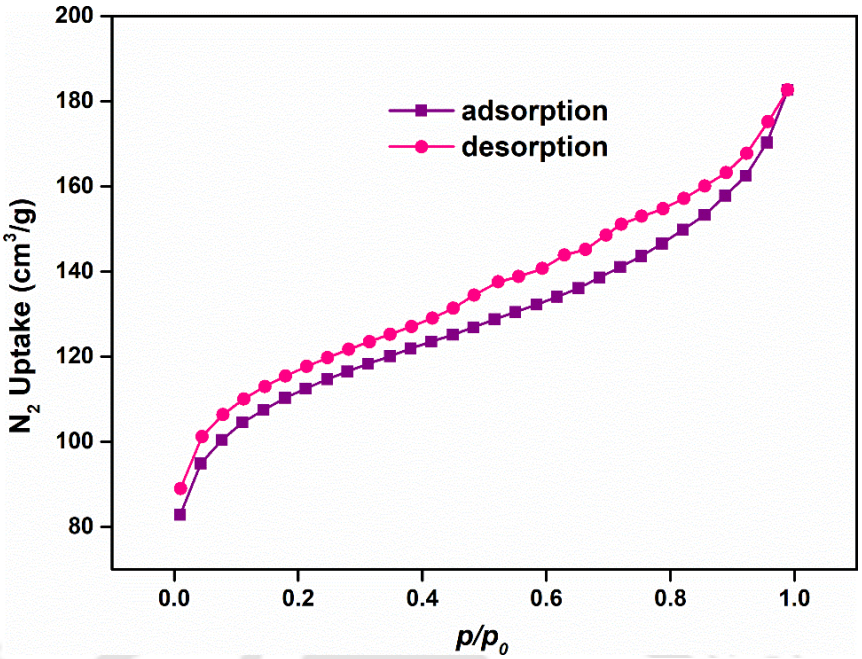

Figure 5.21 Nitrogen adsorption and desorption isotherms of **4′@CF₃@melamine** recorded at -196 °C.

Most conclusive evidence of the uniform immobilization of **4′@CF₃** on the surface of the sponge was received from the FE-SEM images of the polymer coated sponge (Figure 5.22) and the sponge obtained after treatment with **4′@CF₃** (Figure 5.23a-d). From Figure 5.22, it is clear that the polymer coated sponge has a smooth surface, but the **4′@CF₃@melamine** composite has a rough surface. The roughness of the surface of the melamine sponge in **4′@CF₃@melamine** significantly increased after the treatment with **4′@CF₃** MOF. The roughness on the sponge surface was produced by the random arrangement of **4′@CF₃** particles, making the surface hydrophobic. All the above-discussed experiments strongly supported the integration of **4′@CF₃** MOF on the surface of the melamine sponge.

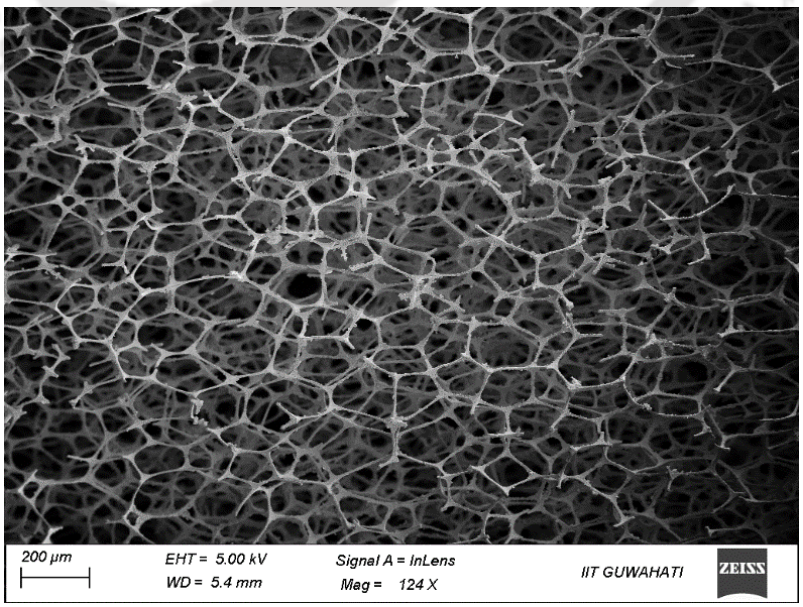

Figure 5.22 High resolution FE-SEM images of melamine sponge.

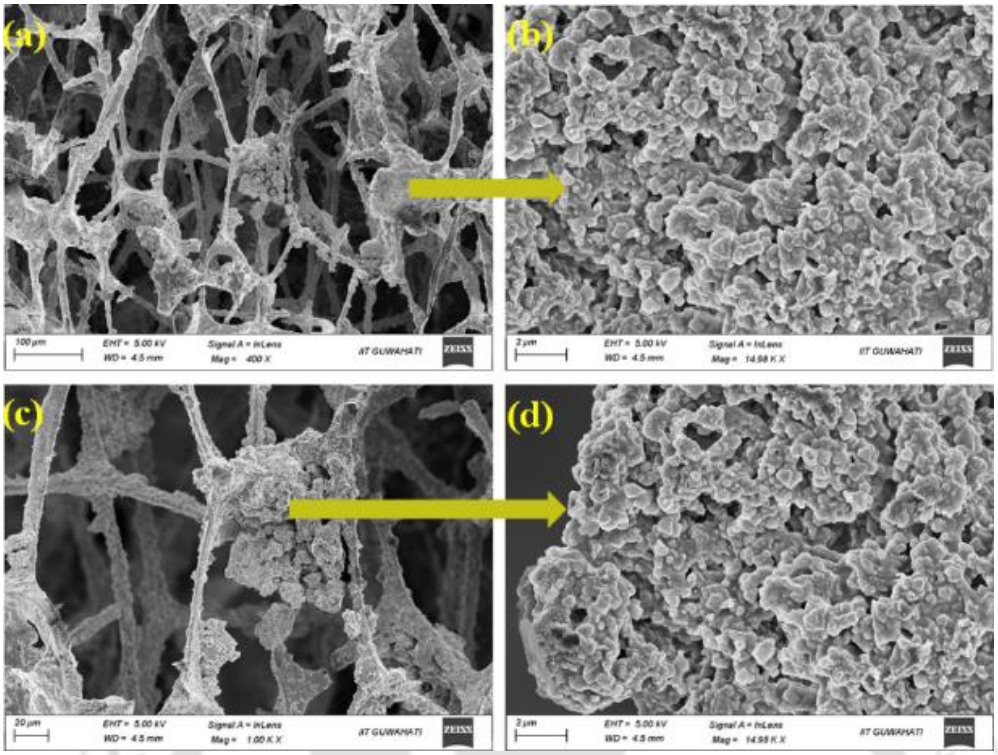

Figure 5.23 High resolution FE-SEM images of **4′@CF$_3$@melamine** composite (a-d).

5.3.10 Hydrophobicity Assessment for 4′@CF$_3$@melamine Composite

After the verification of successful immobilization of the MOF on the surface of the melamine sponge, we verified the hydrophobic nature of the composite. For the same, initially, we carefully added a red colored (red color was added to make the droplet visible) water droplet on the surface of the **4′@CF$_3$@melamine** composite (Figure 5.24). An immediate formation of the spherical droplet was observed on the surface of the composite. But, for a polymer coated sponge, water droplets are readily absorbed by the sponge surface (Figure 5.24). The static WCA of the **4′@CF$_3$@melamine** composite was 145 ± 1°. Such value of WCA evidenced the hydrophobic nature of the **4′@CF$_3$@melamine** composite (Figure 5.24). Water repealing nature of the **4′@CF$_3$** was the reason behind the observation. Next, we verified the self-floating nature of the composite and the polymer coated dopamine treated sponge. Figure 5.25a displays, the surface-modified sponge was floated on the surface of the water, but the polymer coated sponge immersed into the bulk of water after soaking the water. Now, when we forcefully immersed the **4′@CF$_3$@melamine** composite into the bulk of water, a silver-colour shining was observed on the contact point of the sponge and water (Figure 5.25b). A similar phenomenon is also observed when one forcefully immerses a lotus leaf into water. [28]

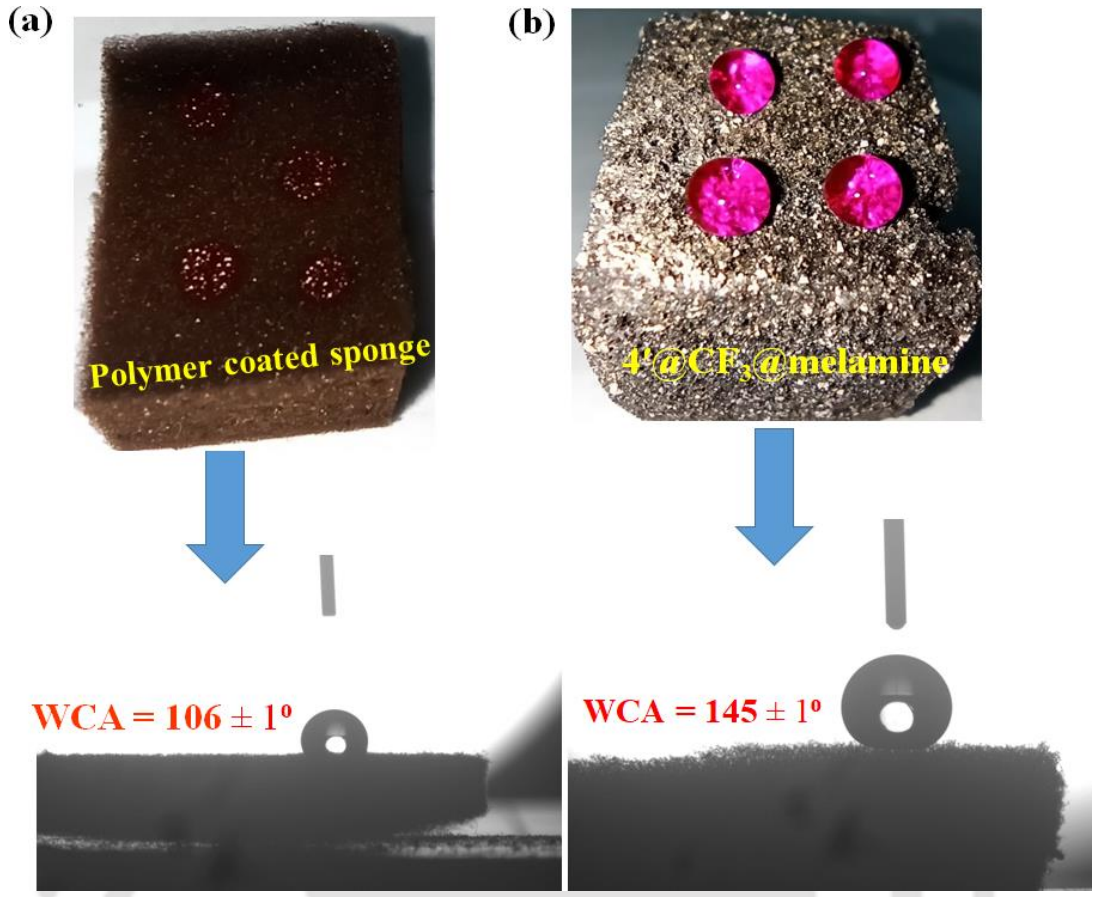

Figure 5.24 Visual images of water droplets (red colour helps visual inspection) suspended on (a) polymer coated sponge and (b) **4′@CF₃@melamine** composite. The measured WCA of the polymer coated sponge and **4′@CF₃@melamine** composite are shown below.

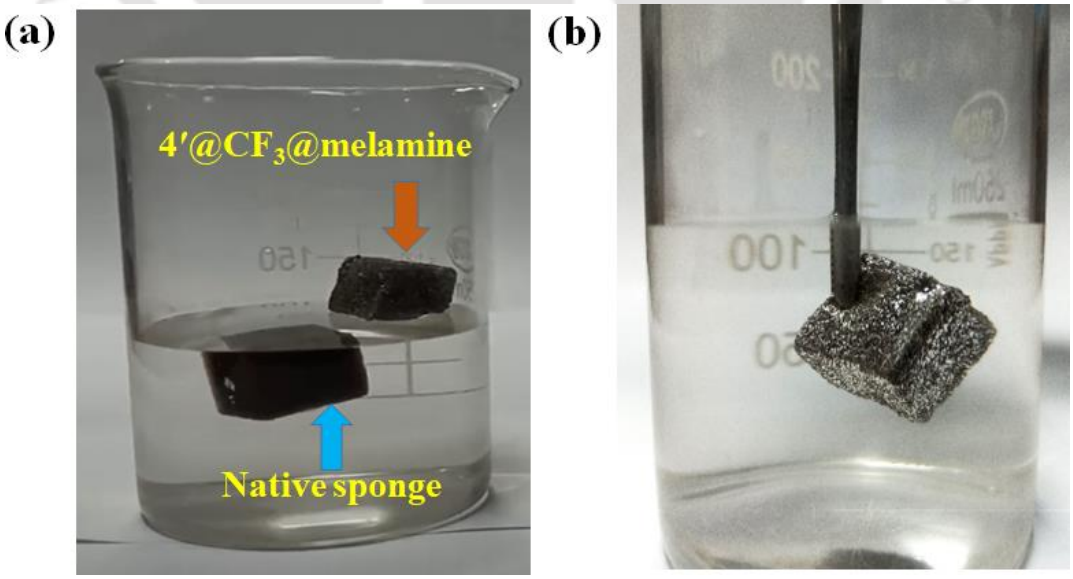

Figure 5.25 (a) Digital images of floating **4′@CF₃@melamine** composite on water and immersion of polymer coated melamine sponge in water and (b) digital image of forcefully submerged **4′@CF₃@melamine** composite under water showed Cassie-Baxter state.

5.3.11 Stability of 4′@CF_3@melamine Composite in Different Oils and Water Media

The composite should be stable in various harsh conditions for actual field application. To know the stability of the composite, it was kept in various oils (CH_2Cl_2, $CHCl_3$, CCl_4, toluene, ethyl acetate, hexane, kerosene, motor oil, silicon oil and gasoline), water (pond, seawater, river, cold water and hot water) and pH (pH = 1 and 10) media for 2 h at room temperature and after 2 h, the composites were dried and the WCA of the composites were collected. Table 5.3 shows that the water repelling ability of the composite remained almost the same as the fresh composite after being exposed to all possible harsh conditions.

Table 5.3 Water Contact angle (WCA) of **4′@CF_3@melamine** after treatment with different types of water and oil specimens.

Sl No.	Oil/Water Types	Average WCA (°)
1	sea water	142 ± 1.8
2	lake water	142 ± 1.5
3	tap water	143 ± 1.9
4	river water	144 ± 1.7
5	hot water	140 ± 1.9
6	cold water	143 ± 1.2
7	pH = 1	143 ± 2.0
8	pH = 10	144 ± 1.9
9	CH_2Cl_2	140 ± 1.1
10	$CHCl_3$	144 ± 1.2
11	CCl_4	141 ± 1.3
12	EtOAc	144 ± 1.5
13	hexane	145 ± 1.8
14	toluene	142 ± 1.0
15	motor oil	147 ± 1.0
16	gasoline	147 ± 1.2
17	kerosene	145 ± 1.3

5.3.12 Selective Separation of Oils by 4′@CF_3@melamine Composite from Oil-Water Mixtures

The stability of the composite in various drastic conditions and its hydrophobic as well as lipophilic nature motivated us to utilize it for the selective separation of oils from the oil-water mixtures. For this task, we chose $CHCl_3$ as a heavy oil (denser than water) and kerosene as light oil (less dense than water). To differentiate the oil and water layers, we made the oil colourful. Kerosene and $CHCl_3$ were made blue and red coloured after the addition of a pinch of Solvent *Blue* 35 and Rhodamine B dyes to a 5 mL volume of oil samples.

Around 100 mL of water and 5 mL of light oil (kerosene) was added in a 250 mL beaker. As the density of kerosene is lower than that of water, it floats on the surface of water. When the **4′@CF_3@melamine** composite was brought into contact with the mixture's upper oil layer, it immediately soaked up all of the light oil (kerosene) in a selective manner (Figure 5.26-i). Next, in a 250 mL beaker, 5 mL of heavy model oil ($CHCl_3$) was added to roughly 100 mL of distilled water. When we put the **4′@CF_3@melamine** composite into the mixture with force, it absorbed all of the heavy oil selectively (Figure 5.26-ii). These findings suggested that **4′@CF_3@melamine** will be beneficial for separating both the heavy and light oils from the oil-water mixture.

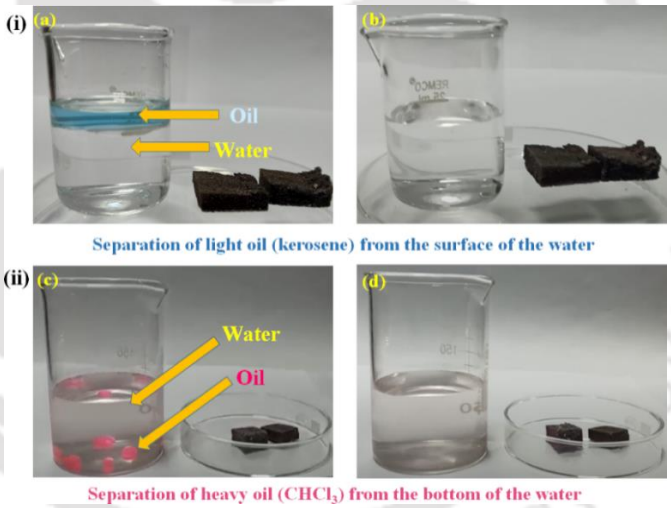

Figure 5.26 Digital photographs of the selective separation of (i) floating oil and (ii) underwater oil by **4′@CF_3@melamine** composite.

This selective and quantitative separation of the **4′@CF_3@melamine** composite for both the heavy and light oils inspired us to evaluate its separation efficiency for various heavy and light oils. Separation efficiency for different oils were determined by the formula: separation efficiency (%) = $V_f/V_i \times 100$ where, V_i is the total volume of oil (mL) used and V_f is the volume of oil absorbed by **4′@CF_3@melamine** composite. The obtained separation efficiency was in the range of 95-99% for the oils tested (Figure 5.27a). The separation efficiency remained almost the same (Figure 5.27b) when we carried out similar experiments (using EtOAc as a reference oil) for various real water samples (tap water, artificial seawater and river water) and pH media (pH 1 and pH 10). After each experiment, the oil absorbed by the **4′@CF_3@melamine** composite was collected by the manual squeezing.

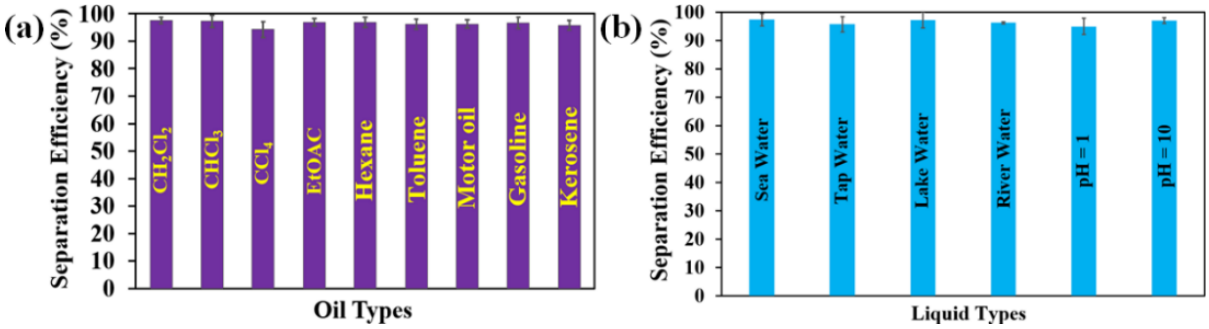

Figure 5.27 Bar plot of separation efficiency (%) of **4′@CF3@melamine** composite towards separation of: (a) various oils from oil-water mixtures, and (b) EtOAc from different types of aqueous media. Each measurement was repeated six times.

Our main aim was to develop a composite to make the oil-water separation process easier, cheaper, effective and less time-consuming. From the above discussion, it is clear that our composite is highly effective in separating various oils with 95-99% efficiency even in harsh conditions. The absorbed oil can be easily collected by mechanical squeezing of the composite within a few seconds. The results show that our material meets all the criteria of an excellent and effective oil-water separation material.

Reusability of the composite is another crucial factor to consider when we select a material for oil-water separation. We tested the reusability of **4′@CF3@melamine** composite up to the 50th cycle and found that the loss of separation efficiency after the 50th cycle was only ~10% (Figure 5.28). After the 50th cycle of the separation experiment, the EDX spectrum and elemental mapping of **4′@CF3@melamine** composite were recorded. The obtained results revealed that the Zr, O, C and F elements were present in the composite (Figure 5.29). We also conducted the FE-SEM analysis of the **4′@CF3@melamine** composite after the 50th cycle of separation. The FE-SEM image of **4′@CF3@melamine** composite exhibited a homogeneous distribution of particles (Figure 5.30). The characteristic PXRD peaks of **4′** were also found in reused **4′@CF3@melamine** (Figure 5.31). All of the findings pointed to the usefulness of the composite for oil-water separation up to the 50th cycle. The recyclability of the composite is much better than the recently reported MOF based composite from our group, which was only up to 10 cycles.[29]

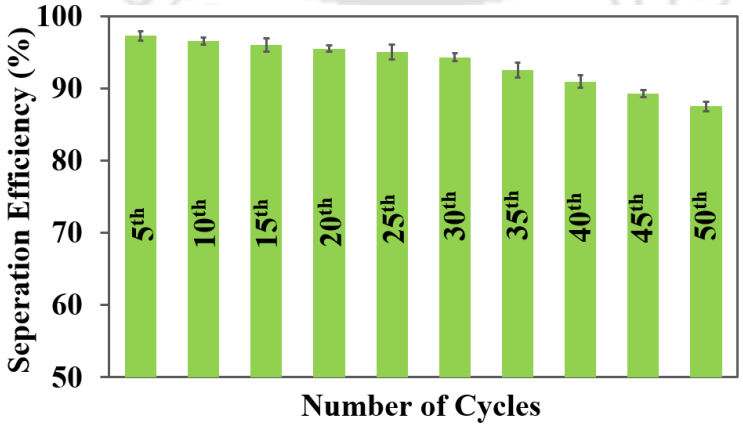

Figure 5.28 Reusabiity of **4′@CF3@melamine** composite for oil-water separation experiment (model oil: kerosene).

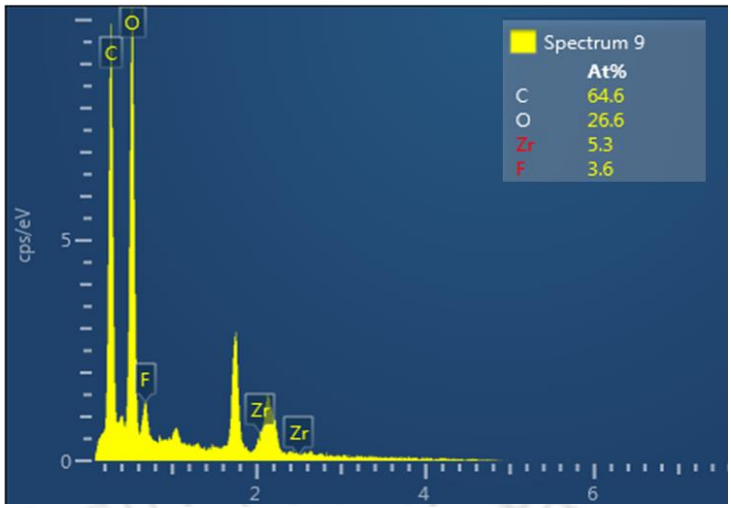

Figure 5.29 EDX spectrum of **4′@CF$_3$@melamine** composite after 50th cycle of oil-water separation experiment.

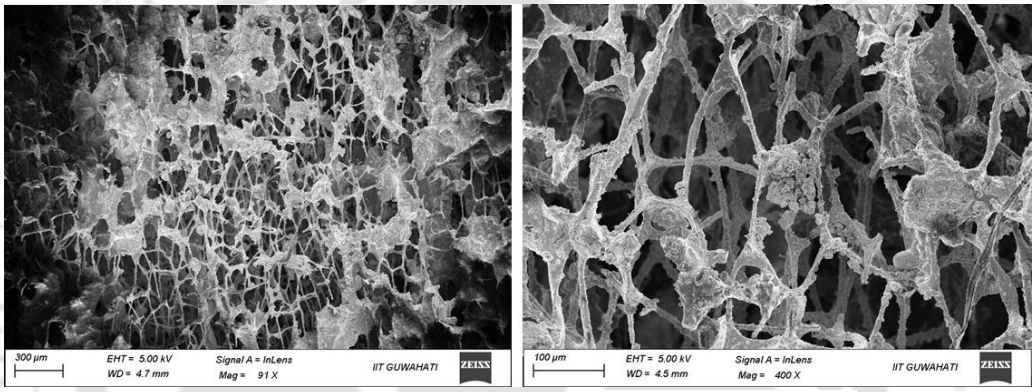

Figure 5.30 High resolution FE-SEM images of **4′@CF$_3$@melamine** composite after 50th cycle of oil-water separation experiment.

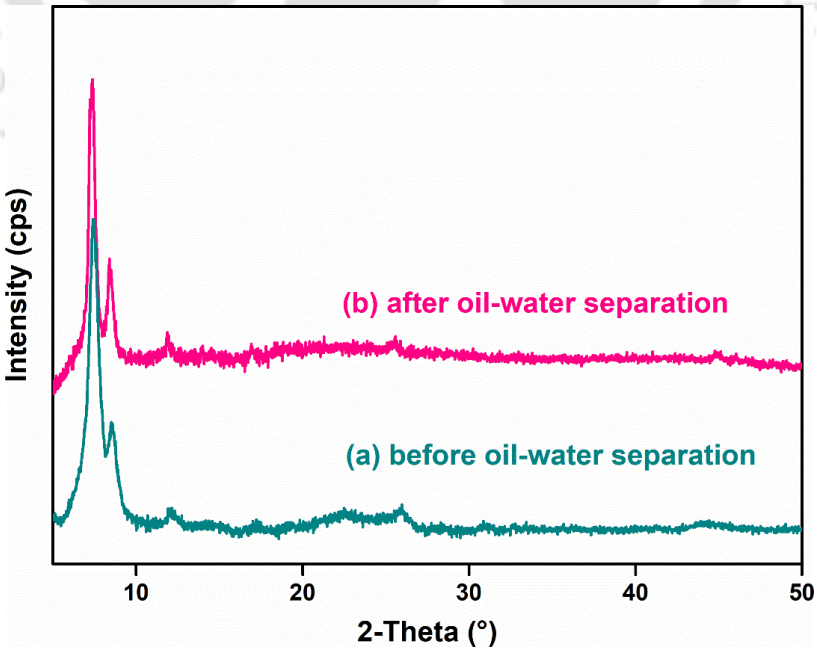

Figure 5.31 PXRD patterns of **4′@CF$_3$@melamine** composite (a) before and (b) after oil-water separation experiments (model oil: EtOAc).

5.3.13 Absorption Capacity of 4′@CF_3@melamine Composite for Various Oils

The extraordinary high separation efficiency of the **4′@CF_3@melamine** composite for different oils and various aqueous media as well as recyclability of the composite up to 50th cycles encouraged us to examine the absorption capacity of the **4′@CF_3@melamine** composite for various oils. For this study, cubic composite pieces were immersed in various oils and kept inside the oils for 1 min. The weights of the composites were measured before and after the absorption of oils. Finally, we calculated the absorption capacity of the composites in terms of g/g unit (mass of oil absorbed by each gram of composite). The composites displayed negligible water absorption capacity but excellent absorption capacity for various oils. The obtain absorption capacities for various oils were water: 1.04 ±0.09, CCl_4: 37.3 ± 1.2 g/g, $CHCl_3$: 36.0 ± 2.6 g/g, CH_2Cl_2: 35.2 ± 2.4 g/g, EtOAc: 32.2 ± 1.2 g/g, kerosene: 28.0 ± 0.8 g/g, gasoline: 26.1 ± 1.2 g/g, toluene: 26.9 ± 1.8 g/g, hexane: 28.3 ± 0.8 g/g and motor oil: 27.5 ± 1.7 g/g (Figure 5.32). The absorption capacity obtained for various oils are similar to previously reported oil-water separation materials and the absorption capacities for various oils are directly proportional to the density of the absorbed oil (Table 5.4).[29]

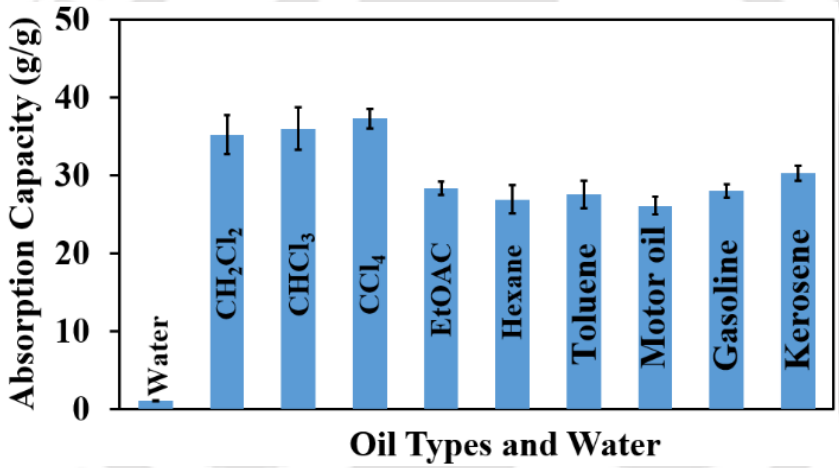

Figure 5.32 Bar plot of absorption capacity (%) of **4′@CF_3@melamine** composite for various oils.

Table 5.4. Absorption capacities (in g/g) of various absorbents for oil absorption.

Sl. No.	Absorbents	Type of Oil	Absorption Capacity (g/g)	Ref.
1	**1′@CF_3@melamine composite**	gasoline oil motor oil kerosene	26.1 ± 1.2 27.5 ± 1.8 28 ± 0.80	this work
2	PDMS-TiO_2-PU sponge	diesel oil	14.20	30
3	SH-UiO-66@CFs	motor oil silicone oil gasoline kerosene	45.23 38.06 31.87 29.41	31
4	superhydrophobic/superoleophilic sawdust	crude oil	17.50	32
5	cotton fiber modified via the sol-gel method	diesel oil lubrication oil crude oil	25.61 44.24 57.01	33

6	modified jute fiber via the sol-gel method	crude oil diesel oil lubricatiom oil	7.41 8.48 10.29	34
7	mesoporous silica aerogel	petrol oil diesel oil	19.1 18.6	35
8	ultralight cellulose-based aerogel	pump oil diesel oil	22.60 20.9	36
9	cellulose-based aerogel	crude oil diesel oil lubrication oil silicone oil	77.08 91.82 105.83 89.72	37

5.3.14 Gravity Driven Filtration-Based Separation of Oils by 4′@CF_3@melamine Composite

We also developed a gravity-driven oil-water separation technique that is very simple and does not require any energy or sophisticated instrumental supports. Firstly, a mixture of 5 mL of $CHCl_3$ and 5 mL of water was prepared ($CHCl_3$ was made colourful to differentiate the liquids). Afterwards, the mixture was poured into a column in which a piece of composite was plugged at the bottom part. It is evident from Figure 5.33a, that the red-coloured chloroform, which has a greater density than water, was filtered or separated through **4′@CF_3@melamine**. However, the water layer remained over **4′@CF_3@melamine**. The hydrophobic feature of the composite did not allow to pass the water through the composite. This observation proved the oil separation capability of the composite from the oil-water mixture via a gravity-driven, zero energy consumption process.

5.3.15 Against Gravity Based Separation of Oils by 4′@CF_3@melamine Composite

The removal technique of heavy oils from the bottom of water using **MOF@cotton** composite against the gravity pathway was recently devoted by our group.[29] Using a similar protocol, we also verified the capability of the **4′@CF_3@melamine** composite to separate sedimentary oil from the bottom of water. In this easy approach, a 6 mL mixture of $CHCl_3$ and water was taken in a 15 mL test tube (again, we made the colour of $CHCl_3$ as red to discriminate the liquids). Afterwards, a Pasteur pipette plugged with the **4′@CF_3@melamine** composite was slowly dipped inside the test tube. The composite did not soak any water when it came in contact with water, but as it touched the $CHCl_3$ layer, it immediately started to absorb $CHCl_3$. After absorbing all the $CHCl_3$, the opposite side of the Pasteur pipette was capped and slowly taken out from the test tube. Red coloured $CHCl_3$ readily came out from the pipette when it was uncapped to another test tube by the force of gravity (Figure 5.33b). The Pasture pipette with composite was then ready for the next cycle of sedimentary oil separation. This experiment clearly evidenced the selective separation ability of the composite for the heavy oils against the gravity.

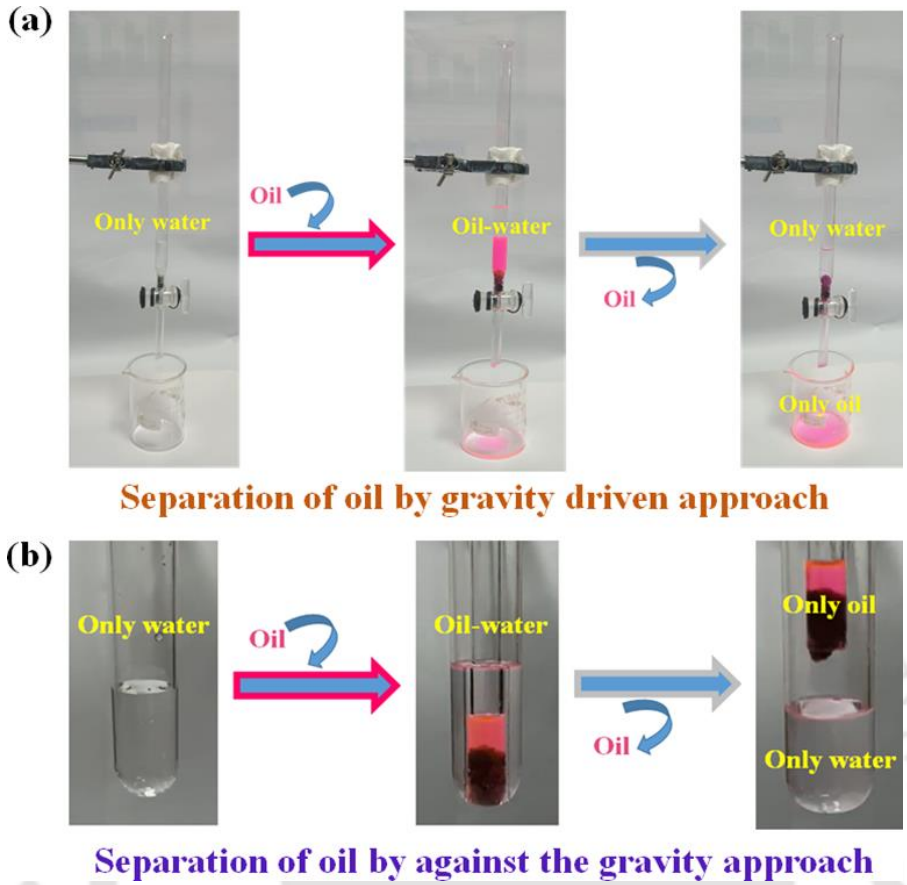

Figure 5.33 Digital photographs of selective separation of oil by gravity-driven method (a) and against the gravity method (b) by **4′@CF$_3$@melamine** composite.

5.3.16 Selective Separation of Oil from Water-in-Oil Emulsions

Large amounts of oil in a small amount of water form emulsion. The separation of oil from water-in-oil emulsion is equally crucial as the water-in-oil separation. Extraordinary separation efficiency, considerable absorption capacity and high reusability of the composite towards the selective separation of oils from water-in-oil mixture prompted us to carry out the water-in-oil emulsion separation experiment**.**

For the separation of emulsions different water-in-oil emulsions were prepared (water/toluene, water/$CHCl_3$, water/ kerosene and water/gasoline) by sonicating the water-oil mixtures for 60 min. To make the emulsion stable, 50 µL of surfactant (Triton X-100) was added to the oil-water mixture before sonication. Then, 4 mL (3.5 mL of oils + 0.5 mL of water) of different water-in-oil emulsions were allow to pass through a chromatographic column and the bottom of the column was packed by hydrophobic **4′@CF$_3$@melamine** composite. The time required for all the separation process were recorded.

Separation efficiency (%) for various water-in-oil emulsion were calculated using the following formula:

Separation efficiency (%) = $V_2/V_1 \times 100\%$

where V_1 was the amount of oil used (mL) for the preparation of the water in oil emulsion and V_2 was the obtained volume of oil (mL) after the separation experiment.

The flux for various emulsions was calculated using the formula: Flux = V/A × T (where V = volume of separated oil, A = area of the composite and T = time required for the separation of oil from water-in-oil emulsion).

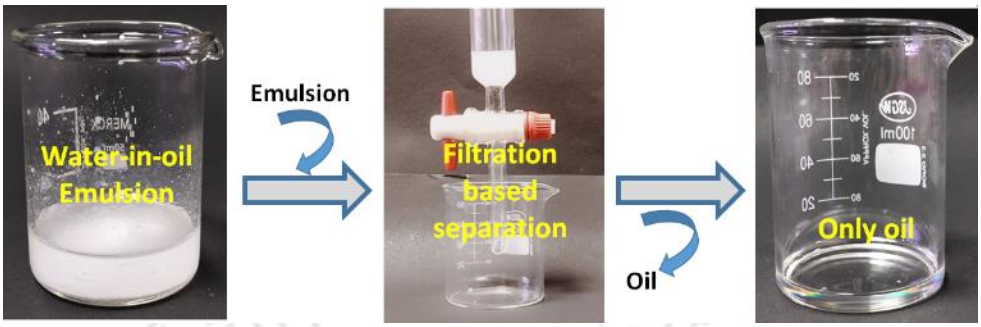

Figure 5.34 Digital photographs of selective separation of oil by gravity-driven method from water-in-oil emulsion.

The readily prepared emulsions were poured into a chromatographic column (the bottom of the column was tightly packed by the composite). Now, the emulsion was allowed to pass through the **4′@CF$_3$@melamine** composite. The emulsion droplets readily demulsified after touching the composite. The composite permitted to pass only the oil components and the water droplets remained above the composite (Figure 5.34). Because of the hydrophobic nature of the **4′@CF$_3$@melamine** composite as the water-in-oils emulsions contact the composite, only the oil phase immediately permeated to go through the hydrophobic layer and formed an oil phase layer, which led to the water droplets being rejected. The lipophilic nature of the composite was the main reason behind the selective separation of oils through the composite.

The efficiency of emulsion separation and flux of the composites towards different water-in-oil emulsions were calculated to verify the capability of the composite towards emulsion separation. The obtain separation efficiencies for water/toluene, water/$CHCl_3$, water/kerosene and water/ gasoline emulsions were 98.5 ± 1.4, 97± 1, 97.2 ± 1 and 98.3 ± 1.5, respectively (Figure 5.35a). The **4′@CF$_3$@melamine** composite exhibited very high flux for all the emulsions. The obtained average flux for water/toluene, water/$CHCl_3$, water/kerosene and water/gasoline emulsions under the atmospheric pressure were 1959, 1931, 1957 and 2028 L/m^{2}h, respectively (Figure 5.35b). The obtained flux is much better than the previously reported emulsion separators.[38]

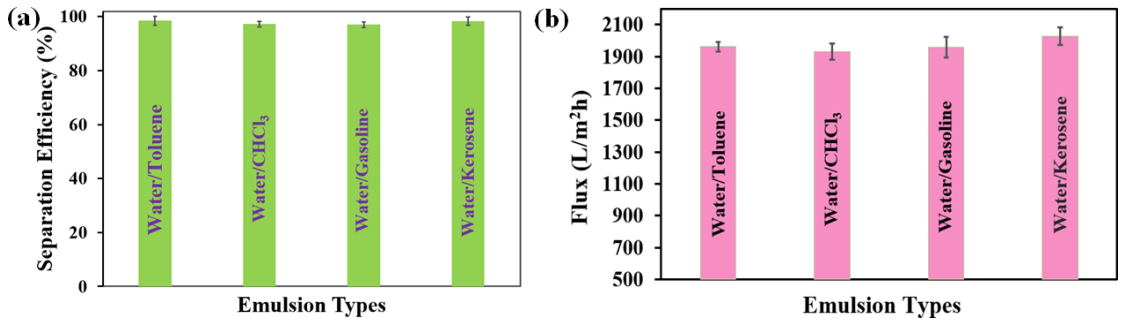

Figure 5.35 (a) Bar plot for separation efficiency (%) and (b) flux of **4′@CF$_3$@melamine** composite for various water-in-oil emulsions.

The reusability performance of the composite for the emulsion separation was also examined up to 30th cycles. After the 30th cycle, the loss of separation efficiency was 9% (Figure 5.36). The stability of the composite was verified after the 30th cycle of separation by collecting the PXRD, EDX, WCA and FE-SEM data of the reused composite (Figure 5.37-5.38). The reused composite displayed similar PXRD pattern as the fresh one (Figure 5.39). All the desired elements were obtained from the elemental analysis and the crystalline nature of **4′@CF$_3$** MOF was further confirmed by the FE-SEM images of the used composites. The WCA data after the emulsion separation experiment are summarized in Table 5.5 All the above results suggested appreciable stability of the composite after the recyclability experiments.

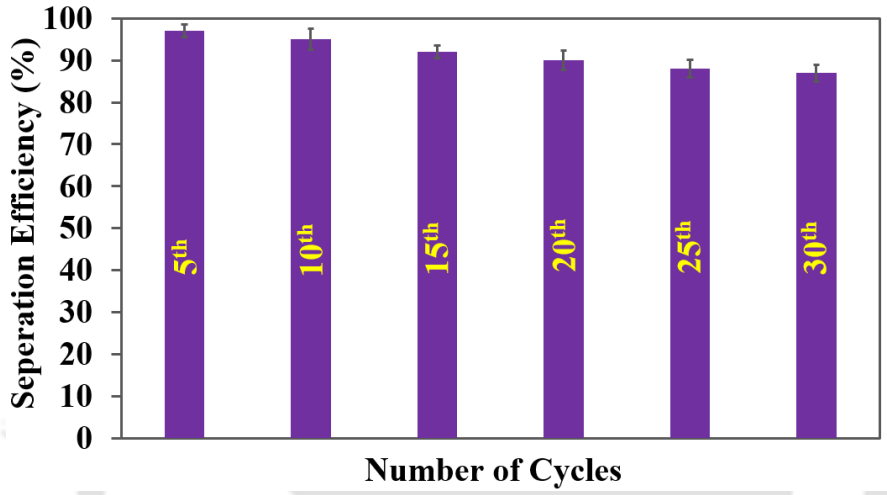

Figure 5.36 Reusabiity of **4′@CF$_3$@melamine** composite for emulsion separation experiment (model oil: kerosene).

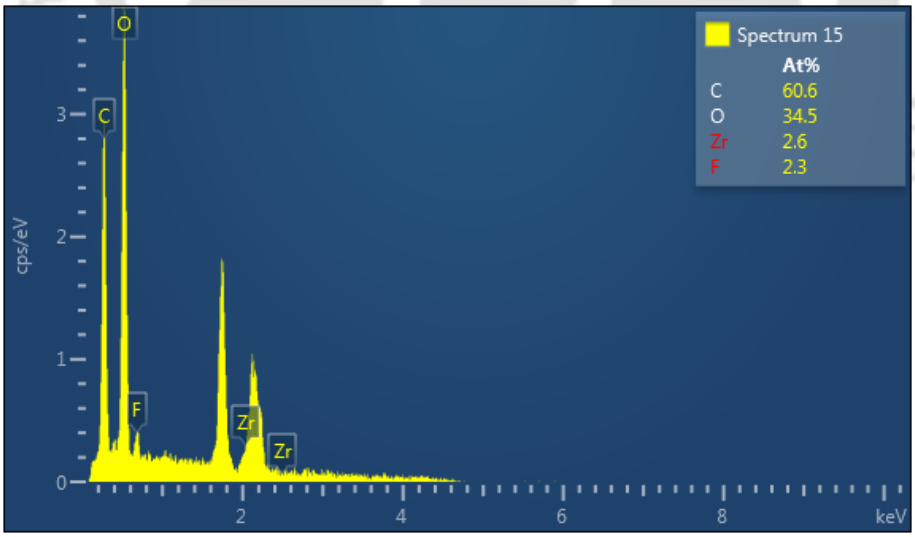

Figure 5.37 EDX spectrum of **4′@CF$_3$@melamine** composite after 30th cycle of emulsion separation experiment.

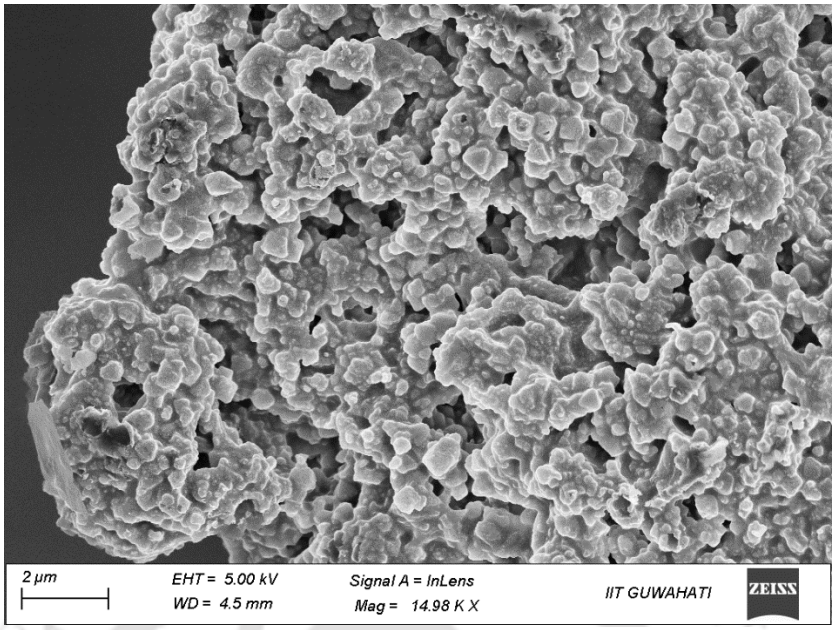

Figure 5.38 High resolution FE-SEM images of **4′@CF$_3$@melamine** composite after 30th cycle of emulsion separation experiment.

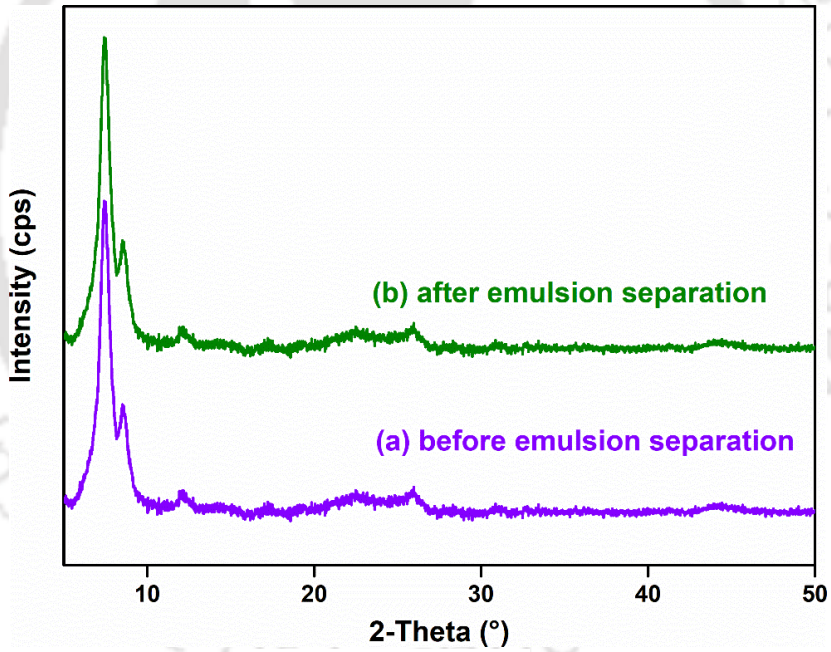

Figure 5.39 PXRD patterns of **4′@CF$_3$@melamine** composite before and after emulsion separation experiments (model oil: kerosene).

Table 5.5 Water Contact angle (WCA) of **4′@CF$_3$@melamine** after emulsion separation experiments.

Sl No.	Emulsion Types	WCA (°)
1	water/toluene	144 ± 1.1
2	water/$CHCl_3$	143 ± 1.3
3	water/gasoline	146 ± 1.0
4	water/kerosene	143 ± 1.4

5.3.17 Self-cleaning Ability of 4′@CF_3

In nature, many plants and animals possess hydrophobic surfaces such as the leaf of lotus, wings of butterfly, pitcher plant, skin of a shark and feet of a gecko. Such hydrophobic surfaces help them to stay sanitary and clean even in a polluted environment. Fungus and bacteria cannot grow on them due to their hydrophobic nature. The possession of a hydrophobic surface prompted us to look into our material's ability to self-clean.

In modern construction transparent glazing materials are regularly used as a building envelope, including doors and windows in the external walls. Glasses are also used for various internal partitions and as an architectural feature including skylights, display cases, mirrors, and glass table-tops. Therefore, glass has huge utilization in modern civilization. Due to regular expose of that glass plates by air, dust particles are continuously deposited on the surface of the glass which hampered the optical transparency of glasses. To get rid of such problem, coating of hydrophobic material on the surface of the glass become very popular in the recent years. To display such applicability of our hydrophobic MOF, we used **polymer@4′@CF_3** coating on the surface of a glass plate. The **polymer@4′@CF_3** coated glass plate displayed good dust removal property just by washing the sand partial containing surface of glass by water (Figure 5.40). For this experiment, a **polymer@4′@CF_3** coated glass slide was prepared. The **polymer@4′@CF_3** was prepared using a suspension of **4′@CF_3**, PMHS and PDMS in above stated procedure. The suspension was then coated over a glass slide by spin-coating method. Afterwards, some dry sand particles were kept on the surface of the slide. When the water droplets were added to the surface, the sand particles were immediately removed from the surface of the glass slide by the droplets (Figure 5.40). Figure 5.41, clearly displays the hydrophobic nature of the **polymer@4′@CF_3** coated glass surface. Again, we verified the stability of the coating by measuring the PXRD profiles and WCA of the **polymer@4′@CF_3** coated glass after performing the self-cleaning experiment (Figure 5.41-5.42). The obtained WCA were 145 ± 1° and 143 ± 1°, respectively (Figure 5.43).

We also demonstrate the self-cleaning ability of the **4′@CF_3@melamine** composite for the practical applications. For the experiment aforementioned procedure (used in case of glass slide) was followed. Similar to the glass slide, all the sand particles immediately removed from the surface of the composite by the addition of water droplets (Figure 5.44). Such experiment clearly displayed the self-cleaning ability of the **4′@CF_3@melamine** composite. The PXRD and WCA of the composite were measured after the self-cleaning experiment, which suggested the robust nature of the composite after the self-cleaning experiment (Figure 5.45-5.46). All the obtained results suggested about the genuine scope of the material in real-world self-cleaning purpose.

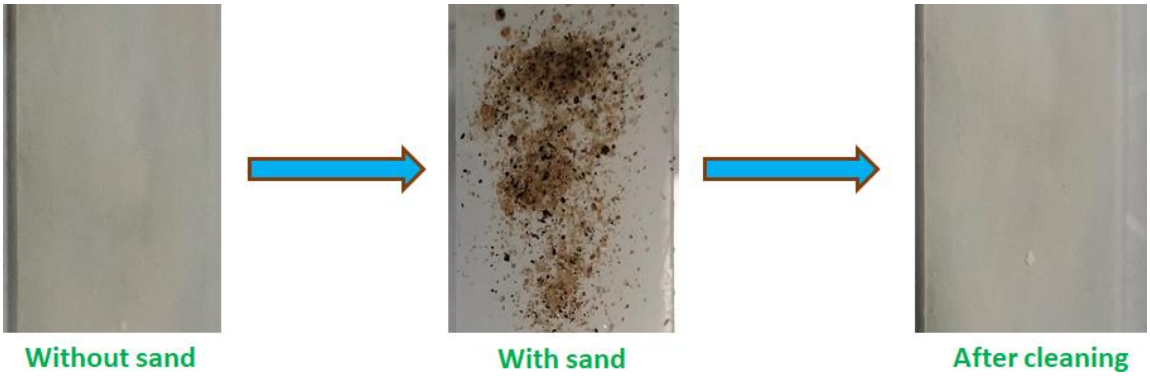

Figure 5.40 Digital image of **polymer@4′@CF$_3$** glass slide displaying self-cleaning nature.

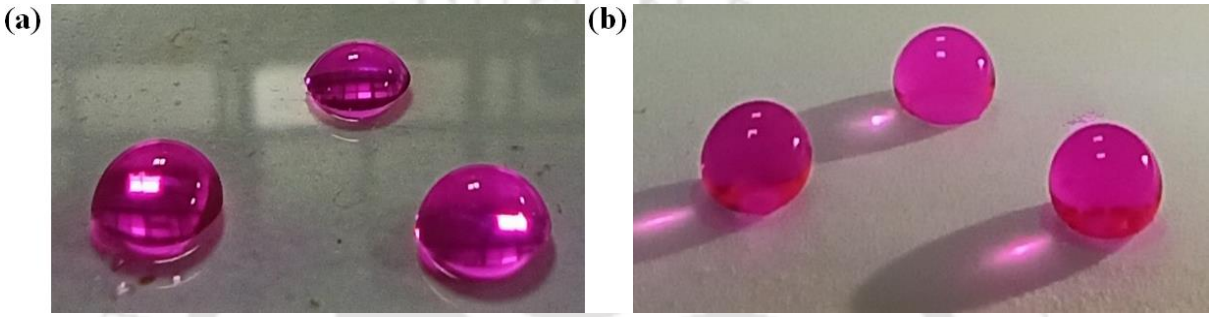

Figure 5.41 Digital imiages of water droplet on (a) only polymer coated glass and (b) **polymer@4′@CF$_3$** coated glass.

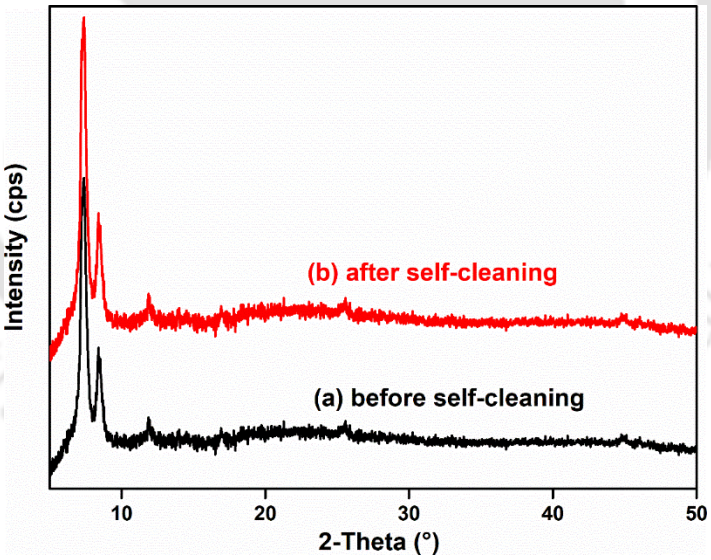

Figure 5.42 PXRD patterns of **polymer@4′@CF$_3$** coated glass (a) before and (b) after self-cleaning.

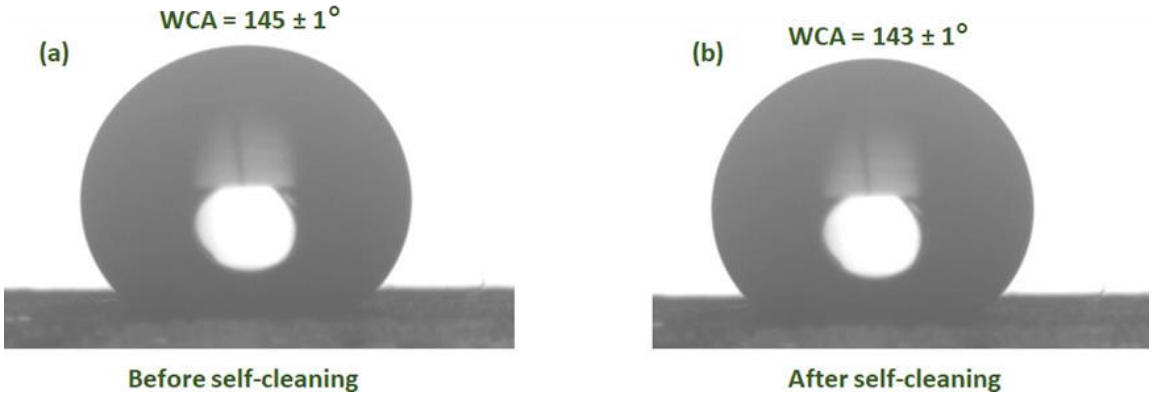

Figure 5.43 Digital images of contact angle of a water droplet on (a) water contact angle of polymer@**4′@CF₃** coated glass before self cleaning and (b) polymer@**4′@CF₃** coated glass after self-cleaning.

Figure 5.44 Digital image of **4′@CF₃@melamine** composite displaying self-cleaning nature.

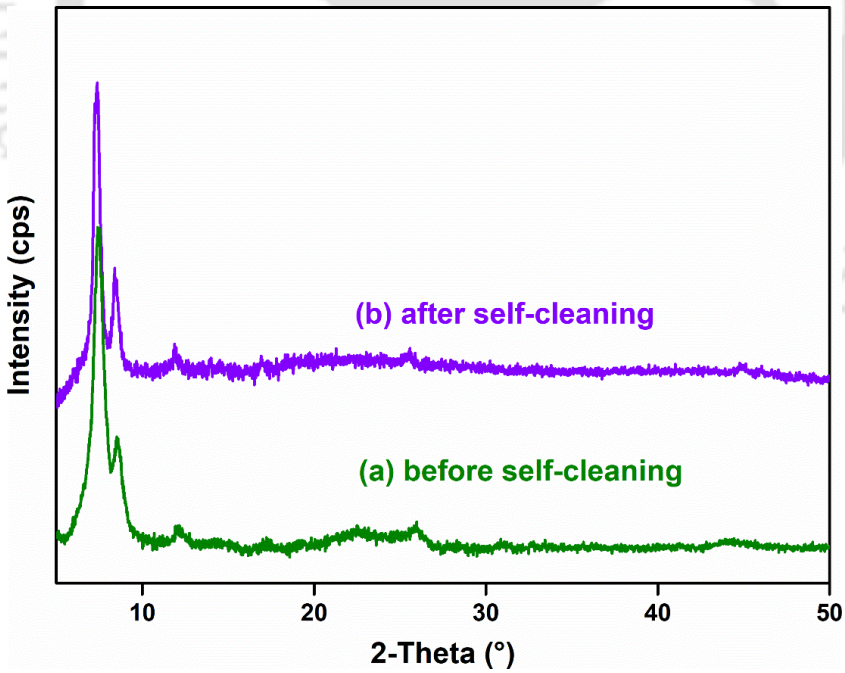

Figure 5.45 PXRD patterns of **4′@CF₃@melamine** composite (a) before and (b) after self-cleaning.

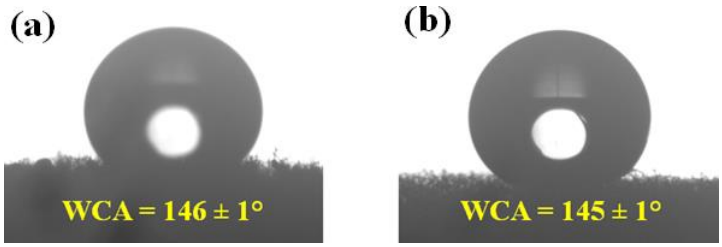

Figure 5.46 Digital images of contact angle of a water droplet on **4′@CF$_3$@melamine** composite (i) before and (ii) after self-cleaning.

5.4 Conclusion

This chapter represents an environment friendly, fast, efficient and cost-effective strategy for separation of various oils from water and oil-water emulsions under different drastic conditions with great efficiency and high recyclability. A hydrophobic MOF derived composite called **4′@CF$_3$@melamine** was fabricated which was utilized for absorption and filtration-based separation processes of oils from oil-water mixtures and water-in-oil emulsions. The obtained separation efficiency for various oils has remained in the range of 95-99%. The separation efficiency for oils remained almost unaltered in various drastic aqueous environments. The absorption capacity achieved for various oils was in the range of 27-40 g/g. The ultra-robust composite showed extraordinary recyclability for both oil-water mixtures (50 times) and water-in-oil emulsions (30 times). The hydrophobic **polymer@4′@CF$_3$** coated on glass substrate also exhibited noticeable self-cleaning ability. In addition to absorption based separation, facile and inexpensive filtration methods were developed for the separation of variety of oils.

5.5 References

1. S. E. Chang, J. Stone, K. Demes and M. Piscitelli, *Ecol. Soc.*, 2014, **19**, 1-25.
2. H. Khordagui and D. Al-Ajmi, *Environ. Manage*, 1993, **17**, 557–562.
3. L. A. Soto, A. V. Botello, S. L. Durán, M. L. L. Partida and A. Y. Arancibia, *Front. Mar. Sci.*, 2014.
4. N. Andrews, N. J. Bennett, P. L. Billon, S. J. Green, A. M. C. Montemayor, S. Amongin, N. J. Gray and U. R. Sumaila, *Energy Res. Soc. Sci.*, 2021, **75**, 102009.
5. P. N. H. Wassenaar and E. M. J. Verbruggen, *Chemosphere*, 2021, **276**, 130113.
6. T. K. Collier, B. F. Anulacion, M. R. Arkoosh, J. P. Dietrich, J. P. Incardona, L. L. Johnson, G. M. Ylitalo and M. S. Myers, *Fish Physiol.*, 2013, **33**, 195-255.
7. N. C. Duke, *Mar. Pollut. Bull.*, 2016, **109**, 700-715.
8. S. A. Zengel, J. Michel and J. A. Dahlin, *Spill Sci. Technol. Bull.*, 2003, **8**, 373-377.
9. R. M. Atlas and T. C. Hazen, *Environ. Sci. Technol.*, 2011, **45**, 6709–6715.
10. S. A. Raya, I. M. Saaid, A. A. Ahmed and A. A. Umar, *J. Pet. Explor. Prod. Technol.*, 2020, **10**, 1711–1728.
11. H. J. Kwon, M. Lee, S. K. Hong, C. Park, S. J. Cho and G. Lim, *ACS Nano*, 2021, **15**, 15815–15823.
12. Y. Paz, Z. Luo, L. Rabenberg and A. Heller, *J. Mater. Res.*, 1995, **10**, 2842 - 2848.
13. H. Chen, F. Wang, H. Fan, R. Hong and W. Li, *Chem. Eng. J.*, 2021, **408**, 127343.

14. M. Wang, Y. Zi, J. Zhu, W. Huang, Z. Zhang and H. Zhang, *Chem. Eng. J.*, 2021, **417**, 129265.
15. Z. Jin, H. Mei, L. Pan, H. Liu and L. Cheng, *ACS Sustain. Chem. Eng.*, 2021, **9**, 4111–4121.
16. C. Y, D. Chen, N. Li, Q. Xu, H. Li, J. He and J. Lu, *ACS Sustain. Chem. Eng.*, 2019, **7**, 2709–2717.
17. H. Li, L. Li, R. Lin, W. Zhou, Z. Zhang, S. Xiang and B. Chen, *EnergyChem*, 2019, **1**, 100006.
18. B. Li, H. Wen, W. Zhou and B. Chen, *J. Phys. Chem. Lett.*, 2014, **5**, 3468–3479.
19. H. D. Lawson, S. P. Walton and C. Chan, *ACS Appl. Mater. Interfaces*, 2021, **13**, 7004–7020.
20. A. Rana, C. Gogoi, S. Ghosh, S. Nandi, S. Kumar, U. Manna and S. Biswas, *New J. Chem.*, 2021, **45**, 20193-20200.
21. D. Himsl, D. Wallacher and M. Hartmann, *Angew. Chem. Int. Ed.*, 2009, **48**, 4639-4642.
22. M. J. Katz, Z. J. Brown, Y. J. Colón, P. W. Siu, K. A. Scheidt, R. Q. Snurr, J. T. Hupp and O. K. Farha, *Chem. Commun.*, 2013, **49**, 9449-9451.
23. N. M. Kreienborg and C. Merten, *Phys. Chem. Chem. Phys.*, 2019, **21**, 3506-3511.
24. J. Winart, B. Shan, S. M. Mcintyre, L. Ye, C. Wang, J. Liu and B. Mu, *Cryst. Growth Des.*, 2020, **20**, 1347–1362.
25. M. Usman, A. Helal, M. M. Abdelnaby, A. M. Alloush, M. Zeama and Z. H. Yamani, *Chem. Rec*, 2021, **21**, 1771-1791.
26. S. Ghosh and S. Biswas, *Microporous Mesoporous Mater.*, 2022, **329**, 111552.
27. R. Dalapati, S. Nandi and S. Biswas, *Dalton Trans.*, 2020, **49**, 8684-8692.
28. M. Yamamoto, N. Nishikawa and Y. N. H. Mayama, Satoshi Yokojima, Shinichiro Nakamura, and Kingo Uchida, *Langmuir*, 2015, **31**, 7355–7363.
29. R. Dalapati, S. Nandi, C. Gogoi, A. Shome and S. Biswas, *ACS Appl. Mater. Interfaces*, 2021, **13**, 8563–8573.
30. Q. Shuai, X. Yang, Y. Luo, H. Tang, X. Luo, Y. Tan and M. Ma, *Mater. Chem. Phys.*, 2015, **162**, 94-99.
31. R. Dalapati, S. Nandi, C. Gogoi, A. Shome and S. Biswas, *ACS Appl. Mater. Interfaces*, 2021, **13**, 8563-8573.
32. D. Zang, F. Liu, M. Zhang, Z. Gao and C. Wang, *Chem. Eng. Res. Des.* , 2015, **102**, 34-41.
33. N. Lv, X. Wang, S. Peng, L. Luo and R. Zhou, *RSC Adv.*, 2018, **8**, 30257-30264.
34. N. Lv, X. Wang, S. Peng, H. Zhang and L. Luo, *Int. J. Environ. Res. Public Health*, 2018, **15**, 969.
35. C. Zhang, C. Dai, H. Zhang, S. Peng, X. Wei and Y. Hu, *Mar. Pollut. Bull.* , 2017, **122**, 129-138.
36. H. Zhang, Y. Li, Y. Xu, Z. Lu, L. Chen, L. Huang and M. Fan, *Phys. Chem. Chem. Phys.* , 2016, **18**, 28297-28306.
37. T. Yin, X. Zhang, X. Liu and C. Wang, *Mar. Pollut. Bull.*, 2017, **118**, 267-274.
38. Y. Cai, D. Chen, N. Li, Q. Xu, H. Li, J. He and J. Lu, *ACS Sustain. Chem. Eng.*, 2019, **7**, 2709−2717.

Conclusions:

Metal-organic frameworks (MOFs) are a special type of organic-inorganic hybrid porous, crystalline coordination architectures. The porosity of MOFs has traditionally been utilized for gas storage, separation, for the separation and storage of miscible and immiscible liquids and even for the selective separation of soluble organic and inorganic compounds. The scope of easy functionalization made MOFs materials highly efficient for the heterogeneous catalysis, proton conduction, and other applications. MOFs have recently gained significant attention in the field of detection and accurate quantification of bio-active and toxic chemicals. This interest stems from the deliberate and rational incorporation of various chemical functionalities into MOF frameworks. In the context of detecting environmental toxins and biomolecules, studies must be conducted in aqueous media to reflect real environmental conditions. However, the synthesis of aqua-stable MOFs that display exceptional selectivity and sensitivity toward specific analytes remains a challenging task in current research. This thesis focuses on the design, synthesis, and characterization of aqua-stable MOFs, with a particular emphasis on conducting comprehensive sensing studies of environmental and biological threats. Moreover, the potential applicability of a hydrophobic MOF coated sponge composite for the selective removal of oil (organic pollutant) from environmental water bodies was also successfully investigated.

To achieve this objective, hard Zr(IV) metal ion and hard carboxylate group containing organic linkers were utilized for the synthesis of aqua-stable MOFs. The frameworks were judiciously functionalized with specific functionalities through specially designed linkers or post-synthetic modification. These specific functionalities serve as recognition sites for targeted analytes, enabling site-specific detection of environmental toxins and biological compounds and also provides the hydrophobicity for the selective capture of lipophilic oil spills.

In my first work, I have presented the fabrication of an exceptionally stable, porous zirconium metal-organic framework functionalized with diamino groups. This framework serves as an effective probe for the selective 'turn-on' fluorometric detection of surfactant; sodium dodecyl sulfate (SDS) in aqueous medium and vitamin B_{12} in HEPES buffer medium. The probe exhibits rapid response times of 50 s and 5 s, setting a new benchmark for detection limits with values of 108 nM for SDS and 45.3 nM for vitamin B_{12}, respectively. Moreover, the applicability of the probe extends to real-world scenarios, as demonstrated in the detection of SDS in environmental water specimens and its capability to analyze different bio-fluids, such as human urine and blood serum for vitamin B_{12}. The probe consistently delivered impressive performance across all detection experiments, and rigorous statistical analyses were conducted to ascertain the reproducibility, originality, and precision of the measurements. To facilitate rapid and on-site detection of both targeted analytes, a MOF-coated cotton composite was engineered. This cost-effective and reusable cotton composite exhibited nanomolar-level sensing capabilities for both SDS and vitamin B_{12}. The experimental results strongly suggested that the electrostatic/H-bonding type interaction between $–NH_2$ of the linker and $–SO^{3-}$ of SDS was responsible for the ‘turn-on’ response of the probe and photo induced energy transfer from

probe to vitamin B_{12} was responsible for the quenching in fluorescence in presence of vitamin B_{12}.

My second work outlines the synthesis and characterization of a new zirconium (Zr) metal-organic framework (MOF) featuring UiO-66 topology by incorporating the rigid benzo[1,2-b:4,5-b']dithiophene-2,6-dicarboxylic acid linker. Solid structures of the MOF were thoroughly examined through X-ray powder diffraction and Rietveld refinement techniques. Additional characterization methods, including thermogravimetric analysis, FE-SEM, EDX, Fourier transform infrared spectroscopy, and elemental analysis, were employed to validate the compound's phase purity. Both the as-synthesized and activated compounds demonstrated thermal stability up to 415 °C in a nitrogen (N_2) environment. The BET surface area of the MOF was determined to be 1228 m^2 g^{-1}. Fluorescence titration experiments revealed that the material exhibited a highly selective and sensitive fluorescence turn-off response to mercury (Hg^{2+}) and nitroantibiotics (nitrofurazone and nitrofurantoin). Interference experiments demonstrated that other cations and antibiotics did not disrupt the detection of Hg^{2+} and nitroantibiotics. Additionally, the probe demonstrated rapid response times (1 min) for both sensing experiments. Remarkably low limits of detection (LODs) were observed for all targeted analytes (LOD values for Hg^{2+}, nitrofurazone, and nitrofurantoin were 5, 156.7, and 96.3 nM, respectively). These LOD values are below the limits regulated by WHO and surpass those reported for most chemodetectors for Hg^{2+} and nitroantibiotics. The on-site detection capability towards the targeted analytes was also demonstrated using a portable MOF-coated paper strips. Experimental studies on the turn-off sensing mechanism of Hg^{2+} suggested that energy transfer through coordination of soft Hg^{2+} with the soft sulfur atoms of the linker was responsible for the fluorescence switch-off response. This proposed reaction mechanism was substantiated by PXRD, XPS, TRPL, EDX, and UV-Vis analyses. Furthermore, resonance energy transfer from MOF to the nitroantibiotics was identified as the probable cause for the fluorescence intensity quenching in presence of nitroantibiotics. The mechanism was supported by a decrease in fluorescence lifetime and maximum overlap between the absorption spectra of nitro-antibiotics and the emission spectra of MOF. Theoretical HOMO-LUMO energy calculations using Gaussian 09 software exhibited good agreement with experimental results. The sensor demonstrated reusability for all the sensing experiments up to five cycles with no significant change in selectivity and sensitivity. The structural integrity and morphology of the reused solids remained similar to the fresh solid, as confirmed by PXRD analysis.

My next work summarized the construction of a highly stable, porous zirconium metal-organic framework functionalized of UiO-67 family with thiourea functional group which serving as a potential probe for the selective 'turn-off' fluorometric detection of adrenaline in HEPES buffer (pH = 7.4) and 6-mercaptopurine (6-MP) in an aqueous medium. The probe exhibited rapid response times of 5 s for both analytes, showcasing the lowest reported detection limits of 1.9 nM and 3.9 nM for adrenaline and 6-MP, respectively. Moreover, the probe's versatility was demonstrated by successfully detecting adrenaline in different bio-fluids (human urine and blood serum) and 6-MP in real environmental water samples. The probe consistently delivered impressive performance across all detection experiments. Rigorous statistical analyses were conducted to ascertain the reproducibility, originality, and precision of the measurements. To facilitate rapid and on-site detection of both targeted analytes, a MOF-

coated cotton composite was fabricated. This cost-effective and reusable cotton composite exhibited nanomolar-level sensing abilities for both adrenaline and 6-MP. Systematic investigations were undertaken to understand the plausible reasons for the 'turn-off' behaviours of the probe in the presence of the quencher. Various instrumental outcomes directed that FRET in presence of adrenaline and IFE in presence of 6-MP are the most possible reasons behind the quenching of fluorescence intensities of the MOF.

In my last work, I have demonstrated the post-synthetic modification of a Zr-UiO-66-OH metal-organic framework with a 2,2,2-trifluoroacetyl (-$COCF_3$) group. The resulting modified MOF, designated as **4′@CF₃**, was utilized to create a hydrophobic composite, named **4′@CF₃@melamine**, employing a commercially available melamine sponge. The melamine sponge was initially coated with polydopamine (PDA) and then immersed in a mixture of **4′@CF₃** and a PDMS-co-PMHS polymer suspension. The addition of **4′@CF₃** enhanced the water contact angle (WCA) of the composite from 106 ± 1° to 145 ± 1°. The hydrophobic **4′@CF₃@melamine** composite demonstrated outstanding efficiency in separating both heavy and light oils from oil-water mixtures (97-99%), maintaining this efficiency over 50 reuse cycles. The absorption capacity for various oils ranged from 27-38 g/g. The composite's oil-water separation performance remained unchanged even in challenging conditions, such as different environmental water samples and varying pH solutions. For water-in-oil emulsions, the emulsion separation efficiency of the **4′@CF₃@melamine** composite ranged from 95-99%, with a flux range of 1461-2288 L/m^2h. The emulsion separation efficiency remained consistent over 30 consecutive cycles of separation. Additionally, the hydrophobic surface of the **4′@CF₃** MOF was exploited for self-cleaning purposes, further showcasing the versatility and effectiveness of the modified MOF-based composite.

Therefore, this thesis focuses on the development of aqua-stable MOFs which can potentially be applicable in environmental remediation and bio-molecule detection. It extensively explores the complex structures of various functionalized Zr(IV) metal ion-containing MOFs. The MOF's functionality is intentionally incorporated into the MOF linker, facilitating its practical use in fluorescence-based detection and quantification of bioactive compounds and organo-toxins. The research also delves into the synthetic methods for producing hydrophobic MOFs tailored for the selective and efficient adsorption of oil spills from oil-water mixture. The presented findings in this thesis are crucial for advancing sustainable environmental practices and aiding in the accurate diagnosis of diseases linked to the uncontrolled release of specific bio-molecules.

Future Prospects:

While the synthesis of numerous aqua MOFs has become feasible through the augmentation of coordination bonds and the utilization of high oxidation state metal ions, but their stability in highly acidic and basic media remains questionable. Thus, my future focus will be directed toward synthesizing MOFs that exhibit stability in extreme pH conditions. I plan to explore the synthesis of MOFs employing redox-active metal ions such as Cr(III), Cu(II), Ni(II), Zn(II), Cd(II), etc. This approach aims to delve into the electrocatalytic applications of MOFs. Furthermore, I intend to investigate MOFs with photoactive linkers and metal ions to explore their potential in photocatalytic reactions and photon upconversion. It is worth noting that MOFs with hard metals are highly labile towards ions like PO_4^{3-}, AsO_4^{3-}, and $O_2^{-\cdot}$, posing limitations for their sensing and adsorption capabilities. Overcoming these limitations will require a strategic approach. Exploring alternative coordinating sites, such as phthalimide, acetoxy, boronic, maleimide, allyloxy, etc., could be useful to overcome such limitations of the applicability of MOFs. Finally, it can be concluded that the journey which inaugurated by the hand of Prof. Robson and Prof. Yagi and his team has now grown enough and its diverse applicability continuously uphill's by various prominent researchers all over the world. I strongly believe that the beautiful affairs between the metal ions and organic linkers will cultivate some more interesting chemistry in the future. I consider myself fortunate to be a modest contributor to this ongoing and expanding journey in metal-organic framework chemistry.

SPRINGER NATURE LICENSE
TERMS AND CONDITIONS

Feb 02, 2024

This Agreement between Mr. Subhrajyoti Ghosh ("You") and Springer Nature ("Springer Nature") consists of your license details and the terms and conditions provided by Springer Nature and Copyright Clearance Center.

License Number	5721131430500
License date	Feb 02, 2024
Licensed Content Publisher	Springer Nature
Licensed Content Publication	Nature
Licensed Content Title	Reticular synthesis and the design of new materials
Licensed Content Author	Omar M. Yaghi et al
Licensed Content Date	Jun 12, 2003
Type of Use	Thesis/Dissertation
Requestor type	non-commercial (non-profit)
Format	print and electronic
Portion	figures/tables/illustrations
Number of figures/tables/illustrations	2
Would you like a high resolution image with your order?	no

Will you be translating?	no
Circulation/distribution	50000 or greater
Author of this Springer Nature content	no
Title of new work	Synthesis Characterization and Applications of Aqua-Stable Metal-Organic Frameworks and their Composites for the Environmental Remediation and Bio-Molecule Sensing
Institution name	Indian Institute of Technology Guwahati
Expected presentation date	Jul 2024
Order reference number	1
Portions	Figure 1a and 1c
Requestor Location	Mr. Subhrajyoti Ghosh IIT Guwahati Guwahati, 781039 India Attn: Mr. Subhrajyoti Ghosh
Total	0.00 USD

Terms and Conditions

Springer Nature Customer Service Centre GmbH Terms and Conditions

The following terms and conditions ("Terms and Conditions") together with the terms specified in your [RightsLink] constitute the License ("License") between you as Licensee and Springer Nature Customer Service Centre GmbH as Licensor. By clicking 'accept' and completing the transaction for your use of the material ("Licensed Material"), you confirm your acceptance of and obligation to be bound by these Terms and Conditions.

1. Grant and Scope of License

1. 1. The Licensor grants you a personal, non-exclusive, non-transferable, non-sublicensable, revocable, world-wide License to reproduce, distribute, communicate to the public, make available, broadcast, electronically transmit or create derivative

works using the Licensed Material for the purpose(s) specified in your RightsLink Licence Details only. Licenses are granted for the specific use requested in the order and for no other use, subject to these Terms and Conditions. You acknowledge and agree that the rights granted to you under this License do not include the right to modify, edit, translate, include in collective works, or create derivative works of the Licensed Material in whole or in part unless expressly stated in your RightsLink Licence Details. You may use the Licensed Material only as permitted under this Agreement and will not reproduce, distribute, display, perform, or otherwise use or exploit any Licensed Material in any way, in whole or in part, except as expressly permitted by this License.

1. 2. You may only use the Licensed Content in the manner and to the extent permitted by these Terms and Conditions, by your RightsLink Licence Details and by any applicable laws.

1. 3. A separate license may be required for any additional use of the Licensed Material, e.g. where a license has been purchased for print use only, separate permission must be obtained for electronic re-use. Similarly, a License is only valid in the language selected and does not apply for editions in other languages unless additional translation rights have been granted separately in the License.

1. 4. Any content within the Licensed Material that is owned by third parties is expressly excluded from the License.

1. 5. Rights for additional reuses such as custom editions, computer/mobile applications, film or TV reuses and/or any other derivative rights requests require additional permission and may be subject to an additional fee. Please apply to journalpermissions@springernature.com or bookpermissions@springernature.com for these rights.

2. Reservation of Rights

Licensor reserves all rights not expressly granted to you under this License. You acknowledge and agree that nothing in this License limits or restricts Licensor's rights in or use of the Licensed Material in any way. Neither this License, nor any act, omission, or statement by Licensor or you, conveys any ownership right to you in any Licensed Material, or to any element or portion thereof. As between Licensor and you, Licensor owns and retains all right, title, and interest in and to the Licensed Material subject to the license granted in Section 1.1. Your permission to use the Licensed Material is expressly conditioned on you not impairing Licensor's or the applicable copyright owner's rights in the Licensed Material in any way.

3. Restrictions on use

3. 1. Minor editing privileges are allowed for adaptations for stylistic purposes or formatting purposes provided such alterations do not alter the original meaning or intention of the Licensed Material and the new figure(s) are still accurate and representative of the Licensed Material. Any other changes including but not limited to, cropping, adapting, and/or omitting material that affect the meaning, intention or moral rights of the author(s) are strictly prohibited.

3. 2. You must not use any Licensed Material as part of any design or trademark.

3. 3. Licensed Material may be used in Open Access Publications (OAP), but any such reuse must include a clear acknowledgment of this permission visible at the same time as the figures/tables/illustration or abstract and which must indicate that the Licensed Material is not part of the governing OA license but has been reproduced with permission. This may be indicated according to any standard

referencing system but must include at a minimum 'Book/Journal title, Author, Journal Name (if applicable), Volume (if applicable), Publisher, Year, reproduced with permission from SNCSC".

4. STM Permission Guidelines

4. 1. An alternative scope of license may apply to signatories of the STM Permissions Guidelines ("STM PG") as amended from time to time and made available at https://www.stm-assoc.org/intellectual-property/permissions/permissions-guidelines/.

4. 2. For content reuse requests that qualify for permission under the STM PG, and which may be updated from time to time, the STM PG supersede the terms and conditions contained in this License.

4. 3. If a License has been granted under the STM PG, but the STM PG no longer apply at the time of publication, further permission must be sought from the Rightsholder. Contact journalpermissions@springernature.com or bookpermissions@springernature.com for these rights.

5. Duration of License

5. 1. Unless otherwise indicated on your License, a License is valid from the date of purchase ("License Date") until the end of the relevant period in the below table:

Reuse in a medical communications project	Reuse up to distribution or time period indicated in License
Reuse in a dissertation/thesis	Lifetime of thesis
Reuse in a journal/magazine	Lifetime of journal/magazine
Reuse in a book/textbook	Lifetime of edition
Reuse on a website	1 year unless otherwise specified in the License
Reuse in a presentation/slide kit/poster	Lifetime of presentation/slide kit/poster. Note: publication whether electronic or in print of presentation/slide kit/poster may require further permission.
Reuse in conference proceedings	Lifetime of conference proceedings
Reuse in an annual report	Lifetime of annual report
Reuse in training/CME materials	Reuse up to distribution or time period indicated in License
Reuse in newsmedia	Lifetime of newsmedia
Reuse in coursepack/classroom materials	Reuse up to distribution and/or time period indicated in license

6. Acknowledgement

6. 1. The Licensor's permission must be acknowledged next to the Licensed Material in print. In electronic form, this acknowledgement must be visible at the same time as the figures/tables/illustrations or abstract and must be hyperlinked to the journal/book's homepage.

6. 2. Acknowledgement may be provided according to any standard referencing system and at a minimum should include "Author, Article/Book Title, Journal

name/Book imprint, volume, page number, year, Springer Nature".

7. Reuse in a dissertation or thesis

7. 1. Where 'reuse in a dissertation/thesis' has been selected, the following terms apply: Print rights of the Version of Record are provided for; electronic rights for use only on institutional repository as defined by the Sherpa guideline (www.sherpa.ac.uk/romeo/) and only up to what is required by the awarding institution.

7. 2. For theses published under an ISBN or ISSN, separate permission is required. Please contact journalpermissions@springernature.com or bookpermissions@springernature.com for these rights.

7. 3. Authors must properly cite the published manuscript in their thesis according to current citation standards and include the following acknowledgement: '*Reproduced with permission from Springer Nature*'.

8. License Fee

You must pay the fee set forth in the License Agreement (the "License Fees"). All amounts payable by you under this License are exclusive of any sales, use, withholding, value added or similar taxes, government fees or levies or other assessments. Collection and/or remittance of such taxes to the relevant tax authority shall be the responsibility of the party who has the legal obligation to do so.

9. Warranty

9. 1. The Licensor warrants that it has, to the best of its knowledge, the rights to license reuse of the Licensed Material. **You are solely responsible for ensuring that the material you wish to license is original to the Licensor and does not carry the copyright of another entity or third party (as credited in the published version).** If the credit line on any part of the Licensed Material indicates that it was reprinted or adapted with permission from another source, then you should seek additional permission from that source to reuse the material.

9. 2. EXCEPT FOR THE EXPRESS WARRANTY STATED HEREIN AND TO THE EXTENT PERMITTED BY APPLICABLE LAW, LICENSOR PROVIDES THE LICENSED MATERIAL "AS IS" AND MAKES NO OTHER REPRESENTATION OR WARRANTY. LICENSOR EXPRESSLY DISCLAIMS ANY LIABILITY FOR ANY CLAIM ARISING FROM OR OUT OF THE CONTENT, INCLUDING BUT NOT LIMITED TO ANY ERRORS, INACCURACIES, OMISSIONS, OR DEFECTS CONTAINED THEREIN, AND ANY IMPLIED OR EXPRESS WARRANTY AS TO MERCHANTABILITY OR FITNESS FOR A PARTICULAR PURPOSE. IN NO EVENT SHALL LICENSOR BE LIABLE TO YOU OR ANY OTHER PARTY OR ANY OTHER PERSON OR FOR ANY SPECIAL, CONSEQUENTIAL, INCIDENTAL, INDIRECT, PUNITIVE, OR EXEMPLARY DAMAGES, HOWEVER CAUSED, ARISING OUT OF OR IN CONNECTION WITH THE DOWNLOADING, VIEWING OR USE OF THE LICENSED MATERIAL REGARDLESS OF THE FORM OF ACTION, WHETHER FOR BREACH OF CONTRACT, BREACH OF WARRANTY, TORT, NEGLIGENCE, INFRINGEMENT OR OTHERWISE (INCLUDING, WITHOUT LIMITATION, DAMAGES BASED ON LOSS OF PROFITS, DATA, FILES, USE, BUSINESS OPPORTUNITY OR CLAIMS OF THIRD PARTIES), AND WHETHER OR NOT THE PARTY HAS BEEN ADVISED OF THE POSSIBILITY OF SUCH DAMAGES. THIS LIMITATION APPLIES NOTWITHSTANDING ANY FAILURE OF ESSENTIAL PURPOSE OF ANY LIMITED REMEDY PROVIDED HEREIN.

10. Termination and Cancellation

10. 1. The License and all rights granted hereunder will continue until the end of the applicable period shown in Clause 5.1 above. Thereafter, this license will be terminated and all rights granted hereunder will cease.

10. 2. Licensor reserves the right to terminate the License in the event that payment is not received in full or if you breach the terms of this License.

11. General

11. 1. The License and the rights and obligations of the parties hereto shall be construed, interpreted and determined in accordance with the laws of the Federal Republic of Germany without reference to the stipulations of the CISG (United Nations Convention on Contracts for the International Sale of Goods) or to Germany's choice-of-law principle.

11. 2. The parties acknowledge and agree that any controversies and disputes arising out of this License shall be decided exclusively by the courts of or having jurisdiction for Heidelberg, Germany, as far as legally permissible.

11. 3. This License is solely for Licensor's and Licensee's benefit. It is not for the benefit of any other person or entity.

Questions? For questions on Copyright Clearance Center accounts or website issues please contact springernaturesupport@copyright.com or +1-855-239-3415 (toll free in the US) or +1-978-646-2777. For questions on Springer Nature licensing please visit https://www.springernature.com/gp/partners/rights-permissions-third-party-distribution

Other Conditions:

Version 1.4 - Dec 2022

Questions? customercare@copyright.com.

ELSEVIER LICENSE
TERMS AND CONDITIONS

Feb 03, 2024

This Agreement between Mr. Subhrajyoti Ghosh ("You") and Elsevier ("Elsevier") consists of your license details and the terms and conditions provided by Elsevier and Copyright Clearance Center.

License Number	5721140629766
License date	Feb 03, 2024
Licensed Content Publisher	Elsevier
Licensed Content Publication	Sensors and Actuators B: Chemical
Licensed Content Title	Europium-based metal-organic framework containing characteristic metal chains: A novel turn-on fluorescence sensor for simultaneous high-performance detection and removal of tetracycline
Licensed Content Author	Yijian Zhao,Qinzhi Wang,Haihua Wang,Hui Zhangsun,Xinyu Sun,Tong Bu,Yingnan Liu,Wenze Wang,Zhihao Xu,Li Wang
Licensed Content Date	1 May 2021
Licensed Content Volume	334
Licensed Content Issue	n/a
Licensed Content Pages	1
Start Page	129610
End Page	0

Type of Use	reuse in a thesis/dissertation
Portion	figures/tables/illustrations
Number of figures/tables/illustrations	1
Format	both print and electronic
Are you the author of this Elsevier article?	No
Will you be translating?	No
Title of new work	Synthesis Characterization and Applications of Aqua-Stable Metal-Organic Frameworks and their Composites for the Environmental Remediation and Bio-Molecule Sensing
Institution name	Indian Institute of Technology Guwahati
Expected presentation date	Jul 2024
Order reference number	2
Portions	Graphical abstract
Requestor Location	Mr. Subhrajyoti Ghosh IIT Guwahati Guwahati, 781039 India Attn: Mr. Subhrajyoti Ghosh
Publisher Tax ID	GB 494 6272 12
Total	0.00 USD
Terms and Conditions	

INTRODUCTION

1. The publisher for this copyrighted material is Elsevier. By clicking "accept" in connection with completing this licensing transaction, you agree that the following terms and conditions apply to this transaction (along with the Billing and Payment terms and conditions established by Copyright Clearance Center, Inc. ("CCC"), at the time that you opened your RightsLink account and that are available at any time at https://myaccount.copyright.com).

GENERAL TERMS

2. Elsevier hereby grants you permission to reproduce the aforementioned material subject to the terms and conditions indicated.

3. Acknowledgement: If any part of the material to be used (for example, figures) has appeared in our publication with credit or acknowledgement to another source, permission must also be sought from that source. If such permission is not obtained then that material may not be included in your publication/copies. Suitable acknowledgement to the source must be made, either as a footnote or in a reference list at the end of your publication, as follows:

"Reprinted from Publication title, Vol /edition number, Author(s), Title of article / title of chapter, Pages No., Copyright (Year), with permission from Elsevier [OR APPLICABLE SOCIETY COPYRIGHT OWNER]." Also Lancet special credit - "Reprinted from The Lancet, Vol. number, Author(s), Title of article, Pages No., Copyright (Year), with permission from Elsevier."

4. Reproduction of this material is confined to the purpose and/or media for which permission is hereby given. The material may not be reproduced or used in any other way, including use in combination with an artificial intelligence tool (including to train an algorithm, test, process, analyse, generate output and/or develop any form of artificial intelligence tool), or to create any derivative work and/or service (including resulting from the use of artificial intelligence tools).

5. Altering/Modifying Material: Not Permitted. However figures and illustrations may be altered/adapted minimally to serve your work. Any other abbreviations, additions, deletions and/or any other alterations shall be made only with prior written authorization of Elsevier Ltd. (Please contact Elsevier's permissions helpdesk here). No modifications can be made to any Lancet figures/tables and they must be reproduced in full.

6. If the permission fee for the requested use of our material is waived in this instance, please be advised that your future requests for Elsevier materials may attract a fee.

7. Reservation of Rights: Publisher reserves all rights not specifically granted in the combination of (i) the license details provided by you and accepted in the course of this licensing transaction, (ii) these terms and conditions and (iii) CCC's Billing and Payment terms and conditions.

8. License Contingent Upon Payment: While you may exercise the rights licensed immediately upon issuance of the license at the end of the licensing process for the transaction, provided that you have disclosed complete and accurate details of your proposed use, no license is finally effective unless and until full payment is received from you (either by publisher or by CCC) as provided in CCC's Billing and Payment terms and conditions. If full payment is not received on a timely basis, then any license preliminarily granted shall be deemed automatically revoked and shall be void as if never granted. Further, in the event that you breach any of these terms and conditions or any of CCC's Billing and Payment terms and conditions, the license is automatically revoked and shall be void as if never granted. Use of materials as described in a revoked license, as well as any use of the materials beyond the scope of an unrevoked license, may constitute copyright infringement and publisher reserves the right to take any and all action to protect its copyright in the materials.

9. Warranties: Publisher makes no representations or warranties with respect to the licensed material.

10. Indemnity: You hereby indemnify and agree to hold harmless publisher and CCC, and their respective officers, directors, employees and agents, from and against any and all claims arising out of your use of the licensed material other than as specifically authorized pursuant to this license.

11. No Transfer of License: This license is personal to you and may not be sublicensed, assigned, or transferred by you to any other person without publisher's written permission.

12. No Amendment Except in Writing: This license may not be amended except in a writing signed by both parties (or, in the case of publisher, by CCC on publisher's behalf).

13. Objection to Contrary Terms: Publisher hereby objects to any terms contained in any purchase order, acknowledgment, check endorsement or other writing prepared by you, which terms are inconsistent with these terms and conditions or CCC's Billing and Payment terms and conditions. These terms and conditions, together with CCC's Billing and Payment terms and conditions (which are incorporated herein), comprise the entire agreement between you and publisher (and CCC) concerning this licensing transaction. In the event of any conflict between your obligations established by these terms and conditions and those established by CCC's Billing and Payment terms and conditions, these terms and conditions shall control.

14. Revocation: Elsevier or Copyright Clearance Center may deny the permissions described in this License at their sole discretion, for any reason or no reason, with a full refund payable to you. Notice of such denial will be made using the contact information provided by you. Failure to receive such notice will not alter or invalidate the denial. In no event will Elsevier or Copyright Clearance Center be responsible or liable for any costs, expenses or damage incurred by you as a result of a denial of your permission request, other than a refund of the amount(s) paid by you to Elsevier and/or Copyright Clearance Center for denied permissions.

LIMITED LICENSE

The following terms and conditions apply only to specific license types:

15. **Translation**: This permission is granted for non-exclusive world **English** rights only unless your license was granted for translation rights. If you licensed translation rights you may only translate this content into the languages you requested. A professional translator must perform all translations and reproduce the content word for word preserving the integrity of the article.

16. **Posting licensed content on any Website**: The following terms and conditions apply as follows: Licensing material from an Elsevier journal: All content posted to the web site must maintain the copyright information line on the bottom of each image; A hyper-text must be included to the Homepage of the journal from which you are licensing at http://www.sciencedirect.com/science/journal/xxxxx or the Elsevier homepage for books at http://www.elsevier.com; Central Storage: This license does not include permission for a scanned version of the material to be stored in a central repository such as that provided by Heron/XanEdu.

Licensing material from an Elsevier book: A hyper-text link must be included to the Elsevier homepage at http://www.elsevier.com . All content posted to the web site must maintain the copyright information line on the bottom of each image.

Posting licensed content on Electronic reserve: In addition to the above the following clauses are applicable: The web site must be password-protected and made available only

to bona fide students registered on a relevant course. This permission is granted for 1 year only. You may obtain a new license for future website posting.

17. **For journal authors:** the following clauses are applicable in addition to the above:

Preprints:

A preprint is an author's own write-up of research results and analysis, it has not been peer-reviewed, nor has it had any other value added to it by a publisher (such as formatting, copyright, technical enhancement etc.).

Authors can share their preprints anywhere at any time. Preprints should not be added to or enhanced in any way in order to appear more like, or to substitute for, the final versions of articles however authors can update their preprints on arXiv or RePEc with their Accepted Author Manuscript (see below).

If accepted for publication, we encourage authors to link from the preprint to their formal publication via its DOI. Millions of researchers have access to the formal publications on ScienceDirect, and so links will help users to find, access, cite and use the best available version. Please note that Cell Press, The Lancet and some society-owned have different preprint policies. Information on these policies is available on the journal homepage.

Accepted Author Manuscripts: An accepted author manuscript is the manuscript of an article that has been accepted for publication and which typically includes author-incorporated changes suggested during submission, peer review and editor-author communications.

Authors can share their accepted author manuscript:

- immediately
  - via their non-commercial person homepage or blog
  - by updating a preprint in arXiv or RePEc with the accepted manuscript
  - via their research institute or institutional repository for internal institutional uses or as part of an invitation-only research collaboration work-group
  - directly by providing copies to their students or to research collaborators for their personal use
  - for private scholarly sharing as part of an invitation-only work group on commercial sites with which Elsevier has an agreement
- After the embargo period
  - via non-commercial hosting platforms such as their institutional repository
  - via commercial sites with which Elsevier has an agreement

In all cases accepted manuscripts should:

- link to the formal publication via its DOI
- bear a CC-BY-NC-ND license - this is easy to do
- if aggregated with other manuscripts, for example in a repository or other site, be shared in alignment with our hosting policy not be added to or enhanced in any way to appear more like, or to substitute for, the published journal article.

Published journal article (JPA): A published journal article (PJA) is the definitive final record of published research that appears or will appear in the journal and embodies all value-adding publishing activities including peer review co-ordination, copy-editing, formatting, (if relevant) pagination and online enrichment.

Policies for sharing publishing journal articles differ for subscription and gold open access articles:

Subscription Articles: If you are an author, please share a link to your article rather than the full-text. Millions of researchers have access to the formal publications on ScienceDirect, and so links will help your users to find, access, cite, and use the best available version.

Theses and dissertations which contain embedded PJAs as part of the formal submission can be posted publicly by the awarding institution with DOI links back to the formal publications on ScienceDirect.

If you are affiliated with a library that subscribes to ScienceDirect you have additional private sharing rights for others' research accessed under that agreement. This includes use for classroom teaching and internal training at the institution (including use in course packs and courseware programs), and inclusion of the article for grant funding purposes.

Gold Open Access Articles: May be shared according to the author-selected end-user license and should contain a CrossMark logo, the end user license, and a DOI link to the formal publication on ScienceDirect.

Please refer to Elsevier's posting policy for further information.

18. **For book authors** the following clauses are applicable in addition to the above: Authors are permitted to place a brief summary of their work online only. You are not allowed to download and post the published electronic version of your chapter, nor may you scan the printed edition to create an electronic version. **Posting to a repository:** Authors are permitted to post a summary of their chapter only in their institution's repository.

19. **Thesis/Dissertation**: If your license is for use in a thesis/dissertation your thesis may be submitted to your institution in either print or electronic form. Should your thesis be published commercially, please reapply for permission. These requirements include permission for the Library and Archives of Canada to supply single copies, on demand, of the complete thesis and include permission for Proquest/UMI to supply single copies, on demand, of the complete thesis. Should your thesis be published commercially, please reapply for permission. Theses and dissertations which contain embedded PJAs as part of the formal submission can be posted publicly by the awarding institution with DOI links back to the formal publications on ScienceDirect.

Elsevier Open Access Terms and Conditions

You can publish open access with Elsevier in hundreds of open access journals or in nearly 2000 established subscription journals that support open access publishing. Permitted third party re-use of these open access articles is defined by the author's choice of Creative Commons user license. See our open access license policy for more information.

Terms & Conditions applicable to all Open Access articles published with Elsevier:

Any reuse of the article must not represent the author as endorsing the adaptation of the article nor should the article be modified in such a way as to damage the author's honour or reputation. If any changes have been made, such changes must be clearly indicated.

The author(s) must be appropriately credited and we ask that you include the end user license and a DOI link to the formal publication on ScienceDirect.

If any part of the material to be used (for example, figures) has appeared in our publication with credit or acknowledgement to another source it is the responsibility of the

user to ensure their reuse complies with the terms and conditions determined by the rights holder.

Additional Terms & Conditions applicable to each Creative Commons user license:

CC BY: The CC-BY license allows users to copy, to create extracts, abstracts and new works from the Article, to alter and revise the Article and to make commercial use of the Article (including reuse and/or resale of the Article by commercial entities), provided the user gives appropriate credit (with a link to the formal publication through the relevant DOI), provides a link to the license, indicates if changes were made and the licensor is not represented as endorsing the use made of the work. The full details of the license are available at http://creativecommons.org/licenses/by/4.0.

CC BY NC SA: The CC BY-NC-SA license allows users to copy, to create extracts, abstracts and new works from the Article, to alter and revise the Article, provided this is not done for commercial purposes, and that the user gives appropriate credit (with a link to the formal publication through the relevant DOI), provides a link to the license, indicates if changes were made and the licensor is not represented as endorsing the use made of the work. Further, any new works must be made available on the same conditions. The full details of the license are available at http://creativecommons.org/licenses/by-nc-sa/4.0.

CC BY NC ND: The CC BY-NC-ND license allows users to copy and distribute the Article, provided this is not done for commercial purposes and further does not permit distribution of the Article if it is changed or edited in any way, and provided the user gives appropriate credit (with a link to the formal publication through the relevant DOI), provides a link to the license, and that the licensor is not represented as endorsing the use made of the work. The full details of the license are available at http://creativecommons.org/licenses/by-nc-nd/4.0. Any commercial reuse of Open Access articles published with a CC BY NC SA or CC BY NC ND license requires permission from Elsevier and will be subject to a fee.

Commercial reuse includes:

- Associating advertising with the full text of the Article
- Charging fees for document delivery or access
- Article aggregation
- Systematic distribution via e-mail lists or share buttons

Posting or linking by commercial companies for use by customers of those companies.

20. **Other Conditions**:

v1.10

Questions? customercare@copyright.com.

ELSEVIER LICENSE
TERMS AND CONDITIONS

Feb 03, 2024

This Agreement between Mr. Subhrajyoti Ghosh ("You") and Elsevier ("Elsevier") consists of your license details and the terms and conditions provided by Elsevier and Copyright Clearance Center.

License Number	5721150777855
License date	Feb 03, 2024
Licensed Content Publisher	Elsevier
Licensed Content Publication	Energy Storage Materials
Licensed Content Title	Metal organic frameworks for energy storage and conversion
Licensed Content Author	Yang Zhao,Zhongxin Song,Xia Li,Qian Sun,Niancai Cheng,Stephen Lawes,Xueliang Sun
Licensed Content Date	Jan 1, 2016
Licensed Content Volume	2
Licensed Content Issue	n/a
Licensed Content Pages	28
Start Page	35
End Page	62
Type of Use	reuse in a thesis/dissertation

Portion	figures/tables/illustrations
Number of figures/tables/illustrations	1
Format	both print and electronic
Are you the author of this Elsevier article?	No
Will you be translating?	No
Title of new work	Synthesis Characterization and Applications of Aqua-Stable Metal-Organic Frameworks and their Composites for the Environmental Remediation and Bio-Molecule Sensing
Institution name	Indian Institute of Technology Guwahati
Expected presentation date	Jul 2024
Order reference number	4
Portions	Figure 2
Requestor Location	Mr. Subhrajyoti Ghosh IIT Guwahati Guwahati, 781039 India Attn: Mr. Subhrajyoti Ghosh
Publisher Tax ID	GB 494 6272 12
Total	0.00 USD
Terms and Conditions	

INTRODUCTION

1. The publisher for this copyrighted material is Elsevier. By clicking "accept" in connection with completing this licensing transaction, you agree that the following terms

and conditions apply to this transaction (along with the Billing and Payment terms and conditions established by Copyright Clearance Center, Inc. ("CCC"), at the time that you opened your RightsLink account and that are available at any time at https://myaccount.copyright.com).

GENERAL TERMS

2. Elsevier hereby grants you permission to reproduce the aforementioned material subject to the terms and conditions indicated.

3. Acknowledgement: If any part of the material to be used (for example, figures) has appeared in our publication with credit or acknowledgement to another source, permission must also be sought from that source. If such permission is not obtained then that material may not be included in your publication/copies. Suitable acknowledgement to the source must be made, either as a footnote or in a reference list at the end of your publication, as follows:

"Reprinted from Publication title, Vol /edition number, Author(s), Title of article / title of chapter, Pages No., Copyright (Year), with permission from Elsevier [OR APPLICABLE SOCIETY COPYRIGHT OWNER]." Also Lancet special credit - "Reprinted from The Lancet, Vol. number, Author(s), Title of article, Pages No., Copyright (Year), with permission from Elsevier."

4. Reproduction of this material is confined to the purpose and/or media for which permission is hereby given. The material may not be reproduced or used in any other way, including use in combination with an artificial intelligence tool (including to train an algorithm, test, process, analyse, generate output and/or develop any form of artificial intelligence tool), or to create any derivative work and/or service (including resulting from the use of artificial intelligence tools).

5. Altering/Modifying Material: Not Permitted. However figures and illustrations may be altered/adapted minimally to serve your work. Any other abbreviations, additions, deletions and/or any other alterations shall be made only with prior written authorization of Elsevier Ltd. (Please contact Elsevier's permissions helpdesk here). No modifications can be made to any Lancet figures/tables and they must be reproduced in full.

6. If the permission fee for the requested use of our material is waived in this instance, please be advised that your future requests for Elsevier materials may attract a fee.

7. Reservation of Rights: Publisher reserves all rights not specifically granted in the combination of (i) the license details provided by you and accepted in the course of this licensing transaction, (ii) these terms and conditions and (iii) CCC's Billing and Payment terms and conditions.

8. License Contingent Upon Payment: While you may exercise the rights licensed immediately upon issuance of the license at the end of the licensing process for the transaction, provided that you have disclosed complete and accurate details of your proposed use, no license is finally effective unless and until full payment is received from you (either by publisher or by CCC) as provided in CCC's Billing and Payment terms and conditions. If full payment is not received on a timely basis, then any license preliminarily granted shall be deemed automatically revoked and shall be void as if never granted. Further, in the event that you breach any of these terms and conditions or any of CCC's Billing and Payment terms and conditions, the license is automatically revoked and shall be void as if never granted. Use of materials as described in a revoked license, as well as any use of the materials beyond the scope of an unrevoked license, may constitute copyright infringement and publisher reserves the right to take any and all action to protect its copyright in the materials.

9. Warranties: Publisher makes no representations or warranties with respect to the licensed material.

10. Indemnity: You hereby indemnify and agree to hold harmless publisher and CCC, and their respective officers, directors, employees and agents, from and against any and all claims arising out of your use of the licensed material other than as specifically authorized pursuant to this license.

11. No Transfer of License: This license is personal to you and may not be sublicensed, assigned, or transferred by you to any other person without publisher's written permission.

12. No Amendment Except in Writing: This license may not be amended except in a writing signed by both parties (or, in the case of publisher, by CCC on publisher's behalf).

13. Objection to Contrary Terms: Publisher hereby objects to any terms contained in any purchase order, acknowledgment, check endorsement or other writing prepared by you, which terms are inconsistent with these terms and conditions or CCC's Billing and Payment terms and conditions. These terms and conditions, together with CCC's Billing and Payment terms and conditions (which are incorporated herein), comprise the entire agreement between you and publisher (and CCC) concerning this licensing transaction. In the event of any conflict between your obligations established by these terms and conditions and those established by CCC's Billing and Payment terms and conditions, these terms and conditions shall control.

14. Revocation: Elsevier or Copyright Clearance Center may deny the permissions described in this License at their sole discretion, for any reason or no reason, with a full refund payable to you. Notice of such denial will be made using the contact information provided by you. Failure to receive such notice will not alter or invalidate the denial. In no event will Elsevier or Copyright Clearance Center be responsible or liable for any costs, expenses or damage incurred by you as a result of a denial of your permission request, other than a refund of the amount(s) paid by you to Elsevier and/or Copyright Clearance Center for denied permissions.

LIMITED LICENSE

The following terms and conditions apply only to specific license types:

15. **Translation**: This permission is granted for non-exclusive world **English** rights only unless your license was granted for translation rights. If you licensed translation rights you may only translate this content into the languages you requested. A professional translator must perform all translations and reproduce the content word for word preserving the integrity of the article.

16. **Posting licensed content on any Website**: The following terms and conditions apply as follows: Licensing material from an Elsevier journal: All content posted to the web site must maintain the copyright information line on the bottom of each image; A hyper-text must be included to the Homepage of the journal from which you are licensing at http://www.sciencedirect.com/science/journal/xxxxx or the Elsevier homepage for books at http://www.elsevier.com; Central Storage: This license does not include permission for a scanned version of the material to be stored in a central repository such as that provided by Heron/XanEdu.

Licensing material from an Elsevier book: A hyper-text link must be included to the Elsevier homepage at http://www.elsevier.com . All content posted to the web site must maintain the copyright information line on the bottom of each image.

Posting licensed content on Electronic reserve: In addition to the above the following clauses are applicable: The web site must be password-protected and made available only

to bona fide students registered on a relevant course. This permission is granted for 1 year only. You may obtain a new license for future website posting.

17. **For journal authors:** the following clauses are applicable in addition to the above:

Preprints:

A preprint is an author's own write-up of research results and analysis, it has not been peer-reviewed, nor has it had any other value added to it by a publisher (such as formatting, copyright, technical enhancement etc.).

Authors can share their preprints anywhere at any time. Preprints should not be added to or enhanced in any way in order to appear more like, or to substitute for, the final versions of articles however authors can update their preprints on arXiv or RePEc with their Accepted Author Manuscript (see below).

If accepted for publication, we encourage authors to link from the preprint to their formal publication via its DOI. Millions of researchers have access to the formal publications on ScienceDirect, and so links will help users to find, access, cite and use the best available version. Please note that Cell Press, The Lancet and some society-owned have different preprint policies. Information on these policies is available on the journal homepage.

Accepted Author Manuscripts: An accepted author manuscript is the manuscript of an article that has been accepted for publication and which typically includes author-incorporated changes suggested during submission, peer review and editor-author communications.

Authors can share their accepted author manuscript:

- immediately
  - via their non-commercial person homepage or blog
  - by updating a preprint in arXiv or RePEc with the accepted manuscript
  - via their research institute or institutional repository for internal institutional uses or as part of an invitation-only research collaboration work-group
  - directly by providing copies to their students or to research collaborators for their personal use
  - for private scholarly sharing as part of an invitation-only work group on commercial sites with which Elsevier has an agreement
- After the embargo period
  - via non-commercial hosting platforms such as their institutional repository
  - via commercial sites with which Elsevier has an agreement

In all cases accepted manuscripts should:

- link to the formal publication via its DOI
- bear a CC-BY-NC-ND license - this is easy to do
- if aggregated with other manuscripts, for example in a repository or other site, be shared in alignment with our hosting policy not be added to or enhanced in any way to appear more like, or to substitute for, the published journal article.

Published journal article (JPA): A published journal article (PJA) is the definitive final record of published research that appears or will appear in the journal and embodies all value-adding publishing activities including peer review co-ordination, copy-editing, formatting, (if relevant) pagination and online enrichment.

Policies for sharing publishing journal articles differ for subscription and gold open access articles:

Subscription Articles: If you are an author, please share a link to your article rather than the full-text. Millions of researchers have access to the formal publications on ScienceDirect, and so links will help your users to find, access, cite, and use the best available version.

Theses and dissertations which contain embedded PJAs as part of the formal submission can be posted publicly by the awarding institution with DOI links back to the formal publications on ScienceDirect.

If you are affiliated with a library that subscribes to ScienceDirect you have additional private sharing rights for others' research accessed under that agreement. This includes use for classroom teaching and internal training at the institution (including use in course packs and courseware programs), and inclusion of the article for grant funding purposes.

Gold Open Access Articles: May be shared according to the author-selected end-user license and should contain a CrossMark logo, the end user license, and a DOI link to the formal publication on ScienceDirect.

Please refer to Elsevier's posting policy for further information.

18. **For book authors** the following clauses are applicable in addition to the above: Authors are permitted to place a brief summary of their work online only. You are not allowed to download and post the published electronic version of your chapter, nor may you scan the printed edition to create an electronic version. **Posting to a repository:** Authors are permitted to post a summary of their chapter only in their institution's repository.

19. **Thesis/Dissertation**: If your license is for use in a thesis/dissertation your thesis may be submitted to your institution in either print or electronic form. Should your thesis be published commercially, please reapply for permission. These requirements include permission for the Library and Archives of Canada to supply single copies, on demand, of the complete thesis and include permission for Proquest/UMI to supply single copies, on demand, of the complete thesis. Should your thesis be published commercially, please reapply for permission. Theses and dissertations which contain embedded PJAs as part of the formal submission can be posted publicly by the awarding institution with DOI links back to the formal publications on ScienceDirect.

Elsevier Open Access Terms and Conditions

You can publish open access with Elsevier in hundreds of open access journals or in nearly 2000 established subscription journals that support open access publishing. Permitted third party re-use of these open access articles is defined by the author's choice of Creative Commons user license. See our open access license policy for more information.

Terms & Conditions applicable to all Open Access articles published with Elsevier:

Any reuse of the article must not represent the author as endorsing the adaptation of the article nor should the article be modified in such a way as to damage the author's honour or reputation. If any changes have been made, such changes must be clearly indicated.

The author(s) must be appropriately credited and we ask that you include the end user license and a DOI link to the formal publication on ScienceDirect.

If any part of the material to be used (for example, figures) has appeared in our publication with credit or acknowledgement to another source it is the responsibility of the

user to ensure their reuse complies with the terms and conditions determined by the rights holder.

Additional Terms & Conditions applicable to each Creative Commons user license:

CC BY: The CC-BY license allows users to copy, to create extracts, abstracts and new works from the Article, to alter and revise the Article and to make commercial use of the Article (including reuse and/or resale of the Article by commercial entities), provided the user gives appropriate credit (with a link to the formal publication through the relevant DOI), provides a link to the license, indicates if changes were made and the licensor is not represented as endorsing the use made of the work. The full details of the license are available at http://creativecommons.org/licenses/by/4.0.

CC BY NC SA: The CC BY-NC-SA license allows users to copy, to create extracts, abstracts and new works from the Article, to alter and revise the Article, provided this is not done for commercial purposes, and that the user gives appropriate credit (with a link to the formal publication through the relevant DOI), provides a link to the license, indicates if changes were made and the licensor is not represented as endorsing the use made of the work. Further, any new works must be made available on the same conditions. The full details of the license are available at http://creativecommons.org/licenses/by-nc-sa/4.0.

CC BY NC ND: The CC BY-NC-ND license allows users to copy and distribute the Article, provided this is not done for commercial purposes and further does not permit distribution of the Article if it is changed or edited in any way, and provided the user gives appropriate credit (with a link to the formal publication through the relevant DOI), provides a link to the license, and that the licensor is not represented as endorsing the use made of the work. The full details of the license are available at http://creativecommons.org/licenses/by-nc-nd/4.0. Any commercial reuse of Open Access articles published with a CC BY NC SA or CC BY NC ND license requires permission from Elsevier and will be subject to a fee.

Commercial reuse includes:

- Associating advertising with the full text of the Article
- Charging fees for document delivery or access
- Article aggregation
- Systematic distribution via e-mail lists or share buttons

Posting or linking by commercial companies for use by customers of those companies.

20. **Other Conditions**:

v1.10

Questions? customercare@copyright.com.

SPRINGER NATURE LICENSE
TERMS AND CONDITIONS

Feb 03, 2024

This Agreement between Mr. Subhrajyoti Ghosh ("You") and Springer Nature ("Springer Nature") consists of your license details and the terms and conditions provided by Springer Nature and Copyright Clearance Center.

License Number	5721151202674
License date	Feb 03, 2024
Licensed Content Publisher	Springer Nature
Licensed Content Publication	Korean Journal of Chemical Engineering
Licensed Content Title	Synthesis of metal-organic frameworks: A mini review
Licensed Content Author	Yu-Ri Lee et al
Licensed Content Date	Aug 17, 2013
Type of Use	Thesis/Dissertation
Requestor type	non-commercial (non-profit)
Format	print and electronic
Portion	figures/tables/illustrations
Number of figures/tables/illustrations	1
Will you be translating?	no
Circulation/distribution	50000 or greater

Author of this Springer Nature content	no
Title of new work	Synthesis Characterization and Applications of Aqua-Stable Metal-Organic Frameworks and their Composites for the Environmental Remediation and Bio-Molecule Sensing
Institution name	Indian Institute of Technology Guwahati
Expected presentation date	Jul 2024
Order reference number	4
Portions	Scheme 8
Requestor Location	Mr. Subhrajyoti Ghosh IIT Guwahati Guwahati, 781039 India Attn: Mr. Subhrajyoti Ghosh
Total	0.00 USD

Terms and Conditions

Springer Nature Customer Service Centre GmbH Terms and Conditions

The following terms and conditions ("Terms and Conditions") together with the terms specified in your [RightsLink] constitute the License ("License") between you as Licensee and Springer Nature Customer Service Centre GmbH as Licensor. By clicking 'accept' and completing the transaction for your use of the material ("Licensed Material"), you confirm your acceptance of and obligation to be bound by these Terms and Conditions.

1. Grant and Scope of License

1. 1. The Licensor grants you a personal, non-exclusive, non-transferable, non-sublicensable, revocable, world-wide License to reproduce, distribute, communicate to the public, make available, broadcast, electronically transmit or create derivative works using the Licensed Material for the purpose(s) specified in your RightsLink Licence Details only. Licenses are granted for the specific use requested in the order and for no other use, subject to these Terms and Conditions. You acknowledge and agree that the rights granted to you under this License do not include the right to modify, edit, translate, include in collective works, or create derivative works of the Licensed Material in whole or in part unless expressly stated in your RightsLink

Licence Details. You may use the Licensed Material only as permitted under this Agreement and will not reproduce, distribute, display, perform, or otherwise use or exploit any Licensed Material in any way, in whole or in part, except as expressly permitted by this License.

1. 2. You may only use the Licensed Content in the manner and to the extent permitted by these Terms and Conditions, by your RightsLink Licence Details and by any applicable laws.

1. 3. A separate license may be required for any additional use of the Licensed Material, e.g. where a license has been purchased for print use only, separate permission must be obtained for electronic re-use. Similarly, a License is only valid in the language selected and does not apply for editions in other languages unless additional translation rights have been granted separately in the License.

1. 4. Any content within the Licensed Material that is owned by third parties is expressly excluded from the License.

1. 5. Rights for additional reuses such as custom editions, computer/mobile applications, film or TV reuses and/or any other derivative rights requests require additional permission and may be subject to an additional fee. Please apply to journalpermissions@springernature.com or bookpermissions@springernature.com for these rights.

2. Reservation of Rights

Licensor reserves all rights not expressly granted to you under this License. You acknowledge and agree that nothing in this License limits or restricts Licensor's rights in or use of the Licensed Material in any way. Neither this License, nor any act, omission, or statement by Licensor or you, conveys any ownership right to you in any Licensed Material, or to any element or portion thereof. As between Licensor and you, Licensor owns and retains all right, title, and interest in and to the Licensed Material subject to the license granted in Section 1.1. Your permission to use the Licensed Material is expressly conditioned on you not impairing Licensor's or the applicable copyright owner's rights in the Licensed Material in any way.

3. Restrictions on use

3. 1. Minor editing privileges are allowed for adaptations for stylistic purposes or formatting purposes provided such alterations do not alter the original meaning or intention of the Licensed Material and the new figure(s) are still accurate and representative of the Licensed Material. Any other changes including but not limited to, cropping, adapting, and/or omitting material that affect the meaning, intention or moral rights of the author(s) are strictly prohibited.

3. 2. You must not use any Licensed Material as part of any design or trademark.

3. 3. Licensed Material may be used in Open Access Publications (OAP), but any such reuse must include a clear acknowledgment of this permission visible at the same time as the figures/tables/illustration or abstract and which must indicate that the Licensed Material is not part of the governing OA license but has been reproduced with permission. This may be indicated according to any standard referencing system but must include at a minimum 'Book/Journal title, Author, Journal Name (if applicable), Volume (if applicable), Publisher, Year, reproduced with permission from SNCSC'.

4. STM Permission Guidelines

4. 1. An alternative scope of license may apply to signatories of the STM Permissions Guidelines ("STM PG") as amended from time to time and made available at https://www.stm-assoc.org/intellectual-property/permissions/permissions-guidelines/.

4. 2. For content reuse requests that qualify for permission under the STM PG, and which may be updated from time to time, the STM PG supersede the terms and conditions contained in this License.

4. 3. If a License has been granted under the STM PG, but the STM PG no longer apply at the time of publication, further permission must be sought from the Rightsholder. Contact journalpermissions@springernature.com or bookpermissions@springernature.com for these rights.

5. Duration of License

5. 1. Unless otherwise indicated on your License, a License is valid from the date of purchase ("License Date") until the end of the relevant period in the below table:

Reuse in a medical communications project	Reuse up to distribution or time period indicated in License
Reuse in a dissertation/thesis	Lifetime of thesis
Reuse in a journal/magazine	Lifetime of journal/magazine
Reuse in a book/textbook	Lifetime of edition
Reuse on a website	1 year unless otherwise specified in the License
Reuse in a presentation/slide kit/poster	Lifetime of presentation/slide kit/poster. Note: publication whether electronic or in print of presentation/slide kit/poster may require further permission.
Reuse in conference proceedings	Lifetime of conference proceedings
Reuse in an annual report	Lifetime of annual report
Reuse in training/CME materials	Reuse up to distribution or time period indicated in License
Reuse in newsmedia	Lifetime of newsmedia
Reuse in coursepack/classroom materials	Reuse up to distribution and/or time period indicated in license

6. Acknowledgement

6. 1. The Licensor's permission must be acknowledged next to the Licensed Material in print. In electronic form, this acknowledgement must be visible at the same time as the figures/tables/illustrations or abstract and must be hyperlinked to the journal/book's homepage.

6. 2. Acknowledgement may be provided according to any standard referencing system and at a minimum should include "Author, Article/Book Title, Journal name/Book imprint, volume, page number, year, Springer Nature".

7. Reuse in a dissertation or thesis

7. 1. Where 'reuse in a dissertation/thesis' has been selected, the following terms apply: Print rights of the Version of Record are provided for; electronic rights for

use only on institutional repository as defined by the Sherpa guideline (www.sherpa.ac.uk/romeo/) and only up to what is required by the awarding institution.

7. 2. For theses published under an ISBN or ISSN, separate permission is required. Please contact journalpermissions@springernature.com or bookpermissions@springernature.com for these rights.

7. 3. Authors must properly cite the published manuscript in their thesis according to current citation standards and include the following acknowledgement: '*Reproduced with permission from Springer Nature*'.

8. License Fee

You must pay the fee set forth in the License Agreement (the "License Fees"). All amounts payable by you under this License are exclusive of any sales, use, withholding, value added or similar taxes, government fees or levies or other assessments. Collection and/or remittance of such taxes to the relevant tax authority shall be the responsibility of the party who has the legal obligation to do so.

9. Warranty

9. 1. The Licensor warrants that it has, to the best of its knowledge, the rights to license reuse of the Licensed Material. **You are solely responsible for ensuring that the material you wish to license is original to the Licensor and does not carry the copyright of another entity or third party (as credited in the published version).** If the credit line on any part of the Licensed Material indicates that it was reprinted or adapted with permission from another source, then you should seek additional permission from that source to reuse the material.

9. 2. EXCEPT FOR THE EXPRESS WARRANTY STATED HEREIN AND TO THE EXTENT PERMITTED BY APPLICABLE LAW, LICENSOR PROVIDES THE LICENSED MATERIAL "AS IS" AND MAKES NO OTHER REPRESENTATION OR WARRANTY. LICENSOR EXPRESSLY DISCLAIMS ANY LIABILITY FOR ANY CLAIM ARISING FROM OR OUT OF THE CONTENT, INCLUDING BUT NOT LIMITED TO ANY ERRORS, INACCURACIES, OMISSIONS, OR DEFECTS CONTAINED THEREIN, AND ANY IMPLIED OR EXPRESS WARRANTY AS TO MERCHANTABILITY OR FITNESS FOR A PARTICULAR PURPOSE. IN NO EVENT SHALL LICENSOR BE LIABLE TO YOU OR ANY OTHER PARTY OR ANY OTHER PERSON OR FOR ANY SPECIAL, CONSEQUENTIAL, INCIDENTAL, INDIRECT, PUNITIVE, OR EXEMPLARY DAMAGES, HOWEVER CAUSED, ARISING OUT OF OR IN CONNECTION WITH THE DOWNLOADING, VIEWING OR USE OF THE LICENSED MATERIAL REGARDLESS OF THE FORM OF ACTION, WHETHER FOR BREACH OF CONTRACT, BREACH OF WARRANTY, TORT, NEGLIGENCE, INFRINGEMENT OR OTHERWISE (INCLUDING, WITHOUT LIMITATION, DAMAGES BASED ON LOSS OF PROFITS, DATA, FILES, USE, BUSINESS OPPORTUNITY OR CLAIMS OF THIRD PARTIES), AND WHETHER OR NOT THE PARTY HAS BEEN ADVISED OF THE POSSIBILITY OF SUCH DAMAGES. THIS LIMITATION APPLIES NOTWITHSTANDING ANY FAILURE OF ESSENTIAL PURPOSE OF ANY LIMITED REMEDY PROVIDED HEREIN.

10. Termination and Cancellation

10. 1. The License and all rights granted hereunder will continue until the end of the applicable period shown in Clause 5.1 above. Thereafter, this license will be terminated and all rights granted hereunder will cease.

10. 2. Licensor reserves the right to terminate the License in the event that payment is not received in full or if you breach the terms of this License.

11. General

11. 1. The License and the rights and obligations of the parties hereto shall be construed, interpreted and determined in accordance with the laws of the Federal Republic of Germany without reference to the stipulations of the CISG (United Nations Convention on Contracts for the International Sale of Goods) or to Germany's choice-of-law principle.

11. 2. The parties acknowledge and agree that any controversies and disputes arising out of this License shall be decided exclusively by the courts of or having jurisdiction for Heidelberg, Germany, as far as legally permissible.

11. 3. This License is solely for Licensor's and Licensee's benefit. It is not for the benefit of any other person or entity.

Questions? For questions on Copyright Clearance Center accounts or website issues please contact springernaturesupport@copyright.com or +1-855-239-3415 (toll free in the US) or +1-978-646-2777. For questions on Springer Nature licensing please visit https://www.springernature.com/gp/partners/rights-permissions-third-party-distribution

Other Conditions:

Version 1.4 - Dec 2022

Questions? customercare@copyright.com.

CCC Marketplace

Special Requests > Special Request Details

Add To Cart | Decline Offer

Journal of materials chemistry. A, Materials for energy and sustainability

Article: Nickel-substituted zeolitic imidazolate frameworks for time-resolved alcohol sensing and photocatalysis under visi...

GENERAL INFORMATION

Request ID	**Request Date**
600154850	03 Feb 2024
Request Status	**Price**
Accepted	0.00 USD

ALL DETAILS

ISSN:	2050-7496
Type of Use:	Republish in a thesis/dissertation
Publisher:	Royal Society of Chemistry
Portion:	Chart/graph/table/figure

LICENSED CONTENT

Publication Title	Journal of materials chemistry. A, Materials for energy and sustainability	**Rightsholder**	Royal Society of Chemistry
		Publication Type	e-Journal
Article Title	Nickel-substituted zeolitic imidazolate frameworks for time-resolved alcohol sensing and photocatalysis under visible light	**URL**	http://pubs.rsc.org/en/journals/journalissues/ta
		Start Page	5724
		Issue	16
		Volume	2
Author/Editor	Royal Society of Chemistry (Great Britain)		
Date	01/01/2013		
Language	English		
Country	United Kingdom of Great Britain and Northern Ireland		

REQUEST DETAILS

Number of Charts / Graphs / Tables / Figures Requested	1	**Distribution**	Worldwide
		Translation	Original language of publication
Format (select all that apply)	Print, Electronic		
Who Will Republish the Content?	Not-for-profit entity	**Copies for the Disabled?**	No
		Minor Editing Privileges?	No
Duration of Use	Life of current edition	**Incidental Promotional Use?**	No
Lifetime Unit Quantity	More than 2,000,000	**Currency**	USD
Rights Requested	Main product		

NEW WORK DETAILS

Title	Synthesis Characterization and Applications of Aqua-Stable Metal-Organic Frameworks and their Composites for the Environmental Remediation and Bio-Molecule Sensing	Institution Name	Indian Institute of Technology Guwahati
		Expected Presentation Date	2024-07-19
Instructor Name	Dr. Shyam P. Biswas		

ADDITIONAL DETAILS

Order Reference Number	8	The Requesting Person / Organization to Appear on the License	Subhrajyoti Ghosh

REQUESTED CONTENT DETAILS

Title, Description or Numeric Reference of the Portion(s)	Figure 1	Title of the Article / Chapter the Portion Is From	Nickel-substituted zeolitic imidazolate frameworks for time-resolved alcohol sensing and photocatalysis under visible light
Editor of Portion(s)	Li, Rui; Ren, Xiaoqian; Ma, Hongwei; Feng, Xiao; Lin, Zhengguo; Li, Xingguo; Hu, Changwen; Wang, Bo	Author of Portion(s)	Li, Rui; Ren, Xiaoqian; Ma, Hongwei; Feng, Xiao; Lin, Zhengguo; Li, Xingguo; Hu, Changwen; Wang, Bo
Volume / Edition	2		
Page or Page Range of Portion	5724-5729	Issue, if Republishing an Article From a Serial	16
		Publication Date of Portion	2014-03-25

COMMENTS

Add Comment / Attachment

09 Feb 2024 4:47:55 PM, by Publisher Representative

Permission is granted as long as the figure is fully acknowledged and a link is given back to the article on our Platform. Please go to rsc.li/permissions for details. Please note that if the material specified above or any part of it appears witl View More

Add To Cart | Decline Offer

ELSEVIER LICENSE
TERMS AND CONDITIONS

Feb 03, 2024

This Agreement between Mr. Subhrajyoti Ghosh ("You") and Elsevier ("Elsevier") consists of your license details and the terms and conditions provided by Elsevier and Copyright Clearance Center.

License Number	5721170136518
License date	Feb 03, 2024
Licensed Content Publisher	Elsevier
Licensed Content Publication	Coordination Chemistry Reviews
Licensed Content Title	When defects turn into virtues: The curious case of zirconium-based metal-organic frameworks
Licensed Content Author	Marco Taddei
Licensed Content Date	Jul 15, 2017
Licensed Content Volume	343
Licensed Content Issue	n/a
Licensed Content Pages	24
Start Page	1
End Page	24
Type of Use	reuse in a thesis/dissertation
Portion	figures/tables/illustrations

Number of figures/tables/illustrations	2
Format	both print and electronic
Are you the author of this Elsevier article?	No
Will you be translating?	No
Title of new work	Synthesis Characterization and Applications of Aqua-Stable Metal-Organic Frameworks and their Composites for the Environmental Remediation and Bio-Molecule Sensing
Institution name	Indian Institute of Technology Guwahati
Expected presentation date	Jul 2024
Order reference number	5
Portions	Figure 1 and 2
Requestor Location	Mr. Subhrajyoti Ghosh IIT Guwahati Guwahati, 781039 India Attn: Mr. Subhrajyoti Ghosh
Publisher Tax ID	GB 494 6272 12
Total	0.00 USD
Terms and Conditions	

INTRODUCTION

1. The publisher for this copyrighted material is Elsevier. By clicking "accept" in connection with completing this licensing transaction, you agree that the following terms and conditions apply to this transaction (along with the Billing and Payment terms and conditions established by Copyright Clearance Center, Inc. ("CCC"), at the time that you

opened your RightsLink account and that are available at any time at https://myaccount.copyright.com).

GENERAL TERMS

2. Elsevier hereby grants you permission to reproduce the aforementioned material subject to the terms and conditions indicated.

3. Acknowledgement: If any part of the material to be used (for example, figures) has appeared in our publication with credit or acknowledgement to another source, permission must also be sought from that source. If such permission is not obtained then that material may not be included in your publication/copies. Suitable acknowledgement to the source must be made, either as a footnote or in a reference list at the end of your publication, as follows:

"Reprinted from Publication title, Vol /edition number, Author(s), Title of article / title of chapter, Pages No., Copyright (Year), with permission from Elsevier [OR APPLICABLE SOCIETY COPYRIGHT OWNER]." Also Lancet special credit - "Reprinted from The Lancet, Vol. number, Author(s), Title of article, Pages No., Copyright (Year), with permission from Elsevier."

4. Reproduction of this material is confined to the purpose and/or media for which permission is hereby given. The material may not be reproduced or used in any other way, including use in combination with an artificial intelligence tool (including to train an algorithm, test, process, analyse, generate output and/or develop any form of artificial intelligence tool), or to create any derivative work and/or service (including resulting from the use of artificial intelligence tools).

5. Altering/Modifying Material: Not Permitted. However figures and illustrations may be altered/adapted minimally to serve your work. Any other abbreviations, additions, deletions and/or any other alterations shall be made only with prior written authorization of Elsevier Ltd. (Please contact Elsevier's permissions helpdesk here). No modifications can be made to any Lancet figures/tables and they must be reproduced in full.

6. If the permission fee for the requested use of our material is waived in this instance, please be advised that your future requests for Elsevier materials may attract a fee.

7. Reservation of Rights: Publisher reserves all rights not specifically granted in the combination of (i) the license details provided by you and accepted in the course of this licensing transaction, (ii) these terms and conditions and (iii) CCC's Billing and Payment terms and conditions.

8. License Contingent Upon Payment: While you may exercise the rights licensed immediately upon issuance of the license at the end of the licensing process for the transaction, provided that you have disclosed complete and accurate details of your proposed use, no license is finally effective unless and until full payment is received from you (either by publisher or by CCC) as provided in CCC's Billing and Payment terms and conditions. If full payment is not received on a timely basis, then any license preliminarily granted shall be deemed automatically revoked and shall be void as if never granted. Further, in the event that you breach any of these terms and conditions or any of CCC's Billing and Payment terms and conditions, the license is automatically revoked and shall be void as if never granted. Use of materials as described in a revoked license, as well as any use of the materials beyond the scope of an unrevoked license, may constitute copyright infringement and publisher reserves the right to take any and all action to protect its copyright in the materials.

9. Warranties: Publisher makes no representations or warranties with respect to the licensed material.

10. Indemnity: You hereby indemnify and agree to hold harmless publisher and CCC, and their respective officers, directors, employees and agents, from and against any and all claims arising out of your use of the licensed material other than as specifically authorized pursuant to this license.

11. No Transfer of License: This license is personal to you and may not be sublicensed, assigned, or transferred by you to any other person without publisher's written permission.

12. No Amendment Except in Writing: This license may not be amended except in a writing signed by both parties (or, in the case of publisher, by CCC on publisher's behalf).

13. Objection to Contrary Terms: Publisher hereby objects to any terms contained in any purchase order, acknowledgment, check endorsement or other writing prepared by you, which terms are inconsistent with these terms and conditions or CCC's Billing and Payment terms and conditions. These terms and conditions, together with CCC's Billing and Payment terms and conditions (which are incorporated herein), comprise the entire agreement between you and publisher (and CCC) concerning this licensing transaction. In the event of any conflict between your obligations established by these terms and conditions and those established by CCC's Billing and Payment terms and conditions, these terms and conditions shall control.

14. Revocation: Elsevier or Copyright Clearance Center may deny the permissions described in this License at their sole discretion, for any reason or no reason, with a full refund payable to you. Notice of such denial will be made using the contact information provided by you. Failure to receive such notice will not alter or invalidate the denial. In no event will Elsevier or Copyright Clearance Center be responsible or liable for any costs, expenses or damage incurred by you as a result of a denial of your permission request, other than a refund of the amount(s) paid by you to Elsevier and/or Copyright Clearance Center for denied permissions.

LIMITED LICENSE

The following terms and conditions apply only to specific license types:

15. **Translation**: This permission is granted for non-exclusive world **English** rights only unless your license was granted for translation rights. If you licensed translation rights you may only translate this content into the languages you requested. A professional translator must perform all translations and reproduce the content word for word preserving the integrity of the article.

16. **Posting licensed content on any Website**: The following terms and conditions apply as follows: Licensing material from an Elsevier journal: All content posted to the web site must maintain the copyright information line on the bottom of each image; A hyper-text must be included to the Homepage of the journal from which you are licensing at http://www.sciencedirect.com/science/journal/xxxxx or the Elsevier homepage for books at http://www.elsevier.com; Central Storage: This license does not include permission for a scanned version of the material to be stored in a central repository such as that provided by Heron/XanEdu.

Licensing material from an Elsevier book: A hyper-text link must be included to the Elsevier homepage at http://www.elsevier.com . All content posted to the web site must maintain the copyright information line on the bottom of each image.

Posting licensed content on Electronic reserve: In addition to the above the following clauses are applicable: The web site must be password-protected and made available only to bona fide students registered on a relevant course. This permission is granted for 1 year only. You may obtain a new license for future website posting.

17. **For journal authors:** the following clauses are applicable in addition to the above:

Preprints:

A preprint is an author's own write-up of research results and analysis, it has not been peer-reviewed, nor has it had any other value added to it by a publisher (such as formatting, copyright, technical enhancement etc.).

Authors can share their preprints anywhere at any time. Preprints should not be added to or enhanced in any way in order to appear more like, or to substitute for, the final versions of articles however authors can update their preprints on arXiv or RePEc with their Accepted Author Manuscript (see below).

If accepted for publication, we encourage authors to link from the preprint to their formal publication via its DOI. Millions of researchers have access to the formal publications on ScienceDirect, and so links will help users to find, access, cite and use the best available version. Please note that Cell Press, The Lancet and some society-owned have different preprint policies. Information on these policies is available on the journal homepage.

Accepted Author Manuscripts: An accepted author manuscript is the manuscript of an article that has been accepted for publication and which typically includes author-incorporated changes suggested during submission, peer review and editor-author communications.

Authors can share their accepted author manuscript:

- immediately
  - via their non-commercial person homepage or blog
  - by updating a preprint in arXiv or RePEc with the accepted manuscript
  - via their research institute or institutional repository for internal institutional uses or as part of an invitation-only research collaboration work-group
  - directly by providing copies to their students or to research collaborators for their personal use
  - for private scholarly sharing as part of an invitation-only work group on commercial sites with which Elsevier has an agreement
- After the embargo period
  - via non-commercial hosting platforms such as their institutional repository
  - via commercial sites with which Elsevier has an agreement

In all cases accepted manuscripts should:

- link to the formal publication via its DOI
- bear a CC-BY-NC-ND license - this is easy to do
- if aggregated with other manuscripts, for example in a repository or other site, be shared in alignment with our hosting policy not be added to or enhanced in any way to appear more like, or to substitute for, the published journal article.

Published journal article (JPA): A published journal article (PJA) is the definitive final record of published research that appears or will appear in the journal and embodies all value-adding publishing activities including peer review co-ordination, copy-editing, formatting, (if relevant) pagination and online enrichment.

Policies for sharing publishing journal articles differ for subscription and gold open access articles:

Subscription Articles: If you are an author, please share a link to your article rather than the full-text. Millions of researchers have access to the formal publications on ScienceDirect, and so links will help your users to find, access, cite, and use the best available version.

Theses and dissertations which contain embedded PJAs as part of the formal submission can be posted publicly by the awarding institution with DOI links back to the formal publications on ScienceDirect.

If you are affiliated with a library that subscribes to ScienceDirect you have additional private sharing rights for others' research accessed under that agreement. This includes use for classroom teaching and internal training at the institution (including use in course packs and courseware programs), and inclusion of the article for grant funding purposes.

Gold Open Access Articles: May be shared according to the author-selected end-user license and should contain a CrossMark logo, the end user license, and a DOI link to the formal publication on ScienceDirect.

Please refer to Elsevier's posting policy for further information.

18. **For book authors** the following clauses are applicable in addition to the above: Authors are permitted to place a brief summary of their work online only. You are not allowed to download and post the published electronic version of your chapter, nor may you scan the printed edition to create an electronic version. **Posting to a repository:** Authors are permitted to post a summary of their chapter only in their institution's repository.

19. **Thesis/Dissertation**: If your license is for use in a thesis/dissertation your thesis may be submitted to your institution in either print or electronic form. Should your thesis be published commercially, please reapply for permission. These requirements include permission for the Library and Archives of Canada to supply single copies, on demand, of the complete thesis and include permission for Proquest/UMI to supply single copies, on demand, of the complete thesis. Should your thesis be published commercially, please reapply for permission. Theses and dissertations which contain embedded PJAs as part of the formal submission can be posted publicly by the awarding institution with DOI links back to the formal publications on ScienceDirect.

Elsevier Open Access Terms and Conditions

You can publish open access with Elsevier in hundreds of open access journals or in nearly 2000 established subscription journals that support open access publishing. Permitted third party re-use of these open access articles is defined by the author's choice of Creative Commons user license. See our open access license policy for more information.

Terms & Conditions applicable to all Open Access articles published with Elsevier:

Any reuse of the article must not represent the author as endorsing the adaptation of the article nor should the article be modified in such a way as to damage the author's honour or reputation. If any changes have been made, such changes must be clearly indicated.

The author(s) must be appropriately credited and we ask that you include the end user license and a DOI link to the formal publication on ScienceDirect.

If any part of the material to be used (for example, figures) has appeared in our publication with credit or acknowledgement to another source it is the responsibility of the user to ensure their reuse complies with the terms and conditions determined by the rights holder.

Additional Terms & Conditions applicable to each Creative Commons user license:

CC BY: The CC-BY license allows users to copy, to create extracts, abstracts and new works from the Article, to alter and revise the Article and to make commercial use of the Article (including reuse and/or resale of the Article by commercial entities), provided the user gives appropriate credit (with a link to the formal publication through the relevant DOI), provides a link to the license, indicates if changes were made and the licensor is not represented as endorsing the use made of the work. The full details of the license are available at http://creativecommons.org/licenses/by/4.0.

CC BY NC SA: The CC BY-NC-SA license allows users to copy, to create extracts, abstracts and new works from the Article, to alter and revise the Article, provided this is not done for commercial purposes, and that the user gives appropriate credit (with a link to the formal publication through the relevant DOI), provides a link to the license, indicates if changes were made and the licensor is not represented as endorsing the use made of the work. Further, any new works must be made available on the same conditions. The full details of the license are available at http://creativecommons.org/licenses/by-nc-sa/4.0.

CC BY NC ND: The CC BY-NC-ND license allows users to copy and distribute the Article, provided this is not done for commercial purposes and further does not permit distribution of the Article if it is changed or edited in any way, and provided the user gives appropriate credit (with a link to the formal publication through the relevant DOI), provides a link to the license, and that the licensor is not represented as endorsing the use made of the work. The full details of the license are available at http://creativecommons.org/licenses/by-nc-nd/4.0. Any commercial reuse of Open Access articles published with a CC BY NC SA or CC BY NC ND license requires permission from Elsevier and will be subject to a fee.

Commercial reuse includes:

- Associating advertising with the full text of the Article
- Charging fees for document delivery or access
- Article aggregation
- Systematic distribution via e-mail lists or share buttons

Posting or linking by commercial companies for use by customers of those companies.

20. **Other Conditions**:

v1.10

Questions? customercare@copyright.com.

CCC Marketplace

Special Requests > Special Request Details

Add To Cart | Decline Offer

CrystEngComm

Article: Metal-organic Frameworks (MOFs) as Fluorescence Sensors: Principles, Development and Prospects

GENERAL INFORMATION

Request ID	**Request Date**
600154849	03 Feb 2024
Request Status	**Price**
Accepted	0.00 USD

ALL DETAILS

ISSN:	1466-8033
Type of Use:	Republish in a thesis/dissertation
Publisher:	ROYAL SOCIETY OF CHEMISTRY
Portion:	Chart/graph/table/figure

LICENSED CONTENT

Publication Title	CrystEngComm	**Rightsholder**	Royal Society of Chemistry
Article Title	Metal-organic Frameworks (MOFs) as Fluorescence Sensors: Principles, Development and Prospects	**Publication Type**	e-Journal
		URL	http://www.rsc.org/Publishing/Journals/ce/index.asp
Author/Editor	Royal Society of Chemistry (Great Britain)	**Start Page**	7881
		Issue	45
Date	01/01/1999	**Volume**	24
Language	English		
Country	United Kingdom of Great Britain and Northern Ireland		

REQUEST DETAILS

Number of Charts / Graphs / Tables / Figures Requested	1	**Distribution**	Worldwide
		Translation	Original language of publication
Format (select all that apply)	Print, Electronic		
Who Will Republish the Content?	Not-for-profit entity	**Copies for the Disabled?**	No
		Minor Editing Privileges?	No
Duration of Use	Life of current edition	**Incidental Promotional Use?**	Yes
Lifetime Unit Quantity	More than 2,000,000	**Currency**	USD
Rights Requested	Main product		

NEW WORK DETAILS

Title	Synthesis Characterization and Applications of Aqua-Stable Metal-Organic Frameworks and their Composites for the Environmental Remediation and Bio-Molecule Sensing	**Institution Name**	Indian Institute of Technology Guwahati
		Expected Presentation Date	2024-07-19
Instructor Name	Dr. Shyam P. Biswas		

ADDITIONAL DETAILS

Order Reference Number	9	**The Requesting Person / Organization to Appear on the License**	Subhrajyoti Ghosh

REQUESTED CONTENT DETAILS

Title, Description or Numeric Reference of the Portion(s)	Scheme 1	**Title of the Article / Chapter the Portion Is From**	Metal-organic Frameworks (MOFs) as Fluorescence Sensors: Principles, Development and Prospects
Editor of Portion(s)	Wu, Tingting; Gao, Xiang-Jing; Ge, Fa-Yuan; Zheng, Hegen	**Author of Portion(s)**	Wu, Tingting; Gao, Xiang-Jing; Ge, Fa-Yuan; Zheng, Hegen
Volume / Edition	24		
Page or Page Range of Portion	7881-7901	**Issue, if Republishing an Article From a Serial**	45
		Publication Date of Portion	2022-01-01

COMMENTS

Add Comment / Attachment

09 Feb 2024 3:44:08 PM, by Publisher Representative

Permission is granted as long as the figure is fully acknowledged and a link is given back to the article on our Platform. Please go to rsc.li/permissions for details. Please note that if the material specified above or any part of it appears witl View More

Add To Cart Decline Offer

CCC RightsLink

SG

ACS Publications

Highly Efficient Luminescent Metal–Organic Framework for the Simultaneous Detection and Removal of Heavy Metals from Water

Author: Nathan D. Rudd, Hao Wang, Erika M. A. Fuentes-Fernandez, et al

Publication: Applied Materials

Publisher: American Chemical Society

Date: Nov 1, 2016

PERMISSION/LICENSE IS GRANTED FOR YOUR ORDER AT NO CHARGE

This type of permission/license, instead of the standard Terms and Conditions, is sent to you because no fee is being charged for your order. Please note the following:

- Permission is granted for your request in both print and electronic formats, and translations.
- If figures and/or tables were requested, they may be adapted or used in part.
- Please print this page for your records and send a copy of it to your publisher/graduate school.
- Appropriate credit for the requested material should be given as follows: "Reprinted (adapted) with permission from (COMPLETE REFERENCE CITATION). Copyright (YEAR) American Chemical Society." Insert appropriate information in place of the capitalized words.
- One-time permission is granted only for the use specified in your RightsLink request. No additional uses are granted (such as derivative works or other editions). For any uses, please submit a new request.

If credit is given to another source for the material you requested from RightsLink, permission must be obtained from that source.

BACK CLOSE WINDOW

Ultrasensitive Detection of Hg(II) Ions in Aqueous Medium Using Zinc-Based Metal–Organic Framework

Author: Asha Pankajakshan, Denis Kuznetsov, Sukhendu Mandal
Publication: Inorganic Chemistry
Publisher: American Chemical Society
Date: Jan 1, 2019

PERMISSION/LICENSE IS GRANTED FOR YOUR ORDER AT NO CHARGE

This type of permission/license, instead of the standard Terms and Conditions, is sent to you because no fee is being charged for your order. Please note the following:

- Permission is granted for your request in both print and electronic formats, and translations.
- If figures and/or tables were requested, they may be adapted or used in part.
- Please print this page for your records and send a copy of it to your publisher/graduate school.
- Appropriate credit for the requested material should be given as follows: "Reprinted (adapted) with permission from (COMPLETE REFERENCE CITATION). Copyright (YEAR) American Chemical Society." Insert appropriate information in place of the capitalized words.
- One-time permission is granted only for the use specified in your RightsLink request. No additional uses are granted (such as derivative works or other editions). For any uses, please submit a new request.

If credit is given to another source for the material you requested from RightsLink, permission must be obtained from that source.

BACK CLOSE WINDOW

ELSEVIER LICENSE
TERMS AND CONDITIONS

Feb 03, 2024

This Agreement between Mr. Subhrajyoti Ghosh ("You") and Elsevier ("Elsevier") consists of your license details and the terms and conditions provided by Elsevier and Copyright Clearance Center.

License Number	5721171002241
License date	Feb 03, 2024
Licensed Content Publisher	Elsevier
Licensed Content Publication	Inorganic Chemistry Communications
Licensed Content Title	A multifunctional Zn(II)-based four-fold interpenetrated metal-organic framework for highly sensitive sensing 2,4,6-trinitrophenol (TNP), nitrofurazone (NFZ) and nitrofurantoin (NFT)
Licensed Content Author	Hai-Bin Zhu,Yu Shen,Zhan-Zhao Fu,You-Ya Yu,Yu-Fei Jiang,Yue Zhao
Licensed Content Date	May 1, 2019
Licensed Content Volume	103
Licensed Content Issue	n/a
Licensed Content Pages	4
Start Page	21
End Page	24
Type of Use	reuse in a thesis/dissertation

Portion	figures/tables/illustrations
Number of figures/tables/illustrations	1
Format	both print and electronic
Are you the author of this Elsevier article?	No
Will you be translating?	No
Title of new work	Synthesis Characterization and Applications of Aqua-Stable Metal-Organic Frameworks and their Composites for the Environmental Remediation and Bio-Molecule Sensing
Institution name	Indian Institute of Technology Guwahati
Expected presentation date	Jul 2024
Order reference number	6
Portions	Graphical abstract
Requestor Location	Mr. Subhrajyoti Ghosh IIT Guwahati Guwahati, 781039 India Attn: Mr. Subhrajyoti Ghosh
Publisher Tax ID	GB 494 6272 12
Total	0.00 USD
Terms and Conditions	

INTRODUCTION

1. The publisher for this copyrighted material is Elsevier. By clicking "accept" in connection with completing this licensing transaction, you agree that the following terms

and conditions apply to this transaction (along with the Billing and Payment terms and conditions established by Copyright Clearance Center, Inc. ("CCC"), at the time that you opened your RightsLink account and that are available at any time at https://myaccount.copyright.com).

GENERAL TERMS

2. Elsevier hereby grants you permission to reproduce the aforementioned material subject to the terms and conditions indicated.

3. Acknowledgement: If any part of the material to be used (for example, figures) has appeared in our publication with credit or acknowledgement to another source, permission must also be sought from that source. If such permission is not obtained then that material may not be included in your publication/copies. Suitable acknowledgement to the source must be made, either as a footnote or in a reference list at the end of your publication, as follows:

"Reprinted from Publication title, Vol /edition number, Author(s), Title of article / title of chapter, Pages No., Copyright (Year), with permission from Elsevier [OR APPLICABLE SOCIETY COPYRIGHT OWNER]." Also Lancet special credit - "Reprinted from The Lancet, Vol. number, Author(s), Title of article, Pages No., Copyright (Year), with permission from Elsevier."

4. Reproduction of this material is confined to the purpose and/or media for which permission is hereby given. The material may not be reproduced or used in any other way, including use in combination with an artificial intelligence tool (including to train an algorithm, test, process, analyse, generate output and/or develop any form of artificial intelligence tool), or to create any derivative work and/or service (including resulting from the use of artificial intelligence tools).

5. Altering/Modifying Material: Not Permitted. However figures and illustrations may be altered/adapted minimally to serve your work. Any other abbreviations, additions, deletions and/or any other alterations shall be made only with prior written authorization of Elsevier Ltd. (Please contact Elsevier's permissions helpdesk here). No modifications can be made to any Lancet figures/tables and they must be reproduced in full.

6. If the permission fee for the requested use of our material is waived in this instance, please be advised that your future requests for Elsevier materials may attract a fee.

7. Reservation of Rights: Publisher reserves all rights not specifically granted in the combination of (i) the license details provided by you and accepted in the course of this licensing transaction, (ii) these terms and conditions and (iii) CCC's Billing and Payment terms and conditions.

8. License Contingent Upon Payment: While you may exercise the rights licensed immediately upon issuance of the license at the end of the licensing process for the transaction, provided that you have disclosed complete and accurate details of your proposed use, no license is finally effective unless and until full payment is received from you (either by publisher or by CCC) as provided in CCC's Billing and Payment terms and conditions. If full payment is not received on a timely basis, then any license preliminarily granted shall be deemed automatically revoked and shall be void as if never granted. Further, in the event that you breach any of these terms and conditions or any of CCC's Billing and Payment terms and conditions, the license is automatically revoked and shall be void as if never granted. Use of materials as described in a revoked license, as well as any use of the materials beyond the scope of an unrevoked license, may constitute copyright infringement and publisher reserves the right to take any and all action to protect its copyright in the materials.

9. Warranties: Publisher makes no representations or warranties with respect to the licensed material.

10. Indemnity: You hereby indemnify and agree to hold harmless publisher and CCC, and their respective officers, directors, employees and agents, from and against any and all claims arising out of your use of the licensed material other than as specifically authorized pursuant to this license.

11. No Transfer of License: This license is personal to you and may not be sublicensed, assigned, or transferred by you to any other person without publisher's written permission.

12. No Amendment Except in Writing: This license may not be amended except in a writing signed by both parties (or, in the case of publisher, by CCC on publisher's behalf).

13. Objection to Contrary Terms: Publisher hereby objects to any terms contained in any purchase order, acknowledgment, check endorsement or other writing prepared by you, which terms are inconsistent with these terms and conditions or CCC's Billing and Payment terms and conditions. These terms and conditions, together with CCC's Billing and Payment terms and conditions (which are incorporated herein), comprise the entire agreement between you and publisher (and CCC) concerning this licensing transaction. In the event of any conflict between your obligations established by these terms and conditions and those established by CCC's Billing and Payment terms and conditions, these terms and conditions shall control.

14. Revocation: Elsevier or Copyright Clearance Center may deny the permissions described in this License at their sole discretion, for any reason or no reason, with a full refund payable to you. Notice of such denial will be made using the contact information provided by you. Failure to receive such notice will not alter or invalidate the denial. In no event will Elsevier or Copyright Clearance Center be responsible or liable for any costs, expenses or damage incurred by you as a result of a denial of your permission request, other than a refund of the amount(s) paid by you to Elsevier and/or Copyright Clearance Center for denied permissions.

LIMITED LICENSE

The following terms and conditions apply only to specific license types:

15. **Translation**: This permission is granted for non-exclusive world **English** rights only unless your license was granted for translation rights. If you licensed translation rights you may only translate this content into the languages you requested. A professional translator must perform all translations and reproduce the content word for word preserving the integrity of the article.

16. **Posting licensed content on any Website**: The following terms and conditions apply as follows: Licensing material from an Elsevier journal: All content posted to the web site must maintain the copyright information line on the bottom of each image; A hyper-text must be included to the Homepage of the journal from which you are licensing at http://www.sciencedirect.com/science/journal/xxxxx or the Elsevier homepage for books at http://www.elsevier.com; Central Storage: This license does not include permission for a scanned version of the material to be stored in a central repository such as that provided by Heron/XanEdu.

Licensing material from an Elsevier book: A hyper-text link must be included to the Elsevier homepage at http://www.elsevier.com . All content posted to the web site must maintain the copyright information line on the bottom of each image.

Posting licensed content on Electronic reserve: In addition to the above the following clauses are applicable: The web site must be password-protected and made available only

to bona fide students registered on a relevant course. This permission is granted for 1 year only. You may obtain a new license for future website posting.

17. **For journal authors:** the following clauses are applicable in addition to the above:

Preprints:

A preprint is an author's own write-up of research results and analysis, it has not been peer-reviewed, nor has it had any other value added to it by a publisher (such as formatting, copyright, technical enhancement etc.).

Authors can share their preprints anywhere at any time. Preprints should not be added to or enhanced in any way in order to appear more like, or to substitute for, the final versions of articles however authors can update their preprints on arXiv or RePEc with their Accepted Author Manuscript (see below).

If accepted for publication, we encourage authors to link from the preprint to their formal publication via its DOI. Millions of researchers have access to the formal publications on ScienceDirect, and so links will help users to find, access, cite and use the best available version. Please note that Cell Press, The Lancet and some society-owned have different preprint policies. Information on these policies is available on the journal homepage.

Accepted Author Manuscripts: An accepted author manuscript is the manuscript of an article that has been accepted for publication and which typically includes author-incorporated changes suggested during submission, peer review and editor-author communications.

Authors can share their accepted author manuscript:

- immediately
  - via their non-commercial person homepage or blog
  - by updating a preprint in arXiv or RePEc with the accepted manuscript
  - via their research institute or institutional repository for internal institutional uses or as part of an invitation-only research collaboration work-group
  - directly by providing copies to their students or to research collaborators for their personal use
  - for private scholarly sharing as part of an invitation-only work group on commercial sites with which Elsevier has an agreement
- After the embargo period
  - via non-commercial hosting platforms such as their institutional repository
  - via commercial sites with which Elsevier has an agreement

In all cases accepted manuscripts should:

- link to the formal publication via its DOI
- bear a CC-BY-NC-ND license - this is easy to do
- if aggregated with other manuscripts, for example in a repository or other site, be shared in alignment with our hosting policy not be added to or enhanced in any way to appear more like, or to substitute for, the published journal article.

Published journal article (JPA): A published journal article (PJA) is the definitive final record of published research that appears or will appear in the journal and embodies all value-adding publishing activities including peer review co-ordination, copy-editing, formatting, (if relevant) pagination and online enrichment.

Policies for sharing publishing journal articles differ for subscription and gold open access articles:

Subscription Articles: If you are an author, please share a link to your article rather than the full-text. Millions of researchers have access to the formal publications on ScienceDirect, and so links will help your users to find, access, cite, and use the best available version.

Theses and dissertations which contain embedded PJAs as part of the formal submission can be posted publicly by the awarding institution with DOI links back to the formal publications on ScienceDirect.

If you are affiliated with a library that subscribes to ScienceDirect you have additional private sharing rights for others' research accessed under that agreement. This includes use for classroom teaching and internal training at the institution (including use in course packs and courseware programs), and inclusion of the article for grant funding purposes.

Gold Open Access Articles: May be shared according to the author-selected end-user license and should contain a CrossMark logo, the end user license, and a DOI link to the formal publication on ScienceDirect.

Please refer to Elsevier's posting policy for further information.

18. **For book authors** the following clauses are applicable in addition to the above: Authors are permitted to place a brief summary of their work online only. You are not allowed to download and post the published electronic version of your chapter, nor may you scan the printed edition to create an electronic version. **Posting to a repository:** Authors are permitted to post a summary of their chapter only in their institution's repository.

19. **Thesis/Dissertation**: If your license is for use in a thesis/dissertation your thesis may be submitted to your institution in either print or electronic form. Should your thesis be published commercially, please reapply for permission. These requirements include permission for the Library and Archives of Canada to supply single copies, on demand, of the complete thesis and include permission for Proquest/UMI to supply single copies, on demand, of the complete thesis. Should your thesis be published commercially, please reapply for permission. Theses and dissertations which contain embedded PJAs as part of the formal submission can be posted publicly by the awarding institution with DOI links back to the formal publications on ScienceDirect.

Elsevier Open Access Terms and Conditions

You can publish open access with Elsevier in hundreds of open access journals or in nearly 2000 established subscription journals that support open access publishing. Permitted third party re-use of these open access articles is defined by the author's choice of Creative Commons user license. See our open access license policy for more information.

Terms & Conditions applicable to all Open Access articles published with Elsevier:

Any reuse of the article must not represent the author as endorsing the adaptation of the article nor should the article be modified in such a way as to damage the author's honour or reputation. If any changes have been made, such changes must be clearly indicated.

The author(s) must be appropriately credited and we ask that you include the end user license and a DOI link to the formal publication on ScienceDirect.

If any part of the material to be used (for example, figures) has appeared in our publication with credit or acknowledgement to another source it is the responsibility of the

user to ensure their reuse complies with the terms and conditions determined by the rights holder.

Additional Terms & Conditions applicable to each Creative Commons user license:

CC BY: The CC-BY license allows users to copy, to create extracts, abstracts and new works from the Article, to alter and revise the Article and to make commercial use of the Article (including reuse and/or resale of the Article by commercial entities), provided the user gives appropriate credit (with a link to the formal publication through the relevant DOI), provides a link to the license, indicates if changes were made and the licensor is not represented as endorsing the use made of the work. The full details of the license are available at http://creativecommons.org/licenses/by/4.0.

CC BY NC SA: The CC BY-NC-SA license allows users to copy, to create extracts, abstracts and new works from the Article, to alter and revise the Article, provided this is not done for commercial purposes, and that the user gives appropriate credit (with a link to the formal publication through the relevant DOI), provides a link to the license, indicates if changes were made and the licensor is not represented as endorsing the use made of the work. Further, any new works must be made available on the same conditions. The full details of the license are available at http://creativecommons.org/licenses/by-nc-sa/4.0.

CC BY NC ND: The CC BY-NC-ND license allows users to copy and distribute the Article, provided this is not done for commercial purposes and further does not permit distribution of the Article if it is changed or edited in any way, and provided the user gives appropriate credit (with a link to the formal publication through the relevant DOI), provides a link to the license, and that the licensor is not represented as endorsing the use made of the work. The full details of the license are available at http://creativecommons.org/licenses/by-nc-nd/4.0. Any commercial reuse of Open Access articles published with a CC BY NC SA or CC BY NC ND license requires permission from Elsevier and will be subject to a fee.

Commercial reuse includes:

- Associating advertising with the full text of the Article
- Charging fees for document delivery or access
- Article aggregation
- Systematic distribution via e-mail lists or share buttons

Posting or linking by commercial companies for use by customers of those companies.

20. **Other Conditions**:

v1.10

Questions? customercare@copyright.com.

CCC RightsLink

SG

ACS Publications
Most Trusted. Most Cited. Most Read.

Highly Sensitive and Selective Sensing of Free Bilirubin Using Metal–Organic Frameworks-Based Energy Transfer Process

Author: Yaran Du, Xiqian Li, Xueju Lv, et al
Publication: Applied Materials
Publisher: American Chemical Society
Date: Sep 1, 2017

PERMISSION/LICENSE IS GRANTED FOR YOUR ORDER AT NO CHARGE

This type of permission/license, instead of the standard Terms and Conditions, is sent to you because no fee is being charged for your order. Please note the following:

- Permission is granted for your request in both print and electronic formats, and translations.
- If figures and/or tables were requested, they may be adapted or used in part.
- Please print this page for your records and send a copy of it to your publisher/graduate school.
- Appropriate credit for the requested material should be given as follows: "Reprinted (adapted) with permission from (COMPLETE REFERENCE CITATION). Copyright (YEAR) American Chemical Society." Insert appropriate information in place of the capitalized words.
- One-time permission is granted only for the use specified in your RightsLink request. No additional uses are granted (such as derivative works or other editions). For any uses, please submit a new request.

If credit is given to another source for the material you requested from RightsLink, permission must be obtained from that source.

BACK CLOSE WINDOW

JOHN WILEY AND SONS LICENSE
TERMS AND CONDITIONS

Feb 03, 2024

This Agreement between Mr. Subhrajyoti Ghosh ("You") and John Wiley and Sons ("John Wiley and Sons") consists of your license details and the terms and conditions provided by John Wiley and Sons and Copyright Clearance Center.

License Number	5721171454946
License date	Feb 03, 2024
Licensed Content Publisher	John Wiley and Sons
Licensed Content Publication	Chemistry - A European Journal
Licensed Content Title	An Ultrahydrophobic Fluorous Metal–Organic Framework Derived Recyclable Composite as a Promising Platform to Tackle Marine Oil Spills
Licensed Content Author	Soumya Mukherjee, Ankit M. Kansara, Debasis Saha, et al
Licensed Content Date	Jun 30, 2016
Licensed Content Volume	22
Licensed Content Issue	31
Licensed Content Pages	7
Type of use	Dissertation/Thesis

Requestor type	University/Academic
Format	Print and electronic
Portion	Figure/table
Number of figures/tables	1
Will you be translating?	No
Title of new work	Synthesis Characterization and Applications of Aqua-Stable Metal-Organic Frameworks and their Composites for the Environmental Remediation and Bio-Molecule Sensing
Institution name	Indian Institute of Technology Guwahati
Expected presentation date	Jul 2024
Order reference number	7
Portions	Graphical Abstract
Requestor Location	Mr. Subhrajyoti Ghosh IIT Guwahati Guwahati, 781039 India Attn: Mr. Subhrajyoti Ghosh
Publisher Tax ID	EU826007151
Total	0.00 USD

Terms and Conditions

TERMS AND CONDITIONS

This copyrighted material is owned by or exclusively licensed to John Wiley & Sons, Inc. or one of its group companies (each a"Wiley Company") or handled on behalf of a society with which a Wiley Company has exclusive publishing rights in relation to a particular work (collectively "WILEY"). By clicking "accept" in connection with completing this licensing transaction, you agree that the following terms and conditions apply to this transaction (along with the billing and payment terms and conditions established by the Copyright Clearance Center Inc., ("CCC's Billing and Payment terms and conditions"), at the time that you opened your RightsLink account (these are available at any time at http://myaccount.copyright.com).

Terms and Conditions

- The materials you have requested permission to reproduce or reuse (the "Wiley Materials") are protected by copyright.
- You are hereby granted a personal, non-exclusive, non-sub licensable (on a stand-alone basis), non-transferable, worldwide, limited license to reproduce the Wiley Materials for the purpose specified in the licensing process. This license, **and any CONTENT (PDF or image file) purchased as part of your order,** is for a one-time use only and limited to any maximum distribution number specified in the license. The first instance of republication or reuse granted by this license must be completed within two years of the date of the grant of this license (although copies prepared before the end date may be distributed thereafter). The Wiley Materials shall not be used in any other manner or for any other purpose, beyond what is granted in the license. Permission is granted subject to an appropriate acknowledgement given to the author, title of the material/book/journal and the publisher. You shall also duplicate the copyright notice that appears in the Wiley publication in your use of the Wiley Material. Permission is also granted on the understanding that nowhere in the text is a previously published source acknowledged for all or part of this Wiley Material. Any third party content is expressly excluded from this permission.
- With respect to the Wiley Materials, all rights are reserved. Except as expressly granted by the terms of the license, no part of the Wiley Materials may be copied, modified, adapted (except for minor reformatting required by the new Publication), translated, reproduced, transferred or distributed, in any form or by any means, and no derivative works may be made based on the Wiley Materials without the prior permission of the respective copyright owner.**For STM Signatory Publishers clearing permission under the terms of the STM Permissions Guidelines only, the terms of the license are extended to include subsequent editions and for editions in other languages, provided such editions are for the work as a whole in situ and does not involve the separate exploitation of the permitted figures or extracts,** You may not alter, remove or suppress in any manner any copyright, trademark or other notices displayed by the Wiley Materials. You may not license, rent, sell, loan, lease, pledge, offer as security, transfer or assign the Wiley Materials on a stand-alone basis, or any of the rights granted to you hereunder to any other person.
- The Wiley Materials and all of the intellectual property rights therein shall at all times remain the exclusive property of John Wiley & Sons Inc, the Wiley Companies, or their respective licensors, and your interest therein is only that of having possession of and the right to reproduce the Wiley Materials pursuant to Section 2 herein during the continuance of this Agreement. You agree that you own no right, title or interest in or to the Wiley Materials or any of the intellectual property rights therein. You shall have no rights hereunder other than the license as provided for above in Section 2. No right, license or interest to any trademark, trade name, service mark or other branding ("Marks") of WILEY or its licensors is

granted hereunder, and you agree that you shall not assert any such right, license or interest with respect thereto

- NEITHER WILEY NOR ITS LICENSORS MAKES ANY WARRANTY OR REPRESENTATION OF ANY KIND TO YOU OR ANY THIRD PARTY, EXPRESS, IMPLIED OR STATUTORY, WITH RESPECT TO THE MATERIALS OR THE ACCURACY OF ANY INFORMATION CONTAINED IN THE MATERIALS, INCLUDING, WITHOUT LIMITATION, ANY IMPLIED WARRANTY OF MERCHANTABILITY, ACCURACY, SATISFACTORY QUALITY, FITNESS FOR A PARTICULAR PURPOSE, USABILITY, INTEGRATION OR NON-INFRINGEMENT AND ALL SUCH WARRANTIES ARE HEREBY EXCLUDED BY WILEY AND ITS LICENSORS AND WAIVED BY YOU.

- WILEY shall have the right to terminate this Agreement immediately upon breach of this Agreement by you.

- You shall indemnify, defend and hold harmless WILEY, its Licensors and their respective directors, officers, agents and employees, from and against any actual or threatened claims, demands, causes of action or proceedings arising from any breach of this Agreement by you.

- IN NO EVENT SHALL WILEY OR ITS LICENSORS BE LIABLE TO YOU OR ANY OTHER PARTY OR ANY OTHER PERSON OR ENTITY FOR ANY SPECIAL, CONSEQUENTIAL, INCIDENTAL, INDIRECT, EXEMPLARY OR PUNITIVE DAMAGES, HOWEVER CAUSED, ARISING OUT OF OR IN CONNECTION WITH THE DOWNLOADING, PROVISIONING, VIEWING OR USE OF THE MATERIALS REGARDLESS OF THE FORM OF ACTION, WHETHER FOR BREACH OF CONTRACT, BREACH OF WARRANTY, TORT, NEGLIGENCE, INFRINGEMENT OR OTHERWISE (INCLUDING, WITHOUT LIMITATION, DAMAGES BASED ON LOSS OF PROFITS, DATA, FILES, USE, BUSINESS OPPORTUNITY OR CLAIMS OF THIRD PARTIES), AND WHETHER OR NOT THE PARTY HAS BEEN ADVISED OF THE POSSIBILITY OF SUCH DAMAGES. THIS LIMITATION SHALL APPLY NOTWITHSTANDING ANY FAILURE OF ESSENTIAL PURPOSE OF ANY LIMITED REMEDY PROVIDED HEREIN.

- Should any provision of this Agreement be held by a court of competent jurisdiction to be illegal, invalid, or unenforceable, that provision shall be deemed amended to achieve as nearly as possible the same economic effect as the original provision, and the legality, validity and enforceability of the remaining provisions of this Agreement shall not be affected or impaired thereby.

- The failure of either party to enforce any term or condition of this Agreement shall not constitute a waiver of either party's right to enforce each and every term and condition of this Agreement. No breach under this agreement shall be deemed waived or excused by either party unless such waiver or consent is in writing signed by the party granting such waiver or consent. The waiver by or consent of a party to a breach of any provision of this Agreement shall not operate or be construed as a waiver of or consent to any other or subsequent breach by such other party.

- This Agreement may not be assigned (including by operation of law or otherwise) by you without WILEY's prior written consent.

- Any fee required for this permission shall be non-refundable after thirty (30) days from receipt by the CCC.

- These terms and conditions together with CCC's Billing and Payment terms and conditions (which are incorporated herein) form the entire agreement between you and WILEY concerning this licensing transaction and (in the absence of fraud) supersedes all prior agreements and representations of the parties, oral or written. This Agreement may not be amended except in writing signed by both parties. This Agreement shall be binding upon and inure to the benefit of the parties' successors, legal representatives, and authorized assigns.

- In the event of any conflict between your obligations established by these terms and conditions and those established by CCC's Billing and Payment terms and conditions, these terms and conditions shall prevail.

- WILEY expressly reserves all rights not specifically granted in the combination of (i) the license details provided by you and accepted in the course of this licensing transaction, (ii) these terms and conditions and (iii) CCC's Billing and Payment terms and conditions.

- This Agreement will be void if the Type of Use, Format, Circulation, or Requestor Type was misrepresented during the licensing process.

- This Agreement shall be governed by and construed in accordance with the laws of the State of New York, USA, without regards to such state's conflict of law rules. Any legal action, suit or proceeding arising out of or relating to these Terms and Conditions or the breach thereof shall be instituted in a court of competent jurisdiction in New York County in the State of New York in the United States of America and each party hereby consents and submits to the personal jurisdiction of such court, waives any objection to venue in such court and consents to service of process by registered or certified mail, return receipt requested, at the last known address of such party.

WILEY OPEN ACCESS TERMS AND CONDITIONS

Wiley Publishes Open Access Articles in fully Open Access Journals and in Subscription journals offering Online Open. Although most of the fully Open Access journals publish open access articles under the terms of the Creative Commons Attribution (CC BY) License only, the subscription journals and a few of the Open Access Journals offer a choice of Creative Commons Licenses. The license type is clearly identified on the article.

The Creative Commons Attribution License

The Creative Commons Attribution License (CC-BY) allows users to copy, distribute and transmit an article, adapt the article and make commercial use of the article. The CC-BY license permits commercial and non-

Creative Commons Attribution Non-Commercial License

The Creative Commons Attribution Non-Commercial (CC-BY-NC)License permits use, distribution and reproduction in any medium, provided the original work is properly cited and is not used for commercial purposes.(see below)

Creative Commons Attribution-Non-Commercial-NoDerivs License

The Creative Commons Attribution Non-Commercial-NoDerivs License (CC-BY-NC-ND) permits use, distribution and reproduction in any medium, provided the original work is properly cited, is not used for commercial purposes and no modifications or adaptations are made. (see below)

Use by commercial "for-profit" organizations

Use of Wiley Open Access articles for commercial, promotional, or marketing purposes requires further explicit permission from Wiley and will be subject to a fee.

Further details can be found on Wiley Online Library
http://olabout.wiley.com/WileyCDA/Section/id-410895.html

Other Terms and Conditions:

v1.10 Last updated September 2015

Questions? customercare@copyright.com.

Publications

1. **S. Ghosh**[ϰ], A. Rana[ϰ], and S. Biswas, Metal–organic framework-based fluorescent sensors for the detection of pharmaceutically active compounds, Chem. Mater. 2024, 36, 99-131. (IF:10.5) (ϰ = equal contribution)
2. **S. Ghosh**, J. Krishnan, S. Hossain, A. Dhakshinamoorthy, and S. Biswas, MOF-fabric composites based on a multi-functional MOF as luminescent sensor for a neurotransmitter and an anti-cancer drug, ACS Appl. Mater. Interfaces, 2023, 15, 26843–26851. (IF: 9.5)
3. **S. Ghosh**, D Mal, S Mukherjee, and S Biswas, Sustainable fabrication of an eco-friendly, reusable Chitosan@Cotton@MOF composite sensor for 2,4-dichlorophenoxyacetic acid herbicide and nitroxoline antibiotic, ACS Sustainable Chem. Eng. 2023, 11, 13179–13186. (IF: 8.4)
4. **S. Ghosh**, J. Krishnan, V. Karthik, A. Dhakshinamoorthy, and S. Biswas, Functionalized metal-organic framework for selective fluorometric detection of sodium dodecyl sulfate and Vitamin B_{12} using MOF@Cotton composites and Lewis base-catalyzed condensation reaction, Inorg. Chem. 2023, 22, 8605–8614. (IF: 5.4)
5. **S. Ghosh**, R. Lipin, A. Ngoipala, N. Ruser, D. M. Venturi, A. Rana, M. Vandichel, and S. Biswas, Hf-based MOF for rapid and selective sensing of a nerve agent simulant and an aminophenol: insights from experiments and theory, Inorg. Chem. 2023, 62, 14632–14646. (IF: 5.4)
6. **S. Ghosh**[ϰ], A. Rana[ϰ], S. Kumar, C. Gogoi, S. Mukherjee, U. Manna, and S. Biswas, A self-cleaning hydrophobic MOF based composite for highly efficient and recyclable separation of oil from water and emulsion, Mater. Chem. Front., 2022, 6, 2051-2060. (IF: 8.683)
7. **S. Ghosh**, F. Steinke, A. Rana, and S. Biswas, A fluorescent zirconium organic framework displaying rapid and nanomolar level detection of Hg(II) and nitroantibiotics, Inorg. Chem. Front., 2022, 9, 859-869. (IF: 7.779)
8. **S. Ghosh**, N. Nagarjun, and S. Nandi, A. Dhakshinamoorthy, S. Biswas, Two birds with one arrow: functionalized Al(III) MOF acts as a fluorometric sensor of dopamine in bio-fluids and recyclable catalyst for Biginelli reaction, J. Mater. Chem. C, 2022, 10, 6717-6727. (IF: 8.067)
9. A. Rana[ϰ], **S. Ghosh**[ϰ], and S. Biswas, An eco-friendly approach by nonfluorous self-cleaning metal-organic framework composite and membrane for oil-water separation, Inorg. Chem. Front., 2023, 10, 612-620. (IF: 7.779).
10. **S. Ghosh**, A. Das, and S. Biswas, A functionalized UiO-66 MOF acting as a luminescent chemosensor for selective and sensitive turn-on detection of superoxide and acetylacetone, Microporous Mesoporous Mater., 2021, 323, 111251. (IF: 5.876)
11. **S. Ghosh**, and S. Biswas, Ultrafast and nanomolar level detection of H_2S in aqueous medium using a functionalized UiO-66 metal-organic framework based fluorescent chemosensor, Dalton Trans., 2021, 50, 11631. (IF: 4.569)

12. **S. Ghosh**, and S. Biswas, A functionalized UiO-66 metal-organic framework acting as a fluorescent based selective sensor of hydrazine in aqueous medium, Microporous Mesoporous Mater., 2021, 329, 111552. (IF: 5.876)
13. **S. Ghosh**, N. Nagarjun, M. Alam, A. Dhakshinamoorthy and S. Biswas, Friedel-crafts alkylation reaction efficiently catalyzed by a di-amide functionalized Zr(IV) metal-organic framework, Molecular Catalysis, 2022, 517, 112007. (IF: 4.6)
14. **S. Ghosh**, J. Krishnan, V. Karthik, A. Rana, A. Dhakshinamoorthy and S. Biswas, Friedlander condensation reaction catalysed by hafnium-based metal-organic framework, Molecular Catalysis, 2022, 533, 112748. (IF: 4.6)
15. A. Das[x], **S. Ghosh**[x], L. Bourda, M. Sk, K. Banerjee, K. Van Hecke and S. Biswas, A Cd(II)-organic framework as a highly sensitive and rapid fluorometric sensor for ascorbic acid in aqueous medium CrystEngComm, 2022, 24, 4723-4730. (IF: 3.756)
16. **S. Ghosh**, N. Nagarjun, M. Alam, A. Dhakshinamoorthy and S. Biswas, Nanomolar level fluorogenic detection of cyanide with an amide functionalized zirconium metal-organic framework and its application in real-world cyanide monitoring, Eur. J. Inorg. Chem., 2022, 2022, e202200110. (IF: 2.551)
17. **S. Ghosh**, F. Steinke, A. Rana, M. Alam and S. Biswas, A metal-organic framework with allyloxy functionalization for aqueous-phase fluorescence recognition of Pd(II) ion, Eur. J. Inorg. Chem., 2021, 3846. (IF: 2.551)
18. **S. Ghosh**, A. Rana, A. Patel, D. Manna, and S. Biswas, Superhydrophobic nanosize metal-organic framework composites for the targeted removal of hydrophobic pharmaceuticals and outstanding bacterial anti-adhesion, 2024, Environ. Sci. Nano 2024, 11, 1967-1977. (IF: 9.47)
19. **S. Ghosh**, S. Mukherjee, V. Karthik, P. Bera, A. Dhakshinamoorthy, and S. Biswas, A superhydrophobic MOF facilitating efficient solvent-free catalytic chemical fixation of CO_2 and oxidation of hydrocarbons and MOF@cotton@starch composite based selective sensing of an herbicide, J. Mater. Chem. C, 2024, 12, 4460-4472. (IF: 8.067)
20. S. Ghosh, D. Mal, and S. Biswas, Regulating water decontamination and food safety by a reusable, nanosized MOF@cotton@chitosan composite through nanomolar detection of drug nitroxinil and organoarsenic feed additive p-arsanilic acid, Environ. Sci. Nano, 2024, 11, 1967-1977. (IF: 9.47)
21. **S. Ghosh**, P. Laha, and S. Biswas, Sustainable superhydrophobic MOF@starch@cotton composite for fast, selective and nanomolar sensing and adsorptive removal of a fluorinated herbicide from aqueous medium. Environ. Sci. Nano 2024, 10.1039/D4EN00289J.
22. S. Nandi, **S. Ghosh**, M. SK, and S. Biswas, Fluorogenic naked eye turn-on sensing of hypochlorous acid by a Zr-based metal organic framework, New J. Chem., 2021, 45, 14211. (IF: 3.925)
23. A. Rana, C. Gogoi, **S. Ghosh**, S. Nandi, S. Kumar, U. Manna and S. Biswas, Rapid recognition of fatal cyanide in water in a wide pH range by a trifluoroacetamido based metal-organic framework, New J. Chem., 2021, 45, 20193-20200. (IF: 3.925)
24. S. Mukherjee, **S. Ghosh**, and S. Biswas, A MOF chemosensor for highly sensitive and ultrafast detection of folic acid in biofriendly medium, paper Strips and real samples, New J. Chem., 2021, 45, 20193-20200. (IF: 3.925)

25. C. Gogoi[x], A. Rana[x], **S. Ghosh**, R. Fopase, L. M. Pandey and S. Biswas, Superhydrophobic self-cleaning composite of MOF with polypropylene fabric for efficient removal of oils from oil-water mixtures and emulsions, ACS Appl. Nano Mater., 2022, 5, 10003-10014. (IF: 6.14)
26. S. Mukherjee, **S. Ghosh**, and S. Biswas, Amine-rich porous MOF nanocrystals for the selective capture of carcinogenic anions and organo-pollutants from the waste water environment at neutral pH, ACS Appl. Nano Mater., 2023, 6, 22231-22240. (IF: 6.14)

Conferences Attended

1. CRSI-NSC-28: 28th National Symposium in Chemistry, Indian Institute of Technology Guwahati, 2022.
2. Research and Industrial Conclave, Indian Institute of Technology Guwahati, 2022.
3. Frontiers in Chemical Sciences, Indian Institute of Technology Guwahati, 2022.
4. North-East Research Conclave, Indian Institute of Technology Guwahati, 2022.
5. MTIC XIX – Modern Trends in Inorganic Chemistry, Banaras Hindu University, 2022.

THE END